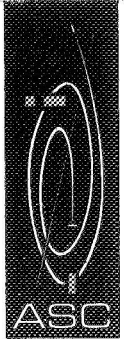


Not in



ASTRO
SCIENCES
CENTER



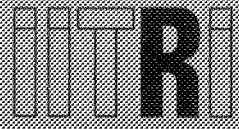
N 70 30919
NASA CR 73450

CASE FILE
COPY

ORBITAL IMAGERY FOR PLANETARY EXPLORATION

VOLUME I

TECHNICAL SUMMARY



IIT RESEARCH INSTITUTE

10 West 35 Street
Chicago, Illinois 60616

ORBITAL IMAGERY FOR PLANETARY EXPLORATION

VOLUME I

TECHNICAL SUMMARY

Written and Compiled by

D. A. Klopp

Contributors


A. Binder
H. Borough
H. Goldman
M. Hopper
J. C. Jones
D. A. Klopp
J. C. Niehoff
D. L. Roberts
K. Uherka
S. Verner
A. Weigandt

for

Mission Analysis Division
National Aeronautics and Space Administration
Office of Advanced Research and Technology
Moffett Field, California

Contract No. NAS2-4494

APPROVED:



D. L. Roberts, Manager
Astro Sciences

February 1970

TABLE OF CONTENTS

	<u>Page</u>
1. INTRODUCTION	1
2. STUDY PROCEDURE	7
2.1 Exploration Objectives	8
2.1.1 Scientific Objectives	8
2.1.2 Engineering Objectives	14
2.2 Measurement Definition	16
2.3 Orbit Selection	21
2.3.1 Interplanetary Transfers	23
2.3.2 Orbit Constraints	26
2.3.3 Measurement Families	27
2.3.4 Candidate Orbits	28
2.3.5 Orbit Selection	28
2.3.6 Orbit Documentation	31
2.4 Imager Scaling Laws	31
2.5 Experiment Support Requirements	37
3. EXPLORATION OBJECTIVES	40
3.1 Goals of Space Exploration	40
3.2 Scientific Objectives	41
3.2.1 Planetary Composition	42
3.2.2 Planetary Structure	46
3.2.3 Active Planetary Processes	49
3.2.4 Atmospheric Composition	54
3.2.5 Atmospheric Structure	57
3.2.6 Active Atmospheric Processes	60
3.2.7 Fields	67
3.2.8 Active Biota	70
3.2.9 Extinct Biota	74
3.3 Engineering Objectives	77

TABLE OF CONTENTS (Continued)

		Page
4.	MEASUREMENT DEFINITION	83
4.1	Ground Resolution	87
4.2	Image Size	88
4.3	Positional Accuracy	89
4.4	Planetary Coverage	89
4.5	Planetary Distribution	90
4.6	Acquisition Times and Repetition Rates	91
4.7	Sensor Types	92
4.8	Spectral Regions	93
4.9	Spectral Bandwidth	94
4.10	Overlap	94
4.11	Sun Elevation	95
4.12	Supporting Measurements	95
4.13	Distribution of Measurements	96
5.	ORBIT SELECTION RESULTS	131
5.1	Mars	131
5.1.1	Interplanetary Transfer Selections	131
5.1.2	Orbit Characteristics and Constraints	140
5.1.3	Orbit Selection	148
5.2	Venus	156
5.2.1	Interplanetary Transfer Selections	156
5.2.2	Orbit Characteristics and Constraints	161
5.2.3	Orbit Selections	175
5.3	Mercury	178
5.3.1	Interplanetary Transfer Selections	178
5.3.2	Orbit Characteristics and Constraints	180
5.3.3	Orbit Selections	197

TABLE OF CONTENTS (Continued)

	Page
5.4 Jupiter	203
5.4.1 Interplanetary Transfer Selections	203
5.4.2 Orbit Characteristics and Constraints	210
5.4.3 Orbit Selections	217
5.5 The Moon	220
6. IMAGING SENSOR SYSTEM SCALING LAWS	223
6.1 Ultraviolet Scanning Systems	225
6.2 Television Systems	239
6.3 Film Camera Systems	254
6.4 Infrared Scanning Systems	267
6.5 Passive Microwave Systems	282
6.6 Noncoherent Radar Systems	293
6.7 Synthetic Aperture Radar Systems	308
7. EXPERIMENT SUPPORT REQUIREMENTS	320
7.1 Ultraviolet Scanning Systems	321
7.2 Visual Imaging Systems	328
7.2.1 Mars	330
7.2.2 Venus	354
7.2.3 Mercury	356
7.2.4 Jupiter	358
7.3 Infrared Scanning Systems	359
7.3.1 Mars	361
7.3.2 Venus	365
7.3.3 Mercury	365
7.3.4 Jupiter	368
7.4 Passive Microwave Scanning Systems	369
7.5 Radar Imaging Systems	373
8. CONCLUSIONS AND RECOMMENDATIONS	379
REFERENCES	388
APPENDIX A ORBIT SELECTION EXAMPLE	392

LIST OF FIGURES

<u>Figure No.</u>		<u>Page</u>
1-1	Spacecraft Subsystems	2
1-2	Study Tasks	4
2-1	Analysis of Scientific Goal	11
2-2	Development of Engineering Observables Planetary Landers	17
2-3	Example of Measurement Specification Worth Curve	22
2-4	Stereographic Projection Definition	30
2-5	Function of Scaling Laws	33
2-6	Logic Diagram for TV Cameras	36
3-3	Development of Engineering Observables Planetary Orbiters	78
3-4	Development of Engineering Observables Atmospheric Probes	79
3-5	Development of Engineering Observables Atmospheric Floaters	80
3-6	Development of Engineering Observables Planetary Landers	81
4-2	A1 to A4: Ground Resolution Worth Curves (Relative Worth vs. Ground Resolution)	99
	A5 to A8: Ground Resolution Worth Curves (Relative Worth vs. Ground Resolution)	100
4-3	B1 to B4: Image Size Worth Curves (Relative Worth vs. Image Size)	101
	B5 to B8: Image Size Worth Curves (Relative Worth vs. Image Size)	102
	B9 to B12: Image Size Worth Curves (Relative Worth vs. Image Size)	103
4-4	C1 to C4: Positional Accuracy Worth Curves (Relative Worth vs. Positional Accuracy)	104
	C5 to C8: Positional Accuracy Worth Curves (Relative Worth vs. Positional Accuracy)	105

LIST OF FIGURES (Continued)

<u>Figure No.</u>		<u>Page</u>
4-4	C9 to C12: Positional Accuracy Worth Curves (Relative Worth vs. Positional Accuracy)	106
4-5	D1 to D4: Planetary Coverage Worth Curves (Relative Worth vs. Planetary Coverage)	107
	D5: Planetary Coverage Worth Curves (Relative Worth vs. Planetary Coverage)	108
4-6	E1 to E4: Time Worth Curves (Relative Worth vs. Time)	109
	E5 to E7: Time Worth Curves (Relative Worth vs. Time)	110
	E8 to E11: Time Worth Curves (Relative Worth vs. Time)	111
	E12 to E15: Time Worth Curves (Relative Worth vs. Time)	112
	E16 to E17: Time Worth Curves (Relative Worth vs. Time)	113
4-7	F1 to F4: Spectral Region Worth Curves (Relative Worth vs. Spectral Region)	114
	F6 to F8: Spectral Region Worth Curves (Relative Worth vs. Spectral Region)	115
	F9 to F12: Spectral Region Worth Curves (Relative Worth vs. Spectral Region)	116
	F13 to F16: Spectral Region Worth Curves (Relative Worth vs. Spectral Region)	117
	F17 to F20: Spectral Region Worth Curves (Relative Worth vs. Spectral Region)	118
	F21 to F22: Spectral Region Worth Curves (Relative Worth vs. Spectral Region)	119
4-8	G1 to G4: Bandwidth Worth Curves (Relative Worth vs. Bandwidth)	120
	G5 to G8: Bandwidth Worth Curves (Relative Worth vs. Bandwidth)	121
	G9 to G12: Bandwidth Worth Curves (Relative Worth vs. Bandwidth)	122
	G13 to G16: Bandwidth Worth Curves (Relative Worth vs. Bandwidth)	123

LIST OF FIGURES (Continued)

<u>Figure No.:</u>		<u>Page</u>
4-8	G17 to G20: Bandwidth Worth Curves (Relative Worth vs. Bandwidth)	124
4-9	H1 to H3: Image Overlap Worth Curves (Relative Worth vs. Image Overlap)	125
4-10	I1 to I4: Solar Elevation Angle Worth Curves (Relative Worth vs. Solar Elevation)	126
	I5 to I8: Solar Elevation Angle Worth Curves (Relative Worth vs. Solar Elevation)	127
4-11	J1 to J4: Vertical Resolution Worth Curves (Relative Worth vs. Vertical Resolution)	128
4-12	Areas to be Observed for Wave of Darkening	129
4-13	Spectral Distribution of Imagery	130
5-2	Mars Capture Occultation Contours (1984)	136
5-3	Mars Aiming Angle/Orbit Orientation Relation- ship (1984)	137
5-4	Mars Capture Occultation Contours (1988)	138
5-5	Mars Aiming Angle/Orbit Orientation Relation- ship (1988)	139
5-6	Mars Orbital Geometry	141
5-7	Mars Illumination Exposure	142
5-8	Mars 50 yr. Orbit Lifetime Curve	144
5-9	Mars Orbit Altitude Ratios	146
5-10	Nodal Precession Due to Mars Oblateness	149
5-11	Argument of Periapse Precession Due to Mars Oblateness	150
5-12	Venus Capture Occultation Contours	159
5-13	Venus Aiming Angle/Orbit Orientation Relation- ship	160
5-14	Venus Rotation/Revolution Relationship	162
5-15	Basic Orbit Definitions	164
5-16	Venus 50-yr Lifetime Orbits	166
5-17	Venus Orbit Altitude Ratios	168
5-18	Venus Impulse Requirements for Complete Daylight Coverage	170

LIST OF FIGURES (Continued)

<u>Figure No.</u>		<u>Page</u>
5-19	Venus Orbit Solar Perturbations: Altitude	172
5-20	Venus Orbit Solar Perturbation: Argument of Periapse	173
5-21	Mercury Capture Occultation Contours (1984)	181
5-22	Mercury Aiming Angle/Orbit Orientation Relationship (1984)	182
5-23	Mercury Capture Occultation Contours (1988)	183
5-24	Mercury Aiming Angle/Orbit Orientation Relationship (1988)	184
5-25	Mercury Rotation/Revolution Relationship	185
5-26	Mercury Orbit Altitude Ratios	190
5-27	Mercury Orbit Solar Perturbations: Altitude	193
5-28	Mercury Orbit Solar Perturbations: Arg. of Periapse	194
5-29	Control Requirements of a Mercury Orbit ($h_p = 500$ km, $e = 0.9$) Under the Influence of Solar Perturbations	196
5-30	Constant Solar Elevation Contours for a Circular 500 km Altitude Polar Mercury Orbit	199
5-31	Jupiter Capture Occultation Contours	208
5-32	Jupiter Aiming Angle/Orbit Orientation	209
5-33	Jupiter 50-year Orbit Lifetime Curve	211
5-34	Jupiter Candidate Orbit Size Constraints	213
5-35	Jupiter Orbit Altitude Range	216
6-1	Logic Diagram for Ultraviolet Scanning Systems	226
6-2	Scaling Laws for Ultraviolet Scanning Systems	227
6-3	Lunar Photometric Function	229
6-4	Logic Diagram for Television Systems	242
6-5	Scaling Laws for Television Systems	243
6-6	TV Tube Operational Resolution	247
6-7	TV Format Sizes	249
6-8	TV Tube Lengths	252

LIST OF FIGURES (Continued)

<u>Figure No.</u>		<u>Page</u>
6-9	Logic Diagram for Photographic Film Systems	256
6-10	Scaling Laws for Photographic Film Systems	257
6-11	Radiation Shielding Weight	265
6-12	Logic Diagram for Infrared Scanning Systems	270
6-13	Scaling Laws for Infrared Scanning Systems	271
6-14	Logic Diagram for Passive Microwave Systems	284
6-15	Scaling Laws for Passive Microwave Systems	285
6-16	Minimum Integration Time	288
6-17	Maximum Antenna Size	290
6-18	Microwave Receiver Weight	291
6-19	Microwave Receiver Power	292
6-20	Logic Diagram for Noncoherent Radar Systems	296
6-21	Scaling Laws for Noncoherent Radar Systems	297
6-22	Side-Looking Radar Geometry	299
6-23	Radar Stereo Modes	303
6-24	Logic Diagram for Synthetic Aperture Radar Systems	310
6-25	Scaling Laws for Synthetic Aperture Radar Systems	311
A-1	Stereographic Projection: Arrival Configura- tion	395
A-2	Stereographic Projection: Constraints	397
A-3	Stereographic Projection: Orbit Options	400
A-4	Stereographic Projection: Orbit Selection	402
A-5	Stereographic Projection: 60 Days After Arrival	404

LIST OF TABLES

<u>Number</u>		<u>Page</u>
2-1	Development of Scientific Objectives	9
2-2	Analysis of Scientific Observables	12
2-3	Development of Engineering Objectives	15
2-4	Example of Measurement Specification Lunar Surface Elevations (Regional)	20
2-5	Development of Planetary Orbit Analysis	24
2-6	Orbit Selection Data Sheet No. 200	32
3-1	Planetary Composition Objectives	43
3-2	Planetary Structure Objectives	47
3-3	Planetary Processes Objectives	50
3-4	Atmospheric Composition Objectives	55
3-5	Atmospheric Structure Objectives	58
3-6	Atmospheric Processes Objectives	61
3-7	Field Objectives	68
3-8	Active Biota	71
3-9	Extinct Biota Objectives	75
4-1	Summary of Measurement Specification	85
5-1	Summary of Minimum VHT Mars Transfers: 1975- 1990	133
5-2	Mars Candidate Orbit Sizes	147
5-3	Measurement Families for Mars	152
5-4	Mars Candidate Orbit Size Coverage Times	153
5-5	Summary of Minimum VHT Venus Transfers: 1975- 1981	157
5-6	Potential Venus Orbit Coverage Characteristics	163
5-7	Venus Candidate Orbit Sizes	167
5-8	Measurement Families for Venus	176
5-9	Summary of Selected Mercury Transfers: 1980 - 1992	179

LIST OF TABLES -continued

<u>Number</u>		<u>Page</u>
5-10	Potential Mercury Orbit Coverage Characteristics	187
5-11	Mercury Candidate Orbit Sizes	189
5-12	Measurement Families for Mercury	198
5-13	Mercury Solar Elevation Restricted Coverage	200
5-14	Minimum Constant Time VHL Transfer and Absolute Minimum VHL Transfers to Jupiter	204
5-15	Summary of 700 ^d Jupiter Transfers: 1975 - 1986	207
5-16	Jupiter Candidate Orbit Sizes	214
5-17	Measurement Families for Jupiter	218
5-18	Jupiter Candidate Orbit Size Coverage Times	219
5-19	Measurement Families for the Moon	221
6-1	Values of r_{ϕ}/r_0	228
6-2	Image Specifications and Orbit Parameters for Ultraviolet Cloud Formation Imagery at Venus	231
6-3	Sample Experiment Support Requirements for an Ultraviolet Scanning System	240
6-4	Image Specifications and Orbit Parameters for Visual Surface Topography Imagery at Mars	244
6-5	Sample Experiment Support Requirements for a Television Imaging System	255
6-6	Image Specifications and Orbital Parameters for Visual Surface Topography Stereo Imagery at Mars	259
6-7	Film Speed and System Resolution	262
6-8	Sample Experiment Support Requirements for a Photographic Film System	268
6-9	Image Specifications and Orbital Parameters for Infrared Surface Thermal Anomaly Imagery at Mars	269
6-10	Infrared Detector Characteristics	274
6-11	Estimates of Planetary Temperatures	275
6-12	Computation of B	277
6-13	Values of C_p and C_t	278

IIT RESEARCH INSTITUTE

LIST OF TABLES -continued

<u>Number</u>		<u>Page</u>
6-14	Sample Experiment Support Requirements for an Infrared Scanning System	281
6-15	Image Specifications and Orbital Parameters for Regional Atmospheric Thermal Anomalies (Venus)	283
6-16	Sample Experiment Support Requirements for a Passive Microwave Imaging System	294
6-17	Image Specifications and Orbit Parameters for Structure of Features (Regional) at Venus	295
6-18	Sample Experiment Support Requirements for Noncoherent Radar Imaging Systems	309
6-19	Image Specifications and Orbital Parameters for Local Scale Structure of Features Imagery (Venus)	313
6-20	Sample Experiment Support Requirements for Synthetic Aperture Radar Imaging Systems	318
7-1	Utility of Orbital Ultraviolet Imagery	322
7-2	Support Requirements for Ultraviolet Scanning Experiments	323
7-3	Utility of Orbital Visual Imagery	329
7-4	Support Requirements for Visual Experiments- Mars (regional)	332
7-5	Support Requirements for Visual Experiments- Mars (local)	342
7-6	Support Requirements for Visual Experiments- Mars (detailed)	347
7-7	Support Requirements for Visual Experiments- Venus	355
7-8	Support Requirements for Visual Experiments- Mercury	357
7-9	Support Requirements for Visual Experiments- Jupiter	360
7-10	Utility of Orbital Infrared Imagery	361
7-11	Support Requirements for Infrared Experiments- Mars	362
7-12	Support Requirements for Infrared Experiments- Venus	366

LIST OF TABLES-continued

<u>Number</u>		<u>Page</u>
7-13	Support Requirements for Infrared Experiments-Mercury and Jupiter	367
7-14	Utility of Orbital Passive Microwave Imagery	369
7-15	Support Requirements for Passive Microwave Imaging Experiments	371
7-16	Utility of Orbital Radar Imagery	374
7-17	Support Requirements for Radar Imaging Experiments-Venus	376
A-1	Measurement Family Specifications	394
A-2	Mars Candidate Orbit Sizes	398

1. INTRODUCTION

"It is better to paint with a wide brush of unknown thickness than to leave the canvas blank."-Gunnar Myrdal

1. INTRODUCTION

The purpose of this study is to estimate the requirements imposed on spacecraft support subsystem technologies by imaging sensor systems used aboard unmanned planetary orbiters. The time frame of interest covers launch opportunities from 1975 to 1995, and the targets considered are Mercury, Venus, the Moon, Mars, and Jupiter. By the definition used here, imaging sensors provide two dimensional information, essentially simultaneously, either by rapid scanning or direct two dimensional rewording.

Knowledge of demands imposed upon spacecraft support subsystems assists in identifying needs for advanced technology development. These needs are made apparent by comparing required subsystem support with projected subsystem capabilities. This study provides the groundwork for such comparison by estimating the support requirements of planetary orbital imaging experiments. Ranger, Surveyor, Lunar Orbiter, and Mariner mission experience has shown that imaging experiments are likely to impose the most crucial demands on spacecraft subsystems in future unmanned planetary exploration. Thus valuable insight pertaining to necessary subsystem technology development is afforded by considering planetary orbital imaging experiments.

Figure 1-1 shows the support interfaces between an imaging experiment and the other spacecraft subsystems. These interfaces can be represented by the following experiment characteristics:

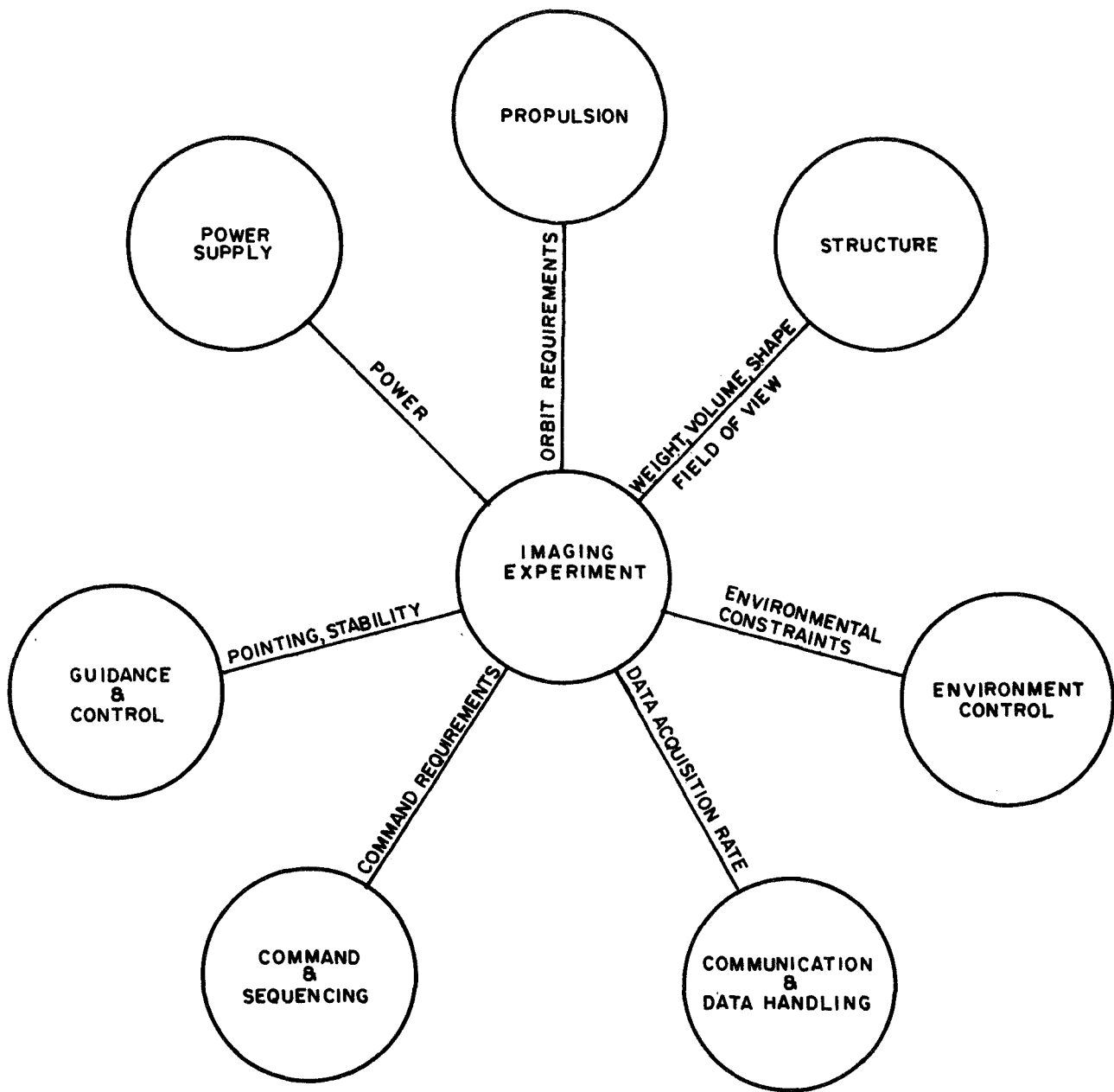


FIGURE I-1. SPACECRAFT SUBSYSTEMS

weight
volume
shape
field of view
environmental constraints
data acquisition rate
command requirements
pointing and platform stability
power
orbit requirements.

The functional relationships between the experiment and the rest of the spacecraft are expressed, in this study, by "scaling laws." Scaling laws express required subsystem capabilities in terms of image characteristics (such as image ground size and resolution) and spacecraft orbit variables (such as altitude and velocity). The image characteristics are necessary to meet the imaging measurement requirements, which are derived directly from the goals of space exploration, and the orbit variables are defined by selecting specific orbits for groups of similar experiments or "families." Thus the study tasks, as shown in Figure 1-2, are:

1. exploration objectives - identify role of remote sensing in total planetary exploration
2. measurement definition - specify imaging measurements in support of exploration objectives
3. orbit selection - determine operational orbits for measurement families
4. imager scaling laws - express experiment characteristics in terms of measurement definition and orbit variables

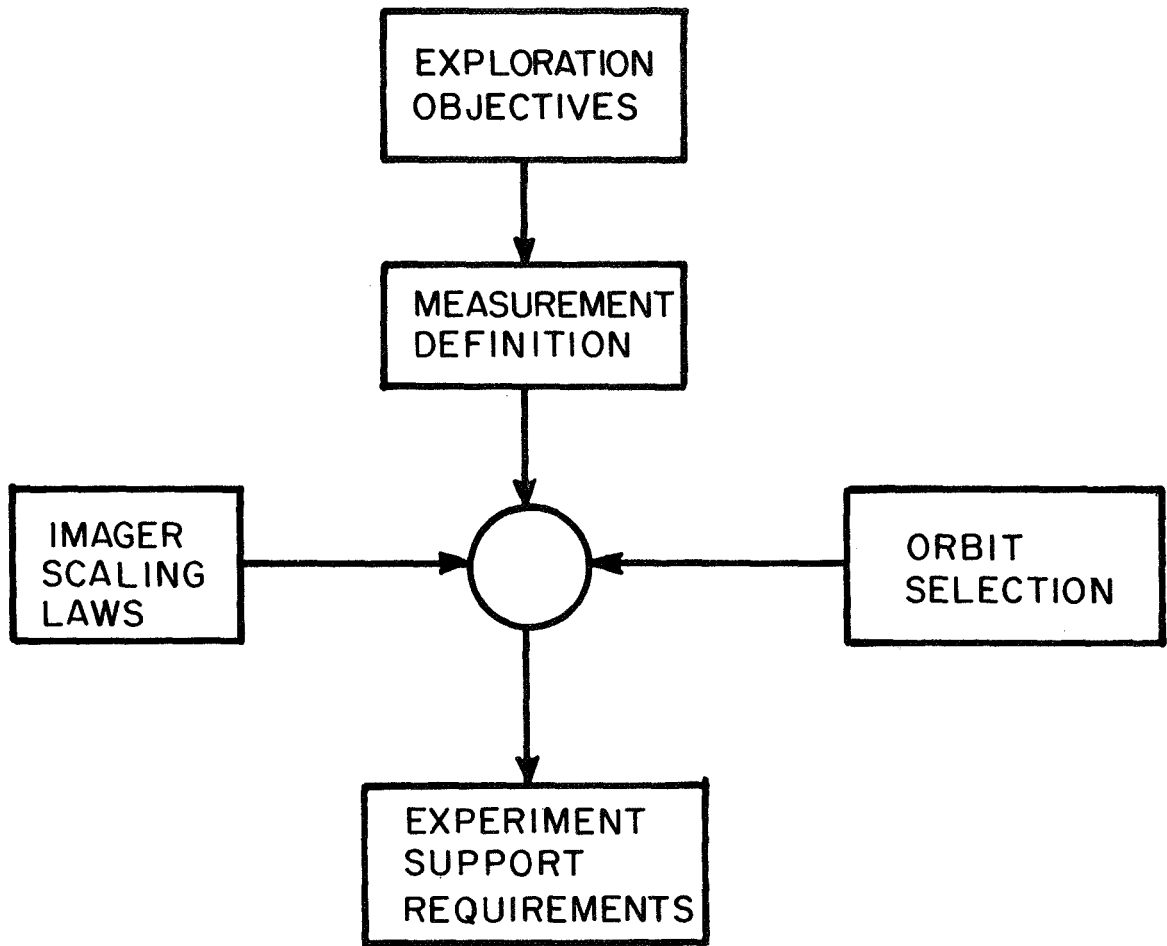


FIGURE 1.2. STUDY TASKS

5. experiment support requirements - use measurement definitions, orbit selections, and scaling laws to estimate typical support requirements.

This volume of the final report summarizes the results of these tasks. The remaining sections of this volume are:

Section 2 (Study Procedure) - reports the method of approach used in each of the study tasks.

Section 3 (Exploration Objectives) - summarizes the scientific and engineering objectives and shows how each objective contributes to the goals of space exploration. Relevant observable properties of the planets are identified in support of the objectives. A detailed description of each observable property, in terms of its geometric, temporal, and spectral characteristics is presented in Vol. II (Definition of Scientific Objectives).

Section 4 (Measurement Definition) - describes the nature and quality of the desired imagery. Image specifications are tabulated for each observable property. The dependence of measurement achievement upon each specified parameter is summarized.

Section 5 (Orbit Selection) - summarizes, for each target planet, the orbital selections for the imaging measurements. Interplanetary transfers are selected for each target planet, and orbits are selected to meet the measurement specifications. A detailed description of each orbit selected for imaging experiments may be found in Volume III (Orbit Selection and Definition).

Section 6 (Imaging Sensor System Scaling Laws) - presents sensor models consisting of a collection of theoretical and empirical expressions suitable for relating the image specifications; orbit parameters; sensor system design variables, and experiment support requirements. For each type of

imaging system, these relations are organized to facilitate the design of an imaging system in sufficient detail that the most important support requirements can be identified. A logic diagram indicates schematically the steps in the design procedure, while a scaling law chart summarizes the theoretical and empirical relations. An illustrative design example is provided for each type of imaging system. A detailed description of the scaling laws is given in Volume IV (Imaging Sensor System Scaling Laws).

Section 7 (Experiment Support Requirements) - discusses the imaging experiment support requirements. Each spectral region is discussed individually. General comments concerning the usefulness of different types of imagers, the degree to which orbital imagery may be successful in obtaining the desired measurements, and correlation of image specifications with support requirements are presented. A detailed list of the support requirements for each individual experiment is given in Volume V (Support Requirements for Planetary Orbital Imaging).

The entire report consists of five volumes:

- I - Technical Summary
- II - Definition of Scientific Objectives
- III - Orbit Selection and Definition
- IV - Imaging Sensor System Scaling Laws
- V - Support Requirements for Planetary
Orbital Imaging.

2. STUDY PROCEDURE

This section describes the techniques that have been used throughout the study. First the relationships between the five major tasks are defined and then the methodologies within each task area are discussed. The importance of a systematized approach cannot be over emphasized in a study of this breadth. The overall relationship between the five major study tasks was shown in Figure 1-2.

The exploration objectives task provides an explicit statement of those objectives of unmanned planetary orbital exploration which might be accomplished by imaging experiments. By considering the goals of space exploration, the current knowledge of planetary phenomena, and conceptual measurement techniques, the analysis identifies those measureable planetary phenomena which can be investigated usefully by remote sensing and by imaging.

The measurement definition task deals with those phenomena for which orbital imagery is useful, describing them in terms of measurement specifications from the viewpoint of the scientist who must interpret the data. A table of detailed measurement specifications provides nominal values for each imaging parameter. The measurement specifications are used in the orbit selection procedure and in the final estimation of experiment support requirements.

The orbit selection task defines operational orbits for each of the required measurements. Where similar measurement requirements exist, they have been grouped into families and orbits selected for these families. The resultant orbital parameters are also used in the estimation of experiment support requirements.

The imager scaling laws provide the quantitative relationships between the imager support requirements (i.e., weight, power, etc.) and its ability to meet given measurement specifications from a given orbit. Useful types of imaging

systems are selected by examining the measurement specifications. For each imager type, a collection of scaling laws which relate the experiment support requirements to the measurement specifications, to the sensor system characteristics, and to the orbit variables, are derived.

The experiment support requirements task combines the results of each of the previous tasks. Both measurement specifications and orbit parameters are used in the scaling laws to estimate typical support requirements demanded by each imaging experiment.

The remainder of this section describes the method of analysis employed in each of the five tasks.

2.1 Exploration Objectives

In identifying useful imaging measurements, a systematic organization of logic reduces the chance of oversight. The rational methodology employed here provides a framework which identifies all the significant objectives of planetary exploration. Both scientific and engineering objectives are considered.

2.1.1 Scientific Objectives

The analysis starts at the highest and most general echelon of space exploration, and proceeds to define the exploration in stages of increasing detail, ultimately translating the information requirements into measurement specifications. This analysis technique is summarized in Table 2-1. As the whole is equal to the sum of its parts, each goal is wholly described by its subgoals, each subgoal by its aspects, each aspect by its objectives, and each objective by its observables. However, no evaluation has been attempted of the relative worth of the components of any category or subcategory. For example, atmospheric composition and planetary structure are assumed to be of equal

Table 2-1

DEVELOPMENT OF SCIENTIFIC OBJECTIVES

Step	Analysis
1. Goal	Define the exploration policy (e.g. understand the origin and evolution of the Solar System).
2. Subgoal	Subdivide the goal into narrower areas of policy (e.g. determine the present status of the planets).
3. Aspect	Develop phenomenological aspects of the subgoals (e.g. to determine planetary structure).
4. Objective	Identify the scientific components (e.g., surface morphology) which together provide understanding of each aspect.
5. Observable	Express the objectives as planetary properties that can be measured (e.g. surface topography).

significance in determining the present state of the planets. They may not be of equal significance, however, in their impact on the orbital imaging support requirements.

In passing from one level of detail to the next, an extremely coarse logic filter prevents the analysis of areas which are manifestly irrelevant to this study. For example, the subgoal of determining the present status of the Sun is shown in Section 3 as a valid and necessary subgoal of "understanding the origin and evolution of the solar system", but is not analyzed in further detail because of its irrelevance to planetary imaging experiments. Figure 2-1 shows, for example, the results of the application of this analysis and filtering to the scientific goal.

In order to recognize those exploration objectives for which orbital imagery is useful, each objective must be described in terms of observable properties. These "observables" define the physical properties whose measurement assists in achieving the objective. For example, an understanding of a planet's surface morphology is furthered by measuring (or observing) surface topography and surface appearance. The properties of the observable are used to determine the usefulness of remote sensing and ultimately the usefulness of imaging. Each observable is analyzed as shown in Table 2-2. The results of this thirteen-step analysis are reported in their entirety in Volume II (Definition of Scientific Objectives). The analysis singles out those exploration objectives for which imagery is useful and discloses those characteristics of the observable which influence the desired nature and quality of the acquired images.

The first two steps of the analysis are self-explanatory. The possible measurement techniques considered in Step 3 do not imply the use of a particular instrument or sensing device, but rather refer to basic physical or chemical

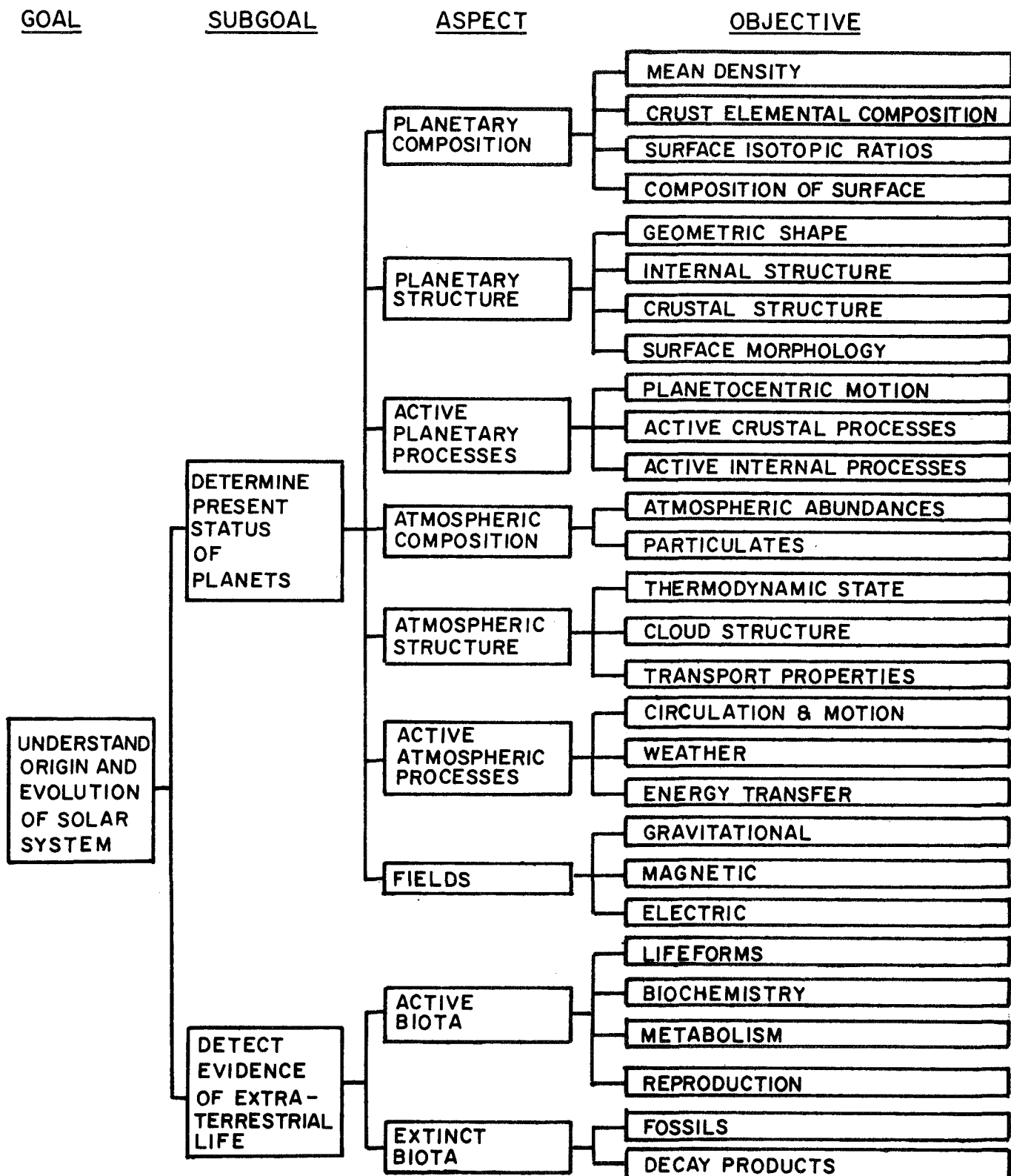


FIGURE 2-1
ANALYSIS OF SCIENTIFIC GOAL

Table 2-2

ANALYSIS OF SCIENTIFIC OBSERVABLES

Step	Analysis
1. Definition	The observable is defined in context of the objective.
2. Phenomena	The phenomena by which the observable manifests itself are identified.
3. Possible Techniques	Conceptual techniques for measuring the phenomena are noted.
4. Remote Sensing	If remote sensing is inapplicable, the observable is not scrutinized further.
5. Measurement Philosophy	The purpose of remote sensing is defined.
6. Planetary Coverage	The planetary distribution of the measurements is suggested.
7. Scale	The characteristic size of the observable is estimated.
8. Spatial Resolution	The desired ground resolution is estimated.
9. Acquisition Time	A maximum time for acquisition of the image is determined.
10. Repetition Rate	A measurement repetition rate is suggested.
11. Spectral Band and Resolution	Spectral regions for remote sensing are identified.
12. Imaging	Items 6-11 are weighed in judging the applicability of orbital imagery.
13. Imagers	Different types of imagers are identified as very useful, useful, or not very useful.

detection techniques, such as neutron activation or measurement of thermal radiation emission. The techniques of interest are not confined to remote sensing nor to the capabilities of available instrumentation. Those techniques involving remote sensing are explicitly identified in Step 4. Remote sensing, in this study, means remote sensing from planetary orbit, and is defined as the detection of electromagnetic radiation of any wavelength from orbital altitudes. In situ measurements and Earth-based remote sensing are specifically excluded. Thus the measurement of the magnetic field vector at the position of the spacecraft is not considered remote sensing. If any potentially useful remote sensing techniques are identified, the analysis proceeds further. Otherwise no further consideration is given to the observable in connection with the exploration objective at hand. However, the same observable may be considered further with relation to a different exploration objective.

The information desired by remote sensing of the observable is summarized in Step 5. The purpose of the measurements may differ from one planet to another. The purpose of observing surface topography on Mars, Venus, Mercury, and the Moon is to define the detailed shape of the surface; the purpose of observing surface topography on Jupiter is to determine if a surface exists. The differences between one planet and another are insignificant at earlier, less-detailed, stages of analysis. However, analysis of the observable from this point on proceeds on an individual planet basis and reflects the current scientific knowledge of each target planet.

The analysis represented by Step 6 identifies the fractional area of the planet which should be observed and how the observation should be distributed over the planet. The analysis is not confined to a single mission, but may reflect a hierarchy of missions. Thus differing planetary coverages are required for regional, local, and detailed scale

surface topography. Steps 7-10 further describe the observable, while Step 11 suggests which parts of the electromagnetic spectrum are suitable for remote sensing.

At this point, a judgment is made concerning the applicability of orbital imagery. Imagery is defined as the collection of two-dimensional data, by remote sensing, in an essentially simultaneous manner. If images can be expected to contribute materially to the achievement of the exploration objective, imaging experiments are useful. Thus if the observable can be expected to exhibit significant geometric or temporal variations (e.g., cloud formation), imagery is essential, or at least exceedingly useful. For some observables (e.g., surface topography), the collection of data from a large number of points over a short period of time is rendered particularly expedient by use of orbital imagery. The usefulness of orbital imagery, as determined in this study, depends upon the characteristics of the observable rather than upon the capabilities of available imaging devices. The usefulness of imagery is, however, highly dependent upon the interpretability of the image. Imagery is useless unless appropriate interpretation techniques are available for obtaining the desired information. Finally, in those cases where imagery is useful, a crude estimate of the relative efficacy of various imaging sensor types (such as IR, or radar stereo) is provided. The spectrum of applicability is confined to very useful, useful, and not very useful.

2.1.2 Engineering Objectives

The purpose of this task is to define the planetary measurements which should be made, so that the most appropriate engineering performance can be achieved. A similar procedure has been used in defining the engineering objectives as for the scientific objectives. The major steps are shown in Table 2-3. The highest echelon is the statement of engineering

Table 2-3

DEVELOPMENT OF ENGINEERING OBJECTIVES

Step	Analysis
1. Goal	Define engineering policy for exploration (e.g. maximum effectiveness in fulfilling exploration plans).
2. Subgoal	Subdivide goal into narrower engineering areas.
3. Aspect	Define concepts for meeting the subgoals (e.g. Mars Lander definition).
5. Objective	Specify engineering criteria which contribute to an aspect (e.g. aeroshell design criteria).
5. Observable	Express objectives in terms of planetary properties which can be measured (e.g. atmospheric density profile).

policy which has been assumed to be the achievement of maximum effectiveness in fulfilling the exploration plans. This is considered in succeeding levels of detail until observables can be defined. The engineering observables are planetary properties which must be measured in order that such systems can be designed in accordance with the engineering goal. However, at all levels in the procedure there are close relationships between the scientific and the engineering objectives. The requirements imposed on the engineering systems and subsystems are determined in large measure by the scientific objectives. The link is particularly close at an observables level where, in fact, scientific measurements are required for engineering purposes.

A full definition of engineering observables requires, as a first step, the specification of an exploration plan. Such a plan was not available, so it was decided to start the procedure at the aspects level. Four mission concepts are considered (orbiters, atmospheric probes, atmospheric floaters and landers) and the objectives and observables are then developed. As an example, Figure 2-2 shows the development of the engineering observables for planetary landers.

The limited definition of the mission concepts makes it impossible to define the observables in detail. Thus no detailed measurement specifications are derived for the engineering observables. Instead, they are compared with the scientific requirements and those scientific observables which can contribute to the engineering objectives are noted.

2.2 Measurement Definition

The study procedure described above identifies the need for imaging experiments meeting the exploration goals of the five planets being considered. The next step requires

ENG. ASPECT
(MISSION CONCEPT)

ENG. OBJECTIVES
(SUB SYSTEM DESIGN)

ENG. OBSERVABLES
(PLANETARY ENVIRONMENT)

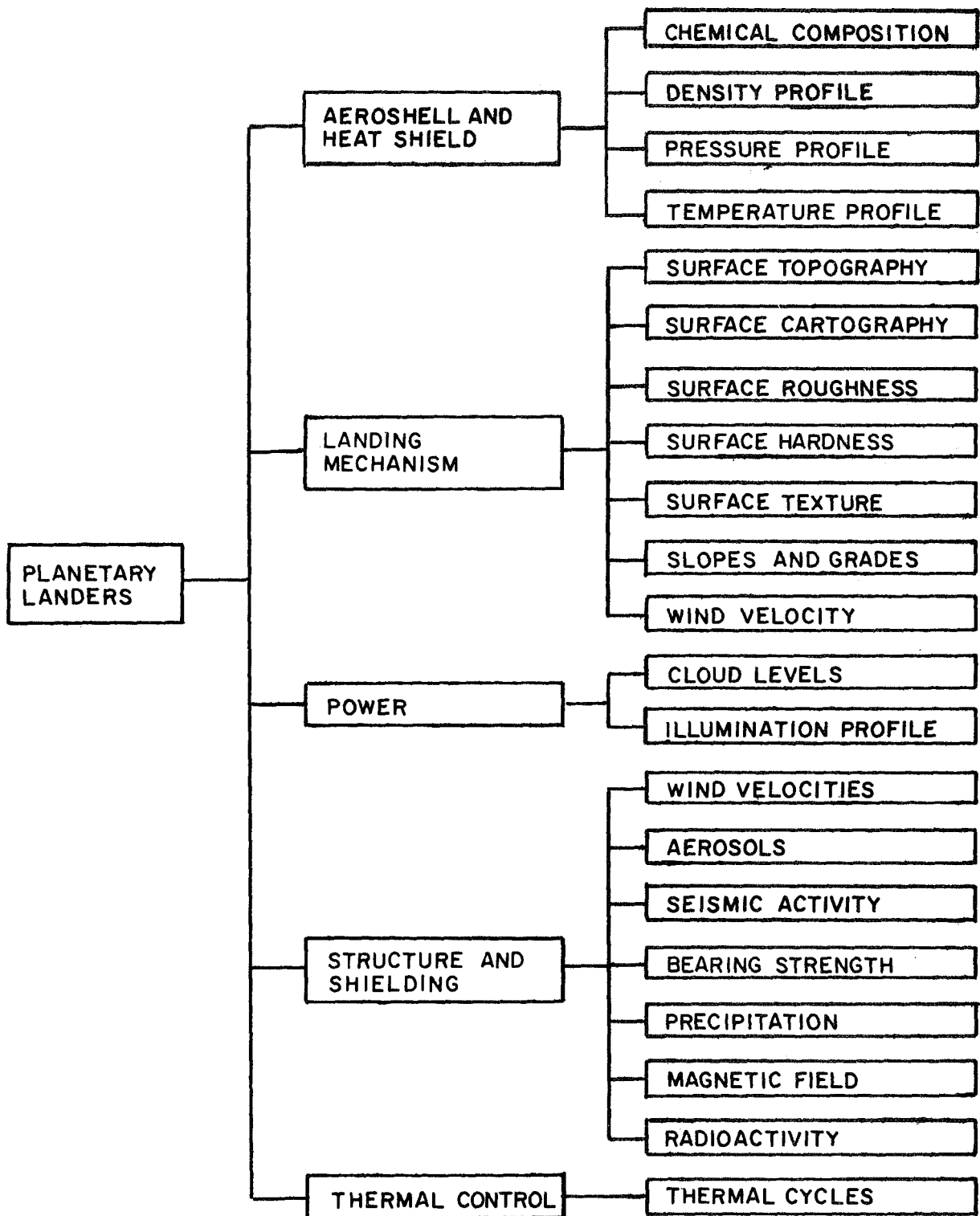


FIGURE 2-2. DEVELOPMENT OF ENGINEERING OBSERVABLES
PLANETARY LANDERS.

the precise definition of measurement specifications for each of the possible imaging experiments.

The specifications are based on (1) the present scientific understanding of the respective planets as indicated in Volume II (Definition of Scientific Objectives), and (2) the nature of the desired image and the way in which it is to be interpreted.

In specifying the measurement requirements, the following specifications have been derived from current planetary knowledge and theory as expressed by the observable description given in Volume II:

- Spectral Region
- Spectral Bandwidth
- Ground Resolution
- Planetary Coverage
- Planetary Distribution of the Measurements
- Acquisition Time
- Repetition Rate

The resolution, planetary coverage, and planetary distribution of the measurements are self explanatory. Acquisition time is related to the rate of change of a feature so that the image is not smeared by changes in the spectral appearance or shape of the object during the exposure. The repetition rate is also related to the rate of change, but it is governed by the need to measure the rate of change of the observable by comparison of successive images. It is analogous to time lapse photography. The spectral region and bandwidth are specified only in relation to the phenomena being observed and the pattern of its radiation spectra. They express the scientist's requirement for data over a given spectral range and not the capability of the state-of-the-art. In these specifications no account is taken, at this point, of whether or not orbits can be found to meet the coverage

or the time requirements nor whether instruments can be designed to meet the ground resolution or spectral requirements. Such considerations are left for a later phase of the study.

The following specifications have been derived from consideration of the interpretation of images;

Ground Image Size
Overlap
Positional Accuracy
Sun Elevation

The image size, on the planetary surface, is related to the anticipated physical scale of the observable and, to some extent to past experience in interpreting the relationships between similar type objects or events. This specification simply states the image size which the scientist wants placed in front of him for interpretation. It does not necessarily imply the size of the raw data frame. The overlap requirements ensure adequate continuity between adjacent frames. Positional accuracy and sun elevation are self explanatory. An example of a set of measurement specifications for observing lunar surface elevations is given in Table 2-4.

There is one more important step in the development of scientific measurement specifications. This is the development of "worth curves" for each of the specified parameters. A single nominal value does not adequately represent the scientific requirements. For instance, the nominal ground resolution specified for measurements of surface elevations on the moon has been determined as 5 kilometers. However, the scientific requirements could probably be met with a resolution of anywhere between 1 and 20 kilometers, and even beyond 20 kilometers the falloff in worth is not very steep. This situation requires the development of measurement specification "worth curves". They are intended to lend flexibility to the measurement

Table 2-4

EXAMPLE OF MEASUREMENT SPECIFICATION
LUNAR SURFACE ELEVATIONS (REGIONAL)

	Spec (i)	Spec (ii)	Spec (iii)	Spec (iv)
Spectral Region:	6000 Å	6000 Å	1-100 cm	1-100 cm
Spectral Bandwidth:	1000 Å	1000 Å	-----	-----
Sensor Type:	Visible	Vis Stereo	Radar	Radar Stereo
Ground Resolution (horiz):	5 km	5 km	5 km	5 km
(vert):	1 km	1 km	1 km	1 km
Image Size:	500 km	500 km	500 km	500 km
Positional Accuracy:	10 km	10 km	10 km	10 km
Planetary Coverage:	100%	100%	100%	100%
Planetary Distribution:	----	----	----	----
Acquisition Rate:	----	----	----	----
Repetition Rate:	----	----	----	----
Overlap:	20%	60%	20%	60%
Sun Elevation:	20°	80°	----	----
Supporting Measurements:		Spacecraft altitude and local time.		

specifications, and to ensure that this flexibility is constrained only by the scientific requirements. Figure 2-3 shows, for example, a "worth curve" related to the ground based resolution requirements for lunar surface elevations. The abscissa is the resolution requirement and the ordinate is the relative scientific worth of the measurement. The plateau gives the range over which the estimated scientific worth of the measurement is the same. At the ends of the plateau the worth falls off, and the slope of the line is used to indicate the rate at which the worth decreases. The dashed line indicates an extrapolation where no real experience exists. In general the nominal specifications are selected on the basis of current scientific experience.

It is very important that the true meaning of these "worth curves" be understood. They represent the range of scientific usefulness of each measurement specification. They do not imply the value of obtaining the data as a contribution to the objectives, since they are all normalized to a maximum value of unity. Nor do they constrain the way in which the data is obtained, except by indicating the worth of the data as it is presented for interpretation.

2.3 Orbit Selection

An understanding of orbital characteristics and the constraints they impose on objectives and subsystems is essential to an accurate definition of orbital imagery potential. The orbital mechanics task requires an analysis of the interaction of orbit characteristics at specific planets with orbit related measurement specifications. The objective of this analysis is to identify compatible orbit/observable groupings so that subsequent experiment definitions including subsystem requirements and mission operations can be made.

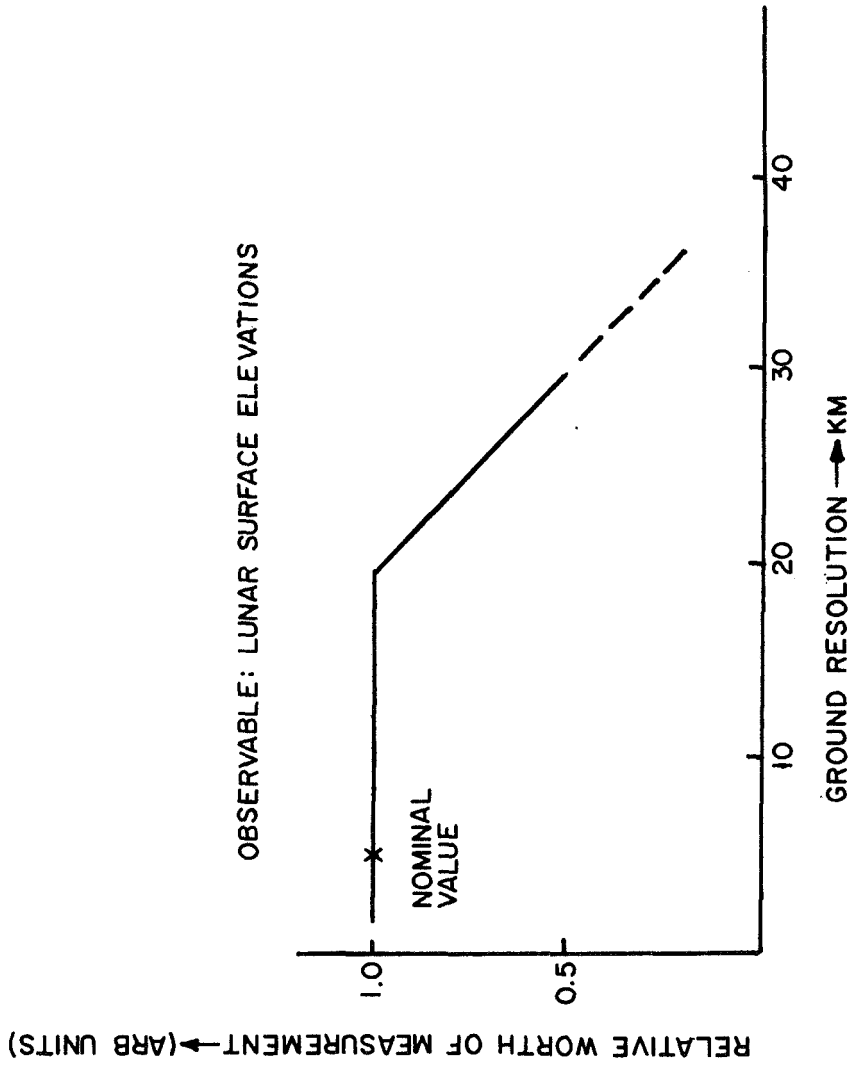


FIGURE 2-3. EXAMPLE OF MEASUREMENT SPECIFICATION WORTH CURVE

Many factors are involved in relating the characteristics of orbits to the accomplishment of an objective. The conditions of planet approach, the capture maneuver, subsequent orbit maneuvers, the time/space relation between orbiting spacecraft and rotating planet, and orbit stability in the planetary environment all play a part in determining the location, amount, and frequency of coverage, the resolution of the image, and the solar illumination conditions during measurement. In order to give each interaction the proper attention, and do so efficiently, it was necessary to formulate procedures and methodologies for the analysis. This is done by organizing the task into a series of sequential steps proceeding from the most general characteristics of orbits to specific orbit selections for observables, grouped according to similar orbit related measurement specifications. These steps are described in Table 2-5.

2.3.1 Interplanetary Transfers

It is necessary to investigate and select interplanetary transfers from Earth to the target planet in order to determine typical arrival conditions from which orbits can be established. The characteristics of planetary transfers are cyclical, approximately repeating themselves after a fixed number of launch opportunities. This opportunity cycle is considered for each target planet in the time period 1975-1995. Emphasis is placed upon those transfers which would yield maximum payload in orbit. Mars and Venus transfers are selected on the basis of the minimum sum of hyperbolic excess speeds at Earth and the target planet. Mercury transfer selection is based on the minimum sum of escape and capture velocity increments, since this data is readily available (Manning 1967). Both direct and Venus swingby transfers are considered. For Jupiter, maximum orbit payload type transfers can take as long as three years to reach the planet. Therefore

Table 2-5

DEVELOPMENT OF PLANETARY ORBIT ANALYSIS

	Step	Analysis
1.	Interplanetary Transfer	Analyze interplanetary transfers to determine typical planet arrival conditions for planetary orbiter missions.
2.	Orbit Constraints	Analyze orbit behavior in the planet environment and assignment of orbit constraints necessary to mission success.
3.	Measurement Families	Sort all observables to which imagery is useful into families of similar orbit related specifications.
4.	Candidate Orbits	Select a parametric set of candidate orbit sizes capable of satisfying measurement specifications (Step 3) and orbit constraints (Step 2).
5.	Orbit Selection	Determine one or more complete orbit definitions (size and orientation) for each observable grouping using techniques of stereographic projections and computerized orbital ground traces.
6.	Orbit Documentation	Document each orbit selection (orbit data sheets) including measurements specifications (required and obtained) imager type/observable combinations, orbit parameters, selection rationale and explanations of incomplete achievement.

shorter trip time transfers, as well as minimum summed excess speed transfers, are considered in the selection process.

For these classes of maximum payload transfers the parameters of most interest are (1) the magnitude and declination (planet centered) of the asymptotic approach velocity to determine locations of periapse, minimum inclination, and magnitude of the capture maneuver, (2) location of the subsolar point to determine orbit ground trace illumination characteristics, and (3) location of the planet in its orbit to determine the season (Mars) or location of surface features (Venus) on the planet at arrival. Other parameters of interest in mission planning which are recorded are planet-Earth communication range, Earth-Sun separation angle, and days after arrival to planet-Earth conjunction (point of maximum communication distance and solar interference).

A tabulation of these data for the selected transfer within each opportunity of a cycle is prepared. The range of variation and average values for each pertinent arrival parameter is computed. Depending upon the variation and number of parameters considered, one or two transfers are selected to provide typical arrival conditions to be used in subsequent orbit determinations.

For each selected transfer, encounter occultation contours are presented in the hyperbolic impact plane for the following references:

<u>Object</u>	<u>Object/near-limb angles</u>
Sun	0°, 5°
Earth	0°
Canopus	0°, 20°

Any specific encounter geometry (assuming fixed approach conditions) is represented by an aiming point in the hyperbolic impact plane. A secondary figure is also prepared relating the aiming angle coordinate of the aiming point to

the consequent orbit inclination and ascending node (assuming a co-planar capture maneuver). Thus it is possible to determine the capture occultation characteristics of any orbit selected from the same approach conditions.

2.3.2 Orbit Constraints

Each planet has different characteristics. Mars, Venus, and Jupiter have atmospheres which can shorten orbit lifetime. Mars and Jupiter rotate rapidly; Venus and Mercury rotate very slowly. Venus and Mercury are close to the Sun causing appreciable solar perturbations on the periapse altitude. The oblateness of Mars and Jupiter perturbs the orbit ascending nodes and arguments of periapse. The rotation axis of Mars is tilted 25° to its orbit plane causing seasonal surface variations. Jupiter has intensive radiation belts, perhaps as far as 3 planet radii from the surface. Capture impulse requirements are different at every planet, being generally considered most severe at Mercury and Jupiter.

Obviously each planet has its own set of traits creating a unique environment for orbital imagery. Therefore, orbital behavior relating to orbit stability, maneuver requirements, surface coverage, resolution, and illumination must be studied, for each planet, before intelligent orbit selections can be attempted. These interactions and resulting orbit constraints are discussed as part of the orbit selection presentations in Section 5 of this volume. Several orbit constraints serve as general guidelines to all orbit selections. These are:

- a. Maximum capture impulse limited to 6.5 km/sec,
- b. Minimum orbit lifetime due to atmospheric drag set at 50 years,
- c. Measurement altitude ranges usually limited to a factor of less than 5 and never exceed a factor of 10,

IIT RESEARCH INSTITUTE

- d. Discrete contiguous imaging is the only coverage technique considered, i.e., coverage is accomplished by obtaining adjacent images (not necessarily from adjacent orbits) with close to the minimum image size and overlap.

2.3.3 Measurement Families

The first step taken toward defining operationally compatible families of experiments is to formulate observable groupings, with similar orbit-related measurement specifications, prior to orbit selection. Those measurement specification categories considered are:

- a. minimum image size
- b. minimum image overlap
- c. percent planet coverage
- d. solar illumination (elevation angle^{*})
- e. coverage time
- f. image interval
- g. coverage interval

By grouping observables it is possible to avoid a great many redundant orbit selections. The measurement specifications representing each observable grouping are made up of what appears to be the most restrictive of each of the specifications. It is possible that some experiments might have "over-designed" orbits. This is not considered a serious problem, however, since the groupings are formulated, to begin with, on the basis of their similarities.

*Elevation angle $= (90^\circ - \text{zenith angle})$

2.3.4 Candidate Orbits

Candidate orbit sizes are characterized by periapse altitude (h_p) and eccentricity (e). A basic groundrule used in setting up these candidate sizes is to keep h_p as low as possible. For Mars and Venus, the lower limit is set by the 50-year orbit lifetime constraint. For Jupiter, h_p is constrained by the radiation belts. At Mercury, h_p is fixed at 500 km.

It is then possible to vary the orbit period by changing e . To assure contiguous coverage at the rapidly rotating planets Mars and Jupiter it is necessary to select e such that the candidate orbit periods are approximately subinteger (Mars) or integer (Jupiter) values of the rotation period. In fact, at Mars the observable minimum image size and overlap are used to select exact values of e which will meet the measurement specifications. For Venus and Mercury, which rotate quite slowly, it is more sensible to ignore the orbit period/image size relationship and simply generate a set of orbits by changing e in equal increments.

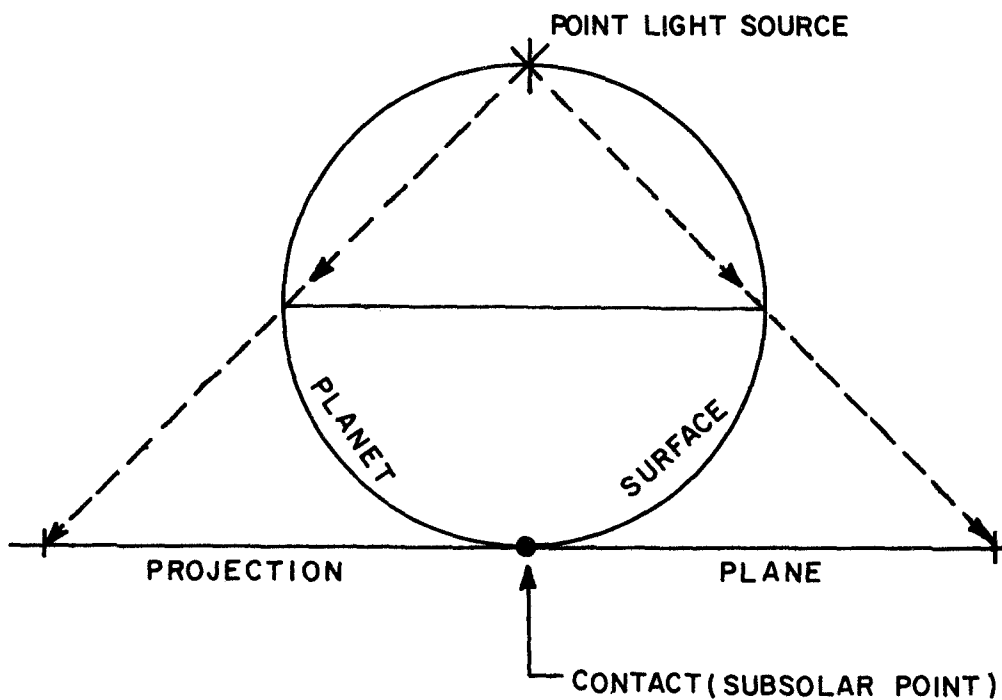
Once the combination of h_p and e are selected to determine the orbit size, a number of additional orbit parameters useful to the subsequent selection process are computed. Included among these are the apoapse altitude, the variation of altitude with central angle from periapse, orbit period, longitudinal lapse rate/coverage, and the number of days to complete 100% longitudinal coverage.

2.3.5 Orbit Selection

The results of the previous steps are combined into orbit selections which satisfy the remaining measurement specifications of each measurement family, including the percent coverage, the solar illumination conditions, the distribution of coverage, time for coverage, and image and

coverage repetition rates. In addition to these requirements, it is important to define what kind and how many maneuvers were necessary to establish the desired orbit, what the range of measurement altitude is, how the conditions and location of coverage change with time in orbit, and a rationale describing the selection process.

The single most useful tool in accomplishing this task was found to be the graphical technique of stereographic projection. These projections permit the orbit analyst to clearly understand the spatial/time relationships involved in obtaining imagery data within such specific constraints as solar illumination, orbit altitude, and location of coverage. A schematic diagram of a stereographic projection is illustrated in Figure 2-4. Planet coordinates, orbit traces, locations of sub-body points, and velocity and position directions which can be located on the planet surface are projected onto a plane tangent to this surface. The ease of subsequent analysis depends upon the selection of the point of tangency. As shown in the figure, all lines and points on the surface are projected as shadows produced by a point of light source on the surface opposite the point of tangency. In order to keep the projection finite, only the lower hemisphere is projected for the orbit selection analysis. Accurate locations (periapse, specific altitude, etc.) and angles (inclination, argument of periapse, ascending node, etc.) can be measured directly from the projection by virtue of the two theorems given in Figure 2-4. An example of the orbit selection procedure employing the stereographic projection technique is given in Appendix A.



THEOREM 1: CIRCLES OF THE SPHERE GO INTO CIRCLES AND STRAIGHT LINES OF THE PROJECTION PLANE.

THEOREM 2: ANGLES ARE PRESERVED, ie. STEREOGRAPHIC PROJECTIONS ARE ISOGONAL TRANSFORMATIONS.

FIGURE 2-4. STEREOGRAPHIC PROJECTION DEFINITION

2.3.6 Orbit Documentation

Certain information, which is useful to other study tasks, is developed during the orbit selection process and is recorded on a data sheet. The completed data sheet for the example discussed in Appendix A is presented as Table 2-6. In addition to the required measurement family specifications, and the orbit elements, the data sheet contains information on the obtained measurement specifications, the selection rationale behind the particular orbit selection, orbit/measurement characteristics (including a brief set of measurement profile data and orbit impulse data), and explanations for differences between required and obtained measurement specifications. A detailed description of the orbit selection data sheet, and its relation to other areas of the study, is included in Volume IV (Orbit Selection and Definition) which is a compilation of orbit selection data sheets for all orbit selections which were made.

2.4 Imager Scaling Laws

The purpose of this task is to provide scaling laws which can translate the measurement specifications into experiment support requirements, provided that an orbit has been selected. This section describes the method of analysis used in obtaining imaging system scaling laws.

The scaling laws are used to interpolate between, and to extrapolate beyond, the point designs of existing or projected imaging systems. Their function is depicted in Figure 2-5. Only those image specifications and support requirements which are directly related to the sensor system design variables are listed in the figure. Other support requirements, such as the necessary operating environment, depend only upon the type of imaging system. Scaling laws have been developed only for those types of imaging systems

TABLE 2-6

ORBIT SELECTION DATA SHEET NO. 200

Mars (1984)

FAMILY NO. 7

ORBIT NO. 6

GROUP MEASUREMENT SPECIFICATIONS:	Required	Obtained
Minimum Image Size (km).....	600	600
Minimum Image Overlap (%).....	20	27.763
Total Planet Coverage (%).....	> 70	76.7
Solar Elevation Range (deg).....	30-60	30-60
Image Interval.....	< 2 hr	10 days ¹
Time for % Coverage (days).....	-	60 days
Coverage Interval.....	> 4/yr	once/10 days
Distribution.....	-	-63° to 40° lat.

ORBIT ELEMENTS:	Final	Intermediate
Eccentricity.....	.4633	.9
Periapse Alt. (km).....	425	425
Apoapse Alt. (km).....	6995	68,915
Inclination (deg).....	110	38
Ascending Node (deg).....	253.7	61.7
Arg. of Periapse (deg).....	349.5	200

SELECTION RATIONALE:

The location of the asymptotic approach direction with respect to the solar illumination area of interest makes it necessary to use an off-periapse insertion maneuver into an intermediate orbit. A plane change of 141° and eccentricity adjustment establish the final orbit for measurements. The final orbit is sun-synchronous with periapse near the center of the area of desired illumination.

ORBIT/MEASUREMENT CHARACTERISTICS:

Orbits to Contiguous Images.....	5
Measurement Orbit Frequency.....	every orbit
Orbit Period (hrs).....	5.03
Measurement Alt. Range (km).....	425 to 1014
Max. Measurement Arc (deg).....	-54.5 to 54.5
Max. Sensor on Time (min/orb).....	3.27
No. of Impulses (ΔV).....	3
Capture ΔV (km/sec).....	1.36 (5.5°)
Plane Change ΔV (km/sec).....	.46
Size Adjustment ΔV (km/sec).....	.57 (141°)
Total ΔV (km/sec).....	2.38

MEASUREMENT ACHIEVEMENT:

¹The time between side-by-side images is equal to 5 orbit periods or 25.15 hours. The time between image repetitions equals 10 days which is the time for one complete cycle of longitudinal coverage.

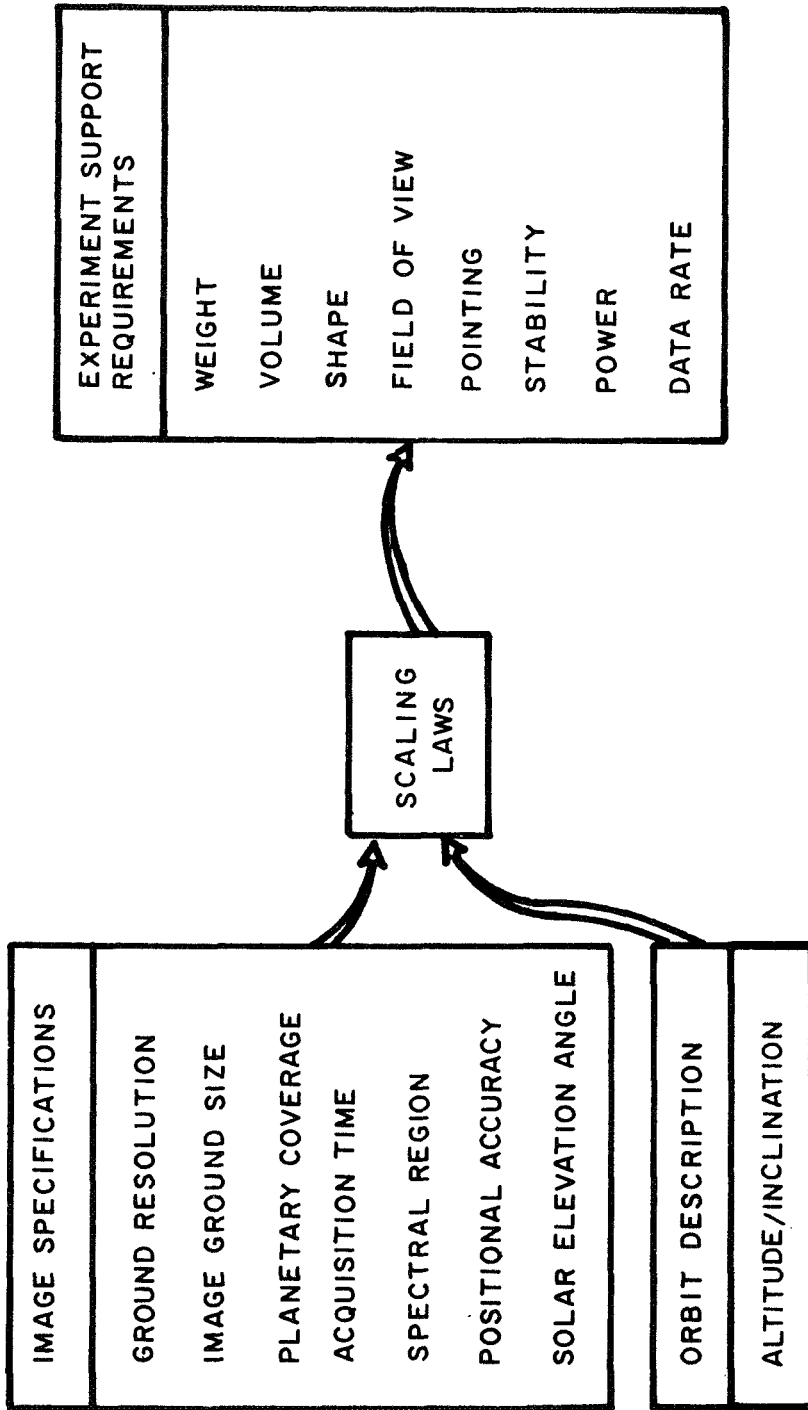


FIGURE 2-5. FUNCTION OF SCALING LAWS

for which (1) a need exists (as expressed by the measurement definitions) and (2) adequate design experience is available. Unless a sensor system is useful, there is no point in developing scaling laws, and unless characteristics of a sensor system can be predicted over fairly wide ranges, scaling laws cannot be developed.

The first step in obtaining scaling laws for a given type of imaging sensor is the collection and correlation of empirical data, in an attempt to relate the support requirements to various characteristics of the sensor system. In many cases, it is convenient to regard the imaging system as composed of different subsystems such as sensing elements, optics, image motion compensation equipment, etc. Empirical relations between the subsystems requirements and the sensor system characteristics, for example the weight of a TV camera system as a function of TV tube diameter, reflect current or past technological capability. Future capabilities must necessarily be speculative. In those few cases where sources of increased capability can be clearly foreseen, the presumed effect of state-of-the-art advances on the scaling laws are noted.

If insufficient empirical data is available, or if no satisfactory empirical correlation between support requirements and the sensor system characteristics can be discovered, theoretical relations are developed. In most cases, the weight, volume, power, and possibly shape requirements are based on empirical scaling laws, while the field of view, pointing, stability, and data acquisition rate requirements are based on physical principles.

The support requirements are most directly related to the characteristics of the imaging system. The weight of a TV imaging system is directly related to the diameter of the image tube, the power requirement of a radar imaging system is related to the peak transmitted power, pulse width, and

pulse repetition frequency. The operation of the sensor system is then analyzed to determine the dependence of the characteristics upon the image specifications. The image specifications are coupled to the support requirements by the sensor system variables.

There is no unique solution to the sensor design problem, however. It is important in the analysis of the system to make no artificial selection of the sensor system variables. For example, the image acquisition time (exposure time) in an orbital TV system must be long enough to result in a satisfactory signal-to-noise ratio and must be short enough that motion of the system or the imaged object does not degrade the spatial resolution. These constraints are identified by the scaling laws and their employment, but no specific acquisition time is implied by the scaling laws. Such freedom of choice can be used by the experiment designer to effect tradeoffs between the support requirements.

The scaling laws for each type of imaging system are organized in a manner which facilitates the estimation of experiment support requirements, identifies those image specifications and orbital parameters which affect the support requirements, and delineates the sensor system variables which may be manipulated by the experiment designer. This systematic organization is expressed in a "logic diagram" for each imager type. For example, Figure 2-6 shows a logic diagram for orbital TV systems. Each box in the diagram represents a computational step in the system design, the reference number in the corner referring to a specific scaling law. Similarly, each balloon represents estimation of an experiment support requirement. The logic diagram also indicates those tradeoffs which may be made internal to the sensor system.

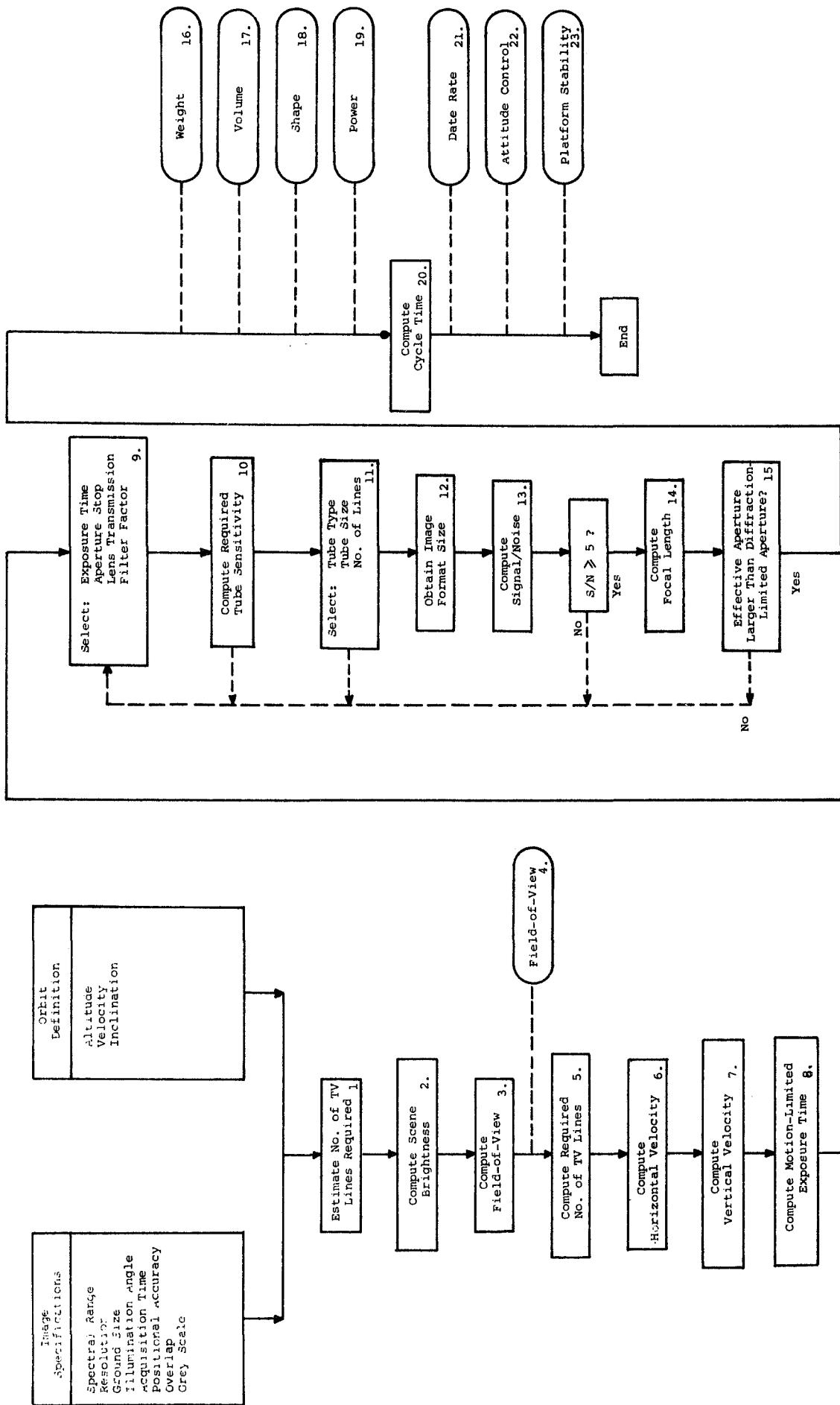


FIGURE 2-6. LOGIC DIAGRAM FOR TV CAMERAS

2.5 Experiment Support Requirements

Once the measurement specifications have been defined, and an orbit selected for achievement of the measurements, the sensor system scaling laws are used to estimate the support requirements imposed upon the spacecraft by the experiment. Each experiment consists of a specific imaging system operating in a specific mode providing imaging data to achieve a specific objective. Thus the support requirements represent a synthesis of exploration objectives, orbital mechanics, and sensor system design.

As previously described, the analysis of space exploration goals results in identification of planetary exploration objectives and planetary phenomena whose observation by orbital imagery is expected to contribute to achievement of the exploration objectives. The measurement definition analysis produces image specifications for each relevant combination of an observable and an imaging system. Some of these image specifications (notably the minimum acceptable image ground size, minimum overlap, solar elevation angle, planetary coverage and distribution, and coverage acquisition time) play a determining role in orbit selection. The spectral region and bandwidth specifications determine the type of imaging system to be used. The sensor system scaling laws are then used with the image specifications (resolution, image size, image acquisition time, overlap, positional accuracy, solar elevation angle, grey scale, and planetary coverage) and the selected orbit (imaging altitudes and velocities) to estimate the experiment support requirements.

Different support requirements may be obtained by selecting a different orbit or by changing the design of the sensor system. If such changes are skillfully made, the measurement achievement need not suffer. No attempt is made

in this analysis to define the limits of experiment flexibility. Thus, the support requirements obtained must be regarded as representative of requirements demanded in an actual mission. In some individual cases, however, similar experiments are compared with one another as a guide to how representative the requirements are.

As implied above, the experiment can be perturbed in many ways which do not affect mission achievement. For example, the data acquisition rate may be decreased at the risk of increasing the time required to achieve full coverage of the planet. Optimization of any experiment is beyond the scope of this analysis. Although all the tools required for optimization are provided by the study procedures, a definition of what one means by an optimum experiment is lacking. An optimum experiment might be defined as one which obtains the required imaging data with the least expenditure of instrument weight, or instrument power, or spacecraft weight, or even advanced technological development costs. The analysis used here ensures only that the experiment is designed to collect the desired imagery.

This section has described the major tasks of the study, and the analytical procedures used to complete these tasks. A structured technique for critical examination of the goals of space exploration has been presented, and methods for analyzing exploration objectives in terms of observable planetary properties has been formulated. It

has been shown that the observable properties must be described from two points of view: that of the scientist who knows what kind of data contributes to his understanding of the origin and evolution of the planets, and that of the image interpreter who knows how the mode of measurement affects his capability to properly interpret the acquired imagery. A method for analyzing the critical functions of imaging sensor systems has been discussed, and procedures for orbit selection have been detailed. Finally, a means for combining the measurement requirements, sensor system characteristics, and orbital constraints into experiments and estimating the resultant support requirements has been evolved. The remainder of this volume presents the results obtained by these analytical procedures.

3. EXPLORATION OBJECTIVES

The support requirements demanded by planetary orbital imaging experiments depend directly upon the objectives of planetary exploration. This section provides an explicit statement of those objectives which might be accomplished by imaging experiments. The relation of this task to the other study tasks was shown in Figure 1-2. The method of analysis has been discussed in Section 2.1. The analysis results in a selection of planetary phenomena which can be usefully investigated by imaging sensor systems in orbit about the planet.

3.1 Goals of Space Exploration

The goals of space exploration represent the formulation of policy, and constitute the highest and most general echelon of an exploration plan. The goals of the United States space exploration effort have been taken to be:

1. To understand the origin and evolution of the solar system.
2. To understand the origin and evolution of the universe outside our solar system.
3. To sustain the technological and economic preeminence of the United States.
4. To achieve the scientific and national space exploration goals in an efficient manner.

The first two goals are scientific goals, the third is a national goal, while the fourth is an engineering goal. These goals are useful primarily as a basis for further analysis. The next level of increasing detail is division of the goals into subgoals. Only the first (scientific) and last (engineering) goals are analyzed in this study.

3.2 Scientific Objectives

The origin and evolution of the solar system are not directly observable. Only the present state is observable, and must be used as the key to the past. Scientific theory is used to infer the origin and evolution of the solar system from its observed condition. Thus the goal of understanding the origin and evolution of the solar system may be expressed in terms of the following subgoals:

1. Determine the present status of the planets.
2. Detect evidence of extraterrestrial life.
3. Determine the present status of the Sun.
4. Determine the present status of the inter-planetary medium.

Only the first two subgoals are pertinent to this study.

Figure 3-2 shows the analysis of these scientific subgoals. The major distinctions at an aspect level are planetary versus atmospheric; composition and structure versus active processes; active versus extinct biota. The aspect of planetary composition deals with the chemical and isotopic constitution of the surface and interior of the planet, while planetary structure relates to the physical and structural properties of the surface and interior. Active planetary processes deal with all dynamic processes (exogenetic and endogenetic) which tend to change the planetary composition or structure. Similarly, the aspect of atmospheric composition refers to the chemical and isotopic composition of the atmosphere, atmospheric structure treats the physical and thermodynamic properties of the atmosphere, and active atmospheric processes relates to dynamic processes which tend to change the atmospheric composition or structure. The aspect of fields includes all those potential fields or particle distributions associated with the planet. The aspect of active biota refers

to detection of viable organisms ranging from self-replicating polymers to elephants, while extinct biota refers to any evidence of past biology.

The following subsections describe the analysis of each scientific aspect identified above into objectives, and the dissection of each objective into observable properties, or "observables," for which orbital imagery may or may not be a useful investigative technique. Briefly, an objective treats the understanding of a scientific area of limited scope. Those planetary phenomena whose observation contributes to the understanding are described as observables. Consideration of the geometric and temporal characteristics of those observables for which remote sensing is useful leads to a judgment on the applicability of orbital imagery. This section summarizes the results of the analysis, aspect by aspect. A detailed description of each observable is given in Volume II (Definition of Scientific Objectives).

3.2.1 Planetary Composition

This aspect deals with the gross composition of the planet and the elemental, isotopic, and mineralogic composition of the crustal materials. The gross elemental composition of the planet may be interpreted in the context of various cosmogonical theories. For example, a significant difference in the planetary iron abundance as a function of distance from the Sun may indicate that some type of differentiation process occurred in the solar nebula either before or while the planets were being formed. Various isotopic ratios may lead to inferences concerning the age of the planet, while mineralogic data may shed light on the planet's development. The aspect of planetary composition is analyzed in terms of the objectives shown in Table 3-1. Each of these objectives will now be treated in further detail.

Table 3-1

PLANETARY COMPOSITION OBJECTIVES

Objective	Observables	Remote Sensing	Orbital Imagery
Mean Density	1. Mass	-	-
	2. Radius	✓	-
	3. Oblateness	✓	-
Elemental Composition of Crust	1. Elemental Abundances	✓	-
Surface Isotopic Ratios	1. Isotopic Abundances	-	-
Composition of Surface Materials	1. Petrology	✓	-
	2. Mineralogy	-	-
	3. Liquids	✓	-

3.2.1.1 Mean Density of the Planet

The mean density of a planet may be inferred from the observables of (1) mass, (2) radius, and (3) oblateness, and is a key parameter used in the classification and inter-comparison of the planets. For example, the low average density of Jupiter is generally regarded as indicating a predominant hydrogen composition. The oblateness is determined by measuring both the equatorial and polar radii and may be used to compute the planetary moment of inertia (Jeffreys 1962). The known moment of inertia may then be compared to moments based on different models of planetary composition, and the most likely composition may be inferred. Orbital imagery is not particularly useful in investigation of these observables, because the properties are virtually time-independent and few measurements are required. The detailed descriptions of these observables, and the analysis leading to this judgement, is given in Volume II (Definition of Scientific Objectives).

3.2.1.2 Elemental Composition of the Crust

Elemental abundances on the surface are the observable properties of this objective. The elemental composition of the crust, and the large-scale spatial variation of the composition, indicate the degree of differentiation which has occurred at the surface and perhaps in the interior. Elemental composition is independent of time and only a small number of geometrically distributed data points are required. Also there is no known interpretation technique for obtaining elemental composition from imagery. Thus orbital imagery is neither required nor especially useful.

3.2.1.3 Surface Isotopic Ratios

The relevant observables are isotopic abundances. These abundances may be used to compute ratios of abundance for radioactive and stable isotopes. Some of the ratios involving radioactive species may be used to infer the length of time since formation of the planet, or since the isotopes were buried. Other ratios may be used to infer the past activity of physiochemical processes which selectively concentrate isotopes (Adams et al. 1967). Variation of specific isotopic ratios from one planet to another, and with respect to solar or cosmic isotopic ratios, may indicate whether fractionation occurred in the solar nebula when the planet was formed. However, remote sensing from orbital altitudes does not appear to be a feasible investigative technique, where even very thin atmospheres exist.

3.2.1.4 Composition of Surface Materials

This objective is to determine the kinds of rocks, minerals, or fluids, present on the surface in large or moderate quantities. The observables are (1) petrologic, (2) mineralogic, and (3) liquid composition. The petrologic composition is defined by the abundance and distribution of various rock units, while the mineralogic composition is defined by the abundance and distribution of various minerals. Rock and mineral forming processes which may have been active are deduced from the surface petrology and mineralogy. For example, granitic rocks might indicate a high degree of crustal differentiation, while basaltic rocks might indicate a low degree of differentiation. Similarly, the presence of sedimentary rocks would imply past action of erosional, solutional, and depositional processes. The composition of any surface liquids present may also lead to inferences of past history. Again, since planetary composition is expected to be independent of time, orbital imagery is unessential. Furthermore, although remote sensing may be of some value in pursuit of this objective

no known image interpretation techniques can provide the desired compositional information.

The applicability of both remote sensing and orbital imagery is summarized in Table 3-1 for all objectives dealing with planetary composition. For details, the reader is referred to Volume II. It is concluded that orbital imagery is useless for determining planetary composition.

3.2.2 Planetary Structure

Examination of planetary structure determines those forces and movements which have taken place within and on the planet. Knowledge of these forces is vital to an understanding of the nature and history of the planet, and provides a framework for the generation and testing of planetary development theories. Table 3-2 shows the objectives dealing with planetary structure.

3.2.2.1 Geometric Shape

The observables of interest are (1) surface elevations and (2) center of mass. Although the geometric shape is not determined by "observing" the center of mass, a comparison of the location of the geometric center with the location of the center of mass will lead to conclusions concerning planet rigidity, hydrostatic equilibrium, and rotation rate history (Goude et al. 1966). Observations of surface elevations will define regional deviations from the basic ellipsoidal shape of the planet (Kaula 1966). Although a global network of elevation measurements are required, the data are independent of time, and thus orbital imagery is unessential. However, orbital imagery would be useful if available: otherwise simple altimetry would suffice. Imagery is useless in determining the center of mass.

Table 3-2

PLANETARY STRUCTURE OBJECTIVES

Objective	Observable	Remote Sensing	Orbital Imagery
Geometric Shape	1. Surface Elevations	✓	✓
	2. Center of Mass	-	-
Internal Structure	1. Density Distribution	✓	-
	2. Discontinuities	-	-
Crustal Structure	1. Layering	✓	✓
	2. Contacts	✓	✓
	3. Attitude of Rock Units	-	-
	4. Structure of Features	✓	✓
Surface Morphology	1. Surface Topography	✓	✓
	2. Surface Appearance	✓	✓

3.2.2.2 Internal Structure

A determination of planetary internal structure will indicate the nature and degree of differentiation, is valuable in the construction of planetary models, and may suggest similarities or dissimilarities in the development and evolution of the planets. The internal structure has observable properties of (1) density distribution and (2) discontinuities. No orbital imaging techniques are useful. The detailed density distribution can best be determined by measuring the paths and speed of seismic waves, although limited data can be obtained by gravimetry and satellite tracking (Anderson and Kovach 1966, Kovach 1966). Discontinuities and phase changes can be detected by seismometry.

3.2.2.3 Crustal Structure

A major portion of the history of a planet may be recorded in the outer few kilometers of its crust, particularly if large structures of rock exist. The general structure of the surface and near-surface is important in understanding the formation of any lithologic units within the crust, and the processes which formed or modified the crustal materials and structural features. The relevant observables in determining the crustal structure are (1) layering, (2) contacts, (3) attitude of rock units, and (4) structure of features.

By mapping rock outcroppings, rock attitudes (dip and strike), and contacts, interpretations can be made regarding the subsurface structure and the processes responsible for the formation and modification of rock units. A study of surface structural features facilitates understanding of the structure and history of the planet's crust. Layering is predominantly a subsurface phenomena, and is best investigated by seismometry and in situ mapping utilizing coring and on-site study of outcroppings. If available, visual and radar imagery from orbit might be useful. In the past, terrestrial

contacts have been studied by in situ mapping. Thorough study of planetary contacts will probably require data collection at many points over extensive areas, hence orbital imagery (most notably visual and multispectral) is particularly expedient. The attitude of rock units is best investigated by in situ mapping and seismometry. Remote sensing techniques do not provide true attitudes. Finally, the structure of surface (and near-surface) features is best obtained by seismometry, gravimetry, magnetometry, and in situ mapping. However, orbital imagery (visual and radar) would be useful, particularly when supplemented by ground truth.

3.2.2.4 Surface Morphology

The morphology of land forms is a function of the near-surface structure and the active processes which build up or tear down the surface. The observable properties are (1) surface topography and (2) surface appearance. Accurate information requires a dense network of data over extensive portions of the planetary surface. Orbital imagery is particularly expedient in the collection of such data. Surface topography requires three-dimensional data which may be obtained by shadowing or stereo coverage.

3.2.3 Active Planetary Processes

All processes which change the physical or chemical properties of the planet are regarded here as active processes. Included are such phenomena as magnetic activity, tidal activity, chemical reactions, seismic activity, tectonic activity, erosion, and deposition. Table 3-3 lists the relevant objectives.

Table 3-3

PLANETARY PROCESSES OBJECTIVES

Objective	Observable	Remote Sensing	Orbital Imagery
Planetocentric Motion	1. Rotation Period	-	-
	2. Tidal Effects	-	-
	3. Polar Wandering	-	-
Crustal Processes	1. Surface Winds	✓	✓
	2. Surface Liquid Motion	✓	-
	3. Topographic Changes	✓	✓
	4. Thermal Anomalies	✓	✓
	5. Seismic Waves	-	-
Internal Processes	1. Magnetic Field	-	-
	2. Heat Flow	-	-
	3. Seismic Waves	-	-
	4. Mass Motion	-	-

3.2.3.1 Planetocentric Motion

This objective includes those dynamic motions which affect the planet as a whole, and is analyzed here in terms of (1) rotation period, (2) tidal effects, and (3) polar wandering. Other observable properties, such as geometric shape of the planet, which may be related to planet dynamics, have been discussed elsewhere. The observed period of rotation allows inferences to be made concerning rotational history. In the case of the Earth, the variations in the length of the day are caused by interaction with the Sun and the Moon and possibly by change in the moment of inertia due to growth of the Earth's core. The period of rotation may be determined by Doppler shift techniques or by stellar tracking from the surface of the planet. However, since the rotational period of the planets are already well known, remote sensing is not very useful. It may be noted that the accuracy of rotational period measurements is more sensitive to the duration of the observations rather than to the distance from which observations are made.

Measurements of tidal variations are significant since they affect the rotational period, and tidal friction provides a mechanism for energy transfer from the planet to its satellites or the Sun. The effectiveness of tidal forces in removing energy from the planet depends upon the phase lag of the tidal bulge and upon the energy dissipation coefficient of the planet. Remote sensing from orbit is not useful in measuring the tidal activity, since no conceivable remote sensing technique affords the required accuracy.

Terrestrial polar wandering has occurred, and is thought to be due to the Earth's response to unequal distribution of land surfaces. Such changes in the position of the poles, together with changes in the rotational velocity, result in large scale fracture features in the surface. Polar wandering is best deduced from paleomagnetic measurements; remote sensing is not useful.

3.2.3.2 Active Crustal Processes

Many dynamic processes such as erosion, faulting, folding, and volcanism produce characteristic surface features. The identification of such processes may lead to inferences regarding planet evolution. For example, if the subdued structure of Martian craters is the result of water erosion, the past presence of a hydrosphere is indicated. Although a clear division between surface modification and internal processes is not always possible, the observable properties relating to active crustal processes are considered to be (1) surface winds, (2) surface liquid motions, (3) topographic changes, (4) thermal anomalies, and (5) seismic waves. Visual imagery from orbit is particularly useful at Mars (and perhaps Mercury) for observing sand and dust storms. The velocity and extent of surface liquid motions could be ascertained by tracking buoys, but only Jupiter is expected to show significant large scale surface fluid motion. Orbital imagery is not especially useful in this regard. Topographic changes are the result of both crustal and internal processes. Rapid and unpredictable topographic changes are due to meteorite impacts, land slides, volcanic eruptions, etc. The deliberately planned detection of such activity would require continuous planet-wide observation. Slow and semi-predictable topographic changes due to soil creep and some volcanic eruptions could be detected by periodic observation from orbit. Very slow and large scale topographic changes could be detected only by observations extending over many years duration. The heat produced by volcanism, faulting, and intrusion of magma could well be detected as a thermal anomaly long after the process has ceased. Extensive areas of the planet could be thermally mapped from orbit. These processes also produce large amounts of seismic energy, but seismic activity cannot be detected from orbit.

3.2.3.3 Active Internal Processes

Dynamic activity in a planet's interior may be deduced from the observed surface structure. For example, thermal convection in the Earth's mantle is thought to have influenced the development of the continents and ocean basins. The observed distribution of lunar surface features (many maria on the near side, but few maria on the far side) may also be the result of internal dynamic processes. However, the recent discovery (Muller and Sjogren 1968) of mass concentrations associated with some of the larger mare suggests the predominance of external effects. The observable properties convenient for studying internal processes are (1) magnetic fields, (2) heat flow, (3) seismic waves, and (4) mass motion. Thermal convection in a fluid metallic core is thought to generate a magnetic field. Therefore, mapping of a planetary magnetic field may lead to inferences concerning thermal convection patterns in the interior. Mars, Venus, and the Moon do not appear to have any appreciable magnetic field. Jupiter does possess a strong magnetic field, but orbital imagery is not a useful investigative technique. Surface heat flow may indicate the general thermal state of the interior, convection in the outer regions, subsurface molten magma, buried extrusive materials, and internal heat generation from meteoritic impacts. However, remote sensing of heat flow depends upon thermal conductivity measurements which must be made by surface sampling. Orbital imagery is only useful in detecting thermal anomalies. Seismic waves cannot be detected remotely, while mass motion of subcrustal materials is inferred from secular variation of the magnetic field and the distribution of surface structures.

3.2.4 Atmospheric Composition

Planetary atmospheric composition yields valuable information as to the origin and past history of the solar system. A massive planet (e.g. Jupiter) will retain most of its gaseous constituents through gravitational attraction, and hence its atmospheric composition may be representative of conditions at an early stage of evolution. Any atmosphere associated with a small planet (e.g. Mars) may be expected to have a composition largely dependent upon surface and internal activity during past geological eras. The aspect of atmospheric composition is analyzed here in terms of the objectives shown in Table 3-4.

3.2.4.1 Gross Atmospheric Abundances

This objective deals with planet-wide atmospheric composition on an atomic or molecular scale. The observables are (1) mean molecular weight, (2) elemental and molecular abundances, and (3) isotopic abundances. The mean molecular weight may be used to infer the general nature of the atmospheric composition. The terrestrial planets appear to have oxidized, secondary atmospheres derived from crustal outgassing (Kuiper 1952). The Jovian planets have reducing atmospheres containing large amounts of hydrogen, thus suggesting an origin closely associated with that of the solar system (Owen 1965). The mean molecular weight of the atmosphere of Mars and Venus is about forty, while at Jupiter a value of about four is generally accepted. Since the mean molecular weight is not exhibited directly by electromagnetic radiation phenomena, remote sensing is not useful. The elemental and molecular constituents of most interest are H, H₂, He, O, O₂, O₃, N, N₂, H₂O, CO, CO₂, CH₄, NH₃, Xe, Ar, and organic molecules (Brandt and Hodge 1964). Since atmospheric composition is not expected to vary appreciably over the planet

Table 3-4

ATMOSPHERIC COMPOSITION OBJECTIVES

Objective	Observable	Remote Sensing	Orbital Imagery
Atmospheric Abundances	1. Mean molecular weight	-	-
	2. Elemental and molecular abundances	✓	-
	3. Isotopic abundances	✓	-
Atmospheric Particulates	1. Aerosol and crystal composition	-	-
	2. Particulate sizes and distribution	✓	-

(except for highly localized anomalies considered in the context of active processes), instantaneous two-dimensional data is not especially useful. Composition as a function of altitude which is particularly desired, cannot be obtained by orbital imagery. Isotopic abundance ratios can be used to infer the extent of fractionation that occurred in the early history of the solar system. Isotopic ratios of particular interest are H^1/H^2 , He^3/He^4 , C^{12}/C^{13} , and Ar^{40}/Ar^{38} . As with elemental and molecular abundances, few data points are required, vertical profile data is desired, and orbital imagery is not useful. Atmospheric sampling is the most effective technique for studying atmospheric composition.

3.2.4.2 Atmospheric Particulates

Determinations of the size, composition, and spatial variations of aerosols and particulates suspended in the atmosphere are of utmost importance in resolving disagreements between various atmospheric models. This is especially true for Venus, since a variety of conflicting theories have been presented (Kellogg and Sagan 1962, Opik 1961, Newell 1967) and have yet to be resolved. The suggested Jovian cloud layers of ammonia droplets and ice crystals require confirmation (Opik 1962, Michaux 1967). The relevant observable properties are (1) aerosol and crystal composition and (2) particulate sizes and distribution. Aerosols refer to non-solid particulates such as liquid droplets, while crystals refer to the solid particulates such as suspended ice or dust. Atmospheric particulates do not exhibit unique absorption lines from which their composition can be readily determined by remote sensing. Atmospheric sampling is required. Remote sensing techniques (especially polarimetry) are useful in determining particulate sizes and planetary distribution. However, since few data points are required, and vertical profiles are desired, orbital imagery is not useful.

3.2.5 Atmospheric Structure

Since the atmosphere is the only barrier between solar radiation and the solid surface of the planet, a knowledge of atmospheric structure permits an evaluation of the role played by solar radiation in the evolution of a planet.

The aspect of atmospheric structure deals with the thermodynamic and physical properties of the atmosphere, and is analyzed in terms of the objectives shown in Table 3-5.

3.2.5.1 Atmospheric Thermodynamic State

The relevant observables are (1) temperature, (2) density, and (3) pressure profiles, (4) vapor content, (5) global thermal balance, and (6) thermal anomalies. The temperature, pressure, and density profiles, along with atmospheric composition data, may indicate the existence of internal heat sources and the achievement of convective or radiative atmospheric equilibrium. However, pressure and density cannot be measured accurately by remote techniques. Orbital imagery is not useful since vertical profiles are required. The global variations of vapor content (notably H_2O and NH_3) are vital to an understanding of planetary weather and the associated condensation and evaporation cycles. Vapor content also influences the transport properties of the atmosphere and assists in determining the proper equation of state (Fleagle and Businger 1963). Vapor content is best determined by atmospheric sampling and chemical analysis or by remote detection of vapor absorption lines (Goody 1964). Since vertical profiles are required, orbital imagery is not useful. A determination of the global heat balance between absorbed solar energy and emitted thermal energy may indicate the presence of heat sources or sinks in the atmosphere or interior, and is related to atmospheric circulation patterns (Mintz 1961). However, heat flux cannot be determined remotely and orbital

Table 3-5

ATMOSPHERIC STRUCTURE OBJECTIVES

Objective	Observable	Remote Sensing	Orbital Imagery
Thermodynamic State	1. Temperature profile	✓	—
	2. Density profile	—	—
	3. Pressure profile	—	—
	4. Vapor content	✓	—
	5. Global thermal balance	—	—
	6. Thermal anomalies	✓	✓
Cloud Structure	1. Extent of global cloud coverage	✓	✓
	2. Cloud layers	✓	—
Transport Properties	1. Coefficient of viscosity	—	—
	2. Thermal conductivity	—	—
	3. Diffusion coefficients	—	—
	4. Radiation transfer coefficients	—	—

imagery is valueless. Detection of thermal anomalies will assist in the location of regions of large viscous and ohmic energy dissipation, volcanic outgassing, and abnormal precipitation. Orbital IR and microwave imaging would be particularly useful in this regard.

3.2.5.2 Cloud Structure

Clouds have been observed on Mars, Venus, and Jupiter. A knowledge of the cloud structure reveals information on the aerosol and dust content of the planetary environment, which in turn largely determines the planet's radiation balance. The observables are (1) extent of global cloud coverage and (2) cloud layers. Earth satellite experience has shown that orbital imagery is essential in studying global cloud coverage. The location and thickness of various cloud layers are related to the detailed radiative balance. Since vertical profile data is required, orbital imagery is not useful. The dynamic aspects of cloud formation and circulation are treated under the aspect of Active Atmospheric Processes.

3.2.5.3 Atmospheric Transport Properties

The observables are (1) coefficient of viscosity, (2) thermal conductivity, (3) diffusion coefficients, and (4) radiation transfer coefficients. The coefficient of viscosity and the thermal conductivity are required in the evaluation of theoretical models describing atmospheric structure and circulation. Since the viscosity and thermal conductivity are functions of the thermodynamic variables and atmospheric constituents, any experimental determination of the viscosity or thermal conductivity offers a useful check on separate data obtained for the thermodynamic variables and atmospheric composition. Diffusion coefficients are needed for theoretical

studies of the various atmospheric layers, particularly the exosphere where diffusion is the dominant process. The radiation transfer coefficients are required if the physical structure of the atmosphere is to be completely understood. In situ atmospheric experiments are essential for determining atmospheric transport properties; orbital imagery is useless. This is a major reason why the Earth's atmospheric structure is still not completely understood.

3.2.6 Active Atmospheric Processes

Atmospheric dynamics is perhaps the most important aspect in understanding the planetary evolution of Venus and Jupiter. The evolution of life on Earth is closely coupled to terrestrial atmospheric processes. Active atmospheric processes are examined here by considering objectives shown in Table 3-6.

3.2.6.1 Atmospheric Circulation and Motion

The general circulation trends and mass motions in a planet's atmosphere can be characterized by the following observables: (1) global wind velocities, (2) convective cells and turbulence, and (3) cloud formation and associated motion. Theoretical and observational data on general atmospheric circulation patterns for the planets are in their initial phases, and the first orbital missions should provide a wealth of information in this area.

The global wind velocities are valuable in establishing the general regime of circulation that exists in a planet's atmosphere. Global circulation patterns can be classified as being in either a "symmetric" or a "wave" regime, depending on the rotation rate and the extent of differential heating between the equator and poles (Mintz 1961). For a slowly rotating planet, the important parameter is the amount of differential heating between the subsolar and anti-solar

Table 3-6

ATMOSPHERIC PROCESSES OBJECTIVES

Objective	Observable	Remote Sensing	Orbital Imagery
Atmospheric Circulation and Motion	1. Global wind velocities	✓	-
	2. Convective Cells and Turbulence	✓	✓
	3. Cloud Formation and Motion	✓	✓
Weather	1. Precipitation Type and Nature	-	-
	2. Precipitation Rate and Variations	✓	✓
	3. Thunderstorms	✓	✓
	4. Cyclone Formations	✓	✓
	5. Atmosphere-Surface Interaction	-	-
Atmospheric Energy Transfer Processes	1. Solar Radiation	-	-
	2. Airglow	✓	-
	3. alpha particles, electrons, and protons	-	-
	4. Cosmic rays	-	-
	5. Meteoroids	✓	-
	6. Ionization and recombination rates	-	-
	7. Surface-atmosphere transfer	✓	✓

IIT RESEARCH INSTITUTE

points (Sagan and Kellogg 1963, Mintz 1962). Since the global circulation pattern is instrumental in establishing the momentum and energy balances in a planet's atmosphere, it is important to establish the flow regime along with the associated rate of mass and heat flow. Orbital imagery, however, cannot measure wind velocities directly. Wind velocities may be inferred from cloud formation and motion.

To thoroughly understand the dynamics and physics of a planet's atmosphere, a knowledge of convective activity other than global circulation and wind patterns is necessary. Turbulence consists of a cascade of energy to smaller and smaller eddies, transforming mechanical energy into internal energy through dissipation, and occurs when the fluid motion exceeds a certain critical value. The most common mode arises in the case of large wind shears in horizontal motion (Lamley and Panofsky 1964). Another type of convective transfer is due to the thermal instability of a stratified fluid heated from below. This can result in adjacent vertical columns of warm and cool fluid alternately ascending and descending, called "Benard cells" when the process is orderly (Chandrasekhar 1961). Under more extreme conditions, this type of natural convection becomes chaotic and is completely turbulent. The existence of vertical convective columns or cells in an atmosphere would indicate that either a significant amount of the solar radiation was being absorbed at low atmospheric levels or else a significant amount of internal heat generation was present. Orbital imagery is useful for studying convective cells and turbulence.

A knowledge of the cloud motions at various atmospheric levels is a direct indication of the wind velocities existing at that altitude. Cloud formation also yields indirect information as to the pressure variations necessary to induce such motions. The time history of cloud formation

enables estimates to be made of the atmospheric temperature and compositional dynamics from theoretical models of aerosol and ice formation (Dufour and Defay 1963, Rosinski 1967). Similarly, for atmospheres in which clouds may be composed principally of dust, a knowledge of cloud variations with time would give an indication of possible interactions between the atmosphere and the surface. Imagery is essential for examining cloud formation and motions.

3.2.6.2 Weather

Weather activity is associated with both local and global phenomena indicating that both condensation and evaporation cycles might be occurring, and that both gases and particulate matter may be involved in mass movement. Other active weather processes might include chemical and other activity occurring through interactions within the near-surface atmospheric regions. The relevant observables are discussed below and can be stated as: (1) precipitation type and nature, (2) precipitation rate and variations, (3) thunderstorms, (4) cyclone formations, and (5) atmosphere-surface interactions.

The type and chemical phase of the precipitation particulates is essential to understanding of the precipitation processes. The mass rate of material exchange can vary appreciably depending on whether the particulates are in a droplet, ice, or snow-flake form. Also, it is important to determine whether or not the particulates are in the form of dust or sand, since this might imply the possible existence of either extensive winds or volcanic activity (Davidson and Anderson, 1967). However, the composition of precipitation cannot be readily determined by remote sensing.

A knowledge of precipitation cycles and their seasonal variations indicates the degree and extent of activity which occurs between various atmospheric levels and

the planet's surface. For example, a high frequency of precipitation indicates that significant variations in the vapor and temperature profiles occur over a relatively short time span in order to accomplish the condensation-evaporation cycle. Radar imagery from orbit may be useful in determining precipitation rate and its spatial and temporal variation.

The intensity of atmospheric processes can be gauged by determining the extent of thunderstorm activity and the associated lightning discharges. Monitoring the lightning activity by spheric imagery from orbit might determine the variability and intensity of atmospheric thunderstorms. The presence of intense cyclonic activity indicates that relatively large pressure differentials and velocity gradients exist within a limited region. A knowledge of these processes is essential for evaluating the activities which are influencing the planet's present and past evolutionary trends. Terrestrial experience has proven that cyclone formations are best studied by orbital imagery.

Atmospheric-surface interactions include determining the amount and extent of chemical and physical interaction associated with crustal outgassing, volcanic activity, and the enhancement of chemical reactions through mixing in the boundary region (Mueller 1964). These processes essentially indicate the present state of stability of the lower atmospheric regions with the surface. Remote sensing cannot provide detailed data on atmospheric-surface interactions.

3.2.6.3 Atmospheric Energy Transfer Processes

The active mechanisms through which energy is added to or extracted from the atmosphere are vital to a complete understanding of atmospheric processes. The observable properties of this objective can be stated as: (1) solar radiation, (2) airglow, (3) α -particles, protons and electrons,

(4) cosmic rays, (5) meteoroids, (6) ionization and recombination rates, and (7) surface to atmosphere transfer.

The global heat balance of a planet is a function of the incident solar radiation. The resultant thermal state of the atmosphere will depend upon how this energy is absorbed, transmitted, and reflected. While the incoming energy of solar radiation peaks at visible wavelengths, it is also important to know the extent of γ -ray, UV, IR, and RF radiation because absorption at various altitudes can affect the stability of atmospheric layers (Fleagle and Businger 1963).

Solar radiation may be instrumental in connection with airglow, i.e. luminescence of the atmosphere. Some atomic species will absorb incident radiation and de-excite by emission of visible light. Accurate measurements of the emission spectrum may identify atmospheric constituents. Although remote spectroscopy might be useful, imaging is not.

In addition to electromagnetic radiation, incident charged particles such as protons, electrons, and α -particles can play an important part in the dynamics and understanding of atmospheric physics and in the formation of radiation belts. The interaction of these particles, or the solar wind, with a planet's atmosphere depends greatly on the magnetic field strength and configuration. A knowledge of the charged particle flux yields useful information relative to the electric and magnetic fields which exist in the atmosphere. Also, for a planet with little or no magnetic field, the solar wind would interact directly with the atmospheric constituents, or with the surface, if the atmosphere is transparent to these particles. A knowledge of these activities is necessary to fully assess the dynamical processes occurring in the atmosphere.

The solar and galactic cosmic ray flux yields information vital to the interpretation of some solar system origin and evolution theories (Dungey 1958). It is also

important in the study of planetary atmospheres because of their high energies and their high penetration capabilities. Of equal importance is the distribution and flux density of meteors and meteorites entering the atmosphere. A knowledge of this flux is necessary in estimating the mass accretion during the past epochs. For a dense atmosphere, much of the meteorite material will be added to the atmospheric constituents at the time of entry due to burnup from viscous heating.

Ionization and recombination processes are important for understanding ionospheric phenomena, aurora, airglow, and other radiative processes. A full understanding of these phenomena requires the determination of collision cross-sections, reaction rates, and the energy budget available in radiation belts and other active regions of the atmosphere.

Active processes involving energy release and dissipation, other than those mentioned above, must be recognized and explained in order to completely understand the physical processes acting in a planetary atmosphere. The most important of these would be energy addition through large scale volcanic activity, such as might exist on Venus (Davidson and Anderson 1967). Not so evident is the possibility of large scale magnetic dynamo activity in the lower atmospheric regions and the resultant ohmic dissipation (Hide 1965) as may exist on Jupiter. Imaging of volcanic dust and vapors and the associated thermal anomalies might be useful, if such activity exists. Ground truth would be particularly useful in connection with atmosphere-surface interactions. None of the other observables in connection with atmospheric energy transfer processes can be usefully investigated by orbital imagery.

3.2.7 Fields

The study of potential fields associated with a planet contributes to an understanding of active processes in the planet interior and atmosphere. Together with seismology and the observation of planetary motion and heat flow, determination of the gravitational, magnetic, and electric fields of a planet provides the only means of evaluating conditions in the planet interior. The gravitational field influences atmospheric composition, structure, and dynamics. The magnetic field influences the interaction between the planet, the interplanetary medium, and the Sun. The objectives related to planetary fields are shown in Table 3-7.

3.2.7.1 Gravitational Field

The gravitational field of a planet is used to determine the figure of the planet in terms of harmonics. The 0th order harmonic is associated with a spherical shape, the 1st order with an oblate ellipsoid, the 2nd order with a pear shape, and so on. The departure of a planet from a sphere is a function of its internal structure (mass distribution), its rotational velocity, and the rigidity of the crust and upper mantle. The observables are (1) field vector, (2) temporal and secular variations, and (3) gravitational waves. In situ detection is required for all three observables; satellite tracking is considered an in situ measurement.

3.2.7.2 Magnetic Field

Understanding of a planetary magnetic field is furthered by observing (1) field vector, (2) temporal and secular variations, (3) radiation belts, (4) auroras, (5) paleomagnetism, and (6) radio burst. The dynamo theory of planetary magnetic fields suggests that the origin and maintenance of the field is related to fluid convective currents in the planetary interior. Therefore the presence of

Table 3-7

FIELD OBJECTIVES

Objective	Observable	Remote Sensing	Orbital Imagery
Gravitational Field	1. Field vector	-	-
	2. Temporal and secular variations	-	-
	3. Gravitational waves	-	-
Magnetic Field	1. Field vector	-	-
	2. Temporal and secular variations	-	-
	3. Radiation belts	-	-
	4. Auroras	✓	✓
	5. Paleomagnetism	-	-
	6. Radio bursts	✓	✓
Electric Field	1. Field vector	-	-
	2. Temporal and secular variations	-	-
	3. Ionospheric ring currents	✓	-
	4. Telluric currents	-	-

a magnetic field is assumed indicative of such currents. Temporal variations in the field may be correlated with the rotational period of the Sun or of planetary satellites, while secular (long-term) variations may result from internal or crustal motion. In situ measurement is required for directly observing the field and its variations. Radiation belts are the result of charged particles being trapped by the planetary magnetic field. Only Jupiter is expected to possess strong radiation belts. In situ techniques are required for detection. Terrestrial auroras are produced by charged particles leaking from the radiation belts, traveling along magnetic field lines, and exciting atoms in the upper atmosphere. Auroras on other planets may have a different origin. The light of the aurora is characteristic of the spectra of the excited species. Remote sensing, and especially visual imagery, would be useful in auroral observation. The past history of magnetic fields may be deduced from paleomagnetic data. Such data may also bear on past crustal history (Runcorn 1962). However, rock paleomagnetism can be measured only by direct surface sampling and testing. The origin of the decametric radio bursts from Jupiter is one of the most significant contemporary problems of planetary phenomena. It has been proposed that the bursts are due to explosions in the Jovian atmosphere (Sagan and Miller 1960), Cerenkov radiation (Warwick 1963), or cyclotron radiation at magnetic field anomalies (Ellis and McCullough 1963), among other reasons. Because of the localization of the activity, and its rapid variations, radio frequency imaging experiments from orbit would be invaluable.

3.2.7.3 Electric Field

Here the observables are (1) field vector, (2) temporal and secular variations, (3) ionospheric ring currents, and (4) telluric currents. The electric field of the Earth, and its variations, do not appear to play a significant role

in planetary phenomena on the Earth. This is probably true on the other planets. In any event, electric field measurements require in situ observation. Ionospheric ring currents might be measured by radio frequency remote sensing, and the resultant data might provide data on electron concentrations in the ionosphere. Imagery, however, is not useful. Telluric currents flow through the crust and mantle of the Earth; similar electric currents may flow in the crust and mantle of the other planets. Such currents might provide information on the electrical and thermal conductivity. Telluric currents are best measured by surface voltage gradient measurements, imagery is not useful.

3.2.8 Active Biota

The detection of a thriving extraterrestrial biology would be the most important scientific discovery in the age of civilization. One can scarcely comprehend the impact of such a discovery upon the direction and magnitude of the space exploration program. The major measurement problem is the design of an experiment which can unambiguously determine that life does or does not exist on a planet. It is possible that extraterrestrial life exists in a form which is both functionally and chemically different from that to which we are accustomed. The most popular exotic suggestions are that extraterrestrial life may be based upon silicon bonds rather than carbon bonds, or on a solvent system other than water, say ammonia. Nonetheless, the objectives and observables formulated here consider detection of an Earth-type biology since no other system has been adequately described to allow experiments to be defined. The objectives are listed in Table 3-8.

Table 3-8

ACTIVE BIOTA

Objective	Observable	Remote Sensing	Orbital Imagery
Life Forms	1. Animal life	-	-
	2. Plant life	-	-
	3. Microscopic life forms	✓	✓
	4. Living cells	✓	✓
Biochemistry	1. Macromolecules	-	-
	2. Complex molecular structures	-	-
	3. Biochemical systems	✓	✓
Metabolism	1. Environmental exchange	-	-
	2. Growth	-	-
	3. Heat generation	-	-
Reproduction	1. Birth	-	-
	2. Number density	-	-
	3. Cellular division	-	-
	4. Genetic codes	-	-

3.2.8.1 Life Forms

The relevant observables are (1) animal life, (2) plant life, (3) microscopic life forms, and (4) living cells. Even the most casual observer on Earth is able to perceive the difference between life and death, the alive and the inert. If terrestrial-like animal or plant life exists on the other planets, the property of life may be recognized with equal ease. For extraterrestrial animal life, the identifying characteristic may be that of mobility, and therefore imaging experiments of high resolution would be essential. Extraterrestrial plant life might exhibit characteristic absorption spectra similar to that of Earth forms. Orbital imagery would be useful, but not essential. Remote sensing of microscopic life forms (spores, viruses, etc.) and living cells appears to be useless because of the microscopic scale.

3.2.8.2 Biochemistry

In order of increasing characteristic size, the observables are (1) macromolecules, (2) complex molecular structure, and (3) biochemical systems. The detection of macromolecules, such as DNA, or complex molecular structures, such as a helix, is not proof of life, but the more complex the molecules, the more indicative of life. It would be highly desirable if experiments could be designed which would detect biologically created molecules, or systems of molecules, without having to identify the molecules. The greatest possibility in this regard appears to be the detection of internal molecular structure. However, because of the molecular scale of the observables, remote sensing is inapplicable. It is possible that biochemical systems may exist on planets or in their atmospheres, especially where complex molecules are densely packed and continuous chemical activity is present.

Such systems may be analogous to the primordial soup which has been suggested as preceding life on Earth. Orbiting imagery experiments might be useful for detecting biochemical systems.

3.2.8.3 Metabolism

A living organism is continually involved in an interchange with its environment. It is dependent upon its surroundings for energy and nutrients, and it deposits the by-products of its metabolism into its environment. It may be irritated, made dormant, and killed, or it may be induced to grow and reproduce prolifically. The observables considered here are (1) environmental exchanges, (2) growth, and (3) heat generation. It has been suggested (Hitchcock and Lovelock 1967) that the entropy of living systems is low relative to their dead environments. Life drives its environment into disequilibrium, and an entropy gradient exists between living and non-living matter. The environmental exchanges between life and non-living matter require close-hand investigation and remote sensing is not useful. All active life grows within its life cycle as a direct result of its metabolism. This growth may be small, as in the case of cells and microorganisms, or large, as in the case of animals. The detection of growth requires continuous, or periodic, observation of specific, individual life forms and remote sensing is not helpful without tracing of individuals. Metabolic activity always produces heat, even though often in minute quantities. However, the remote detection of metabolic heat production does not appear to be a promising remote life detection technique.

3.2.8.4 Reproduction

The demonstration of reproduction must be one of the most convincing proofs of life. The relevant observable properties are (1) birth, (2) number density, (3) cellular division, and (4) genetic codes. The probability of observing the birth of higher forms of life must be extremely small. However, it might be possible to monitor population growth as a function of time. Carefully controlled samples are essential to proper data interpretation. The most probable method of detecting reproduction is on a cellular level, since cells are common to all forms of life and subdivide with a rapid periodicity. Perhaps at the fringe of detection is the identification of reproduction codes on a macromolecular level. Remote sensing is not useful in detecting any of these observable properties.

3.2.9 Extinct Biota

The clear identification of biological remains is extremely difficult. Controversy still rages over the interpretation in meteorites. This is further complicated if the environmental history of the material is not adequately understood. The task on the planets is initially one of sifting surface materials to detect pieces with shapes and constructions reminiscent of biological species on a microscopic and macroscopic scale. In addition, it may be possible to identify chemicals and substances created by the decay of biological materials. The objectives relevant to extinct biota are shown in Table 3-9.

Table 3-9

EXTINCT BIOTA OBJECTIVES

Objective	Observable	Remote Sensing	Orbital Imagery
Fossils	1. Animal and Plant fossils	-	-
	2. Molecular fossils	-	-
Biological Decay Products	1. Hydrocarbons	✓	✓

3.2.9.1 Fossils

The relevant observables are (1) animal and plant fossils and (2) molecular fossils. Fossils found on the Earth of animals, insects, and plants are readily identifiable as extinct life forms even when only partially complete. Such fossils on any planet, even though of unknown species, would be equally easily recognized. One of the problems, however, is knowing where to look for them. This will be dependent on the erosional and depositional history of the surface materials and should be determined as part of the exploration of the planet. The remote possibility exists that artifacts of an intelligent biota could be fossilized, but a specific search for these is not proposed. Molecules, as well as organisms can be fossilized. The types of molecule that are generated depend on the particular ambient conditions at the time of their formation. As conditions change it is possible for these molecules to become trapped and inactive. The detection of complex biological molecules within rocks will be indicative of, rather than proof of, an extinct biota. Surface sampling is required for fossil detection.

3.2.9.2 Biological Decay Products

Hydrocarbons and petrochemicals in the Earth's crust have been attributed to the decay of biological material. However, this origin is probably not unique and the detection of oil, coal, and natural gas (methane, butane, etc.) in a planetary crust would lend credence to a biological history rather than prove it. There is a possibility that pools of hydrocarbons exist on Venus, in particular. Orbital imagery might be useful in detecting accumulations of hydrocarbons.

3.3 Engineering Objectives

The engineering goal requires that the exploration plans be performed with maximum effectiveness. Broadly speaking this requires that the right experiments be performed, at the right times, in the right places and presumably for the minimum cost.

Engineering objectives and observables have been developed for four mission concepts. Figure 3-3 shows the development of engineering objectives for planetary orbiters. In considering each of the orbiter subsystems, it was found that the design of the four subsystems shown (guidance and control, structure and shielding, altitude control and thermal control) all were dependent on the environment in which they were to function. The particular environmental properties of interest are shown as observables. The environmental interfaces with other subsystems either did not involve planetary observables or, if they did, they were adequately known already. Within the constraints of the study, it was not possible to consider the engineering observables in any further detail, either as a function of specific spacecraft designs or in terms of each of the planets. Figures 3-4, 3-5 and 3-6 provide the development of engineering observables for atmospheric probes, atmospheric floaters and landers respectively.

The engineering observables were not considered in sufficient detail to define measurement specifications, but they were correlated with the scientific observables. Those measurement specifications which could conceivably contribute to the engineering objectives were noted. Even the limited results presented here have demonstrated the feasibility of defining engineering measurement requirements. It is strongly recommended that the method and results be carefully reviewed, changed where necessary and then applied

ENG. CONCEPT
(MISSION CONCEPT)

ENG. OBJECTIVES
(SUB SYSTEM DESIGN)

ENG. OBSERVABLES
(PLANETARY ENVIRONMENT)

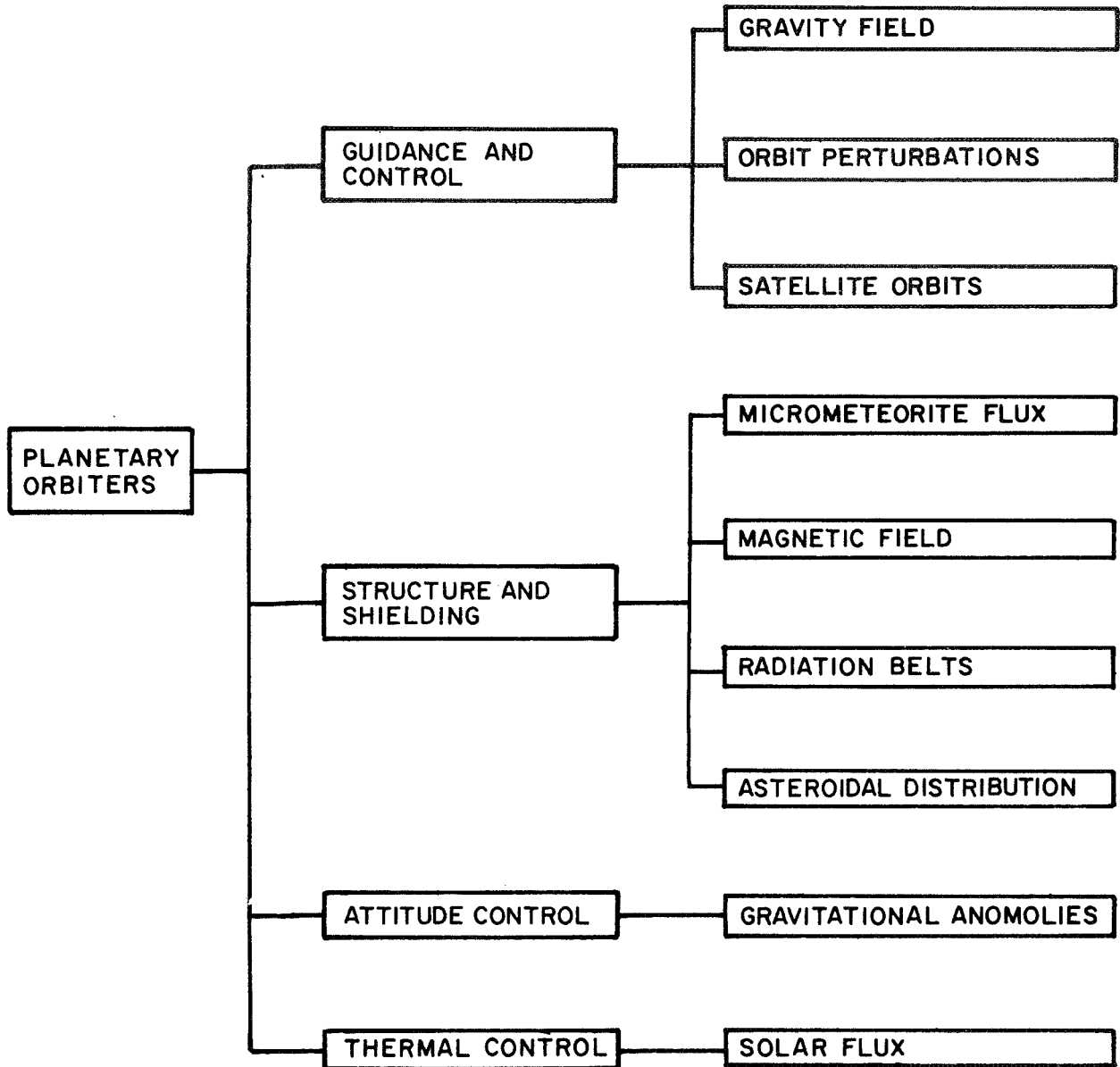


FIGURE 3-3. DEVELOPMENT OF ENGINEERING OBSERVABLES
PLANETARY ORBITERS

ENG. ASPECT
(MISSION CONCEPT)

ENG. OBJECTIVES
(SUB SYSTEM DESIGN)

ENG. OBSERVABLES
(PLANETARY ENVIRONMENT)

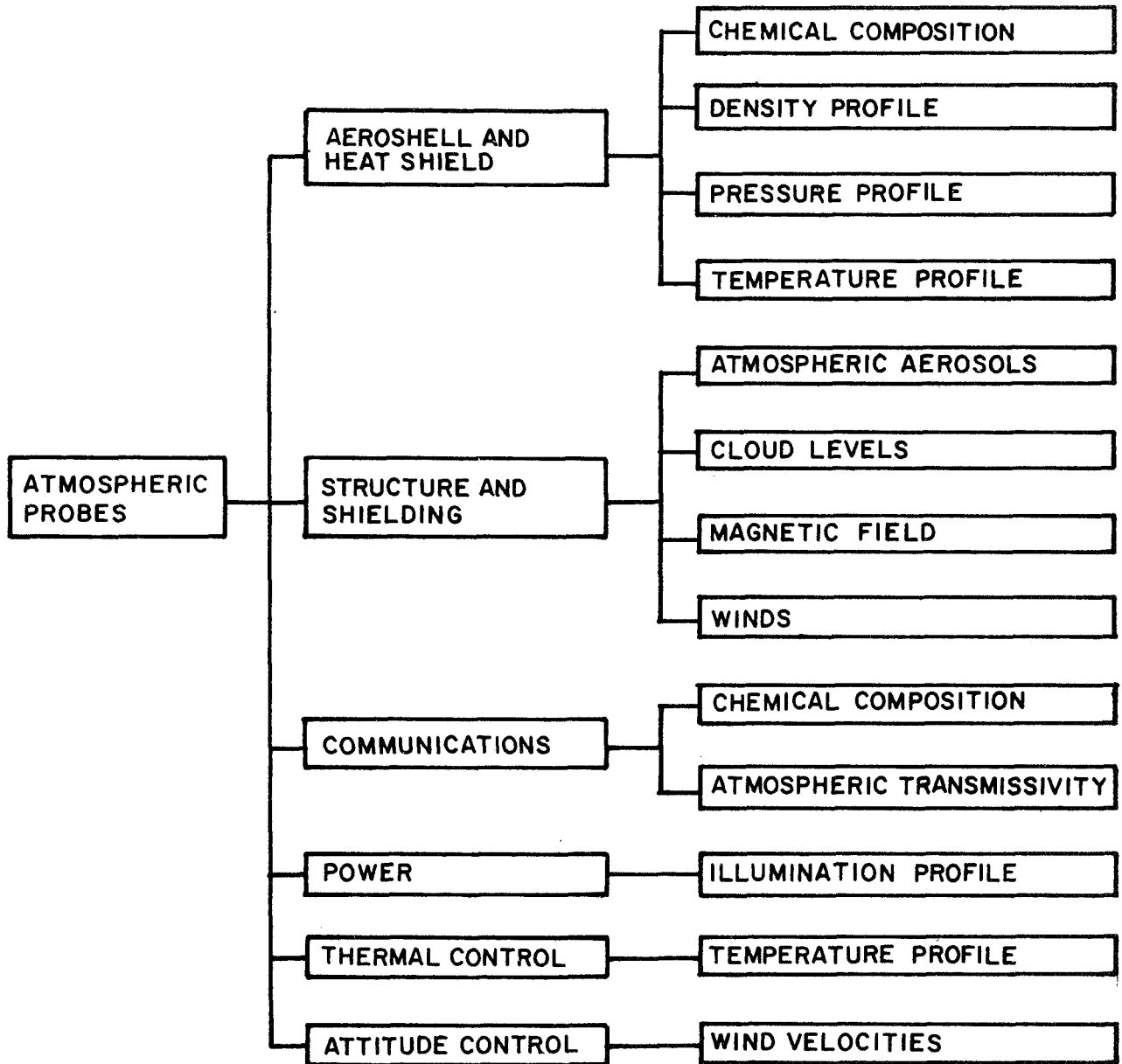


FIGURE 3-4. DEVELOPMENT OF ENGINEERING OBSERVABLES
ATMOSPHERIC PROBES

ENG. ASPECT
(MISSION CONCEPT)

ENG. OBJECTIVES
(SUB SYSTEM DESIGN)

ENG. OBSERVABLES
(PLANETARY ENVIRONMENT)

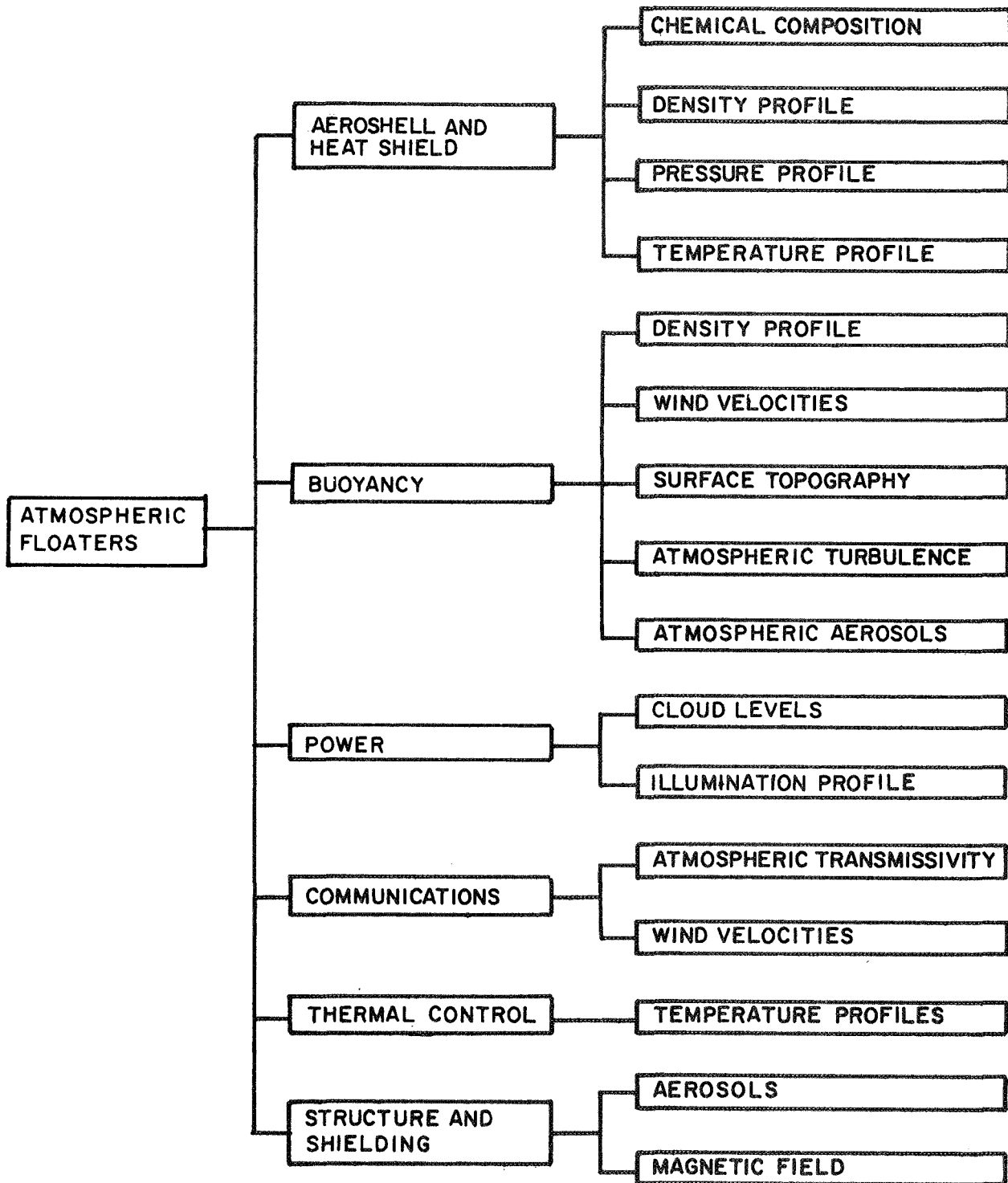


FIGURE 3-5. DEVELOPMENT OF ENGINEERING OBSERVABLES
ATMOSPHERIC FLOATERS

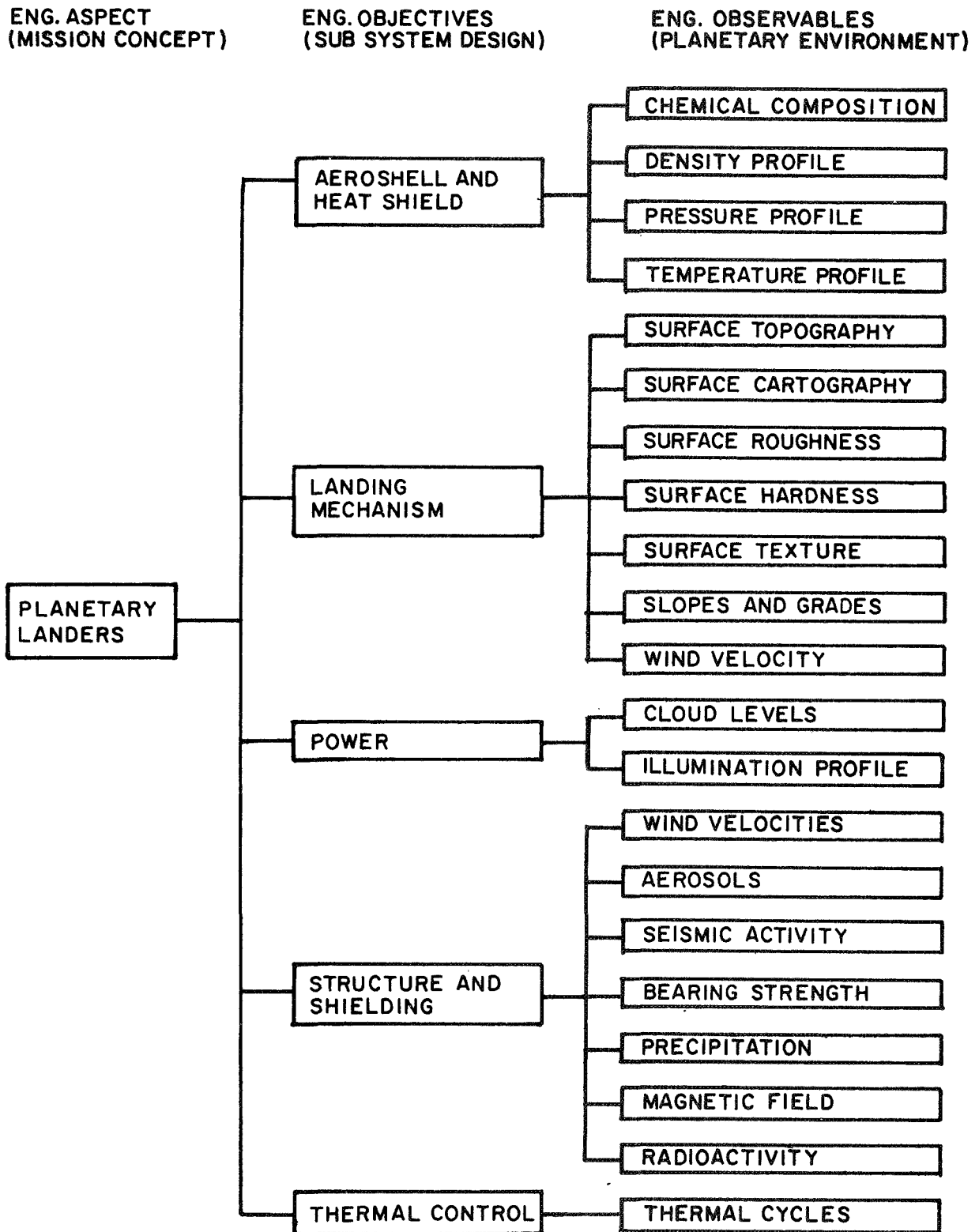


FIGURE 3-6. DEVELOPMENT OF ENGINEERING OBSERVABLES
PLANETARY LANDERS

from the top down. It is felt that many measurement requirements will arise which are not identified by scientific considerations. These may have an impact on the subsystem requirements and on the need for advanced technology developments. An example may be measurements of surface bearing strength or angles of repose which relate to the design of a lander but have little intrinsic scientific value.

4. MEASUREMENT DEFINITION

The detailed description of the observables, as given in Section 3 and in the data sheets of Volume II, provide a firm basis for the identification of the need for imaging experiments. The measurement definition task is to take each observable and to generate a quantitative set of measurement specifications for each imaging experiment and for each of the planets. The parts can be summarized as follows:

- (a) Specify the nominal measurement requirements as defined by the need to extend current scientific knowledge by approximately one order of magnitude.
- (b) Specify the nominal measurement requirements as defined by the need to interpret the images scientifically.
- (c) Identify the relative worth of the measurement as the above measurement specifications deviate on either side of nominal.

It must be emphasized that the specifications are based solely on the scientific requirements. No account is taken here of the difficulty of meeting these requirements.

Table 4-1 summarizes the measurement specifications for all the observables for which imaging was found to be useful. They embrace the geometrical, temporal, and spectral characteristics of the measurement. To the limited extent that the spectral specifications define a type of sensing system, this is also included under the column "sensor type."

The first column identifies the observable to which imaging applies and the second column, the planet to which the ensuing specifications refer. The next sixteen columns are used to specify the scientific measurement

requirements. Each entry consists of a number and a reference. The number is the nominal specification and the reference relates to a "worth curve" from which the scientific degradation in the measurement can be assessed for other than nominal specifications. Each column will be discussed in turn, but first it is important to discuss the concept and application of the worth curves.

In specifying a scientific measurement requirement it was apparent that although a nominal value could be found in all cases, a single value did not adequately represent the flexibility of the scientific requirements. Furthermore, since the measurement specifications were being determined while carefully avoiding any consideration of the ease or difficulty of implementation, it was felt necessary to provide limits that a scientific investigator would consider acceptable. This is the context in which the worth curves were developed.

It will be readily appreciated that each specification, for each observable, for each planet must be considered independently. Simply because nominal specifications are the same for two observables, does not imply that the worth of both experiments varies in the same fashion for variation in the specifications on either side of nominal. Families of worth curves are presented in Figures 4-2 to 4-11 at the end of this section for each of the measurement requirements. In each case the plateau represents the range of the parameter over which the measurement has maximum value (normalized to unity). The slopes at the ends indicate how rapidly the measurement degrades, again from a purely scientific standpoint. Finally, the dashed lines are extrapolations into regions where no real experience is available.

The worth curves refer to each specified parameter considered one at a time. It is not apparent how a measurement would degrade if two or more specified parameters were moved off the plateau simultaneously. No effort was expended in this area, since the context of the study was such that the

TABLE 4-1 SUMMARY OF MEASUREMENT SPECIFICATIONS

OBSERVABLE	PLANET	GROUND RESOLUTION	IMAGE SIZE	POSITIONAL ACCURACY	PLANETARY COVERAGE	PLANETARY DISTRIBUTION	ACQUISITION TIME		SENSOR REFERENCES	SENSOR TYPE	SPECTRAL REGION	BANDWIDTH	OVERLAP	SUN ELEVATION	SUPPORT MEASUREMENTS	COMMENTS
							IMAGE	COVERAGE								
1) Surface Elevations	Moon	5 km A7	500 km B5	10 km C7	100% D1	-	-	-	a Visible	5750Å F3	1000Å G3	20% H1	20° I1	S/C Altitude, Local Time	Vertical resolution for all bodies is 1 km (J1) except Jupiter which is 4 km (J2).	
	Mercury	5 km A7	800 km B6	10 km C7	100% D1	-	-	-	b Visible Stereo	5750Å F3	1000Å G3	20% H2	20° I1	S/C Altitude, Local Time		
	Mars	5 km A7	1000 km B6	10 km C7	100% D1	-	-	-	c Visible Stereo	5750Å F3	1000Å G3	60% H3	20° I1	S/C Altitude, Local Time		
	Venus	5 km A7	2000 km B8	10 km C7	100% D1	-	-	-	d Visible Stereo	5750Å F3	1000Å G3	60% H3	80° I4	S/C Altitude, Local Time		
	Jupiter	50 km A8	20000 km B11	50 km C9	100% D1	-	-	-	e Radar	20 cm F18	-	20% H1	-	S/C Altitude		
2) Layering	Moon	10 cm A1	1 km B2	10 m C2	<1% D2	Determined by prior mapping	-	-	a Visible	5750Å F3	1000Å G2	20% H1	45° I2	-		
	Mercury	10 cm A1	1 km B2	10 m C2	<1% D2	Determined by prior mapping	-	-	b Visible	5750Å F3	1000Å G2	20% H2	45° I2	-		
	Mars	10 cm A1	1 km B2	10 m C2	<1% D2	Determined by prior mapping	-	-	c Radar	10 cm F17	-	20% H1	-	-		
	Venus	10 cm A1	1 km B2	10 m C2	<1% D2	Determined by prior mapping	-	-	d Multifreq. Radar	50 cm F18	3 bands G16	20% H1	-	-		
	Jupiter	1 m A3	1 km B2	10 m C2	<1% D2	Determined by prior mapping	-	-	e Radar	60 cm F18	3 bands G16	20% H2	-	-		
3) Contacts (Regional)	Mercury	1 km A6	800 km B6	10 km C6	100% D1	-	-	-	a Ultraviolet	2250Å F1	500Å G1	20% H1	90° I5	-		
	Mars	1 km A6	1000 km B6	10 km C6	100% D1	-	-	-	b Visible	5750Å F3	1000Å G2	20% H1	20° I1	-		
	Venus	1 km A6	2000 km B8	10 km C6	100% D1	-	-	-	c Visible	5750Å F3	1000Å G2	20% H1	20° I1	-		
	Jupiter	10 km A7	20000 km B11	50 km C9	5% D3	Global	-	-	d Visible	5750Å F3	1000Å G2	20% H2	20° I1	-		
	Moon	100 m A5	100 km B4	1 km C4	100% D1	-	See regional maps	-	e Infrared	1.75µ F6	0.1µ G2	20% H1	20° I1	-		
4) (Local)	Mercury	100 m A5	100 km B4	1 km C4	10% D2	See regional maps	-	-	f Infrared	1.75µ F6	0.1µ G2	20% H2	20° I1	-		
	Mars	100 m A5	100 km B4	1 km C4	10% D2	See regional maps	-	-	g Infrared	1.75µ F6	0.1µ G2	20% H2	20° I1	-		
	Venus	100 m A5	100 km B4	1 km C4	10% D2	See regional maps	-	-	h Radar	120µ F12	20µ G9	20% H1	90° I5	-		
	Moon	1 m A3	1 km B2	10 m C2	<1% D2	See local maps	-	-	i Radar	10 cm F17	-	20% H1	-	-		
	Mercury	1 m A3	1 km B2	10 m C2	<1% D2	See local maps	-	-	j Multiband	15-21µ F1,3,7	6 bands G19	20% H1	45° I2	-		
5) (Detailed)	Venus	1 m A3	1 km B2	10 m C2	<1% D2	See local maps	-	-	k Multiband	15-21µ F1,3,7	6 bands G19	20% H1	45° I2	-		
	Mercury	1 km A6	800 km B6	10 km C6	100% D1	-	-	-	a Visible	5750Å F3	1000Å G2	20% H1	20° I1	-		
	Mars	1 km A6	1000 km B6	10 km C6	100% D1	-	-	-	b Visible Stereo	5750Å F3	1000Å G2	20% H2	20° I1	-		
	Venus	1 km A6	2000 km B8	10 km C6	100% D1	-	-	-	c Visible Stereo	5750Å F3	1000Å G2	20% H2	20° I1	-		
	Jupiter	10 km A7	20000 km B11	200 km C10	5% D3	Global	-	-	d Visible Color	5750Å F3	1000Å G2	60% H3	80° I4	-		
6) Structure of Features (Regional)	Mercury	100 m A5	100 km B4	1 km C4	100% D1	-	See regional maps	-	e Visible Color	5750Å F3	3 bands G4,17	20% H1	20° I1	-	Vertical resolution same as horizontal	
	Mars	100 m A5	100 km B4	1 km C4	10% D2	See regional maps	-	-	f Visible Color	5750Å F3	3 bands G4,17	20% H1	20° I1	-		
	Venus	100 m A5	100 km B4	1 km C4	10% D2	See regional maps	-	-	g Radar	20 cm F18	3 bands G4,17	20% H2	20° I1	-		
	Moon	1 m A3	1 km B2	10 m C2	<1% D2	See local maps	-	-	h Radar	50 cm F18	3 bands G4,17	20% H1	-	-		
	Mercury	1 m A3	1 km B2	10 m C2	<1% D2	See local maps	-	-	i Radar Stereo	50 cm F18	3 bands G4,17	20% H2	-	-		
7) (Local)	Venus	1 m A3	1 km B2	10 m C2	<1% D2	See local maps	-	-	j Radar Stereo	50 cm F18	3 bands G4,17	20% H2	-	-		
	Mercury	1 km A6	800 km B6	10 km C6	100% D1	-	-	-	a Visible	5750Å F3	1000Å G2	20% H1	20° I1	-		
	Mars	1 km A6	1000 km B6	10 km C6	100% D1	-	-	-	b Visible	5750Å F3	1000Å G2	20% H2	20° I1	-		
	Venus	1 km A6	2000 km B8	10 km C6	100% D1	-	-	-	c Visible Stereo	5750Å F3	1000Å G2	20% H2	20° I1	-		
	Jupiter	10 km A7	20000 km B11	200 km C10	5% D3	Global	-	-	d Visible Stereo	5750Å F3	1000Å G2	60% H3	80° I4	-		
8) (Detailed)	Mercury	100 m A5	100 km B4	1 km C4	100% D1	-	See regional maps	-	e Visible Stereo	5750Å F3	1000Å G2	20% H1	20° I1	-	Vertical resolution: (Regional) - 1 km (J1) for all except Jupiter at 4 km (J2) 30 m (J3) (Local) - 10 m (J4) (Detailed) - 10 m (J4)	
	Mars	100 m A5	100 km B4	1 km C4	10% D2	See regional maps	-	-	f Radar	50 cm F18	3 bands G4,17	20% H2	20° I1	-		
	Venus	100 m A5	100 km B4	1 km C4	10% D2	See regional maps	-	-	g Radar	50 cm F18	3 bands G4,17	20% H2	20° I1	-		
	Moon	1 m A3	1 km B2	10 m C2	<1% D2	See local maps	-	-	h Radar Stereo	50 cm F18	3 bands G4,17	20% H1	-	-		
	Mercury	1 m A3	1 km B2	10 m C2	<1% D2	See local maps	-	-	i Radar Stereo	50 cm F18	3 bands G4,17	20% H2	-	-		
9) Surface Topography (Regional)	Venus	1 m A3	1 km B2	10 m C2	<1% D2	See local maps	-	-	j Radar Stereo	50 cm F18	3 bands G4,17	20% H2	-	-		
	Mercury	1 km A6	800 km B6	10 km C6	100% D1	-	-	-	a Visible	5750Å F3	1000Å G2	20% H1	20° I1	-		
	Mars	1 km A6	1000 km B6	10 km C6	100% D1	-	-	-	b Visible	5750Å F3	1000Å G2	20% H2	20° I1	-		
	Venus	1 km A6	2000 km B8	10 km C6	100% D1	-	-	-	c Visible Stereo	5750Å F3	1000Å G2	20% H2	20° I1	-		
	Jupiter	10 km A7	20000 km B11	200 km C10	5% D3	Global	-	-	d Visible Stereo	5750Å F3	1000Å G2	60% H3	80° I4	-		
10) (Local)	Mercury	100 m A5	100 km B4	1 km C4	100% D1	-	See regional maps	-	e Visible Stereo	5750Å F3	1000Å G2	20% H1	20° I1	-		
	Mars	100 m A5	100 km B4	1 km C4	10% D2	See regional maps	-	-	f Radar	50 cm F18	3 bands G4,17	20% H2	20° I1	-		
	Venus	100 m A5	100 km B4	1 km C4	10% D2	See regional maps	-	-	g Radar	50 cm F18	3 bands G4,17	20% H2	20° I1	-		
	Moon	1 m A3	1 km B2	10 m C2	<1% D2	See local maps	-	-	h Radar Stereo	50 cm F18	3 bands G4,17	20% H1	-	-		
	Mercury	1 m A3	1 km B2	10 m C2	<1% D2	See local maps	-	-	i Radar Stereo	50 cm F18	3 bands G4,17	20% H2	-	-		
11) (Detailed)	Venus	1 m A3	1 km B2	10 m C2	<1% D2	See local maps	-	-	j Radar Stereo	50 cm F18	3 bands G4,17	20% H2	-	-		
	Mercury	1 km A6	800 km B6	10 km C6	100% D1	-	-	-	a Visible	5750Å F3	1000Å G2	20% H1	20° I1	-		
	Mars	1 km A6	1000 km B6	10 km C6	100% D1	-	-	-	b Visible	5750Å F3	1000Å G2	20% H2	20° I1	-		
	Venus	1 km A6	2000 km B8	10 km C6	100% D1	-	-	-	c Visible Color	5750Å F3	1000Å G2	20% H2	20° I1	-		
	Jupiter	10 km A7	20000 km B11	200 km C10	5% D3	Global	-	-	d Visible Color	5750Å F3	1000Å G2	60% H3	80° I4	-		
12) Surface Appearance (Regional)	Mercury	100 m A5	100 km B4	1 km C4	100% D1	-	See regional maps	-	e Visible Color	5750Å F3	3 bands G4,17	20% H1	20° I1	-		
	Mars	100 m A5	100 km B4	1 km C4	10% D2	See regional maps	-	-	f Radar	50 cm F18	3 bands G4,17	20% H2	20° I1	-		
	Venus	100 m A5	100 km B4	1 km C4	10% D2	See regional maps	-	-	g Radar	50 cm F18	3 bands G4,17	20% H2	20° I1	-		
	Moon	1 m A3	1 km B2	10 m C2	<1% D2	See local maps	-	-	h Radar	50 cm F18	3 bands G4,17	20% H1	-	-		
	Mercury	1 m A3	1 km B2	10 m C2	<1% D2	See local maps	-	-	i Radar	50 cm F18	3 bands G4,17	20% H2	-	-		
13) (Local)	Venus	1 m A3	1 km B2	10 m C2	<1% D2	See local maps	-	-	j Radar	50 cm F18	3 bands G4,17	20% H2	-	-		
	Mercury	1 km A6	800 km B6	10 km C6	100% D1	-	-	-	a Visible	5750Å F3	1000Å G2	20% H1	20° I1	-		
	Mars	1 km A6	1000 km B6	10 km C6	100% D1	-	-	-	b Visible	5750Å F3	1000Å G2	20% H2	20° I1	-		
	Venus	1 km A6	2000 km B8	10 km C6	100% D1	-	-	-	c Visible Color	5750Å F3	1000Å G2	20% H2	20° I1	-		
	Jupiter	10 km A7	20000 km B11	200 km C10	5% D3	Global	-	-	d Visible Color	5750Å F3	1000Å G2	60% H3	80° I4	-		
14) (Detailed)	Mercury	100 m A5	100 km B4	1 km C4	100% D1	-	See regional maps	-	e Visible Color	5750Å F3	3 bands G4,17	20% H1	20° I1	-		
	Mars	100 m A5	100 km B4	1 km C4	10% D2	See regional maps	-	-	f Radar	50 cm F18	3 bands G4,17	20% H2	20° I1	-		
	Venus	100 m A5	100 km B4	1 km C4	10% D2	See regional maps	-	-	g Radar	50 cm F18	3 bands G4,17	20% H2	20° I1	-		
	Moon	1 m A3	1 km B2	10 m C2	<1% D2	See local maps	-	-	h Radar	50 cm F18	3 bands G4,17	20% H1	-	-		
	Mercury	1 m A3	1 km B2	10 m C2	<1% D2	See local maps	-	-	i Radar	50 cm F18	3 bands G4,17	20% H2	-	-		
15) Variable (Reg)	Venus	1 m A3	1 km B2	10 m C2	<1% D2	See local maps	-	-	j Radar	50 cm F18	3 bands G4,17	20% H2	-	-		
	Mercury	1 km A6	800 km B6	10 km C6	100% D1	-	-	-	a Visible	5750Å F3	1000Å G2	20% H1	20° I1	-		
	Mars	1 km A6	1000 km B6	10 km C6	100% D1	-	-	-	b Visible	5750Å F3	1000Å G2	20% H2	20° I1	-		
	Venus	1 km A6	2000 km B8	10 km C6	100% D1	-	-	-	c Visible Color	5750Å F3	1000Å G2	20% H2	20° I1	-		
	Jupiter	10 km A7	20000 km B11	200 km C10	5% D3	Global	-	-	d Visible Color	5750Å F3	1000Å G2	60% H3	80° I4	-		
16) Surface (Local)	Mercury	100 m A5	100 km B4	1 km C4	100% D1	-	See regional maps	-	e Visible Color	5750Å F3	3 bands G4,17	20% H1	20° I1	-		
	Mars	100 m A5	100 km B4	1 km C4	10% D2	See regional maps	-	-	f Radar	50 cm F18	3 bands G4,17	20% H2	20° I1	-		
	Venus	100 m A5	100 km B4	1 km C4	10% D2	See regional maps	-	-	g Radar	50 cm F18	3 bands G4,17	20% H2	20° I1	-		
	Moon	1 m A3	1 km B2	10 m C2	<1% D2	See local maps	-	-	h Radar	50 cm F18	3 bands G4,17	20% H1	-	-		
	Mercury	1 m A3	1 km B2	10 m C2	<1% D2	See local maps	-	-	i Radar	50 cm F18	3 bands G4,17	20% H2	-	-		
17) Appearance (Det)	Venus	1 m A3	1 km B2	10 m C2	<1% D2	See local maps	-	-	j Radar	50 cm F18	3 bands G4,17	20% H2	-	-		
	Mercury	1 km A6	800 km B6	10 km C6	100% D1	-	-	-	a Visible	5750Å F3	1000Å G2	20% H1	20° I1	-		
	Mars	1 km A6	1000 km B6	10 km C6	100% D1	-	-	-	b Visible	5750Å F3	1000Å G2	20% H2	20° I1	-		
	Venus	1 km A6	2000 km B8	10 km C6	10											

TABLE 4-1 SUMMARY OF MEASUREMENT SPECIFICATIONS (Continued)

OBSERVABLE	PLANET	GROUND RESOLUTION	IMAGE SIZE	POSITIONAL ACCURACY	PLANETARY COVERAGE	PLANETARY DISTRIBUTION	ACQUISITION TIME		REPETITION RATE		SENSOR REFERENCE	SENSOR TYPE	SPECTRAL REGIONS	BANDWIDTH	OVERLAP	SUN ELEVATION	SUPPORT MEASUREMENTS	COMMENTS
							IMAGE	COVERAGE	IMAGE	COVERAGE								
21) Surface Thermal Anomalies (Regional)	Moon	1 km	A6 500 km	10 km	C6 100% D1	-	1 hr	E7	10 hr	E10	a, c, f	a IR	10μ	20% H1	-	-	Desired Temperature Resolution: 1K Moon Mercury 5K Mars 2K Venus 5K Jupiter 2K	
	Mars	1 km	A6 800 km	10 km	C6 100% D1	-	1 hr	E7	10 hr	E10	b, d, g	b Microwave	10μ	20% H2	-	-		
	Mars	1 km	A6 1000 km	10 km	C6 100% D1	-	1 hr	E7	10 hr	E10	b, d, g	c Microwave	10 cm	20% H1	-	-		
	Venus	1 km	A6 2000 km	10 km	C6 100% D1	-	1 hr	E7	10 hr	E10	d, h	d	10 cm	20% H2	-	-		
	Jupiter	10 km	A7 10000 km	100 km	C9 100% D1	-	1 hr	E7	10 hr	E10	e	e	10 cm	20% H2	-	-		
22) (Local)	Moon	100 m	A5 100 km	1 km	C4 5% D3	See regional maps	1 hr	E7	10 hr	E10	a, c, f	f Multiband	4 bands	20% H1	-	-		
	Mars	100 m	A5 100 km	1 km	C4 5% D3	See regional maps	1 hr	E7	10 hr	E10	b, d, g	g	4 bands	20% H1	-	-		
	Mars	100 m	A5 100 km	1 km	C4 5% D3	See regional maps	1 hr	E7	10 hr	E10	b, d, g	h	3 bands	20% H2	-	-		
	Venus	100 m	A5 100 km	1 km	C4 5% D3	See regional maps	1 hr	E7	10 hr	E10	d, h							
	Venus	100 m	A5 100 km	1 km	C4 5% D3	See regional maps	1 hr	E7	10 hr	E10								
23) (Detailed)	Moon	1 m	A3 1 km	10 m	C2 1% D4	See local maps	1 hr	E7	10 hr	E10	a, c, f	a IR	6μ	20% H2	-	-	Desired Temperature Resolution: Same as above	
	Mars	1 m	A3 1 km	10 m	C2 <1% D2	See local maps	1 hr	E7	10 hr	E10	b, d, g	b Microwave	10 mm	20% H2	-	-		
	Mars	1 m	A3 1 km	10 m	C2 <1% D2	See local maps	1 hr	E7	10 hr	E10	b, d, g	c	10 mm	20% H2	-	-		
	Venus	1 m	A3 1 km	10 m	C2 <1% D2	See local maps	1 hr	E7	10 hr	E10	d, h	d	4 bands	20% H2	-	-		
	Venus	1 m	A3 1 km	10 m	C2 <1% D2	See local maps	1 hr	E7	10 hr	E10		e	4 bands	20% H2	-	-		
24)* Atmos. Thermal Anomalies (Regional)	Mars	10 km	A7 1200 km	50 km	C8 100% D1	Polar regions	1 hr	E7	10 yr	E17	a, b, d	a IR	6μ	20% H2	-	-	Desired Temperature Resolution: Same as above	
	Venus	10 km	A7 2000 km	50 km	C8 100% D1	Cloud belts, red spot	1 hr	E7	10 yr	E17	a, c, e	b Microwave	10 mm	20% H2	-	-		
	Jupiter	10 km	A7 20000 km	200 km	C10 100% D1	See regional maps	1 hr	E7	10 yr	E17	a, c, e	c	10 mm	20% H2	-	-		
	Venus	1 km	A6 100 km	10 km	C6 10% D2	See regional maps	1 hr	E7	1 day	E13	a, b, d	d Multiband	4 bands	20% H2	-	-		
	Jupiter	1 km	A6 2000 km	20 km	C8 20% D2	See regional maps	1 hr	E7	1 day	E13	a, c, e	e	4 bands	20% H2	-	-		
26) Global Cloud Coverage	Mars	10 km	A7 1200 km	50 km	C8 100% D1	Polar regions	15 min	E6	1 day	E13	a, b, c, d, e	a UV	1000A	20% H2	Day	I6	Desired Temperature Resolution: Same as above	
	Venus	10 km	A7 2000 km	50 km	C8 100% D1	Subsolar and polar areas	15 min	E6	100 hr	E13	a, b, c, d, e	b Visible (BW & 5750A color)	1000A	20% H2	Day	I6		
	Jupiter	10 km	A7 20000 km	200 km	C10 100% D1	See regional maps	2 min	E6	1 day	E13	a, b, c, d, e	c IR	1μ	20% H2	Day	I6		
	Venus	1 km	A6 100 km	10 km	C6 10% D2	See regional maps	1 hr	E7	1 day	E13	a, b, c, d	d	8μ	20% H2	Day	I6		
	Jupiter	1 km	A6 1000 km	10 km	C8 20% D2	See regional maps	1 hr	E7	1 day	E13	a, b, c, d, e, f	e	6 cm	20% H2	Day	I8		
27)* Convective Cells and Turbulence (Regional)	Mars	10 km	A7 1000 km	50 km	C8 100% D1	Equatorial and polar areas	1 hr	E7	10 yr	E16	a, b, c, d	a UV	1000A	20% H2	Day	I6	Desired Temperature Resolution: Same as above	
	Venus	10 km	A7 1000 km	50 km	C8 100% D1	Solar and anti-solar points	1 hr	E7	10 yr	E16	a, b, c, d, e, f	b Visible	1000A	20% H2	Day	I6		
	Jupiter	10 km	A7 10000 km	100 km	C9 100% D1	Cloud belts, red spot	1 hr	E7	10 yr	E16	a, b, c, d, e, f	c IR	8μ	20% H2	Day	I6		
	Venus	1 km	A6 100 km	10 km	C5 20% D2	See regional maps	1 hr	E7	1 day	E13	a, b, c, d	d	8μ	20% H2	Day	I6		
	Jupiter	1 km	A6 1000 km	10 km	C8 20% D2	See regional maps	1 hr	E7	100 hr	E13	a, b, c, d, e, f	e	6 cm	20% H2	Day	I8		
29) Cloud Formation	Mars	1 km	A6 1000 km	10 km	C6 20% D2	Subsolar and polar areas	1 min	E5	10 min	E6	a, b, c, d, e	a UV	1000A	20% H2	Day	I6	Desired Temperature Resolution: Same as above	
	Venus	1 km	A6 1000 km	10 km	C6 20% D2	Equatorial and polar areas	1 min	E5	10 min	E6	a, b, c, d, e, f	b Visible (BW & 5750A color)	1000A	20% H2	Day	I6		
	Jupiter	10 km	A7 10000 km	100 km	C9 20% D2	Belts, red spot, tropics	10 sec	E5	2 min	E8	a, b, c, e, f	c IR	10μ	20% H2	Day	I6		
	Venus	1 km	A6 100 km	10 km	C5 20% D2	See regional maps	1 min	E5	10 min	E6	a, b, c, d, e, f	d	2μ	20% H2	Day	I6		
	Jupiter	10 km	A7 10000 km	100 km	C9 20% D2	See regional maps	10 min	E5	2 min	E8	a, b, c, d, e, f	e	6 bands	20% H2	Day	I8		
30)* Precipitation Rate	Mars	10 km	A7 1000 km	50 km	C8 100% D1	Wave of darkening and poles	1 min	E5	10 min	E6	a	a Radar	3 bands	20% H2	-	-	Desired Temperature Resolution: Same as above	
	Venus	10 km	A7 1000 km	50 km	C8 100% D1	Equator, poles and mountains	1 min	E5	10 min	E6	b	b	3 bands	20% H2	-	-		
	Jupiter	10 km	A7 10000 km	100 km	C9 100% D1	Equatorial and temperate zones	10 μsec	E1	1 min	E8	a	a Passive RF	1 m	20% H2	-	-		
	Venus	10 km	A7 1000 km	50 km	C8 100% D1	See regional maps	10 μsec	E1	1 min	E8	b	b	1 m	20% H2	-	-		
	Jupiter	10 km	A7 10000 km	100 km	C9 100% D1	See regional maps	10 μsec	E1	1 min	E8	a	a	1 m	20% H2	-	-		
31) Thunderstorms (Regional)	Mars	10 km	A7 1000 km	50 km	C8 100% D1	Subsolar point	10 min	E6	10 min	E6	a, b, c, d	a Visible	1000A	20% H2	Day	I6	Desired Temperature Resolution: Same as above	
	Venus	10 km	A7 1000 km	50 km	C8 100% D1	Cloud belts, red spot	10 min	E6	10 min	E6	a, b, c, d	b IR	1μ	20% H2	Day	I6		
	Jupiter	10 km	A7 10000 km	100 km	C9 100% D1	See regional maps	10 min	E6	10 min	E6	a, b, c, d	c	10μ	20% H2	Day	I6		
	Venus	1 km	A6 100 km	10 km	C5 20% D2	See regional maps	10 min	E6	10 min	E6	a, b, c, d	d	6 bands	20% H2	Day	I8		
	Jupiter	1 km	A6 500 km	5 km	C5 20% D2	See regional maps	10 min	E6	10 min	E6	a, b, c, d	e	6 bands	20% H2	Day	I8		
33) Cyclone Formations (Regional)	Mars	10 km	A7 1000 km	50 km	C8 100% D1	Subsolar point	10 min	E6	10 min	E6	a, c	a Visible	1000A	20% H2	Day	I6	Desired Temperature Resolution: Same as above	
	Venus	10 km	A7 1000 km	50 km	C8 100% D1	Cloud belts, red spot	10 min	E6	10 min	E6	b, d	b IR	1μ	20% H2	Day	I6		
	Jupiter	10 km	A7 10000 km	100 km	C9 100% D1	See regional maps	10 min	E6	10 min	E6	b, d, e	c Vis. Color	10μ	20% H2	Day	I6		
	Venus	1 km	A6 100 km	10 km	C6 20% D2	See regional maps	10 min	E6	10 min	E6	e, f	d	3 bands	20% H2	Day	I6		
	Jupiter	1 km	A6 1000 km	10 km	C6 20% D2	See regional maps	10 min	E6	10 min	E6	e, f	e IR	8μ	20% H2	Day	I6		
35) Surface to Atmosphere Transfer	Moon	1 km	A6 500 km	10 km	C6 100% D1	Red spot and tropical regions	1 min	E5	10 min	E5	a, b, c, d	a Visible	1000A	20% H2	Day	I6	Desired Temperature Resolution: Same as above	
	Mars	1 km	A6 500 km	10 km	C6 100% D1	Subsolar point	1 min	E5	10 min	E5	b, d	b IR	1μ	20% H2	Day	I6		
	Venus	1 km	A6 200 km	10 km	C6 100% D1	Cloud belts, red spot	1 min	E5	10 min	E5	b, d, e	c Vis. Color	10μ	20% H2	Day	I6		
	Mars	1 km	A6 200 km	10 km	C6 100% D1	See regional maps	1 min	E5	10 min	E5	e, f	d	3 bands	20% H2	Day	I6		
	Jupiter	10 km	A7 1000 km	100 km	C9 100% D1	See regional maps	1 min	E5	10 min	E5	e, f	e IR	8μ	20% H2	Day	I6		
36) Radio Bursts	Jupiter	100 km	A8 50000 km	500 km	C11 100% D1	Subsatellite pts. of satellites	1 msec	E2	1 min	E8	a	a Passive RF	3 bands	20% H2	-	-	Local Time	
	Mars	10 km	A7 1000 km	50 km	C8 100% D1	Polar regions	1 min	E5	10 min	E5	a, b	a Visible	1000A	20% H2	Night	I7		
	Venus	10 km	A7 1000 km	50 km	C8 100% D1	Polar regions	1 min	E5	10 min	E5	a, b	b Vis. Color	1000A	20% H2	Night	I7		
	Jupiter	10 km	A7 10000 km	100 km	C9 100% D1	Polar regions	1 min	E5	10 min	E5	a, b	a	3 bands	20% H2	Night	I7		
	Venus	20 cm	A2 400 m	100 m	C3 - D5	Wave of darkening and poles	1 sec	E4	10 sec	E5	a, b, c, d	a Visible	1000A	20% H2	Day	I6		
38) Animal Life	Mars	100 m	A5 200 km	1 km	C4 10% D2	Wave of darkening and poles	1 hr	E7	10 yr	E16	a, b, c	a Visible	1000A	20% H2	Day	I6	Desired Temperature Resolution: Same as above	
	Venus	100 m	A5 200 km	1 km	C4 10% D2	Mountains and poles	1 hr	E7	10 yr	E16	d	b Vis. Color	1000A	20% H2	Day	I6		
	Mars	1 km	A6 800 km	10 km	C7 10% D2	Wave of darkening and poles	1 hr	E7	10 yr	E16	a	a Multiband	10 bands	20% H2	Day	I6		
	Venus	1 km	A6 1000 km	10 km	C7 10% D2	Mountains and poles	1 hr	E7	10 yr	E16	b	b	10 bands	20% H2	Day	I6		
	Jupiter	1 km	A6 2000 km	20 km	C8 5% D3	Global	1 hr	E7	10 yr	E16	b	b	10 bands	20% H2	Day	I6		
40) Biochemical Systems	Mars	1 km	A6 800 km	10 km	C7 10% D2	Global	1 hr	E7	10 yr	E16	a	a Multiband	10 bands	20% H2	Day	I6	Desired Temperature Resolution: Same as above	
	Venus	1 km	A6 1000 km	10 km	C7 10% D2	Global	1 hr	E7	10 yr	E16	a	a	10 bands	20% H2	Day	I6		
	Jupiter	1 km	A6 2000 km	20 km	C8 5% D3	Global	1 hr	E7	10 yr	E16	b	b	10 bands	20% H2	Day	I6		
	Moon	1 km	A6 500 km	10 km	C7 10% D2	Global	1 hr	E7	10 yr	E16	a	a	10 bands	20% H2	Day	I6		
	Mars	1 km	A6 800 km	10 km	C7 10% D2	Global	1 hr	E7	10 yr	E16	b	b	10 bands	20% H2	Day	I6		

*Measurements made on this observable may be applicable to engineering objectives.

intention was always to stay on the operating plateaus. The worth curves simply define the end limits of the plateaus and how sharply degradation sets in beyond these limits.

Each of the measurement specifications is discussed in the following subsections.

4.1 Ground Resolution

Ground resolution is used to describe the length, on the surface, of an assumed square element that can be resolved in the final image. It is determined on the basis of the geometrical scale of the feature or event being observed. This specification is that required by the scientist for the image he will have to interpret.

For instance, the ground resolution of five kilometers required for imaging of lunar surface elevations is based on the need for contour maps of the whole moon, on a regional (approximately 100 km) scale. In fact, referring to the worth curve in Figure 4-2 it is found that ground resolutions up to 20 km are acceptable in a worst case. In practice the resolution may not be constant over a whole image, in which case the scientist will need to be aware of its variation from one part of the image to another.

Ground resolution requirements for Mercury, Mars, and Venus are similar for almost all observables, since in each case regional data is needed initially. For the Moon, the regional data is currently available and the need is for higher resolution local information. At the other extreme, Jupiter is hardly known at all; although regional data are required, the required resolution is an order of magnitude larger than that required on the inner planets because of Jupiter's size. In addition, the question of surface measurements for Jupiter is somewhat moot. At present it is not at all clear that there is a definable surface beneath the visible ammonia clouds, rather than just

an atmosphere which gradually becomes thicker and thicker with depth. In some cases the required ground resolution would appear to be completely out of keeping with the reality of orbital measurements (e.g., 20 cm or less for imaging of animal life). It should be made quite clear that this is the scientific requirement if animal life is to be detected by imaging. Whether or not it is reasonable ever to set up an experiment to meet this imaging requirement is left to a later phase of the study where both orbital constraints and support requirements are considered. The specification and its associated worth curve simply implies that it is not worth attempting to fulfill this observable unless a resolution of 20 cm or less can be achieved.

The ground resolution used here refers to the horizontal surface. In those cases where a vertical resolution requirement exists, such as for Surface Elevations, the vertical resolution is specified in the comments column of Table 4-1. The associated worth curves are given in Figure 4-11.

4.2 Image Size

This specification identifies the length, on the planetary surface, of an assumed square image which will be required for scientific interpretation. There is no implication as to the image format of the image itself. The required size of the final image is based only on the scale of the feature or event being observed and the need to correlate features or events over regions of the planet. Clearly there is some relationship between the required resolution and the required image size. In general, for ease in interpretation, an image should contain at least 40,000 resolution elements (200 x 200).

The image size requirements are very similar for Mars, Venus, and Mercury, because of the similar scale of the information required. In general terms, the lunar requirements

are an order of magnitude smaller and the Jupiter requirements are an order of magnitude larger. The worth curves indicate that the major scientific constraint is on the smallness of the image. In no case has an upper limit been identified for an acceptable image. Larger images simply would require larger displays to maintain their resolution requirements, but this is a physical rather than a scientific problem.

4.3 Positional Accuracy

This specifies the accuracy with which it is necessary to know the location on the planet of the feature or event being investigated. It is based, in some cases, on the need to know which part of the planet is being imaged, but in other cases, it reflects a need to image a pre-selected feature because of its particular properties. The accuracy requirements are defined so that the impact of the measurement on the support subsystems (attitude control, pointing) can be determined later in the study.

The positional accuracy requirements are most stringent for the detailed investigations of the Moon and most relaxed for the global measurements of Jupiter. The worth curves are shown in Figure 4-4. The high accuracy end of the plateau continue right up to the axis. Although such high accuracy may be unnecessary, it certainly is not detrimental to the scientific worth of the image. On the other hand, it would seem pointless to demand, on scientific grounds, a pointing accuracy which exceeds the ground resolution of the image. As an approximate guideline, an accuracy of 10 times the resolution is found to be adequate. The worth curves reflect this criteria at the low accuracy end of the plateau.

4.4 Planetary Coverage

Planetary coverage is used to describe the total percentage area of the planet which should be observed during

the course of the measurement. It is based on the need either to map the planet or to obtain average data on its properties, as discussed in the observable definition of Volume II.

However, in some cases where specific features or events are being observed, the coverage is related directly to their probable distribution over the planet. Mapping requirements are defined in terms of regional, local, and detailed scales. The coverage requirements are related to these scales, i.e., total coverage regionally, 10% coverage locally, and less than 1% coverage at a detailed scale. The worth curves express, at the low end of the plateau any definable limits to acceptable coverage. At the upper end however, 100% is the only limit to worthwhile coverage. From a scientific viewpoint a measurement cannot be degraded because it gives information over a larger area than is absolutely necessary.

4.5 Planetary Distribution

The distribution of a planetary coverage specification is closely coupled to the percentage of planetary coverage. The distribution is based on the anticipated distribution of observables and also the geometrical effects which may occur as a result of seasonal processes. In many instances however, the distribution cannot be defined at the present time. The distribution requirements for local and detailed measurements can only be identified after regional maps have been scientifically studied and interpreted. While Earth experience may be adequate to estimate the percentage of high resolution coverage, it is unlikely to identify its distribution. Thus, fairly general descriptives are used to define the distribution e.g., polar regions, cloud belts, etc., and no worth curves are presented. In the case of regional scale observables at Mars, some indication of planetary distributions can be obtained from Earth-based observation. Thus Figure 4-12 shows on a

map of Mars, the distribution of primary and secondary areas of interest in connection with the wave of darkening.

4.6 Acquisition Times and Repetition Rates

Time constraints may be required for observables which change with time. Four types of time constraints are considered.

The image acquisition time is similar in concept to exposure time, but is based on the rate of change of the observable itself. It is a time short enough to prevent changes in the feature from causing a blur in the image. No allowance is made here for such things as image motion due to relative spacecraft velocity.

Coverage acquisition time means the time which can be allowed for fulfilling the complete coverage requirement. It is a time considerably shorter than that in which major changes can take place over all the areas of interest on the planet. It ensures a set of images providing full coverage of the planet in the same state. The coverage acquisition time is often related to seasonal effects, but it may also be related to diurnal effects, as is the case with global cloud coverage.

The repetition rate is required to provide an analog to time lapse photography, and allows changes on the planet to be measured. Again a distinction is made between image repetition rate and the repetition rate for total coverage. Image repetition rate is specified to allow changes in an observable to be identified and is based directly on the rate of change of a single feature or event being investigated. The coverage repetition rate is included to allow large scale features or events to be monitored with respect to time. These are usually seasonal effects and occur over planetary areas which are large compared to an image.

For many of the measurements of surface properties, there are no time constraints specified; significant observable

changes are not anticipated in periods of 10 or 20 years. Some active surface processes are however included, in the sense that the wave of darkening should be observed on Mars, and possibly active volcanism on Venus. Otherwise the time constraints apply mostly to atmospheric events, ranging from the global cloud pattern to the emission of decameter radio bursts from Jupiter.

The worth curves for acquisition time and repetition rate are shown in Figure 4-6. In general, there is no limit on how quickly the image or the coverage requirements can be met. However, upper limits on both times are specified.

4.7 Sensor Types

The measurement specifications discussed thus far deal with the geometrical and temporal measurement requirements. It is now necessary to identify the spectral properties of the required images. For each observable (at each target), the spectral regions in which the observable radiates or reflects, are identified. In general, there are multiple regions which are of scientific interest, and a cross reference system has been introduced in Table 4-1. Following each of the repetition rate specifications is a series of sensor references. These refer to all the remaining specifications as indicated in the adjacent "sensor type" column. The identification of sensor types at this point in the specifications would appear to be premature, but in fact it has been done quite purposefully. Once the spectral regions have been identified it is convenient to classify them by the standard nomenclature used to identify the gamma ray, X-ray, UV, visible, IR, microwave (passive), radar (active microwave), and radio regions of the spectrum. This not only makes the spectral regions more readily recognizable, but provides an advantage for a later phase of the study. Each of the above regions are, for fundamental physics reasons, normally detected by quite different sensing elements, which are part of quite different sensing systems.

Thus, indirectly, and purely on the basis of scientific requirements, the sensor types for which scaling laws will have to be generated later, have been identified. Included in the designations are an indication of whether stereoscopic or monoscopic images could be useful. Multi-band as a sensor type is used when the spectral region of scientific interest falls into more than one of the above designations.

As mentioned above, more than one sensor type is applicable to each of the observables. For instance, surface elevations can be measured by using:

- a. Shadows in visible images,
- b. Stereo-visible images,
- c. Radar-altimetry or,
- d. Stereo-radar images.

In practice not all of these would be used. However, the selection is one that can be made only after the orbit and subsystem requirements have been clearly identified. Thus specifications for all possibilities are carried through, and no selections have been made at this point in the analysis.

4.8 Spectral Regions

The approximate center wavelength of the spectral region of interest is specified. It is determined by considering both the phenomenological radiation pattern of the observable, and the absorption path between the feature and the sensor. Examples of the latter constraints are the 5000 Å cutoff by the blue haze on Mars, and the requirements for very long wavelengths at Jupiter (to penetrate the very dense atmosphere). The worth curves are shown in Figure 4-7. They reflect an uncertainty about the spectral regions from which useful interpretation can be made. This is because Earth experience of planetary phenomenon is strongly conditioned by

the windows in the Earth's atmosphere to visible, IR, and microwave radiation. Thus, in many cases, the plateau shows where scientists are accustomed to operating and continues into somewhat indeterminate regions by extrapolation.

4.9 Spectral Bandwidth

This is used to define the width of the band, in which all the spectral information should be contained. It is derived in conjunction with the spectral region as discussed in the observables data sheets. However, for the multi-band requirements, it identifies how many equal bands into which the quoted spectral region should be divided. The multi-band worth curves then show the scientific worth of the measurements as a function of the number of bands.

In general, the worth curves show that broad-band low spectral resolution is all that is required in all cases. In fact, this is typical of conventional imaging experiments as opposed to , say, spectrophotometric measurements.

4.10 Overlap

This identifies the amount of geometrical redundancy which is required between adjacent images. It is based on the general need to locate features of scientific interest on a scale larger than that of a single image. An image overlap of about 20% is generally adequate for this purpose. In addition, there is a need for overlap between the images of a stereoscopic pair, so that adequate interpretation can be achieved. This should be a minimum of 60%. The 20% overlap will then apply between adjacent stereoscopic pairs.

The worth curves are shown in Figure 4-9 and give only a lower limit to the acceptable overlap. From a purely scientific standpoint, there is no degradation as the overlap increased, even up to nearly 100% provided the other specifications of coverage, etc., are met. It may indeed be wasteful

to provide unnecessarily high overlap, but such judgments can only be made with a knowledge of the subsystem support requirements, which are defined in a later phase of the study.

4.11 Sun Elevation

The specification identifies the nominal height of the Sun above the horizon when measurements are being made. It is based on one of three considerations: shadowing, excitation, or illumination. Where shadows are to be used as part of the scientific interpretation process, it is necessary not only to know the Sun elevation angle, but for it to be quite low (approximately 20°). For excitation (surface or atmospheric), it is important to have a large proportion of the imaged area exposed to solar radiation, so that the maximum effect can be observed, and the maximum secondary radiation obtained. The angle which reduces shadows to an acceptably low proportion will depend on the roughness and the morphology of the surface. Finally for illumination, the major constraint is for stereoscopic pairs of images where minimum shadows are required. There are also conditions where the maximum illumination is required simply to detect a weak effect. Conversely sometimes the absence of solar illumination is required, since it would obscure an emission of interest.

The worth curves are shown in Figure 4-10. They include defined plateaus for shadowing, lower limits only for solar excitation and illumination, and, in some cases, the identification only between night and day.

4.12 Supporting Measurements

Many of the images which meet the specifications will require additional information, if adequate interpretation is to be possible. In particular, for many experiments it will be necessary to know the spacecraft altitude at which each was obtained as well as the local time.

4.13 Distribution of Measurements

Table 4-1 has suggested a grand total of 401 imaging experiments. These are distributed as follows:

<u>planet</u>	<u>no. of imaging experiments</u>
Moon	59
Mercury	79
Mars	129
Venus	77
Jupiter	57

Mars offers the greatest opportunity for orbital imaging experiments because Earth-based observations are inadequate, no significant amount of imagery has been obtained previously, and the transparent atmosphere facilitates visual imaging of the surface. Furthermore, Mars appears to have the least uncomfortable environment and more extraterrestrial life detection imaging experiments are suggested for Mars than for the other planets. Although the atmosphere is thin, atmospheric phenomena have been observed on Mars and nearly as many atmospheric experiments have been suggested for Mars as for Venus and Jupiter.

Figure 4-13 shows that visual imagery is more useful at Mars than imagery in any other spectral region. The histogram gives the number of experiments listed in Table 4-1 for each spectral region. No distinction is made between regional, local, and detailed scale experiments. The legend along the abscissa is self-explanatory, except that MB signifies multiband imaging experiments. More multiband experiments are suggested at Mars than at any other planet for the detection of extraterrestrial life, mapping of thermal anomalies, and study of atmospheric phenomena.

Orbital imagery at Mercury and Venus is less useful than at Mars, in the sense that there are less phenomena to observe or fewer ways to observe them. Mercury has no

significant atmosphere, hence no experiments contributing to understanding of Mercury's atmosphere have been suggested. Venus has a thick cloud cover which shields the surface from visual observation. Although it has been suggested (Keene 1968) that Venusian surface features might be observed visually from orbital altitudes through breaks in the cloud cover, no measurement definitions have been based upon this speculation. The lack of atmosphere results in only 33 visual imaging experiments at Mercury, as shown in Figure 4-13, while the absence of visual surface imaging results in only 8 visual experiments at Venus. Radar imaging of the surface leads to about 25 experiments at Venus, at Mars, and at Mercury.

Only 59 imaging experiments have been defined for study of the Moon. This is because the Moon has no atmosphere to observe and sufficient regional scale imagery of the surface has already been obtained. Only 57 imaging experiments have been suggested for Jupiter. As with Venus, the heavy cloud cover is presumed to prohibit visual imaging of the surface from orbital altitudes. In addition, no local and detailed radar imagery of the surface has been proposed, since a surface may not even exist.

The measurement specifications presented here represent a major contribution to advanced mission planning. They bridge the large gap between the scientific statements of the goals and objectives of space exploration and the detailed type of information that a mission analyst needs, if

he is going to be able to fulfill the goals and objectives as part of an exploration plan. It is absolutely imperative that it is the scientist who defines the measurement specifications, and that they provide a description of those measurements the scientist needs to make, rather than what he thinks he could make. It is equally imperative that they be expressed in terms that the mission analyst can understand. At the same time, they must not be influenced by the practical constraints of the mission analysis. In the process of defining the scientific measurement requirements, it became clear that, in most cases, there was no unambiguous definition of the scientific requirements. Rather a range is acceptable and there is no clear way of narrowing down the range, on purely scientific grounds. The worth curves represent a valuable step insolving this problem. They provide an effective way of expressing tolerances on the nominal specifications, again from a purely scientific standpoint. In all the specifications, there is only one which has been left in an indeterminate state. It is impossible to foresee clearly the planetary distribution required for imagery of observables on a local and detailed scale. Only when regional scale information is available, can the preferred distribution of imagery for local and detailed scale studies be determined.

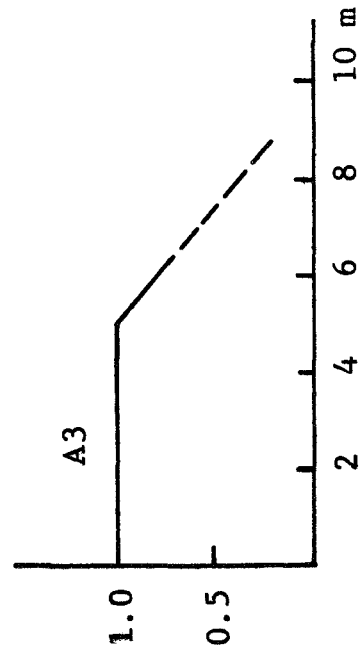
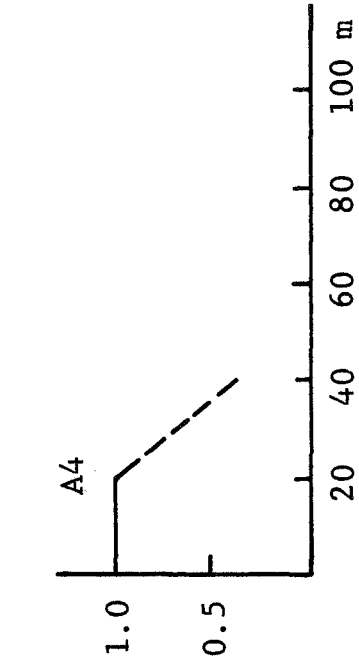
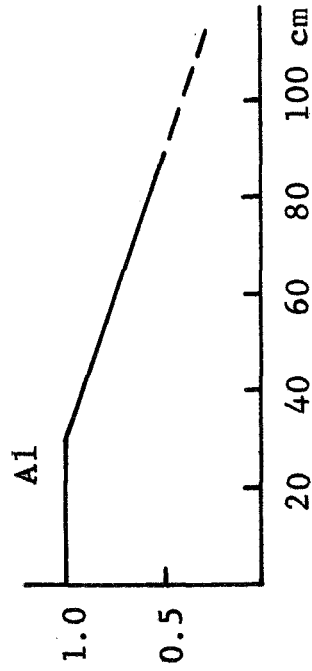
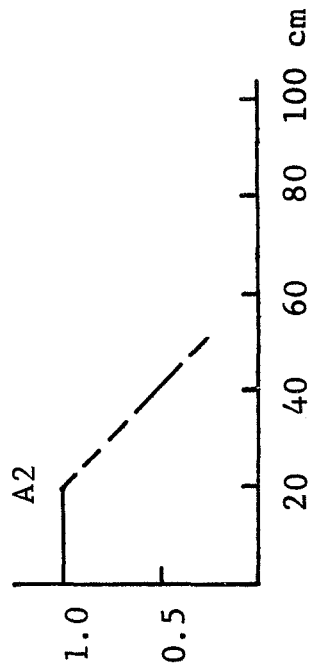


Figure 4.2 - A1 to A4: GROUND RESOLUTION WORTH CURVES
(Relative Worth vs. Ground Resolution)

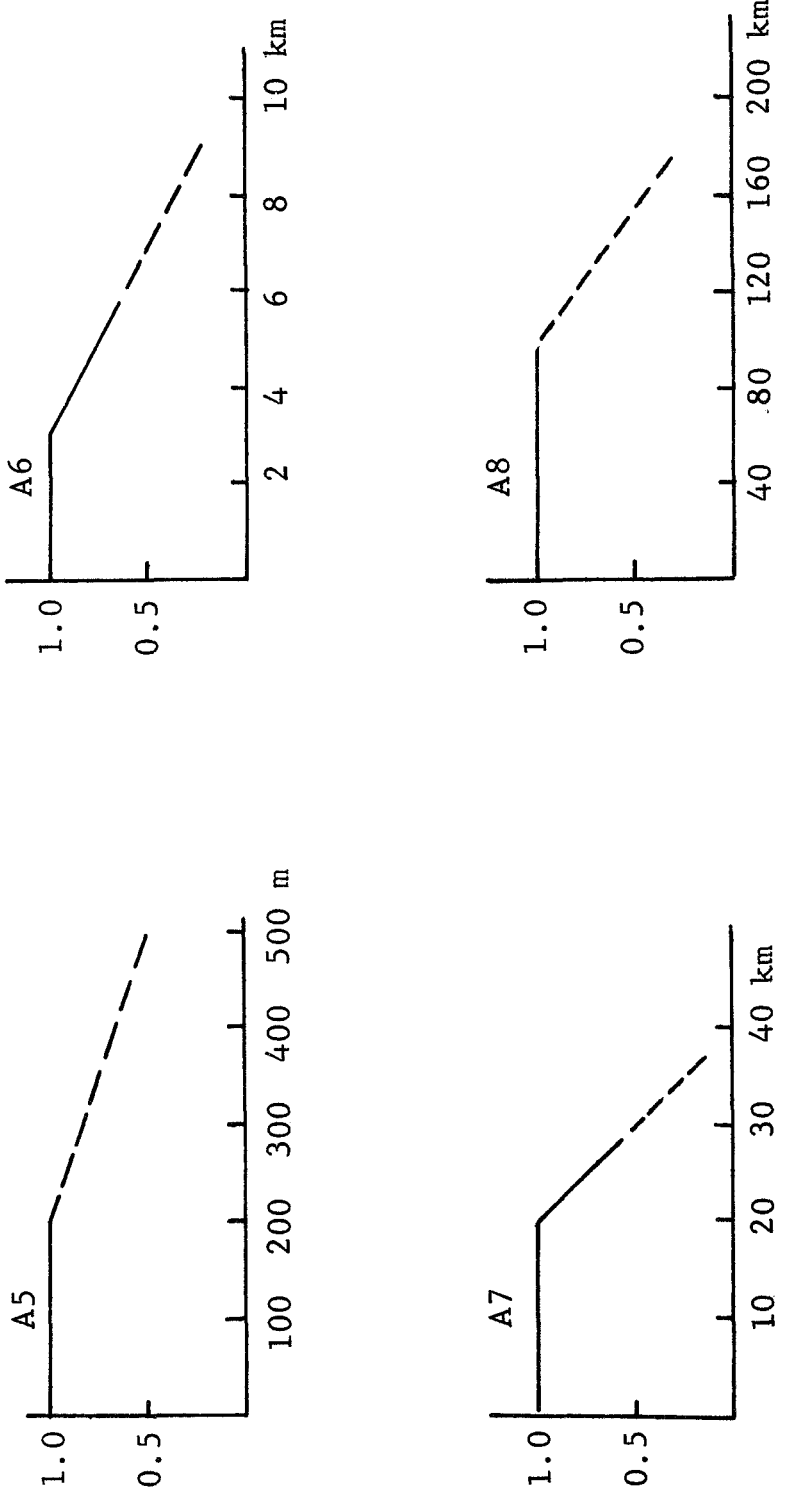


Figure 4.2 - A5 to A8: GROUND RESOLUTION WORTH CURVES
(Relative Worth vs. Ground Resolution)

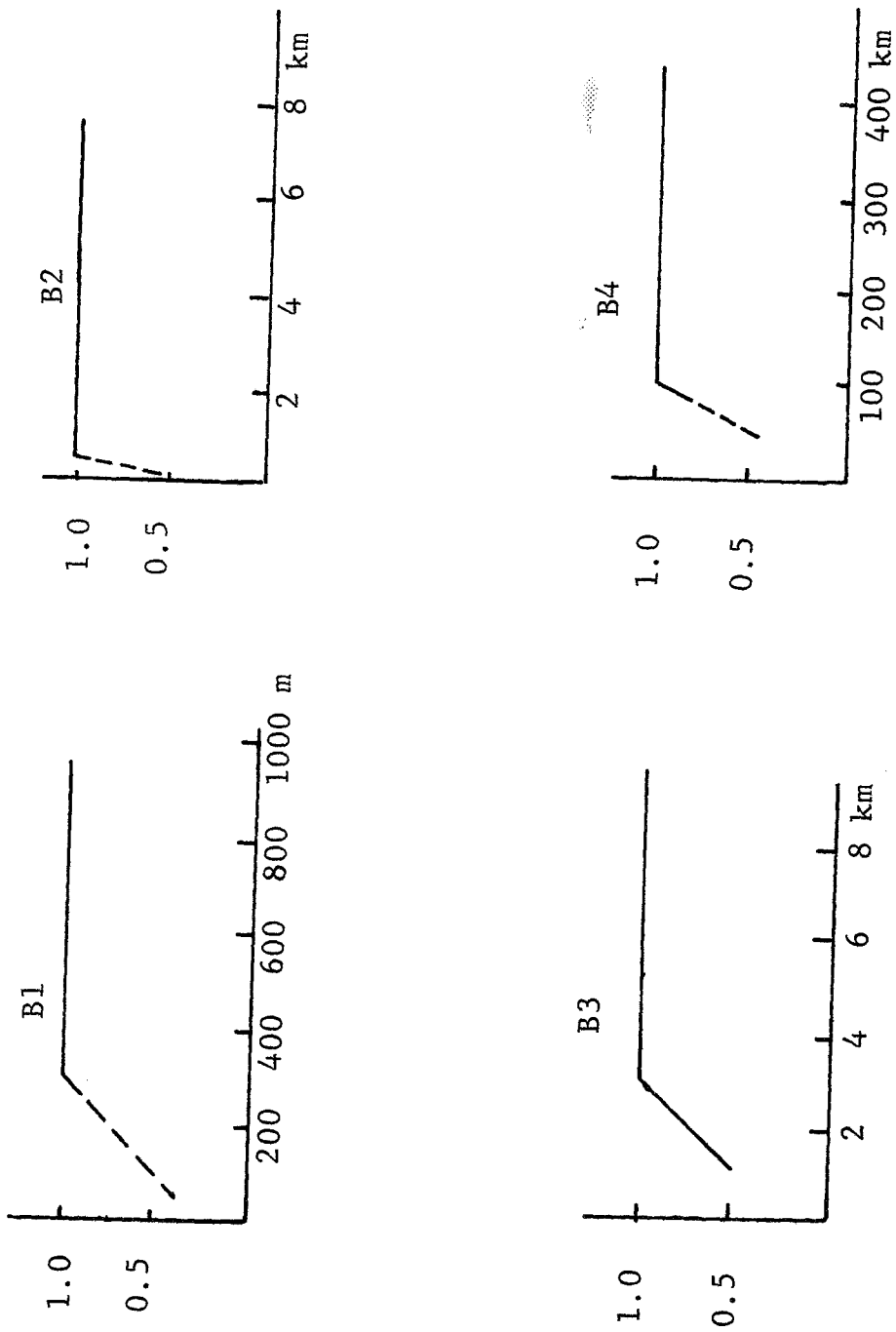


Figure 4.3 - B1 to B4: IMAGE SIZE WORTH CURVES
(Relative Worth vs. Image Size)

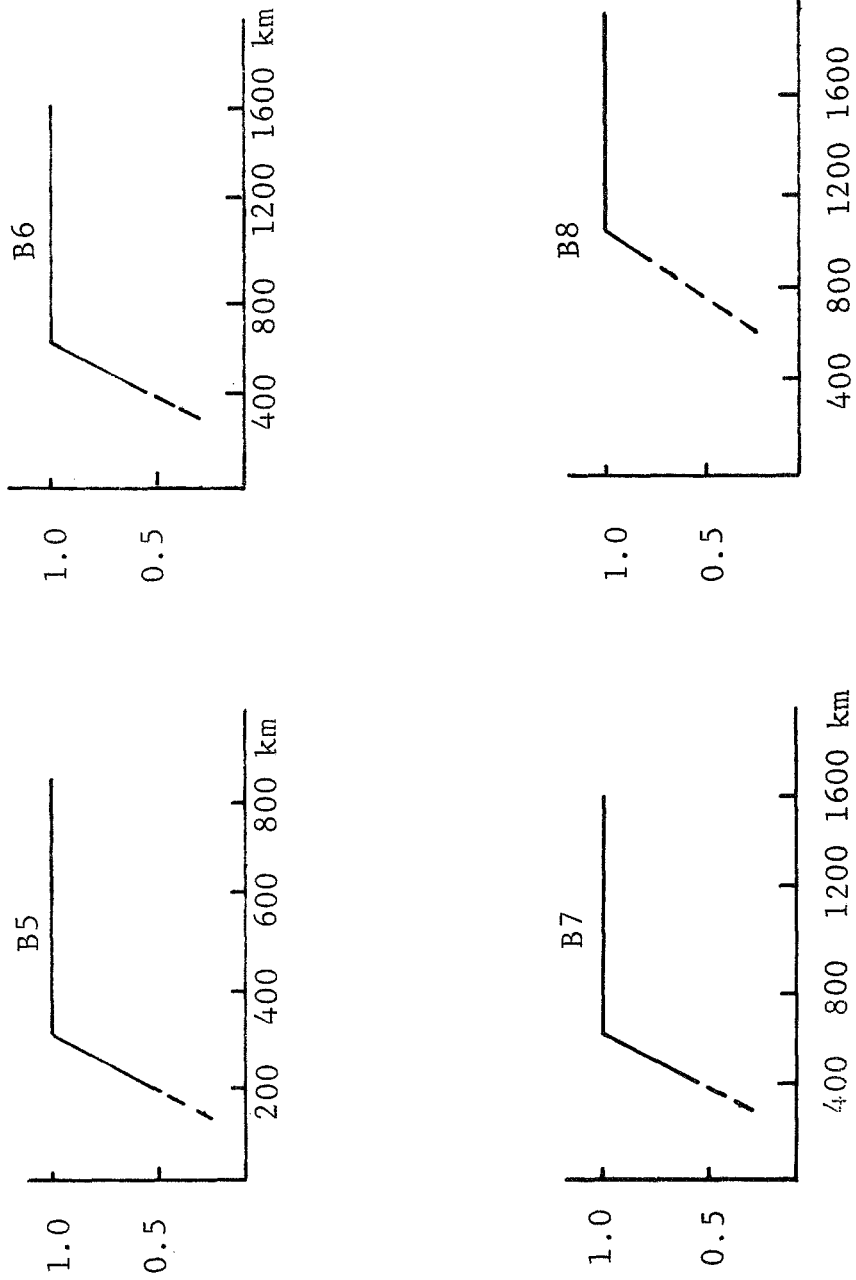


Figure 4.3 - B5 to B8: IMAGE SIZE WORTH CURVES
(Relative Worth vs. Image Size)

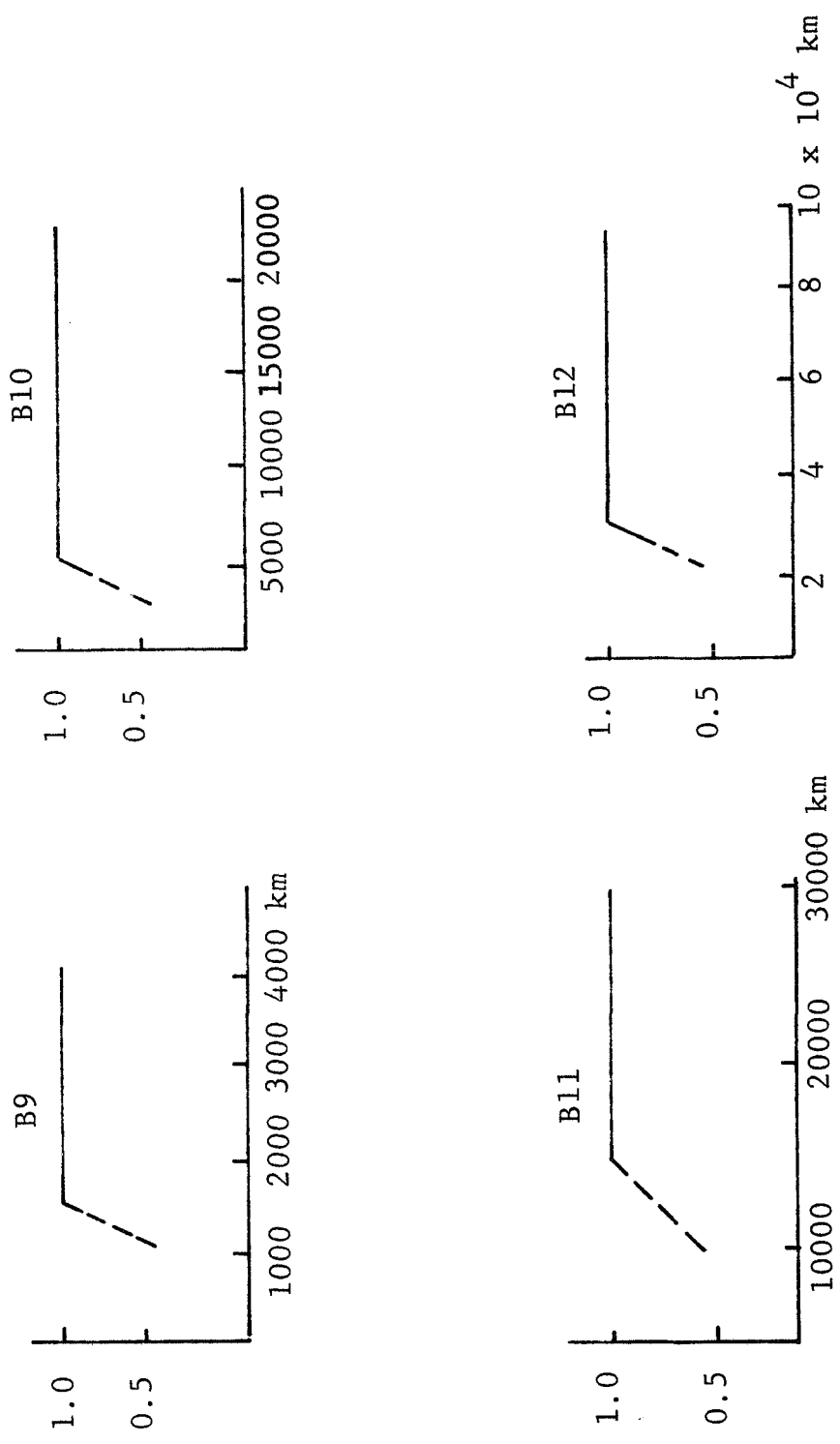


Figure 4.3 - B9 to B12: IMAGE SIZE WORTH CURVES
(Relative Worth vs. Image Size)

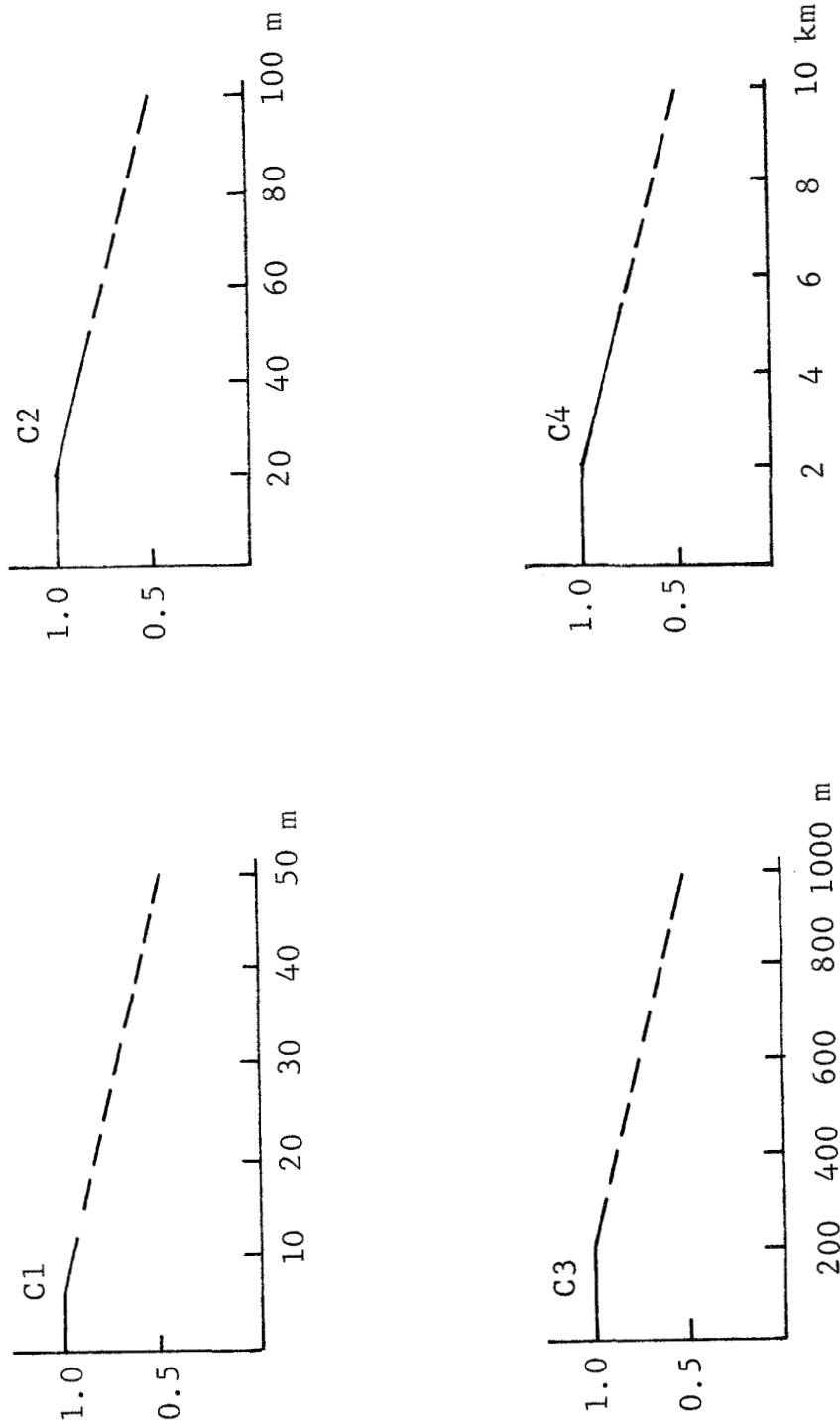


Figure 4.4 - C1 to C4: POSITIONAL ACCURACY WORTH CURVES
(Relative Worth vs. Positional Accuracy)

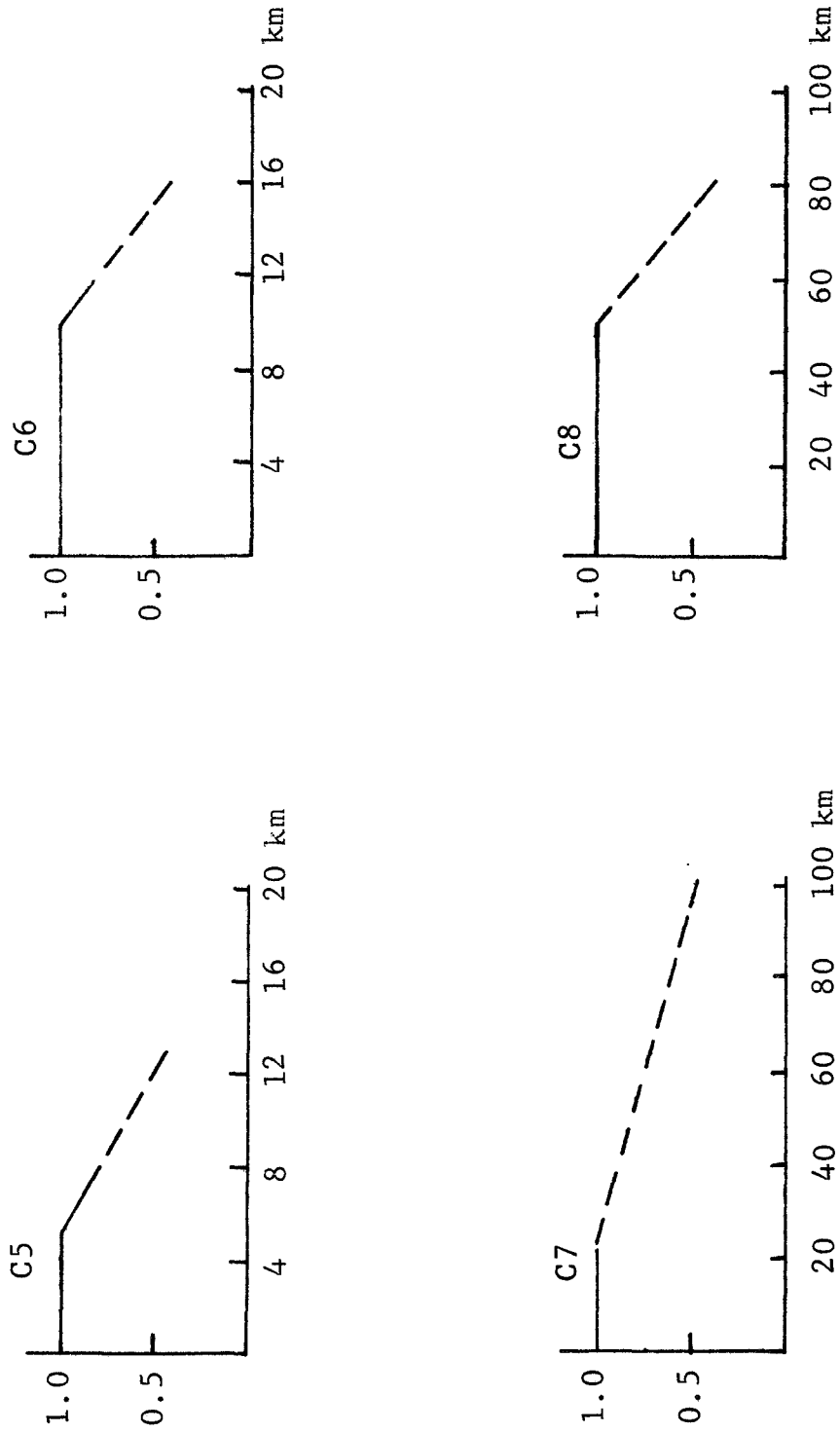


Figure 4.4 - C5 to C8: POSITIONAL ACCURACY WORTH CURVES
(Relative Worth vs. Positional Accuracy)

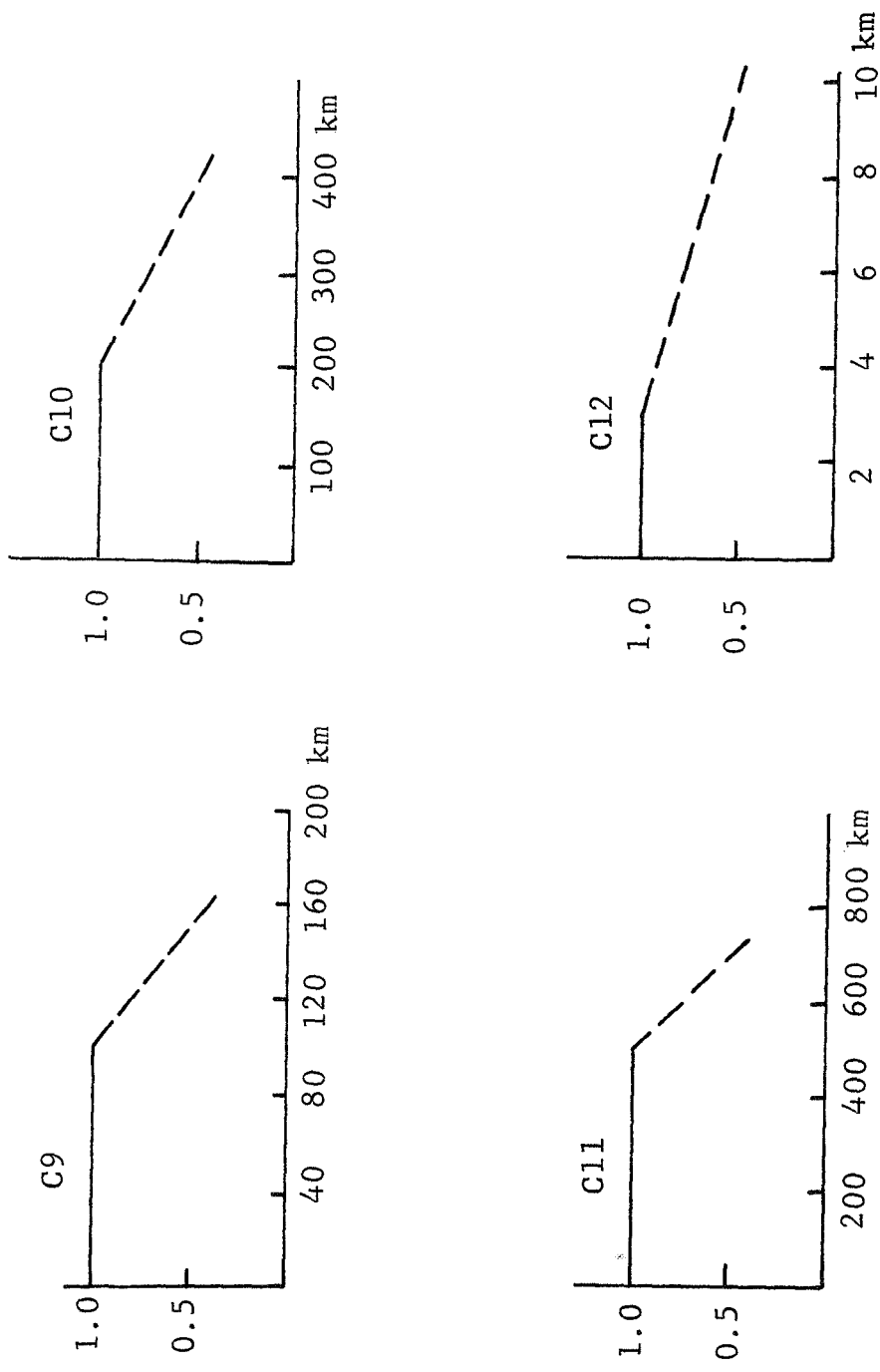


Figure 4.4 - C9 to C12: POSITIONAL ACCURACY WORTH CURVES
(Relative Worth vs. Positional Accuracy)

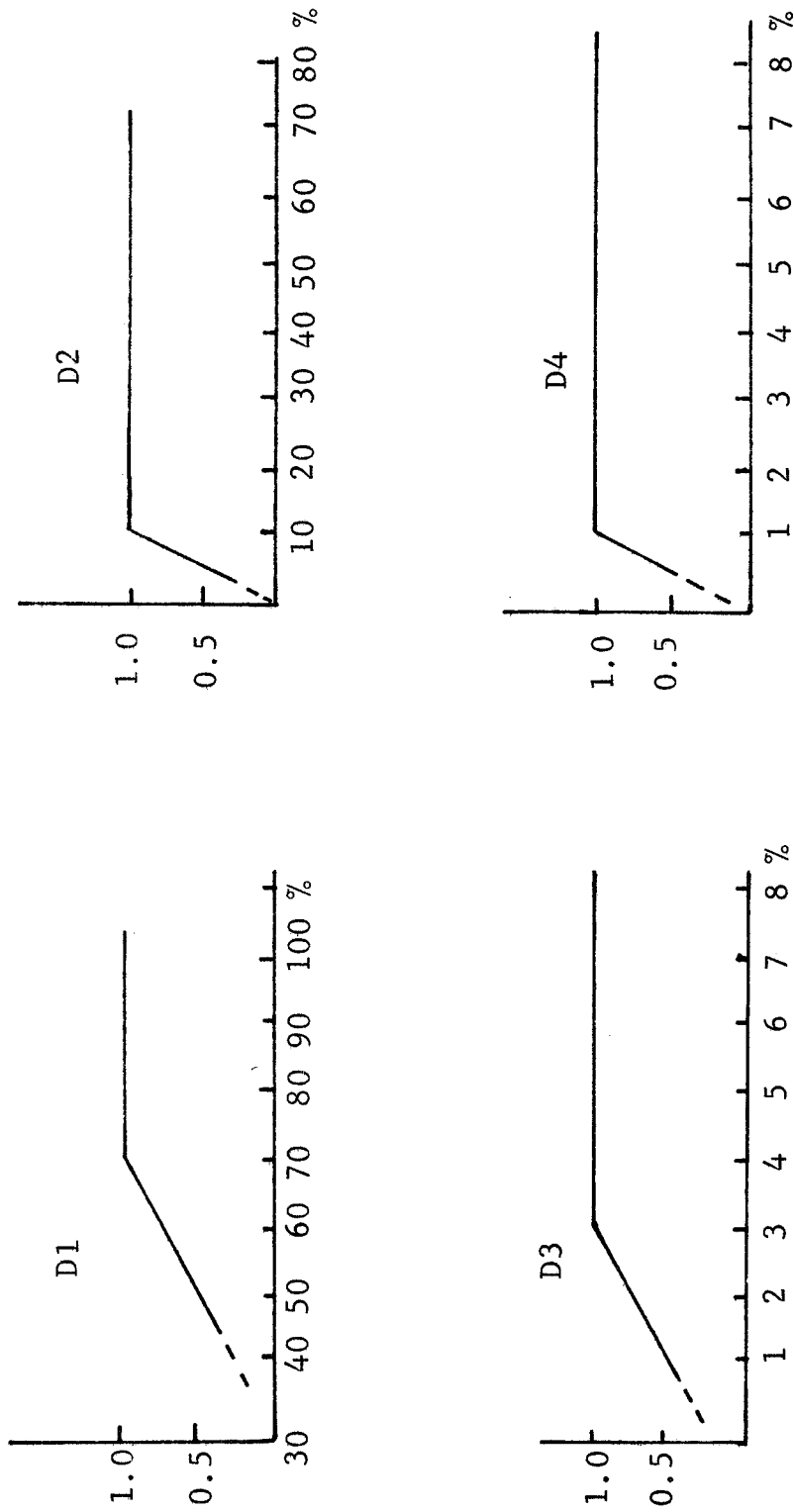


Figure 4.5 - D1 to D4: PLANETARY COVERAGE WORTH CURVES
(Relative Worth vs. Planetary Coverage)

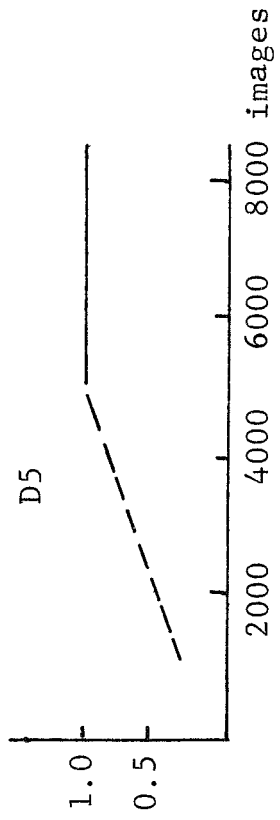


Figure 4.5 - D5: PLANETARY COVERAGE WORTH CURVES
(Relative Worth vs. Planetary Coverage)

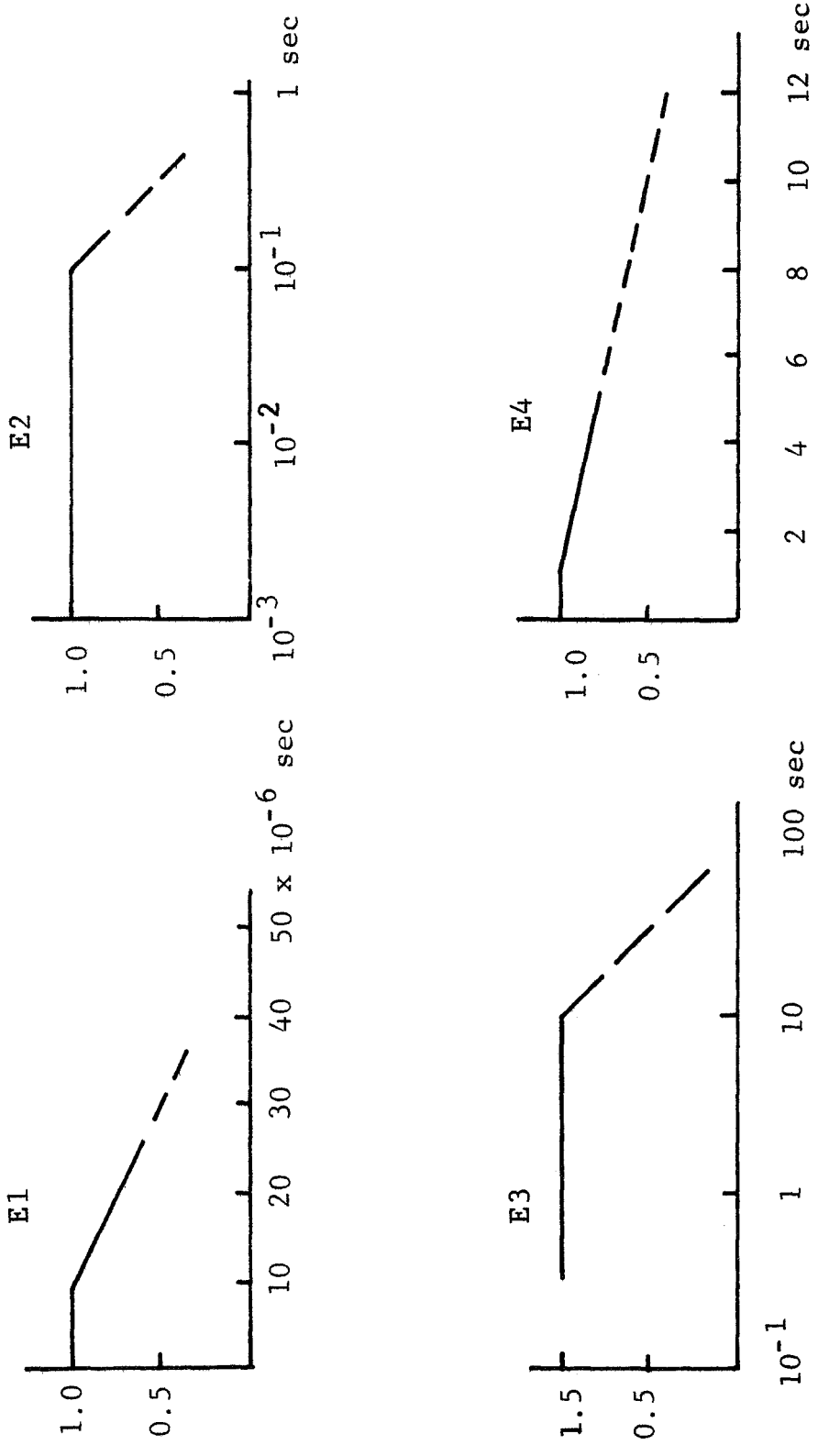


Figure 4.6 - E1 to E4: TIME WORTH CURVES
(Relative Worth vs. Time)

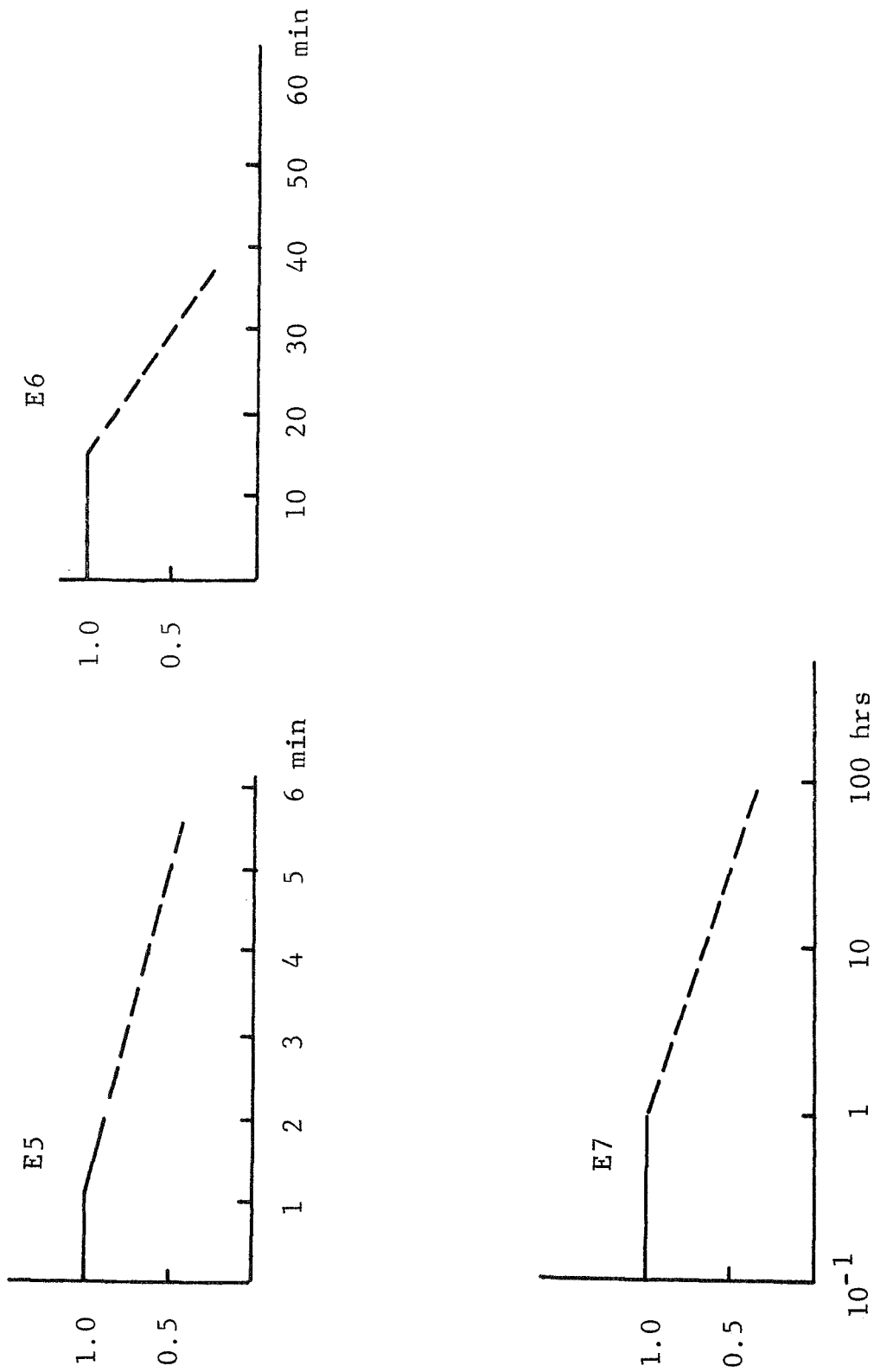


Figure 4.6 - E5 to E7: TIME WORTH CURVES
(Relative Worth vs. Time)

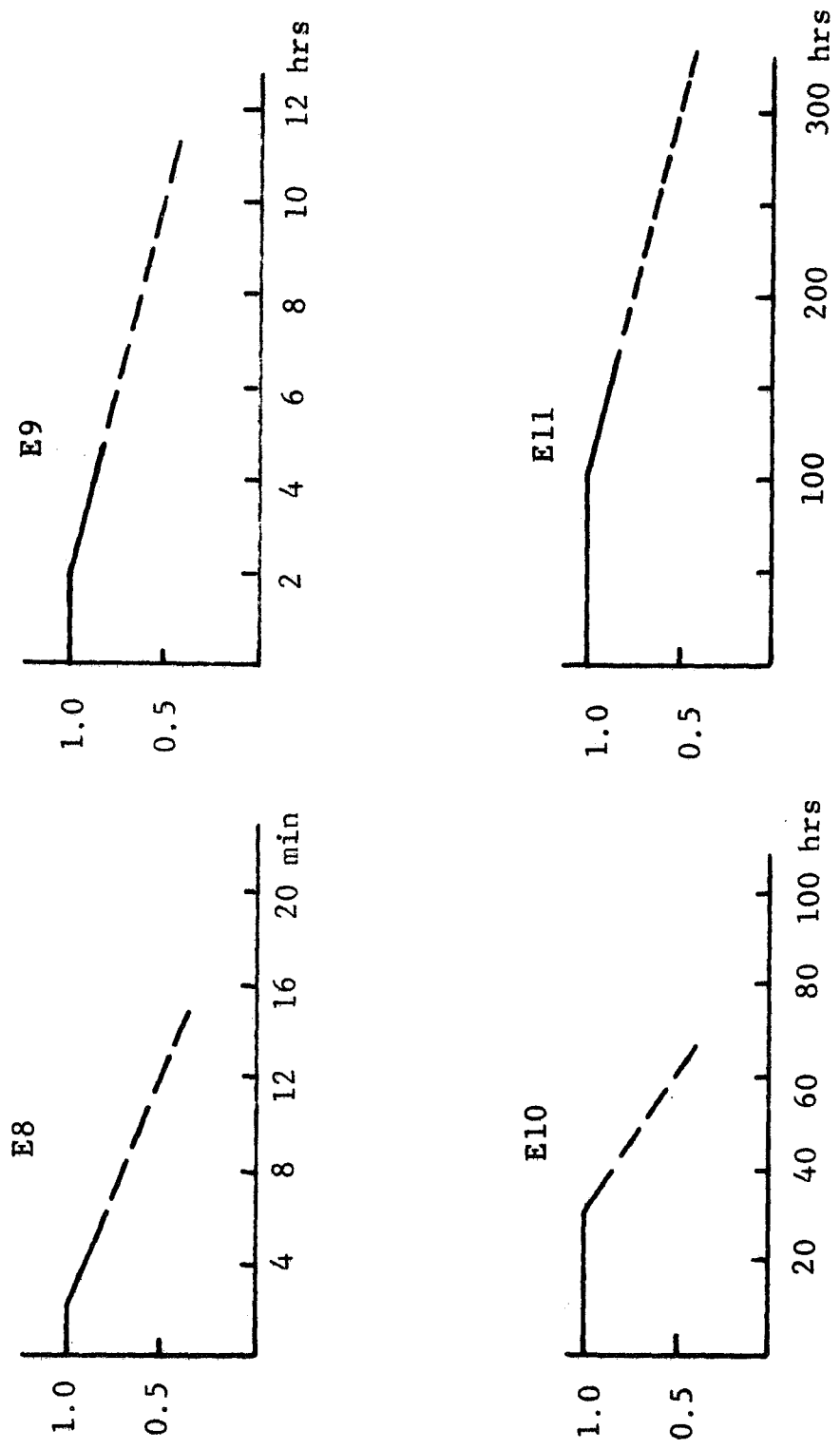


Figure 4.6 - E8 to E11: TIME WORTH CURVES
(Relative Worth vs. Time)

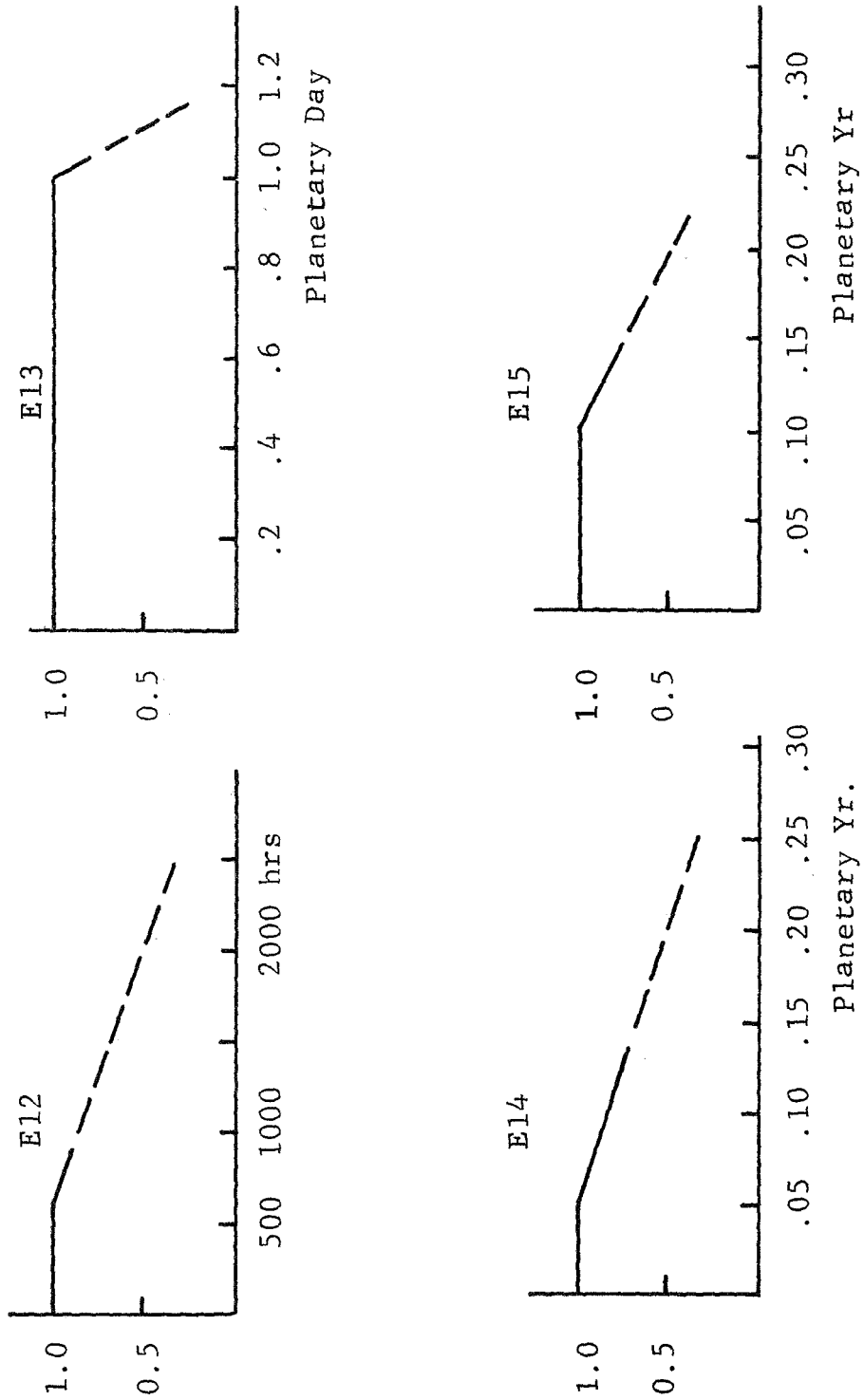


Figure 4.6 - E12 to E15: TIME WORTH CURVES
(Relative Worth vs. Time)

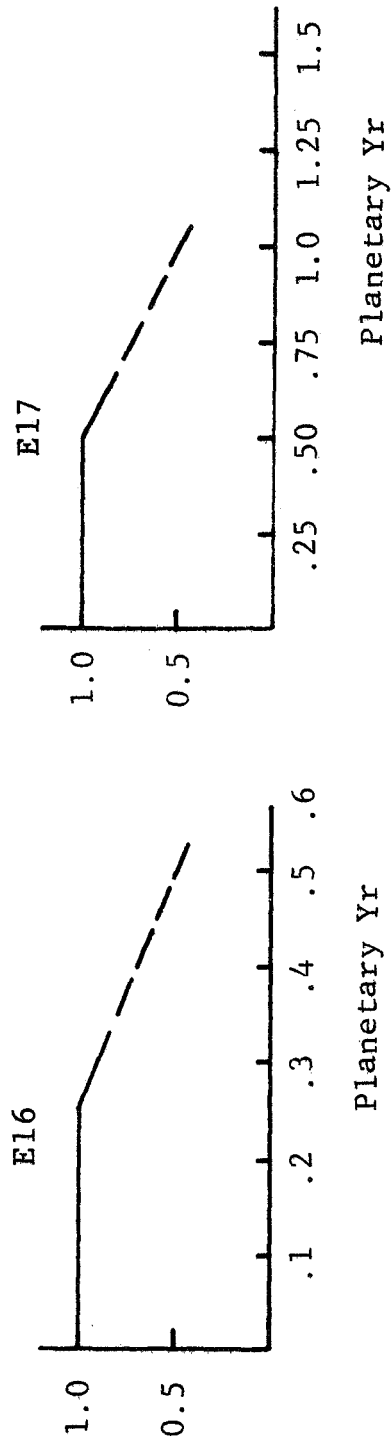


Figure 4.6 - E16 to E17: TIME WORTH CURVES
(Relative Worth vs. Time)

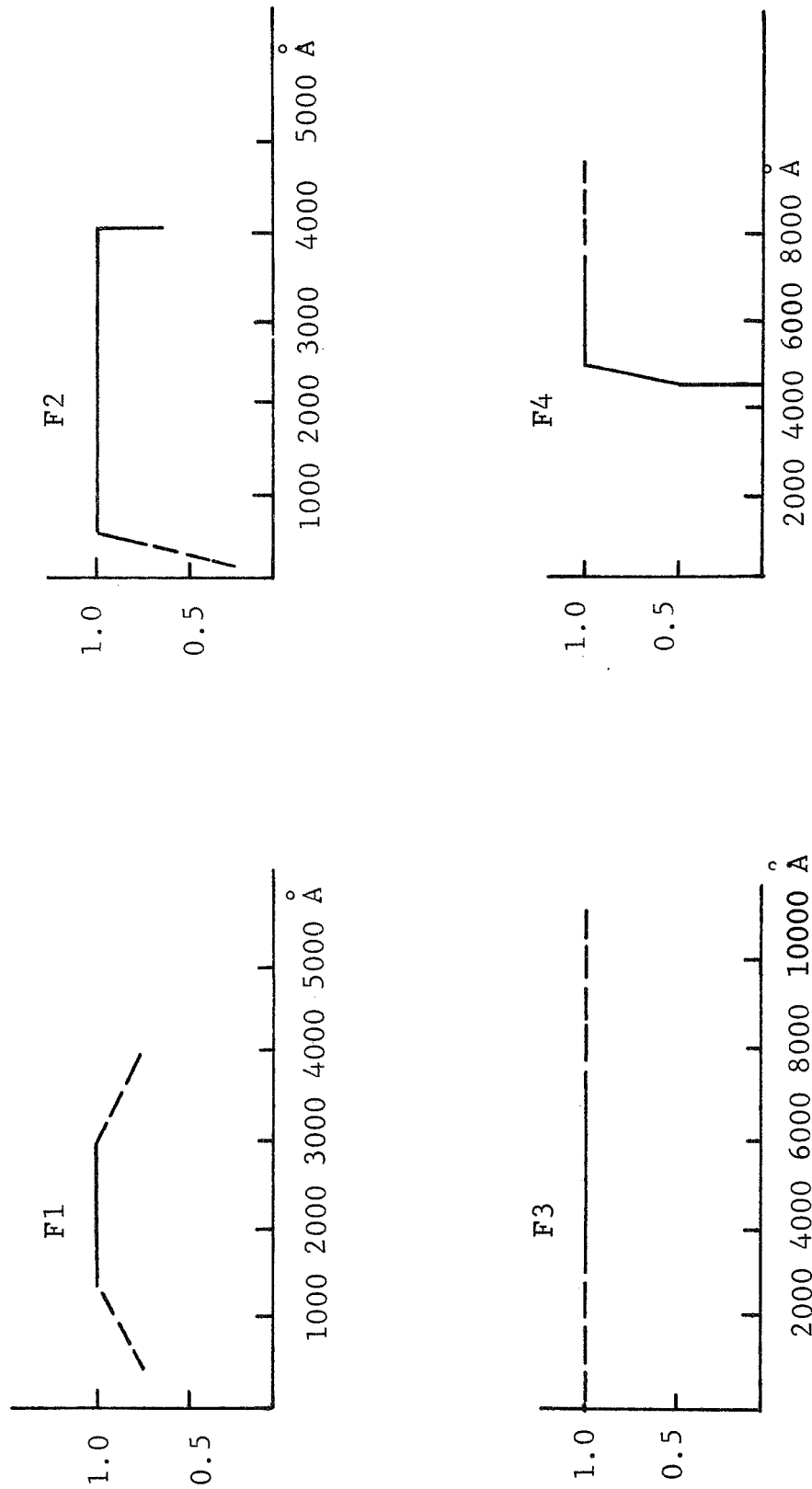


Figure 4.7 - F1 to F4: SPECTRAL REGION WORTH CURVES
(Relative Worth vs. Spectral Region)

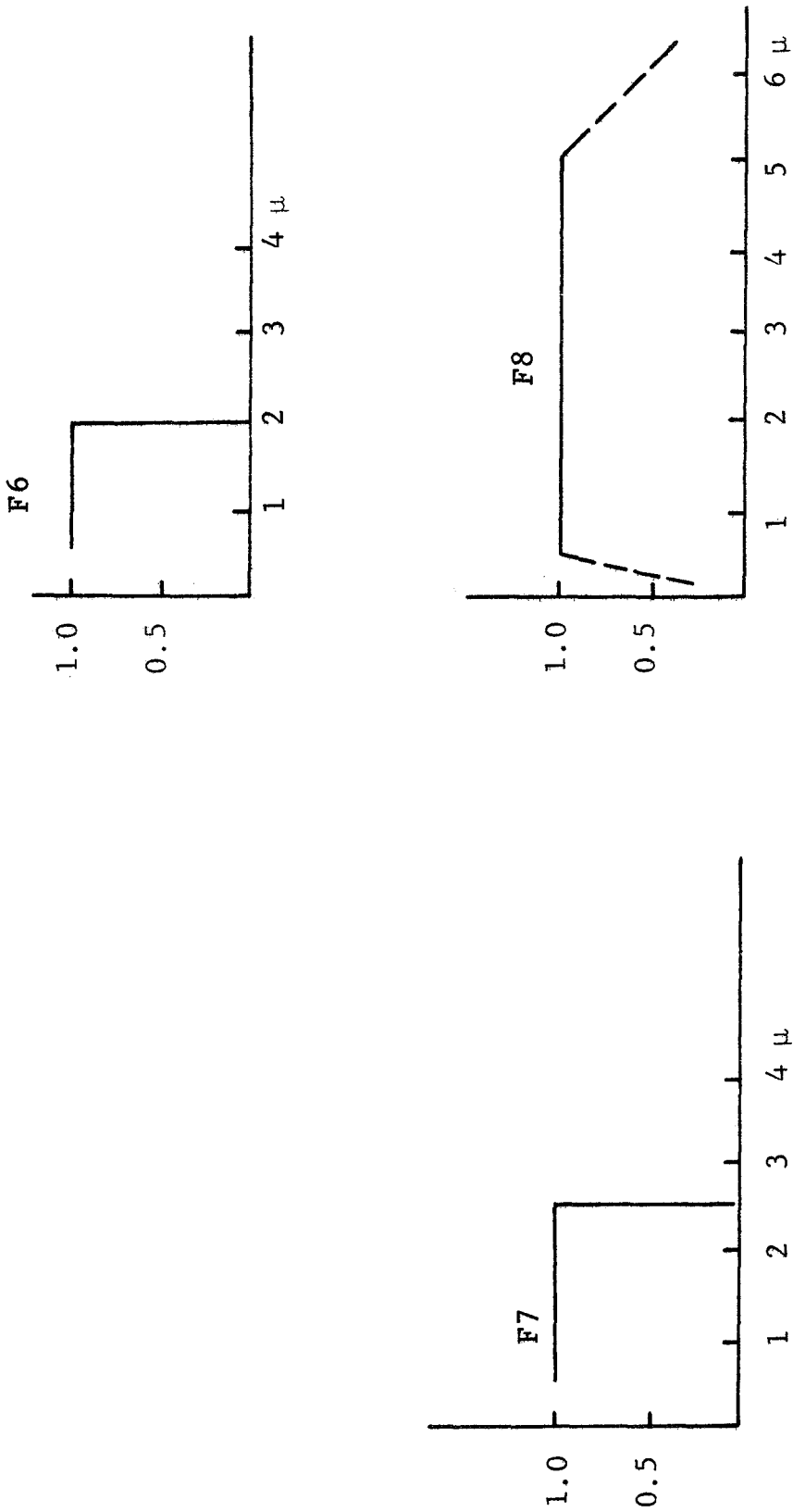


Figure 4.7 - F6 to F8: SPECTRAL REGION WORTH CURVES
(Relative Worth vs. Spectral Region)

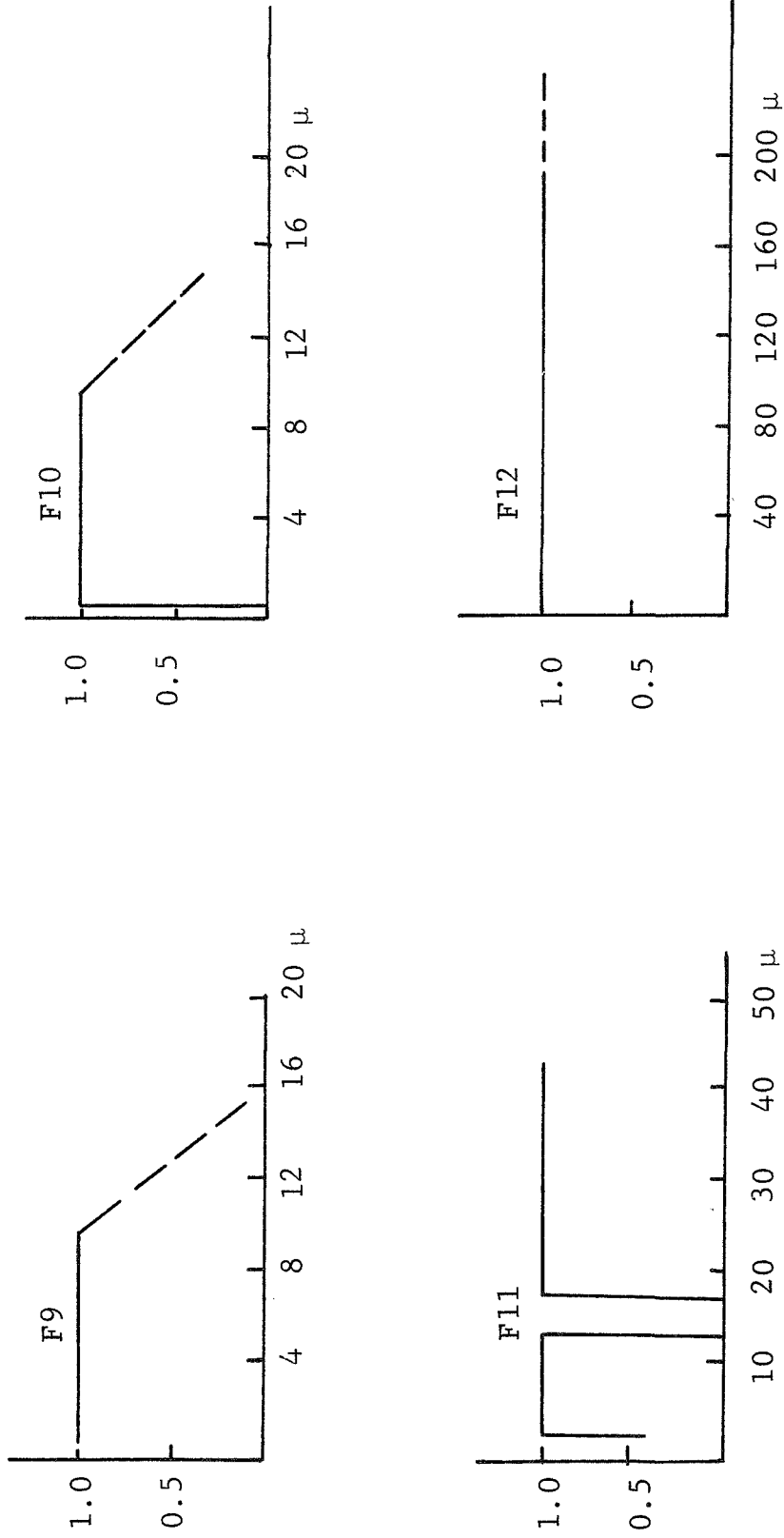


Figure 4.7 - F9 to F12: SPECTRAL REGION WORTH CURVES
 Relative Worth vs. Spectral Region)

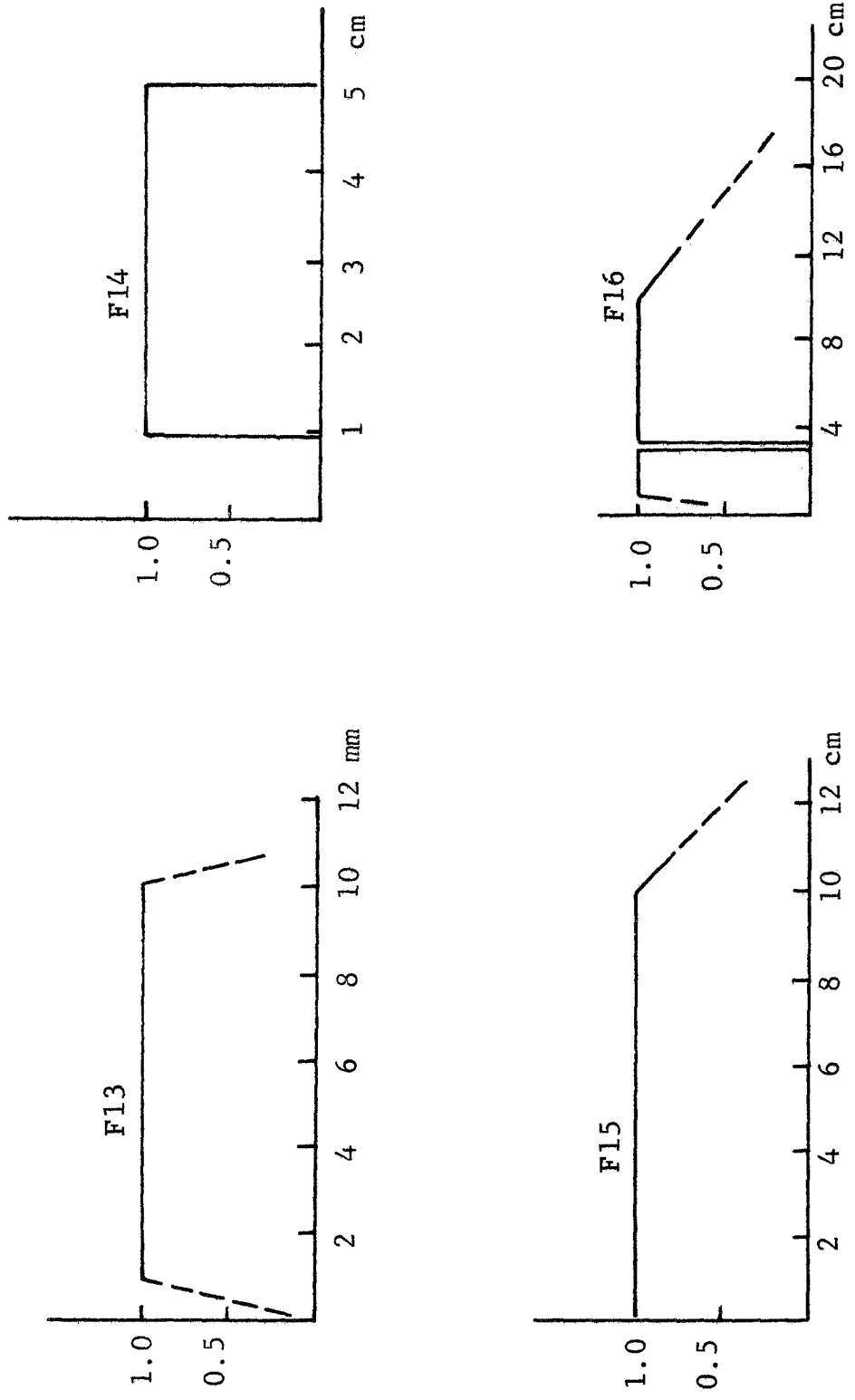


Figure 4.7 - F13 to F16: SPECTRAL REGION WORTH CURVES
(Relative Worth vs. Spectral Region)

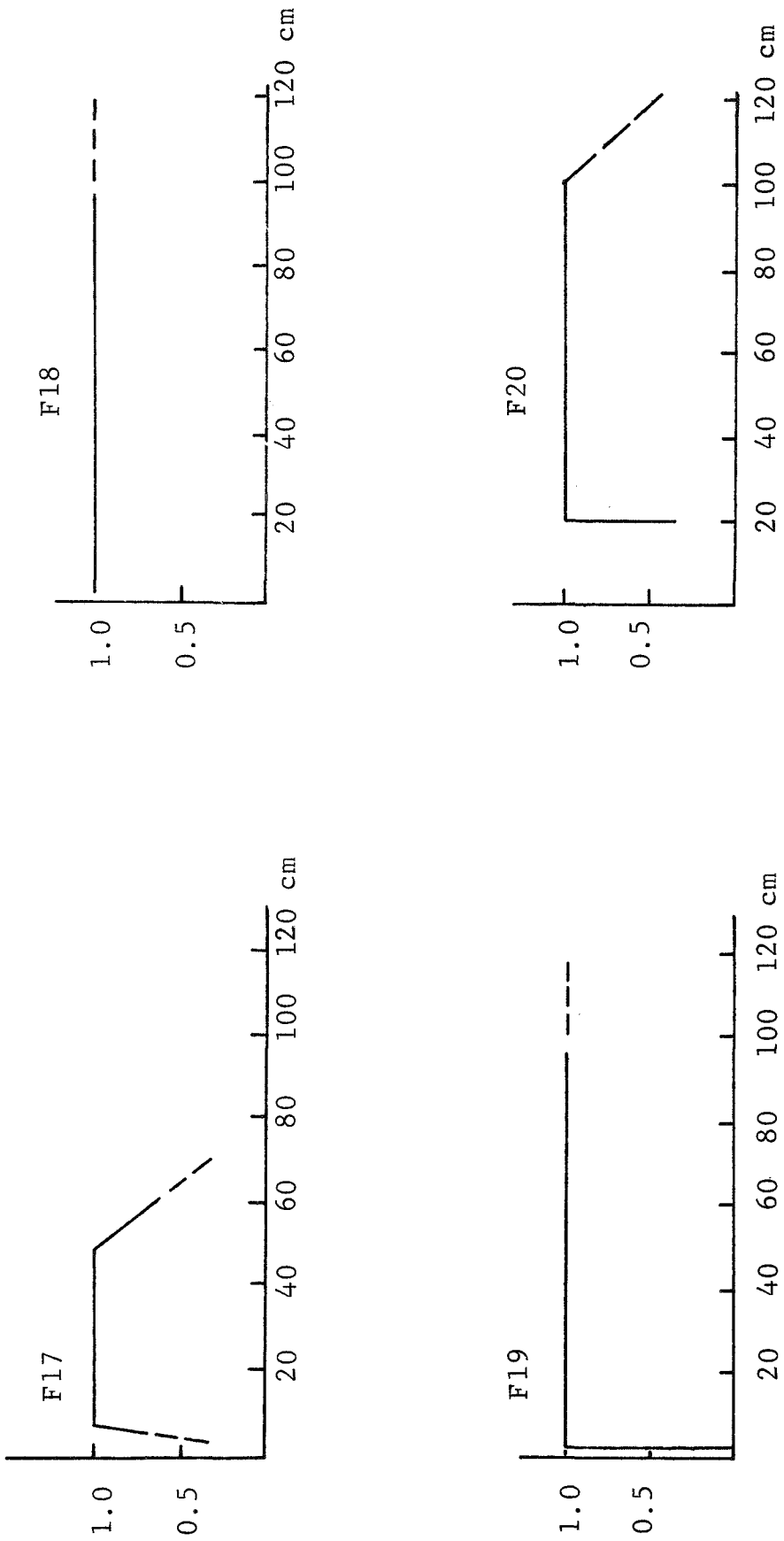


Figure 4.7 - F17 to F20: SPECTRAL REGION WORTH CURVES
(Relative Worth vs. Spectral Region)

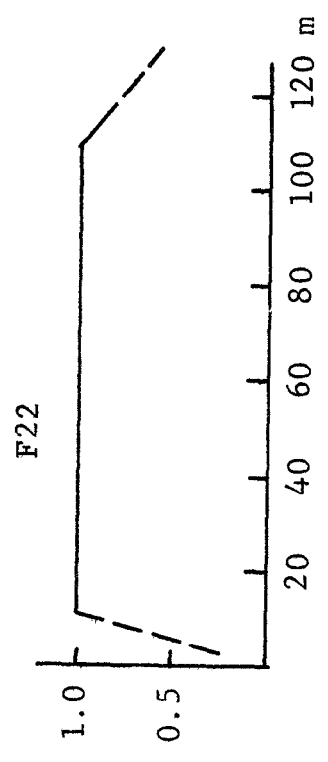
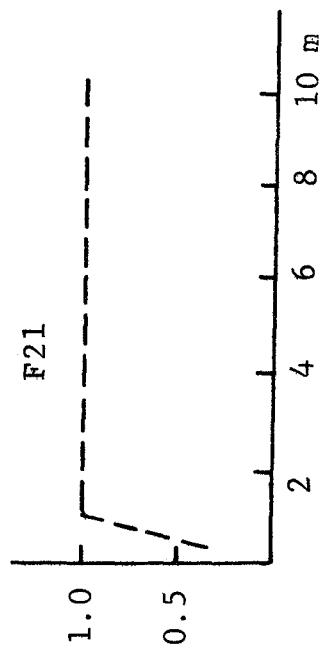


Figure 4.7 - F21 to F22: SPECTRAL REGION WORTH CURVES
(Relative Worth vs. Spectral Region)

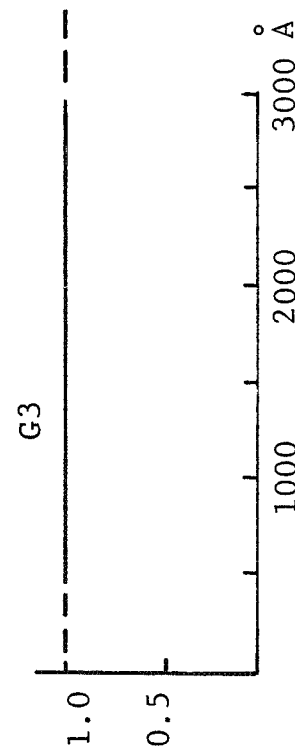
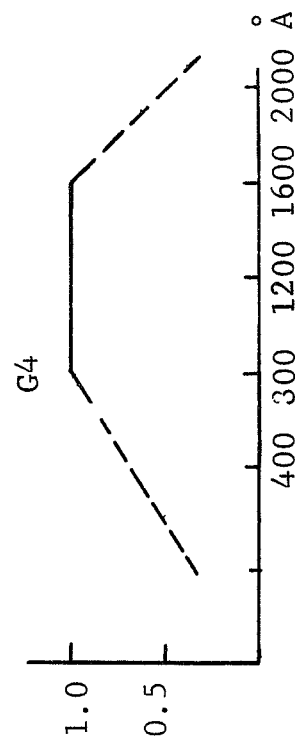
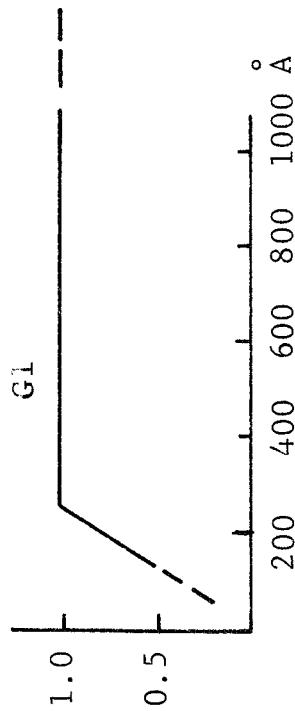
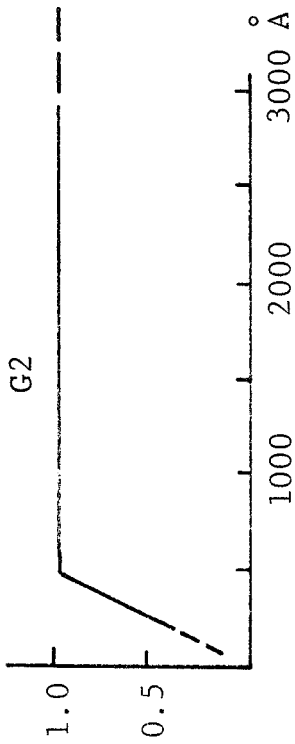


Figure 4.8 - G1 to G4: BANDWIDTH WORTH CURVES
(Relative Worth vs. Bandwidth)

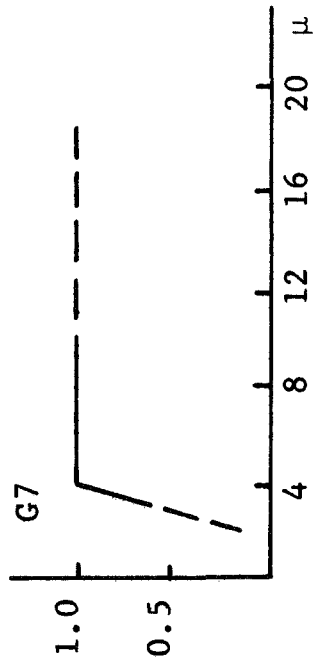
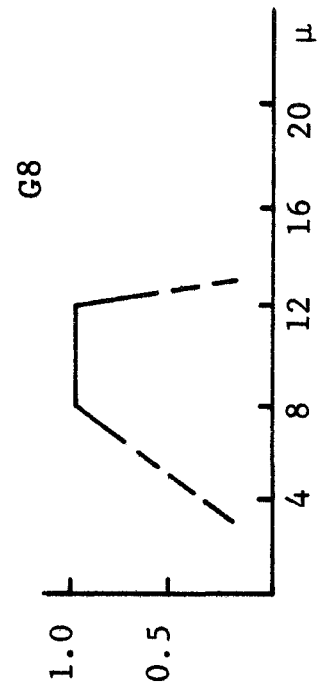
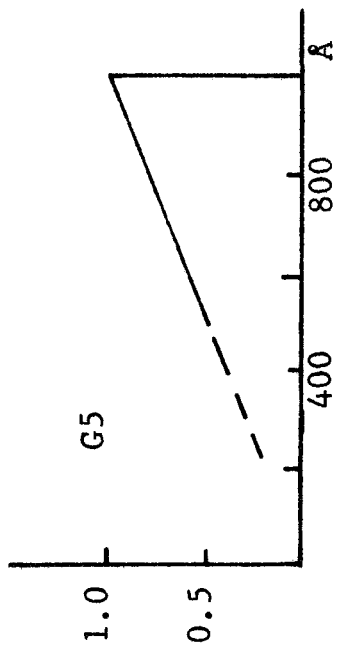
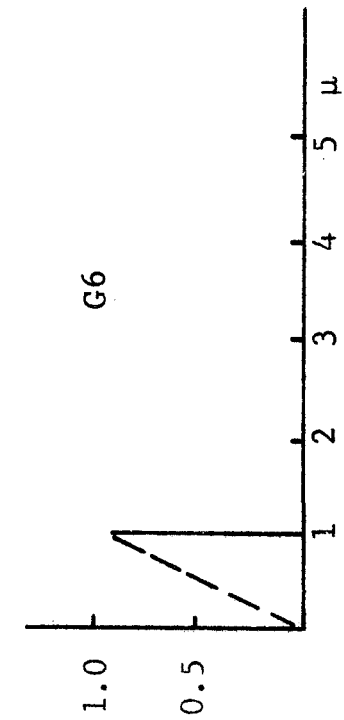


Figure 4.8 - G5 to G8: BANDWIDTH WORTH CURVES
(Relative Worth vs. Bandwidth)

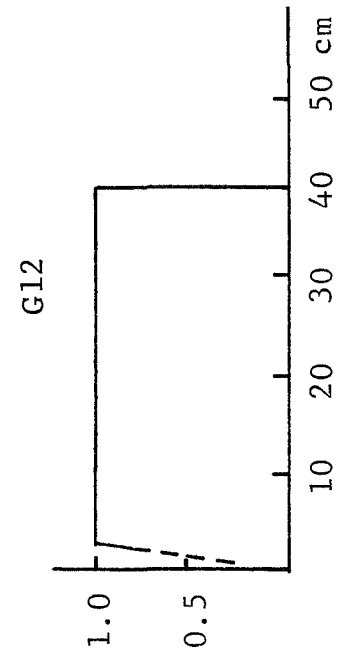
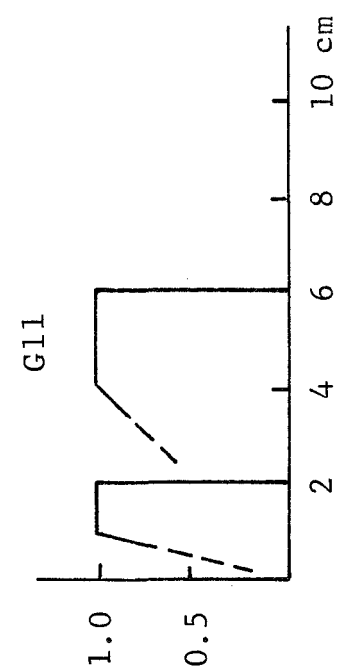
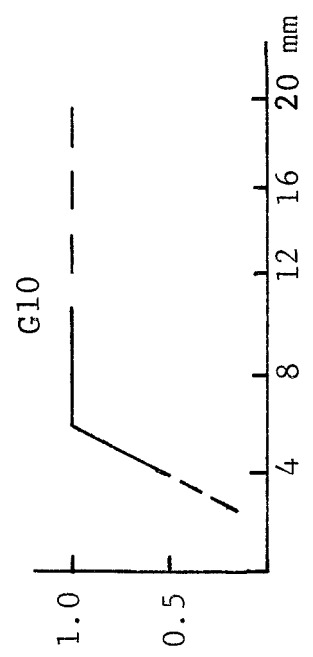
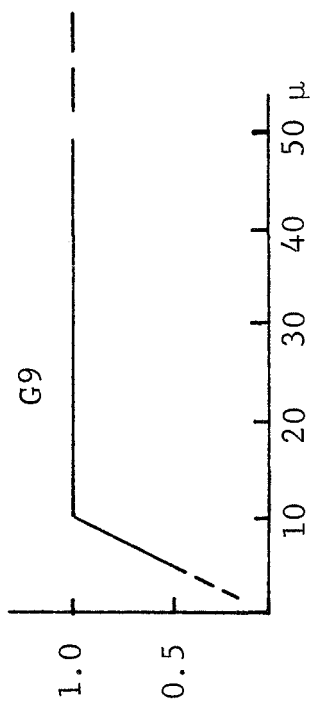


Figure 4.8 - G9 to G12: BANDWIDTH WORTH CURVES
(Relative Worth vs. Bandwidth)

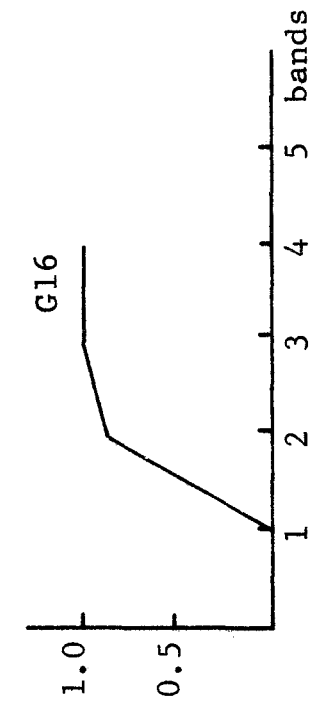
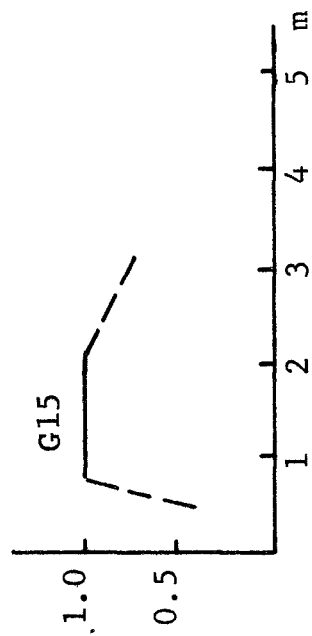
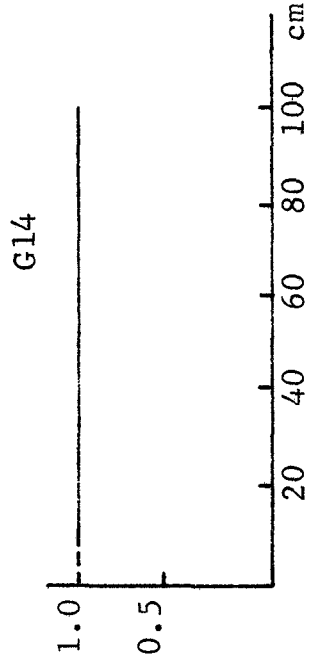
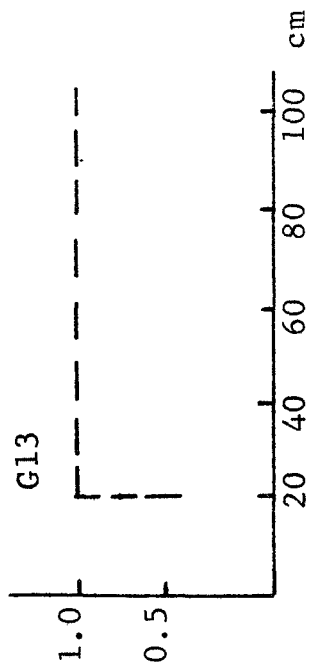


Figure 4.8 - G13 to G16: BANDWIDTH WORTH CURVES
(Relative Worth vs. Bandwidth)

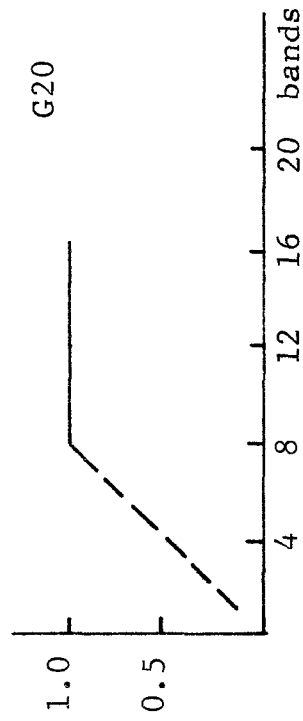
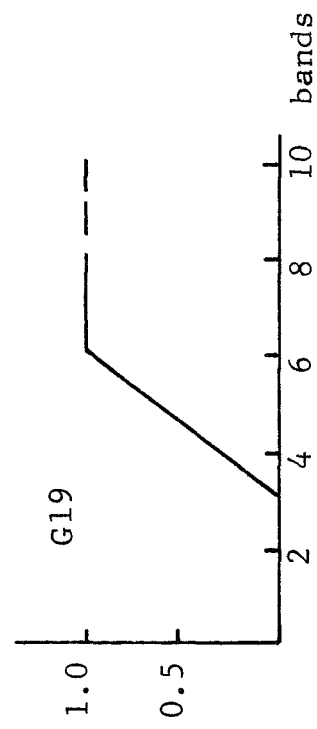
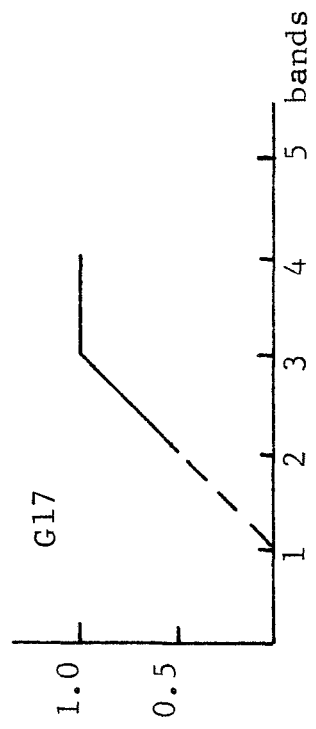
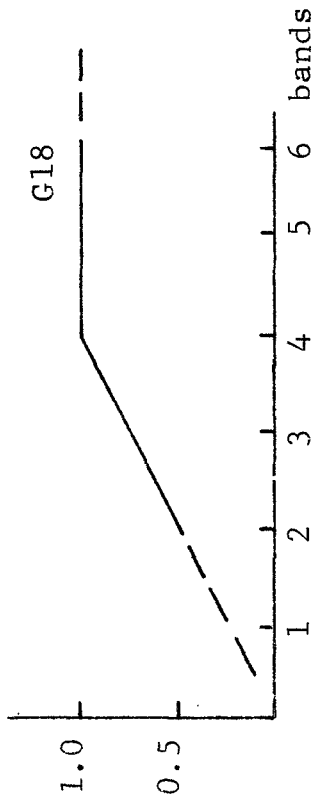


Figure 4.8 - G17 to G20: BANDWIDTH WORTH CURVES
(Relative Worth vs. Bandwidth)

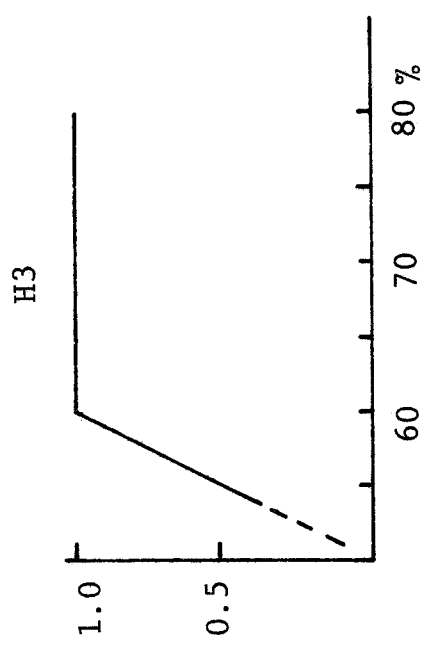
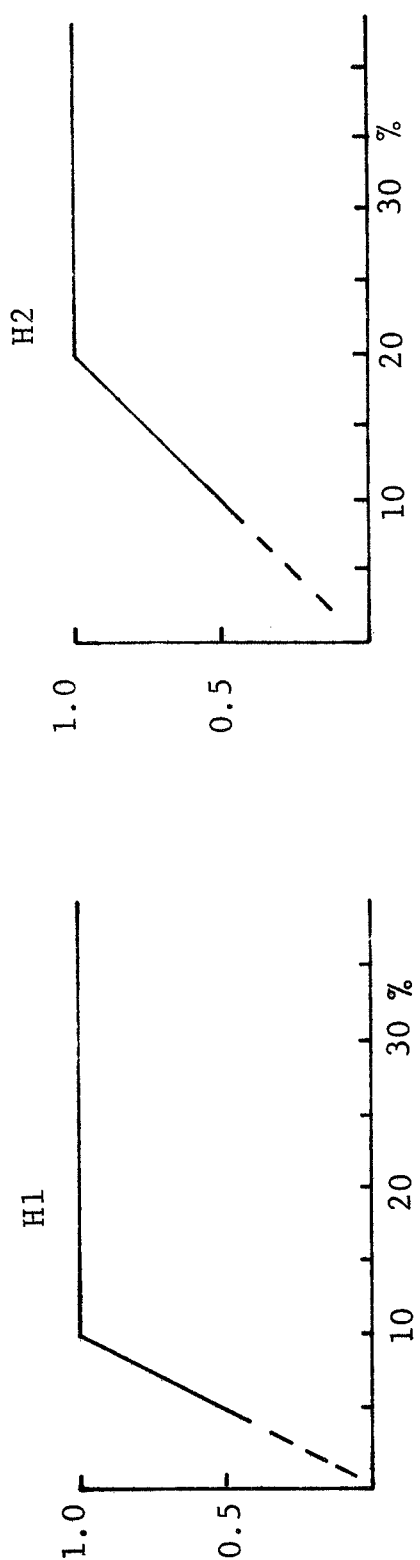


Figure 4.9 - H1 to H3: IMAGE OVERLAP WORTH CURVES
(Relative Worth vs. Image Overlap)

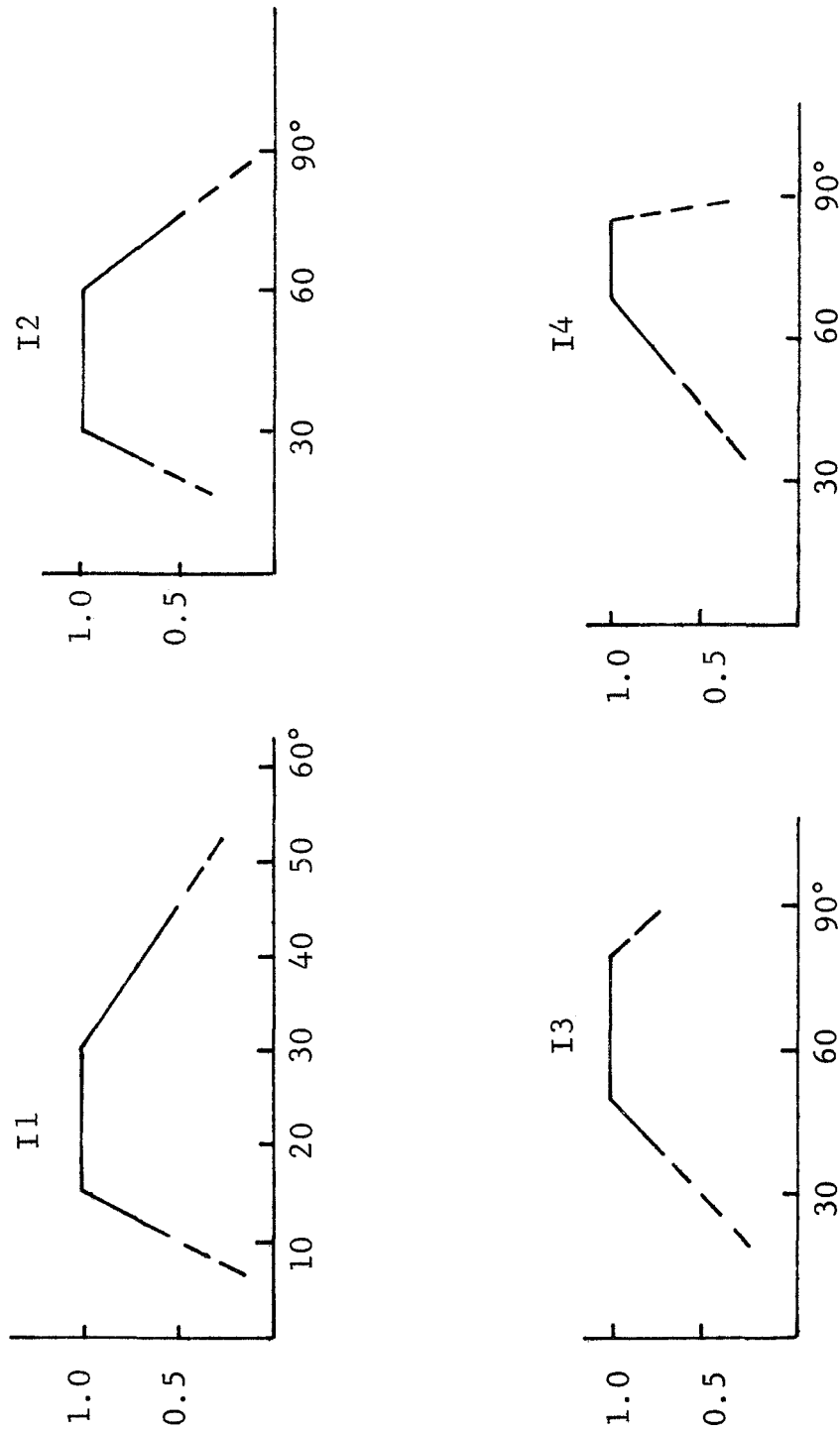


Figure 4.10 - I1 to I4: SOLAR ELEVATION ANGLE WORTH CURVES
(Relative Worth vs. Solar Elevation)

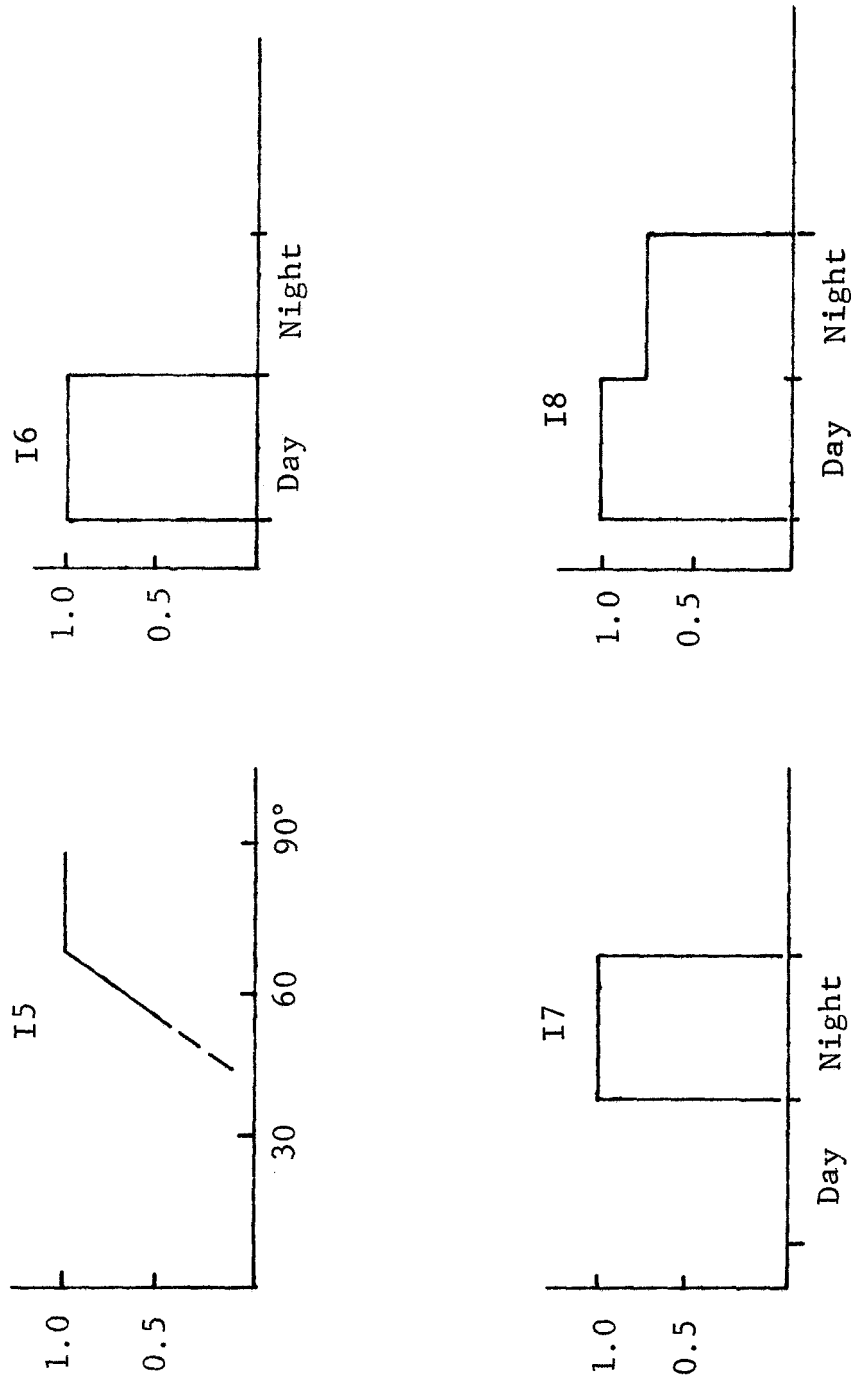


Figure 4.10 - I5 to I8: SOLAR ELEVATION ANGLE WORTH CURVES
(Relative Worth vs. Solar Elevation)

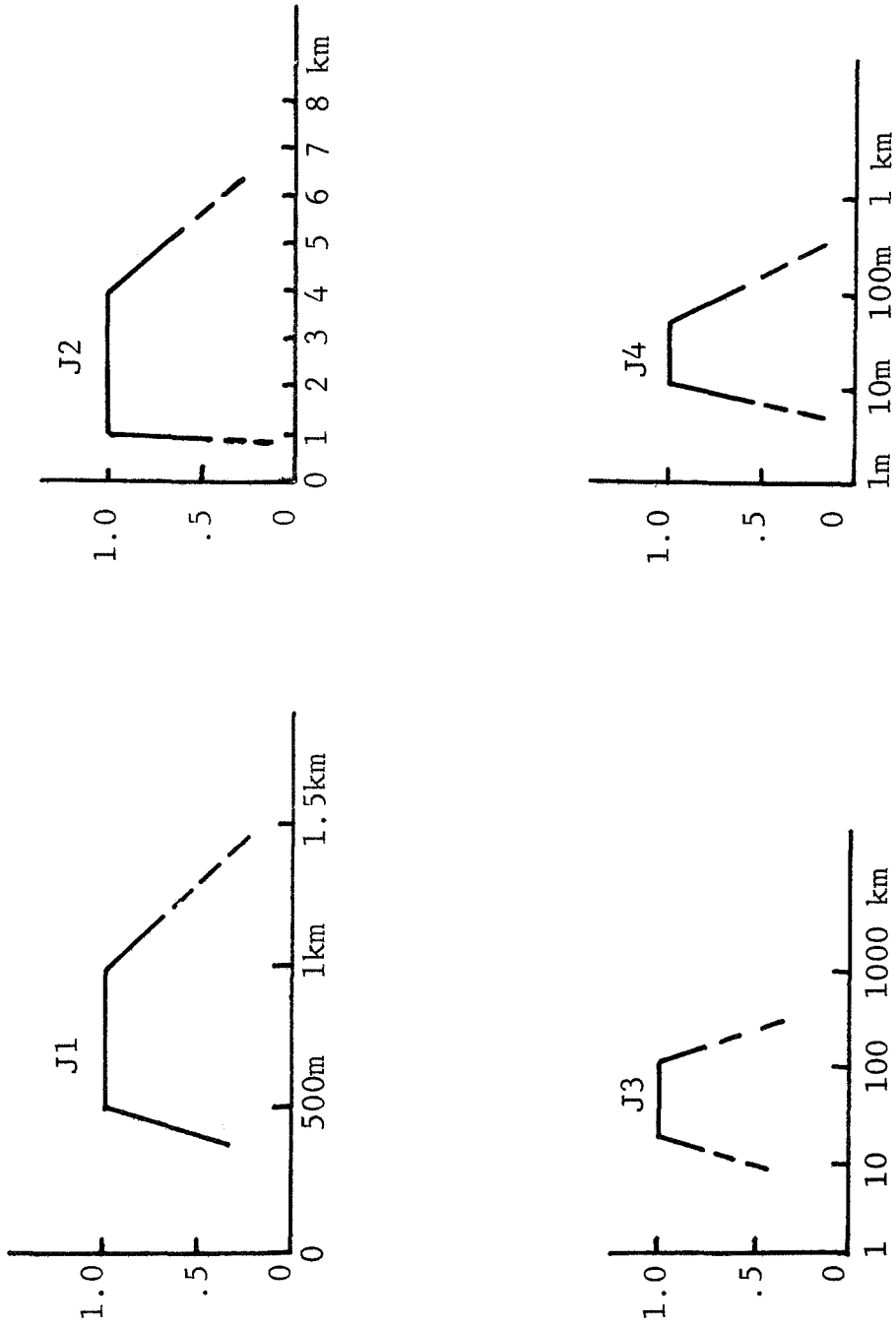
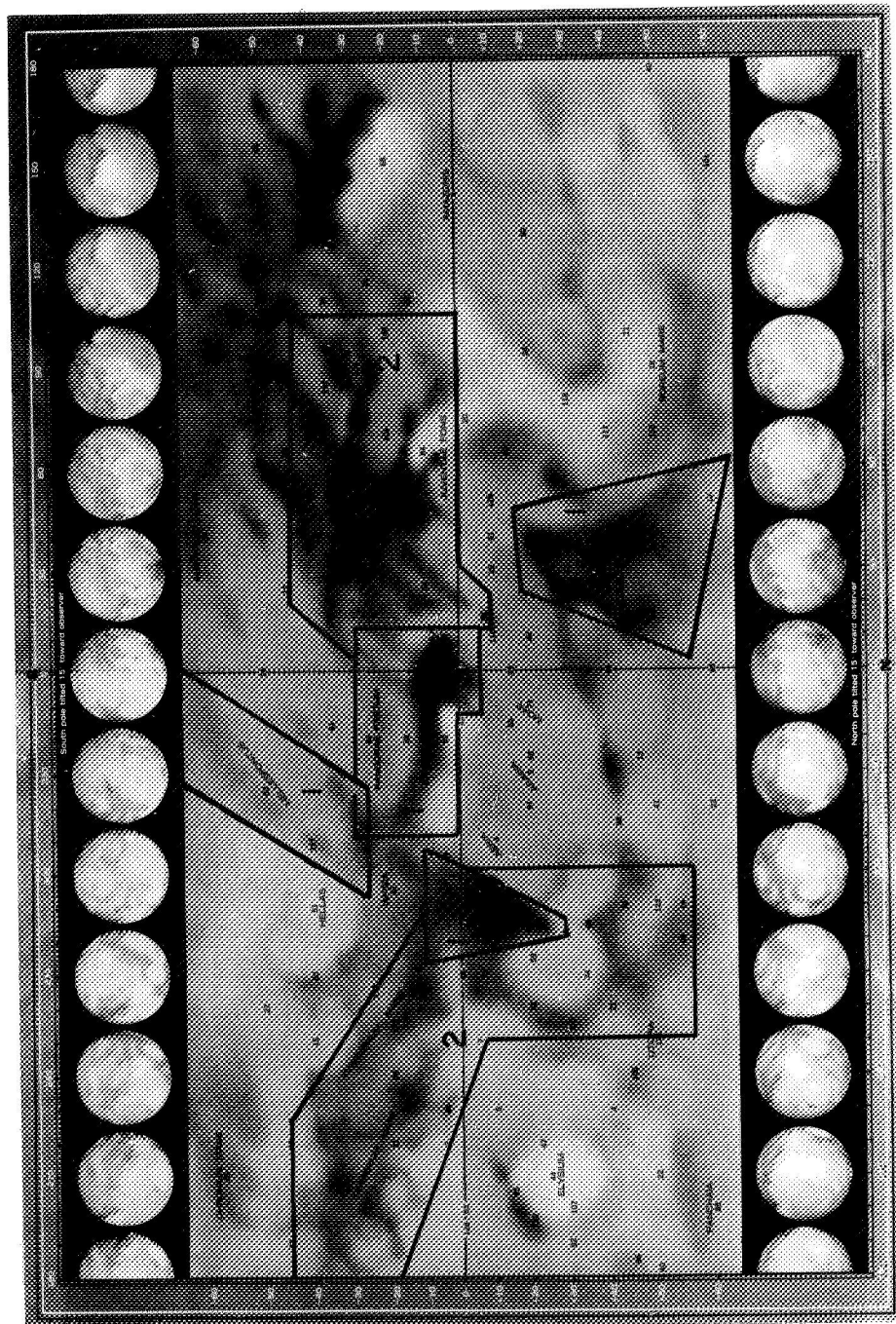


Figure 4.11 - J1 to J4: VERTICAL RESOLUTION WORTH CURVES
(Relative Worth vs. Vertical Resolution)



PRIMARY AREAS: 1
 SECONDARY AREAS: 2

FIGURE 4-12 . AREAS TO BE OBSERVED FOR WAVE OF DARKENING

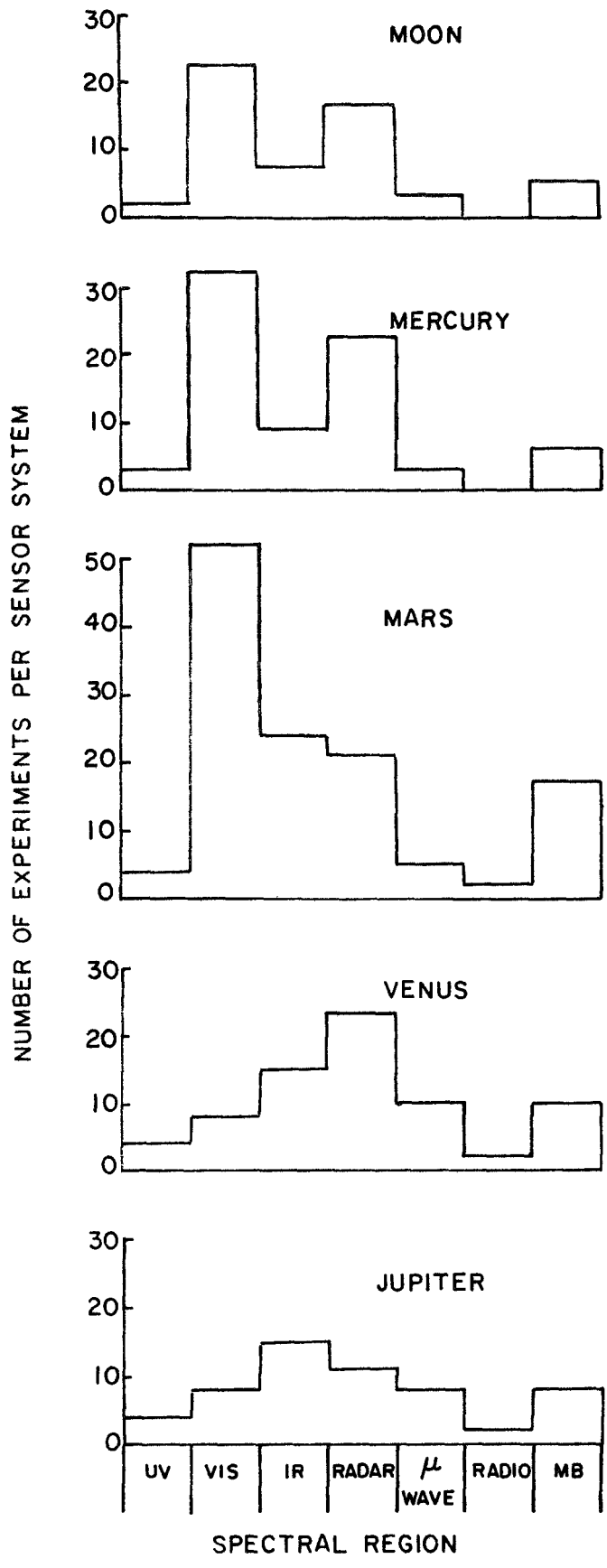


FIGURE 4-13. SPECTRAL DISTRIBUTION OF IMAGERY

5. ORBIT SELECTION RESULTS

The relationship of the orbit selection task to the study tasks was shown in Figure 1-2. The procedure and methods used to select orbits for imaging experiments have been described above (Section 2.3). The results achieved by applying those techniques to grouped measurement families are presented here. The discussion is divided into three subtopics for each planet: (1) interplanetary transfer selections, (2) orbit characteristics and constraints, and (3) orbit selections. The orbit selection data sheets detailing each individual orbit selection are presented in Volume III.

5.1 Mars

5.1.1 Interplanetary Transfer Selections

Maximum payload in orbit was a guideline to the selection of typical Mars transfers. Where no specification of orbit sizes or propulsion systems are available, a suitable approximation to minimum energy transfers is one which minimizes the sum of the hyperbolic excess speeds at Earth (VHL) and Mars (VHP). Previous analyses have shown that these transfers can be found within 30 launch days of minimum Earth escape transfers to Mars.

Eight launch opportunities over the period 1975-1990 were considered as a selection base. Mars transfers have approximately cyclical characteristics over this period. Both Type I and Type II transfers were investigated. Type I transfers (heliocentric angles less than 180°) are characterized by shorter trip times and smaller communication distances at arrival than for Type II transfers (heliocentric angles greater than 180°).

Within each opportunity, one type transfer is usually preferred due to its smaller value of total hyperbolic excess speed (VHT). However, it is necessary to also consider the equatorial declination of the geocentric departure asymptote, δ_{\oplus} . Absolute values of δ_{\oplus} in excess of about 45° imply serious violations of range safety limits during launch (AMR) which may only be remedied by payload consuming dog-leg maneuvers. Minimum VHT transfers were found by generating daily minimum VHL trajectories over a range of dates about the absolute minimum VHL launch date. A search was then made for the trajectory with the smallest VHT. While it may be possible to find even smaller VHT's by searching non-minimum VHL transfers, several investigations show that the VHT's resulting from the first search were within 5 percent of any further minimizations. Hence, these results were retained for the final selection process. The associated transfer characteristics are tabulated in Table 5-1.

It may be noted that on the bases of minimum VHT and $|\delta_{\oplus}| < 45^{\circ}$ Type II transfers are preferred. Only in 1986 is it necessary to use a Type II transfer instead of a Type I because δ_{\oplus} was greater than 45° . This causes an increase in VHT for that year of less than 8%.

The following parameters were considered in selecting transfers from Table 5-1 which have typical Mars arrival conditions:

- VHP - hyperbolic excess speed at Mars arrival, km/sec
- δ_{\oplus} - declination of the approach asymptote to the Mars equatorial plane, deg (this is the minimum orbit inclination which can be established with a co-planar capture maneuver),

TABLE 5-1

SUMMARY OF MINIMUM VHT MARS TRANSFERS: 1975 - 1990

Launch Date (Min. VHT)	Type	Flt. Time (days)	δ_{\oplus} (deg)	VHL (KPS)	VHP (KPS)	VHT (KPS)	δ_{\oplus} (deg)	ρ (deg)	θ (deg)	RC (AU)	DTC (Days)	Season (North Hemf)
Sep 3, 1975	II	356	9.3	3.80	2.60	6.40	26.45	60.40	17.40	2.44	92	Mid-Sum
Oct 5, 1977	II	335	18.9	3.30	2.46	5.76	4.07	78.32	23.32	2.23	137	Mid-Sum
Oct 30, 1979	II	296	24.3	3.01	2.75	5.76	-16.10	109.73	33.44	1.84	224	Late-Sum
Nov 27, 1981	II	303	25.3	3.04	3.07	6.11	-30.69	86.00	37.96	1.61	250	Early-Fall
Jan 1, 1984	II	286	9.9	3.33	3.62	6.95	-32.92	77.94	44.15	1.25	278	Late-Fall
May 8, 1986	II	261	-14.8	2.79	3.95	6.74	-7.44	45.86	38.05	1.54	213	Mid-Win
Jul 9, 1988	I	193	13.1	3.42	2.68	6.10	3.57	112.48	40.33	1.14	255	Late-Win
Aug 23, 1990	II	361	5.6	3.96	2.77	6.73	33.52	53.03	15.54	2.49	81	Early-Sum

- ρ_{\odot} - planar angle between the approach asymptote and the planet subsolar point, deg (for values less than 90° the approach is from the sunlit side of the planet but periapse is near or beyond the solar terminator, i.e., in darkness),
- $\theta_{\oplus\oplus}$ - the planar angle between the Sun and Earth as seen from Mars at arrival, deg (when this angle becomes less than 10° it may be difficult for the spacecraft to receive transmissions from the Earth),
- R_C - communication distance between Earth and Mars at arrival, AU,
- DTC - days to conjunction of Earth and Mars from the arrival date (conjunction is the time of maximum communication distance as well as communication blackout),
- Season - the northern hemisphere season on the Martian surface at arrival (Earth-based observations of Mars indicate that changes in surface conditions are most apparent during the Spring seasons of the hemispheres. These changes include retreat of the polar "ice cap" and the "wave of darkening" across mare regions at mid-latitudes).

The parameters VHP, δ_{\oplus} , ρ_{\odot} and Season were given the most weight in the selection process, since they most directly affect how and what can be measured on the planet. Two transfers were selected to represent typical Mars arrival conditions for the subsequent orbit selection analysis: 1984 Type II and the 1988 Type I.

The 1984 Type II arrival conditions are characterized by

- (a) a moderately high approach velocity,
- (b) periapse locations which favor the southern hemisphere,
- (c) approach from the dark side, but periapse favoring the sunlit side of the planet, and
- (d) arrival at a seasonally inactive period, season is late fall in the northern hemisphere.

The 1988 Type I arrival conditions are characterized by

- (a) a low approach velocity,
- (b) periapse locations equally available in both hemispheres,
- (c) approach from the sunlit side but periapse near the terminator or in darkness, and
- (d) arrival at a seasonally active period in the northern hemisphere, Season is late winter beginning the northern "wave of darkening."

Once the transfer selections are made the insertion occultation characteristics can be presented without any further information about the orbit to be selected. Contours of occultation are mapped on the hyperbolic impact plane in Figure 5-2 for the 1984 Type II transfer. The planar spherical coordinates are the asymptotic miss distance, B_I and the aiming angle, θ measured from the reference T axis, which is the intersection of the impact and ecliptic planes. Contours for occultation beginning at 5° and 0° from the planet near limb are given for the Sun, 0° for Earth, and 20° and 0° for the star Canopus. The relation between the aiming angle θ , orbit inclination, and ascending node in the Mars equatorial system are given in Figure 5-3. With these curves it is possible to relate orbit selections made in the Mars equatorial reference system to the occultation contours. Similar graphs for the 1988 Type I transfer selection are given in Figures 5-4 and 5-5.

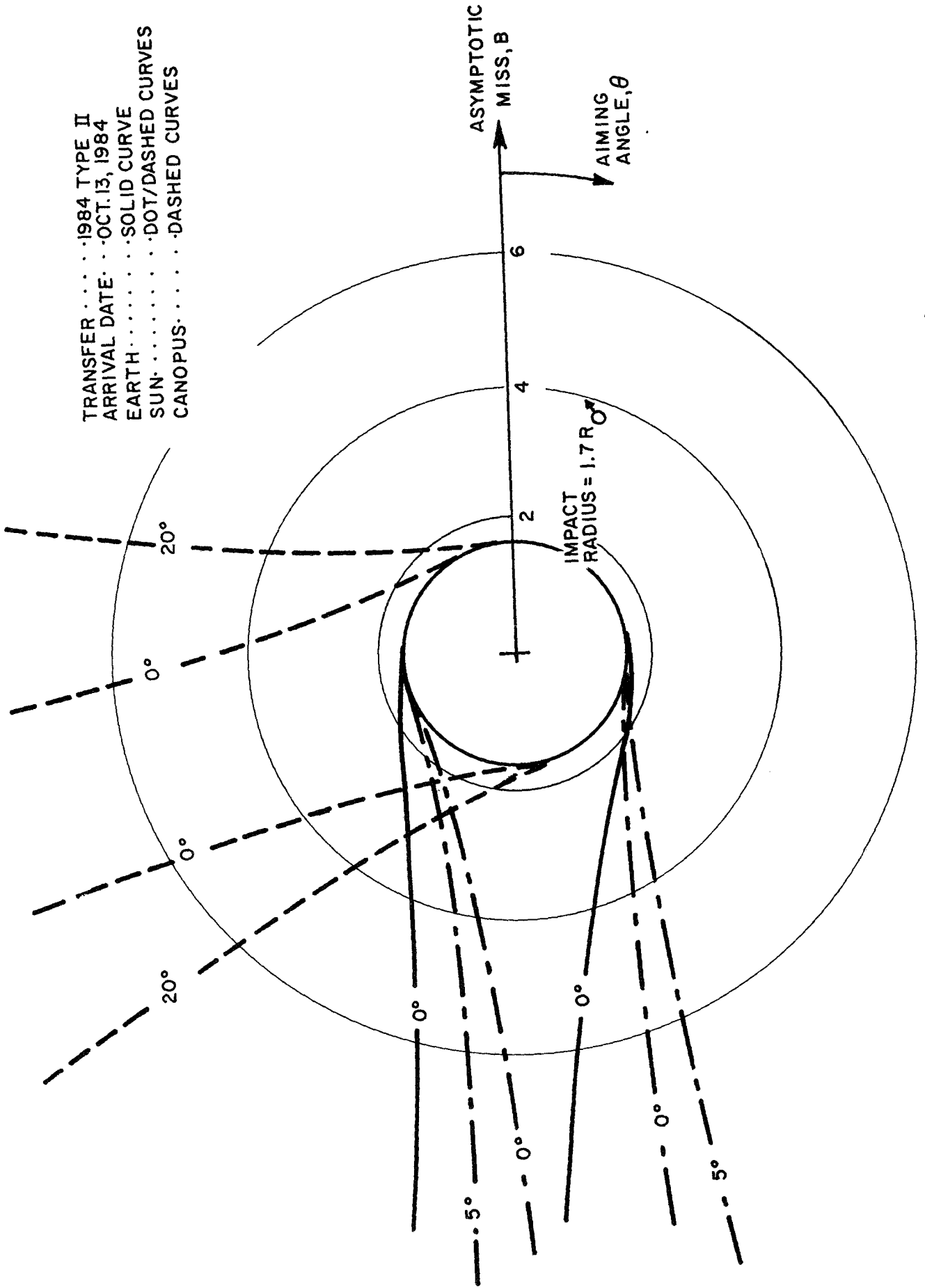


FIGURE 5-2. MARS CAPTURE OCCULTATION CONTOURS (1984)

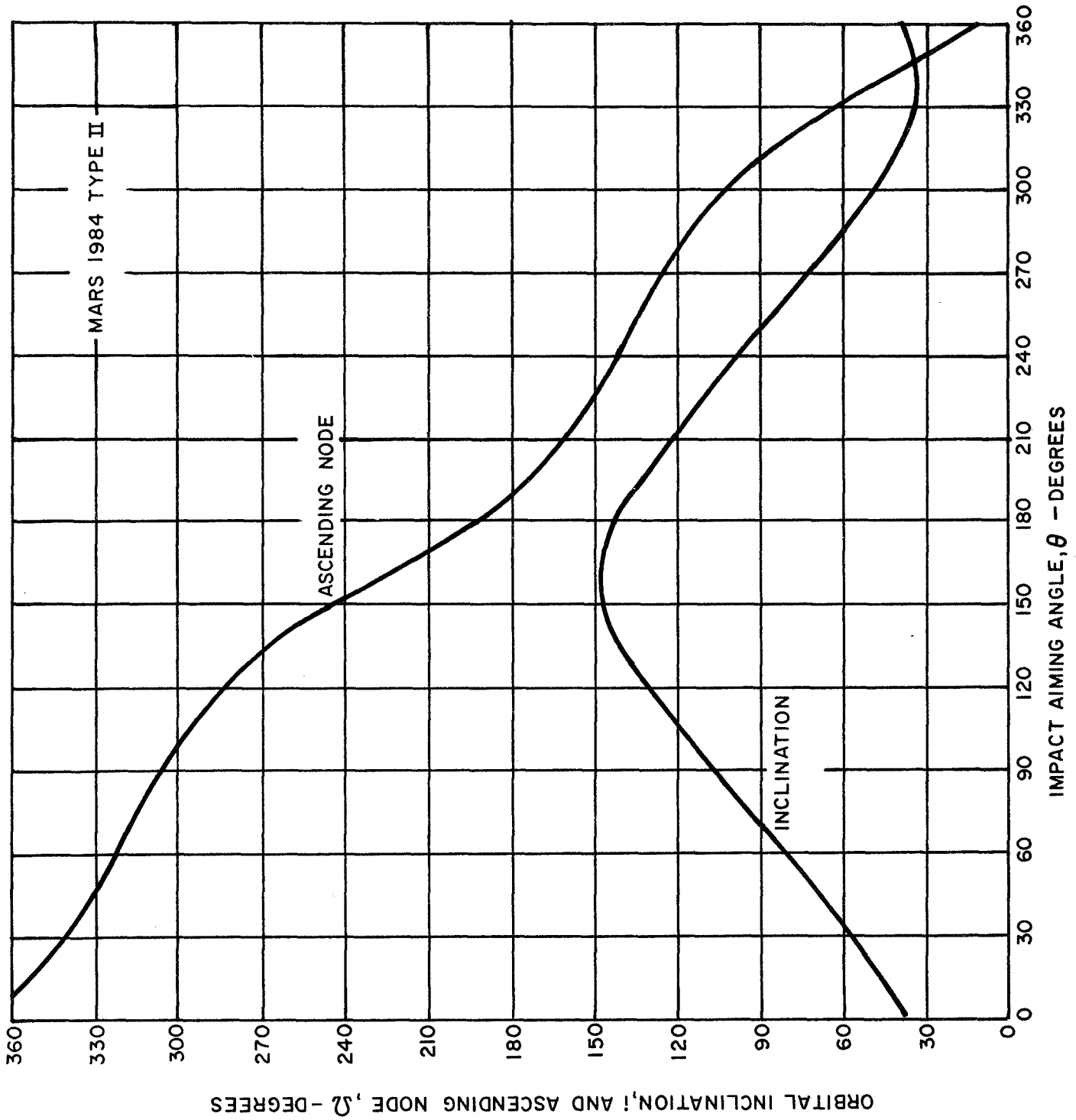


FIGURE 5-3. MARS AIMING ANGLE/ORBIT ORIENTATION RELATIONSHIP (1984)

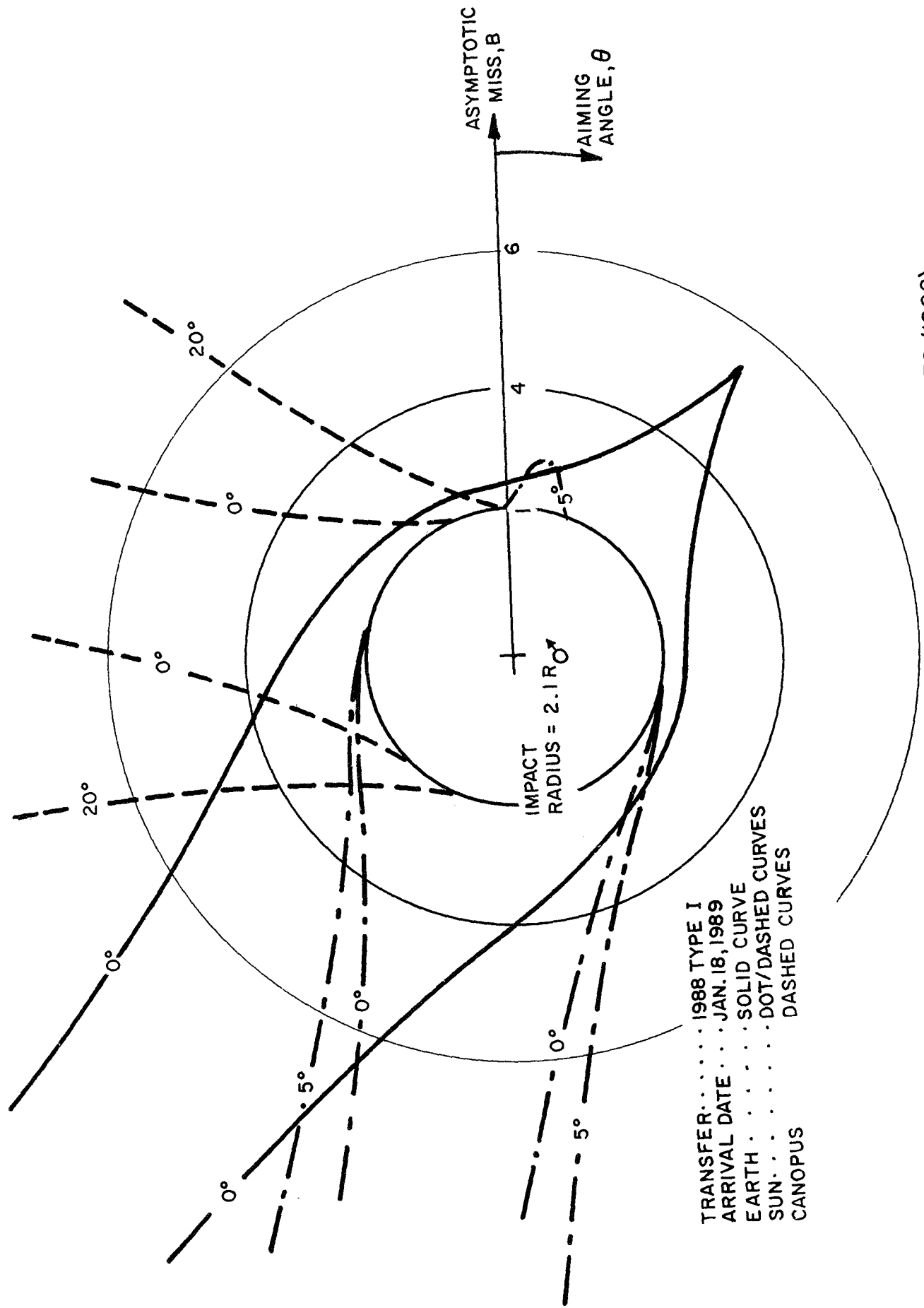


FIGURE 5-4. MARS CAPTURE OCCULTATION CONTOURS (1988)

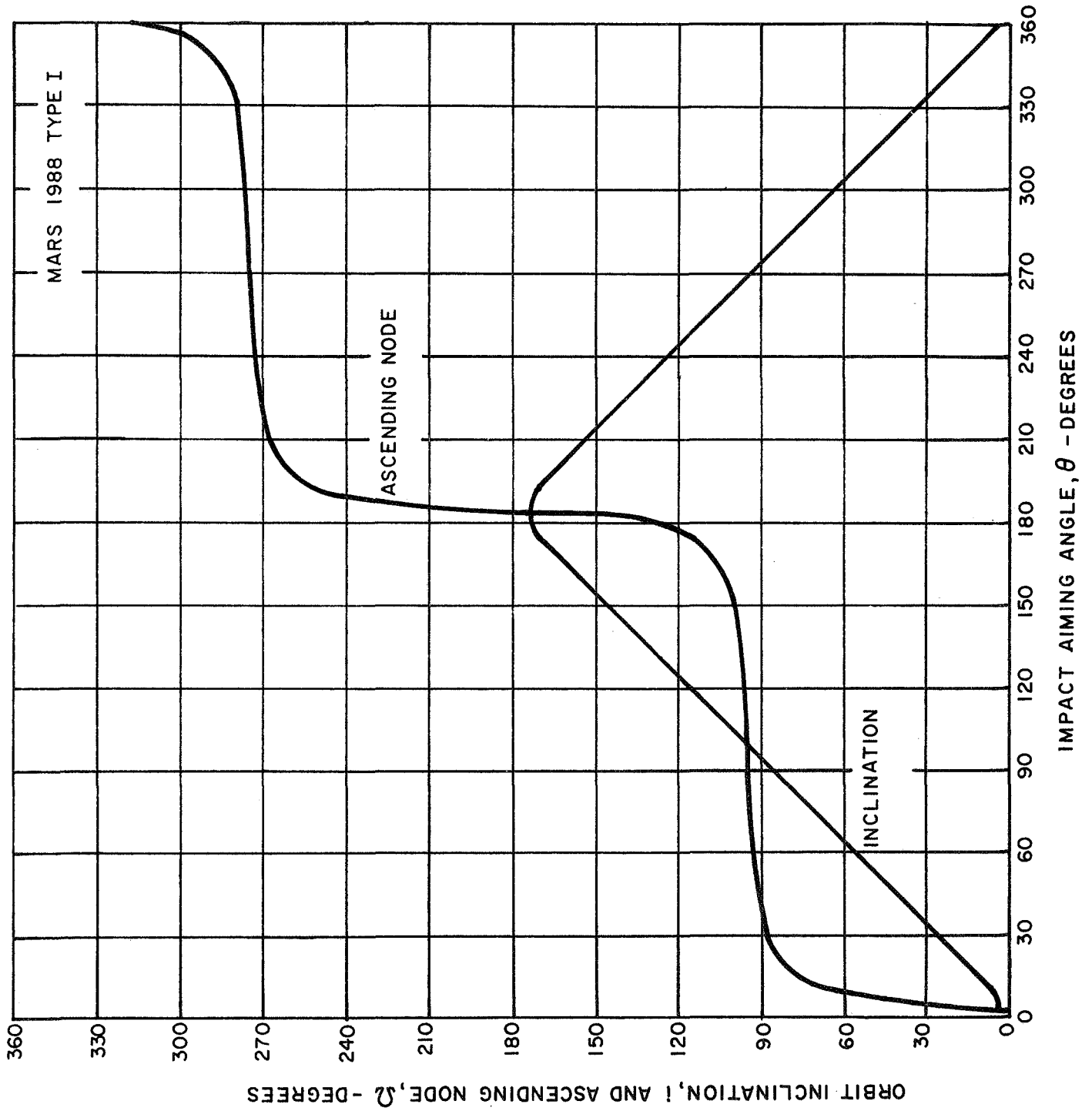


FIGURE 5-5. MARS AIMING ANGLE/ORBIT ORIENTATION RELATIONSHIP (1988)

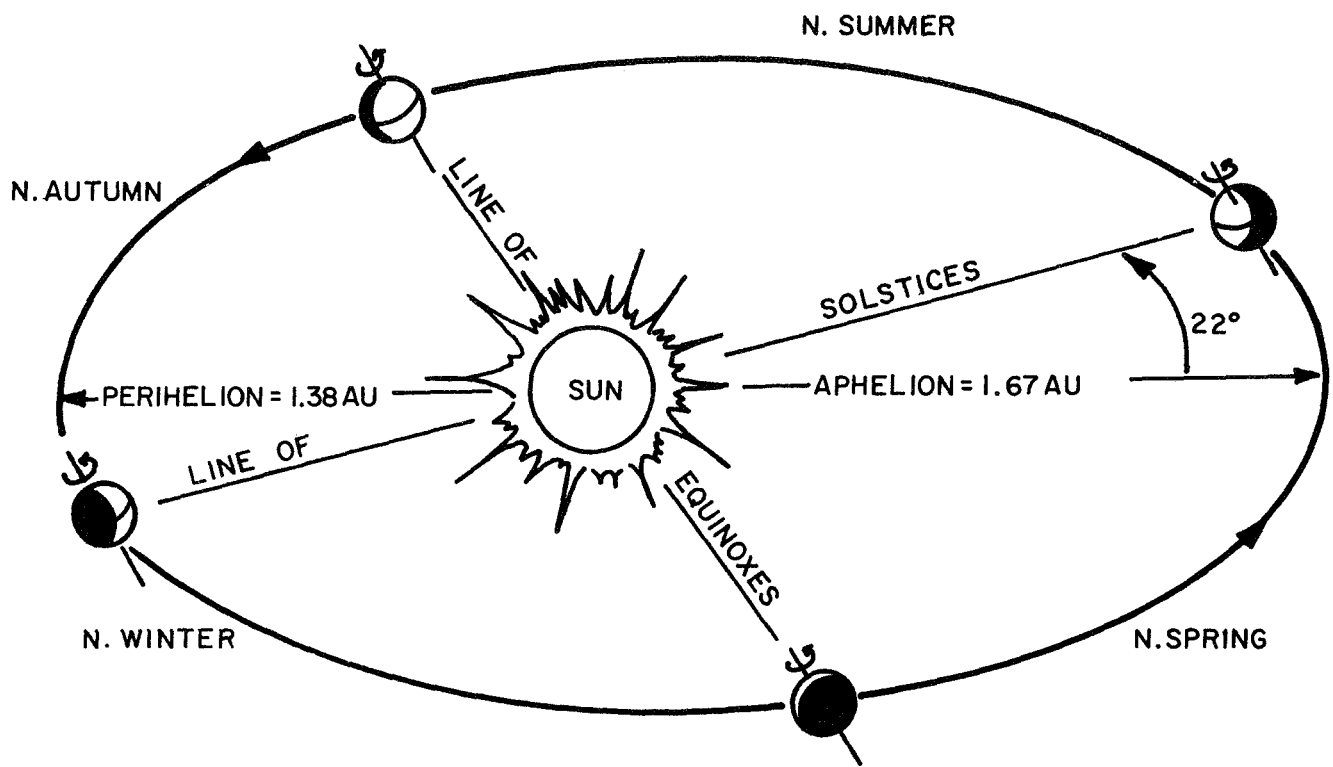
It should be reiterated that these transfer selections were not made with regard to optimum arrival conditions or with any preference to year of opportunity. Rather the transfers were picked with the objective of representing the ranges and combinations of values of arrival parameters at Mars.

5.1.2 Orbit Characteristics and Constraints (Mars)

The Mars environment provides a dynamic background for imaging experiments. Its transparent atmosphere permits visual imaging of the surface. The planet's rapid rotation period, 24.6 hrs, makes it possible to image large areas under similar conditions of solar illumination. A schematic diagram of the planets motion about the Sun is illustrated in Figure 5-6. The inclination of Mars' rotation axis of about 25° to its orbit plane causes seasonal variation in the hemispheres as the planet moves around the Sun. Because the Mars orbit is eccentric, the duration of seasons varies as can be seen in the figure. As has been noted, the type of seasonal coverage which can be achieved is directly dependent upon the location of Mars in its orbit at the time of arrival. Mars has a moderate oblateness which is the dominating perturbation on orbital imaging.

Many Mars surface imaging experiments are subject to solar illumination constraints. The percent of Mars surface exposure to any specific solar elevation angle* is described in Figure 5-7. The rapid rotation rate, coupled with the fact that the planet's rotation axis is inclined 25° to the orbit plane, permits a significant 42% of the planet to be observed

* Elevation angle = (90° - zenith angle)



● MARS ROTATION

INCLINED 25° TO ORBIT PLANE

ONE MARS DAY = 24 HRS. 37 MIN. 22.6 SEC. = 1.029 EARTH DAYS.

● MARS SEASONS (NORTHERN HEMISPHERE)

SPRING ····199 EARTH DAYS
 SUMMER ····182
 AUTUMN ····146
 WINTER ····160
 YEAR ····687

FIGURE 5-6. MARS ORBITAL GEOMETRY

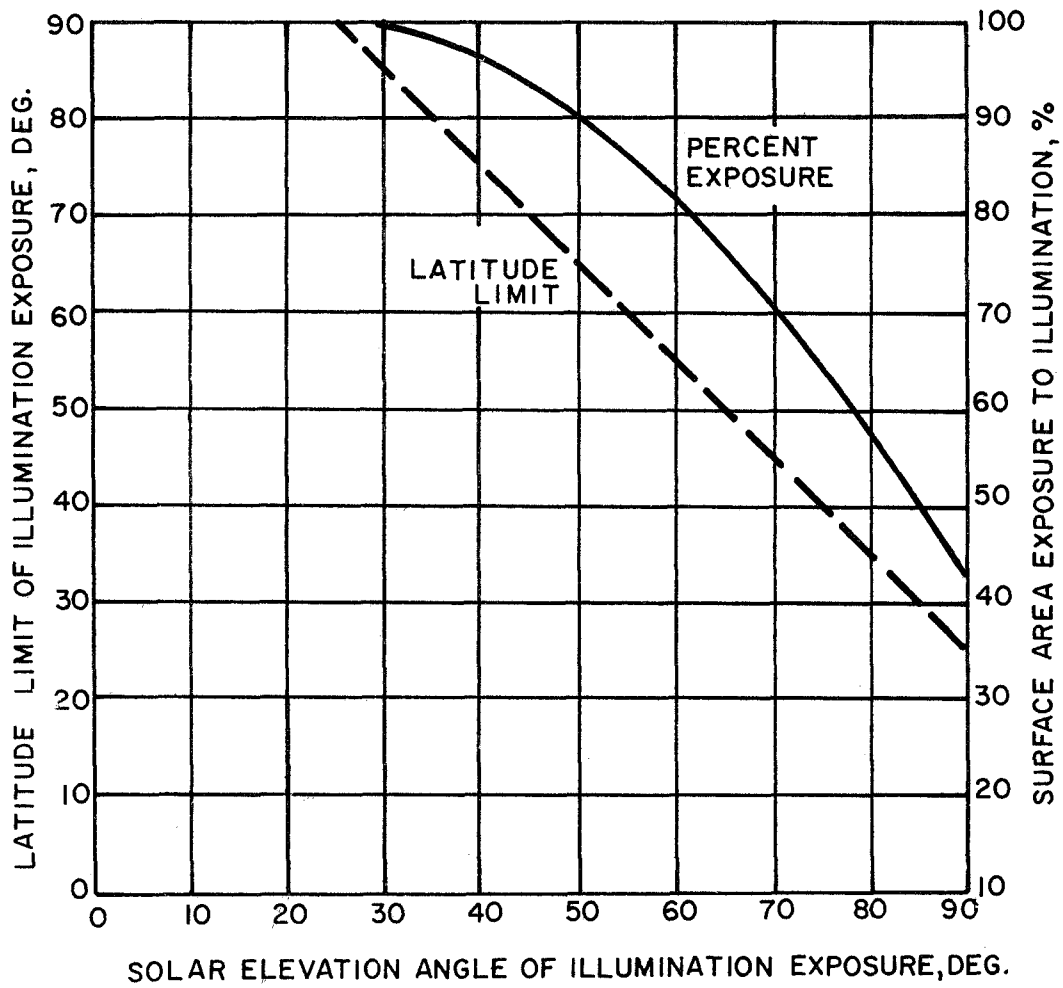


FIGURE 5-7. MARS ILLUMINATION EXPOSURE

at a noon sun illumination at some time during the Mars year. In terms of orbital imaging, however, this is somewhat misleading, since measurements would have to be continued for a minimum of 300 days to obtain this amount of coverage. The entire surface of Mars is, at one time or other, exposed to a solar elevation angle of up to 25° . Also shown in Figure 5-7 are the limiting latitudes (north and south), at which solar elevation angles with less than 100% exposure occur.

The selection of a set of candidate orbit sizes was constrained to satisfy 50-year lifetimes due to atmospheric drag. The 50-year Mars orbit lifetime curve (Lockheed 1968) used in the study is shown in Figure 5-8. Any combination of periapse altitude (hp) and eccentricity (e) which lies above the curve is assumed to have a lifetime, based only on atmospheric drag considerations, of greater than 50 years.

There are a number of measurement techniques which provide complete imaging coverage over large areas of a planet. The only technique assumed for the orbit selection process was that of contiguous coverage. Contiguous coverage, as used in this study, is defined as data collection at or near the specified minimum image size (inferring maximum resolution) and minimum overlap, with large area coverage being obtained from a composite of many small (by comparison) images. At Mars it is not possible to perform this type of imaging consecutively unless orbit periods of integer Mars days are used. That is, for orbits less than a Mars day it is not possible to overlap images on consecutive orbits. Orbits with periods greater than one Mars day are not attractive because of the long coverage acquisition times. Therefore orbits for the candidate orbit size selections were chosen with periods approximately equal to subintervals of a Mars day, i.e.,

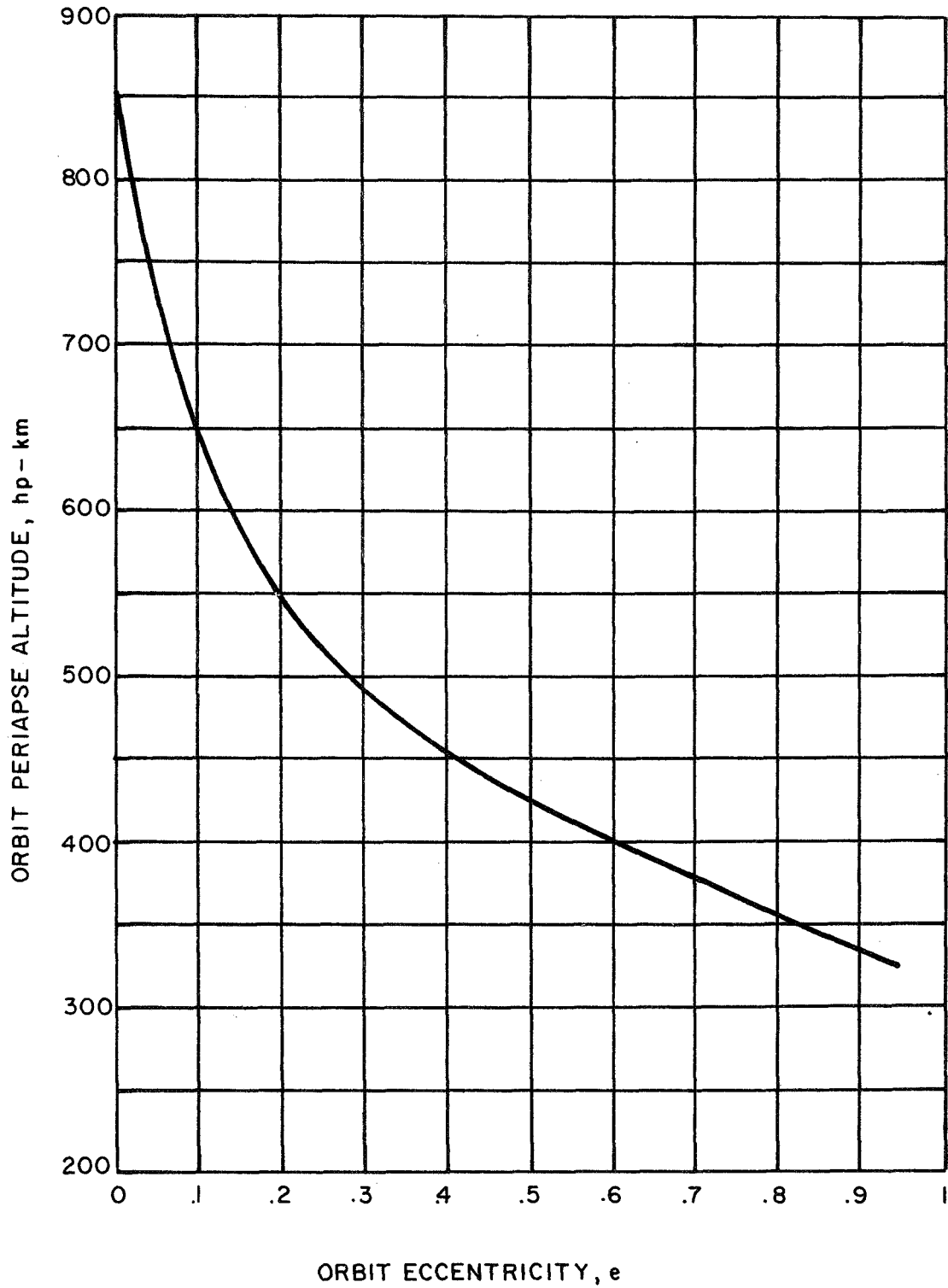


FIGURE 5-8. MARS 50 YR. ORBIT LIFETIME CURVE

$$n = \frac{\text{Mars day}}{\text{Orbit period}} = 1, 2, 3, \dots, 10 \text{ orbits/day.}$$

In this way up to 10 separated imaging passes are made across the planet surface in one Mars day. On each successive day, overlapping images are obtained with images of the respective pass of the previous day.

A second factor of importance in the orbit size selection process is measurement altitude. For non-circular orbits, measurement altitude varies with location on the orbit. It is convenient to express this variation as the ratio:

$$h/h_p = \frac{\text{local altitude}}{\text{periapse altitude}} .$$

Orbit measurement arcs limited by maximum values of h/h_p are presented in Figure 5-9. The orbits used to construct the graph lie along the 50-year lifetime curve of Figure 5-8. The variation of measurement arc (ordinate) is shown as a function of subinteger orbit periods of a Mars day for maximum h/h_p 's of 2, 5 and 10. All orbits cover one-half of the planet surface (if periapse is at the equator) with values of h/h_p less than 10. However, only an orbit period equivalent to 10 orbits/day can measure across this same arc with values of h/h_p less than 2.

A list of the candidate orbits representing orbit sizes for imaging orbit selection is presented in Table 5-2. All of these orbits have lifetimes equal to or greater than 50 years. In addition to the parameters already discussed, the average required capture impulse is given in the table. This is based on a coplanar capture maneuver, assuming a hyperbolic approach speed (VHP) of 2.98 km/sec averaged from the VHP data presented in Table 5-1.

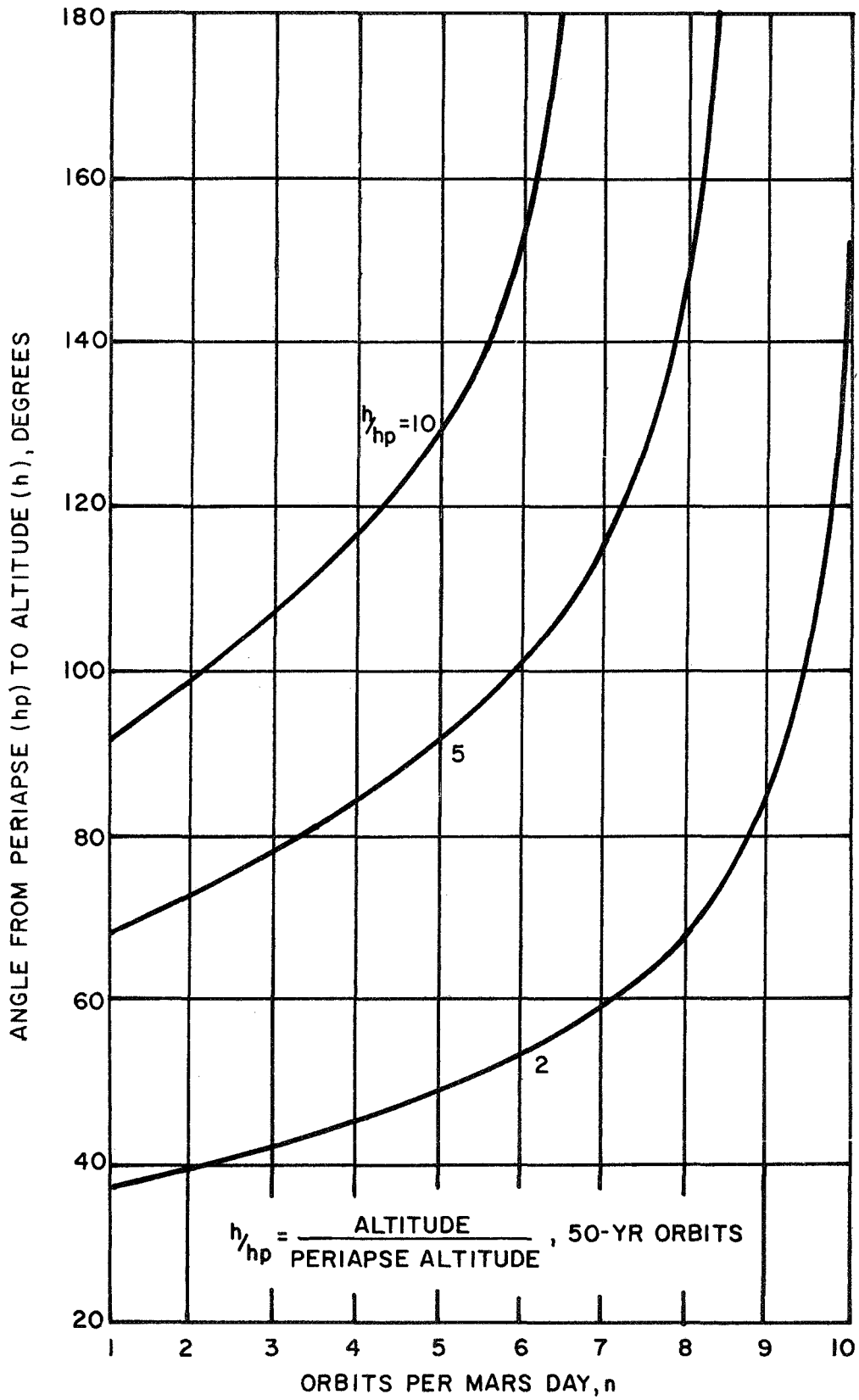


FIGURE 5-9. MARS ORBIT ALTITUDE RATIOS.

TABLE 5-2

MARS CANDIDATE ORBIT SIZES

Orbit No.	Orbits Per Day (n)	Eccentricity	Periapse Altitude (km)	Maximum Altitude Ratio, h/hp	Orbit Period (hrs)	Average* Capture ΔV (km/sec)
1	10	.0000	1025	1.0	2.46	2.205
2	9	.1622	580	3.6	2.74	1.979
3	8	.2362	525	5.6	3.08	1.870
4	7	.3075	490	8.0	3.52	1.765
5	6	.3800	460	11.2	4.10	1.661
6	5	.4538	440	15.4	4.92	1.558
7	4	.5318	420	21.6	6.16	1.450
8	3	.6155	400	31.3	8.21	1.337
9	2	.7081	380	49.0	12.31	1.215
10	1	.8174	355	95.2	24.62	1.075

* Capture ΔV Based on a Surveyed Average Hyperbolic Approach Speed, VHP = 2.98 km/sec.

The dominant perturbation on these orbits is that of planetary oblateness which causes precession of the orbit node and argument of periapse. The magnitude and direction of these perturbations varies with orbit inclination as well as size. This variation is presented in Figure 5-10 for nodal precession, and in Figure 5-11 for precession of the argument of periapse as functions of orbit inclination. Not all orbit sizes in Table 5-2 are shown since the perturbations become quite small as the orbit becomes large and highly elliptical, i.e., as n approaches 1. Nodal perturbations (Figure 5-10) are symmetric about the origin, i.e. (0,90). Perturbations in the argument of periapse are symmetric about an inclination of 90° . A nodal precession rate equal to that of the average rate of the Sun's motion about Mars (0.5420 deg/day) will establish sun-synchronous orbits. Such orbits can be useful in expanding coverage within high solar elevation limits (e.g. 70° - 90°) by following the subsolar point as it moves north or south across the Mars surface.

5.1.3 Orbit Selection (Mars)

Orbit selection as used here, is defined as the selection of a candidate orbit size and the determination of the remaining orbit parameters (inclination, ascending node, and argument of periapse) designed to meet a set of specifications pertaining to a measurement family. The objectives of selection were

- (a) to provide orbit data necessary in determining experiment subsystem requirements,
- (b) to determine operational characteristics of the selected orbits, e.g., orbit duration, capture and maneuver impulses, perturbations, etc.,
- (c) to assess the commonality of orbit/observable combinations.

An important initial step in the orbit selection process was grouping observables into measurement families

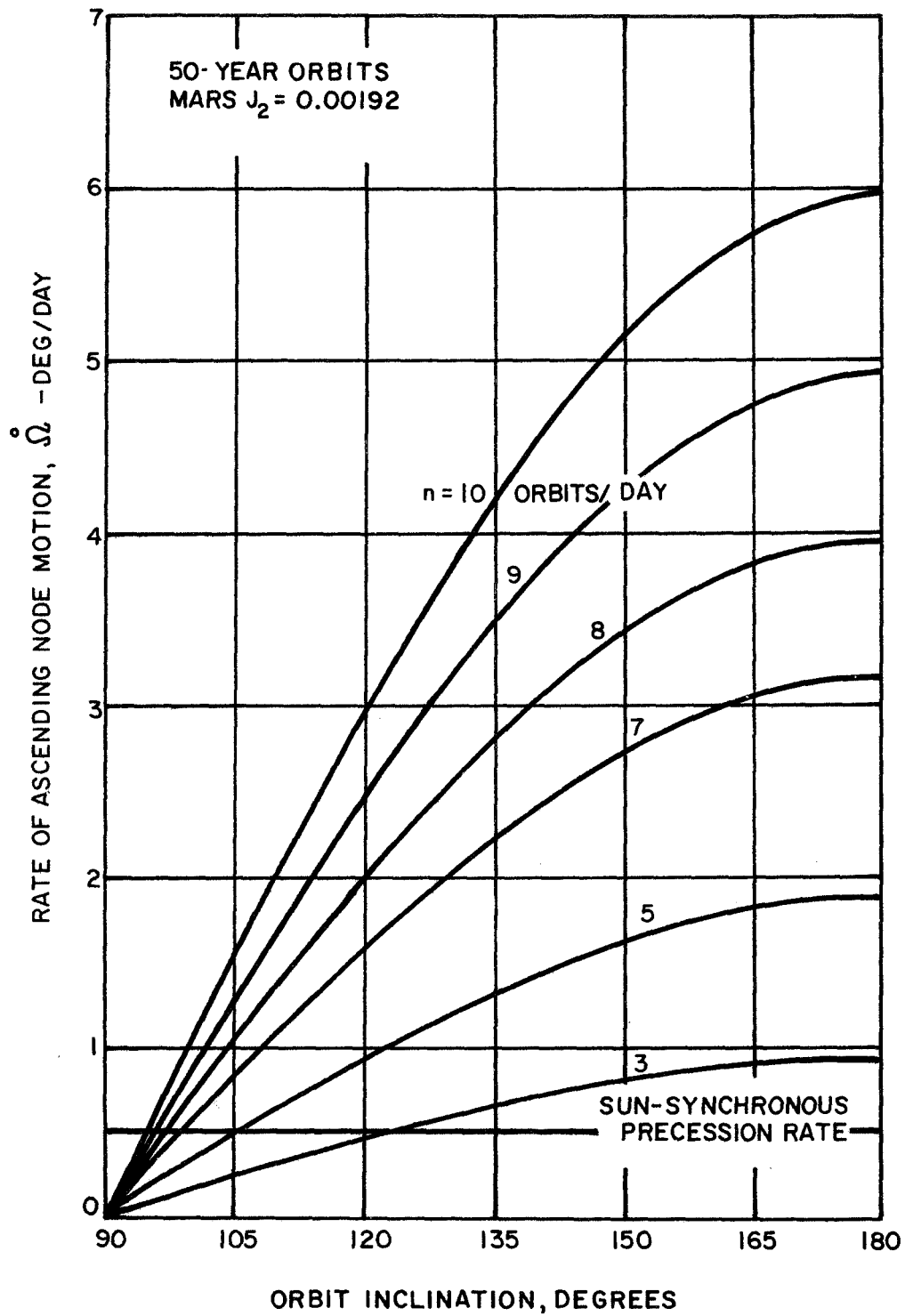


FIGURE 5-10. NODAL PRESSION DUE TO MARS OBLATENESS

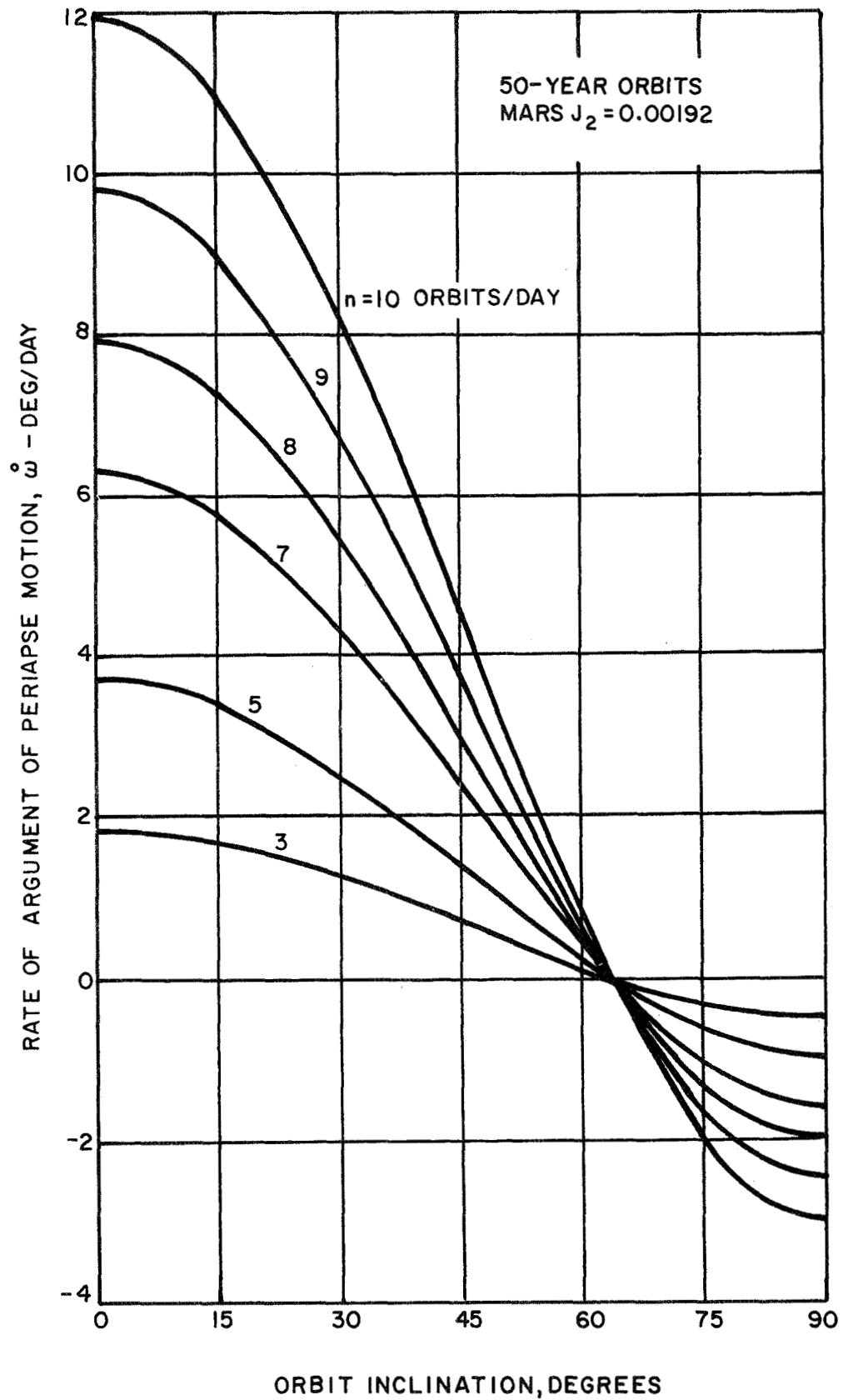


FIGURE 5-11. ARGUMENT OF PERIAPSE PRECESSION DUE TO MARS OBLATENESS

according to similar measurement specifications. This procedure (a) provides the first basis for commonality between orbits and observables, and (b) avoids redundant selections of orbits. The results of this grouping process are presented in Table 5-3. The composite measurement specifications given in the table use the most restrictive specifications from within each group of observable/imager combinations. Both Table 4-1 and the worth curves were used in constructing Table 5-3. The 34 groups are organized according to image size and overlap with the least demanding combinations coming first. Hence regional measurements of moderate resolution will be found near the top of the table, and detailed measurements with high resolution will be found at the bottom. All specifications in the table are taken into consideration in selecting orbits. Definitions for each specification, and the relation of the measurement families to individual observables and measurement specifications, are presented in Volume III of this report.

The length of time required to obtain 100% longitudinal coverage at the different image size/overlap combinations in Table 5-3 is presented in Table 5-4 for the selected candidate orbit periods. These are minimum times and do not reflect the fact that there must be an integer number of orbits per day in order to obtain contiguous coverage. In fact, in the actual process of orbit selection small variations were made in the candidate orbit size parameters, h_p and e , in order to obtain as nearly as possible the minimum image size and overlap specifications. Also, although the measurement families for local and detailed measurements (families 16-34 in Table 5-3) require only about 10% coverage or less, it is necessary to provide the same coverage capability as for the regional measurements in the absence of a priori information on the locations of coverages.

TABLE 5-3

MEASUREMENT FAMILIES FOR MARS

Family Number	Observable Number(s)	Sensor* Type(s)	Minimum Image Size (km)	Overlap (%)	Minimum Coverage (%)	Solar Elevation Range (deg)	Coverage Distribution	Time for Coverage	Image Interval	Coverage Interval
1	26	UV, V, MB	1000	20	70	Day	Poles	< 1 day	-	20/yr
2	24, 26	IR, μ , MB	1000	20	70	-	Poles	< 1 day	-	20/yr
3	1, 6, 9	V	600	60	70	70-85	-	-	-	-
4	1, 6, 9	R	600	60	70	-	-	-	-	-
5	3	IR	600	20	70	70-90	-	-	-	-
6	6, 12, 15	V	600	20	70	50-80	Mare, Poles	< 100 hr	< 1 day	> 4/yr
7	3, 18, 40	MB, V	600	20	70	30-60	-	-	< 2 hr	> 4/yr
8	1, 3, 6, 9, 12, 15	V, IR	600	20	70	15-30	Mare, Poles	< 100 hr	< 1 day	> 4/yr
9	27, 29, 33, 41	UV, V, MB	600	20	70	Day	Equator, Poles	-	< 15 min	> 4/yr
10	37	V	600	20	70	Night	Poles	-	< 2 hr	> 4/yr
11	1, 3, 6, 9, 12, 21	R, MB, IR, μ	600	20	70	-	Equator, Poles	-	< 30 hr	> 2/yr
12	27, 29, 30, 31, 33	IR, R, RF	600	20	70	-	Equator, Poles, Wave	-	< 2 min	> 10/yr
13	35	V	100	20	70	50-80	Poles, Wave	< 1 day	-	> 4/yr
14	35	V	100	20	70	30-60	Poles, Wave	< 1 day	-	> 4/yr
15	35	IR	100	20	70	-	-	< 1 day	-	-
16	7, 10	V	100	60	10	70-85	-	-	-	> 4/yr
17	7, 10	R	100	60	10	-	-	-	-	-
18	4	IR	100	20	10	70-90	-	-	-	-
19	7, 13, 16, 39	V	100	20	10	50-80	-	< 100hr	< 1 day	> 4/yr
20	4, 19, 39	V, MB	100	20	10	30-60	-	-	< 2 min	> 4/yr
21	4, 7, 10, 13, 16	V, IR	100	20	10	15-30	Mare, Poles	< 100 hr	< 1 day	> 4/yr
22	28, 34	UV, V, IR, MB	100	20	10	Day	-	-	< 2 hr	> 1/day
23	4, 7, 10, 13, 22, 25	R, IR, μ , MB	100	20	10	-	-	-	< 30 hr	> 2/yr
24	28, 32, 34	IR, RF	100	20	10	-	-	-	< 2 min	> 1/day
25	8, 11, 20	V	0.5	60	3	70-85	-	-	-	> 1/300hr
26	8, 11, 20	R	0.5	60	3	-	-	-	-	> 1/300hr
27	5	IR	0.5	20	3	70-90	-	-	-	-
28	8, 14, 18	V	0.5	20	3	50-80	-	< 100 hr	< 1 day	> 4/yr
29	2, 5	V, MB	0.5	20	3	30-60	-	-	-	-
30	5, 8, 11, 14, 17, 20	V, IR	0.5	20	3	15-30	-	< 100 hr	< 1 day	> 4/yr
31	2, 5, 8, 11, 14, 20, 23	R, IR, μ , MB	0.5	20	3	-	-	-	< 30 hr	> 1/300hr
32	38	V	0.3	60	-	70-85	Mare, Poles, Mountains	-	< 1 min	-
33	38	V	0.3	-	-	50-80	Mare, Poles, Mountains	-	< 1 min	-
34	38	V, MB	0.3	-	-	30-60	Mare, Poles, Mountains	-	< 1 min	-

* Sensor Type Definitions are:
 UV...Ultraviolet
 V...Visible
 IR...Infrared
 μ ...Microwave
 R...Radar
 RF...Radio Frequency
 MB...Multi-band

TABLE 5-4

MARS CANDIDATE ORBIT SIZE COVERAGE TIMES

Minimum Image Size (km)	% Overlap	Swath Width (km)	No. of Degrees Longitude	No. of Orbits To Cover Surface	Minimum Earth Days to Cover 360° Longitude									
					n=10	n=9	n=8	n=7	n=6	n=5	n=4	n=3	n=2	n=1
1000	20	800	13.56	27	2.6	2.9	3.3	3.8	4.4	5.2	6.5	8.7	13.1	26.2
600	20	480	8.14	45	4.4	4.9	5.4	6.2	7.3	8.7	10.9	14.6	21.9	43.7
600	60	240	4.07	89	8.7	9.6	10.8	12.3	14.4	17.3	21.6	26.8	43.3	86.5
100	20	80	1.36	266	25.9	28.8	32.4	36.9	43.1	51.7	64.6	86.1	129	259
100	60	40	0.68	531	51.6	57.3	64.5	73.7	86	103	129	172	258	516

The individual orbit selections for the families in Table 5-3 are presented in moderate detail on orbit selection data sheets in Volume III to the report. Those results are summarized here as follows, first for low and medium resolution experiments (families 1-24):

- (a) Most measurement families could be satisfied with either elliptical or circular orbits with periods less than one Mars day and orbit durations of less than 60 days.
- (b) Some measurements which are restricted to high solar elevation angles require extended orbit durations of 100-250 days in order to increase the amount of coverage by taking advantage of the Sun's latitude motion across the Mars surface.
- (c) Circular orbits tend to provide greater amounts of coverage at lower altitudes in less time while elliptical orbits require less capture impulse.
- (d) Polar or near polar orbits are used to avoid redundant imaging and obtain the maximum available coverage; inclinations less than or greater than 90° are used only to maintain Sun-synchronous orbits, or to reach an area of restricted solar elevations without a plane change.
- (e) Approximately half of the families require only a single coplanar periapse capture maneuver,
- (f) A coplanar capture maneuver followed by plane change and orbit size adjustment maneuvers is required by the majority of the solar elevation restricted families for one or more of the following reasons: (1) high solar elevation

limits (e.g. 70-90°) provide only a small measurement area which is inaccessible to polar type orbits using only a coplanar periapse capture, (2) Sun-synchronous orbits must be established at a specific point in the restricted area to provide sufficient time to obtain local coverage detail or observe seasonal changes and (3) for the 1988 Type I transfer the approach direction is along the Mars equator, but about 110° from the subsolar point, making polar type orbits inaccessible to most restricted areas of solar elevation with only a coplanar capture.

- (g) Off-periapse insertion maneuvers are required with 1988 Type I transfer arrival conditions and elliptical orbit selections, in order to obtain solar elevation restricted coverage at minimum altitudes since approach is from the day side of the planet, placing the periapse of polar or near-polar orbits in darkness.
- (h) Maximum total impulse requirement is less than 3 km/sec.
- (i) Most frequent measurement specifications not achieved are image repetition rate (the rate at which images of the same object are to be repeated) and percent surface coverage of solar elevation restricted measurements.

For high resolution experiments (families 25-34), where no a priori information is known about the locations of coverage, the orbits selected are summarized as follows:

- (a) Specific orbit selections are not possible because of lack of information.

- (b) Orbit durations will probably be longer than 60 days, particularly if the areas of interest are dispersed.
- (c) Multiple orbit impulses in excess of three in number and 3 km/sec in magnitude may be required to move from one location to the next rapidly and still be able to collect high resolution data within each area.

5.2 Venus

5.2.1 Interplanetary Transfer Selections

The same guidelines and selection methodology used in selecting Mars transfers were used for Venus. Earth-Venus transfer opportunities have very nearly repetitive characteristics every sixth opportunity, or eight years. Minimum VHT (sum of hyperbolic excess speeds at Earth and Venus) Type I and Type II transfers within five opportunities over the period 1975-1981 were considered as a selection base. The values of the geocentric departure asymptote, δ_o , for these transfers in no case exceeded 45° , the maximum value which avoids serious launch safety problems.

The six best transfers (minimum VHT) from this group are listed in Table 5-5. Both type transfers are presented for the 1975 opportunity, since they are too similar to indicate a preference. Note that these preferred transfers are equally split between Type I and Type II for the five opportunities considered.

The arrival parameters considered in making the final transfer selection, which are presented in Table 5-5, were VHP, δ_ϕ , ρ_o and DTC.* The transfer chosen was the 1977

*These and other arrival parameters in the table are defined on page 135 of the Mars transfer selection discussion.

TABLE 5-5

SUMMARY OF MINIMUM VHT VENUS TRANSFERS: 1975 - 1981

Launch Date (Min. VHT)	Type	Flt. t _{ym} (Days)	δ_{\oplus} (deg)	VHI (KPS)	VHP (KPS)	VHT (KPS)	δ_{\ominus} (deg)	ρ_{\ominus} (deg)	θ_{\oplus} (deg)	R _c (AU)	DTC (Days)
Jun 8, 1975	I	144	10.3	2.50	3.55	6.05	-37.89	100.20	94.03	0.63	231
Jun 1, 1975	II	152	6.3	2.42	3.49	5.91	-36.10	102.27	93.79	0.64	231
Jan 10, 1977	I	127	0.5	2.75	4.39	7.14	36.87	53.43	112.61	0.48	250
Aug 22, 1978	I	111	-0.7	2.93	5.26	8.19	-32.26	43.16	120.58	0.40	257
Mar 17, 1980	II	179	42.6	3.08	5.11	8.19	-34.18	133.97	78.89	0.85	207
Nov 10, 1981	II	156	-17.2	2.74	4.33	7.07	31.10	131.82	82.90	0.79	203

- Type I. The arrival conditions are characterized by
- (a) an intermediate asymptotic approach velocity,
 - (b) periapse locations which favor the northern hemisphere,
 - (c) an approach from the dark side with orbit periapse locations favoring the sunlit side, and
 - (d) as for all transfers, the time to superior conjunction with Earth is about one Venus revolution about the sun.

With the exception of ρ_{\odot} , the 1977 Type I arrival conditions are typical of all values presented in Table 5-5. It is difficult to select a single transfer which typifies all approach directions (ρ_{\odot} 's) encountered. For values of ρ_{\odot} greater than 90° , the approach is just opposite to that described above, i.e., from the sunlit side with orbit periapse favoring the dark side. It would be necessary to select another transfer to represent this case. This was not done. Rather it was confirmed that values of ρ_{\odot} greater than 90° only affect the orbit duration and sequence in which coverage is obtained, but otherwise do not influence the experiment definitions or subsystems and operational requirements.

Contours of insertion occultation for the 1977 Type I transfer are presented in Figure 5-12 mapped on the hyperbolic impact plane. Occultation contours with minimum near limb angles of 5° and 0° are shown for Sun, 0° for Earth, and 20° and 0° for the star Canopus. The relation between the aiming angle θ and orbit inclination and orbit ascending node in the Venus equatorial system are given in Figure 5-13.

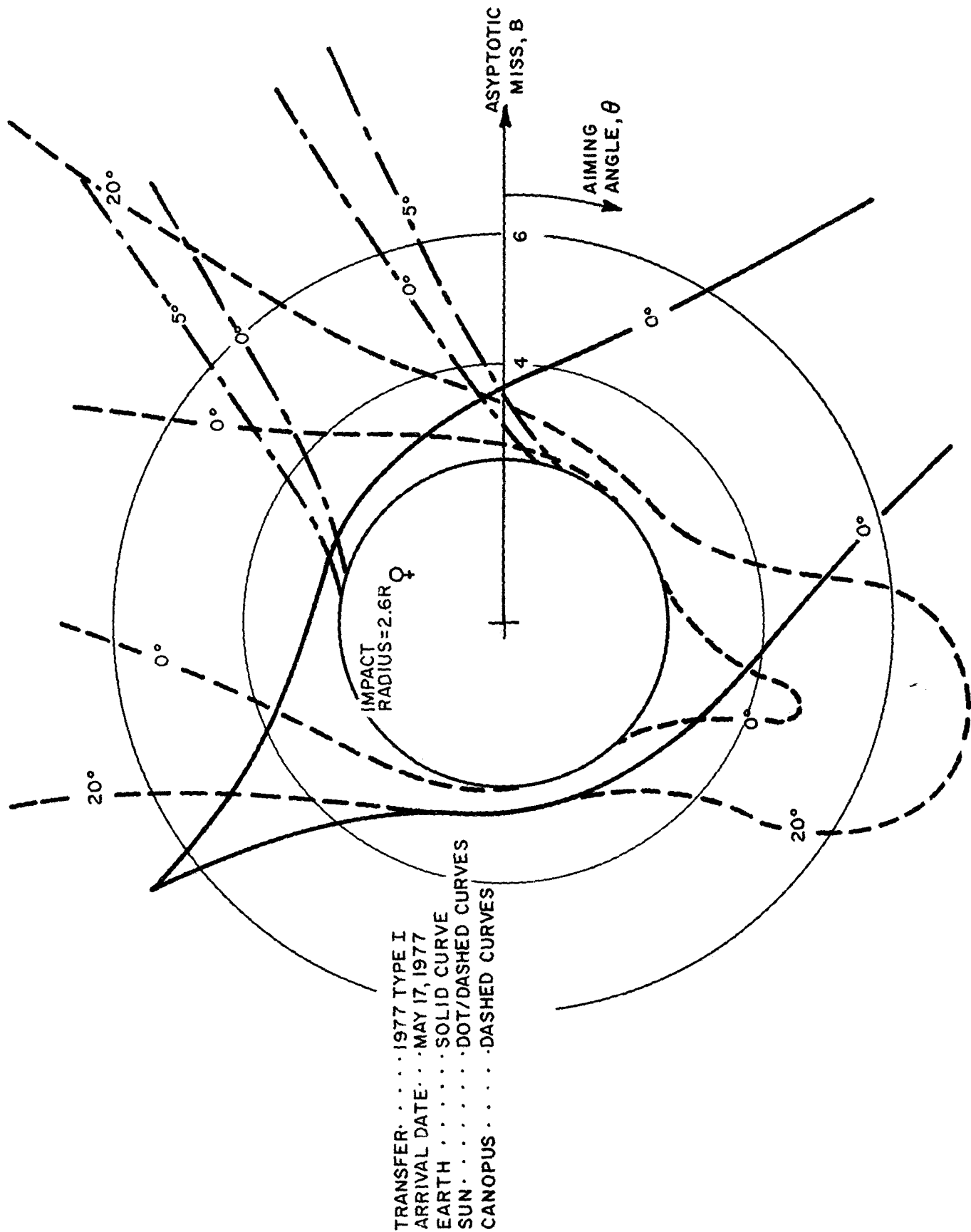


FIGURE 5-12. VENUS CAPTURE OCCULTATION CONTOURS

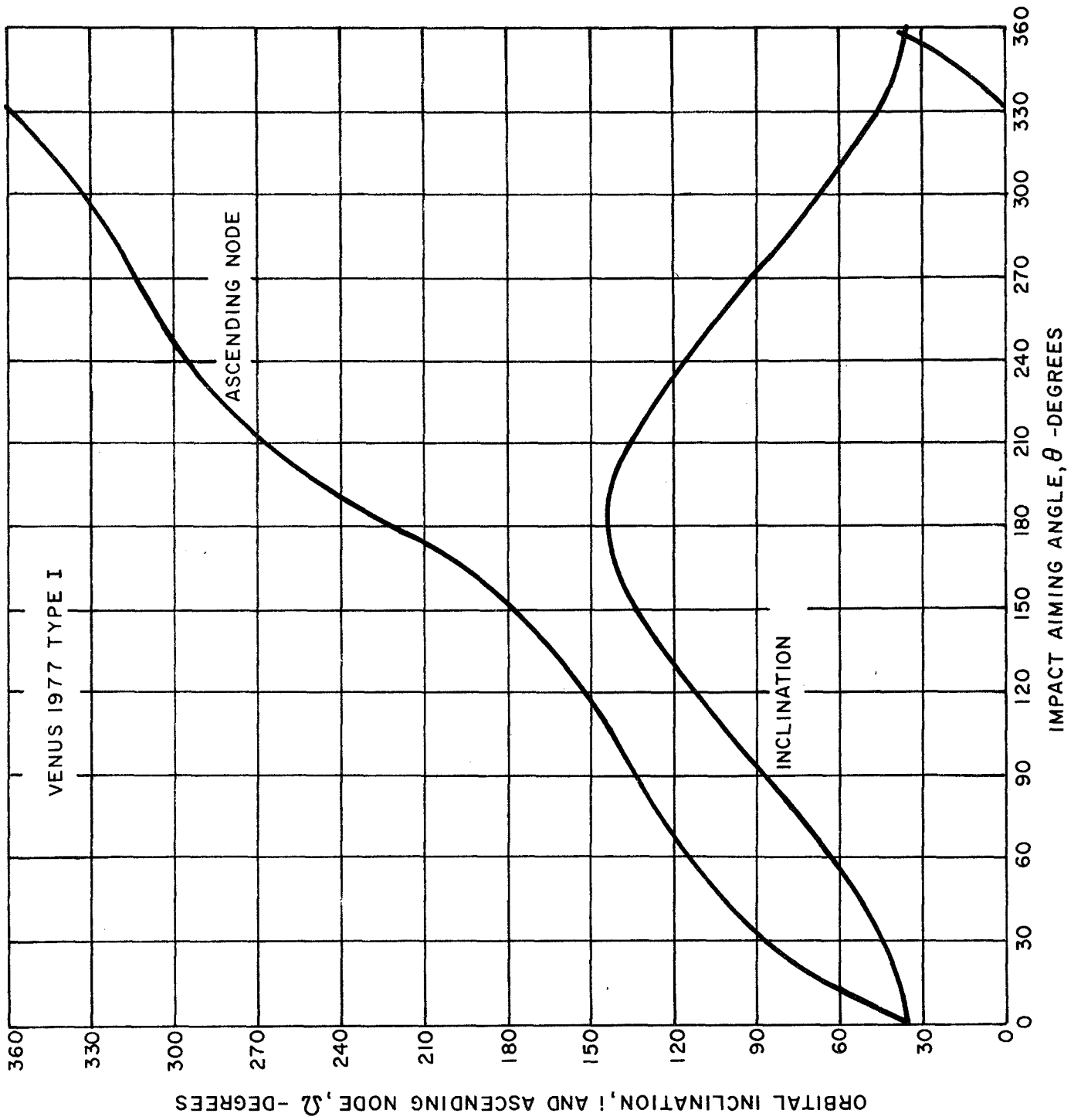


FIGURE 5-13. VENUS AIMING ANGLE/ORBIT ORIENTATION RELATIONSHIP

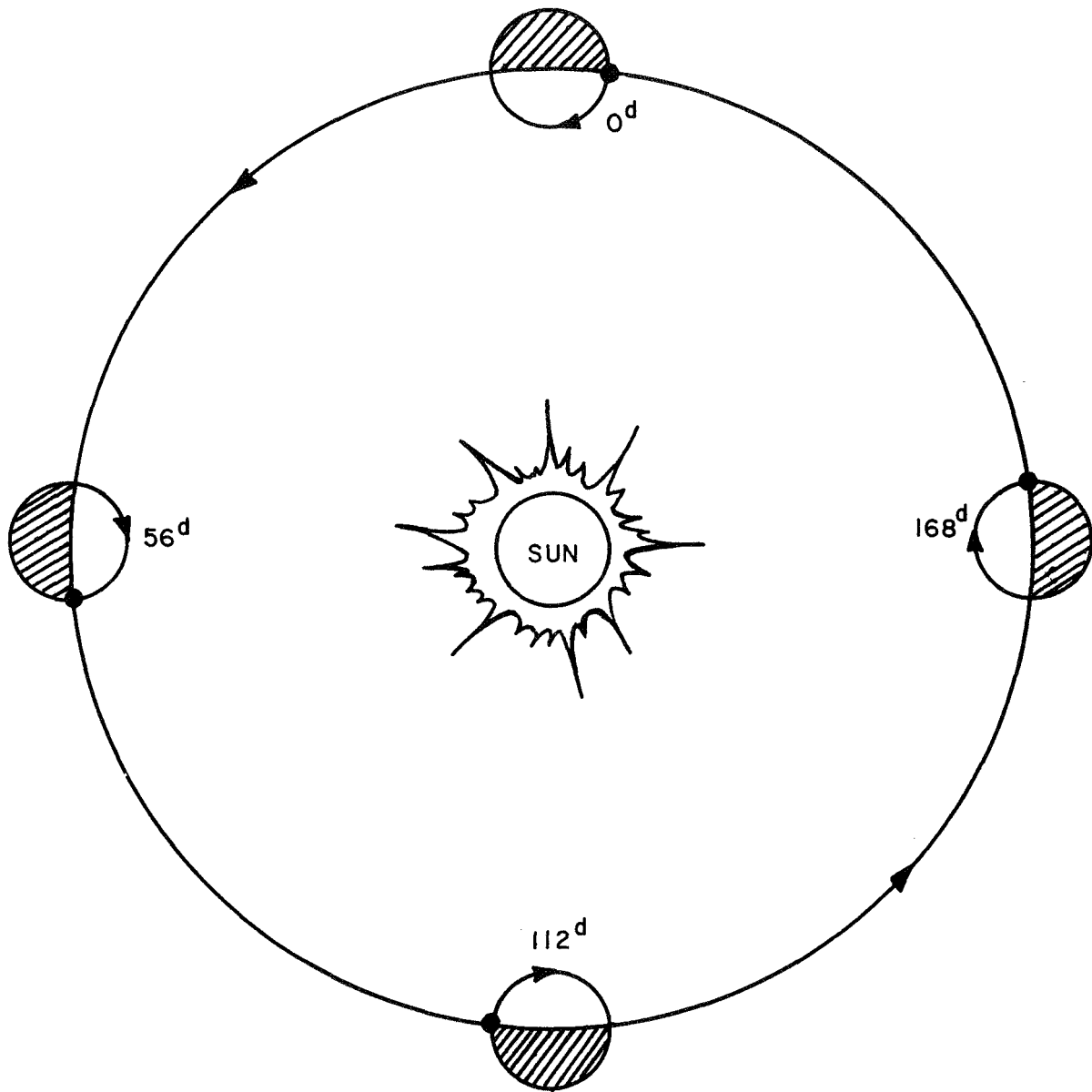
5.2.2 Orbit Characteristics and Constraints (Venus)

Orbital or flyby imagery has, to date, been studied and used for investigation of Earth, Mars, and the Moon. All of these bodies have transparent or nonexistent atmospheres and reasonably rapid rotation rates, factors which obviously enhance orbital imagery. In contrast, Venus has a slow retrograde rotation of about 243 days/rotation and an optically opaque atmosphere. Hence, one expects Venus imagery from orbit to be characterized by longer mission times and different imaging systems (particularly radar) than have been common to previous orbital missions.

The relationship between Venus' inherent rotation and its revolution about the sun is graphically illustrated in Figure 5-14. The relative motion of a fixed point on the surface with respect to the Sun is about 3 deg/day resulting in a Venus day of approximately 120 Earth days. The potential orbital coverage characteristics which result from this motion are itemized in Table 5-6, considering both inertial and sun-synchronous orbits. A geometrical definition of minimized altitude coverage is illustrated in Figure 5-15. Minimized altitude coverage is defined as coverage from polar orbits with periapse at the planet equator and measurement arcs ≤ 180 degrees centered at periapse. The constraints of daylight coverage infers no specific elevation angle, just daylight. This is consistent with daylight investigations of Venus which are limited to atmospheric phenomena, where specific illumination conditions are usually not required.

Several conclusions can be drawn about orbital coverage from Table 5-6:

- a. Circular orbits provide coverage in the shortest time if measurement altitudes are restricted.



RATES OF MOTION

TERMINATOR	1.6 DEG/DAY
SURFACE	-1.48 DEG/DAY
RELATIVE	3.08 DEG/DAY

VENUS DAY \approx 120 EARTH DAYS

FIGURE 5-14. VENUS ROTATION/REVOLUTION RELATIONSHIP

TABLE 5-6

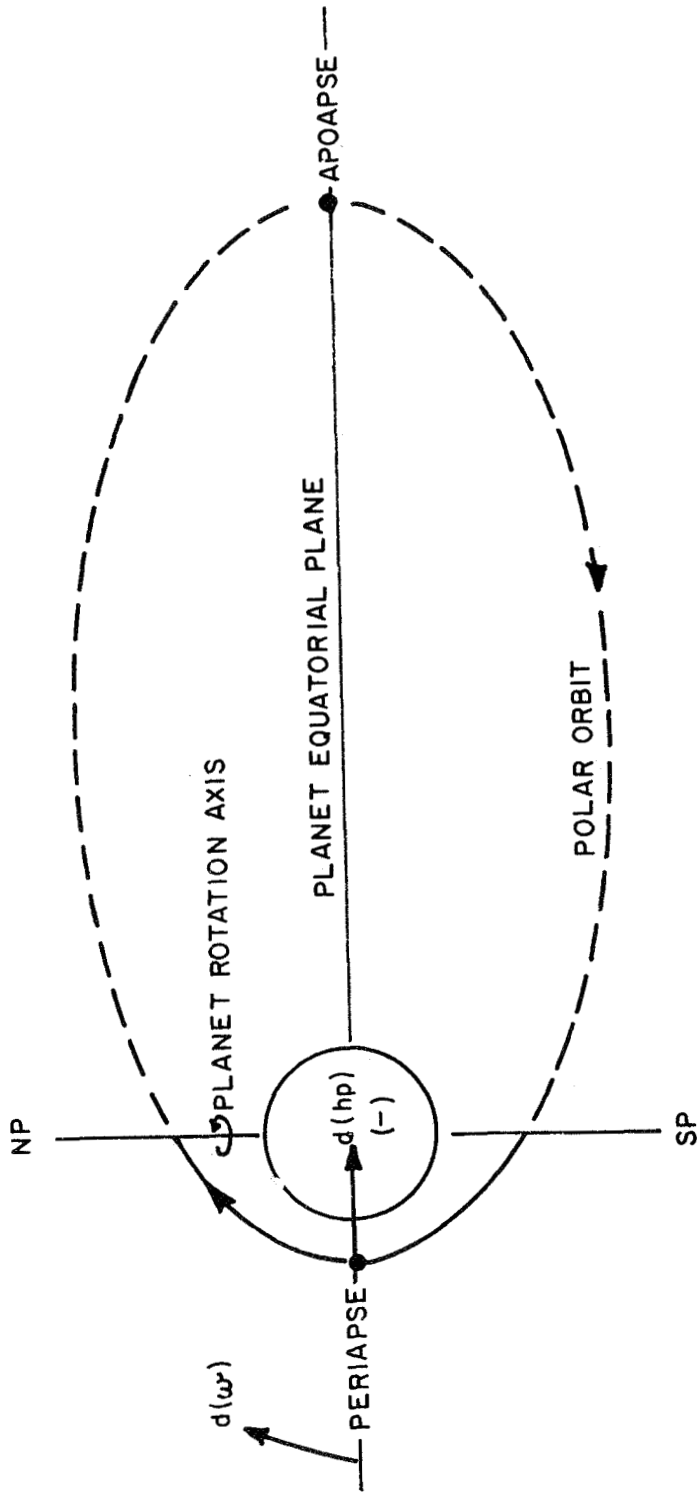
POTENTIAL VENUS ORBIT COVERAGE CHARACTERISTICS

- INERTIAL ORBITS, NO LIGHTING CONSTRAINTS:
 - 100% LONGITUDE COVERAGE POSSIBLE
 - IN 120 DAYS IF ALL ORBIT ALTITUDES ARE USED
 - IN 240 DAYS IF MINIMIZED ALTITUDE COVERAGE IS EMPLOYED

- INERTIAL ORBITS, DAYLIGHT COVERAGE CONSTRAINT:
 - APPROXIMATELY 50% COVERAGE POSSIBLE
 - IN 112 DAYS IF ALL ORBIT ALTITUDES ARE USED
 - IN 224 DAYS IF MINIMIZED ALTITUDES COVERAGE IS EMPLOYED (THIS INCLUDES A 112-DAY 'NO-DATA' WAITING PERIOD)
 - NO FURTHER DAYLIGHT COVERAGE IS OBTAINED UNLESS A PLANE CHANGE (90° FOR REMAINING 50% LONGITUDE COVERAGE) IS MADE IN THE ORBIT ASCENDING NODE

- SUN-SYNCHRONOUS ORBITS:
 - 100% LONGITUDE COVERAGE IN 116 DAYS AT CONSTANT SOLAR ELEVATION ANGLE AND MINIMUM ALTITUDES

IIT RESEARCH INSTITUTE



- ORBIT ARC FOR MINIMIZED ALTITUDE COVERAGE
- $d(\text{hp})$ SECULAR PERIAPSE ALTITUDE SOLAR PERTURBATION
- $d(\omega)$ SECULAR ARG. OF PERIAPSE SOLAR PERTURBATION

FIGURE 5-15. BASIC ORBIT DEFINITIONS

- b. Only about half of the planet is covered in daylight with an inertial orbit, regardless of the stay time.
- c. Sunsynchronous orbits would provide 100 percent longitudinal daylight coverage, and do so most rapidly for measurement altitude restricted elliptical orbits.

Potential orbit sizes for Venus imagery were constrained to have a lifetime of equal to or greater than 50 years considering only atmospheric drag. The 50-year orbit lifetime curve (Lockheed 1968) for Venus is presented in Figure 5-16. The very slow rotation of Venus makes it easily possible to obtain contiguous images on consecutive orbits. In fact, for large images (> 1000 km) and tight orbits (circular), measurements can be separated by more than 100 orbits still satisfying a contiguous imaging requirement. Therefore, rather than relating the candidate orbit size selection to imaging requirements, a range of orbit eccentricities of 0 to 0.9 was used to represent as broad a range in orbits as possible.

Ten candidate orbit sizes and related data are presented in Table 5-7. The periapse altitude for each eccentricity was determined from the 50-year lifetime curve in Figure 5-16. The maximum orbit altitude ratio, h/h_p , increases rapidly with larger values of eccentricity. Figure 5-17 illustrates the relation of measurement arc (twice the angle from periapse) to eccentricity for maximum measurement altitude ratios of $h/h_p = 2, 5, \text{ and } 10$. Considering minimized altitude coverage as described in Figure 5-15 (angle from periapse = 90°), it is seen from Figure 5-17 that the limiting eccentricities for maximum measurement altitude ratios of 2, 5, and 10 are 0.055, 0.193, and 0.405, respectively.

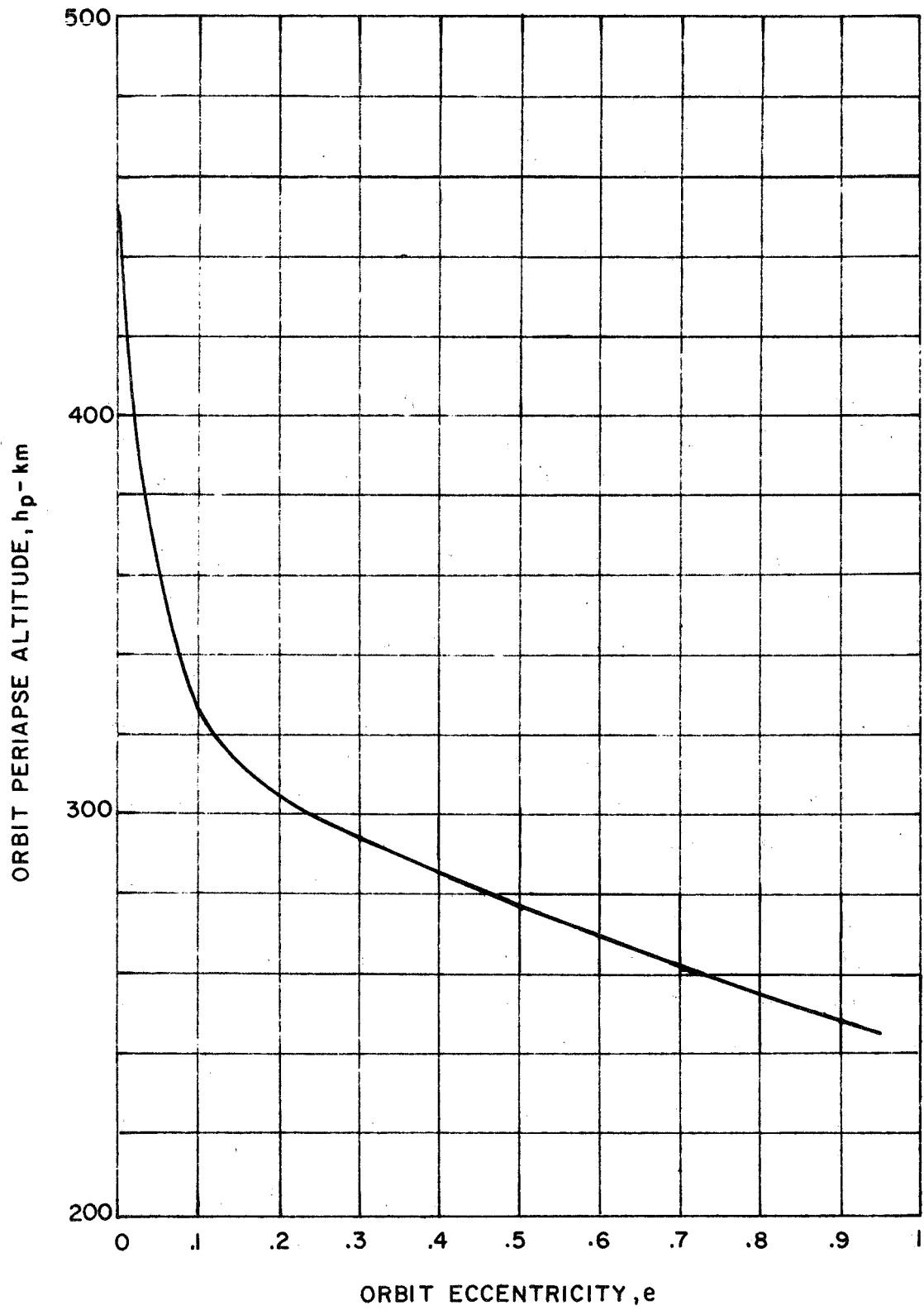


FIGURE 5-16. VENUS 50-YEAR LIFETIME ORBITS

TABLE 5-7

VENUS CANDIDATE ORBIT SIZES

Orbit No.	Eccentricity	Periapse Altitude (km)	Maximum Altitude Ratio, h/hp	Orbit Period (hrs)	Lapse Rate Per Orbit (km)	Average* Capture ΔV (km/sec)
1	0.0	454	1.0	1.608	10.5	3.902
2	0.1	327	5.3	1.829	11.9	3.574
3	0.2	305	11.4	2.171	14.2	3.244
4	0.3	294	19.5	2.645	17.2	2.925
5	0.4	285	30.7	3.326	21.7	2.618
6	0.5	277	46.7	4.364	28.5	2.321
7	0.6	269	71.5	6.087	39.7	2.033
8	0.7	261	113.9	9.354	61.0	1.754
9	0.8	255	199.0	17.160	111.9	1.483
10	0.9	248	458.5	48.456	316.0	1.219

* Capture ΔV Based on a Surveyed Average Hyperbolic Approach Speed, $V_{HP} = 4.52$ km/sec.

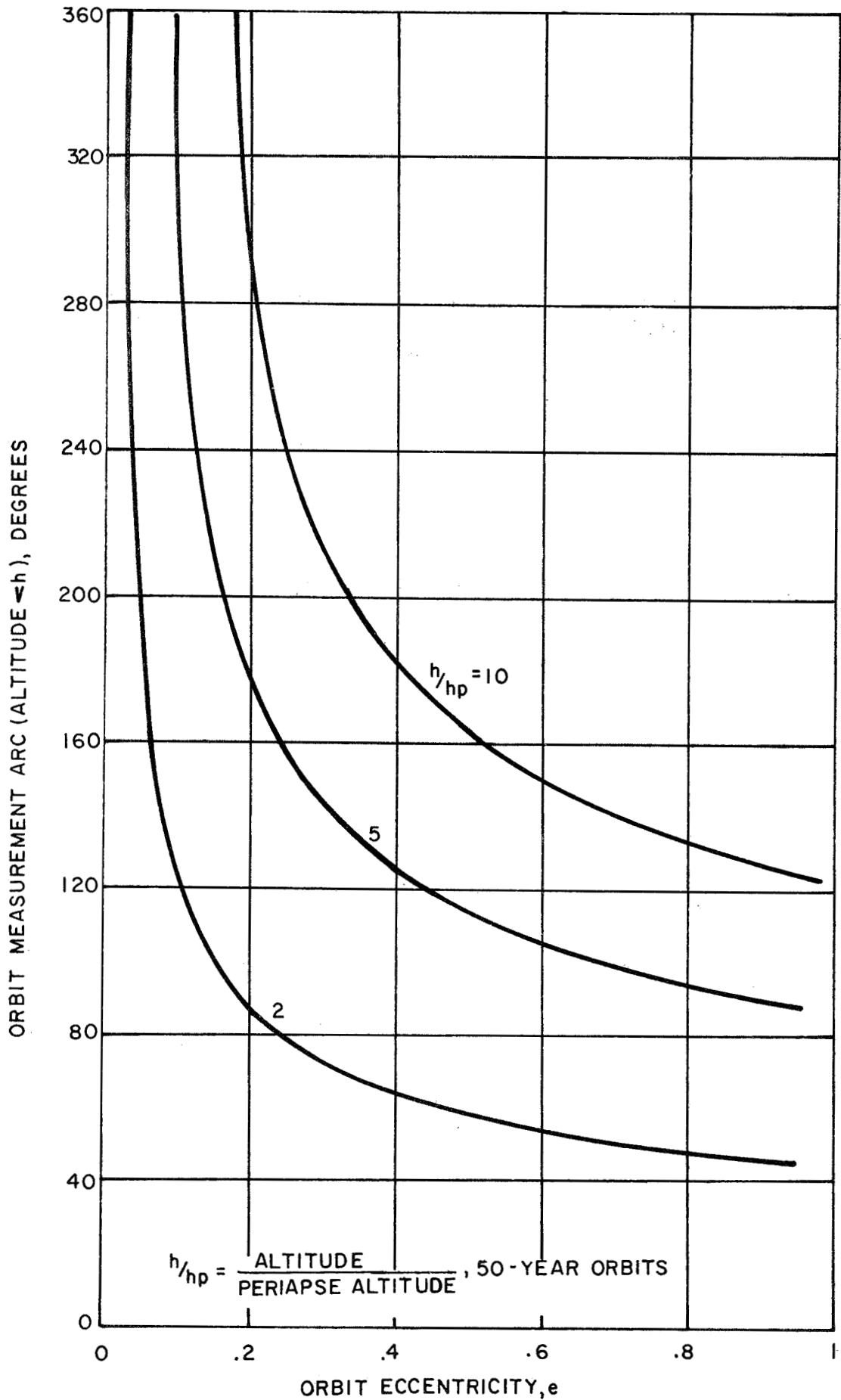


FIGURE 5-17. VENUS ORBIT ALTITUDE RATIOS

The last column in Table 5-7 lists the average capture impulses required to establish the candidate orbit sizes, using a coplanar periapse capture maneuver and assuming a hyperbolic approach speed (VHP) of 4.52 km/sec averaged from the VHP data presented in Table 5-5. The difference in capture impulse between the circular orbit and the $e = 0.9$ elliptical orbit is 2.683 km/sec, which gives the highly elliptical orbit a considerable weight savings advantage.

One of the coverage characteristics presented in Table 5-6 is that only about 50 percent of Venus can be covered in daylight from an inertial orbit. To obtain complete daylight coverage requires a plane change of approximately 90 degrees in the orbit ascending node. The total impulse required to do this is presented in Figure 5-18 for the candidate orbit sizes. Two plane change techniques were considered, assuming that the initial orbit had an inclination of 90 degrees and periapse was at the equator (as shown in Figure 5-15). The maneuvers for the solid curve in the figure are:

- a. adjustment to a large elliptical orbit of the same periapse but apoapse equal to 119,757 km^{*},
- b. a 90° plane change at apoapse to a circular equatorial orbit of radius 119,757 km,
- c. a 90° plane change back to the large elliptical orbit 90° later
- d. adjustment back to the original orbit size.

The maneuvers for the dotted curve are:

- a. transfer to a large eccentricity orbit at the pole with a periapse equal to the radius at the pole and an apoapse of 119,757 km,

* This is the apoapse radius of the $e = 0.9$ candidate orbit which eliminates this and the last maneuver of this sequence for that orbit size.

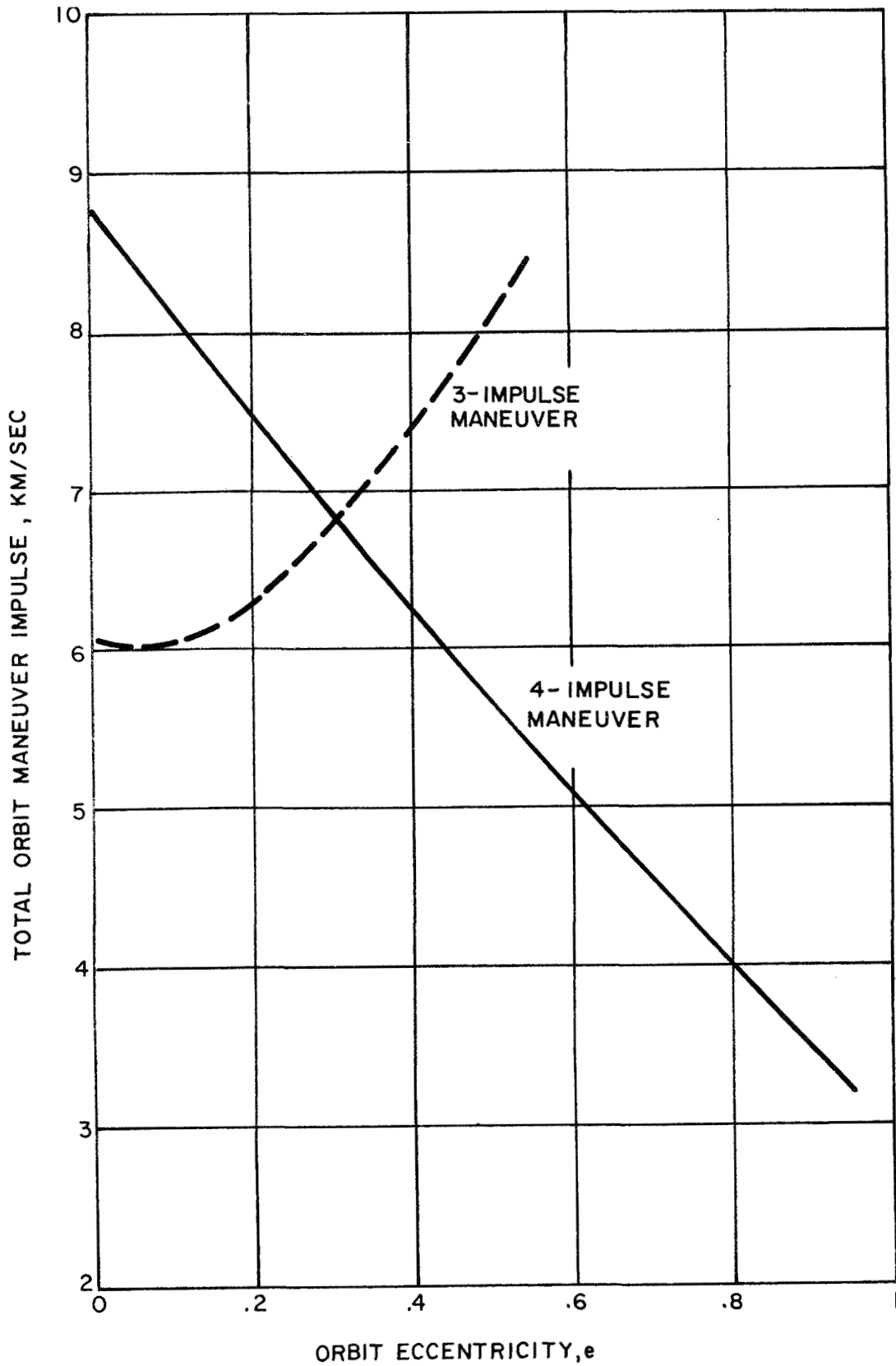


FIGURE 5-18. VENUS IMPULSE REQUIREMENTS FOR COMPLETE DAYLIGHT COVERAGE.

- b. a 90° plane change at apoapse of the new orbit,
- c. a transfer back to the initial orbit size similar to the first impulse.

From Figure 5-18, even at an initial orbit eccentricity of 0.9, the added impulse requirement of 3.5 km/sec appears to be a costly penalty for obtaining more than 50 percent coverage of Venus' cloud tops in daylight. It should be pointed out that no effort was made to determine how efficient the maneuver policies used in Figure 5-18 are. Hence, this conclusion could change if significantly better techniques of changing the orbit plane are found.

The coverage characteristics cited in Table 5-6, for inertial orbits, do not consider orbit perturbations. For Venus two sources of perturbations are considered: a) the Sun's mass, and b) planetary oblateness. Taking the Sun's mass first, and considering just polar orbits (best latitude coverage), results for the secular rate of change in periapse altitude, $d(h_p)$, and argument of periapse, $d(\omega)$ are presented in Figures 5-19 and 5-20.* $d(h_p)$ is shown in Figure 5-19 as a function of orbit eccentricity for three values of ω . $d(h_p)$ is symmetric about $\omega = \frac{\pi}{4}$, and symmetric in magnitude about $\omega = \frac{\pi}{2}$, but with a change in sign. Hence values of $d(h_p)$ are repeated every n , where $n = 1, 2, 3, \dots$. Maximum values of $d(h_p)$ are found at $\frac{n\pi}{4}$, where $n = 1, 3, 5, \dots$

The secular rate of change in the argument of periapse, $d(\omega)$, shown in Figure 5-20 as a function of ω for values of eccentricity between 0.5 and 0.9, is symmetric about $\omega = \pi$. Although the magnitudes of $d(\omega)$ are very small, they are important in two respects. First, $d(\omega)$ reaches a maximum value at $\omega = 0$, where $d(h_p)$ changes sign. This is also a desirable value of ω for elliptical orbit imaging (i.e.,

* See Figure 5-15 for geometric definitions of $d(h_p)$ and $d(\omega)$.

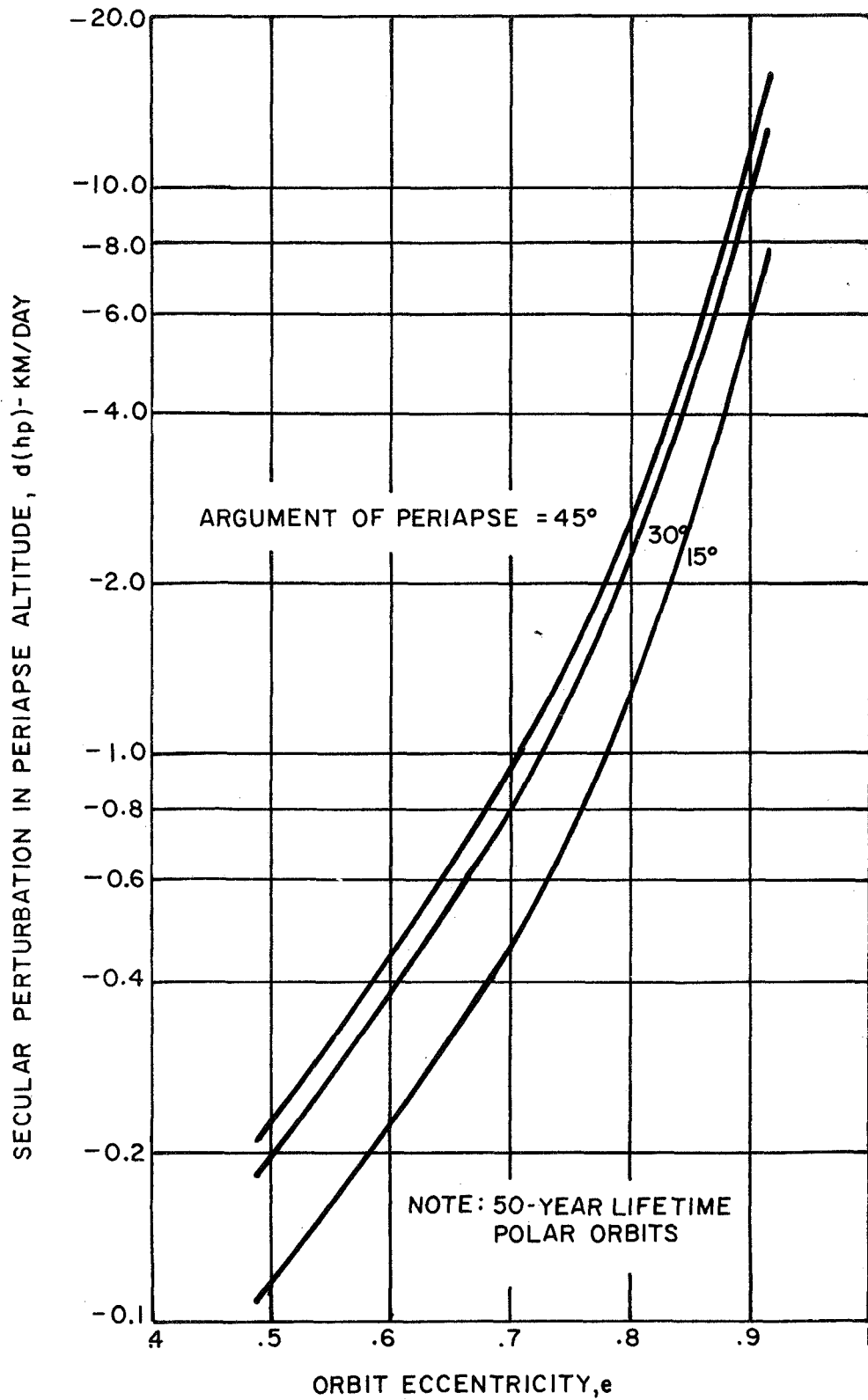


FIGURE 5-19. VENUS ORBIT SOLAR PERTURBATIONS: ALTITUDE.

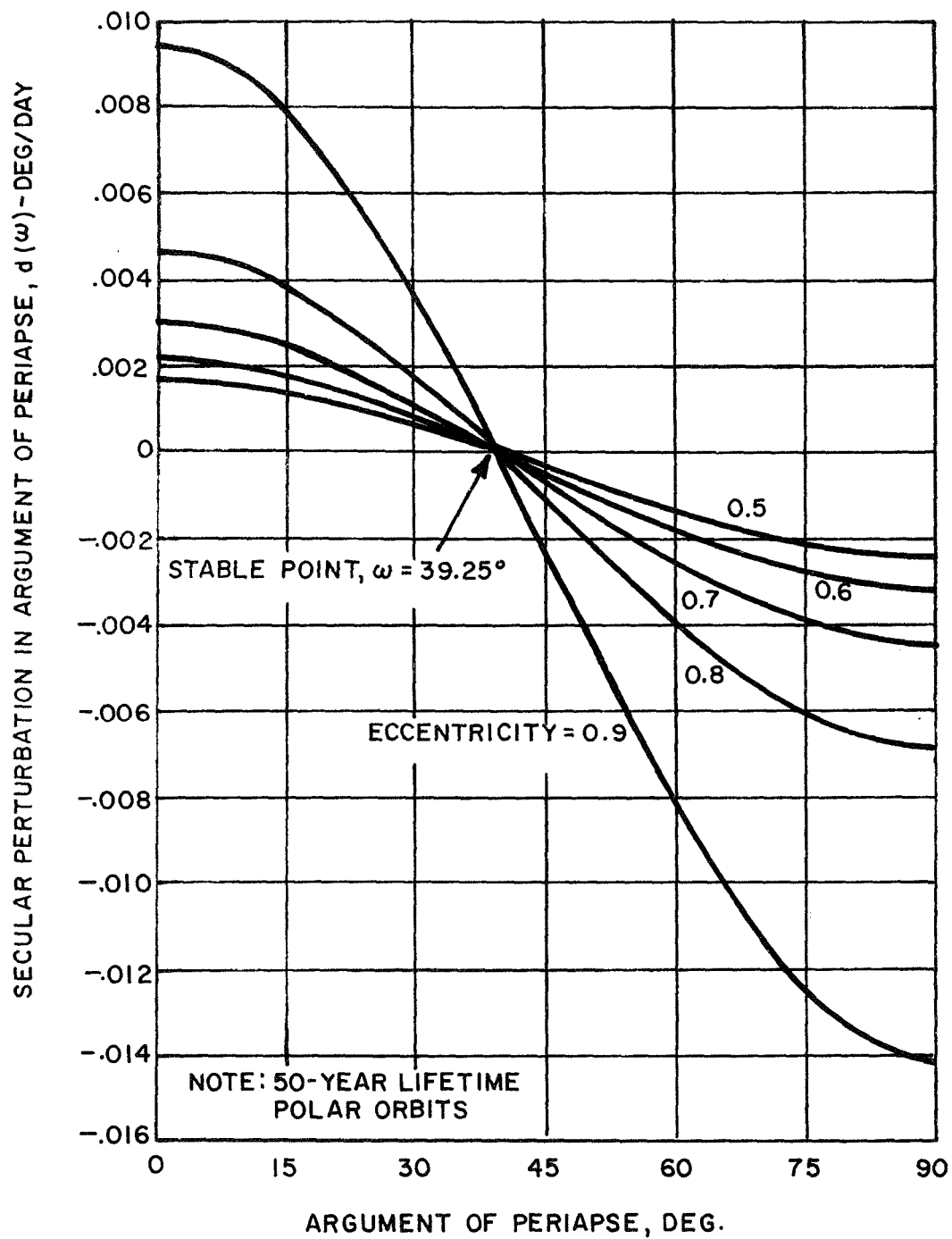


FIGURE 5-20. VENUS ORBIT SOLAR PERTURBATION: ARGUMENT OF PERIAPSE.

minimized altitude coverage). Knowing the length of orbit duration, ω can be set to a slightly negative value such that solar perturbations move it slowly to zero and then to positive values. In this way $d(h_p)$ is first positive and then negative, allowing the periapse altitude to first increase and then decrease. With the proper initial selection of ω , minimized altitude coverage can be accomplished from highly eccentric orbits without h_p ever falling below a specified value over long orbit durations (i.e., on the order of 250 days).

The second interesting aspect about Figure 5-20 is that the secular portion of $d(\omega)$ always moves ω toward a point of "stability" which for polar orbits exists at 39.25° . However, since $d(\omega)$ approaches 0 as ω approaches 39.25° , an infinite time is required to reach this point from an arbitrary starting point in ω . Also other perturbations, such as Venus oblateness, will affect this behavior as ω gets close to its "stable" value. The important conclusion which can be drawn from these results is that the control of altitude variations caused by solar perturbations is critically dependent upon the initial selection of the orbit argument of periapse.

The second source of perturbations, i.e., oblateness, is incidental for Venus. Tracking data from the recent Mariner V mission (Efron, 1968) indicates a second zonal harmonic for Venus of

$$J_2 = (8.4 \pm 0.4) \times 10^{-6}$$

The maximum rate of nodal regression which can be obtained from this value is 0.0474 deg/day, using the circular candidate orbit and a minimum inclination of about 35 degrees.

The coverage characteristics of sun-synchronous orbits greatly improves the daylight coverage capability of Venus orbits. However, with the very small value of J_2 for Venus,

the maximum possible nodal regression of 0.0474 deg/day is far less than the 1.6 deg/day required to maintain sun-synchronization. Active control systems for maintaining this regression rate were investigated and found to be unreasonable. For a 474 km circular polar orbit, a low thrust system would have to generate an acceleration of more than 3.5×10^{-4} g's. An impulsive form of controlling this same orbit would require about 13 m/sec per orbit, or a total of 23 km/sec for a 116 day orbit duration (100 percent coverage). Based on these preliminary considerations, sun-synchronous orbits do not appear to be feasible for Venus.

5.2.3 Orbit Selections (Venus)

Once the characteristics of orbital coverage and perturbations were understood, it was possible to proceed with the orbit selections in much the same manner that was done for Mars. The measurement families for which orbit selections were made are presented in Table 5-8. Orbit selections were limited to polar orbits, since this at least maximizes the latitudes covered and no apparent reasons emerged in favor of any other inclinations. A stereographic projection using the 1978 Type I transfer arrival conditions was prepared. The two known surface roughness features alpha and beta (Koenig et al. 1967) were located on the projection for coverage consideration.

The candidate circular orbit of 474 km altitude was applied to every observable grouping. Highly elliptical ($e = 0.8$ or 0.9) orbits were also selected for regional observable groups to dramatize the differences in measurement altitude, stay time, coverage, and capture impulse, compared to circular orbits. These elliptical orbit selections also provide examples of the effects of solar perturbations upon orbit stability and how these effects change the selection of the initial orbit orientation. The orbit selection results for Venus imaging experiments are summarized as follows:

TABLE 5-8

MEASUREMENT FAMILIES FOR VENUS

Family Number	Observable Number(s)	Sensor* Type(s)	Minimum Image Size (km)	Overlap (%)	Minimum (%)	Solar Elevation Range (deg)	Coverage Distribution	Time for Coverage	Image Interval	Coverage Interval
1	24	IR, μ , MB	1500	20	70	-	-	-	-	> 2/yr
2	26	IR	1500	20	70	-	-	< 100 hr	-	> 10/yr
3	26	UV, V	1500	20	70	Day	-	< 100 hr	-	> 10/yr
4	26	MB	1500	20	70	Day&Night	-	< 100 hr	-	> 10/yr
5	1, 3, 6, 9, 12, 21	R, μ , MB	1000	20	70	-	-	-	< 30 hr	-
6	1, 6, 9	R	1000	60	70	-	-	-	-	-
7	27, 29, 30, 33, 35	IR, μ , R	500	20	70	-	Equator, Poles	< 100 hr	< 15 min	> 4/yr
8	31	RF	500	20	70	-	-	-	< 2 min	> 10/yr
9	27, 29, 33, 40	UV, V, IR, MB	500	20	70	Day	Equator, Poles	-	-	> 4/yr
10	29, 33	MB	500	20	10	Day&Night	Subsolar, Poles	-	< 15 min	> 4/yr
11	37	V	500	20	70	Night	Poles	-	< 30 hr	> 4/yr
12	4, 7, 10, 13, 22, 25	R, μ , MB, IR	100	20	10	-	-	-	< 30 hr	-
13	28, 34, 39	R, IR, μ	100	20	10	-	-	-	< 2 hr	> 4/yr
14	32	RF	100	20	10	-	-	-	< 2 min	> 10/yr
15	28	UV, V	100	20	10	Day	-	-	< 100 hr	-
16	34	V, IR	100	20	10	Day	-	-	< 2 hr	> 4/yr
17	34	MB	100	20	10	Day&Night	-	-	< 2 hr	> 4/yr
18	7, 10	R	100	60	10	-	-	-	-	-
19	2, 5, 8, 11, 14, 20	R	0.5	20	10	-	-	-	-	> 1/300hr
20	23	μ , MB	0.5	20	10	-	-	-	< 30 hr	-
21	8, 11, 20	R	0.5	60	10	-	-	-	-	> 1/300hr
22	38	R	0.3	-	5000	-	Mountains, Poles	-	< 1 min	-
23	38	R	0.3	60	Images	-	Mountains, Poles	-	< 1 min	-

* Sensor Type Definitions are:
 UV...Ultraviolet
 V....Visible
 IR....Infrared
 μMicrowave
 R....Radar
 RF....Radio Frequency
 MB....Multi-band

- (a) Polar circular orbits work well for all observable groups, accomplishing 100 percent unrestricted coverage and approximately 50 percent daylight coverage in 122 days.
- (b) For regional coverage (net image size > 1200 km), measurements may be spaced as far apart as 145 orbits for circular orbits.
- (c) Elliptical polar orbits were selected only for regional coverage, since the lapse rate per orbit is too large to obtain overlapped images of a detailed scale,
- (d) Elliptical orbits typically take 243 days to complete experiments due to restricted maximum measurement altitudes; because of this restriction and the locations of coverages (poles in particular) only 60-70% unrestricted and 30-40% daylight coverage is possible.
- (e) For the 1978 transfer arrival conditions, daylight coverage on elliptical altitude restricted orbits is interrupted 30 days after polar orbit capture for 113 days.
- (f) The maximum capture impulse required is 3.85 km/sec for circular orbit capture,
- (g) The capture impulse requirement for elliptical orbits saves up to 2.66 km/sec over circular orbits (for the 1978 transfer VHP),
- (h) The minimum total impulse (two maneuvers) to change the orbit node 90° for increased daylight coverage is 3.5 km/sec for a 0.9 eccentricity orbit; smaller eccentricity orbits need four impulses to achieve the nodal change and require larger total impulses.

IIT RESEARCH INSTITUTE

5.3 Mercury

5.3.1 Interplanetary Transfer Selections

The selection of interplanetary transfers to Mercury proceeded in a somewhat different fashion than for Mars and Venus. A recent comprehensive study (Manning 1967) of minimal energy ballistic trajectories to Mercury was used as a data base for the transfer selections. Direct, Venus swingby, and modified pericenter Venus swingby transfers for all opportunities between 1980 and 1992 were considered. The total impulse requirements of orbiter missions exhibit a cyclical variation over a period of 13 years. The trajectories were minimized in total impulse (ΔV), assuming a 1000 km circular orbit at Mercury.

The lowest minimum energy, regardless of the transfer, from each year between 1980 and 1992 was chosen to formulate a set of candidate transfers from which representative transfer selections could be made. These transfers are presented in Table 5-9. The arrival parameters listed in the table have been defined on page 135.

The values of the geocentric departure asymptote in no case approach 45° , a maximum value set to avoid serious launch safety problems. Of the 13 candidate transfers in Table 5-9, 8 use a direct flight mode, 3 utilize a Venus swingby, and 2 involve modified Venus pericenter swingbys. As pointed out by Manning, the direct transfers all use the same opportunity within any year (three are available) to arrive at Mercury near perihelion and its ecliptic ascending node which minimizes the impulse requirements. Hence these direct transfers are all rather similar, and it was only necessary to select one to represent their approach conditions for orbit selection. The 1984 transfer was selected with approach conditions which are characterized by a hyperbolic excess speed very close to

TABLE 5-9

SUMMARY OF SELECTED MERCURY TRANSFERS: 1980 - 1992

Launch Date (From Ref.)	Flight Mode	Time (Days)	δ_{\oplus} (deg)	VHL (KPS)	VHP (KPS)	VHT (KPS)	δ_{\oplus} (deg)	ρ_{\oplus} (deg)	θ_{\oplus} (deg)	RC (AU)	DTC (Days)
Apr 6, 1980	MPVS	124	18.2	5.28	8.13	13.41	-48.05	73.60	71.45	1.07	18
Apr 21, 1981	DIR	85	3.2	9.79	9.47	19.26	19.20	83.46	101.75	0.88	26
Jan 30, 1982	VS	305	24.3	4.75	10.67	15.42	-8.45	97.86	14.99	1.43	115
May 29, 1983	VS	144	-8.6	6.18	11.38	17.56	31.09	183.43	18.24	1.36	10
May 7, 1984	DIR	130	-7.5	11.44	8.31	19.75	-3.67	105.36	90.87	0.95	26
May 10, 1985	DIR	110	-2.8	9.89	7.97	17.86	-8.99	81.05	97.33	0.92	25
May 11, 1986	DIR	95	3.5	9.36	8.18	17.54	-8.09	97.53	88.39	0.97	22
May 2, 1987	DIR	85	4.8	9.82	8.71	18.53	8.96	82.15	99.67	0.90	25
Jun 17, 1988	MPVS	300	-22.1	7.60	6.30	13.90	8.21	107.50	33.52	1.24	95
Jun 2, 1989	VS	242	-28.8	8.72	10.96	19.68	14.44	63.24	86.00	0.94	48
May 10, 1990	DIR	135	-11.2	12.09	8.11	20.20	6.42	89.76	99.81	0.90	30
May 9, 1991	DIR	120	-6.7	10.76	8.00	18.76	-1.91	78.87	103.31	0.90	27
May 9, 1992	DIR	105	-1.4	9.61	7.93	17.54	-4.88	91.10	92.23	0.95	24

the average VHP for direct transfers of 8.34 km/sec and a typical terminator approach almost in the Mercury equatorial plane.

The Venus swingby and modified pericenter Venus swingby transfers differ markedly from each other as well as from direct flight transfers. It is impossible to pick a typical example of these transfers. However, the 1989 Venus swingby transfer was selected to investigate what effects approach conditions different from those of a direct transfer would have on the orbit selections. The approach conditions are characterized by a high hyperbolic excess speed of almost 11 km/sec (this does seem to be typical of at least the Venus swingby flight mode) and approach from the dark side of the planet at an angle pointing 14 degrees above Mercury's equator.

Contours of insertion occultation for the 1984 direct transfer are presented in Figure 5-21 mapped in the hyperbolic impact plane. Contours with minimum near limb angles of 5° and 0° are shown for the Sun, 0° for Earth, and 20° and 0° for the star Canopus. The relationship between the aiming angle θ , orbit inclination, and ascending node in the Mercury equatorial system are given in Figure 5-22. Similar graphs for the 1988 Venus swingby transfer are presented in Figures 5-23 and 5-24.

5.3.2 Orbit Characteristics and Constraints (Mercury)

Like Venus, the usefulness of orbits to scientific investigation of Mercury through imaging systems is largely unstudied. Mercury has a rather unique pattern of motion, which has a profound effect on imaging coverage from orbit. This motion is illustrated in Figure 5-25. The planet completes approximately one rotation on its axis every 60 days, and one revolution about the Sun every 90 days. The relative

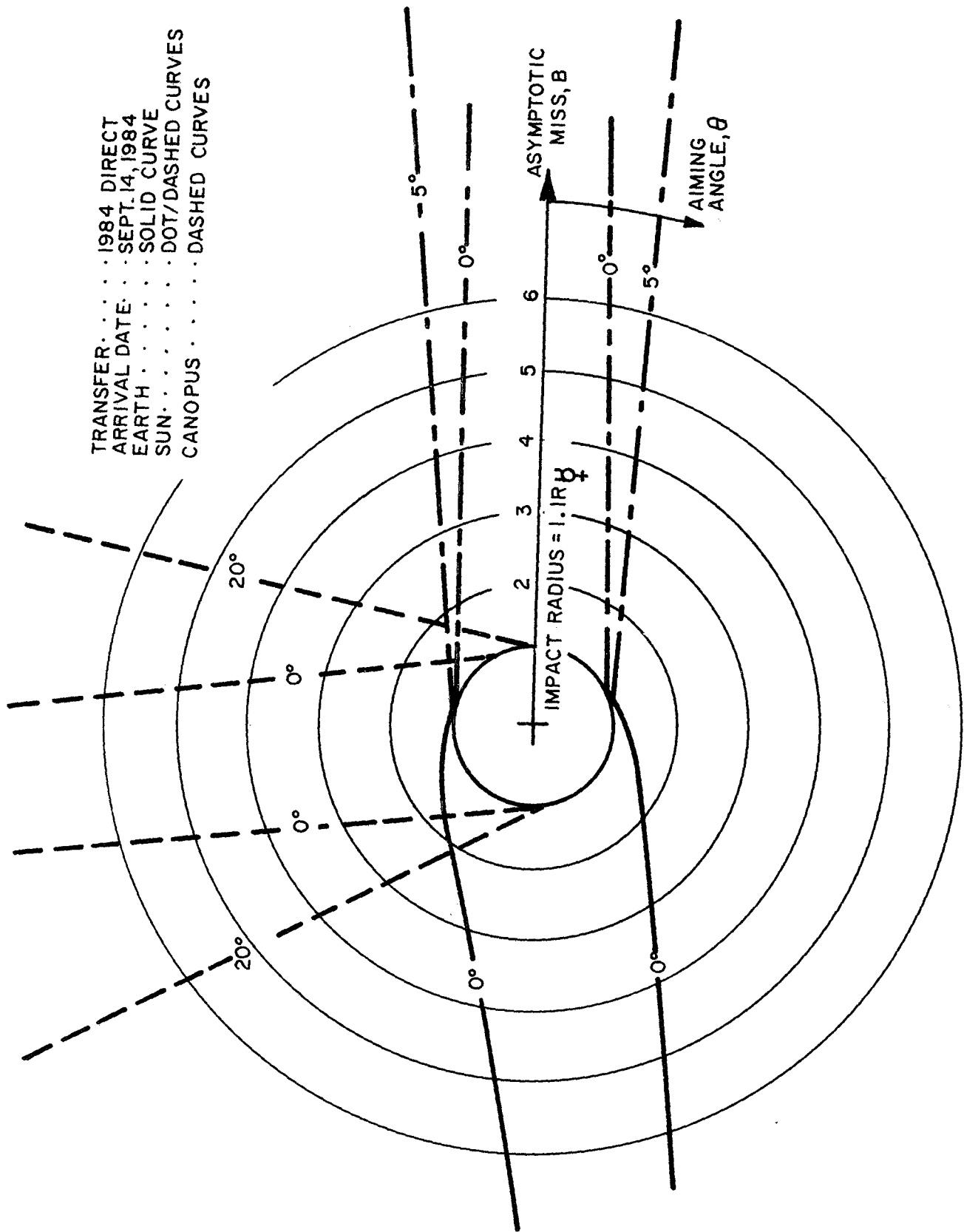


FIGURE 5-21. MERCURY CAPTURE OCCULTATION CONTOURS (1984)

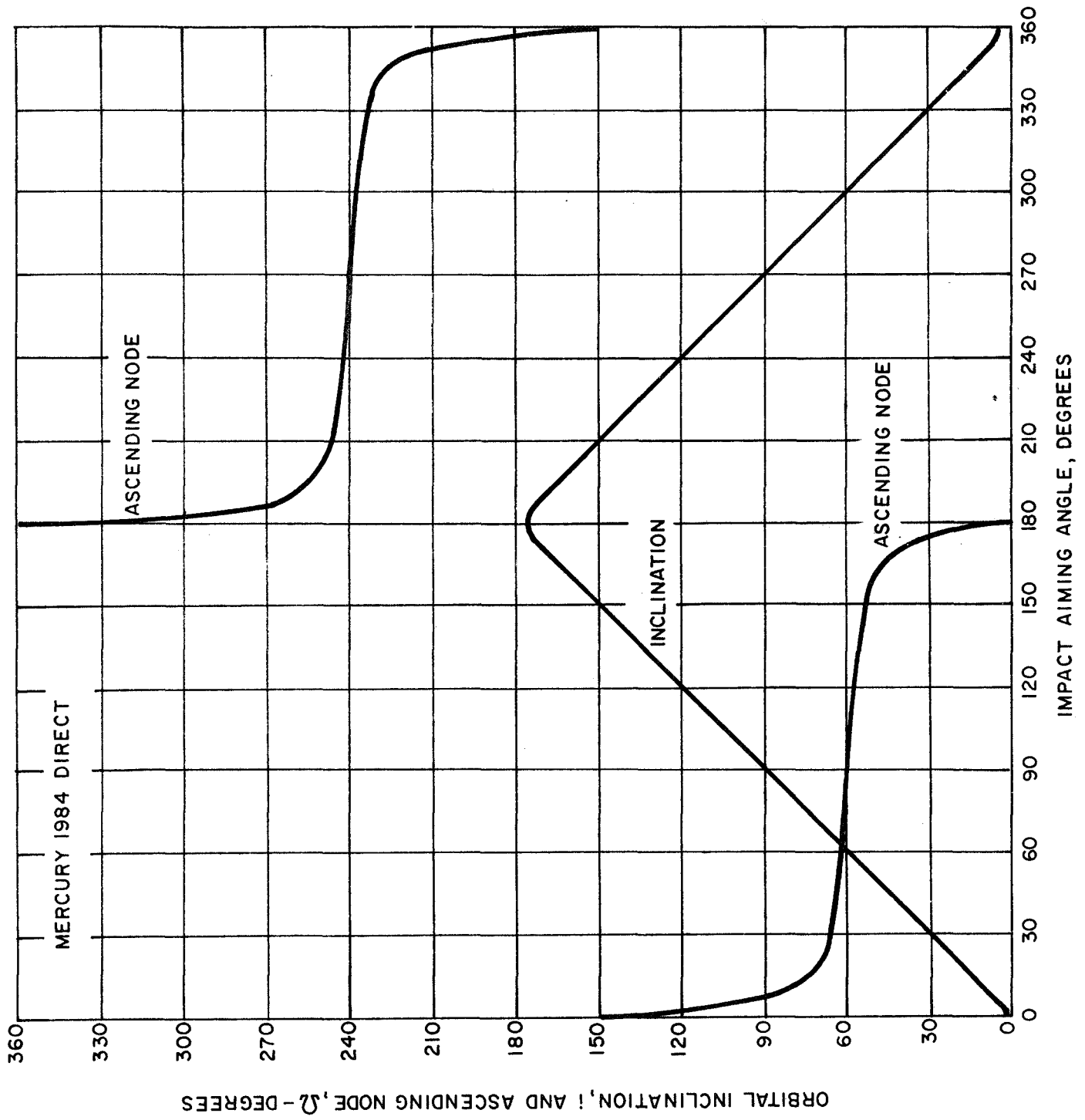


FIGURE 5-22. MERCURY AIMING ANGLE/ORBIT ORIENTATION RELATIONSHIP (1984)

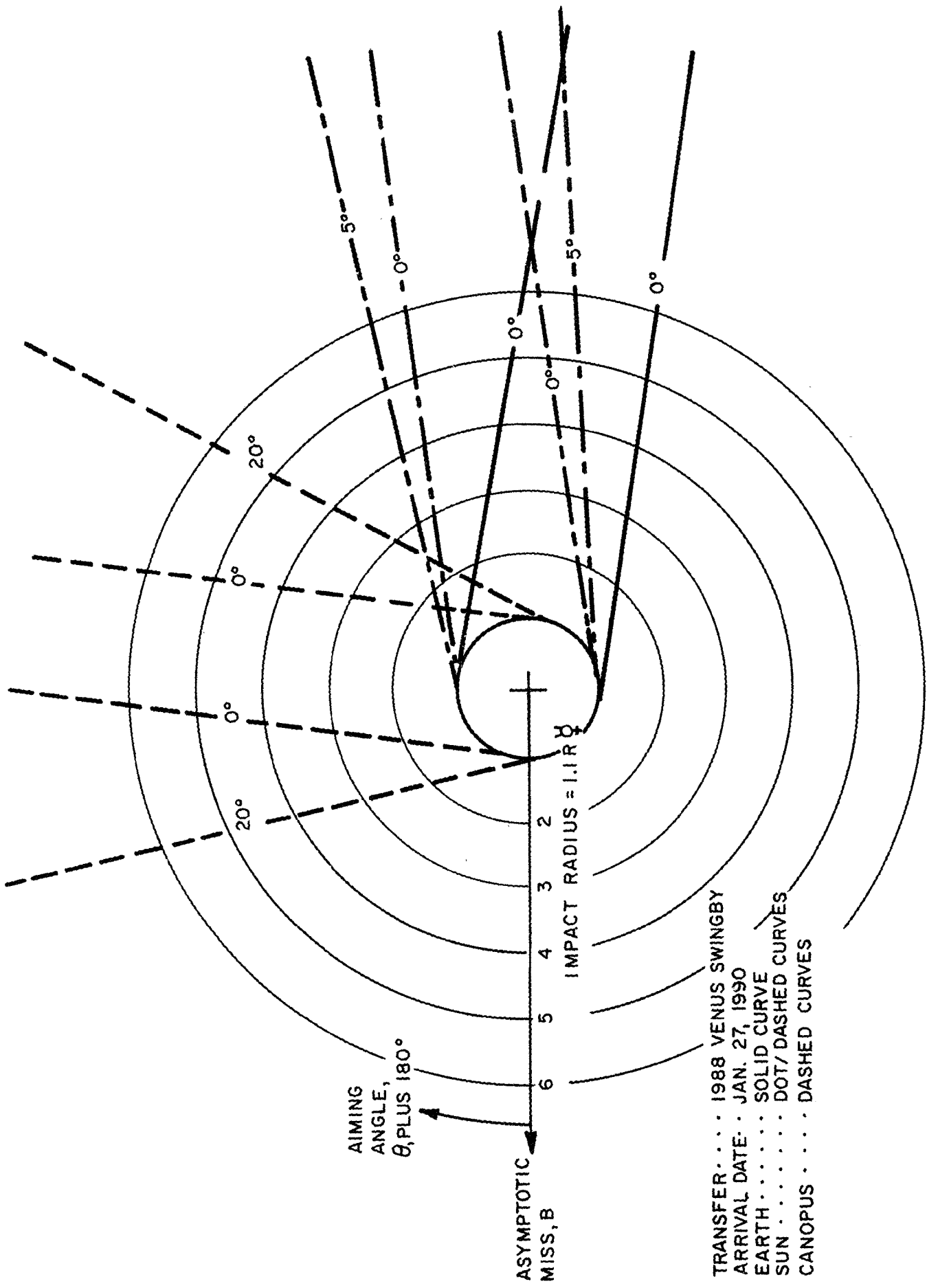
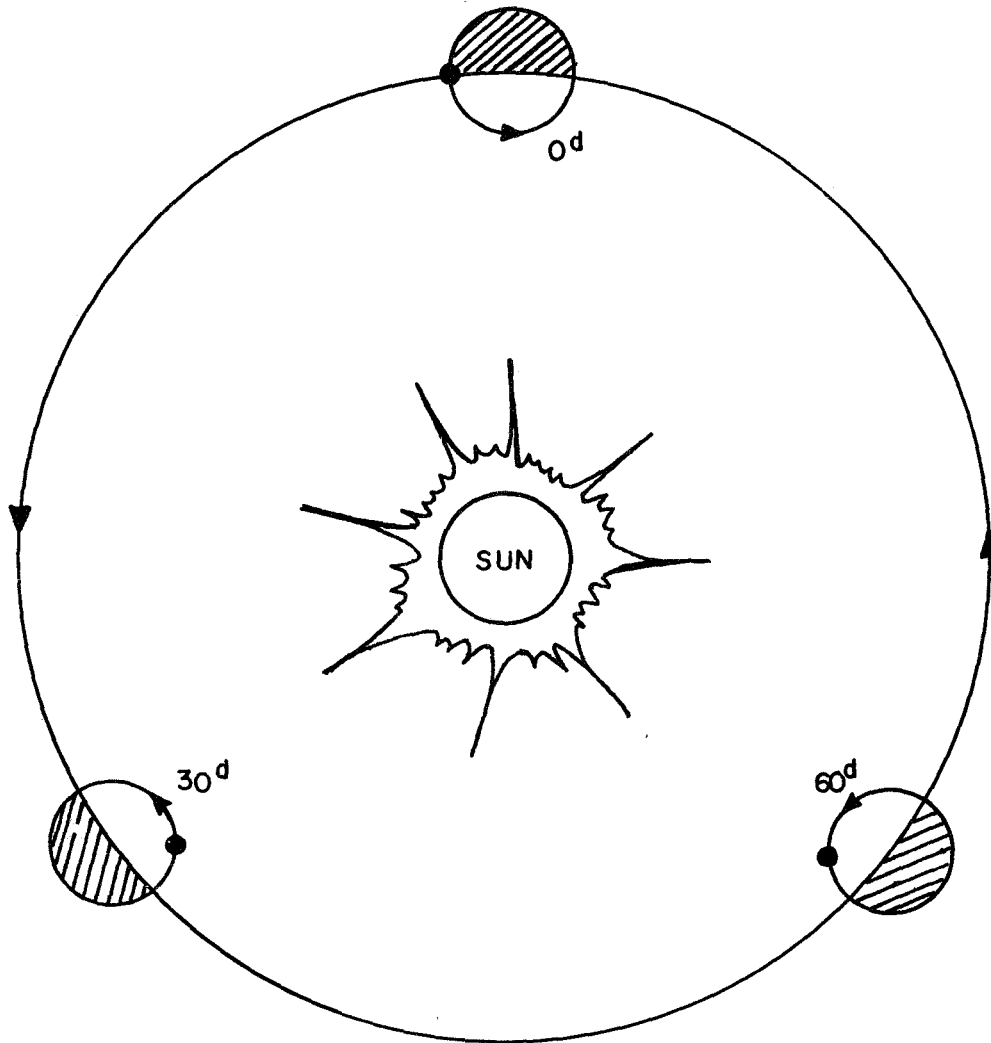


FIGURE 5-23. MERCURY CAPTURE OCCULTATION CONTOURS (1988)



RATES OF MOTION

TERMINATOR	4.09 DEG/DAY
SURFACE	6.10 DEG/DAY
RELATIVE	2.01 DEG/DAY

MERCURY DAY \approx 180 EARTH DAYS

FIGURE 5-25. MERCURY ROTATION/REVOLUTION RELATIONSHIP

motion of the surface with respect to the Sun is about $2^\circ/\text{day}$, resulting in a Mercury day of 180 Earth days. Hence it takes two revolutions of Mercury about the Sun to complete one day on the surface.

The characteristics of potential orbit coverage which result from solar elevation restrictions (or lack of them) with Mercury's motion relative to the Sun are enumerated in Table 5-10. The characteristics differ depending on whether or not the orbit is inertial. For inertial orbits, it was found that surface coverage in the absence of sunlight constraints can be completed (i.e. 360° in longitude) in 30 days with no altitude restrictions, and in 60 days with a minimized altitude* requirement.

The amount of daylight coverage (no specific solar elevation required) which can be obtained within a set period of time after orbit insertion is directly related to the orientation of the orbit with respect to the terminators. The best position yields 75% uninterrupted longitudinal coverage in 45 days.

When solar elevation limits are specified, as was the case with the majority of the Mercury measurement families, the pattern and amount of coverage become a function of the specific limits which are set. Assuming that Mercury's axis of rotation is perpendicular to its orbit plane, an inertial orbit will pass over the surface subsolar point twice every planet revolution ($\sim 90^\text{d}$) at planet orbit positions separated by 180 degrees. With a Mercury day of two solar revolutions, this means that four locations on the planet surface can be observed at 90° solar elevation in 180 days, provided no restriction is made on the maximum altitude of observation. The surface location of these four points depends upon the

* See Figure 5-15, page 164, for the definition of "minimized altitude coverage."

TABLE 5-10

POTENTIAL MERCURY ORBIT COVERAGE CHARACTERISTICS

● INERTIAL ORBITS, NO LIGHTING CONSTRAINTS:

100% LONGITUDE COVERAGE POSSIBLE
IN 30 DAYS IF ALL ORBIT ALTITUDES
ARE USED
IN 60 DAYS IF MINIMIZED ALTITUDE
COVERAGE IS EMPLOYED

● INERTIAL ORBITS, DAYLIGHT COVERAGE CONSTRAINT:

ANYWHERE FROM ZERO TO 75% LONGITUDINAL
COVERAGE IN 45 DAYS AT MINIMIZED ALTITUDES
DEPENDING UPON ORBIT ASCENDING NODE

● INERTIAL ORBITS, FIXED SOLAR ELEVATION CONSTRAINT:

ONE DAYLIGHT PASS PROVIDES FOLLOWING AMOUNTS
OF COVERAGE

ELEV	15-30°	15% COVERAGE
	30-60°	23%
	50-80°	13%
	70-90°	4%

IN LESS THAN 40 DAYS - MAXIMUM COVERAGE (NO
ALTITUDE CONSTRAINT) OBTAINED IN FOUR CON-
SECUTIVE DAYLIGHT PASSES TAKING 180 DAYS

● SUN-SYNCHRONOUS ORBITS:

100% LONGITUDINAL COVERAGE AT CONSTANT SOLAR
ELEVATION ANGLE IN 180 DAYS

position of the orbit nodes on the Mercury equator. About each of these points, rings of lesser solar elevations exist. The coverage percentages presented in Table 5-10 for each set of solar elevation limits which occurred in the observable groupings are typical for one pass over the surface subsolar point.

With a sun-synchronous orbit, it is possible to obtain 100% longitudinal coverage at a fixed elevation angle in 180 days. This would certainly improve the total coverage obtained within a specified range of solar elevation angles using inertial orbits. However, 70% coverage (required for regional experiments) would never be attainable at elevations of 50° - 90° , assuming that the Sun remains in Mercury's equatorial plane. Sun-synchronous orbits would not be advantageous for families without solar elevation restrictions. Since total longitudinal coverage would still take 180 days, a six or three-fold increase in coverage time over inertial orbits would be necessary, depending upon whether or not minimized altitude coverage is required.

The candidate orbit sizes chosen for Mercury were similar to those used for Venus orbit selections. However, an assumption was made that Mercury's atmosphere has negligible effect upon the orbit lifetime. Hence it was necessary to use some other criteria than a 50-year orbit lifetime to establish periapse of the candidate orbits. This was done by somewhat arbitrarily setting the periapse altitude of all orbits to 500 km. The range of eccentricities considered was 0 to 0.9. Pertinent parameters of this set of orbits are presented in Table 5-11 in increments of 0.1 in orbit eccentricity.

The maximum altitude ratios of these orbits (column 4, Table 5-11) is somewhat less than was experienced in the Venus candidate orbit size selections. Measurement arc is plotted in Figure 5-26 as a function of eccentricity for maximum measurement altitude ratios (h/h_p) of 2, 5, and 10.

TABLE 5-11

MERCURY CANDIDATE ORBIT SIZES

Orbit No.	Eccentricity	Periapse Altitude (km)	Maximum Altitude Ratio, h/hp	Orbit Period (hrs)	Lapse Rate Per Orbit (km)	Average* Capture ΔV (km/sec)
1	0.0	500	1.0	1.889	20.5	6.462
2	0.1	500	2.3	2.213	24.0	6.329
3	0.2	500	3.9	2.640	28.6	6.202
4	0.3	500	6.0	3.226	34.9	6.081
5	0.4	500	8.8	4.065	44.0	5.964
6	0.5	500	12.8	5.344	57.9	5.851
7	0.6	500	18.6	7.468	80.9	5.742
8	0.7	500	28.4	11.498	124.5	5.636
9	0.8	500	48.0	21.123	228.7	5.534
10	0.9	500	106.8	59.746	646.8	5.434

*Capture ΔV Based on a Surveyed Average Hyperbolic Approach Speed of Direct Mercury Transfers, VHP = 8.34 km/sec.

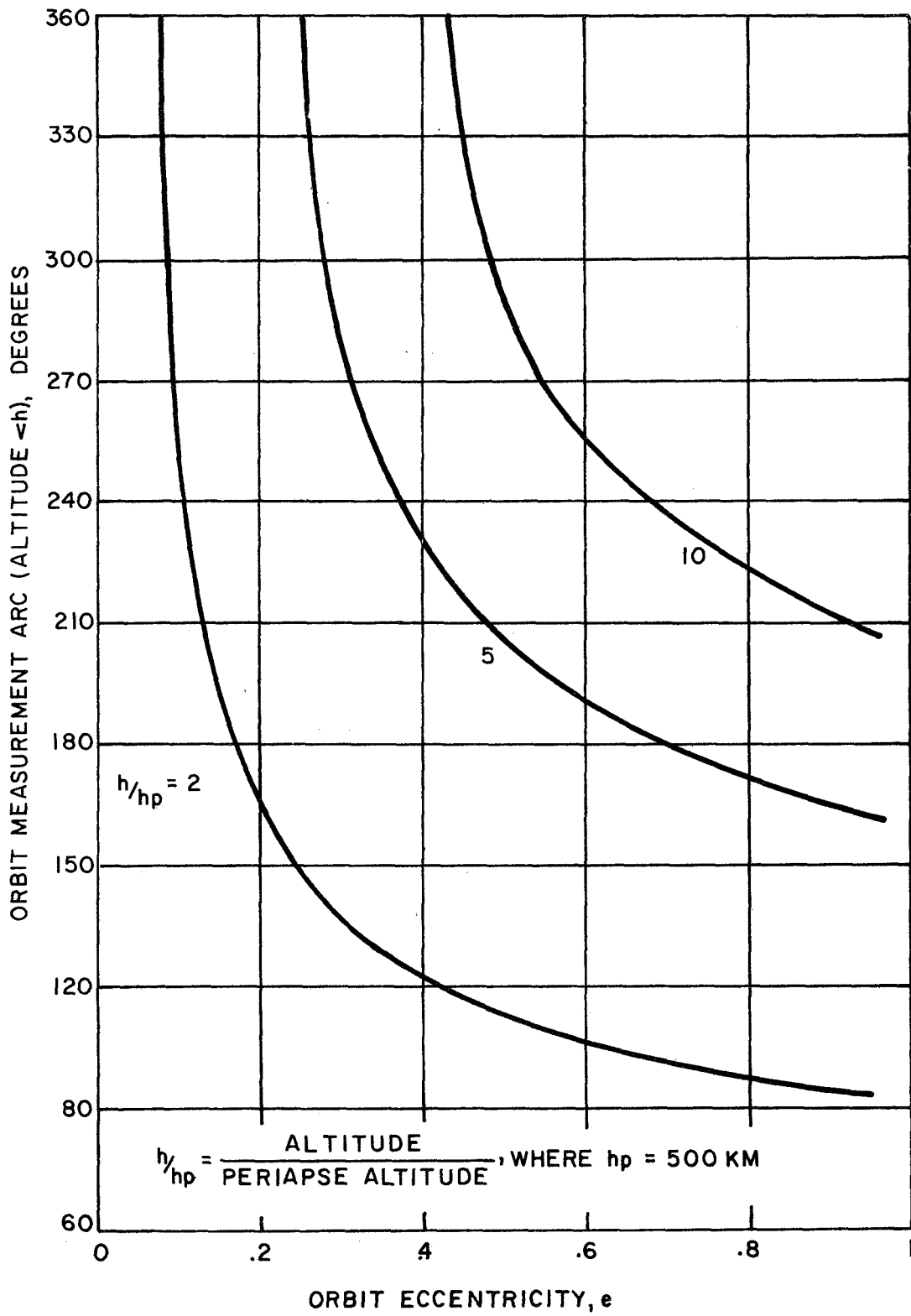


FIGURE 5-26. MERCURY ORBIT ALTITUDE RATIOS

Twice the angle from periapse represents the orbit arc over which measurements can be taken at less than or equal to the specified altitude ratio. Total minimized altitude coverage as defined in Figure 5-15 requires a measurement arc of 180 degrees. From Figure 5-26, minimized altitude coverage of Mercury within maximum altitude ratios of 2, 5, and 10 is possible with orbit eccentricities up to 0.169, 0.685, and > 0.9 respectively.

The orbit capture impulse requirements (last column, Table 5-11) were derived using an asymptotic approach velocity (VHP) of 8.34 km/sec which is averaged from the direct Mercury transfer data presented in Table 5-9. The ΔV savings of a 0.9 eccentricity orbit over a circular orbit is about one km/sec. At magnitudes of 6 km/sec, this can represent an appreciable gain in useful orbit payload. For example, assuming (a) a three-stage equally divided capture maneuver, (b) propellant Isp = 400 sec and (c) 20% of the capture propulsion system allocated to structure, tankage and engines, a useful payload fraction of 10.5% is possible with a circular orbit capture. The payload increases by almost 50% to a fraction of 15.6% for a 0.9 eccentricity elliptical orbit capture.

So far the potential orbit coverage discussion and review of orbit characteristics have not considered the influence of perturbations on an orbit. Mercury's slow rotation (2/3 resonance with orbit period) provides little basis for any appreciable planetary oblateness. This is further supported by the low upper limit of J_2^* determined from Mariner V tracking data past Venus, also a slowly rotating terrestrial planet. Oblateness was therefore neglected in the analysis of Mercury orbit perturbations. Due in part to this

* See page 174.

decision, sun-synchronous orbits were not further considered as a coverage mode. The rapid average rate of solar motion, and the variation in this rate due to Mercury's orbit eccentricity, also contributed to this decision. Hence, the remaining process of orbit selection deals only with inertial orbits and perturbation effects on them.

Solar gravitation was regarded as the dominant perturbing force requiring some form of compensating orbit control, particularly if highly eccentric orbits are to be used. The only orbit parameter significantly affected by solar perturbations is the orbit periaipse altitude. The rate of change of periaipse altitude due to the dominant secular perturbations of solar gravitation is presented in Figure 5-27 as a function of orbit eccentricity for several arguments of periaipse, ω , where ω is the in-plane angle of periaipse measured from the ascending node of the orbit plane on Mercury's equator (assuming Mercury's equator and ecliptic are coplanar). The rate of change of ω , $d(\omega)$, due to secular solar perturbations is presented in Figure 5-28.

These figures are similar to the graph of solar perturbation effects presented in the Venus orbit characteristics discussion (Figures 5-19 and 5-20). Note that the results presented are for polar orbits. The magnitude of $d(h_p)$ decreases with decreasing inclination, but then so also does the amount of surface area covered by the orbit. In the worst case, an 0.9 eccentricity polar orbit ($h_p = 500$ km), with $\omega = 45^\circ$, will degenerate to impact the surface in about 11 days, neglecting periodic effects. Also, although the magnitudes of $d(\omega)$ presented in Figure 5-28 are small, they are important. For example, while it appears to be desirable to place periaipse at Mercury's equator ($\omega = 0$) to nullify solar perturbation effects on altitude ($d(h_p) = 0$), it is obvious that, with time, periaipse will move away from this point and solar perturbations

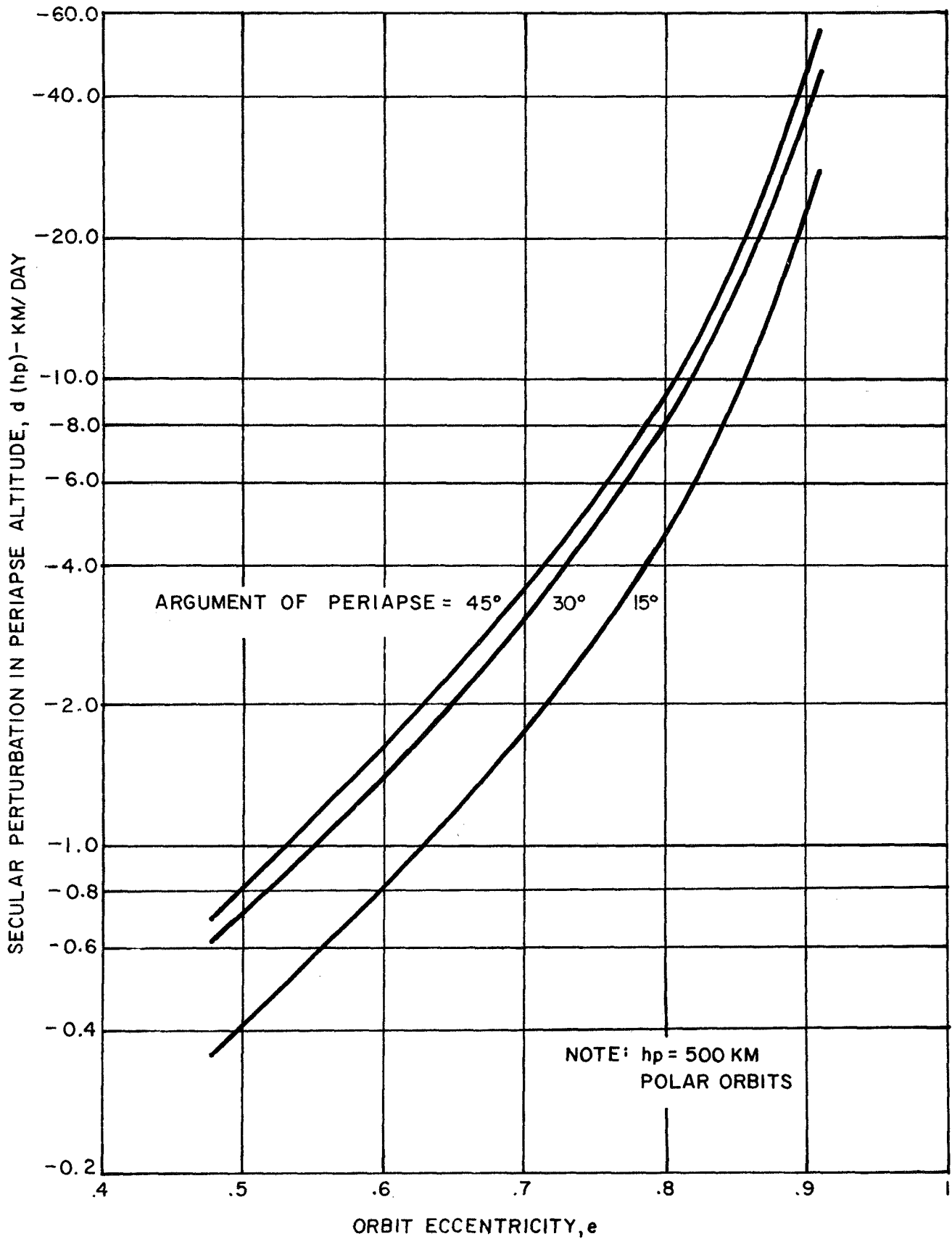


FIGURE 5-27. MERCURY ORBIT SOLAR PERTURBATIONS: ALTITUDE

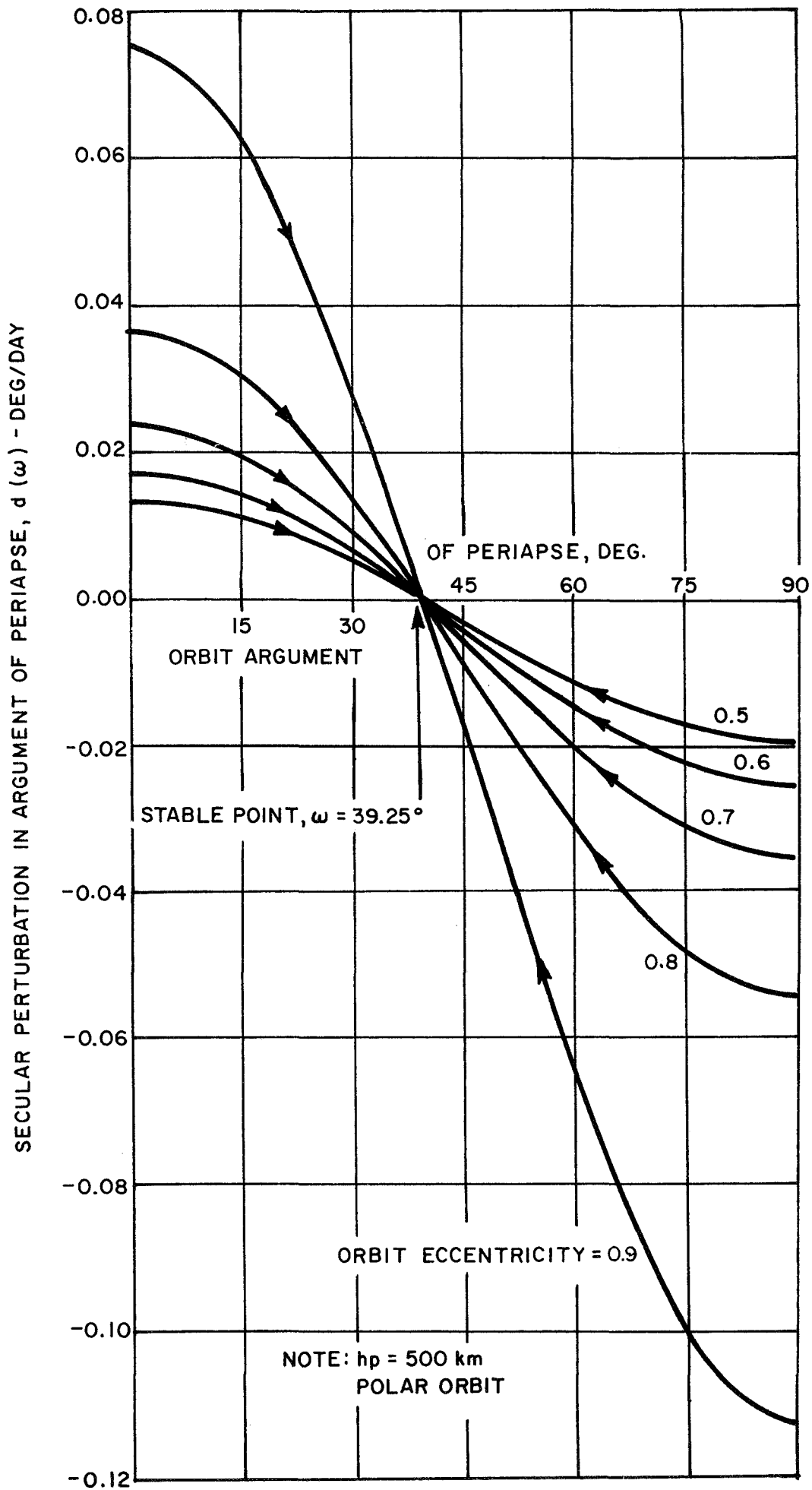


FIGURE 5-28. MERCURY ORBIT SOLAR PERTURBATION: ARG. OF PERIAPSE

will begin to reduce the periapse altitude. Consider a 0.9 eccentricity orbit placed with periapse at the equator and allowed to exist under the influence of secular solar perturbations for 180 days, the longest orbit duration given in Table 5-10 for maximum coverage. At the end of this period the periapse altitude will have degenerated to 998 km below Mercury's surface while ω has only precessed about 12° ! Hence it is clear that if highly eccentric orbits are to be used in the interest of payload savings, some form of solar perturbation control is also necessary.

Two methods of active orbit control were reviewed: (1) correction of periapse altitude, eccentricity, and the argument of periapse and (2) correction of periapse altitude and eccentricity only. The ΔV requirements per orbit (one impulse) of each method are presented for a 0.9 eccentricity orbit ($h_p = 500$ km, $i = 90^\circ$) versus orbit argument of periapse, ω , in Figure 5-29. The requirements are approximately symmetric about $\omega = 90^\circ$. Each method is better than the other over some range of ω . For an initial $\omega = 0^\circ$ and a 180-day orbit duration, it is advisable to correct only h_p and e (dotted curve), since ω precesses only 12° . The ΔV cost is roughly 80 m/sec. The addition of an orbit control propulsion system, and the obvious reliability requirement, are disadvantageous to this solution.

A passive solution (similar to that discussed for Venus) which takes advantage of the changing sign of the perturbation $d(h_p)$ about $\omega = 0$ was considered. By placing periapse at a small negative value of ω , the altitude first increases until ω reaches 0° and then decreases again. It was found that by setting $\omega = -7.0^\circ$, the periapse altitude of an $e = 0.9$ orbit increases initially to a maximum value of about 1050 km and then returns to 500 km by the end of a 180-day orbit duration. This method of control is the one suggested for the elliptic orbit selections made for measurement

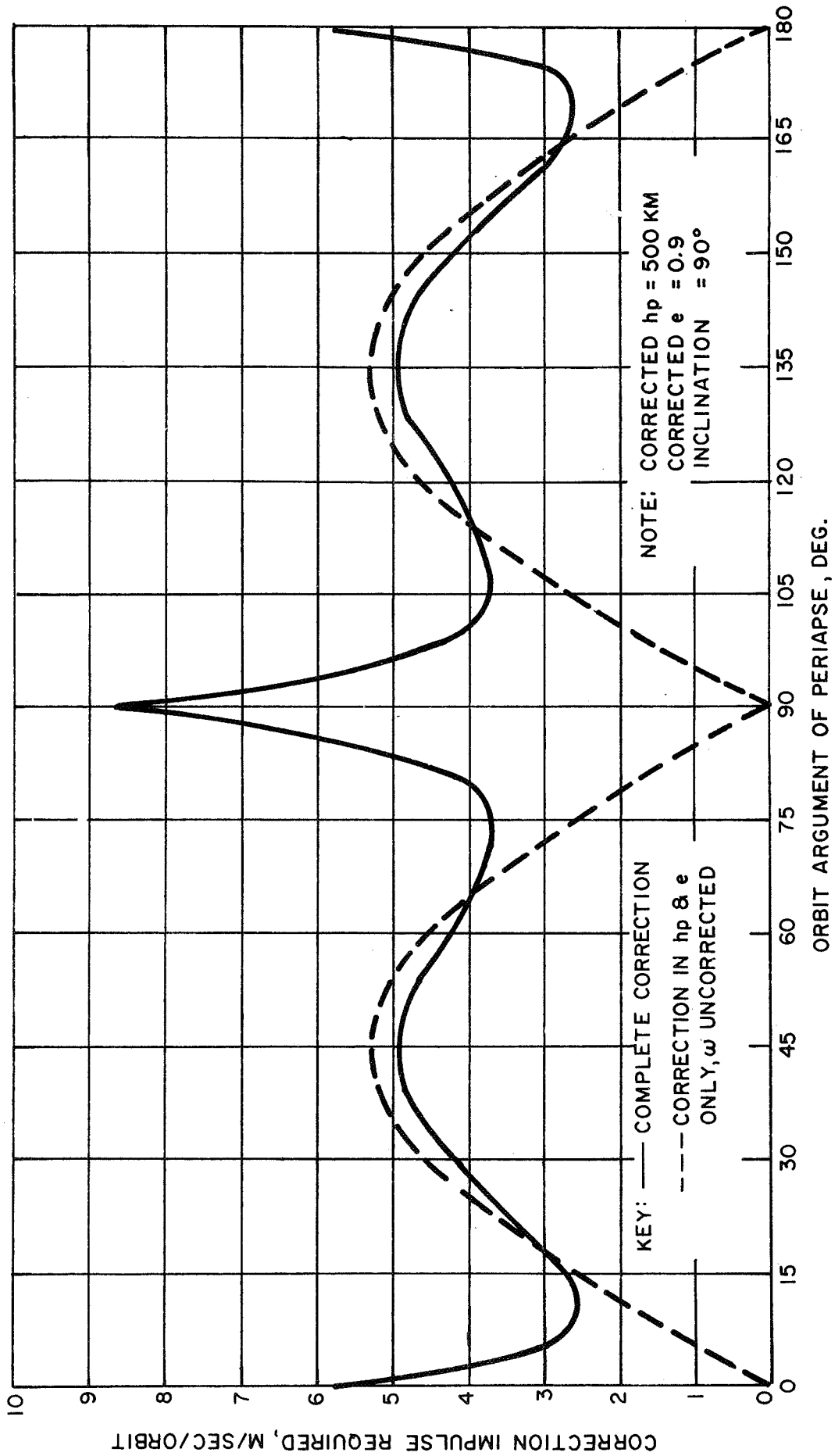


FIGURE 5-29. CONTROL REQUIREMENTS OF A MERCURY ORBIT ($h_p = 500$ KM, $e = 0.9$) UNDER THE INFLUENCE OF SOLAR PERTURBATIONS.

families involving specific solar elevation constraints. Of course, if the mission is continued without active control beyond 180 days, the orbit will degenerate to impact within several additional weeks.

5.3.3 Orbit Selections (Mercury)

The measurement families for which orbit selections were made are presented in Table 5-12. The most important measurement specification pertaining to the potential orbit coverage characteristics is the solar elevation requirement. Of the 24 families given, 6 have no restrictions, 1 requires daylight, and 17 require a specific solar elevation range.

Orbit selections were made for two different approach conditions: a 1984 direct Mercury transfer, and a 1989 Venus swingby transfer. The results of orbit selections for the 1984 transfer arrival conditions are presented in Volume III of the report. Orbit selections are limited to polar orbits since, as with Venus, this will at least maximize the latitude coverage, and no obvious reasons were found favoring other inclinations. The pattern of illumination-constrained coverage obtained during the first subsolar point pass is illustrated in Figure 5-30 on a latitude vs. longitude* map of Mercury's surface. The elevation limits of the annular coverage areas are given in Table 5-11 for the various measurement families. The annular areas of coverage are elliptical in shape, due to Mercury's changing rate of motion on its elliptical path about the Sun. Additional coverage is possible by allowing the orbit to traverse three more subsolar points for an orbit duration of 180 days. The additional amounts of coverage, percentage overlap between successive coverage areas, and total net coverage are summarized in Table 5-13 for each range of

* Zero longitude is set in the direction of Mercury's perihelion at the time of orbit capture.

TABLE 5-12

MEASUREMENT FAMILIES FOR MERCURY

Family Number	Observable Number(s)	Sensor* Type(s)	Minimum Image Size(km)	Overlap (%)	Minimum Coverage (%)	Solar Elevation Range (deg)	Coverage Distribution	Time for Coverage	Image Interval	Coverage Interval
1	3	UV, IR	600	20	70	70-90	-	-	-	-
2	6, 12	V	600	20	70	50-80	-	-	-	-
3	3, 18	MB, V	600	20	70	30-60	-	-	< 2 hr	> 2/yr
4	1, 3, 6, 9, 12	V, IR	600	20	70	15-30	-	-	-	-
5	41	MB	600	20	70	Day	-	-	-	-
6	1, 3, 6, 9, 12, 21	R, IR, μ , MB	600	20	70	-	-	-	< 30 hr	-
7	1, 6, 9	V	600	60	70	70-85	-	-	-	-
8	1, 6, 9	R	600	60	70	-	-	-	-	-
9	35	V	300	20	70	50-80	-	< 1 day	-	> 10/yr
10	35	V	300	20	70	30-60	-	< 1 day	-	> 10/yr
11	4	UV, IR	100	20	10	70-90	-	-	-	-
12	7, 13	V	100	20	10	50-80	-	-	-	-
13	4, 19	MB, V	100	20	10	30-60	-	-	-	-
14	4, 7, 10, 13	V, IR	100	20	10	15-30	-	-	-	-
15	4, 7, 10, 13, 22	R, IR, μ , MB	100	20	10	-	-	-	< 30 hr	-
16	7, 10	V	100	60	10	70-85	-	-	-	-
17	7, 10	R	100	60	10	-	-	-	-	-
18	5	UV, IR	0.5	20	3	70-90	-	-	-	-
19	8, 14	V	0.5	20	3	50-80	-	-	-	-
20	2, 5	V, MB	0.5	20	3	30-60	-	-	-	-
21	5, 8, 11, 14, 20	V, IR	0.5	20	3	15-30	-	-	-	> 1/300hr
22	2, 5, 8, 11, 14, 20, 23	R, IR, μ , MB	0.5	20	3	-	-	-	< 30 hr	> 1/300hr
23	8, 11, 20	V	0.5	60	3	70-85	-	-	-	> 1/300hr
24	8, 11, 20	R	0.5	60	3	-	-	-	-	> 1/300hr

*Sensor Type Definitions are: UV....Ultraviolet
V....Visible
IR....Infrared
 μMicrowave
R....Radar
MB....Multi-band

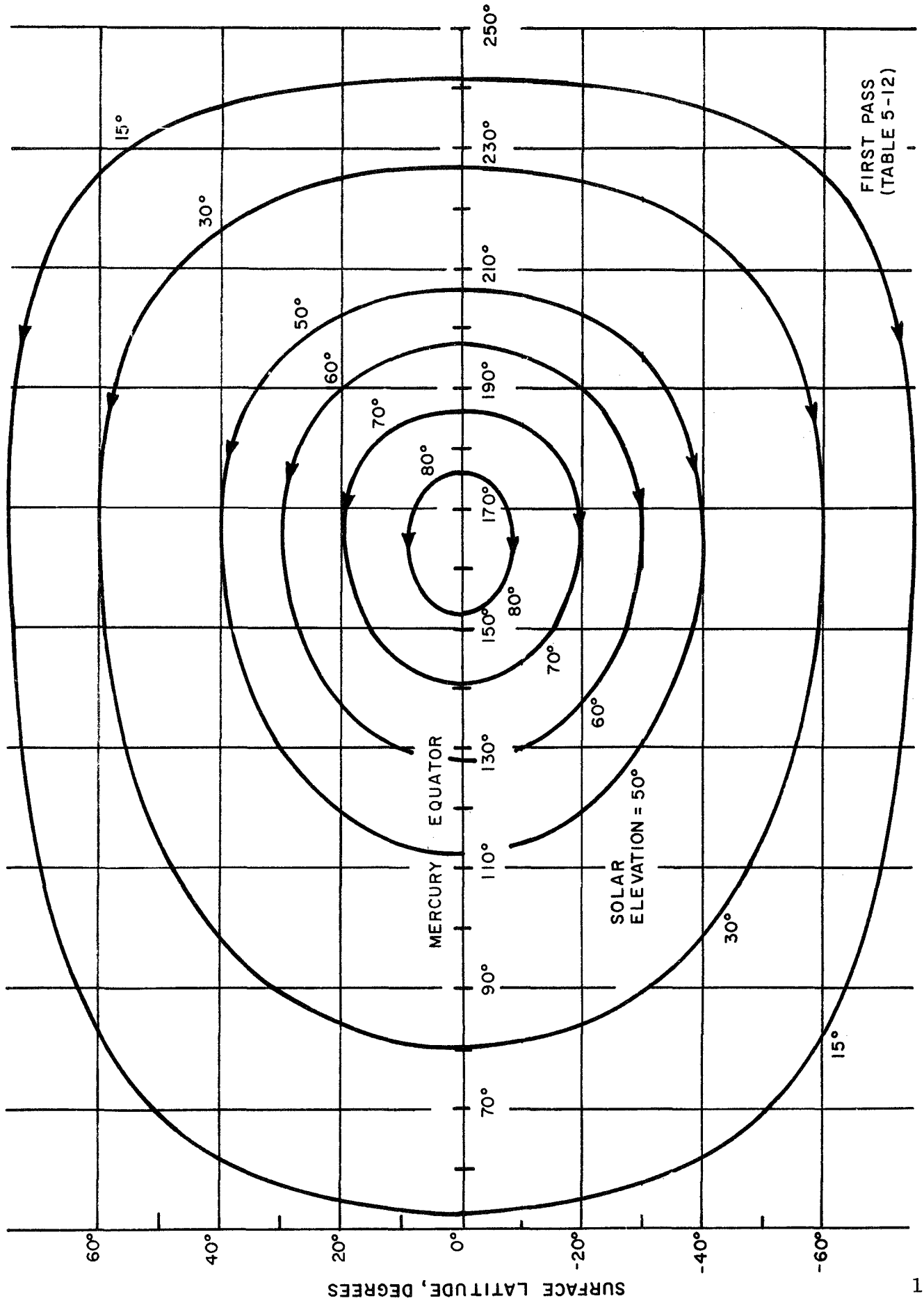


FIGURE 5-30. CONSTANT SOLAR ELEVATION CONTOURS FOR A CIRCULAR 500 km ALTITUDE POLAR MERCURY ORBIT

TABLE 5-13

MERCURY SOLAR ELEVATION RESTRICTED COVERAGE*

Area Description	Solar Elevation Constraints (deg)			
	15-30	30-60	50-80	70-90
First Pass	15.6	22.7	13.2	3.7
Overlap Between First and Second Pass	2.0	7.8	--	--
Second Pass	20.6	31.2	19.3	5.4
Overlap between Second and Third Pass	3.3	11.7	8.2	1.7
Third Pass	16.1	22.1	13.0	3.7
Overlap Between Third and Fourth Pass	2.1	7.8	--	--
Fourth Pass	20.6	31.2	19.3	5.4
Overlap Between Fourth and First Pass	2.8	10.4	7.8	1.6

Total Net Coverage Obtained	62.7	69.5	48.8	14.9
Maximum** Possible Coverage	96.6	86.6	64.3	34.2

* Assuming Polar Orbits and Up to 180-day Stay Time.

** Assuming Mercury's Equator and Ecliptic are Coplanar.

solar elevation angles specified. It should be noted that only the ranges of 15° to 30° and 30° to 60° come close to satisfying a 70% surface coverage requirement specified for many of the families in Table 5-12.

Both circular and maximum elliptical ($e = 0.9$) orbits were selected for the first seven families to study the tradeoffs between altitude, orbit coverage, and capture impulse. Circular orbits were chosen for the remaining families. The results are summarized as follows:

- (a) Circular orbits provide the most coverage in the shortest time; solar elevation restricted coverage (see Table 5-12) is accomplished in 180 days; 100% unrestricted coverage is possible in 30 days.
- (b) Elliptical orbits require a plane change after capture to place periapse at Mercury's equator (the center of restricted solar elevation coverage) but still save about 0.8 km/sec in total impulse over circular orbits,
- (c) The maximum capture impulse is 6.44 km/sec for a circular 500 km altitude orbit,
- (d) Restricted maximum imaging altitudes ($h/h_p < 10$) reduce restricted solar elevation coverage by about half even though the coverage time remains the same, and increase unrestricted coverage by a factor of two, i.e., 60 days,
- (e) Highly elliptical orbits are only useful for regional coverage since their longer periods yield orbit lapse rates too large for detailed (high resolution) overlapping images.

The primary differences between the 1989 Venus swingby transfer and the 1984 direct transfer are the asymptotic approach speed and the approach direction with respect to the subsolar point. The higher approach speed of the 1989 transfer raises the capture ΔV requirement for a circular orbit from 6.44 to 8.90 km/sec. For an elliptical polar orbit, with $e = 0.9$ and $\omega = 0$, the ΔV increases from 5.68 to 8.11 km/sec. It is questionable whether the high ΔV 's associated with the Venus swingby transfer are feasible for chemical propulsion systems. However, assuming they are, resulting polar orbits differ from similar orbits using the 1984 arrival conditions as follows:

- (a) For circular orbit capture, the ground trace at arrival is just leaving an area of constrained solar elevation coverage (maximum solar elevation angle is 28° and decreasing) meaning that some 20 days must be spent in orbit before significant coverage is available at constrained solar elevation angles.
- (b) For elliptical orbit capture, the maximum solar elevation of the ground trace is 65° and increasing meaning that less than half of the first constrained solar elevation area has been missed.

The conditions of the 1984 orbits are roughly reverse of these, with the circular orbit being established right at the onset of a constrained solar elevation area, i.e., maximum solar elevation = 15° . Once coverage from orbit begins, there is little or no difference in the mission profile between the two transfers, except that the actual surface areas being covered at constrained solar elevations are different. Hence, specific orbit selections were not made for the 1989 transfer arrival conditions.

5.4 Jupiter

5.4.1 Interplanetary Transfer Selections

Minimum launch energy (VHP) trajectories provide low total hyperbolic velocities (VHT), but at the expense of long trip times on the order of 1000 days. It was therefore decided to consider shorter constant flight times as well in the Jupiter transfer selection process. The Earth-Jupiter geometry for optimum launches approximately repeats itself every 12th year. Variations in trajectory characteristics for a given type of transfer (i.e., minimum energy or constant flight time) can be adequately investigated by considering 11 successive opportunities. In addition to selecting representative transfers, the selection process also reflects consideration of the relatively high velocity impulses required to obtain low Jupiter orbits.

Taking these factors into consideration three different transfers were initially investigated: (a) 500-day transfers, (b) 700-day transfers, and (c) minimum VHL transfers. The results are tabulated in Table 5-14. The variable definitions for the data presented are as follows:

- Launch Date - Launch date with minimum VHL
- Type - Type I transfer (shortest trip for given VHL)
- Trip - Transfer trip time, days
- δ_{\oplus} - Declination of outgoing geocentric asymptote, deg
- VHL - Geocentric hyperbolic excess speed, km/sec
- VHP - Planet hyperbolic approach speed, km/sec
- VHT - VHL + VHP, km/sec.

Data is shown in Table 5-14 for each transfer every 3rd opportunity over the 11-year period 1975-1986.* With the exception of the parameter δ_{\oplus} , the characteristics of the 500-day and

* These transfers provide a fairly even distribution in the two transfer parameters: trip time and hyperbolic approach speed.

TABLE 5-14

MINIMUM CONSTANT TIME VHL TRANSFERS AND
ABSOLUTE MINIMUM VHL TRANSFERS TO JUPITER

Launch Date	Type	Trip (Days)	δ_{opt} (deg)	VHL (KPS)	VHP (KPS)	VHT (KPS)
Jun 26, 1975	I	500	-4.42	10.38	11.68	22.06
Jun 23, 1975	I	700	-7.36	9.20	7.05	16.25
Jun 30, 1975	I	900	-5.79	8.97	5.69	14.66
Jul 6, 1975	I	1017*	3.69	8.96	5.70	14.66
Oct 10, 1978	I	500	28.70	10.99	13.12	24.11
Oct 5, 1978	I	700	36.49	9.64	7.85	17.49
Oct 14, 1978	I	900	43.69	9.76	5.76	15.52
Oct 8, 1978	I	777*	39.47	9.57	6.75	16.32
Jan 8, 1982	I	500	-1.82	10.72	13.72	24.44
Jan 1, 1982	I	700	1.17	9.15	8.18	17.33
Jan 4, 1982	I	900	-1.95	8.72	6.00	14.72
Jan 5, 1982	I	946*	-6.62	8.68	5.82	14.50
Apr 17, 1985	I	500	-28.56	10.21	12.15	22.36
Apr 16, 1985	I	700	-37.24	9.19	7.30	16.49
Apr 29, 1985	I	900	-42.88	9.52	6.02	15.54
Apr 19, 1985	I	743*	-38.13	9.19	6.77	15.96

* These are the Absolute Minimum VHL Transfers to Jupiter

700-day transfers are fairly stable over the 11-year period. This reduces the number of selections needed to represent all possible Jupiter approach conditions.

The minimum energy transfers show somewhat larger variations from year to year, particularly in the arrival conditions and flight time. (The flight time varies by as much as 16% from an average TF = 870 days). These variations are reduced by selecting a constant time of flight transfer which is representative of the minimum energy transfers. A 900-day transfer is selected for this consideration since its time of flight is close to the average for minimum VHL transfers (870 days). The data for the 900-day transfers are included in Table 5-14. In three of the four 900-day transfers shown, VHT is less than or equal to that for the corresponding minimum VHL transfer. Also, the trajectory characteristics are fairly stable from one opportunity to the next, except again for the variable δ_{\oplus} .

The parameter δ_{\oplus} shows the same pattern of variation with launch opportunity, regardless of the trip time. However, its magnitude of variation does increase with longer trip times. An upper limit on δ_{\oplus} magnitude of 45° has been used in the previous transfer selections to Mars, Venus, and Mercury to avoid serious violations of range safety limits or dog-leg maneuver payload penalties during launch. This limit probably restricts the use of some of the 900-day transfers, since δ_{\oplus} varies through a launch window.

In view of the stability of characteristics exhibited by the 900-day transfers, minimum VHL trajectories were not considered further in the transfer selections. The remaining transfers to be considered have constant flight times of 500, 700, and 900 days. The most significant differences in arrival conditions for these transfers are (a) the magnitude of the hyperbolic approach speed, VHP, (b) the approach

direction, ρ_0^* , and (c) the location of Earth at arrival. In the interest of keeping the number of selections to a minimum, it was decided that the 700-day transfer is sufficiently representative of this set to eliminate the 500 and 900 day transfers. The hyperbolic approach speed for the 700 day transfer, VHP (avg.) = 7.64 km/sec, slightly favors the lower approach speeds of the 900 day transfers. The locations of periapse for coplanar periapse capture are in darkness for all values of ρ_0 for all transfers. The closest periapse gets to daylight is about the sunset terminator for equatorial orbits and the 900 day transfers. Both the 500 day and 900 day transfers arrive near Earth/Jupiter opposition; the 700 day transfers arrive near conjunction. However, for any in-orbit time of more than 200 days Earth will also pass through opposition with a 700 day transfer mission.

An expanded tabulation of transfer and arrival conditions of 700 day transfers for every opportunity of an 11-year cycle is presented in Table 5-15. The 1978 transfer was selected from this list of trajectories to represent a typical transfer to Jupiter for orbiter imaging missions. The approach occultation contours of this transfer for Earth, Sun, and Canopus for minimum near-limb angles of 0° , 0° and 5° , and 0 and 20° , respectively are illustrated in Figure 5-31. The relationships of orbit inclination and orbit ascending nodes with the aiming angle, θ , are given in Figure 5-32.

* See page 132 for definitions of arrival parameters.

TABLE 5-15

SUMMARY OF 700^d JUPITER TRANSFERS: 1975 - 1986

Launch Date (Min. VHL)	δ_{\oplus} (deg)	VHL (KPS)	VHP (KPS)	VHT (KPS)	δ_{\oplus} (deg)	ρ_{\oplus} (deg)	θ_{\oplus} (deg)	RC (AU)	DTC (Days)
Jun 23, 1975	-7.36	9.20	7.05	16.25	-2.11	126.18	1.68	6.06	12
Jul 28, 1976	15.05	9.29	7.20	16.49	-4.88	130.04	1.67	6.21	12
Sep 2, 1977	30.97	9.49	7.51	17.00	-5.24	134.17	1.40	6.34	10
Oct 5, 1978	36.49	9.64	7.85	17.49	-3.64	137.46	1.21	6.43	9
Nov 5, 1979	31.65	9.61	8.13	17.74	-1.30	139.28	1.21	6.45	8
Dec 3, 1980	19.02	9.42	8.25	17.67	1.04	139.39	1.39	6.38	10
Jan 1, 1982	1.17	9.15	8.18	17.33	3.14	137.75	1.69	6.26	12
Feb 2, 1983	-19.10	8.99	7.95	16.94	4.90	134.34	1.87	6.12	13
Mar 9, 1984	-34.49	9.06	7.62	16.68	5.43	129.72	1.70	5.99	11
Apr 16, 1985	-37.24	9.19	7.30	16.49	4.03	125.78	1.53	5.94	10
May 23, 1986	-25.15	9.21	7.08	16.29	0.98	124.53	1.54	5.97	10

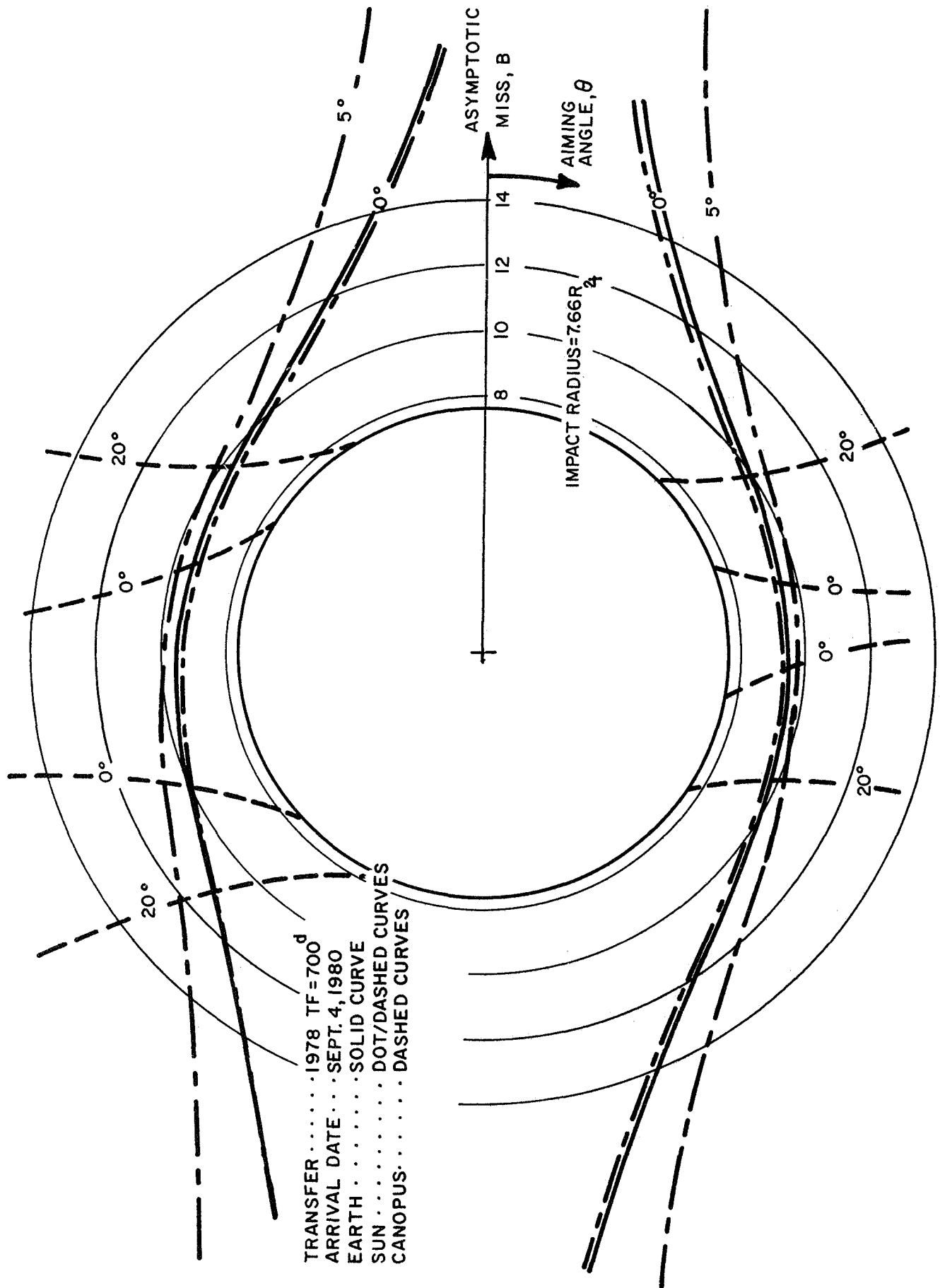


FIGURE 5-31. JUPITER CAPTURE OCCULTATION CONTOURS

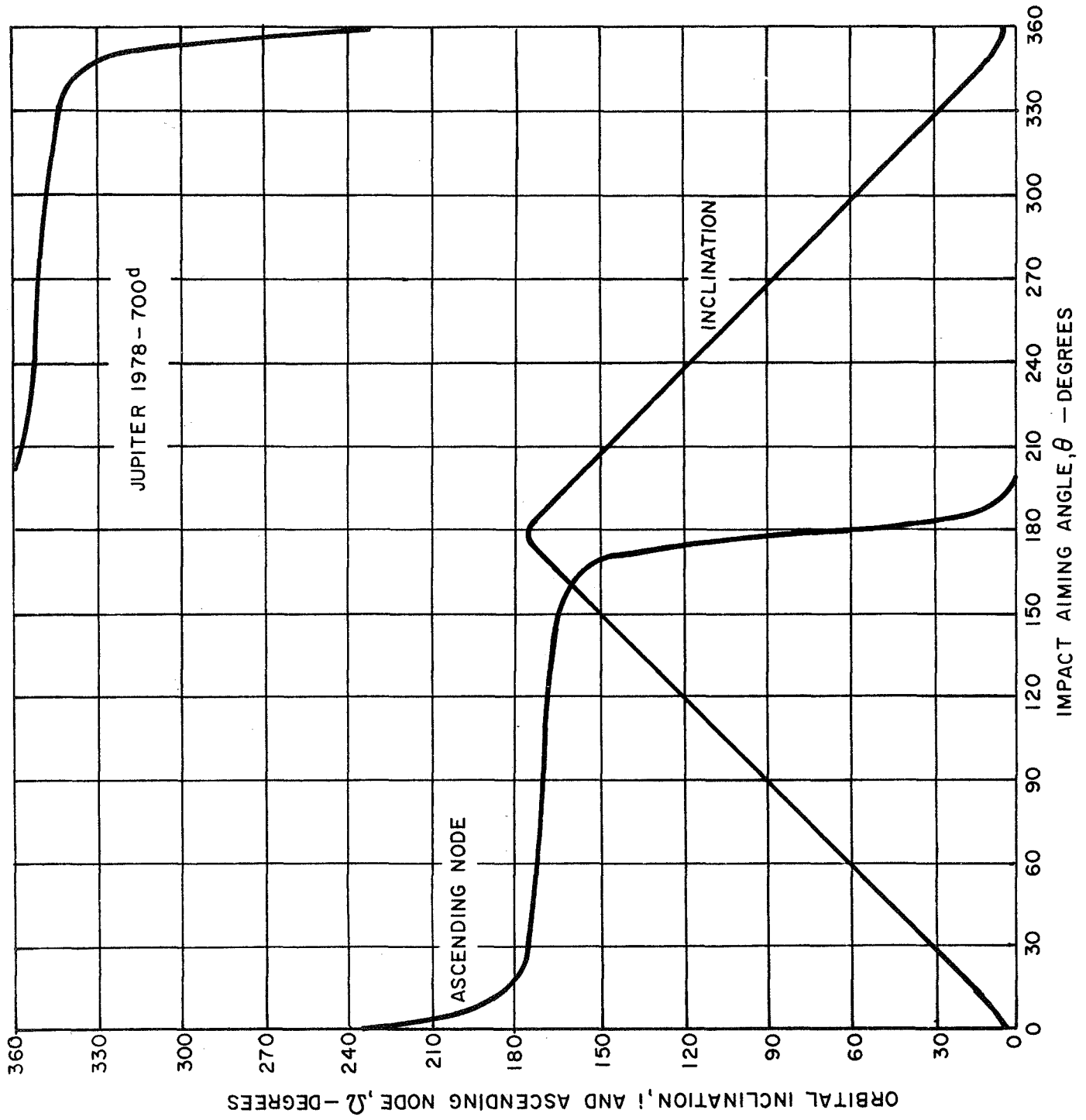


FIGURE 5-32. JUPITER AIMING ANGLE/ORBIT ORIENTATION RELATIONSHIP.

5.4.2 Orbit Characteristics and Constraints (Jupiter)

The three physical characteristics of Jupiter which are most influential in orbit selection at the planet are (a) the existence of radiation belts, (b) the rapid rotation rate of the planet, and (c) the presence of massive satellites. The radiation belts extend to about 3.5 Jupiter radii (Michaux et al. 1965) from the center of the planet and are a potential hazard for the spacecraft. For this reason, it was decided to constrain minimum orbit periapse altitudes (hp) to 2.5 Jupiter radii. Whenever possible, hp is chosen to be equal to this value to minimize measurement altitudes. A 50-year orbit lifetime curve is presented in Figure 5-33 for orbit eccentricities between 0 and 0.9. All Jupiter orbits with periapse altitudes greater than 0.006 Jupiter radii have orbit lifetimes greater than 50 years. The 2.5 Jupiter radii altitude radiation constraint obviously satisfies the 50-year orbit lifetime constraint used for orbit size selections at Mars and Venus.

Imaging measurements are constrained as part of the study procedure to a contiguous coverage technique. With the short rotation period of Jupiter (9.842 hrs), it is not possible to use subinteger Jupiter day orbits (as was shown in the Mars orbit selection) and maintain a minimum orbit altitude of 2.5 Jupiter radii. Hence, for contiguous coverage, candidate orbit sizes were chosen with periods approximately equal to an integer number of Jupiter rotation periods, i.e.,

$$N = \frac{\text{orbit period}}{\text{Jupiter day}} = 1, 2, 3, \dots \text{days/orbit.}$$

A maximum limit of 6.5 km/sec was set as a constraint on orbit capture and maneuvers. To illustrate this limit in terms of payload, an equally distributed 3-stage impulse of 6.5 km/sec using a propellant ISP of 400 sec with an allotment of 20% of the stage weight for structure, tankage, and engines

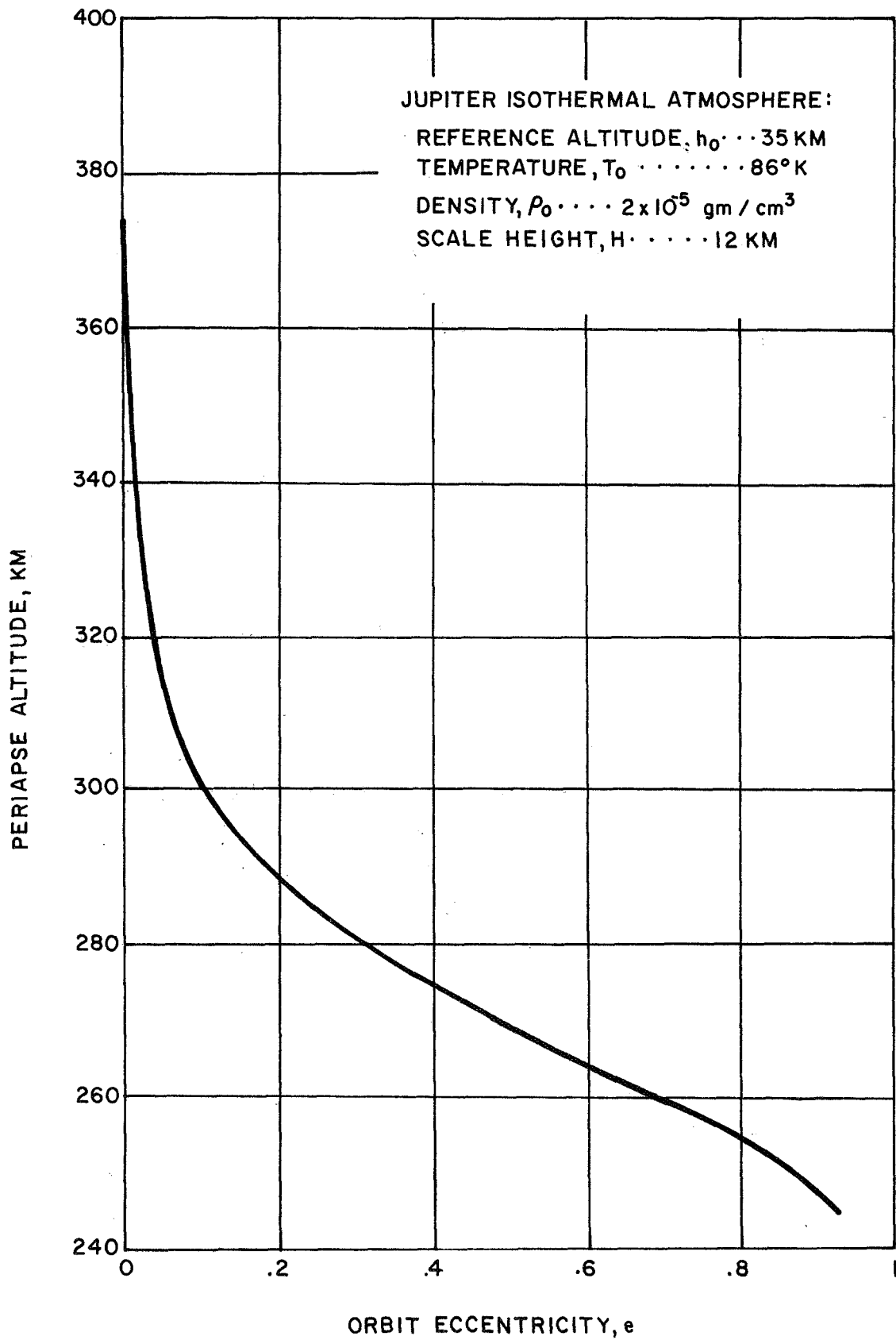


FIGURE 5-33. JUPITER 50-YEAR ORBIT LIFETIME CURVE.

has a useful orbit weight of approximately 10% of the total weight before impulse.

The region of acceptable orbit sizes, taking these constraints into account, is illustrated in Figure 5-34. Orbit period, expressed as Jupiter days per orbit, N , is plotted against periapse altitude with dotted curves of constant orbit eccentricity as a background. Orbit sizes with acceptable combinations of h_p and N are confined to a pie-shaped area in the center of the graph. Orbit periapse altitudes less than 2.5 Jupiter radii violate the radiation constraint. Orbit combinations of h_p and N in the lower right area of the graph (includes all circular orbits) exceed the maximum capture impulse requirement of 6.5 km/sec.

Nine candidate orbit sizes selected from Figure 5-34 are given in Table 5-16. The periapse altitude is fixed at 2.5 Jupiter radii for these orbits. The five inner satellites revolve about the planet in nearly circular, equatorial orbits, with orbit radii ranging from 2.5 to 26.4 planet radii. The satellites both perturb the spacecraft and present a possible collision hazard. If it is assumed that the fixed orbit positions have polar, or nearly polar, orbits with periapse near the equator (this is in fact the case) then only orbit nos. 2, 5, and 6 have a potential satellite collision hazard. The apoapse of orbit 2 comes within about 0.14 Jupiter radii (R) of the satellite Europa ($9.40 R$). Apoapse of orbits 5 and 6 come within 0.66 and 0.81 R of Ganymede ($15.00 R$).

Although orbits 2, 5, and 6 could be significantly perturbed by near misses of Europa or Ganymede, satellite perturbations are not considered in the orbit analysis, because of anticipated polar inclinations for imaging experiments. With orbit inclinations at or near 90 degrees, little time is spent in or near the plane of Jupiter's satellites.

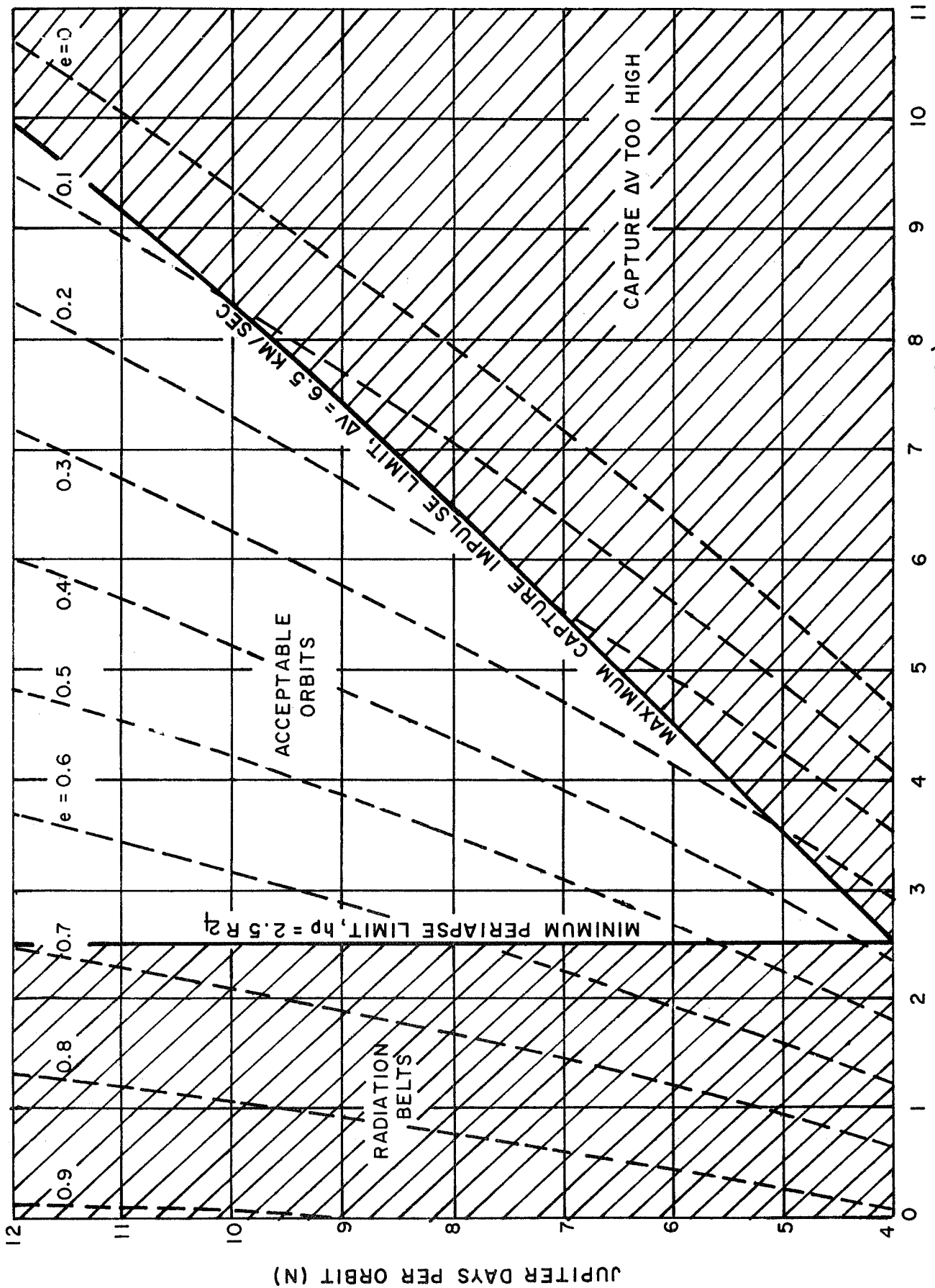


FIGURE 5-34. JUPITER CANDIDATE ORBIT SIZE CONSTRAINTS.

TABLE 5-16

JUPITER CANDIDATE ORBIT SIZES

Orbit No.	Days/ Orbit (N)	Periapse Altitude (km/pl.radii)	Eccen- tricity	Maximum Altitude Ratio, h/hp	Orbit Period (hrs)	Average* Capture ΔV (km/sec)
1	4	178375/2.5	0.3772	2.70	39.36	6.325
2	5	178375/2.5	0.4633	3.42	49.20	5.511
3	6	178375/2.5	0.5247	4.09	59.05	4.945
4	7	178375/2.5	0.5711	4.73	68.89	4.525
5	8	178375/2.5	0.6076	5.34	78.73	4.199
6	9	178375/2.5	0.6373	5.92	88.57	3.937
7	10	178375/2.5	0.6619	6.48	98.41	3.721
8	11	178375/2.5	0.6827	7.02	108.25	3.539
9	12	178375/2.5	0.7006	7.55	118.09	3.385
10	5	249725/3.5	0.3099	2.15	49.20	6.378
11	7	356750/5.0	0.2648	1.86	68.89	6.154

* Capture ΔV Based on Surveyed Average Hyperbolic Approach Speed, VHP = 7.64 km/sec, for 700 Day Jupiter Transfers.

IIT RESEARCH INSTITUTE

The large second zonal harmonic of Jupiter's gravitational potential ($J_2 = 0.0147$) could cause a significant perturbation of orbit ascending node and argument of periapse. However for polar orbits, the orbit sizes in Table 5-16 are so large that these perturbations have negligible effect on orbit stability for imaging measurements. For example, the smallest (most easily perturbed) orbit, orbit number 1, has a perturbation in the argument of periapse of only -0.104 degrees per Earth day at an inclination of 90 degrees. Oblateness perturbations are therefore ignored, except where orbit durations approach 1000 days and low inclinations (~ 30 degrees) are used to provide extensive coverage of Jupiter's red spot.

The altitude characteristics of candidate orbit sizes 1-9 (Table 5-16) are illustrated in Figure 5-35. Measurement arc (ordinate) is twice the true anomaly from periapse to a specified maximum measurement altitude, h . For all Jupiter transfers studied, the location of orbit periapse is on the planet's dark side and near its equator. Hence, from Figure 5-35, it is seen that no candidate orbit sizes using polar orbits can make daylight measurements at altitude ratios (h/h_p) of less than two without additional orbit maneuvers.

In order to provide an alternative to orbit off-periapse insertion and plane change maneuvers for Jupiter daylight experiments, two additional orbit sizes which have maximum altitude ratios of about two, were added to Table 5-16. These orbits are within the acceptable region of orbit sizes on Figure 5-34, but have higher periapse altitudes than the other selections in order to maintain a lower eccentricity and hence imply less altitude variation. The average measurement altitude is consequently larger than some of the other candidate orbit sizes. Notice also that the capture ΔV requirements (last column, Table 5-16) are also near the upper limit of 6.5 km/sec.

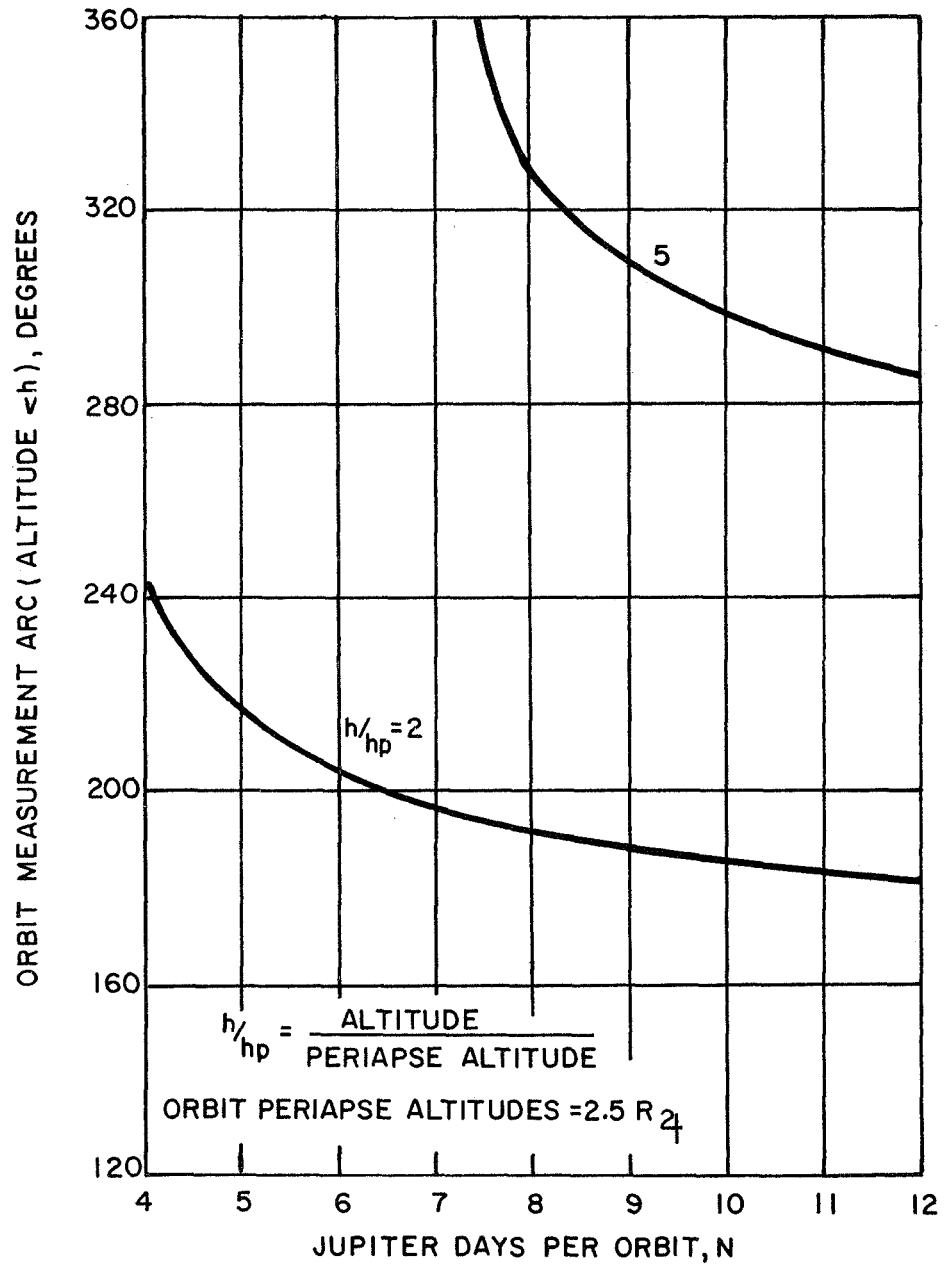


FIGURE 5-35. JUPITER ORBIT ALTITUDE RANGE

5.4.3 Orbit Selections (Jupiter)

The measurement families for which orbit selections were made are presented in Table 5-17. No specific solar elevation restrictions are given. One-third of the measurement families do, however, have a requirement of daylight (or night in some cases) coverage. The number of days to obtain complete longitudinal contiguous coverage is presented in Table 5-18 for all combinations of image size and overlap from Table 5-17 (except for image sizes of less than 1 km) for candidate orbits 1 through 9 of Table 5-16. Those orbits which cannot obtain complete longitudinal coverage at the specified image size and overlap within approximately 1000 days of capture (cross-hatched areas in the Table) were eliminated from consideration for those respective measurement families.

For constant periapse altitude orbits, the capture impulse decreases as the orbit period increases. In general two candidate orbit sizes were selected for each measurement family to study the tradeoff in mission time versus capture impulse. Two methods were used for imaging on the daylight side of the planet:

- (a) low eccentricity orbits so that measurement altitude variations do not exceed a factor of two,
- (b) move periapse to the light side of the planet using an off-periapse insertion on a highly elliptical, low inclination orbit followed by a plane change to high inclination, and finally reduce the eccentricity of the orbit.

The second method was used for measurement families that required daylight coverage only. The orbit selection results can be summarized as follows:

- (a) No circular orbits are possible for 700-day transfers with a maximum capture impulse constraint of 6.5 km/sec.

MIT RESEARCH INSTITUTE

TABLE 5-17

MEASUREMENT FAMILIES FOR JUPITER

Family Number	Observable Number(s)	Sensor* Type(s)	Minimum Image Size (km)	Overlap (%)	Minimum Coverage (%)	Solar Elevation Range (deg)	Coverage Distribution	Time for Coverage	Image Interval	Coverage Interval
1	36	RF	30,000	20	70	-	Subsatellite Points	-	< 2 min	-
2	1, 6, 9, 12, 24	R, IR, μ , MB	15,000	20	70	-	Cloud Belts, Red Spot	-	-	> 2/yr
3	26	IR	15,000	20	70	-	-	< 1 day	-	> 10/yr
4	26	UV, V	15,000	20	70	Day	-	< 1 day	-	> 10/yr
5	26	MB	15,000	20	70	Day&Night	-	< 1 day	-	> 10/yr
6	1, 6, 9	R	15,000	60	70	-	-	-	-	> 2/yr
7	21, 27, 33	IR, μ	5,000	20	70	-	Cloud Belts, Red Spot	-	-	> 4/yr
8	29	IR	5,000	20	10	-	Belts, Red Spot, Tropics	-	< 2 min	-
9	30	R	5,000	20	70	-	-	-	< 15 min	> 4/yr
10	31	RF	5,000	20	70	-	-	-	< 2 min	> 10/yr
11	3	R	5,000	20	3	-	Global	-	-	-
12	27, 33	UV, V, IR	5,000	20	70	Day	Cloud Belts, Red Spot	-	-	> 4/yr
13	29	UV, V, IR	5,000	20	10	Day	Belts, Red Spot, Tropics	-	< 2 min	-
14	29	MB	5,000	20	10	Day&Night	Belts, Red Spot, Tropics	-	< 2 min	-
15	33	MB	5,000	20	70	Day&Night	Cloud Belts, Red Spot	-	-	> 4/yr
16	37	V	5,000	20	70	Night	Polar Regions	-	< 1 hr	> 4/yr
17	25	IR, μ , MB	1,500	20	10	-	Cloud Belts, Red Spot	-	< 1 day	-
18	40	MB	1,500	20	3	Day	Random	-	-	> 4/yr
19	35	IR, μ	1,000	20	70	-	Red Spot, Tropics	< 1 day	-	> 10/yr
20	28	IR, μ	1,000	20	10	-	Cloud Belts, Red Spot	-	< 1 day	-
21	34	IR	1,000	20	10	-	Cloud Belts, Red Spot	-	< 15 min	> 4/yr
22	28, 34	UV, V, IR	1,000	20	10	Day	Cloud Belts, Red Spot	-	< 15 min	> 4/yr
23	34	MB	1,000	20	10	Day&Night	Cloud Belts, Red Spot	-	< 15 min	> 4/yr
24	32	RF	300	20	10	-	-	-	< 2 min	> 10/yr
25	20	R	3	20	1	-	-	-	-	> 1/300hr
26	20	R	3	60	1	-	-	-	-	> 1/300hr
27	2	R	.5	20	3	-	-	-	-	-

*Sensor Type Definitions are: UV...Ultraviolet
V....Visible
IR....Infrared
 μMicrowave
R....Radar
RF....Radio Frequency
MB....Multi-band

TABLE 5-18

JUPITER CANDIDATE ORBIT SIZE COVERAGE TIMES

Image Size (km)	% Overlap	Swath Width (km)	No. of Degrees of Long.	No. of Orbits To Cover Surface	Days to Cover Surface							
					n=4	n=5	n=6	n=7	n=8	n=9	n=10	n=12
30,000	20	25,000	20	18	29.5	36.9	44.3	51.7	59.	66.4	73.8	88.6
15,000	20	12,500	10	36	59.	73.8	88.6	103.3	118.1	132.84	147.6	177.1
15,000	60	9,375	7.5	48	78.7	98.4	118.1	137.8	157.4	177.1	196.8	236.2
5,000	20	4166.7	3.35	107.46	176.2	220.3	264.4	308.4	352.5	396.5	440.6	528.7
1,500	20	1,250	1	360	590.4	738.0	885.6	1033.2	1180.8	1328.4	1476.0	1771.2
1,000	20	833.3	.67	537.3	881.2	1101.5	1321.8	1542.1	1762.3	1982.6	2202.9	2643.5
300	20	250	.20	1,800	2952.	3960.	4428.	5166.	5904.	6642.	7380.	8856.

- (b) Polar orbits are used exclusively, except for extended coverage of Jupiter's Red Spot from an orbit inclination of 30° .
- (c) Coverage time can vary from 30 to 200 days for regional coverage depending upon the orbit size used.
- (d) Daylight coverage takes longer than unconstrained illumination coverage because higher period orbits must be used to insure acceptable measurement altitudes in daylight within a total impulse expense of 6.5 km/sec.
- (e) Local coverage time (minimum image sizes of 1000-5000 km) varies from 200 to 1100 days depending upon image size, overlap, and illumination specifications.
- (f) The maximum total impulse employed is 6.64 km/sec (for daylight coverage) employing an off-periapse insertion, 85° plane change, and orbit eccentricity reduction from 0.95 to 0.70.
- (g) The minimum capture impulse is 3.77 km/sec.
- (h) Orbit altitudes varying between 3.5 and 7.5 Jupiter radii, or between 5 and 9.3 Jupiter radii, are used to obtain daylight and night coverage respectively on the same orbit.

5.5

The Moon

The measurement families and group specifications for the Moon are presented in Table 5-19. These are related to pure science objectives that have been the basis for orbit selections at the planets. However, during the time frame of 1975 to 1995 lunar orbital missions will involve manned operations or be in support of manned (orbital and surface)

TABLE 5-19

MEASUREMENT FAMILIES FOR THE MOON

Family Number	Observable Number(s)	Sensor* Type(s)	Minimum Image Size (km)	Overlap (%)	Minimum Coverage (%)	Solar Elevation Range	Coverage Distribution	Time for Coverage	Image Interval	Coverage Interval
1	35	V	300	10	70	50-80	-	< 1 day	-	> 10/yr
2	35	V	300	10	70	30-60	-	< 1 day	-	> 10/yr
3	1	V	300	10	70	15-30	-	-	-	-
4	41	MB	300	10	70	day	-	-	-	-
5	1	R	300	10	70	-	-	-	-	-
6	21	IR, μ , MB	300	10	70	-	-	-	< 30 hr	-
7	1	V	300	60	70	70-85	-	-	-	-
8	1	R	300	60	70	-	-	-	-	-
9	4	UV, IR	100	10	70	70-90	-	-	-	-
10	7, 13	V	100	10	70	50-80	-	-	-	-
11	4, 7, 10, 13	V, IR, MB	100	10	70	15-30	-	-	-	-
12	4, 7, 10, 13	R	100	10	70	-	-	-	-	-
13	22	IR, μ , MB	100	10	70	-	-	-	< 30 hr	-
14	7, 10	V	100	60	70	70-85	-	-	-	-
15	7, 10	R	100	60	70	-	-	-	-	-
16	5	UV, IR	0.5	10	3	70-90	-	-	-	-
17	8, 14	V	0.5	10	3	50-80	-	-	-	-
18	2	V	0.5	10	3	30-60	-	-	-	-
19	5, 8, 11, 14, 20	V, IR, MB	0.5	10	3	15-30	-	-	-	> 1/300hr
20	41	MB	0.5	10	3	day	-	-	-	-
21	2, 5, 8, 11, 14, 20	R	0.5	10	3	-	-	-	-	> 1/300hr
22	23	IR, μ , MB	0.5	10	3	-	-	-	< 30 hr	-
23	8, 11, 20	V	0.5	60	3	70-85	-	-	-	> 1/300hr
24	8, 11, 20	R	0.5	60	3	-	-	-	-	> 1/300hr

*Sensor Type Definitions are: UV...Ultraviolet
V....Visible
IR...Infrared
 μMicrowave
R....Radar
MB...Multi-band

missions. It is doubtful therefore, that any realistic orbit selections are possible without the consideration of manned mission objectives. The presence of manned lunar operations changes the premise that scientific imaging experiments control orbital mission support requirements. Orbit selections for lunar measurement families were not attempted in this study, and support requirements were not estimated.

6. IMAGING SENSOR SYSTEM SCALING LAWS

In this study, imaging sensor systems are represented by "scaling laws" which provide a quantitative relationship between the imaging system characteristics and the demands imposed upon spacecraft subsystems by imaging experiments. This section summarizes and illustrates the scaling laws for those imaging system which are useful in support of planetary exploration objectives. The scaling laws provide a tool for estimating imaging experiment support requirements, given the specifications of the required imagery and an orbit definition. In this study, the scientific objectives of planetary exploration for which imaging systems are useful have been identified and are summarized in Section 3. The nature and the quality of the desired images have been defined in Section 4, while Section 5 has summarized the procedures used for orbit selection. Section 7, which follows this section, presents the results of using the sensor system scaling laws.

With regard to experiment support requirements, the relevant imaging system characteristics are:

- a. Weight
- b. Volume
- c. Shape
- d. Field of View
- e. Pointing Requirements
- f. Yaw, Pitch, and Roll Rate Control
- g. Power
- h. Data Acquisition Rate
- i. Required Operating Environment
- j. Electromagnetic Interference Generation and Susceptibility
- k. Calibration Requirements
- l. Command and Sequencing Requirements.

Each different type of imaging system is described by a set of sensor scaling laws which are designed to provide items (a) through (h) above. These characteristics are sensitive to the image specifications, the orbit selection, and the details of the imaging system. Items i through k are most sensitive to the type of imaging system, rather than to the image specifications or orbit. For example, high performance optical components require temperature stabilization within 5°F, regardless of the orbit altitude. The command and sequencing characteristics are most sensitive to the details of the selected orbit. The only sequencing aspect considered here is the relation between the orbital altitude, the image size, and the time interval between images. Orbital parameters which affect the sequencing requirements are noted on the orbit selection data sheets in Volume III.

The analysis of scientific objectives, which is summarized in Section 3, has identified the following types of imaging systems as at least marginally useful:

- ultraviolet (2000 - 4000 Å)
- visual (4000 - 7500 Å)
- infrared (0.75 - 200 μ)
- passive microwave (0.1 - 100 cm)
- radar (0.1 - 100 cm)
- radio frequency (1 - 100 m)
- multiband

The following subsections summarize the scaling laws for these types of imagers in the order given above. Scaling laws are given for both television and film photography systems in the visual portion of the spectrum, and for both noncoherent and synthetic aperture radar imaging systems. However, no scaling laws are provided for radio frequency or multiband systems. Scaling laws are valid only if they are based upon a broad range of design or operational experience, and no such experience exists for radio frequency or multiband systems. A complete derivation and discussion of all the scaling laws

is provided in Volume IV of this final report series. Only a scaling law summary and illustrative example for each imager type is presented here. It should be emphasized that the scaling laws are not a substitute for detailed experiment design. They are only intended to provide representative sensor system configurations, thus permitting estimation of typical support requirements demanded by specific imaging experiments.

6.1. Ultraviolet Scanning Systems

Figure 6-1 is a logic diagram which summarizes the design procedures developed in Volume IV for ultraviolet scanning systems. Given a set of image specifications and a set of orbit parameters, the logic diagram indicates each step in the estimation of the support requirements implied by any specific ultraviolet scanning experiment. The specific types of image specifications and orbit parameters which significantly influence the sensor system design are listed in the two large boxes in the upper left hand corner of the logic diagram (Figure 6-1). The design proceeds from the image specifications and orbit definition as shown. The oval boxes represent estimation of experiment support requirements, while the rectangular boxes represent steps in the design procedure. The scaling laws are summarized in Figure 6-2, which is designed for use with the logic diagram. That is, the numbered blocks in the scaling law chart relate to the numbered blocks in the logic diagram, as will be made clear in the example design below. Table 6-1 and Figure 6-3 present data which may be required during system design, as illustrated in the design example given here.

To illustrate the design procedure and estimation of experiment support requirements, consider an ultraviolet imaging experiment for the study of cloud formation processes at Venus. The nominal image specifications for this experiment have been given in Table 4-1. The worth curves given in Section 4 may be used to arrive at a somewhat less demanding

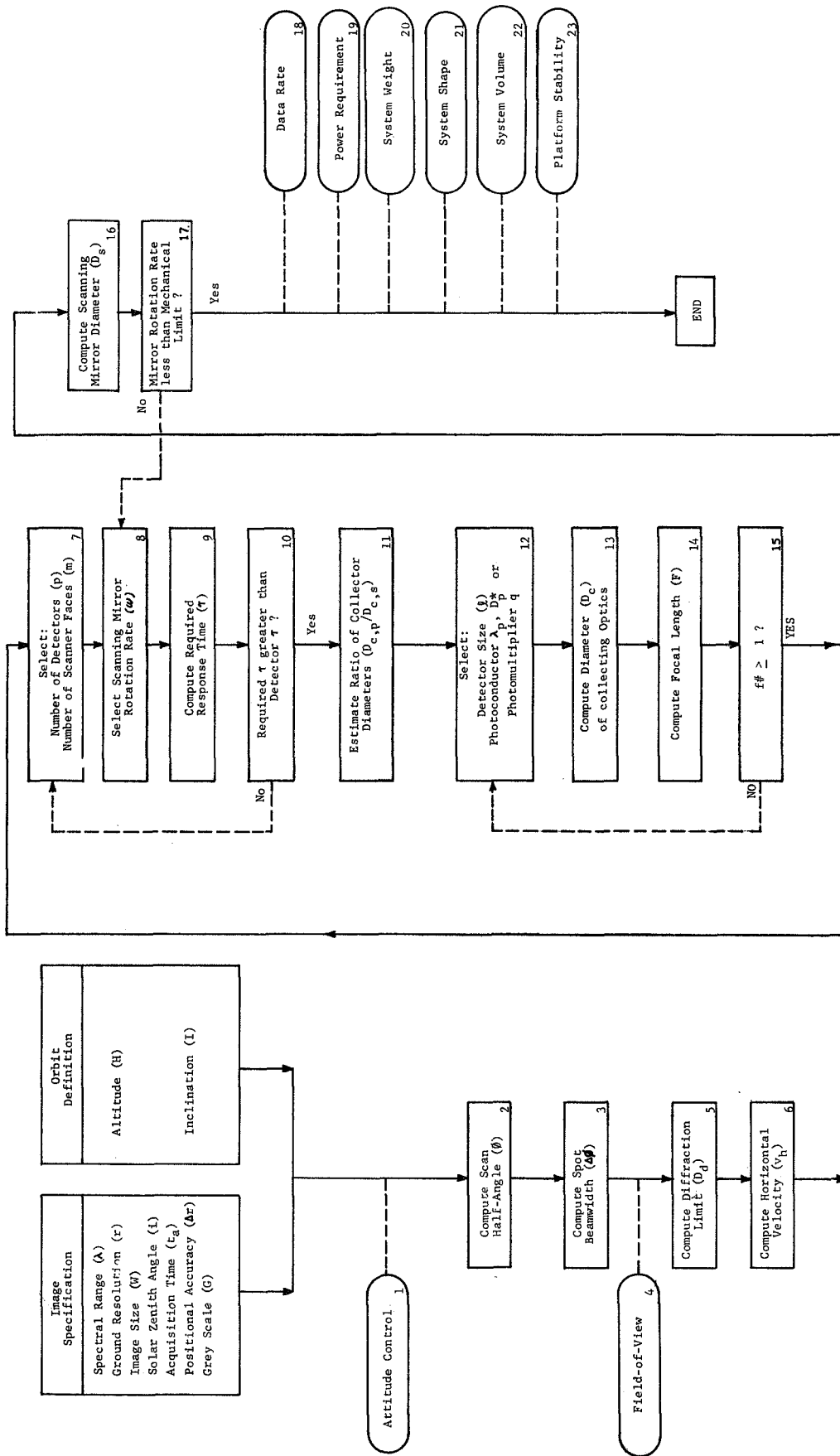


FIGURE 6-1. LOGIC DIAGRAM FOR ULTRAVIOLET SCANNING SYSTEMS

$\Delta\theta = \frac{\Delta r}{R}$ radians $\gamma = \frac{V}{2R}$ If $\gamma \leq 0.1$, $\beta \tan^{-1} \frac{V}{2R}$ Otherwise, $\beta = \cot^{-1} \left(\frac{R+H}{R} \tan \gamma - \cot \gamma \right)$	required $\tau = \frac{\Delta\theta}{\omega}$ detectors τ limited by SOA to: 10^{-3} sec for photoconductors 10^{-6} sec for photomultipliers	$\beta\theta = \frac{R}{R+H} \left(\frac{R+H}{R} \tan \gamma - \cot \gamma \right)$	$\beta\theta = \frac{R}{R+H} \left(\frac{R+H}{R} \tan \gamma - \cot \gamma \right)$
$\Delta\theta = \frac{1.22 \lambda}{2D}$ $V_p = \sqrt{2 - \frac{2H}{R} \cos \gamma}$ $V_h = \sqrt{2 - \frac{2H}{R} \cos I}$ where $V_e = 270$ m/sec for Mars 1.27×10^4 m/sec for Jupiter 0 for Moon, Mercury, Venus Stop if $V_h \geq V$	detectors τ limited by SOA to: 10^{-3} sec for photoconductors 10^{-6} sec for photomultipliers	$D_{C,P} = 3 \times 10^{-12} \left(\frac{S/N}{D} \right)^{\frac{1}{2}} \left(\frac{M}{C_p F} \right)^{\frac{1}{2}}$ or $D_{C,P} = \frac{2.33}{20} \left(\frac{D_p \cdot S/N}{P \cdot C_p \cdot F} \right)^{\frac{1}{2}} \left(\frac{M}{C_p} \right)^{\frac{1}{2}}$ but $D_C \geq D_d$	$V_p = \sqrt{2 - \frac{2H}{R} \cos \gamma}$ $V_h = \sqrt{2 - \frac{2H}{R} \cos I}$ where $V_e = 270$ m/sec for Mars 1.27×10^4 m/sec for Jupiter 0 for Moon, Mercury, Venus Stop if $V_h \geq V$
$P \leq 10$ (SOA limit) m normally < 10	suggested values: Photoconductors $q = 0.2$ $F = 10^{-3}$ $(10^{-4} \leq F \leq 0.1)$	$M_c = 168 D_C^2$ $M_b = \begin{cases} 240 D_C^3 & \text{for } m = 1 \\ 407 D_C^3 & \text{for } m = 2 \\ 27.8 m D_C^3 \sin \frac{\pi m}{2} & \text{for } m \geq 3 \end{cases}$ System Mass = $M_c + M_b + P$	$M_c = 168 D_C^2$ $M_b = \begin{cases} 240 D_C^3 & \text{for } m = 1 \\ 407 D_C^3 & \text{for } m = 2 \\ 27.8 m D_C^3 \sin \frac{\pi m}{2} & \text{for } m \geq 3 \end{cases}$ System Mass = $M_c + M_b + P$
$\omega \geq \frac{2 \pi V_h}{\text{per } H \Delta\theta}$ ω normally selected as minimum	$D_{C,P} = 0.045 \left(\frac{M}{C_p} \right)^{\frac{1}{2}}$ If < 1 , photomultiplier detectors will use smaller collecting optics than solid-state detectors.	$M_c = 168 D_C^2$ $M_b = \begin{cases} 240 D_C^3 & \text{for } m = 1 \\ 407 D_C^3 & \text{for } m = 2 \\ 27.8 m D_C^3 \sin \frac{\pi m}{2} & \text{for } m \geq 3 \end{cases}$ System Mass = $M_c + M_b + P$	$M_c = 168 D_C^2$ $M_b = \begin{cases} 240 D_C^3 & \text{for } m = 1 \\ 407 D_C^3 & \text{for } m = 2 \\ 27.8 m D_C^3 \sin \frac{\pi m}{2} & \text{for } m \geq 3 \end{cases}$ System Mass = $M_c + M_b + P$
$P \leq 10$ (SOA limit) m normally < 10	$D_{C,P} = 0.045 \left(\frac{M}{C_p} \right)^{\frac{1}{2}}$ If < 1 , photomultiplier detectors will use smaller collecting optics than solid-state detectors.	$M_c = 168 D_C^2$ $M_b = \begin{cases} 240 D_C^3 & \text{for } m = 1 \\ 407 D_C^3 & \text{for } m = 2 \\ 27.8 m D_C^3 \sin \frac{\pi m}{2} & \text{for } m \geq 3 \end{cases}$ System Mass = $M_c + M_b + P$	$M_c = 168 D_C^2$ $M_b = \begin{cases} 240 D_C^3 & \text{for } m = 1 \\ 407 D_C^3 & \text{for } m = 2 \\ 27.8 m D_C^3 \sin \frac{\pi m}{2} & \text{for } m \geq 3 \end{cases}$ System Mass = $M_c + M_b + P$

NOMENCLATURE
(MKS units implied)

- D_c - Collecting aperture diameter
- $D_{C,P}$ - D_c for photomultiplier system
- $D_{C,S}$ - D_c for photoconductive system
- D_d - Diffraction limit for D_c
- D_p - Photoconductive detector peak detectivity
- D_s - Scanning mirror diameter
- DR - Data acquisition rate (bits/sec)
- F - Aperture stop (F-number)
- f - Photometric function
- $f\theta$ - Aperture stop (F-number)
- FOV - Field-of-view
- G - Bits per resolution element (normally 6)
- H - Sensor altitude
- H_a - Orbit apogee altitude
- H_p - Orbit perigee altitude
- I - Orbit inclination
- I_s - Solar zenith angle
- L - Detector linear size
- M_c - Mass of collecting optics
- M_b - Mass of scanning mirror
- m - Number of scanning scans
- P - System power requirement
- q - Number of detectors
- q - Photomultiplier quantum efficiency
- R - Planet radius
- r - Ground resolution
- S/N - Signal-to-noise ratio (normally 120)
- V - System volume
- V_h - Apparent horizontal ground speed
- V_p - Speed of subsatellite point
- V_r - Planet equatorial rotational speed
- W - Linear ground size of image
- γ - Planocentric half-angle subtended by W
- Δr - Image location error on planet
- $\Delta\theta$ - Allowable pointing error
- $\Delta\theta$ - Allowable sensor roll or yaw rate
- $\Delta\theta$ - Scanning beam angular size
- λ - Wavelength
- λ_p - Photoconductive detector cutoff wavelength
- β - Half-angle of scan
- τ - Response time
- ω - Scanning mirror rotation rate

FIGURE 6-2. SCALING LAWS FOR ULTRAVIOLET SCANNING SYSTEMS

Table 6-1

Values of r_{ϕ}/r_0

<u>ALTITUDE</u> <u>RADIUS</u>	Half-Angle Field-of-View ϕ (Deg.)							
	10	20	30	40	50	60	70	80
0.01	1.03	1.13	1.34	1.72	2.47	4.19	9.66	69.9
0.02	1.03	1.14	1.35	1.74	2.53	4.40	11.2	--
0.03	1.03	1.14	1.35	1.76	2.59	4.64	13.4	--
0.04	1.03	1.14	1.36	1.78	2.65	4.92	17.0	--
0.05	1.03	1.14	1.37	1.80	2.72	5.24	24.1	--
0.06	1.03	1.15	1.38	1.82	2.79	5.61	51.6	--
0.07	1.03	1.15	1.38	1.84	2.87	6.04	--	--
0.08	1.04	1.15	1.39	1.87	2.95	6.58	--	--
0.09	1.04	1.15	1.40	1.89	3.04	7.24	--	--
0.1	1.04	1.16	1.41	1.92	3.13	8.08	--	--
0.2	1.04	1.18	1.50	2.22	4.80	--	--	--
0.3	1.05	1.21	1.60	2.71	27.3	--	--	--
0.4	1.05	1.25	1.74	3.65	--	--	--	--
0.5	1.06	1.28	1.93	6.66	--	--	--	--
0.6	1.07	1.33	2.18	--	--	--	--	--
0.7	1.07	1.38	2.56	--	--	--	--	--
0.8	1.08	1.43	3.22	--	--	--	--	--
0.9	1.09	1.50	4.74	--	--	--	--	--
1.0	1.10	1.58	--	--	--	--	--	--
2.0	1.23	--	--	--	--	--	--	--
3.0	1.49	--	--	--	--	--	--	--
4.0	2.23	--	--	--	--	--	--	--

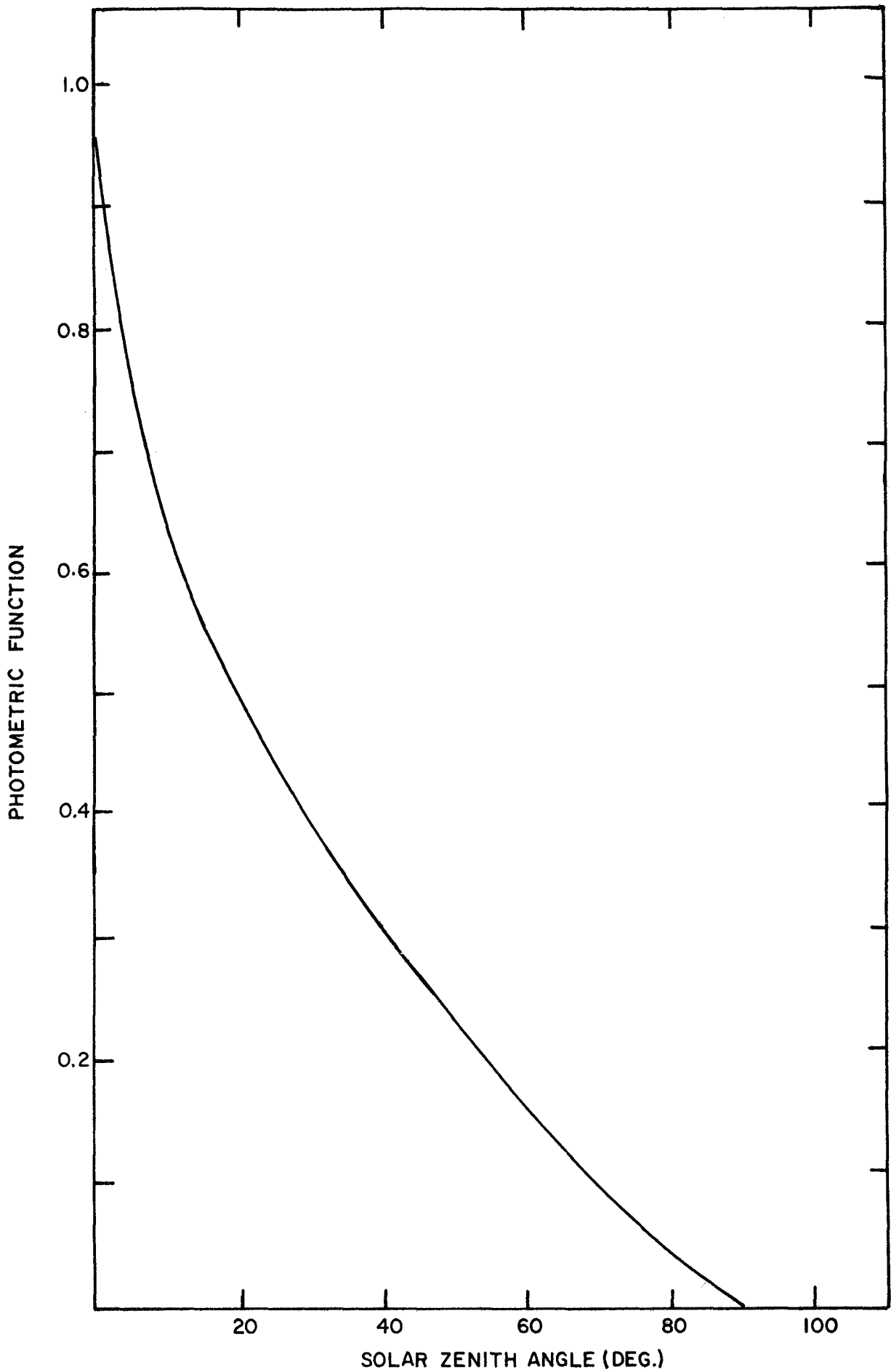


FIGURE 6-3. LUNAR PHOTOMETRIC FUNCTION

set of image specifications, and yet a set which describes imagery having essentially the same scientific value as that associated with the nominal image specifications. These relaxed specifications are summarized in Table 6-2 and are used as the basis of experiment design. Also shown in Table 6-2 are the orbit parameters for a typical orbit suitable for this experiment. This particular orbit was selected to provide maximum planetary coverage under daylight conditions in a minimum amount of time, and is more fully described by orbit data sheet # 101 in Volume III. Table 6-2 gives only those image specifications which significantly influence the sensor system design. Other types of image specifications not shown here have been used to select an appropriate orbit. That is, for cloud formation imagery at Venus, at least seventy percent coverage of the planet is desired four times per planetary year. These requirements have influenced the orbit selection, but do not affect the sensor system design. Using the image specifications and orbit parameters given in Table 6-2, the sensor system design proceeds according to the logic diagram and scaling law chart as follows:

Step 1: The attitude control requirement depends upon the required positional accuracy and the spacecraft altitude. Since the allowable error in the location of the imaged scene is 10 km, the pointing accuracy requirement is $10/454$ or 0.022 radians (1.3 degrees).

Step 2: For an image ground size of 600 km, the half-angle γ subtended at the planet center by a great-circle arc length of 600 km is 0.049 radians, taking the planet radius as 6100 km. Since γ is less than 0.1 radians, the effects of planetary curvature in computing the required field-of-view may be ignored. Thus, the scan half-angle ϕ is simply $\tan^{-1}(W/2H)$ or 0.584 radians (33.5 degrees).

Table 6-2

Image Specifications and Orbit Parameters for
Ultraviolet Cloud Formation Imagery at Venus

Spectral Range	500-4000 Å
Ground Resolution	3 km
Minimum Image Size	600 km
Solar Zenith Angle	0-90 deg
Maximum Acquisition Time	1 min
Positional Accuracy	10 km
Grey Scale	6 bits
Orbit Periapse Altitude	454 km
Orbit Apoapse Altitude	454 km
Orbit Inclination	90 deg

Step 3: Ignoring the effects of planetary curvature, the required angular resolution is simply r/H or 6.6 milliradians (0.39 degrees). However, interpolation in Table 6-1 shows that if the half-angle field-of-view is 33.5 degrees, the ground resolution provided by such an angular resolution is a factor of 1.55 poorer at the edge of the field-of-view than at the nadir or subsatellite point. Thus, the angular resolution, or scanning beam size, must be reduced to 4.26 milliradians (0.24 degrees) if a 3 km ground resolution is to be achieved throughout the entire scan length.

Step 4: Since the scanning beam size is 0.24 degrees, and the scan half-angle is 33.5 degrees, the sensor system field-of-view is 0.24 by 67 degrees.

Step 5: For a wavelength of 4000 \AA and an angular resolution of 4.26 milliradians, the optical system is diffraction-limited to a diameter of 0.011 cm. That is, the optical system diameter must be at least 0.011 cm. Although, in this case, the diffraction limit is not a problem, it is useful to determine the diffraction limit early in the design procedure. Current state-of-art limits the optical system diameter to about one meter. If the diffraction limit exceeds one meter, the design may be abandoned as beyond the current state-of-art. Actually, the optical system could be as large as two meters at the current state-of-art. However, the scanning mirror is state-of-art limited to about two meters, and since the scanning mirror is roughly twice the diameter of the optics, the optical system is limited to about one meter.

Step 6: The gravitational constant of Venus is $3.25 \times 10^{14} \text{ m}^3/\text{sec}^2$ and the planet radius is $6.1 \times 10^6 \text{ m}$. Thus for a circular orbit of altitude $4.54 \times 10^5 \text{ m}$, the speed of the subsatellite point on the surface of a non-rotating planet is $6.55 \times 10^3 \text{ m/sec}$. The effects of planet rotation on apparent ground speed may be neglected for orbital experiments at the

Moon, Mercury, and Venus. Thus the apparent ground speed is taken as 6.55 km/sec. At this ground speed, it will take the subsatellite point $600/6.55$ or 92 seconds to traverse 600 km on the visible surface. That is, for a scanning system, 92 seconds will be required to obtain data from a ground (or cloud) area of 600 by 600 km. The image specifications require that the data be collected in about one minute. By using two sensor systems, one pointing forward, the other aft, the data could be collected in 46 seconds. This would approximately double the experiment weight, volume, power, and data rate support requirements. In this study, the experiment support requirements have been estimated by using a single sensor system and accepting those data acquisition and repetition times provided by the orbit characteristics.

Step 7: As an initial design guess, a single-faced scanning mirror and a single detector may be used. The current state-of-art limits the system to a linear array of no more than ten detectors.

Step 8: The minimum rotation rate of the scanning mirror is determined by the need to avoid gaps between consecutive scans. In this example, with a one-faced mirror and one detector, the minimum rotation rate is 21.3 radians/sec, or about 200 rpm. Although the design rotation rate may be selected as any value which is not less than the minimum value of 21.3 radians/sec, usually the minimum value itself should be selected. Rotation rates larger than necessary will result in larger optical systems but less stringent platform stability requirements, because the amount of time spent observing each scene resolution element decreases as the rotation rate increases. Thus in this example, the scanning mirror rotation rate is taken as 21.3 radians/sec.

Step 9: The response time required of the detector is assumed to be one-half the dwell time per resolution element.

In this example, the detector response time must be 10^{-4} sec, or less.

Step 10: The required detector response time eliminates consideration of solid-state photoconductive detectors at the design mirror rotation rate. Either a photomultiplier tube must be used, or else the dwell time per resolution element must be increased a factor of ten to permit use of a photoconductive detector. The dashed line in the logic diagram indicates this possible iteration. The dwell time may be increased by decreasing the mirror rotation rate, which may be accomplished by increasing the number of detectors or the number of faces on the scanning mirror.

Step 11: If both a photoconductive or photomultiplier detector can be used, it is useful to estimate which type of detector will require the larger optical system. Ignoring detector response time problems for the moment, in this example the ratio of the optical system diameter required by a photomultiplier to that required by a photoconductor is about 0.38. That is, even if a solid-state detector had a sufficiently quick response time, the optical system implied by use of a photomultiplier tube has a diameter only 38 percent of that implied by use of a solid-state detector. This estimate of comparative optical system sizes is quite approximate, and depends upon the specific characteristics of the detectors. Reasonable values have been assumed in deriving the formula shown in the scaling law chart, but by changing the detector characteristics within reasonable bounds (in particular the size of the solid-state detector), the ratio of optical system diameters can be changed by a factor of two. That is, the estimate of comparative optical system sizes is only accurate to within a factor of about two.

Step 12: Once it has been decided to use solid-state or

photomultiplier detectors, the detector characteristics may be determined. For photomultiplier detectors, the quantum efficiency may be taken as about 20 percent over the spectral region from 2000 to 4000 Å. The detector effective size (ℓ) may be initially selected as about one millimeter. Rather wide latitude is permitted in the selection of photomultiplier detector effective size. Use of a field stop permits effective sizes of about 0.1 millimeter, while the photosensitive surface of a multiplier tube could probably be made as large as ten centimeters. For solid-state detectors (in particular, for SnO_2 and $\text{ZnS} - \text{MgS}$), detectivities of $4 \times 10^{11} \text{ cm-Hz}^{1/2}/\text{watt}$ at a long wavelength cutoff of 3000 Å are appropriate. Solid-state detectors cannot be made with uniformly sensitive areas nearly as large as for photomultipliers.

Step 13: The optical system collecting diameter is given by $D_{c,p}$ for photomultiplier tubes and by $D_{c,s}$ for solid-state detectors. The numerical coefficients in the given formulae presume use of MKS units. A value of 120 is recommended for the signal/noise ratio, as this corresponds to detection of scene reflectivity differences of five percent. The solar ultraviolet spectrum has been multiplied by the planetary albedo and the spectral response of the detector, and then integrated over wavelength to obtain the constants C_p and C_s , which also accounts for the heliocentric radius of the planet. For C_p , which is appropriate for photomultiplier detectors, the detector is assumed to have a flat spectral response and the spectral region from 2200 to 4000 Å has been used. For C_s , which is appropriate for solid-state detectors, the detector sensitivity per unit incident energy is taken as proportional to wavelength and the spectral region from 2200 to 3000 Å has been used. The scene photometric function is taken as $\cos i$ for Venus, Mars, and Jupiter, where i is the solar zenith angle. For daylight scenes, in which the zenith angle is not specified, the zenith angle may be taken as sixty degrees. For the Moon

and Mercury, where the surface is visible in the ultraviolet, the lunar photometric function given in Figure 6-3 should be used. The expressions given for the optics collecting diameter assume an optical efficiency of eighty percent. Other values may be used by noting that the diameter is inversely proportional to the square root of the optical efficiency. To continue with the sample design problem, use of a photomultiplier tube at Venus implies that C_p is 3×10^{-5} watts/meter. Using a solar zenith angle of sixty degrees, the value of the photometric function is 0.5. Finally, with a signal/noise ratio of 120 and a quantum efficiency of twenty percent, the required optical system collecting diameter is 3.4×10^{-3} meters. Since the optical system is diffraction-limited to 0.1 millimeter (Step #5), the optical system size is determined by the need to collect adequate energy rather than by resolution constraints. Since Venus is close to the sun, and has a high albedo, the necessary optical size is quite small. It is not necessary (in this case) to estimate the size of the optical system with any greater accuracy, since the optical system clearly has little impact upon the experiment support requirements.

Step 14: With a detector effective size of one millimeter, the optical system focal length is 0.23 meters.

Step 15: Using an optical diameter of 3.4 millimeters, the f-number is $f/69$. In most cases, the f-number can be easily altered by changing the detector size or the collecting aperture diameter. The exact value of the aperture stop is not significant. It is, however, important to ensure that the system can be designed with an f-number of unity or larger. In this particular design example, it is likely that an optical system diameter larger than 3.4 millimeters would be used,

and the f-number is likely to be on the order of $f/10$ or $f/20$. If the estimated aperture stop is less than unity, the easiest design remedy is to increase the effective size of the detector. This iterative loop is shown by the dashed line in the logic diagram. For solid-state detectors, this will also increase the required size of the collecting optics. For photomultiplier systems, the only effect will be to increase the system focal length, and hence the size of the sensor system.

Step 16: The size of the scanning mirror depends upon the number of faces on the mirror and the size of the collecting optics. For a single-sided mirror, as in the design example, the diameter of the scanning mirror is simply 1.414 times the optical collecting diameter. Thus, continuing with the example, the minimum diameter of the scanning mirror is 4.8 millimeters.

Step 17: An upper limit to the permissible rotation rate of the scanning mirror has been estimated on the basis of dynamic distortion of the optically-flat mirror surfaces. For a beryllium scanning mirror, optical distortion may become significant when the rotation rate (radians/sec) is about $193/D_s$, where D_s is the mirror diameter in meters. For the illustrative design problem, this implies that optical distortion will not be serious for rotation rates up to 4×10^4 radians/sec, or about 400,000 rpm, assuming a 4.8 millimeter diameter scanning mirror. An additional constraint is that rotation rates of 10^6 radians/sec may not be feasible, regardless of the size of the mirror. If the initial design rotation rate exceeds $193/D_s$ or 10^6 radians/sec, the rotation rate must be reduced. This will, of course, affect all the steps in the design process from Step #8 onward. On the other hand, if the rotation rate is acceptable, the system design is sufficiently well-defined that the remaining experiment support requirements may be estimated.

Step 18: The rate at which the sensor system acquires data is estimated as shown. For the example, this yields a data acquisition rate of 3.0×10^4 bits/sec, assuming that the data from each resolution element can be described by six binary bits (corresponding to 64 shades of grey).

Step 19: The system average power requirement is approximately one watt, since only one detector is used.

Step 20: The optical system has a mass of about 2 grams (for a 3.4 millimeter aperture), while the scanning system has a mass of about 27 milligrams (for a 4.8 millimeter diameter mirror). The total imaging system mass is estimated as one kilogram, or about two pounds. The scanning system mass estimates presume use of beryllium mirrors. Both the optical system and scanning system mass scaling laws have been based on use of larger systems than encountered during this design example. That is, the optical system and scanning system mass scaling laws are unreliable for small optical or scanning systems. Clearly, it is unreasonable to consider scanning mirror driving motors of less than 27 milligrams! However, for purposes of this study it is immaterial whether the scanning system has a mass of 30 milligrams, 300 milligrams, or even 300 grams. The point is that for the experiment considered here, the optical and scanning subsystems can be made sufficiently small that the detector and its associated electronics dominates the imaging system weight, and hence the total imaging system weight is on the order of two or three pounds.

Step 21: As with the mass scaling laws, the imaging system size estimates are unreliable for very small optical and scanning systems. For the sample design problem, it is sufficient to know that the imaging system can be made small (see next step). However, one dimension of the imaging system must exceed the focal length, which is 0.23 meters.

Step 22: The sensor system volume estimate is based on the required collector diameter, the focal length, and the scanning mirror diameter. The volume estimate is unreliable for very small collectors and scanning mirrors. For this reason, the minimum volume is taken as 10^{-3} m^3 , or about 0.04 cubic feet.

Step 23: An estimate of the maximum allowable sensor system roll, pitch, or yaw rate is provided by permitted the optical axis to rotate through one-half a resolution element during the dwell time on the resolution element. This leads to an allowable sensor system roll, pitch, or yaw rate of one-half the scanning mirror rotation rate. For the example problem considered here, the maximum roll, pitch, or yaw rate is then about 10 radians/sec. It should be noted that, in general, the platform stability requirements are determined by the effects of smear due to an apparent scene motion.

The experiment support requirements implied by the illustrative design problem given here are summarized in Table 6-3, which is taken directly from Volume V of this report series.

6.2 Television Systems

Figure 6-4 presents a logic diagram for the design of orbital television systems, while figure 6-5 presents the scaling laws. The logic diagram shows how the sensor system design proceeds step-by-step from the desired image specifications and an orbit definition. The blocks in the scaling law chart are numbered to correspond to the steps shown in the logic diagram. The scaling laws are best described by considering an illustrative design problem. The scaling laws provided here have been derived from study of space-orbital television systems which have already flown, or have been designed in some detail, and represent the capability provided by currently anticipated equipment under operational conditions. For details, the reader is referred to Volume IV of this report series.

Table 6-3

Sample Experiment Support Requirements
for an Ultraviolet Scanning System

PLANET: Venus

OBSERVABLE: Cloud Formation

Family No. 9a

DETECTOR: Photomultiplier

ORBIT: Data Sheet Number.....101
 Periapse/Apoapse Alt. (km).....454/454
 Inclination (deg)..... 90
 Imaging Altitude Range (km).....454
 Imaging On-Time (min)..... 48

IMAGE: Minimum Image Width (km).....600
 Max. Ground Resolution (km)..... 3
 Positional Accuracy (km)..... 10

SCANNER: Collector Diameter (cm).....0.3
 Aperture Stop.....f/70
 No. of Detectors..... 1
 No. of Scanner Faces..... 1
 Scanner Rotation Rate (rpm).....200

SUPPORT REQUIREMENTS:

Field of View (deg).....0.24x67
 Pointing Accuracy (deg).....1.3
 System Volume (cu. ft.).....0.04
 Max. Roll/Yaw Rate (deg/sec).....570
 Operating Power (watts).....1
 Data Rate (bits/sec).....3.0x10⁴
 System Weight (lbs).....2.2

COMMENTS:

50% planetary coverage can be achieved in daylight without a plane change, while only 10% is required. 1.5 min is required to obtain data from an image area of W x W, while one min is desired. Essentially the same area can be imaged every 96 min, while an image repetition time of 15 min is desired.

The sample design deals with surface topography on a regional scale at Mars, with vertical height differences deduced from measurement of shadow lengths. A similar experiment, but with vertical height differences deduced from measurements of stereo parallax, is used as the illustrative problem in Section 6.3, which describes the scaling laws for film systems. The image specifications and orbit parameters for the example are given in Table 6-4. These specifications are derived from Table 4-1 and the appropriate worth curves. That is, the specifications shown are for a relaxed or "minimal" experiment. In addition to these specifications, Table 4-1 and worth curve D1 indicate that seventy percent planetary coverage is required. A sun-synchronous circular orbit of 969 km altitude provides 74 percent coverage of Mars in a five day period at the proper solar illumination. This particular orbit is described in greater detail by orbit data sheet #14 in Volume III.

Step 1: If the location of the image on Mars is to be known within 3 km from an altitude of 969 km, the required system pointing accuracy is 3.1 milliradians, or 0.18 degrees.

Step 2: The ground resolution required in the imagery may not be the same as the required resolution on the ground horizontal, if some inferences of vertical height differences are to be made. For example, if vertical height differences of one km are to be detected by measurement of shadow lengths produced by a solar zenith angle in the range 60-75 degrees, then the necessary ground resolution is $1 \text{ km} \times \tan 60$ or 1.73 km. Thus in this design example, the required ground resolution is determined by the vertical resolution desired, rather than the horizontal resolution.

Step 3: For a ground resolution of 1.73 km and a minimum image ground size of 600 km, a minimum of 495 TV lines are required. This estimate does not account for effects of planetary curvature on the ground resolution, but it is useful to

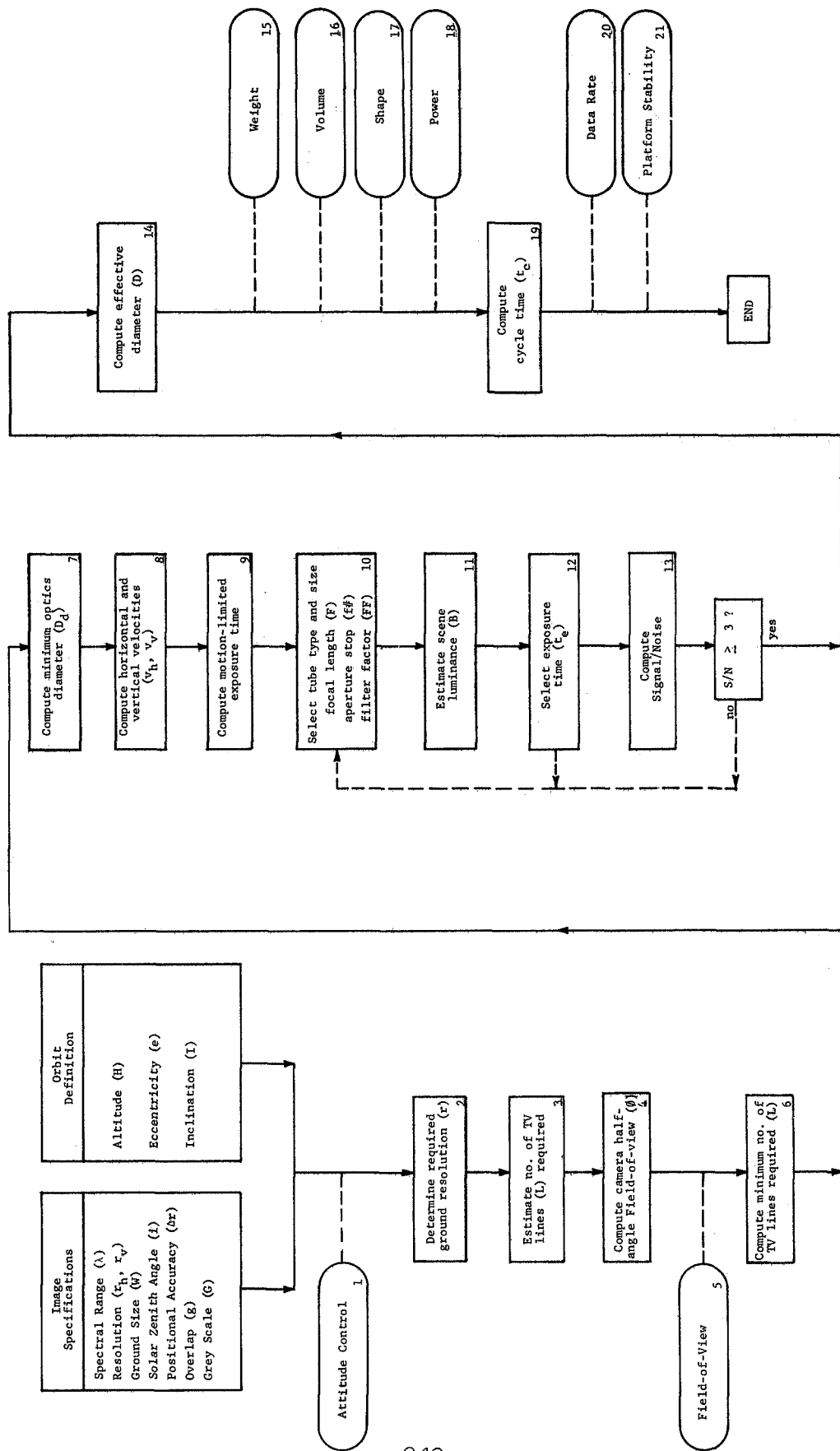


FIGURE 6-4. LOGIC DIAGRAM FOR TELEVISION SYSTEMS.

<p>① $\Delta\theta = \frac{R}{H}$</p> <p>If no vertical resolution required, $r = r_h$. For shadow measurement, r is the smaller of $r_{h, \text{tan } i}$ or r_h. For stereo, r is the smaller of $0.4Hr_h/H$ or r_h.</p>	<p>Planet $R(\text{km})$ $\mu(\text{km}^3/\text{sec}^2)$ $V_e(\text{km/sec})$</p> <table border="1"> <tr><td>Moon</td><td>1740</td><td>4.90×10^6</td><td>-</td></tr> <tr><td>Mercury</td><td>2420</td><td>2.17×10^6</td><td>-</td></tr> <tr><td>Venus</td><td>6100</td><td>3.25×10^6</td><td>0.24</td></tr> <tr><td>Mars</td><td>3380</td><td>4.30×10^6</td><td>0.24</td></tr> <tr><td>Jupiter</td><td>71350</td><td>4.27×10^6</td><td>12.7</td></tr> </table>	Moon	1740	4.90×10^6	-	Mercury	2420	2.17×10^6	-	Venus	6100	3.25×10^6	0.24	Mars	3380	4.30×10^6	0.24	Jupiter	71350	4.27×10^6	12.7	<p>④ $D = \frac{F}{f}$ Limited to 2 meters</p> <p>⑤ Weight is 16 lbs./inch of TV tube diameter. If IMC used, add 15 lbs.; 2 lbs., D in cm. If $h > 10$ cm, add 0.037D² lbs., D in cm. If zoom lens used, add $25 + 0.047 D^2$ lbs., D in cm.</p>
Moon	1740	4.90×10^6	-																			
Mercury	2420	2.17×10^6	-																			
Venus	6100	3.25×10^6	0.24																			
Mars	3380	4.30×10^6	0.24																			
Jupiter	71350	4.27×10^6	12.7																			
<p>② $L \geq \frac{H}{0.7FE}$, but $L \leq 3000$</p> <p>$\gamma = \frac{H}{2K}$</p> <p>If $\gamma < 0.1$, $\beta = \tan^{-1} \frac{H}{2H}$, otherwise $\beta = \cot^{-1} \left(\frac{R}{K} \frac{\sin \gamma}{\sin \gamma} - \cot \gamma \right)$</p>	<p>⑥ $t_e \leq 3 \left(\frac{F}{V_e^2 \tan^2 \beta} \right)$ w/o IMC</p> <p>$t_e \leq 3 \left(0.1V_e + V_e \tan \beta \right)$ w/ IMC</p>	<p>⑥ TV tube length from Figure 6-8. System length $>$ tube length $+ F$ System diameter $>$ tube diameter or D.</p>																				
<p>③ $L \geq \frac{H(V_e/r_0)}{0.7FE}$, but ≤ 3000, where</p> <p>$\frac{r_0}{r_h} = \frac{R}{H} \cdot \left\{ \frac{\cos \theta}{\left[\left(\frac{R}{KH} \right)^2 - \sin^2 \theta \right]^{1/2}} - 1 \right\}$</p> <p>which is given in Table 6-1.</p>	<p>Use Figure 6-6 to select tube type and size. Image format size (f) from Figure 6-7.</p> <p>$r_0 = \frac{f}{2 \tan \beta} \text{ mm}$</p> <p>$1 \leq f \leq \frac{H}{2}$</p> <p>Filter</p> <table border="1"> <tr><td>500mμ</td><td>FF</td></tr> <tr><td>Mercury 47 blue</td><td>3.7</td></tr> <tr><td>Mars 58 green</td><td>9.8</td></tr> <tr><td>Mars 25A red</td><td>27</td></tr> </table>	500m μ	FF	Mercury 47 blue	3.7	Mars 58 green	9.8	Mars 25A red	27	<p>⑦ Input power is 16 watts/inch of TV tube diameter. If IMC used, add 15 watts. If zoom lens used, add 10 watts.</p>												
500m μ	FF																					
Mercury 47 blue	3.7																					
Mars 58 green	9.8																					
Mars 25A red	27																					
<p>④ $D = \frac{1.83 \times 10^{-4} L}{\tan \beta}$ cm but limited to two meters.</p> <p>$a = R + K(R_p + R_h)$</p> <p>$V_p = \frac{R}{R \sin \theta} \left[u \left(\frac{R}{R \sin \theta} - \frac{a}{R} \right) \right]^{1/2}$</p> <p>$V_h = (V_p^2 + V_e^2 - 2V_p V_e \cos \theta)^{1/2}$</p> <p>$V = \left[\frac{u^2}{a(1 - e^2)} \right]^{1/2}$</p>	<p>Planet R_e Zenith Angle (λ) f</p> <table border="1"> <tr><td>Moon</td><td>10°</td><td>0.49</td></tr> <tr><td>Mercury</td><td>30°</td><td>0.31</td></tr> <tr><td>Venus</td><td>15-50°</td><td>0.15</td></tr> <tr><td>Mars</td><td>60°</td><td>0.06</td></tr> <tr><td>Jupiter</td><td>200</td><td></td></tr> </table> <p>Use $f = \cos i$ for Venus, Jupiter</p> <p>⑧ $t_e \geq \frac{4S(FF)^2}{\eta\beta}$</p> <p>See step #9 above, S given in lower right table. Use η of 0.6 for zoom lens, 0.9 otherwise.</p>	Moon	10°	0.49	Mercury	30°	0.31	Venus	15-50°	0.15	Mars	60°	0.06	Jupiter	200		<p>⑧ $t_c = \frac{R(LR)}{V_h}$</p> <p>$DR = \frac{DR^2}{V_e}$</p> <p>where $t = t_c - 0.1$ sec or 100 sec, whichever is smaller. For 3 color filters, $t = \frac{1}{3} t_c - 0.1$ sec or 100 sec, whichever is smaller.</p>					
Moon	10°	0.49																				
Mercury	30°	0.31																				
Venus	15-50°	0.15																				
Mars	60°	0.06																				
Jupiter	200																					
<p>⑤ $S = \frac{4.6 \times 10^5 H L}{L(FF)k} \left(\frac{V_h V_e}{FF} \right)^{1/2}$</p>	<p>⑨ $S = \frac{4.6 \times 10^5 H L}{L(FF)k} \left(\frac{V_h V_e}{FF} \right)^{1/2}$</p>	<p>⑨ Tube Type S(ft-candle-sec) H A</p> <table border="1"> <tr><td>Vidicon</td><td>3A10-3</td><td>2.0</td><td>0.2</td></tr> <tr><td>Plumbicon</td><td>2A10-3</td><td>2.3</td><td>0.2</td></tr> <tr><td>EBW</td><td>1A10-5</td><td>2.0</td><td>0.2</td></tr> <tr><td>SEC</td><td>5A10-5</td><td>1.8</td><td>0.3</td></tr> <tr><td>Image Orthicon</td><td>2A10-6</td><td>2.0</td><td>0.3</td></tr> </table>	Vidicon	3A10-3	2.0	0.2	Plumbicon	2A10-3	2.3	0.2	EBW	1A10-5	2.0	0.2	SEC	5A10-5	1.8	0.3	Image Orthicon	2A10-6	2.0	0.3
Vidicon	3A10-3	2.0	0.2																			
Plumbicon	2A10-3	2.3	0.2																			
EBW	1A10-5	2.0	0.2																			
SEC	5A10-5	1.8	0.3																			
Image Orthicon	2A10-6	2.0	0.3																			

FIGURE 6-5. SCALING LAWS FOR TELEVISION SYSTEMS

- NOMENCLATURE**
- a-orbit semi-major axis, km
 - B-scene luminance, ft-lambert
 - D-optics diameter (F/ff), cm
 - D₀-minimum optics diameter, cm
 - DR-data acquisition rate, bits/sec
 - e-orbit eccentricity
 - f-scene photometric function
 - ff-optics aperture stop (f-number)
 - F-focal length, cm
 - FF-filter factor
 - FOV-field-of-view
 - g-fractional overlap along orbit
 - G-bits per revolution element (normally 5)
 - h-camera altitude, km
 - h₀-orbit apogee altitude, km
 - h_p-orbit perigee altitude, km
 - i-solar zenith angle
 - I-orbit inclination
 - K-number of grey levels (normally 64)
 - L-image format size, cm
 - L₀-number of TV lines
 - M-maximum density difference
 - q-quantum efficiency
 - r₀-desired ground resolution, km
 - r_h-desired horizontal resolution, km
 - r_v-desired vertical resolution, km
 - R-planet radius, km
 - S-min. tube illumination, ft-candle-sec
 - S/R-signal-to-noise ratio
 - t_c-camera cycle time, sec
 - t_e-exposure time, sec
 - V_h-apparent horizontal speed, km/sec
 - V_p-camera ground speed at perigee, km/sec
 - V_e-planet equatorial rotation speed, km/sec
 - V_v-camera vertical speed, km/sec
 - W-camera width (length) on ground, km
 - Y-image half-angle subtended at planet center
 - Δc-allowed image ground positional accuracy, km
 - Δc₀-allowable camera pointing error, radians
 - T-optical system transmission factor
 - θ-allowable camera yaw rate, rad/sec
 - λ-wavelength
 - μ-planet gravitational constant, km³/sec²
 - β-camera half-angle field-of-view
 - β₀-allowable camera pitch or roll rate, rad/sec

Table 6-4

Image Specifications and Orbit Parameters
for Visual Surface Topography Imagery at Mars

Spectral Range	5000-7500 Å
Horizontal Ground Resolution	3 km
Vertical Ground Resolution	1 km
Minimum Image Ground Size	600 km
Solar Zenith Angle	60-75 deg
Image Positional Accuracy	3 km
Overlap	20%
Grey Scale	6 bits
Orbit Periapse Altitude	969 km
Orbit Apoapse Altitude	969 km
Orbit Eccentricity	0
Orbit Inclination	94.8 deg

compute a preliminary estimate to ensure that TV systems might possess the necessary resolution capability before proceeding further with the system design. The analysis of television system design presented in Volume IV concludes that, at the current or near-future state-of-art, only about 3000 TV lines can be provided for operational imagery of a low-contrast planetary scene. If greater than 3000 lines are required, film systems should be considered.

Step 4: Using a Mars radius of 3380 km, a great-circle arc length of 600 km subtends an half-angle of 0.089 radians at the planet's center. Since this value is less than 0.1 radian, the simpler formula for the camera half-angle field-of-view may be used to find the half-angle is 17 degrees.

Step 5: The camera field-of-view is 34 by 34 degrees.

Step 6: Interpolating from Table 6-1, r_{ϕ}/r_o is 1.16, and hence 575 TV lines are required to achieve a ground resolution of 1.73 km over a 600 x 600 km area. (Compare with Step 3 above.)

Step 7: Using 575 TV lines and a view half-angle of 17 degrees, the optical system is resolution-limited to 0.34 cm diameter or larger. The equation shown in this step of the scaling law chart presumes that the optical system lens must be at least five times larger than the classical diffraction limit. For such a distortion-free lens, the modulation transfer function has a value of about 0.78. The current state-of-art limits the lens diameter to something on the order of two meters or less.

Step 8: The apparent camera ground speed is 2.44 km/sec, neglecting Mars' rotation. Since the orbit inclination is 94.8 degrees, the maximum ground speed is estimated to be 2.47 km/sec when the effect of planet rotation is accounted for. For a circular orbit, the camera does not have a vertical velocity component. The expression shown for the vertical speed gives the maximum vertical speed experienced by the spacecraft during

orbital maneuver. If the imaging system is not operating at the time of maximum vertical speed, a lesser value for the vertical speed may be used, as discussed in Volume IV. Usually, it is adequate to consider only the maximum vertical speed.

Step 9: The maximum exposure time is 0.23 seconds if image motion compensation (IMC) is not provided, and about 2.3 seconds if IMC is provided. The design equations given in the scaling law chart presume that an image smear equivalent to one-half resolution element is acceptable. As shown in Volume IV, this corresponds to a value of 0.64 for the image motion modulation transfer function. In particular, one-third of a resolution element is allocated for apparent translational motion, and one-sixth an element for rotational motion (Step #21). The IMC result is predicated on correction for ninety percent of the apparent scene horizontal velocity.

Step 10: The size and type of TV image tube may be selected using Figure 6-6. The data shown in the figure were estimated by assuming that a value of 0.35 is required for the image tube modulation transfer function, as measured at the corners of the image format. This value is consistent with a value of 0.64 for the image motion MTF (modulation transfer function), a value of 0.78 for the lens MTF, an apparent scene contrast of 1.6:1, and a value of 0.04 for the imaging system MTF. Figure 6-6 shows that a two-inch diameter vidicon tube will not quite provide the desired resolution (575 lines), while the 2" RBV has more than adequate resolution. Actually, the method of analysis used here is not sufficiently accurate to eliminate the 2" vidicon from consideration, but the 2" RBV provides 2500 TV lines under the operational conditions considered here. This increased capability may be used to provide a larger image ground size or better ground resolution. The choice is at the discretion of the system designer. In the case considered here, use of a 2" RBV will provide a ground resolution of 400 meters

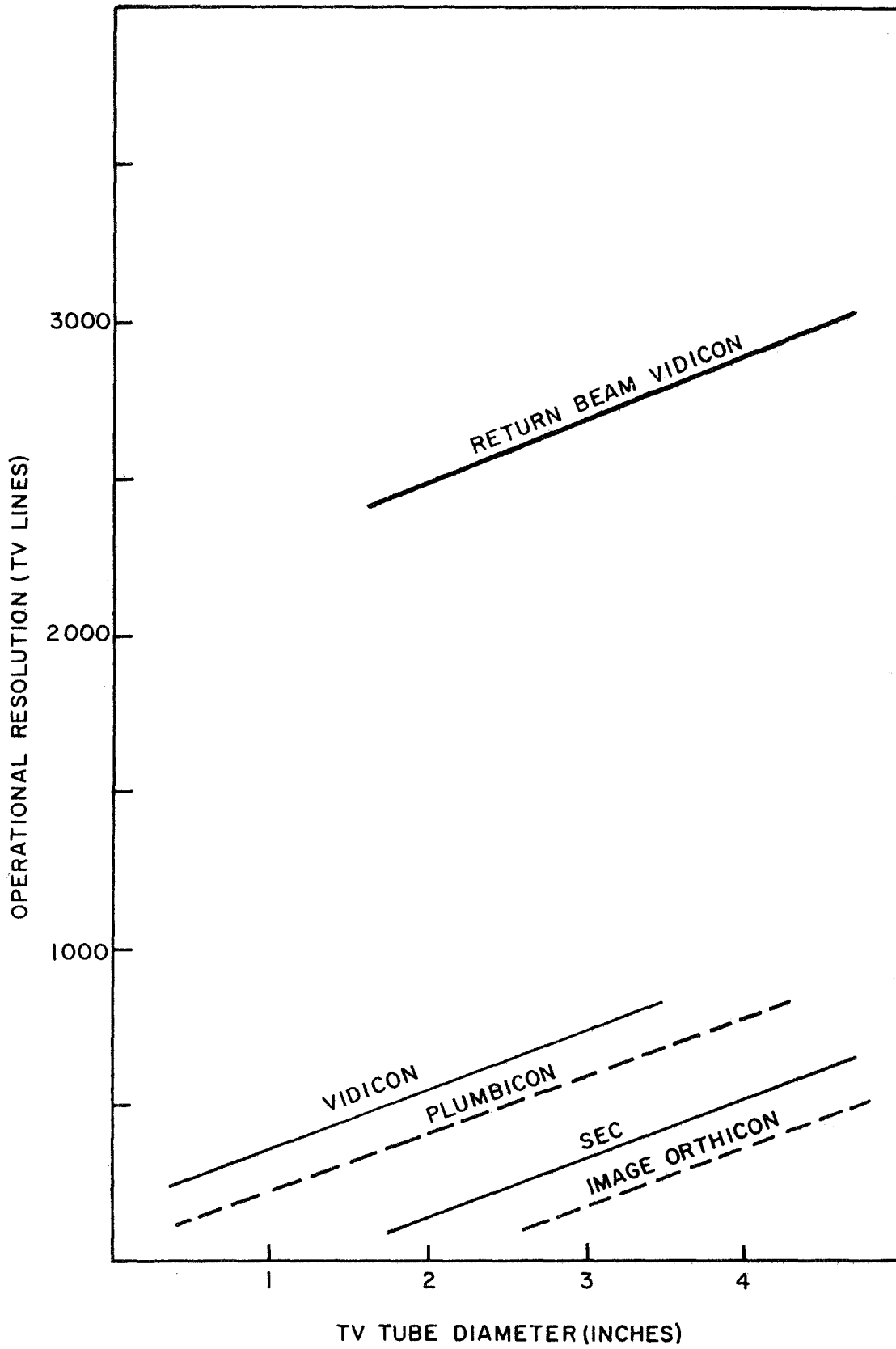


FIGURE 6-6. TV TUBE OPERATIONAL RESOLUTION

over a 600 x 600 km area, or a ground resolution of 1.73 km over a 1500 x 1500 km area. Of course, intermediate combinations are also available. A zoom lens may be useful if imagery from an elliptic orbit is desired. Assuming that such a device will provide focal lengths which can be adjusted over a five-fold range, the camera tube resolution capability can be efficiently used over a five-fold range in imaging altitude. Of course, the zoom lens subsystem adds weight, volume, and power requirements to the basic imaging system, in addition to increasing optical system transmission losses. Imaging a 1500 x 1500 km area from the selected orbit requires a camera field-of-view of 70 by 70 degrees, and at this field-of-view and 2500 TV lines, the resolution-limited lens diameter (Step #7) is 0.65 cm. From Figure 6-7, the image size on the face of a 2" RBV is about 23 millimeters square. Thus the focal length is 16 millimeters, and the relative aperture stop must be f/2.5 or larger. The table in block #10 of the scaling law chart shows that for a 500 m μ filter (required if the spectral range is to be 5000 - 7500 Å), the filter factor is 3.7.

Step 11: For a 75 degree solar zenith angle, the scene photometric function is approximately 0.06 (assuming the Martian surface has a photometric function similar to that of the Moon), and hence the scene luminance is estimated as 48 foot-lamberts.

Step 12: The table in the lower right hand corner of the scaling law chart indicates that a minimum faceplate illumination of 1×10^{-3} foot-candle-sec is required for an RBV tube. Assuming an optical system transmission of ninety percent and an f/2 aperture stop, the minimum exposure time is about 0.0014 seconds. The minimum exposure time should be compared to the maximum times estimated in Step #9. If the minimum time is not less than the maximum time, the minimum time may be reduced by increasing the lens aperture or selecting a more sensitive TV tube. In the design example here, the minimum exposure time of

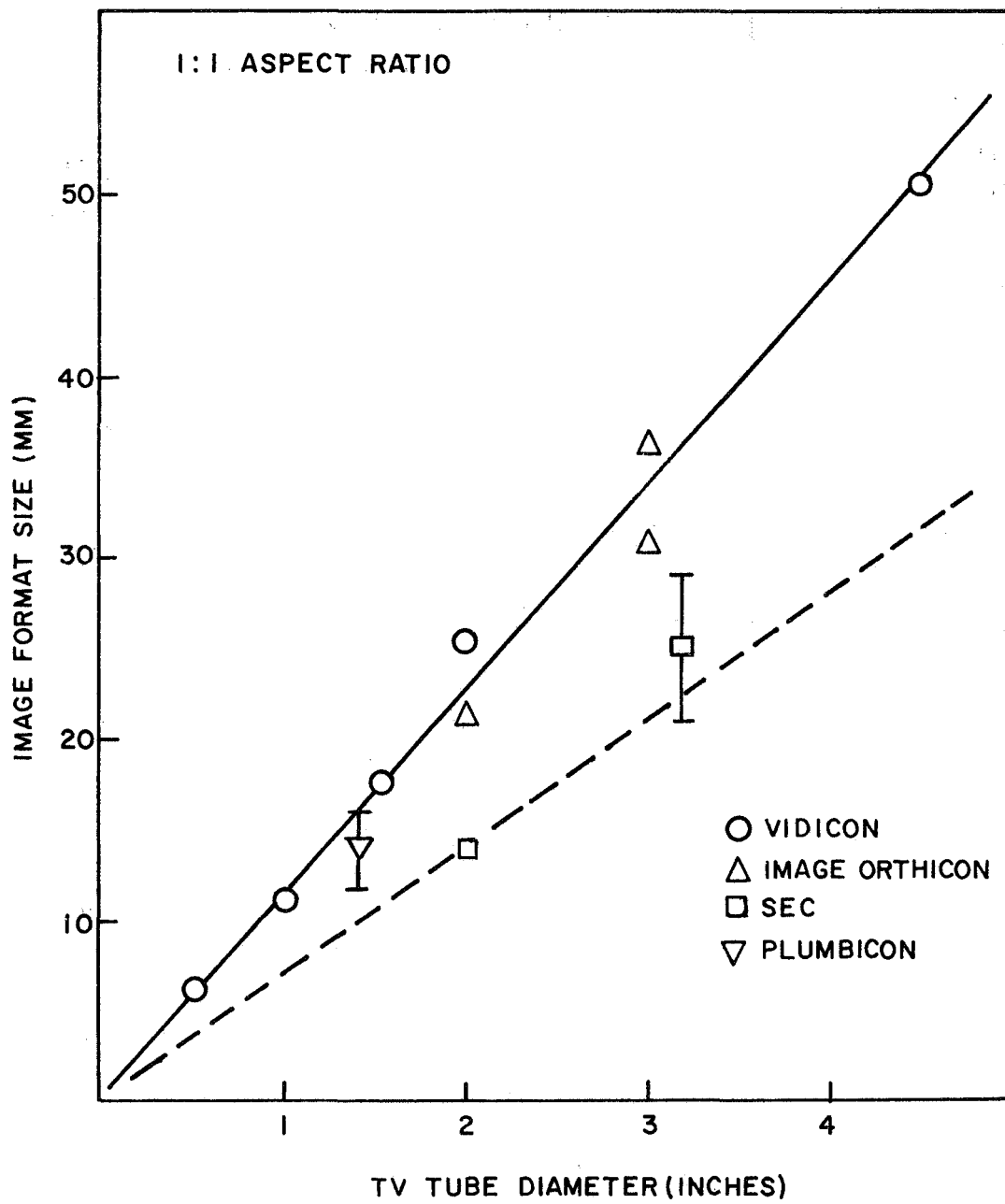


FIGURE 6-7. TV FORMAT SIZES

0.0014 seconds is less than the maximum exposure time of 0.23 seconds without IMC and 2.3 seconds with IMC. If the minimum exposure time were one second, an alternative to choosing a more sensitive tube or opening the lens would be to use IMC. All three design alternatives may have disadvantages. As shown in Figure 6-6, a more sensitive tube may require a larger tube diameter, and hence a heavier system, to provide adequate resolution. Increasing the lens aperture requires a larger lens (since the focal length is already fixed) and may increase the system weight significantly. Use of IMC will add about 15 pounds to the system weight and about 15 watts to the system power requirement. In the current design example, these alternatives are not pertinent and an exposure time of 0.01 seconds may be rather arbitrarily selected.

Step 13: Using the values of M and q for an RBV tube given in the lower right hand corner of the scaling law chart, the signal-to-noise ratio is found to be about ten. The numerical coefficient in the formula shown in the scaling law chart requires that the format size l be in millimeters. The signal-to-noise ratio computed in this design step regards the signal as the difference in brightness or intensity between two adjacent image resolution elements differing by one shade of grey, and the noise as due to the inherent statistical error in photon detection. Noise contributed by the system electronics and the image tube is not considered. That is, the signal-to-noise ratio computed here is that of an idealized imaging system. A signal-to-noise ratio of three is regarded as the minimum acceptable value for adequate image interpretation. Usually the most convenient way to increase the signal-to-noise ratio is to decrease the f-number or increase the exposure time. This design iteration loop is indicated by the dashed lines in the logic diagram.

Step 14: The effective lens or optical system diameter is simply the focal length divided by the f-number. For the design example considered here, the lens diameter is 8 millimeters. The maximum permissible lens diameter is taken as about two meters without grossly exceeding the current state-of-art.

Step 15: For a 2" camera tube, the imaging system weight is about 32 pounds. Additional weight is required for imaging systems using optical systems larger than ten cm diameter, zoom lenses, or IMC.

Step 16: For a 2" camera tube, the imaging system volume is estimated as 1100 cubic inches, or about 0.65 cubic feet. As with the system weight, additional support (volume, in this case) is required for systems using large optics, zoom lenses, or IMC. It is presumed here that the zoom lens focal length is controlled by data from an on-board radar altimeter weighing 25 pounds, of size 10 x 10 x 10 inches, and consuming ten watts of power. If instead the zoom lens is preprogrammed, or under some other means of control, the radar altimeter may be omitted.

Step 17: The dimensions of a television imaging system may be tailored to fit a variety of accommodations. However, one linear dimension is constrained to be somewhat larger than the sum of the camera tube length and the focal length, while the other two dimensions must exceed the larger of the camera tube diameter or the optics diameter. Figure 6-8 shows how camera tube length varies with the diameter of the camera tube, independently of the type of tube. Thus, for the illustrative example considered here, the 2" RBV camera tube is about ten inches long. Adding one inch for the focal length (16 millimeters), the imaging system dimensions must exceed approximately 11 x 2 x 2 inches. The volume estimated above in Step #16 greatly exceeds the volume obtained by multiplying together these system dimensions. This simply means that great latitude is available in designing the shape of the imaging system

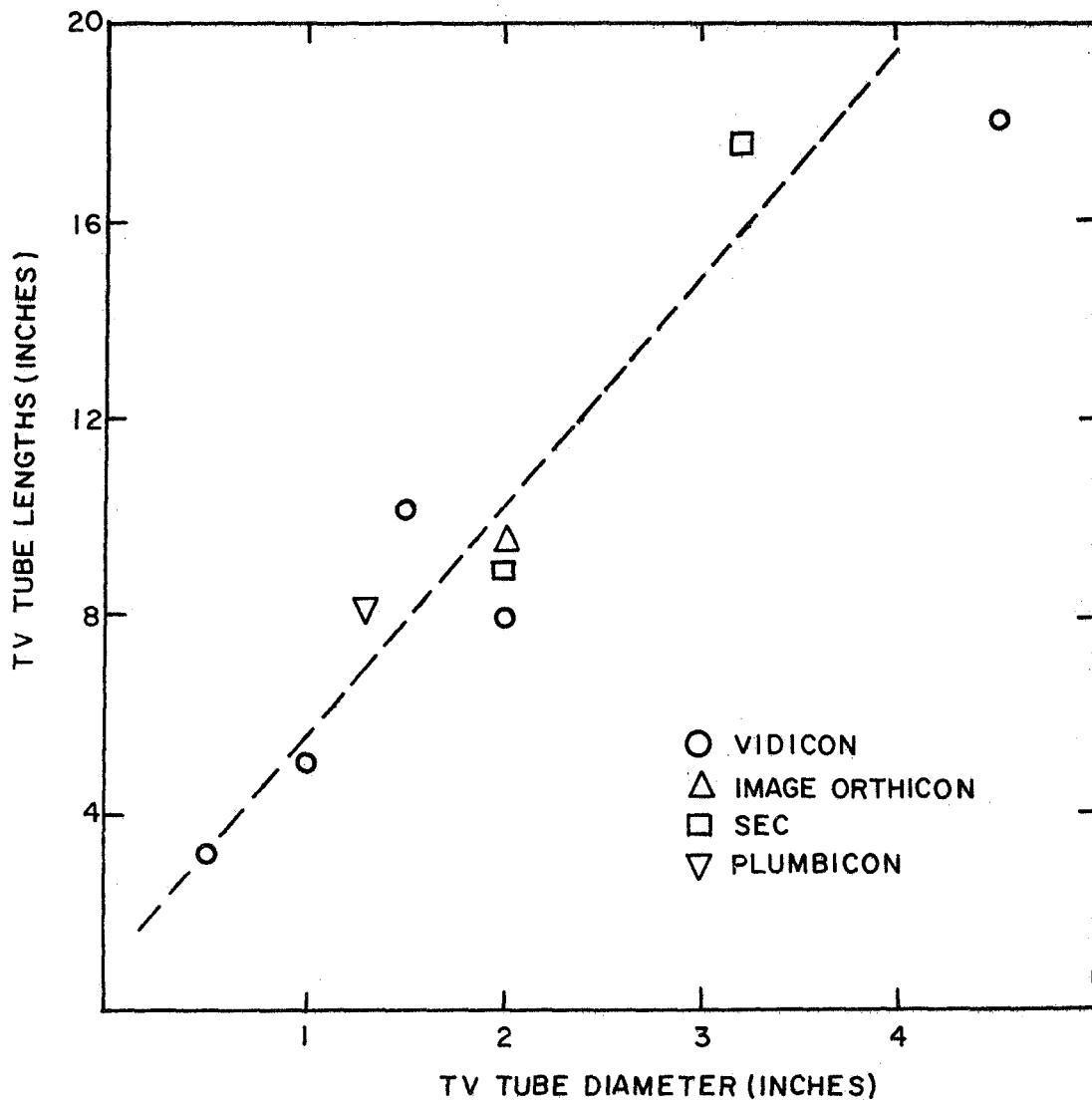


FIGURE 6-8. TV TUBE LENGTHS

package. That is, the total system volume is about 1100 cubic inches; one dimension must exceed 11 inches, the other two dimensions must each exceed two inches.

Step 18: The imaging system average power requirement is estimated as 32 watts for a 2" camera tube. Note that additional power is required for a zoom or IMC capability.

Step 19: The cycle time, or image interval time, depends upon the image ground size, image overlap along the heading line or subsatellite track, and the apparent ground speed of the sensor. For the design example, using a 1500 km image ground size and twenty percent overlap, the cycle time is about 180 seconds, or three minutes.

Step 20: For 64 shades of grey, six binary bits per resolution element are required. Thus, the data acquisition rate is about 3.8×10^5 bits/second. Actually, this is the rate at which data must be removed from the imaging system and placed in a data storage or transmission subsystem, since the data cannot be stored longer than about 100 seconds on the camera tube without loss of information. That is, even though the image interval time is 180 seconds, the data must be dumped in 100 seconds. If the cycle time is less than 100 seconds, a 0.1 second interval should be allowed for preparing the camera tube (erasing the previous image). For image orthicon or SEC vidicon camera tubes, the image storage time on the camera tube can be as long as desired, that is, the time used in computing the data acquisition rate should be essentially the cycle time. For pseudo-color imagery, in which three images of very nearly the same scene are procured through a blue, green, and red filter, three images are acquired during each cycle time, and the data acquisition rate is computed accordingly.

Step 21: Platform stability requirements are based on restricting the apparent image motion. It is assumed that pitching or rolling, but not yawing, can be ninety percent compensated for by IMC. Thus for the illustrative design,

considered here, which does not provide an IMC capability, the allowable yaw rate is estimated as 0.038 radians/sec, or about 2 degrees/sec, while the allowable pitch or roll rate is estimated as 0.030 radians/sec, or about 1.7 degrees/sec. These estimates are based on an allowable image smear of one-sixth a resolution element, due to sensor system rotation, and further, that the rotational effects are not additive.

Table 6-5, taken from Volume V, summarizes the support requirements estimated for this illustrative design example.

6.3 Film Camera Systems

Figures 6-9 and 6-10 summarize the design procedure and scaling laws for film camera systems. Not surprisingly, they are very similar to those presented in the previous section for television systems. Since the Lunar Orbiter photographic system is the only space film system, suitable for unmanned operations, for which operational data is available, the scaling laws have been derived from aerial reconnaissance camera data and have then been modified to force agreement with Lunar Orbiter data and other data derived from orbital mission design studies. In other words, the functional dependence of the camera system support requirements upon the camera design parameters and the system capabilities has been deduced from an analysis of aerial reconnaissance camera characteristics, but the numerical scaling coefficients are based on admittedly sparse data appropriate to space hardware. A complete derivation and explanation of the scaling laws is provided in Volume IV. An example design is presented here to illustrate the procedure.

The design example used here is similar to the television experiment just presented, except that stereo parallax is used to provide vertical height information. Thus the solar illumination angles desired are different from the television experiment in which vertical height differences were to be

Table 6-5

Sample Experiment Support Requirements
for a Television Imaging System

PLANET: Mars

OBSERVABLE: Surface Topography (regional)

Family No. 8b

TV TYPE: 2-inch RBV (shadowing)

ORBIT:	Data Sheet Number.....	14
	Periapse/Apoapse Alt. (km).....	969/969
	Inclination (deg).....	95
	Imaging Altitude Range (km).....	969
	Imaging On-Time (min).....	45
IMAGE:	Minimum Image Width (km).....	600
	Max. Ground Resolution (km).....	3 (1 vert.)
	Positional Accuracy (km).....	3
CAMERA:	Focal Length (mm).....	16
	Aperture Stop.....	f/2
	Exposure Time (sec).....	0.01
	Cycle Time (sec).....	490
	Signal-to-Noise Ratio.....	10

SUPPORT REQUIREMENTS:

Field of View (deg).....	70 x 70
Pointing Accuracy (deg).....	0.18
Camera Volume (cu. ft.).....	0.65
Max. Roll/Yaw Rate (deg/sec).....	1.7/2.2
Operating Power (watts).....	32
Data Rate (bits/sec).....	3.8×10^5
Camera Weight (lbs).....	32

COMMENTS:

This sun-synchronous orbit provides 74% coverage in five days. Image size used is 1500 x 1500 km with ground resolution of 1.7 km permitting detection of vertical height differences of 1 km by shadow measurements.

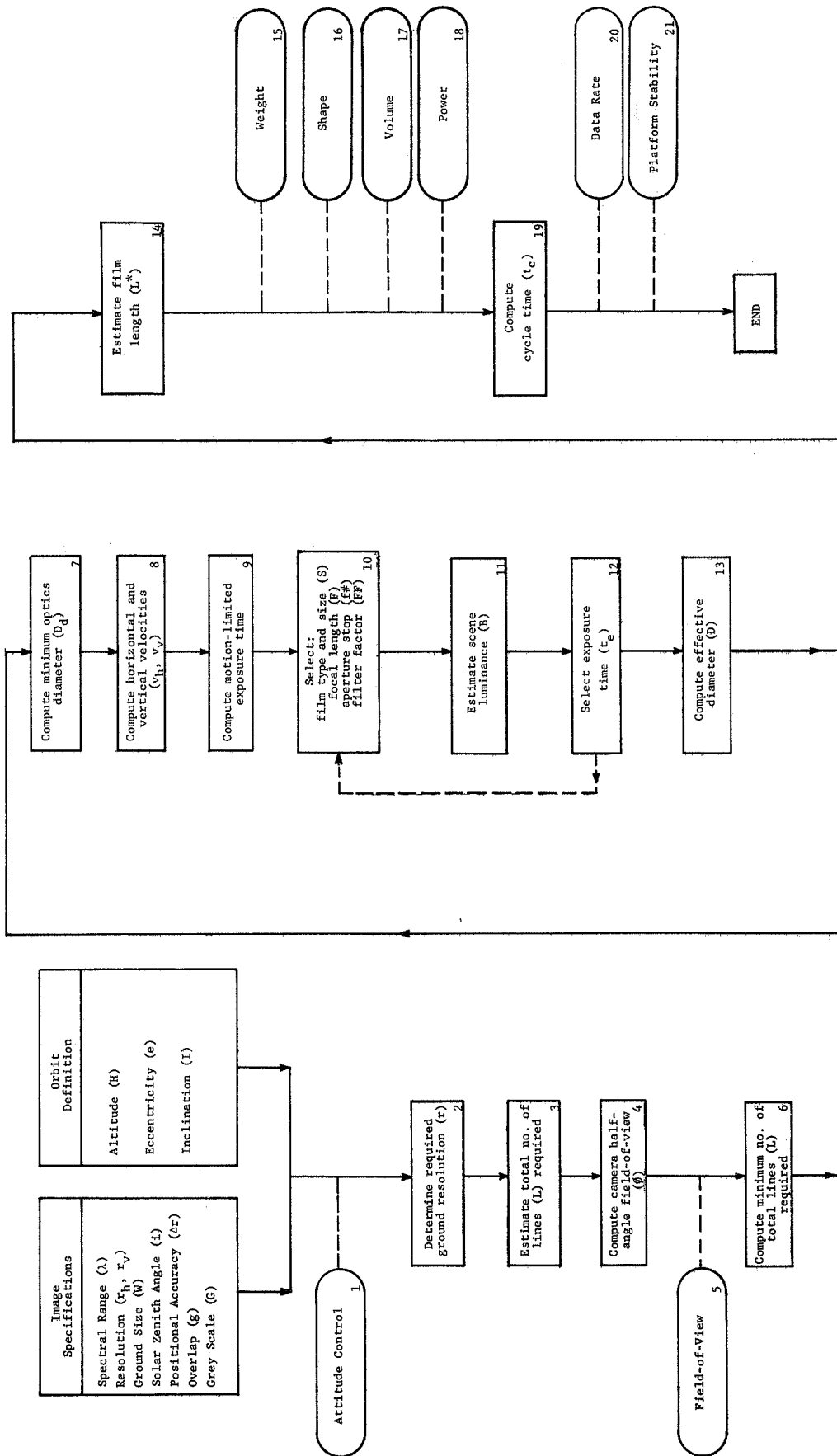


FIGURE 6-9. LOGIC DIAGRAM FOR PHOTOGRAPHIC FILM SYSTEMS.

<p>① $\Delta \theta = \frac{\Delta r}{R}$</p> <p>If no vertical resolution required, $r = r_h$. For shadow measurement, r is the smaller of $r_h \tan \alpha$ or r_v. For stereo, r is the smaller of $0.4W_c/H$ or r_h.</p>	<p>Planet R (km) U (km³/sec²) V_r (km/sec)</p> <p>Moon 1740 4.90 x 10⁴ -</p> <p>Mercury 2420 2.17 x 10⁴ -</p> <p>Venus 6100 3.25 x 10⁴ -</p> <p>Mars 3380 4.30 x 10⁴ 0.24</p> <p>Jupiter 71350 1.27 x 10⁶ 12.7</p>	<p>② System weight (lbs) = $18 + aS^2 + (0.22 - 0.00765)D^2$, where S is film size in inches, D in cm, and a is a constant. Add 0.04 lb/oz of film for processing. Add film weight using Table 6-7. If IMC is used, add 10 lb for V/H sensor. If zoom lens used, add 25 + 0.076² lbs. If $D > 10$ cm for 70mm and 5in film or > 20 cm for 9in film, add 0.037² lbs. For optics</p>	<p>③ $t_e \leq \sqrt{(V_h^2 + V_v^2 \tan^2 \beta)} / w$ I/MC $t_e \leq \sqrt{(0.1V_h + V_v \tan \beta)} / w$ I/MC</p>	<p>④ Use Table 6-7 to select film type & size. V_h is horizontal velocity in in/sec, V_v is vertical velocity in in/sec, and β is film tilt, respectively. $F = \frac{L}{2m \sin \theta}$ $1 \leq F \leq \frac{1}{2}$</p>	<p>⑤ $t_e = \frac{H(L - R)}{V_h}$</p>
<p>⑥ $L > \frac{W}{\tau}$, but $\leq 33,000$</p>	<p>⑦ $\gamma = \frac{W}{2R}$ If $\gamma < 0.1$, $\beta = \tan^{-1} \frac{W}{2H}$, otherwise $\beta = \cot^{-1} \left(\frac{2H}{W} - \cot \gamma \right)$</p>	<p>⑧ Film size Length (in) Width (in) Depth (in)</p> <p>70 mm 4 7 10</p> <p>1 in 4 16 20</p> <p>9in 0 16 20</p>	<p>⑨ $t_e = \frac{H(L - R)}{V_h}$</p>	<p>⑩ $L > \frac{W(C_g/r_0)}{\tau}$ but $\leq 33,000$, where</p> <p>$\frac{r_0}{r} = R \cdot \left[\frac{\cos \beta}{(R/H) - \sin^2 \beta} - 1 \right]$</p> <p>which is given in Table 6-1.</p>	<p>⑪ $D_s = \frac{1.48 \times 10^{-4}}{\sin \theta}$ cm but limited to two meters.</p>
<p>⑫ $L > \frac{W(C_g/r_0)}{\tau}$ but $\leq 33,000$, where</p> <p>$\frac{r_0}{r} = R \cdot \left[\frac{\cos \beta}{(R/H) - \sin^2 \beta} - 1 \right]$</p> <p>which is given in Table 6-1.</p>	<p>⑬ $D_s = \frac{1.48 \times 10^{-4}}{\sin \theta}$ cm but limited to two meters.</p>	<p>⑭ $t_e = \frac{H(L - R)}{V_h}$</p>	<p>⑮ $t_e = \frac{H(L - R)}{V_h}$</p>	<p>⑯ $L > \frac{W(C_g/r_0)}{\tau}$ but $\leq 33,000$, where</p> <p>$\frac{r_0}{r} = R \cdot \left[\frac{\cos \beta}{(R/H) - \sin^2 \beta} - 1 \right]$</p> <p>which is given in Table 6-1.</p>	<p>⑰ $D_s = \frac{1.48 \times 10^{-4}}{\sin \theta}$ cm but limited to two meters.</p>
<p>⑰ $L > \frac{W(C_g/r_0)}{\tau}$ but $\leq 33,000$, where</p> <p>$\frac{r_0}{r} = R \cdot \left[\frac{\cos \beta}{(R/H) - \sin^2 \beta} - 1 \right]$</p> <p>which is given in Table 6-1.</p>	<p>⑱ $D_s = \frac{1.48 \times 10^{-4}}{\sin \theta}$ cm but limited to two meters.</p>	<p>⑲ $t_e = \frac{H(L - R)}{V_h}$</p>	<p>⑳ $t_e = \frac{H(L - R)}{V_h}$</p>	<p>㉑ $L > \frac{W(C_g/r_0)}{\tau}$ but $\leq 33,000$, where</p> <p>$\frac{r_0}{r} = R \cdot \left[\frac{\cos \beta}{(R/H) - \sin^2 \beta} - 1 \right]$</p> <p>which is given in Table 6-1.</p>	<p>㉒ $D_s = \frac{1.48 \times 10^{-4}}{\sin \theta}$ cm but limited to two meters.</p>

NOMENCLATURE

- a-orbit semi-major axis, km
- AEI-film aerial exposure index
- B-scene luminance, ft-lambert
- C-planetary fractional coverage
- D-optics diameter (F/F), cm
- D_g-minimum optics diameter, cm
- DR-data acquisition rate, bits/sec
- e-orbit eccentricity
- f-scene photometric function
- F#-optics aperture stop (F-number)
- F-focal length, cm
- FF-filter factor
- FOV-field-of-view
- G-fractional overlap along orbit
- G-bits per resolution element (normally 6)
- H-camera altitude, km
- H_o-orbit apogee altitude, km
- H_p-orbit perigee altitude, km
- i-solar zenith angle
- I-orbit inclination
- J-image format size
- L-total no. of lines per frame
- L_o-total length of film, feet
- R-desired ground resolution, km
- R_h-desired horizontal resolution, km
- R_v-desired vertical resolution, km
- R-planet radius, km
- s-fractional side overlap
- S-film width, inches
- t_c-cycle time, sec
- t_e-exposure time, sec
- t_h-apparent horizontal speed, km/sec
- t_v-camera ground speed at perigee, km/sec
- v_e-planet equatorial rotation speed, km/sec
- v_v-camera vertical speed, km/sec
- W-image width (length) on ground, km
- Y-image half-angle subtended at planet center
- Δx-desired image ground positional accuracy, km
- Δθ-allowable camera pointing error, radians
- η-optical system transmission factor
- ω-allowable camera yaw rate, rad/sec
- λ-wavelength
- μ-planet gravitational constant, km³/sec²
- β-camera half-angle field-of-view
- β-allowable camera pitch or roll rate, rad/sec

FIGURE 6-10. SCALING LAWS FOR PHOTOGRAPHIC FILM SYSTEMS

inferred from measurement of shadow lengths. The image specifications and orbit parameters for the illustrative design problem are given in Table 6-6. The selected orbit is similar to that used in the television example, and is more fully described by orbit data sheet #5 in Volume III. The orbit has been selected to provide sixty percent overlap at the minimum image ground size. Stereo coverage is obtained by viewing imagery obtained from the n th and the $n + 10$ th orbit, the longitudinal displacement between the two orbit ground traces being 240 km at the Mars equator. This mode of obtaining the stereo coverage is referred to in Volume V as "side stereo", the alternative mode of obtaining sixty percent overlap along the subsatellite path is referred to as "forward stereo".

Step 1: As with the television systems, the required pointing accuracy is simply the image ground positional accuracy divided by the imaging system altitude, giving 3 milliradians, or 0.17 degrees, in this case.

Step 2: For the minimum image ground size of 600 by 600 km, the ground resolution required to infer height differences of one kilometer by measurement of stereo parallax is about 240 meters.

Step 3: An estimate of the required number of lines per image is obtained by dividing the image ground size by the required ground resolution. Thus approximately 2500 lines are required. This is an underestimate because planetary curvature effects are not considered. Comparison with the television scaling laws shows that inclusion of the Kell factor increases the estimate to nearly 3600 lines, which is beyond the resolution capability of currently available television imaging systems.

Step 4: Since the image half-angle subtended at the planet center is less than 0.1 radians, the effects of planetary curvature on computing the field-of-view may be neglected. The camera half-angle field-of-view is then approximately 16.8 degrees,

Table 6-6

Image Specifications and Orbital Parameters for
Visual Surface Topography Stereo Imagery at Mars

Spectral Range	5000-7500 Å
Horizontal Ground Resolution	3 km
Vertical Ground Resolution	1 km
Minimum Image Ground Size	600 km
Solar Zenith Angle	5-20 deg
Image Positional Accuracy	3 km
Overlap (Forward)	20%
Grey Scale	6 bits
Orbit Periapse Altitude	994 km
Orbit Apoapse Altitude	994 km
Orbit Eccentricity	0
Orbit Inclination	94.9 deg

for a 600 x 600 km image size. Including the effects of planetary curvature would result in a half-angle of 16.6 degrees.

Step 5: The camera minimum field-of-view is about 33 by 33 degrees.

Step 6: With this field-of-view, the ground resolution at the edge of the field-of-view is degraded by a factor of 1.16 compared to the ground resolution at the subsatellite point. Thus 2900 lines, rather than the 2500 lines estimated above, are required.

Step 7: A resolution capability of 2900 lines in a field-of-view of half-angle 16.8 degrees requires an optical system no less than 1.76 cm in diameter. As with the television scaling laws, this corresponds to a diameter five times the classical diffraction limit and implies a value of about 0.78 for the lens modulation transfer function.

Step 8: The orbit semi-major axis is 4374 km, and the ground speed of the subsatellite point is 2.42 km/sec, neglecting planet rotation. Since the orbit inclination is 94.9 degrees, and the equatorial speed of planet rotation is 0.24 km/sec, the maximum apparent ground speed is estimated to be 2.45 km/sec. For a circular orbit, the vertical speed of the imaging system vanishes.

Step 9: For a ground resolution of 240 meters, the maximum exposure time is 0.033 seconds without IMC (image motion compensation) or 0.33 seconds with IMC. Just as with the television scaling laws, these exposure time constraints are based on a maximum image smear of one-third a resolution element for smear arising from an apparent horizontal movement of the scene. One-sixth a resolution element smear is presumed to arise from rotation of the imaging system (see Step #21); the total image smear of one-half a resolution element corresponds to a value of about 0.64 for the image motion modulation transfer function.

Step 10: Table 6-7 presents various film characteristics pertinent to system design. In particular, the total number of lines per frame may be used to select a tentative film size. The number of lines per frame shown in the table correspond to the number of lines per millimeter providing a value of about 0.35 for the product of the film modulation transfer function and the flying spot scanner modulation transfer function (the scanner is assumed to have a five micron scanning beam). The transfer functions are given in Volume IV. Thus the product of the transfer functions for the film, scanner, optics, and image motion is about 0.17. For an apparent scene contrast of 1.6:1, the imaging system modulation transfer function has a value of about 0.04, which is assumed here to be the minimum acceptable value. Of course, if the optical system diameter substantially exceeds that computed in Step #7, or if the exposure time is substantially less than that computed in Step #9, the system transfer may be significantly more than 0.04 at the necessary resolution.

Referring to Table 6-7, 70 mm SO-243 film provides 9,300 lines per frame (image), while only 2900 lines per frame are required. Assuming there is sufficient scene luminance, there is not much point in using a faster film because a greater amount of film radiation shielding would be required. The system designer may utilize the excess resolution capability to increase the image ground size or to improve the ground resolution. Since an increased ground size will increase the image cycle time and hence reduce the data acquisition rate, this procedure has been usually followed in estimating film system support requirements. For stereo coverage, the image ground size controls the ground resolution for all image sizes less than $Hr_h / (0.4r_v)$. For any image size less than this value, the number of lines required is independent of image size (except for planet curvature effects). Therefore, when stereo coverage is required, it is generally ineffecient to use any

Table 6-7

Film Speed and System Resolution

Film Type	Aerial Exposure Index	Weight (lbs/sq.ft)	Total Number of Lines per Frame		
			70 mm	5 in	9½ in
SO-243	1.6	0.037	9300	16500	33000
3404	1.6	0.022	9200	16400	32800
SO-230	6	0.022	9200	16400	32800
SO-206	6	0.022	8300	14700	29400
SO-226	6	0.032	8300	14700	29400
SO-130	20	--	8100	14500	29000
3400	20	0.022	7700	13700	27400
SO-136	20	0.033	7700	13700	27400
SO-102	64	--	7600	13600	27100

image ground size less than $Hr_h/(0.4r_v)$. For the experiment under consideration, this limiting image size is 7,455 km. At this image size, a ground resolution of 3 km would enable deduction of vertical height differences of 1 km and (neglecting surface curvature) only 2,485 lines per frame would be required. However, since the radius of Mars is only 3,380 km, surface curvature effects are important for such large image ground sizes. It can be shown that if L lines per frame are provided by the film capability, and if the image ground size is less than $Hr_h/(0.4r_v)$, then the maximum acceptable value of r_ϕ/r_o is $0.4 r_v L/H$. For this example problem, 70 mm SO-243 film provides 9300 lines per frame, hence r_ϕ/r_o must be less than 3.74 to permit use of such film.

Some iteration with Table 6-1 leads to the conclusion that an image ground size of 2300 by 2300 km comes close to utilizing all the available resolution capability of 70 mm SO-243 film. For such an image ground size, the ground resolution required is about one km (actually 0.93 km), the camera field-of-view is about 87 by 87 degrees, and the minimum optics diameter is about 1.8 centimeters. The maximum exposure time is increased to about 0.13 sec without IMC and 1.3 sec with IMC. This type of iteration is not shown on the logic diagram because it is only applicable to stereo experiments with large image ground sizes.

To proceed with Step #10, the image format size is 64 by 64 millimeters for 70 mm film, hence the optics focal length is about 34 millimeters. The relative aperture must be in the range $f/1$ to $f/1.9$. To restrict the spectral range to above 5000 Å, a filter should be used, and the appropriate filter factor is about 1.8.

Step 11: For a solar zenith angle of twenty degrees, the surface photometric function is taken as 0.49, hence the minimum scene luminance is about 400 foot-lamberts.

Step 12: Using an optical system transmission factor of 0.9, an AEI (aerial exposure index) of 1.6 (from Table 6-7), and a lens aperture of f/1.8, the minimum exposure time is 0.0057 seconds. For design purposes, an exposure time of 0.01 seconds may be selected. If the minimum exposure time exceeds the maximum exposure time (Step #9), either the aperture must be opened or a faster film must be used. Apertures of less than f/1 are not feasible, while use of a fast film reduces the resolution capability and may require a larger film size.

Step 13: For an f/1.8 34 mm lens, the lens diameter must be about 1.9 centimeters. For lens diameters larger than about ten centimeters in the case of 70 mm film cameras, and about twenty centimeters in the case of 5 inch or 9½ inch film cameras, oversize optical systems must be used thereby increasing the system weight and volume.

Step 14: Because only a small area is illuminated at the proper solar zenith angle, at any one time, a very long time is required for 70 percent of Mars to be seen at the proper illumination. Orbit data sheet #5 (p.24 in Volume III) indicates that for this experiment only 36 percent of Mars can be imaged in the first 55 days of the mission. There is then a 60 day waiting period before new areas are properly illuminated. To image 70 percent of the planet will require 418 days in orbit. For the initial 36 percent coverage, a film length of 7 feet is required, assuming 60 percent side overlap and 20 percent forward overlap.

Step 15: Since IMC is not required, the basic system weight is $18 + 0.56 (2.76)^2 + 0.199 (1.9)^2$ or 23 pounds. From Table 6-7, the film weighs 0.037 lbs/sq.ft. Since the processing material weighs about 0.04 lbs/sq.ft. of processed film, the total film and processing weight is 0.077 lbs/sq.ft, or about 0.12 pounds for 7 feet of 70 mm film. Figure 6-11 shows that approximately one pound of shielding is required for 70 mm

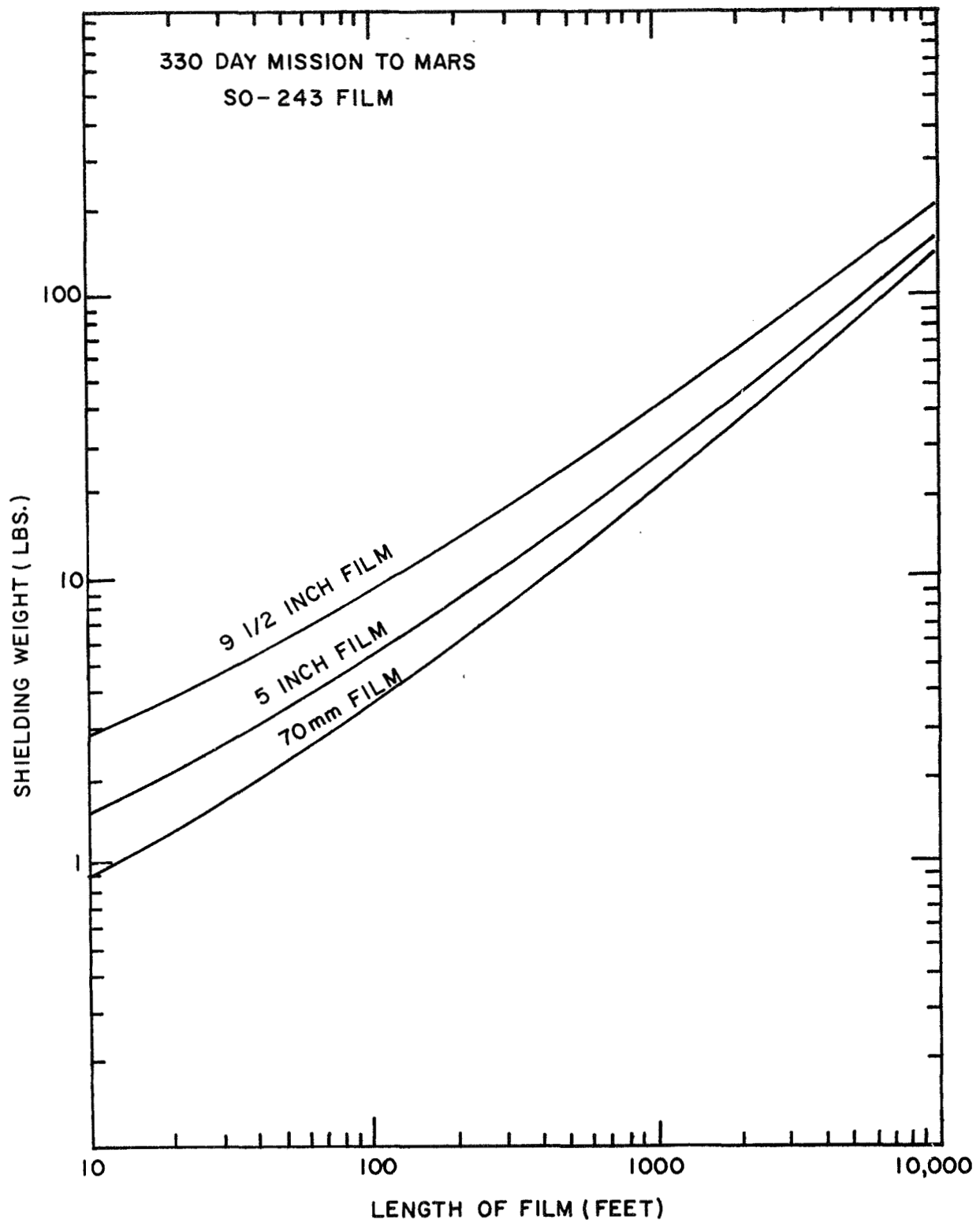


FIGURE 6-II. RADIATION SHIELDING WEIGHT

SO-243 film for a mission duration of 330 days. The flight time to Mars is given in Volume III as about 286 days (1984 opportunity), so that 341 days are required to complete the initial 36 percent coverage. The shielding weight is proportional to the mission duration, so the estimate obtained from Figure 6-11 should be multiplied by 341/330. In this case, this factor is nearly unity and may be ignored. The shielding weight is also proportional to the film speed and is assumed to be inversely proportional to the planet's distance from the Sun. The figure assumes an AEI of 1.6 and a heliocentric distance of 1.52 AU. When, for example, SO-130 film with an AEI of 20 is used on a 120 day mission to Mercury at 0.39 AU, the shielding weight obtained from Figure 6-11 should be multiplied by $(20 \times 120 \times 1.52 \times 1.52) / (1.6 \times 330 \times 0.39 \times 0.39)$. The additional weight, volume, and power requirement estimates appropriate when a zoom lens is added to the system presume that a radar altimeter is required to properly control the lens focal length. If oversize optical systems are employed, additional weight is required. For example, if a 20 cm diameter lens is employed with a 70 mm camera system, an additional weight of $0.037 (20)^2$ or 15 pounds is involved.

Step 16: The minimum size of a 70 mm camera system is 8 x 7 x 10 inches. Since the focal length is about 1.3 inches, and assuming a minimum of seven feet of film, the camera system length must be increased by about 3.7 inches and the depth increased by about 2.6 inches. The camera system size is then about 12 x 7 x 13 inches.

Step 17: The camera system volume is obtained from the linear dimensions as about 1100 cubic inches, or about 0.63 cubic feet.

Step 18: The system average power requirement is 36 watts for a 70 mm camera without IMC.

Step 19: For an image ground size of 2300 km, and a forward overlap of 20 percent, the cycle time is about 750 seconds.

Step 20: Assuming six bits per resolution element, the data acquisition rate is 6.9×10^5 bits/sec. If a forward overlap of 60 percent is used, as would be appropriate for obtaining stereo coverage in the direction of flight (forward stereo), the cycle time would decrease to 375 sec, and hence the data rate would increase to 1.4×10^6 bits/sec. It may also be noted that if the excess resolution capability of SO-243 70 mm film were used solely to improve the ground resolution, the image ground size would be 600 km, the cycle time 196 sec, and the data rate 2.6×10^6 bits/sec rather than 6.9×10^5 bits/sec. Of course, the ground resolution would be about 75 meters.

Step 21: The platform stability requirements are estimated in the same manner as for television systems. In this case, the allowable yaw rate is about 0.77 degrees/sec, while the allowable pitch or roll rate is about 0.89 degrees/sec.

Table 6-8 summarizes the support requirements for the design example.

6.4 Infrared Scanning Systems

Figure 6-12 is a logic diagram for designing infrared scanning systems in sufficient detail that the experiment support requirements may be estimated. Figure 6-13 summarizes the scaling laws which are used in the design procedure and support requirement estimation. These scaling laws have been based on an analysis of currently available equipment, or which could be available as the result of a short development program. A complete derivation and discussion is given in Volume IV. The procedure is illustrated here by a sample design aimed at imagery of Mars surface thermal anomalies on a local scale. The image specifications and orbital parameters are given in Table 6-9. The image specifications have been obtained from Table 4-1 and the appropriate worth curves. That is, the image specifications represent the minimum quality imagery which will satisfy the scientific objectives. The selected orbit is described by

Table 6-8

Sample Experiment Support Requirements
for a Photographic Film System

PLANET: Mars

OBSERVABLE: Surface Topography (regional)

Family No. 3a

CAMERA: 70mm with SO-243 film (side stereo)

ORBIT:	Data Sheet Number.....	5
	Periapse/Apoapse Alt. (km).....	994/994
	Inclination (deg).....	95
	Imaging Altitude Range (km).....	994
	Imaging On-Time (min).....	15
IMAGE:	Minimum Image Size (km).....	600
	Max. Ground Resolution (km).....	3 (1 vert.)
	Positional Accuracy (km).....	3
CAMERA:	Focal Length (mm).....	34
	Aperture Stop.....	f/1.8
	Exposure Time (sec).....	0.01
	Cycle Time (sec).....	750
	Length of Film (ft).....	7
	Shielding Weight (lbs).....	1

SUPPORT REQUIREMENTS:	
Field of View (deg).....	87 x 87
Pointing Accuracy (deg).....	0.17
Camera Volume (cu. ft.).....	0.58
Camera Shape (ft).....	1x0.6x1
Max. Roll/Yaw Rate (deg/sec).....	0.89/0.77
Operating Power (watts).....	36
Data Rate (bits/sec).....	6.9×10^5
Camera Weight (lbs).....	24

COMMENTS:

Image size is 2300 x 2300 km with ground resolution of 0.93 km. Film length based on 36% coverage which is achieved in 55 days. 418 days are required for 70% coverage. Forward stereo would increase data rate to 1.4×10^6 .

Table 6-9

Image Specifications and Orbital Parameters for
Infrared Surface Thermal Anomaly Imagery at Mars

Spectral Range	1-200 μ
Ground Resolution	0.2 km
Minimum Image Ground Size	100 km
Solar Zenith Angle	--
Temperature Resolution	2 deg K
Positional Accuracy	2 km
Maximum Acquisition Time	1 hr
Grey Scale	6 bits
Orbit Periapse Altitude	340 km
Orbit Apoapse Altitude	33,809 km
Orbit Inclination	90 deg
Mission Duration	400 days
Imaging Altitude	340-370 km

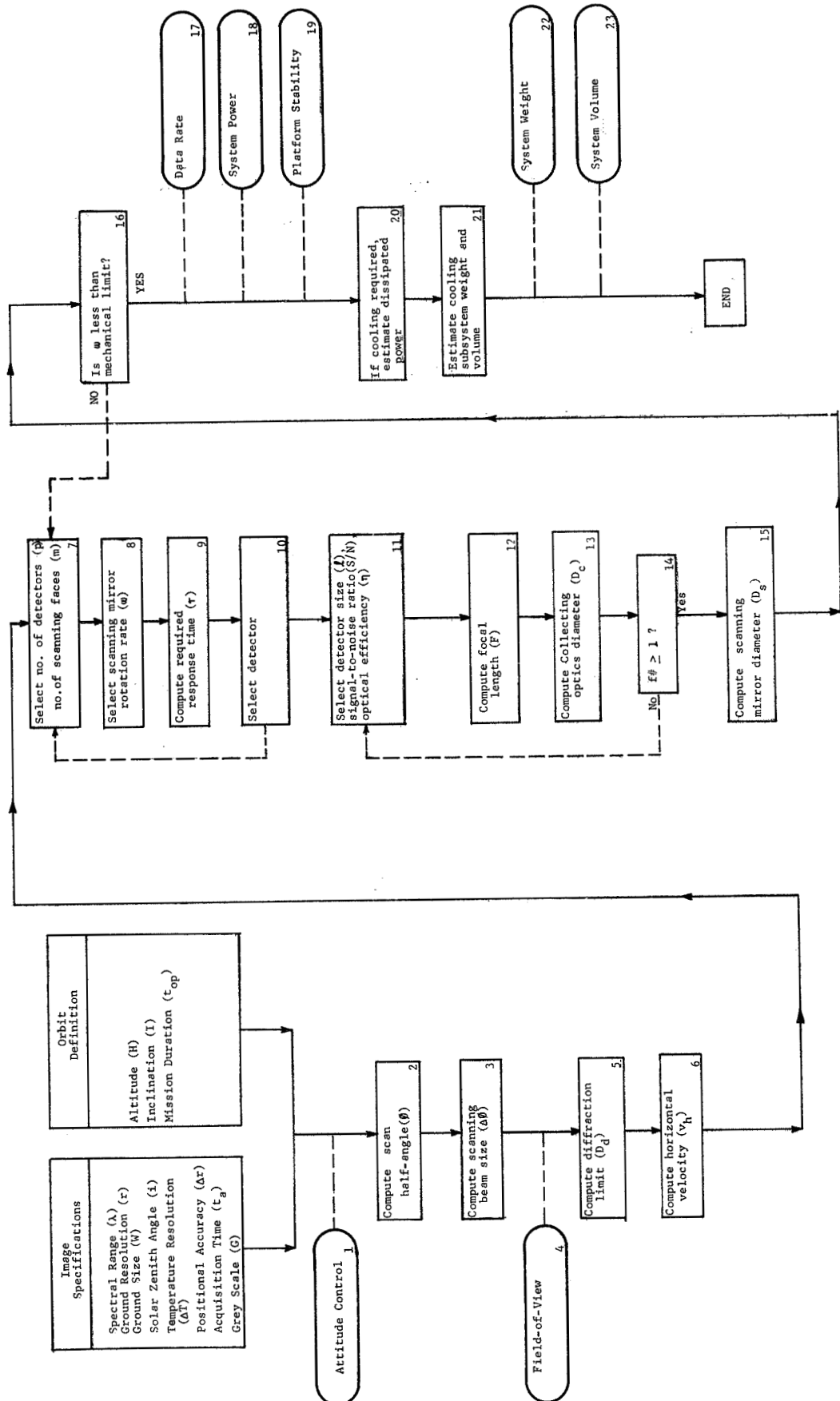


FIGURE 6-12. LOGIC DIAGRAM FOR INFRARED SCANNING SYSTEMS

NOMENCLATURE
(MKS units implied unless stated otherwise)

- a-orbit semi-major axis
- A_r-resistor area
- B-constant from Table 6-12
- C_c-constant from Table 6-13
- D_c-diameter of collecting optics
- D_d-collecting optics diffraction limit
- D_d²-detectivity, see Table 6-10
- D_d²-diameter of scanning mirror
- DR-data acquisition rate
- f₀-optics aperture stop (f-number)
- F-focal length
- FOV-field-of-view
- G-bits per resolution element (normally 6)
- H-sensor system altitude
- H₀ orbit apogee altitude
- H₀ orbit perigee altitude
- i-solar zenith angle
- I-orbit inclination
- l-detector size
- n-no. of faces on scanning mirror
- M_d-mass of collecting optics
- M_d-mass of detector and electronics
- M_g-mass of solid gas cooling system
- M_r-mass of radiative cooling system
- M_s-mass of scanning system
- p-number of detectors
- P-system power requirement
- P_d-power dissipated by cooling
- r-desired ground resolution
- R-planet radius
- SOM-state-of-art
- S/N-signal-to-noise ratio
- t_a-maximum acquisition time
- t₀-mission duration (must be in days)
- T₀-planetary temperature (deg K)
- T_d-detector temperature, see Table 6-10
- v_h-apparent horizontal speed
- v_p-sensor ground speed at perigee
- v_r-pinnet equatorial rotation speed
- V-volume of solid gas cooling system
- W-ground length of scan
- W-scan half-angle subtended at pinnet center
- Δr-desired image ground positional accuracy
- ΔT-desired temperature resolution (deg K)
- Δθ-allowable sensor pointing error
- Δφ-angular width of scanning beam
- τ-optical system transmission factor
- λ-wavelength
- μ-planet gravitational constant
- σ-Stefan-Boltzmann constant (5.67x10⁻⁸)
- τ-response time
- β-allowable sensor rotation rate
- β-scan half-angle
- w-scanning mirror rotation rate

<p>1</p> <p>$\Delta\theta = \frac{\Delta r}{R}$ radians</p> <p>$\gamma = \frac{W}{2R} - 1$ or, otherwise: $\beta = \cot^{-1} \left(\frac{R \sin \gamma}{R \cos \gamma - c \cot} \right)$</p> <p>If $\gamma < 0.1$, $\beta = \tan^{-1} \frac{W}{2R}$, otherwise: $\beta = \cot^{-1} \left(\frac{R \sin \gamma}{R \cos \gamma - c \cot} \right)$</p>	<p>2</p> <p>See Table 6-10</p> <p>If response time of desired detector is longer than response time of scanning mirror, response time by increasing p or n.</p>	<p>3</p> <p>$\Delta\theta = \frac{r}{H}$</p> <p>$\tau/p \leq \frac{1}{2\pi f_0}$ from Table 6-1</p>																		
<p>4</p> <p>FOV is $\Delta\theta$ by 2θ</p>	<p>5</p> <p>$D_d = \frac{1.22\lambda}{\Delta\theta}$</p> <p>should be less than one meter</p>	<p>6</p> <p>$a = R \frac{1}{2} (1 + H_0^2)$</p> <p>$v_p = \frac{R}{R + H_p} \left[\mu \left(\frac{2}{R + H_p} - \frac{1}{a} \right) \right]^{\frac{1}{2}}$</p> <p>$v_h = \left(v_p^2 + 2v_p v_r \cos i \right)^{\frac{1}{2}}$</p> <p>$v_h^2$ should be $\geq N$</p> <table border="1"> <tr> <th>Planet</th> <th>$\frac{R(\mu)}{H(\mu^2/\text{sec}^2)}$</th> <th>$v_r$ (m/sec)</th> </tr> <tr> <td>Moon</td> <td>1.74×10^6</td> <td>4.90×10^{12}</td> </tr> <tr> <td>Mercury</td> <td>2.42×10^6</td> <td>2.17×10^{13}</td> </tr> <tr> <td>Venus</td> <td>6.10×10^6</td> <td>3.25×10^{14}</td> </tr> <tr> <td>Mars</td> <td>3.38×10^6</td> <td>4.30×10^{13}</td> </tr> <tr> <td>Jupiter</td> <td>7.14×10^7</td> <td>1.27×10^{17}</td> </tr> </table>	Planet	$\frac{R(\mu)}{H(\mu^2/\text{sec}^2)}$	v_r (m/sec)	Moon	1.74×10^6	4.90×10^{12}	Mercury	2.42×10^6	2.17×10^{13}	Venus	6.10×10^6	3.25×10^{14}	Mars	3.38×10^6	4.30×10^{13}	Jupiter	7.14×10^7	1.27×10^{17}
Planet	$\frac{R(\mu)}{H(\mu^2/\text{sec}^2)}$	v_r (m/sec)																		
Moon	1.74×10^6	4.90×10^{12}																		
Mercury	2.42×10^6	2.17×10^{13}																		
Venus	6.10×10^6	3.25×10^{14}																		
Mars	3.38×10^6	4.30×10^{13}																		
Jupiter	7.14×10^7	1.27×10^{17}																		
<p>7</p> <p>Try $p = m = 1$</p> <p>p is SOM-limited to 50 or less.</p> <p>m should be ≤ 10</p>	<p>8</p> <p>$\tau \leq \frac{\Delta\theta}{2\pi f_0}$</p> <p>$\tau \leq \frac{\Delta\theta}{2\pi f_0}$</p>	<p>9</p> <p>$D_c = \frac{1}{B} \left(\frac{W}{\Delta\theta} \right)^{\frac{1}{2}} \left(\frac{S/N}{D_p} \right)^{\frac{1}{2}}$</p> <p>See Table 6-12 for B</p>																		
<p>10</p> <p>$\tau \leq \frac{\Delta\theta}{2\pi f_0}$</p>	<p>11</p> <p>Should be from 0.1 to 3mm</p> <p>S/N normally 120 for reflected sunlight images, 3 for thermal imagery.</p> <p>0.8 for $\lambda > 3\mu$.</p>	<p>12</p> <p>$F = \frac{A_r}{\Delta\theta}$</p>																		
<p>13</p> <p>$\tau \leq \frac{\Delta\theta}{2\pi f_0}$</p>	<p>14</p> <p>$\tau \leq \frac{\Delta\theta}{2\pi f_0}$</p>	<p>15</p> <p>$D_c = \frac{1}{B} \left(\frac{W}{\Delta\theta} \right)^{\frac{1}{2}} \left(\frac{S/N}{D_p} \right)^{\frac{1}{2}}$</p> <p>See Table 6-12 for B</p>																		
<p>16</p> <p>$\tau \leq \frac{\Delta\theta}{2\pi f_0}$</p>	<p>17</p> <p>$\tau \leq \frac{\Delta\theta}{2\pi f_0}$</p>	<p>18</p> <p>$D_c = \frac{1}{B} \left(\frac{W}{\Delta\theta} \right)^{\frac{1}{2}} \left(\frac{S/N}{D_p} \right)^{\frac{1}{2}}$</p> <p>See Table 6-12 for B</p>																		
<p>19</p> <p>$\tau \leq \frac{\Delta\theta}{2\pi f_0}$</p>	<p>20</p> <p>$\tau \leq \frac{\Delta\theta}{2\pi f_0}$</p>	<p>21</p> <p>$D_c = \frac{1}{B} \left(\frac{W}{\Delta\theta} \right)^{\frac{1}{2}} \left(\frac{S/N}{D_p} \right)^{\frac{1}{2}}$</p> <p>See Table 6-12 for B</p>																		
<p>20</p> <p>$\tau \leq \frac{\Delta\theta}{2\pi f_0}$</p>	<p>21</p> <p>$\tau \leq \frac{\Delta\theta}{2\pi f_0}$</p>	<p>22</p> <p>$D_c = \frac{1}{B} \left(\frac{W}{\Delta\theta} \right)^{\frac{1}{2}} \left(\frac{S/N}{D_p} \right)^{\frac{1}{2}}$</p> <p>See Table 6-12 for B</p>																		
<p>21</p> <p>$\tau \leq \frac{\Delta\theta}{2\pi f_0}$</p>	<p>22</p> <p>$\tau \leq \frac{\Delta\theta}{2\pi f_0}$</p>	<p>23</p> <p>$D_c = \frac{1}{B} \left(\frac{W}{\Delta\theta} \right)^{\frac{1}{2}} \left(\frac{S/N}{D_p} \right)^{\frac{1}{2}}$</p> <p>See Table 6-12 for B</p>																		
<p>22</p> <p>$\tau \leq \frac{\Delta\theta}{2\pi f_0}$</p>	<p>23</p> <p>$\tau \leq \frac{\Delta\theta}{2\pi f_0}$</p>	<p>24</p> <p>$D_c = \frac{1}{B} \left(\frac{W}{\Delta\theta} \right)^{\frac{1}{2}} \left(\frac{S/N}{D_p} \right)^{\frac{1}{2}}$</p> <p>See Table 6-12 for B</p>																		
<p>23</p> <p>$\tau \leq \frac{\Delta\theta}{2\pi f_0}$</p>	<p>24</p> <p>$\tau \leq \frac{\Delta\theta}{2\pi f_0}$</p>	<p>25</p> <p>$D_c = \frac{1}{B} \left(\frac{W}{\Delta\theta} \right)^{\frac{1}{2}} \left(\frac{S/N}{D_p} \right)^{\frac{1}{2}}$</p> <p>See Table 6-12 for B</p>																		

FIGURE 6-13 SCALING LAWS FOR INFRARED SCANNING SYSTEMS

orbit data sheet #35 in Volume III.

Step 1: The pointing accuracy implied by an allowable 2 km error on the planetary surface is 5.4 milliradians or 0.31 degrees.

Step 2: For a ground scan length of 100 km, the scan half-angle is 8.4 degrees.

Step 3: From Table 6-1, r_{ϕ}/r_o is approximately 1.04, hence the required angular resolution is about 0.52 milliradians or 0.03 degrees.

Step 4: The scanning system field-of-view is 0.03 by 17 degrees.

Step 5: At a wavelength of 50 μ , the diffraction limit is about 12 cm. That is, the optical system must be 12 cm diameter or larger if the proper ground resolution is to be achieved at a wavelength of 50 μ . This value is only an estimate since the detector and hence wavelength have not yet been selected, but it does indicate that the experiment may be feasible. To avoid scanning mirrors which are beyond the current state-of-art, the optical system diameter should be limited to one meter.

Step 6: The orbit semi-major axis is 20,455 km, hence the apparent speed of the subsatellite point at periapse is 4.16 km/sec, neglecting planetary rotation. For a polar orbit, the effect of planetary rotation is to increase the maximum apparent ground speed to 4.17 km/sec.

Step 7: As an initial design selection, one detector and one face on the scanning mirror may be chosen.

Step 8: For p and m each unity, the minimum rotation rate of the scanning mirror is 146 radians/sec.

Step 9: The detector response time must be less than about 1.8 microseconds.

Step 10: Table 6-10 presents characteristics of selected infrared detectors. An initial detector selection may be made on the basis of response time and wavelength. For photon detectors, identified with a P in the table, wavelengths shorter than the value given in the table can be detected. A thermistor detector can be used at any wavelength in the infrared, but is limited to application where the required detector response time is slower than 500 microseconds. The required response time may be increased by increasing the number of detectors or the number of faces on the scanning mirror. If 50 detectors are used ($p=50$) and four faces are used on the scanning mirror ($m=4$), the product pm is 200 and the response time can be increased a factor of 200. Since it is already known (Step #5) that relatively large collecting optics is required, the system weight will increase rapidly with m larger than 4. If m were 6, then pm would be 300, and the required response time would be about 540 μ sec. That is, a linear array of 50 thermistor detectors could be used in conjunction with a six-sided scanning mirror. An alternative design approach, and one which would probably result in less demanding experiment support requirements, is simply to use a detector with a faster time response.

Some consideration must be given to the detector operating temperature and cutoff wavelength. Operating temperatures of 295 deg K will require no additional weight for cooling. Operating temperatures of 195 deg K will require only a small amount of additional weight for radiative cooling, while operating temperatures of 77 or 23 deg K may require a heavy cooling system. Operating temperatures of 4 deg K are probably unfeasible for planetary orbital missions. Selection of the operating wavelength depends upon the type of imagery desired. For detection of reflected solar energy, wavelengths longer than 2.5μ are useless. For thermal imagery, that is, detection of thermal energy emitted by the scene, the selection of wavelength depends upon the scene temperature. Since the amount of thermal power emitted by a

Table 6-10
Infrared Detector Characteristics

Wavelength of Peak Response λ_p (μ)	Detector	Photon or Thermal	Operating Temperature (deg K)	Response Time (μ sec)	Peak Detectivity D_p^* ($m-Hz^{1/2}/watt$)
2.3	PbS	P	295	0.1	1.1×10^9
2.6	PbS	P	195	3.5	5.5×10^9
3.0	InAs	P	77	2	2.5×10^9
3.3	PbS	P	77	3	1.4×10^9
3.5	PbSe	P	295	2	2.5×10^7
4.2	PbSe	P	195	30	2.5×10^8
5.1	InSb	P	77	2	7×10^8
6	Ge: Au	P	77	1	4.5×10^7
11	Ge: Hg	P	23	1	2.3×10^8
12	HgCdTe	P	77	0.01	8×10^7
18	Si: Al*	P	23	0.00005	4×10^8
23	Ge: Cu	P	4	0.003	3×10^8
30	Si: B*	P	23	0.0002	5×10^8
34	Ge: Zn	P	4	1	2×10^8
-	Thermistor	T	295	> 500	$8 \times 10^4 \times [\tau (\mu sec)]^{1/2}$

* in developmental stages

surface increases with temperature, a conservative system design will probably result if the design is based on the minimum scene temperature expected to be observed. This minimum temperature varies from planet to planet and also depends upon whether atmospheric or surface phenomena are to be observed. Estimates of these temperatures are given in Table 6-11. Thus for observing surface thermal anomalies at Mars, the minimum scene temperature expected is about 200 deg K. At this temperature, the peak of the black body spectral emission curve will occur in the vicinity of 15μ , hence a detector which can respond out to 15μ should be selected. Table 6-10 indicates that a heavy cooling system will probably be required for any detector operating at longer than 5μ wavelength. Also all the detectors sensitive to this wavelength region have sufficiently fast response times (even the InSb detector could be used with two faces on the scanning mirror or two detectors). Thus a reasonable detector selection appears to be that of aluminum - doped silicon operating at 23 deg K.

Table 6-11

Estimates of Planetary Temperatures

Planet	Minimum Atmospheric Temperature (deg K)	Minimum Surface Temperature (deg K)	Maximum Temperature (deg K)
Moon	--	120	400
Mercury	--	100	600
Venus	200	550	700
Mars	150	200	300
Jupiter	100	150	200

Step 11: The detector size may be taken as 0.1 mm, the required signal-to-noise ratio as 3, and the optical system efficiency as 80 percent. For imagery of reflected sunlight the

signal-to-noise ratio should be 120 and the optical system efficiency may be increased to 85 percent. The difference in signal-to-noise ratio between thermal and sunlight imagery arises from the definition of signal. For thermal imagery, the signal is regarded as the difference in apparent brightness between two adjacent scene resolution elements whose brightness temperatures differ by ΔT deg K, where ΔT is the desired temperature resolution. For imagery of infrared reflectivity, the signal is regarded as the total amount of energy detected as being reflected from a scene resolution element. To detect reflectivity differences of five percent in a low contrast scene, a high signal-to-noise ratio is required.

Step 12: The system focal length is easily estimated to be about 19 cm for a detector size of 0.1 mm and an angular resolution of 0.52 milliradians.

Step 13: The equation shown in the scaling law chart gives an estimate of the minimum collector aperture diameter which will focus enough energy upon the detector to satisfy the signal-to-noise requirement. Table 6-12 gives a prescription for computing the quantity B which is needed in computing the collector diameter. Actually, the table gives B squared, and the square root must be taken before using the diameter formula. For reflected sunlight imagery, some additional constants given in Table 6-13 are required to compute B. The numerical constants are designed for MKS units. For this reason, the detectivities given in Table 6-10 have been given in unit of meters - $\text{Hz}^{\frac{1}{2}}/\text{watt}$ rather than the more common centimeters - $\text{Hz}^{\frac{1}{2}}/\text{watt}$. For the design example, λT ranges from 4×10^{-4} meter-deg K (at 2μ) to 3.6×10^{-3} meters - deg K (at 18μ). Thus the third formula given in Table 6-12 should be used to compute B^2 . Since x_2 is 4 and x_1 is 36, B^2 is found to be 0.163 watts/m^2 . Using a D_p^* of 4×10^8 meters - $\text{Hz}^{\frac{1}{2}}/\text{watt}$, the collector diameter is estimated to be 10.6 cm. At a wavelength of 18μ , the diffraction limit is

Table 6-12
Computation of B

Detector Type	Energy Source	λT (meters-deg K)	B^2
	Sunlight	any value	$\frac{0.113 \text{ fc}_p}{\lambda_p}$
Photon	Thermal Emission	≥ 0.014	$\frac{1.46 \times 10^{-15} \Delta T}{\lambda_p} \left(\frac{1}{\lambda_1^2} - \frac{1}{\lambda_2^2} \right)$
		≤ 0.014	$\frac{1.41 \times 10^{-11} T^2 \Delta T}{\lambda_p} \left[e^{-x} (x^3 + 3x^2 + 6x + 6) \right]_{x_1}^{x_2}$
	Sunlight	any value	0.113 fc_t
Thermal	Thermal Emission	≥ 0.014	$9.77 \times 10^{-16} \Delta T \left(\frac{1}{\lambda_1^3} - \frac{1}{\lambda_2^3} \right)$
		≤ 0.014	$9.82 \times 10^{-10} T^3 \Delta T \left[e^{-x} (x^4 + 4x^3 + 12x^2 + 24x + 24) \right]_{x_1}^{x_2}$

Note: x_i is $(0.0144 \text{ meters-deg K})/\lambda_i T$; C_p and C_t are given in Table 6-13

4.2 cm. The collector size can be reduced by decreasing the scanning mirror rotation rate as permitted by the response time of the detector. Increasing the number of faces on the scanning mirror to about three or four does not affect the system power requirement and does not greatly increase the weight of the scanning system. Using a four-sided mirror, the scanner rotation rate may be reduced to 36.4 radians/sec and the corresponding collector diameter is 7.5 cm.

Table 6-13

Values of C_p and C_t

Planet	Spectral Interval (microns)	Photon Detectors C_p (watts/m)	Thermal Detectors C_t (watts/m ²)
Moon	0.8-2.5	2.22×10^{-4}	143
Mercury	0.8-2.0	1.26×10^{-3}	852
Venus	0.8-2.5	6.38×10^{-4}	525
Mars	0.8-2.5	1.00×10^{-4}	77.3
Jupiter	0.8-2.5	3.71×10^{-6}	3.55

Step 14: The f-number is simply 19cm/7.5 cm, or f/2.5. If the f-number comes out less than one, the focal length should be increased by increasing the detector size, or the collector diameter decreased.

Step 15: For a four-sided scanning mirror, the mirror base has a diameter of 2.3 times the collector diameter, if the scan half-angle is 8.4 degrees. Thus, the scanning mirror diameter is about 17.3 cm. Mirror diameters of more than two meters are regarded as beyond the state-of-art.

Step 16: The rotation rate is limited to $193/D_s$, by optical distortion. In this case, the limit is about 1100 rad/sec, while the design rate is 36.4 rad/sec. If the design rate is not less than $193/D_s$, the rotation rate must be reduced by increasing the number of detectors or the number of mirror faces.

Step 17: With a single detector and six binary bits per resolution element, the data acquisition rate is 4.1×10^5 bits/sec. This estimate does not take into account the duty cycle of the scanning mirror, and hence is the maximum data acquisition rate.

Step 18: The system average power requirement is estimated to be four watts.

Step 19: The maximum allowable pitch, roll, or yaw rate is estimated as 18.2 radians/sec. This estimate is based on an allowable image smear of one-half resolution element.

Step 20: Since cooling is required, an estimate must be made of the dissipated power. It is assumed that 20 milliwatts are delivered to each detector by conduction, and 500 watts per square meter of detector area by radiation. The remaining term accounts for reflected and thermally emitted energy focused on the detector by the collector. In computing this contribution, the maximum expected planetary temperature should be used and is given in Table 6-11. Thus, in this example, 20 milliwatts are delivered to the detector by conduction, 5 microwatts by radiation, and about 0.2 microwatts by the optical system. In most cases, the conductive term will completely dominate the power which must be dissipated, and hence the dissipated power is 0.02 watts.

Step 21: The cooling system weight and volume estimates for detector temperatures less than 195 deg K are based on the use of solid gas cryogenic systems. Thus for a detector temperature of 23 deg K, 0.02 watts of dissipated power, and an operating time of 400 days, the cooling system has a mass of 16 kilograms

and a volume of 0.012 cubic meters. The 400 day operating time is based on an interplanetary flight time of nearly 300 days and an orbit operating time a little more than 100 days. The numerical scaling coefficients given in the scaling law chart presumes that the operating time is expressed in days. That is, for a 23 deg K system, 2 kilograms of cooling per watt-day are required. Note that a 13 deg K system is lighter but much bulkier. Had radiative cooling been possible for this experiment, the cooling system mass and radiating area would have been estimated as 0.2 kilograms and 0.1 square meters, respectively.

Step 22: For the design example, approximately one kilogram is required for the detector and the associated electronics. The mass of the optical system is about 9.4 kilograms, for a 7.5 cm diameter collector. For a four-faced mirror of 17.3 cm base diameter, the scanning system has a mass of about 0.6 kilograms. Thus, the imaging system total mass is about 27 kilograms, or 60 pounds.

Step 23: The volume of the optical, scanning, and detecting systems is roughly 0.004 cubic meters, hence the total volume (including the cooling system) is estimated to be 0.016 cubic meters, or nearly 0.6 cubic feet.

Table 6-14, which is taken from Volume V, summarizes the experiment support requirements for this illustrative design example.

Table 6-14
 Sample Experiment Support Requirements
 for an Infrared Scanning System

PLANET: Mars

OBSERVABLE: Surface Thermal Anomalies (local)

Family No. 23

DETECTOR: Si: Al at 23 deg K (2-18 μ)

ORBIT:	Data Sheet Number.....	35
	Periapse/Apoapse Alt. (km).....	340/33,809
	Inclination (deg).....	90
	Imaging Altitude Range (km).....	340-370
	Imaging On-Time (min).....	10
IMAGE:	Minimum Image Width (km).....	100
	Max. Ground Resolution (km).....	0.2
	Positional Accuracy (km).....	2
SCANNER:	Collector Diameter (cm).....	7.5
	Aperture Stop.....	f/2.5
	No. of Detectors.....	1
	No. of Scanner Faces.....	4
	Scanner Rotation Rate (rpm).....	350

SUPPORT REQUIREMENTS:	
Field of View (deg).....	0.03 x 17
Pointing Accuracy (deg).....	0.31
System Volume (cu. ft.).....	0.6
Max. Roll/Yaw Rate (deg/sec).....	1000
Operating Power (watts).....	4
Data Rate (bits/sec).....	410,000
System Weight (lbs).....	60

COMMENTS:

Solid neon cooling system weighs 35 pounds, based on 0.02 watts dissipated for 400 days.

6.5 Passive Microwave Systems

Figure 6-14 and 6-15 present a suggested design procedure and associated scaling laws for passive microwave imaging systems. The scaling laws are similar to those for ultraviolet and infrared scanning systems, since the imagery is obtained by scanning across the planetary surface normal to the direction of flight. Rather than a scanning mirror, a scanning antenna is used. Mechanically-scanned antennas may be employed if relatively long scan times are permitted, otherwise electrically-scanned antennas should be used. Selection of an operating frequency may be made on the basis of the available integration time per resolution element. A complete discussion of the design procedure, and derivation of the scaling laws, is presented in Volume IV. Only a design example is given here.

To illustrate the design procedure, consider the image specifications for imagery of atmospheric thermal anomalies at Venus on a regional scale. The specifications, as derived from Table 4-1 and the appropriate worth curves, are shown in Table 6-15, along with selected orbit parameters. As with the other design examples, the worth curves have been used to select values for the image specifications which would appear to result in the least demanding support requirements without significantly degrading the scientific value of the imagery. The orbit selected is more fully described by orbit data sheet #85 in Volume III. From this orbit, total coverage of Venus can be achieved in 122 days.

Step 1: The required sensor system pointing accuracy is $50/454$ radians, or 6.3 degrees.

Step 2: Since the angle subtended at the planet center by one-half the scan length is 0.123 radians, computation of the scan half-angle should include the effects of planet curvature. The scan half-angle is then 56 degrees.

Table 6-15

Image Specifications and Orbital Parameters
for Regional Atmospheric Thermal Anomalies (Venus)

Ground Resolution	20 km
Minimum Image Ground Size	1500 km
Temperature Resolution	5 deg K
Positional Accuracy	50 km
Maximum Acquisition Time	1 hr
Grey Scale	6 bits
Orbit Periapse Altitude	454 km
Orbit Apoapse Altitude	454 km
Orbit Inclination	90 deg

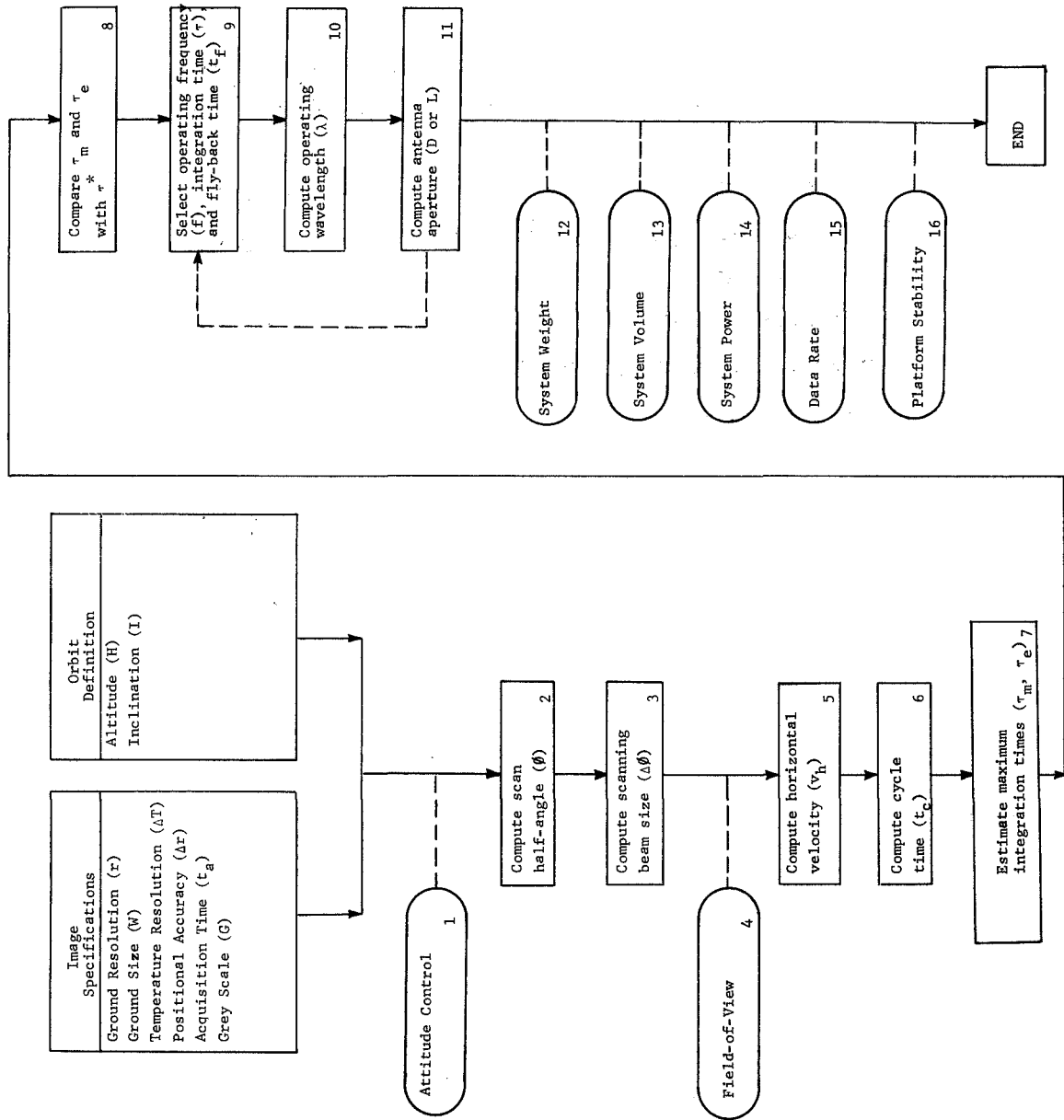


FIGURE 6-14. LOGIC DIAGRAM FOR PASSIVE MICROWAVE SYSTEMS

<p>1</p> $\Delta\theta = \frac{\alpha^2}{H^2} \text{ radians}$ $Y = \frac{H}{2R}$ <p>If $Y < 0.1$, $\beta = \tan^{-1} \frac{H}{2R}$, otherwise $\beta = \cot^{-1} \left(\frac{R+H}{R} \sin Y - \cot Y \right)$</p>	<p>2</p> $\Delta\theta = \frac{R}{H} \left(\frac{1}{\cos \beta} - \sin^2 \beta \right)$ <p>which is given in Table 4-1.</p>	<p>3</p> <p>FOV is $\Delta\theta$ by 28</p> $a = R + \frac{1}{2}(H_p + H_s)$ $V_p = \frac{R}{R_{HP}} \left[\frac{R}{R_{HP}} - \sin^2 \beta \right]^{\frac{1}{2}}$ $V_s = \sqrt{V_p^2 - 2V_p V_c \cos \beta}$ <p>Note: V_a must $\geq V$</p> <table border="1"> <thead> <tr> <th>Planet</th> <th>$\frac{R}{H}$</th> <th>$\frac{R}{R_{HP}}$</th> <th>$\frac{R}{R_{HP}} \left(\frac{R}{R_{HP}} - \sin^2 \beta \right)^{\frac{1}{2}}$</th> <th>$V_c$ (m/sec)</th> </tr> </thead> <tbody> <tr> <td>Moon</td> <td>1.78×10^6</td> <td>4.90×10^{12}</td> <td>-</td> <td>-</td> </tr> <tr> <td>Mercury</td> <td>2.42×10^6</td> <td>2.17×10^{14}</td> <td>-</td> <td>-</td> </tr> <tr> <td>Venus</td> <td>6.10×10^6</td> <td>3.25×10^{14}</td> <td>-</td> <td>-</td> </tr> <tr> <td>Mars</td> <td>3.38×10^6</td> <td>4.30×10^{13}</td> <td>2.60×10^2</td> <td>-</td> </tr> <tr> <td>Jupiter</td> <td>7.14×10^7</td> <td>1.27×10^{17}</td> <td>1.27×10^4</td> <td>-</td> </tr> </tbody> </table>	Planet	$\frac{R}{H}$	$\frac{R}{R_{HP}}$	$\frac{R}{R_{HP}} \left(\frac{R}{R_{HP}} - \sin^2 \beta \right)^{\frac{1}{2}}$	V_c (m/sec)	Moon	1.78×10^6	4.90×10^{12}	-	-	Mercury	2.42×10^6	2.17×10^{14}	-	-	Venus	6.10×10^6	3.25×10^{14}	-	-	Mars	3.38×10^6	4.30×10^{13}	2.60×10^2	-	Jupiter	7.14×10^7	1.27×10^{17}	1.27×10^4	-	<p>4</p> $t_c = \frac{H \Delta\theta}{V_a}$ $T_m = \frac{t_c \Delta\theta}{\omega}$ $T_e = \frac{\Delta\theta}{2\omega} (t_c - 2 \times 10^{-4}) \cdot 10^{-4}$	<p>5</p> <p>* given in Figure 7-6 If $t_m > t_e$, use mechanically-scanned antenna If $t_m < t_e$, use electrically-scanned antenna If neither t_m or $t_e > t_e$, comp. resolution implied by Figure 7-6 cannot be achieved.</p> <p>Use T_m or T_e with Figure 7-6 to select f. elec. scan: $t_e = 2 \times 10^{-4}$ sec $t = t_e$ mech. scan: $t_e \leq t_c = \frac{4\theta \Delta\theta}{\omega}$ $t = \frac{\Delta\theta}{\omega} (t_c - t_e) \geq t_e$</p>	<p>6</p> <p>Receiver weight (M_R) from Figure 7-7. mech. scan: $M_R = 5.80^2$ elec. scan: $d = \frac{1}{1 + \frac{1}{\pi} \pi \omega \theta}$ $M = \frac{1}{d} + 1$ $M_R = M(0.046 + \frac{0.492}{f})$ System weight $= M_R + M_A$</p>
Planet	$\frac{R}{H}$	$\frac{R}{R_{HP}}$	$\frac{R}{R_{HP}} \left(\frac{R}{R_{HP}} - \sin^2 \beta \right)^{\frac{1}{2}}$	V_c (m/sec)																															
Moon	1.78×10^6	4.90×10^{12}	-	-																															
Mercury	2.42×10^6	2.17×10^{14}	-	-																															
Venus	6.10×10^6	3.25×10^{14}	-	-																															
Mars	3.38×10^6	4.30×10^{13}	2.60×10^2	-																															
Jupiter	7.14×10^7	1.27×10^{17}	1.27×10^4	-																															
<p>7</p> <p>Antenna area D^2 or 1.212 100 cu in for $f \leq 1$ GHz 200 cu in for $1 < f \leq 30$ GHz 300 cu in for $30 < f < 100$ GHz 500 cu in for $f > 100$ GHz</p>	<p>8</p> <p>Receiver power requirement (P_R) from Figure 7-8. mech. scan: $P_R = \frac{40M(0.04)^2}{t_c^2}$ elec. scan: $P_R = 0.194N$</p>	<p>9</p> <p>Receiver power requirement (P_R) from Figure 7-8. mech. scan: $P_R = \frac{40M(0.04)^2}{t_c^2}$ elec. scan: $P_R = 0.194N$</p>	<p>10</p> <p>Receiver power requirement (P_R) from Figure 7-8. mech. scan: $P_R = \frac{40M(0.04)^2}{t_c^2}$ elec. scan: $P_R = 0.194N$</p>	<p>11</p> <p>Receiver power requirement (P_R) from Figure 7-8. mech. scan: $P_R = \frac{40M(0.04)^2}{t_c^2}$ elec. scan: $P_R = 0.194N$</p>	<p>12</p> <p>Receiver power requirement (P_R) from Figure 7-8. mech. scan: $P_R = \frac{40M(0.04)^2}{t_c^2}$ elec. scan: $P_R = 0.194N$</p>																														
<p>13</p> <p>Receiver power requirement (P_R) from Figure 7-8. mech. scan: $P_R = \frac{40M(0.04)^2}{t_c^2}$ elec. scan: $P_R = 0.194N$</p>	<p>14</p> <p>Receiver power requirement (P_R) from Figure 7-8. mech. scan: $P_R = \frac{40M(0.04)^2}{t_c^2}$ elec. scan: $P_R = 0.194N$</p>	<p>15</p> <p>Receiver power requirement (P_R) from Figure 7-8. mech. scan: $P_R = \frac{40M(0.04)^2}{t_c^2}$ elec. scan: $P_R = 0.194N$</p>	<p>16</p> <p>Receiver power requirement (P_R) from Figure 7-8. mech. scan: $P_R = \frac{40M(0.04)^2}{t_c^2}$ elec. scan: $P_R = 0.194N$</p>	<p>17</p> <p>Receiver power requirement (P_R) from Figure 7-8. mech. scan: $P_R = \frac{40M(0.04)^2}{t_c^2}$ elec. scan: $P_R = 0.194N$</p>	<p>18</p> <p>Receiver power requirement (P_R) from Figure 7-8. mech. scan: $P_R = \frac{40M(0.04)^2}{t_c^2}$ elec. scan: $P_R = 0.194N$</p>																														

NONERGLATURE

(MKS units throughout unless specified otherwise)

- a-orbit semi-major axis
- c-speed of light
- d-antenna element spacing
- D-parabolic antenna diameter
- DR-data acquisition rate
- F-operating frequency (in GHz)
- FOV-field-of-view
- G-binary bits per resolution element (normally 6)
- H-antenna altitude
- H-orbit apogee altitude
- H-orbit perigee altitude
- I-orbit inclination
- L-antenna active length
- M-antenna weight
- M-receiver weight
- N-number of antenna elements
- P-antenna power requirement
- P-receiver power requirement
- R-desired ground resolution
- R-planet radius
- T-maximum permitted acquisition time
- t-antenna cycle time
- V_a-apparent horizontal ground speed
- V_g-ground speed of antenna at perigee
- V_p-planet equatorial rotation speed
- W-ground length of scan line
- Y-half-angle subtended by R at planet center
- Δθ-required ground positional accuracy
- Δβ-angular size of scanning beam
- β-maximum permissible platform rotation rate
- λ-operating wavelength
- μ-planet gravitational constant
- T-integration time actually used
- T-integration time required
- T_e-integration time afforded by electrical scan
- T_m-integration time afforded by mechanical scan
- β-scan half-angle

FIGURE 6-15. SCALING LAWS FOR PASSIVE MICROWAVE SYSTEMS

Step 3: Since r_{ϕ}/r_0 changes rapidly with ϕ in the vicinity of 60 degrees, r_{ϕ}/r_0 should be computed using the formula given in the scaling law chart rather than obtained by interpolation from Table 6-1. The formula yields a value of 4.41, hence the required angular resolution, or scanning beam size, is 10 milliradians, or 0.57 degrees. It should be noted that, contrary to the situation in the case of a flat planet, if the sensor system were operated at a higher altitude, the required angular resolution would actually be less demanding since a more vertical view angle could be used at the edge of the field-of-view.

Step 4: The sensor system field-of-view is then 0.57 by 112 degrees.

Step 5: The ground speed of the subsatellite point is about 6.55 km/sec. Therefore, data from a 1500 km length along the subsatellite track will be acquired in about 230 seconds, which is considerably less than the desired maximum of one hour.

Step 6: The cycle time is 0.69 seconds. That is, in order to prevent gaps between adjacent scan lines, each scan line must be swept out and the antenna in position to start the next scan within 0.69 seconds.

Step 7: The maximum integration time per resolution element permitted by a mechanically-scanned antenna has been estimated by assuming that the data integration time can only be one-half or less of the antenna dwell time per resolution element, and the antenna fly-back time has been neglected. Thus the integration time estimate is an upper limit; in practice something like one-half the estimated time is available when one allows for a reasonable antenna fly-back time. Very short fly-back times increase rapidly the power requirement for a mechanically-scanned antenna (Step #14). The integration time estimate for an electrically-scanned antenna is based on a beam-switching time of 0.1 milliseconds and a fly-back or calibration time of 0.2 milliseconds.

Step 8: Figure 6-16 shows the integration time per resolution element required to achieve a temperature resolution of one deg K at the Moon, two deg K at Mars or Jupiter, and five deg K at Venus or Mercury as a function of the system operating frequency. The data given in the figure are based on a number of assumptions regarding the receiver bandwidth, radiometer constant, signal-to-noise ratio, background temperature, and amplifier noise temperature which are discussed in Volume IV. The figure shows that 5 milliseconds integration time is required to achieve a 5 deg K temperature resolution at Venus if the operating frequency is 30 GHz. Also, if any other frequency is used, the integration time must be longer. Even if an electrically-scanned antenna is used, The available integration time is only 3.4 milliseconds. In other words, the desired temperature resolution cannot be achieved. The discussion in Volume IV shows that the minimum integration time plotted in the figure is inversely proportional to the square of the temperature resolution. Thus the temperature resolution afforded by a 3.4 millisecond integration time is $(5 \text{ m sec}/3.4 \text{ m sec})^{\frac{1}{2}} \times (5 \text{ deg K})$ or about 6 deg K.

Step 9: Since figure 6-16 shows that for atmospheric thermal emission at Venus, the minimum integration time occurs at 30 GHz, this implies that if the integration time is fixed, the best temperature resolution is achieved at 30 GHz. Thus the operating frequency should be about 30 GHz, the integration time 3.4 milliseconds, and the fly-back or calibration time 0.2 milliseconds. In situations where the available integration time from Step 7 exceeds the minimum integration time shown in the figure, some flexibility is available in the selection of operating frequency. For example, if the required ground resolution were only 40 km, instead of 20 km, the angular resolution would be 20 milliradians. The maximum integration times would then be 6.8 milliseconds for a mechanically-scanned antenna and about 14 milliseconds for an electrically-scanned

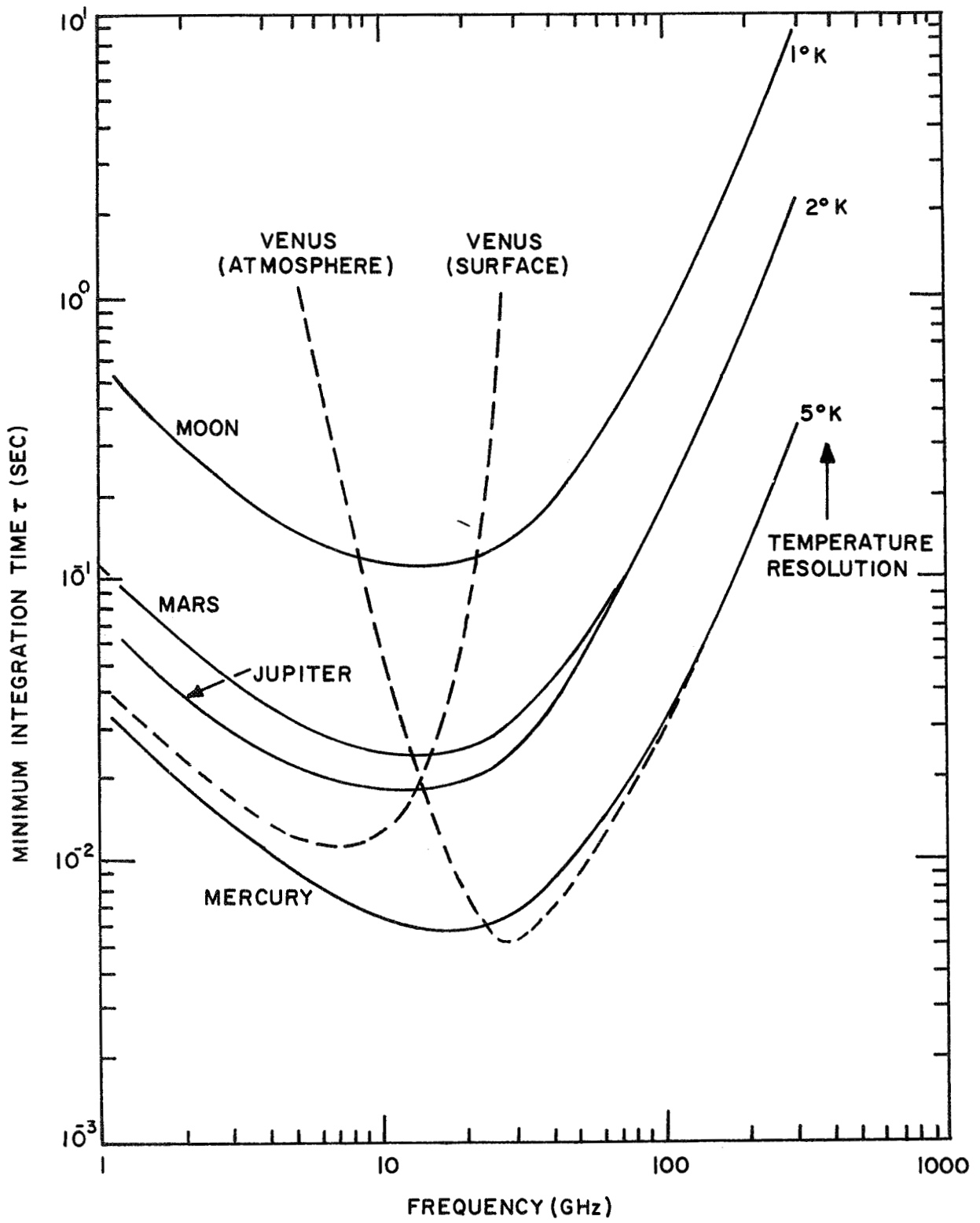


FIGURE 6-16. MINIMUM INTEGRATION TIME

antenna. Then, for an electrically-scanned antenna, the operating frequency should lie in the range 15-66 GHz. Selection of a low operating frequency will tend to decrease the receiver support requirements, while selection of a high operating frequency will tend to decrease the antenna support requirements.

Step 10: For an operating frequency of 30 GHz, the corresponding operating wavelength is 0.01 meters, or one centimeter.

Step 11: For an electrically-scanned antenna, the active length L is about 2 meters. Figure 6-17 shows that at 30 GHz, the current state-of-art limits the antenna size to about 5.5 meters, hence a 2 meter antenna is well within the current state-of-art. If the required antenna size exceeds the state-of-art capability, the operating frequency should be increased, if possible. This iterative loop is indicated by the dashed line in the logic diagram.

Step 12: Figure 6-18 indicates that a 30 GHz receiver weighs about 15 pounds. For an electrically-scanned antenna, the elements should be spaced at intervals of about 0.55 cm, and hence there should be about 370 elements. The antenna mass is then about 40 kg, or 87 pounds. The total imaging system weight is then about 100 pounds.

Step 13: The total antenna area is about 4.8 square meters, while the receiver volume is about 250 cubic inches.

Step 14: Figure 6-19 shows that a 30 GHz receiver has an average power requirement of about ten watts. Since there are 370 elements, the antenna power requirement is about 70 watts. The system average power requirement is then about 80 watts.

Step 15: For six binary bits per resolution element, the data acquisition rate is about 1700 bits/sec.

Step 16: The allowable pitch, roll, or yaw rate is estimated as 1.4 radians/sec, or 80 deg/sec. This will result in an image smear of one-half a resolution element.

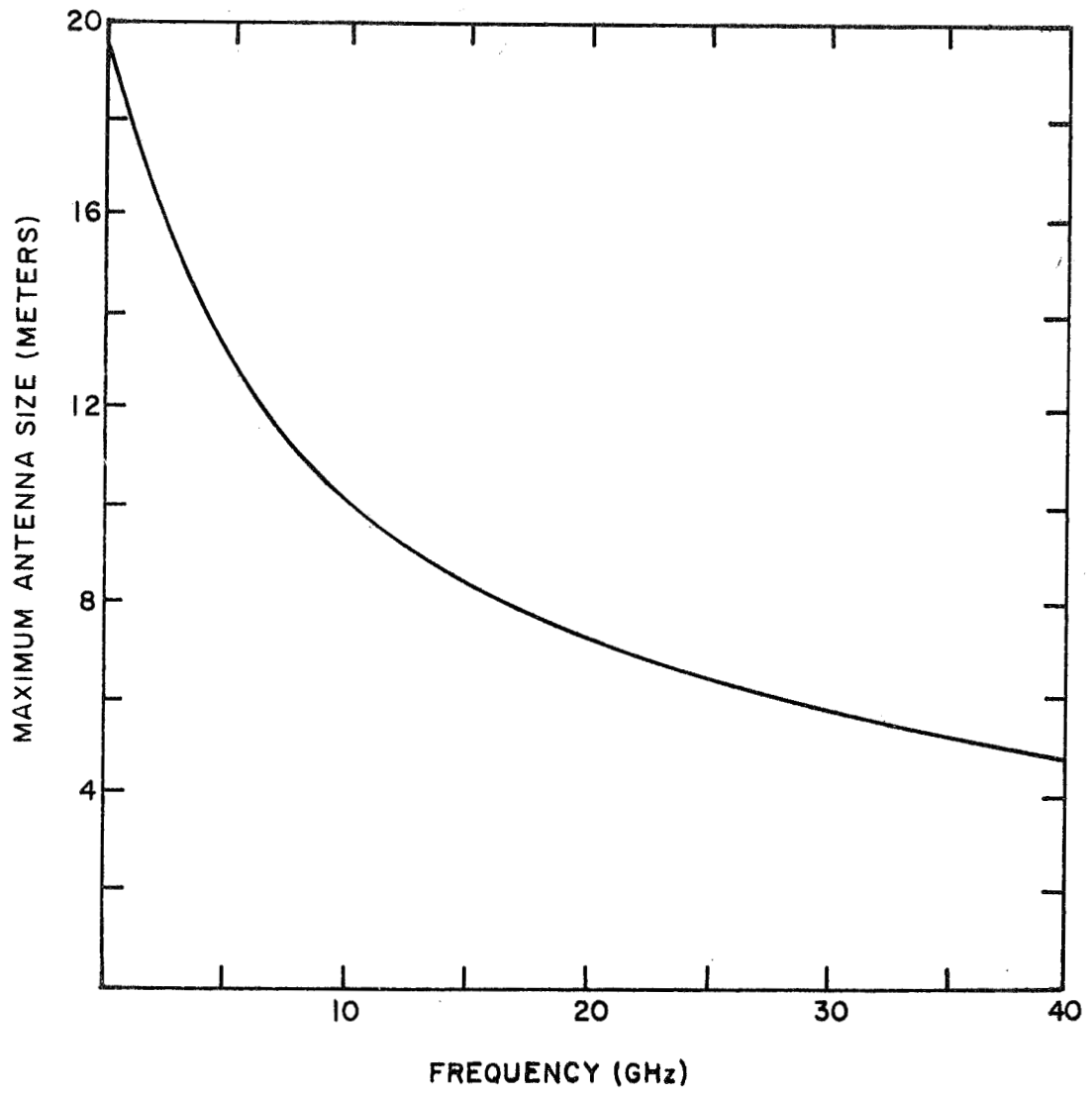


FIGURE 6-17. MAXIMUM ANTENNA SIZE

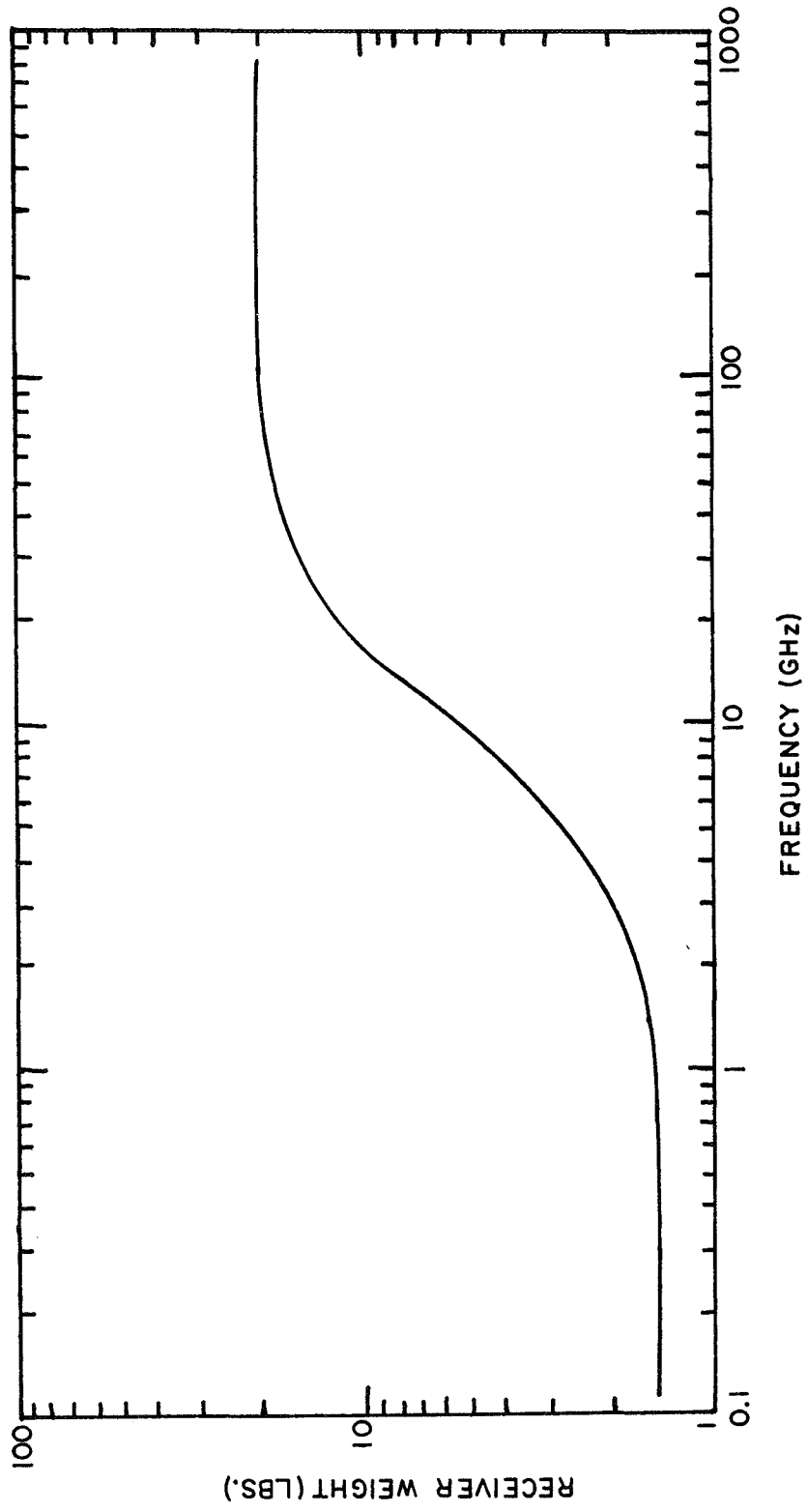


FIGURE 6-18. MICROWAVE RECEIVER WEIGHT

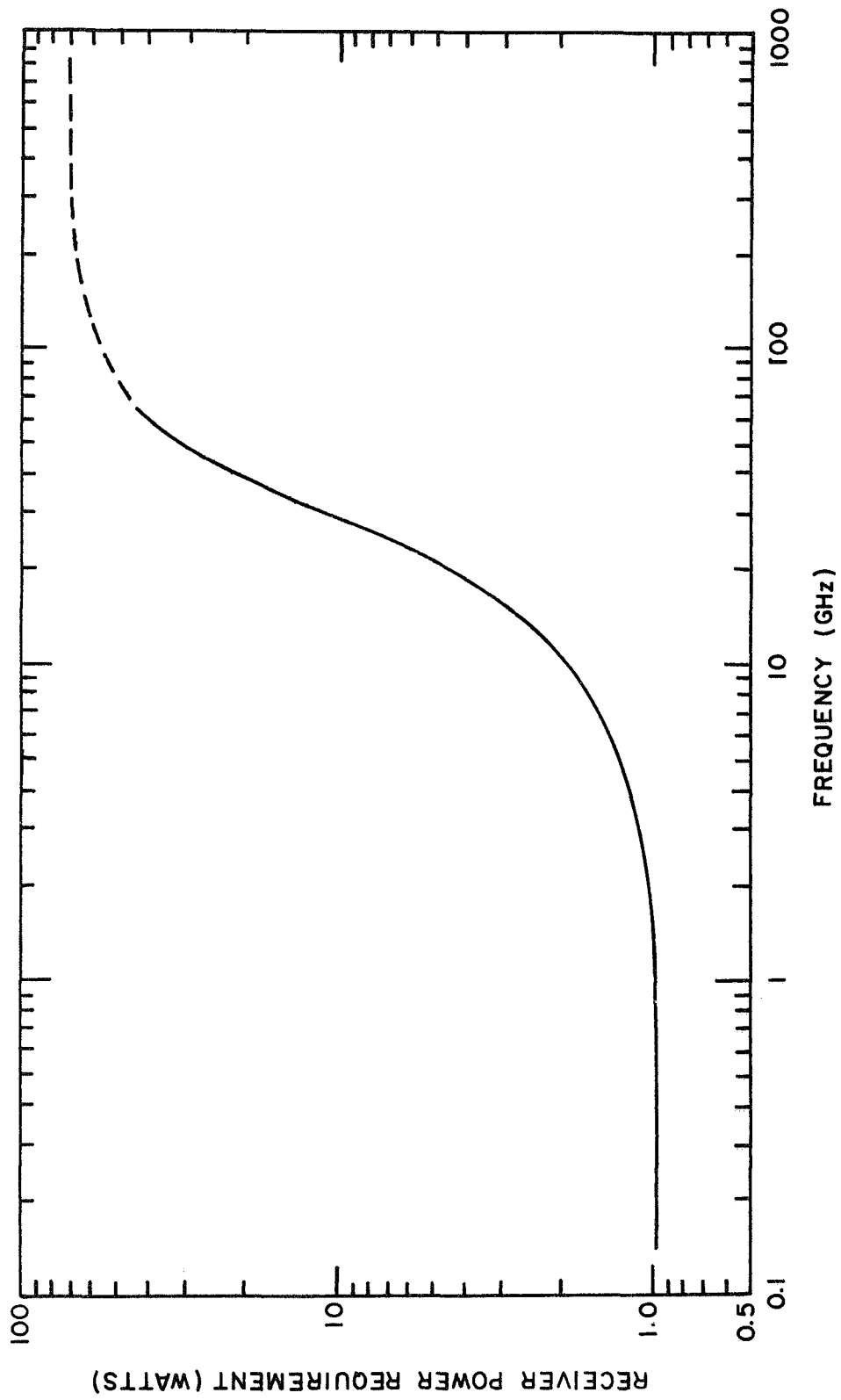


FIGURE 6-19. MICROWAVE RECEIVER POWER

Table 6-16 summarizes the experiment support requirements for this illustrative design example.

6.6 Noncoherent Radar Systems

Figure 6-20 presents a logic diagram for the design of a noncoherent radar imaging system, while Figure 6-21 summarizes the associated scaling laws. The design procedure and scaling laws are described in detail in Volume IV. To illustrate the estimation of experiment support requirements, consider a radar experiment for the study of structure of features on a regional scale at Venus. Table 6-16 summarizes the image specifications obtained from Table 4-1 and the appropriate worth curves. The selected orbit is more fully described by orbit data sheet #95 in Volume III. For a side-looking radar system, the minimum image ground size is interpreted as the minimum ground swath width.

Step 1: It is recommended that an operating wavelength of ten centimeters be initially selected for imaging experiments at Venus. At this wavelength, the atmospheric attenuation is a minor effect, while at longer wavelengths the antenna length becomes unwieldy. Similar comments apply to Jupiter and a 30 cm wavelength, however the estimates of atmospheric absorption at Jupiter are unreliable. In general, there is a tradeoff between system power requirement and antenna size which is sensitive to the operating wavelength. Short wavelengths tend to minimize the antenna size at the expense of the system average power requirement, while long wavelengths decrease the atmospheric absorption and power requirement but may require large antennas.

Step 2: Because the feasibility of a noncoherent radar system in a given situation is largely controlled by the antenna length, it is useful to obtain an early estimate of the length. In particular, a lower limit on the antenna azimuth aperture, which is approximately equal to the antenna length, is easily

Table 6-16

Sample Experiment Support Requirements for
A Passive Microwave Imaging System.

PLANET: Venus
 OBSERVABLE: Atmospheric Thermal Anomalies (regional)
 Family No. 1a
 ANTENNA TYPE: Electrical scan
 ORBIT: Data Sheet Number..... 85
 Periapse/Apoapse Alt. (km)..... 454/454
 Inclination (deg)..... 90
 Imaging Altitude Range (km)..... 454
 Imaging On-Time (min)..... 96
 IMAGE: Minimum Scan Length (km).....1500
 Max. Ground Resolution (km)..... 20
 Temperature Resolution (deg K)..... 5
 Positional Accuracy (km)..... 50
 SENSOR: Operating Frequency (GHz)..... 30
 Integration Time (sec).....0.0034
 Fly-Back Time (sec).....0.0002

SUPPORT REQUIREMENTS:	
Field of View (deg).....	0.57 x 112
Pointing Accuracy (deg).....	6.3
Max. Rotation Rate (deg/sec).....	81
Antenna Size (ft).....	6.7
Receiver Volume (cu in).....	250
Operating Power (watts).....	82
Data Rate (bits/sec).....	1700
Antenna Weight (lbs).....	87
Receiver Weight (lbs).....	15

COMMENTS:

The minimum integration time required to achieve a temperature resolution of 5 deg K is 5.2 m sec. Therefore, only a 6.2 deg K resolution is achieved. The entire planet may be mapped twice a year as desired. Orbit described on data sheet #86 affords only one coverage per year at poorer temperature resolution.

Table 6-17

Image Specifications and Orbit Parameters for
Structure of Features (Regional) at Venus

Wavelength Range	1-100 cm
Ground Horizontal Resolution	3 km
Ground Vertical Resolution	3 km
Minimum Image Ground Size	1000 km
Grey Scale	6 bits
Positional Accuracy	10 km
Maximum Acquisition Time	—
Orbit Periapse Altitude	454 km
Orbit Apoapse Altitude	454 km
Orbit Inclination	90 deg

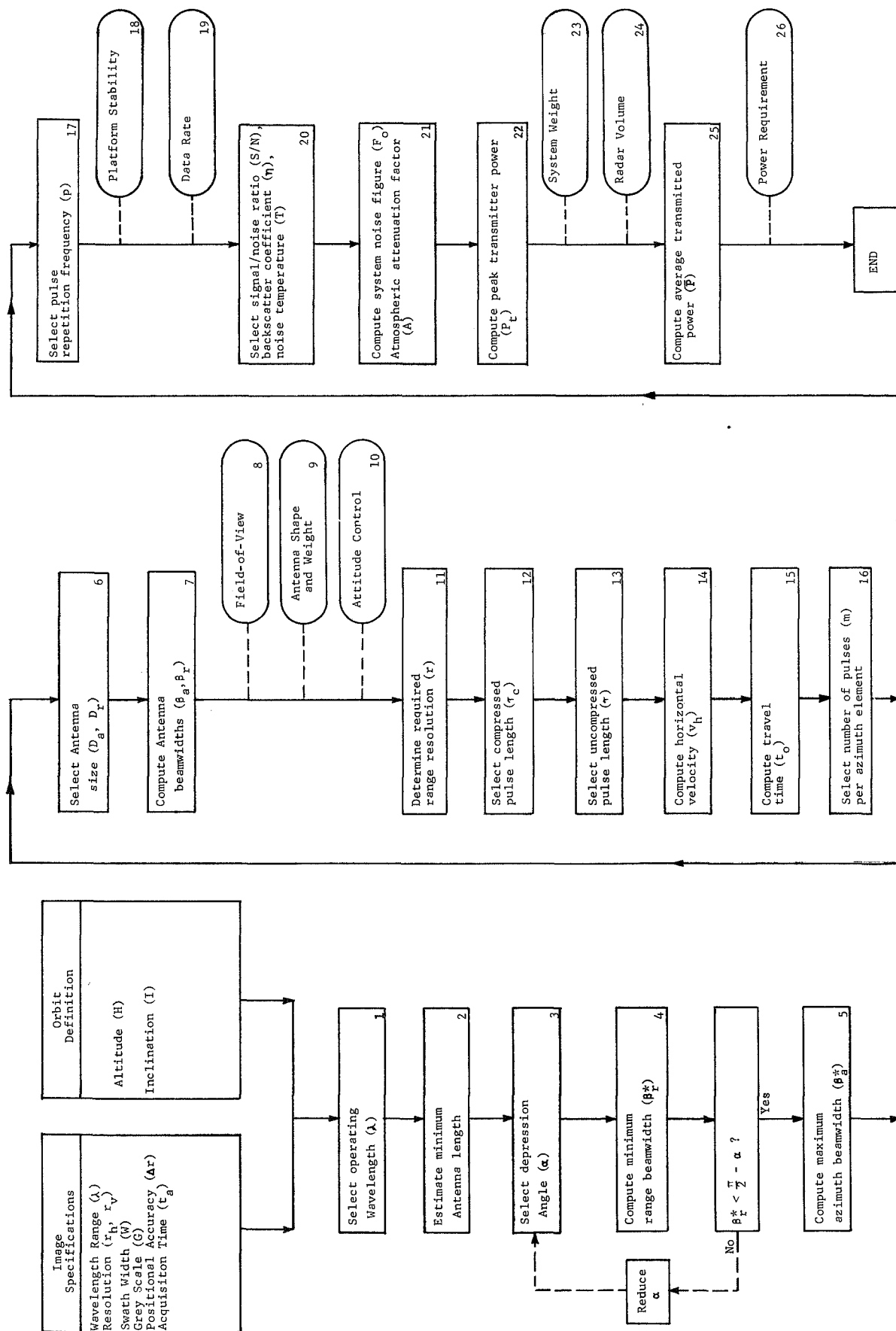


FIGURE 6-20. LOGIC DIAGRAM FOR NONCOHERENT RADAR SYSTEMS

NONCOHERENT (MKS units used throughout)																																													
<p>1. λ must be in range given by Image Specs. Suggested values are about 1 cm for Moon, Mars, Mercury, 10 cm for Venus, 30 cm for Jupiter.</p> <p>2. $D_a > \frac{1.46\lambda H}{h}$ SMA-limited to smaller of 1000A or 160 meters.</p> <p>3. Suggested α near 45°, but $\alpha > \cos^{-1} \frac{R}{R+H}$</p> <p>4. $\delta = \frac{W}{2R}$ $W = \frac{W}{\sin \delta}$ $V_p = \cos^{-1} \left(\frac{R+H}{R} \cos \alpha \right)$ $R_p = \frac{R \sin(\alpha - \beta)}{\cos \alpha}$ $\beta = \tan^{-1} \left[\frac{W \sin(\beta_2 + \delta)}{R_2 - W \cos(\beta_2 + \delta)} \right]$</p> <p>5. $\beta_a = \frac{0.87\lambda h}{R_2}$ $D_a \geq \frac{1.25\lambda}{\beta_a}$ Maximum D_a and Minimum D_a normally used.</p> <p>6. $\beta_r = \frac{1.25\lambda}{D_r}$ $\beta_a = \frac{1.25\lambda}{D_a} < 2 \cos^{-1} \frac{R}{R_1}$</p> <p>7. FOV is β_a by β_r</p> <p>8. Antenna Area is D_a by D_r. Antenna Height = $4.9D_a D_r$ kg.</p>	<p>9. $\Delta \theta = \frac{2\lambda c}{R_1 R_2}$ where $R_1 = W \sin(\beta_2 + \delta) / \sin \beta_a$ $R_2 = \frac{2\lambda c}{\Delta \theta}$</p> <p>10. If τ_v not given, $\tau_r = W \tau_v$. Shadowing: $\tau_r = \frac{\tau_v}{\tan \beta_1}$ where $\beta_1 = \beta_2 + \beta_a + 2\delta$ One-sided stereo: $\tau_r = \frac{0.4M\tau_v}{H}$ Two-sided stereo: $\tau_r = \frac{0.4M\tau_v}{H(1 + \beta)}$ ($\alpha = \beta + \beta_2$)</p> <p>11. $\frac{10\lambda}{c} \left[\frac{1}{5 \times 10^{-12}} \right] \leq \tau_c \leq \left[\frac{2r_c \cos \beta_1}{\lambda} \right]$ τ_c normally chosen as large as possible.</p> <p>12. $\tau_c \leq \tau \leq 200\tau_c$ τ normally chosen as large as possible.</p> <p>13. $a = R \frac{H}{R+H}$ $V_p = \frac{R}{R+H} \left[1 + \frac{2}{R+H} \left(\frac{R}{2} - \frac{1}{2} \right) \right]^{\frac{1}{2}}$ $V_h = \left(V_p^2 + 2V_p V_c \cos \beta \right)^{\frac{1}{2}}$</p> <table border="1"> <tr> <td>Planet</td> <td>$\frac{R}{R+H}$</td> <td>$\frac{H}{R+H}$</td> <td>V_p (m/sec)</td> <td>V_h (m/sec)</td> </tr> <tr> <td>Moon</td> <td>1.74 x 10⁶</td> <td>4.90 x 10¹²</td> <td>-</td> <td>-</td> </tr> <tr> <td>Mercury</td> <td>2.42 x 10⁶</td> <td>2.17 x 10¹³</td> <td>-</td> <td>-</td> </tr> <tr> <td>Venus</td> <td>6.10 x 10⁶</td> <td>3.23 x 10¹⁴</td> <td>-</td> <td>-</td> </tr> <tr> <td>Mars</td> <td>3.38 x 10⁶</td> <td>4.30 x 10¹³</td> <td>2.40 x 10²</td> <td>2.40 x 10²</td> </tr> <tr> <td>Jupiter</td> <td>7.14 x 10⁷</td> <td>1.27 x 10¹⁷</td> <td>1.27 x 10⁴</td> <td>1.27 x 10⁴</td> </tr> </table> <p>Note: V_h should be $> W$.</p> <p>14. $\tau_c = \frac{2R}{V_h} \sin^{-1} \left[\frac{R \sin(\beta/2)}{R+R_1 \sin(\alpha + \beta)} \right]$</p> <p>15. A large value of m decreases P_r but increases P_t, hence m normally chosen near 1.</p> <p>16. $P_r = \frac{m^2 P_t}{L_0}$ Power requirement = 100 + 3F watts</p>	Planet	$\frac{R}{R+H}$	$\frac{H}{R+H}$	V_p (m/sec)	V_h (m/sec)	Moon	1.74 x 10 ⁶	4.90 x 10 ¹²	-	-	Mercury	2.42 x 10 ⁶	2.17 x 10 ¹³	-	-	Venus	6.10 x 10 ⁶	3.23 x 10 ¹⁴	-	-	Mars	3.38 x 10 ⁶	4.30 x 10 ¹³	2.40 x 10 ²	2.40 x 10 ²	Jupiter	7.14 x 10 ⁷	1.27 x 10 ¹⁷	1.27 x 10 ⁴	1.27 x 10 ⁴	<p>17. $\frac{P_r}{P_t} \leq P \leq \frac{P_r}{L_0} (200\tau_c)^{-1}$ where: $\frac{R_2 - R_1}{R_2} \leq R - \alpha \tau$ then $\frac{Q}{R_2 - R_1}$ $\geq 200\tau$ none of above If $m=1$, then $P=1/L_0$.</p> <p>18. $\frac{m}{L_0} > \frac{1}{200\tau}$ or $\frac{c\beta}{2R_2 \tau \cos \beta}$ $\beta = \frac{c\beta}{m}$ or $\frac{c\beta}{2R_2 \tau \cos \beta}$</p> <p>19. $DR = \frac{M}{c^2 L_0} (\cos^2 \beta \cos^2 \beta_2)$</p> <p>20. S/N normally chosen as 10 η normally chosen as 5 x 10⁻⁴</p> <table border="1"> <tr> <td>Planet</td> <td>$\frac{M}{L_0}$</td> </tr> <tr> <td>Moon</td> <td>400</td> </tr> <tr> <td>Mercury</td> <td>600</td> </tr> <tr> <td>Venus</td> <td>700</td> </tr> <tr> <td>Mars</td> <td>300</td> </tr> <tr> <td>Jupiter</td> <td>200</td> </tr> </table> <p>21. $F_0 = \exp(3.80 - 0.344 \ln(1000))$ $A = \exp(a/\lambda^2 \sin \beta_2)$ $a = 6.5 \times 10^{-4}$ for Venus, .0266 for Jupiter, 0 for Moon, Mercury, Mars</p> <p>22. $P_t = \frac{10^{-30} (S/N)^2 R_2^2 \beta_a^2 \cos \beta_2}{\tau_c^2 \eta^2 \lambda^2}$ SMA limit is 4 x 10⁸ watts if λ in meters.</p> <p>23. Radar weight = 13.6 + 9.1 ln(0.1P_t) kg System weight = Radar weight + Antenna weight</p> <p>24. Radar volume = 0.0039 x Radar weight</p>	Planet	$\frac{M}{L_0}$	Moon	400	Mercury	600	Venus	700	Mars	300	Jupiter	200	<p>25. $P_r = \frac{m^2 P_t}{L_0}$</p> <p>26. Power requirement = 100 + 3F watts</p>
Planet	$\frac{R}{R+H}$	$\frac{H}{R+H}$	V_p (m/sec)	V_h (m/sec)																																									
Moon	1.74 x 10 ⁶	4.90 x 10 ¹²	-	-																																									
Mercury	2.42 x 10 ⁶	2.17 x 10 ¹³	-	-																																									
Venus	6.10 x 10 ⁶	3.23 x 10 ¹⁴	-	-																																									
Mars	3.38 x 10 ⁶	4.30 x 10 ¹³	2.40 x 10 ²	2.40 x 10 ²																																									
Jupiter	7.14 x 10 ⁷	1.27 x 10 ¹⁷	1.27 x 10 ⁴	1.27 x 10 ⁴																																									
Planet	$\frac{M}{L_0}$																																												
Moon	400																																												
Mercury	600																																												
Venus	700																																												
Mars	300																																												
Jupiter	200																																												

FIGURE 6-21. SCALING LAWS FOR NONCOHERENT RADAR SYSTEMS

calculated as shown. For the design example, the estimate yields a lower limit of about 22 meters for the antenna length. Current state-of-art limitations on the fabrication and alignment of long antennas permit antennas which are approximately one thousand times as long as the wavelength, in this case 100 meters for a 10 cm operating wavelength. However, an upper limit of 500 feet, or 160 meters, has rather arbitrarily been applied. If antennas in excess of either 1000 times the wavelength or 160 meters are required for a noncoherent system, the design should probably be abandoned and consideration given to a synthetic aperture radar system (see following section for design procedure and scaling laws).

Step 3: A lower limit on the antenna depression angle is given by the depression angle to the apparent planetary horizon. The geometry is shown in Figure 6-22. That is, the radar beam should be directed towards the planetary surface rather than above the horizon. For the example problem, the depression angle to the horizon is about 21.5 degrees, hence the antenna should be depressed more than 21.5 degrees. For a given beam size, the azimuth resolution (the resolution parallel to the subsatellite track) is enhanced by large depression angles, while the range resolution (perpendicular to the subsatellite track) is enhanced by small depression angles. Thus a depression angle of about 45 degrees is often a suitable compromise.

Step 4: To obtain a swath width of 1000 km, as measured along a great-circle arc, the half-angle δ subtended by the swath width at the center of Venus is 0.082 radians. The planetary chord length W' corresponding to a great-circle arc-length of 1000 km is then very nearly 1000 km. For most applications, the distinction between chord length and arc length may be ignored (if the swath width is less than ten percent of the planet diameter). Assuming a depression angle of 45 degrees, the grazing angle ψ_2 at the far edge of the swath width is

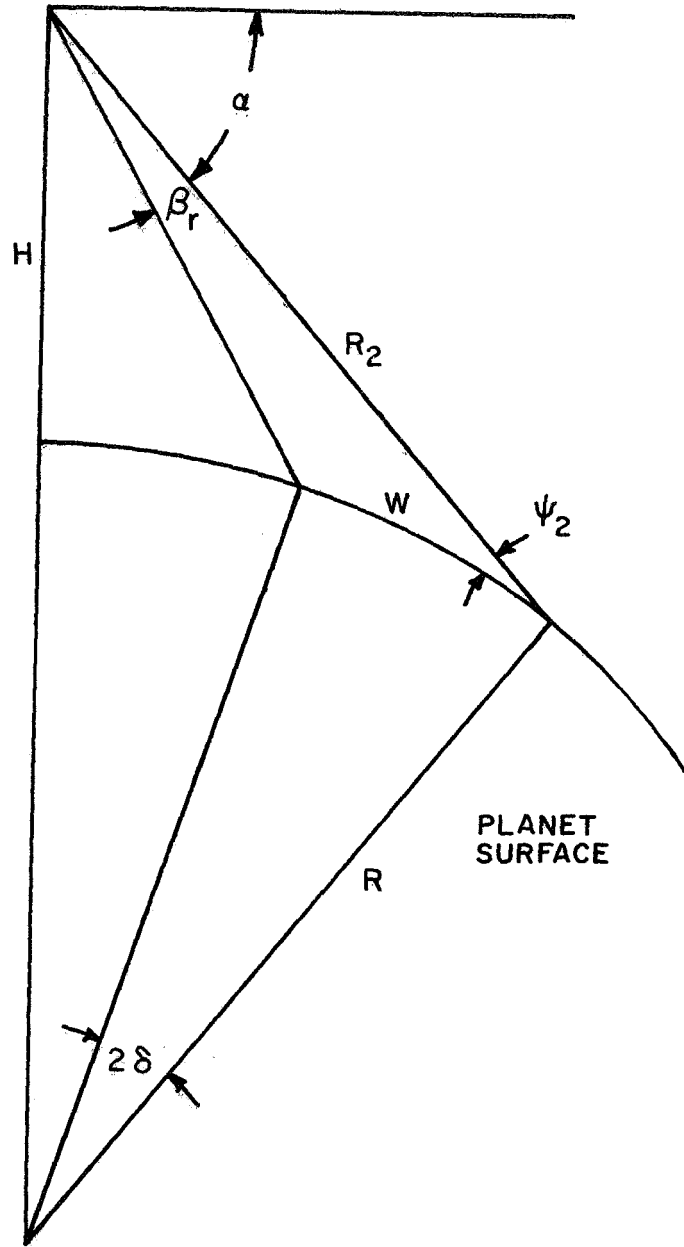


FIGURE 6-22. SIDE-LOOKING RADAR GEOMETRY

about 40.6 degrees or 0.708 radians. The slant range R_2 from the antenna to the far edge of the swath width is 670 km. Finally, the antenna range beamwidth required to intercept a great-circle arc-length of 1000 km at an antenna depression angle of 45 degrees is 92.8 degrees. Since the minimum azimuth beamwidth β_r^* is not less than $(90-\alpha)$ degrees, the swath width includes the subsatellite track. In such a situation, the ground range resolution approaches infinity in the vicinity of the subsatellite track. Thus the swath width must be moved off the subsatellite track by reducing the antenna depression angle. By reducing the depression angle to 25 degrees, the grazing angle at the far edge of the swath width becomes 13.2 degrees, the slant range to the far edge of the swath width 1380 km, and the minimum range beamwidth 35.4 degrees or 0.618 radians. The near edge of the swath is then about 30 degrees off the subsatellite track.

Step 5: For a ground horizontal resolution of 3 km at a slant range of 1380 km, the required antenna azimuth beamwidth is about 1.89 milliradians.

Step 6: The antenna range aperture corresponding to a range beamwidth of 0.618 radians is 0.20 meters, while the antenna azimuth aperture corresponding to an azimuth beamwidth of 1.89 milliradians is 66 meters (for a ten centimeter wavelength). That is, the antenna is about 0.20 meters wide and 66 meters long. The antenna length estimate used in Step 2 is based on a slant range equal to the orbit altitude, and is thus a lower limit to the antenna length. In cases, such as the design example, when the slant range is considerably longer than the orbit altitude, the estimate given by Step 2 will be poor. Since, in the design example, the actual slant range is nearly three times the altitude, the actual antenna length required is three times the earlier estimate.

For very small swath widths, very wide antennas are required. However, by imaging larger areas of ground than

demanded by the scientific requirements, the antenna range beamwidth may be increased, and hence the antenna width (and weight) decreased. Of course, if the beam size is increased, the transmitted power, and hence the system average power requirement, must also be increased. A similar tradeoff is possible with the antenna length. By increasing the antenna length, the transmitted power is focused on a small ground area, thus decreasing the power requirement and improving the system resolution. For imaging ground areas in excess of on the order of one hundred kilometers, the system support requirements are usually minimized by using an antenna width corresponding to the minimum acceptable swath width and an antenna length corresponding to that determined by the required ground resolution.

Step 7: If it is decided that the antenna width should be decreased or the antenna length should be increased, the beam size should be adjusted accordingly. In any event, the azimuth beamwidth should satisfy the inequality shown on the scaling law chart if the radar return from the vicinity of the sub-satellite point is not to interfere with the return from the swath width.

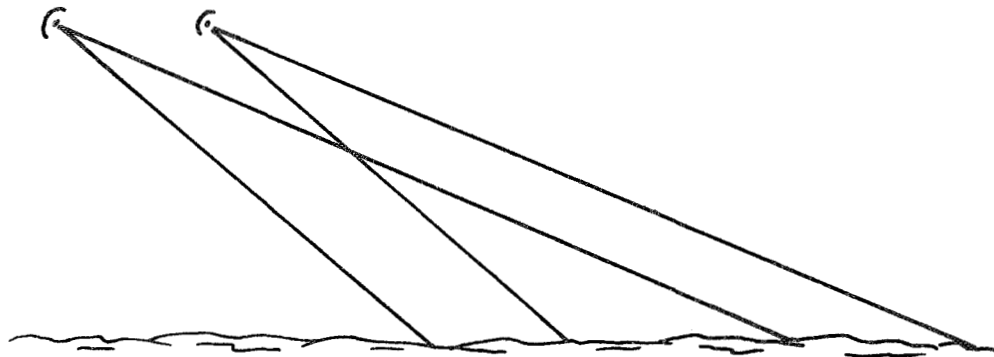
Step 8: The sensor system field-of-view is simply described by the antenna beamwidth. That is, in the design example, the field-of-view is 1.89 milliradians by 0.618 radians.

Step 9: The antenna area is approximately the azimuth aperture times the range aperture, while the weight estimate is based on one pound per square foot of antenna area. To continue with the example, the antenna area is about 13 square meters with a mass of 65 kilograms.

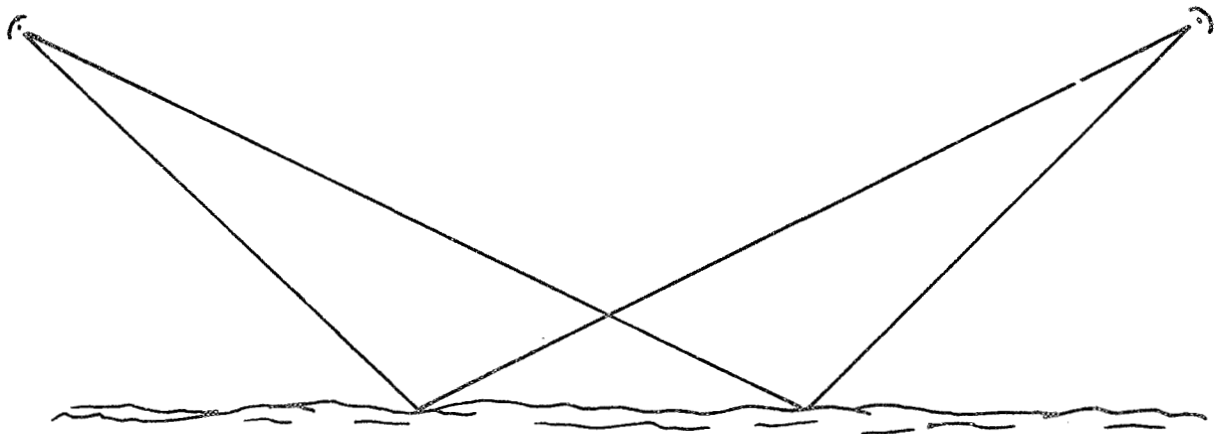
Step 10: The slant range to the near edge of the swath width is about 530 km. If the location of the image is to be known within an accuracy of 10 km, the implied antenna pointing accuracy is about ten milliradians.

Step 11: The required range resolution depends upon whether or not vertical height information is desired. If not, the range resolution may be taken as equal to the desired ground resolution. Vertical height differences can be deduced from measurements of shadow lengths or stereo parallax in radar imagery, just as with imagery obtained in the visible region of the spectrum. For shadowing, the grazing angle of the radar beam is analogous to the solar elevation angle. For stereo coverage, the stereo parallax may be obtained by keeping the antenna depression angle fixed and overlapping swath widths by proper selection of the orbit to provide sixty percent overlap from one swath width to the next, or by imaging essentially the same swath width on the ground from one side and then the other. These two modes, one-sided and two-sided, are illustrated in Figure 6-23. The two-sided mode requires a careful adjustment of antenna pointing with ground coverage and clearly involves a more complicated command and control sequence than the one-sided mode. This added complexity is not fully reflected in the support requirements estimated here. The orbit selected for the design example is based on sixty percent overlap from one 1000 km strip to the next, hence the range resolution should be computed using the one-sided stereo formula shown. That is, for detection of vertical height differences of 3 km, the range resolution should be 2.64 km. If a similar orbit were to be used to obtain two-sided stereo coverage or heights by radar shadowing, the required range resolutions would be 5.37 and 1.88 km, respectively. The range resolution should be equal to, or less than, the desired ground horizontal resolution, hence the range resolution provided for in the two-sided stereo mode should be 3 km.

Step 12: To achieve the desired range resolution throughout the swath width and to avoid excessive frequency shifts in the pulse return due to planet rotation, the compressed pulse length must be equal to, or less than, both upper limits shown on the



(A) ONE-SIDED STEREO COVERAGE



(B) TWO-SIDED STEREO COVERAGE

FIGURE 6-23. RADAR STEREO MODES

scaling law chart. Similarly, the current state-of-art limits the compressed pulse length to values equal to, or larger than, both lower limits. Thus in the design example, the compressed pulse length must lie between about three nanoseconds and 9.4 microseconds. The support requirements are usually least stringent if the compressed pulse length is selected to be as large as consistent with the upper limits shown. In other words, the design compressed pulse length should be 9.4 microseconds.

Step 13: The uncompressed, or transmitted, pulse length can be as large as 200 times the compressed pulse length. To put it the more logical way, the current state-of-art in pulse processing technology permits compression ratios of 200. That is, by pulse compression techniques, the range resolution obtained from the processed data is equivalent to a pulse length a factor of 200 shorter than the pulse length actually transmitted. Because the resolution depends directly upon the compressed length, it is convenient to determine the compressed length before determining the transmitted length. Since the peak transmitted power required to achieve a specific signal-to-noise ratio is inversely proportional to the pulse length, it is usually good practice to use as long a pulse length as possible. However, in some cases, a more desirable mode of pulse timing (Step 17) can be attained if the pulse length is decreased. In the illustrative example, the compression ratio may be taken as 200, and hence the transmitted pulse length is about 1.9 milliseconds.

Step 14: The orbit semi-major axis is 6554 km. For Venus, the effects of planet rotation are negligible, and hence the radar system apparent ground speed is 6.55 km/sec. As with any scanning system, the amount of time required to observe an area W by W km, is simply the amount of time required for the sub-satellite point to travel W km. In this case, the data from a 1000 x 1000 km area is collected in about 150 seconds. This

time should be less than any maximum image acquisition time given in the image specifications.

Step 15: If the antenna is considered fixed, and the observed scene is regarded as moving, the time required for a point target to move through the radar beam is the observation or travel time t_o . Since this time increases with slant range, the observation time is computed for the slant range to the near edge of the swath. In order for all targets to be observed, at least one pulse must be transmitted in each time interval equal to the travel time. Of course, more pulses may be transmitted, if desired. For the design example, the travel time is about 0.15 seconds.

Step 16: The number of pulses transmitted during the travel time, or the number of hits per target, may be selected by the system designer. The peak transmitted power decreases as the square root of the number of pulses m , and hence to keep the peak power within feasible limits it may be necessary to increase m . However, the average transmitted power increases with the square root of m , hence m should be kept at a minimum to decrease the system average power requirement. Thus, unless high peak powers are anticipated, m should be chosen initially as one. The value of m is assumed not to influence the data acquisition rate, since the data is integrated over the observation time.

Step 17: The pulse repetition frequency must provide for m pulses in the time t_o , hence a lower limit on the pulse rate is simply m/t_o . Thus for the example design with m equal one, the pulse repetition frequency is $1/t_o$ or 6.6 pulses per second. Pulse rates on the order of 10^5 per second are attainable with current transmitter technology. However, the pulse rate is also limited by timing constraints connected with pulse return ambiguity and interference between the transmitted and received pulse. The scaling law chart gives a prescription for estimating the maximum pulse rate. The details of the various pulse timing

modes are discussed in Volume IV. For the example design, $R_2 - R_1$ is about 850 km while $H - c\tau$ is negative so that $R_2 - R_1$ is not less than $H - c\tau$. Also $20 c\tau$ is about 11,000 km so that $R_2 - R_1$ is not greater than $20 c\tau$. Therefore the parameter Q is equal to R_2 (1380 km), and hence the maximum pulse repetition rate is about 90 pulses per second. That is, the design pulse repetition frequency must lie between 6.6 and 90 pulses per second. There is not much point in pulsing faster than necessary, or transmitting more pulses than are received and recorded. Thus, since m is one, p is chosen as 6.6 per second. If it is desired to increase m , it should be noted that m can be no greater than pt_0 . Since p is limited to 90 per second, m can be no greater than about 13. This provides a limit to how much the peak transmitted power can be reduced by increasing m .

Step 18: The maximum permissible antenna roll and yaw rates are estimated by assuming that antenna rotation be limited to less than one beamwidth during the time required to transmit and receive m pulses. If m is one and the parameter Q in Step 17 has been set equal to R_2 , the computation is simplified by noting the allowable rotation rate is simply the maximum pulse repetition frequency from Step 17 times the appropriate beamwidth. Since this is the case in the design example, the allowable roll rate is 90 per second times 0.618 radians or about 56 radians per second (3200 degrees per second), while the allowable yaw rate is 90 per second times 1.89 milliradians or about 0.17 radians per second (9.7 degrees per second).

Step 19: The data acquisition rate represents the amount of data collected during the travel time t_0 . For the design example, the data rate is 2.1×10^4 bits per second.

Step 20: It is suggested that the radar system be designed for a signal-to-noise ratio of ten, a target backscatter coefficient of 0.0005, and an input noise temperature equivalent to black body thermal emission from a planetary surface at the temperatures given in the scaling law chart.

Step 21: For the design example, the system noise figure is about 20. It is essential that in the formula shown, the wavelength be expressed in meters. A noise figure of 20 corresponds to about 13 dB. This includes about 7 dB loss in the receiver and about 6 dB loss from system degradation, transmission line losses, etc. The receiver loss is assumed to vary with operating frequency, while the other losses are independent of frequency, the result being the formula shown. Thus from the standpoint of noise, long wavelength systems are more efficient than short wavelength systems. For ten centimeter wavelength at Venus, with ψ_2 equal to 13.2 degrees, the atmospheric attenuation factor is 1.33. That is, there is a 33 percent signal loss due to atmospheric absorption, hence the transmitted power must be increased by a factor of 1.33 over the power required if there were no atmosphere. Again it is essential that the wavelength be expressed in meters in the formula given. There is no significant atmospheric or ionospheric absorption at the Moon, Mercury, and Mars.

Step 22: The peak power in the transmitted radar pulse is estimated using the rather messy expression in the scaling law chart. The numerical coefficient of 10^{-30} has units of (seconds)² / (meter-deg K), hence to avoid errors in computation, lengths should be expressed in meters (both the range and the wavelength). For the design example, the power in each transmitted pulse is about four kilowatts. This is well below the capability of transmitter technology, since current technology is on the verge of 40 megawatts at ten centimeter wavelength. If the design transmitted power exceeds the state-of-art limit, the number of hits per target can be increased as pointed out earlier. This will, however, also increase the system average power requirement.

Step 23: The radar mass (excluding the antenna) is estimated to be about 47 kilograms, or 100 pounds, hence the total system weight (including the antenna) is about 240 pounds.

Step 24: An estimate of the radar system volume (excluding the antenna) is based on a packing density of 16 pounds per cubic foot. In this case, the radar volume is a little more than six cubic feet.

Step 25: The average transmitted power is quickly estimated from the power in each pulse, since there are m pulses of length τ during the time t_0 . For the design example, the average transmitted power is 49 watts.

Step 26: The system average power requirement is based on a transmitter power conversion efficiency of 33 percent and a receiver requirement of 100 watts. Thus the input power is estimated to be about 250 watts.

Table 6-18, taken directly from Volume V, summarizes the experiment support requirement for the illustrative design example.

6.7 SYNTHETIC APERTURE RADAR SYSTEMS

Figure 6-24 is a logic diagram which presents a suggested procedure for the design of synthetic aperture side-looking radar systems. Figure 6-25 is a scaling law chart, designed for use with the logic diagram, which summarizes the design equations for synthetic aperture systems and the scaling laws for estimation of experiment support requirements. The synthetic aperture technique involves transmitting a number of pulses and processing the pulse return data in such a manner that the data appears to represent a single pulse return from a long antenna. That is, if m pulses are transmitted and processed, and the antenna moves the distance d between pulse transmissions, the data can be processed to appear as if a non-coherent radar antenna of length md had been used. Thus, in many respects, the scaling laws for a synthetic aperture system are similar to those for a noncoherent system except that m is a design variable associated with the azimuth resolution rather than the antenna length.

Table 6-18

Sample Experiment Support Requirements for
Noncoherent Radar Imaging Systems

PLANET: Venus

OBSERVABLE: Structure of Features (regional)

Family No. 6a

RADAR TYPE: Noncoherent (one-sided stereo)

ORBIT:	Data Sheet Number.....	95
	Periapse/Apoapse Alt. (km).....	454/454
	Inclination (deg).....	90
	Imaging Altitude Range (km).....	454
	Imaging On-Time (min).....	97
IMAGE:	Minimum Swath Width (km).....	1000
	Max. Ground Resolution (km).....	3 (2.6 range)
	Positional Accuracy (km).....	10
RADAR:	Operating Wavelength (cm).....	10
	Depression Angle (deg).....	25
	Compressed Pulse Width (μsec).....	9.4
	Pulse Repetition Freq. (/sec).....	6.6
	No. of Integrated Pulses.....	1
	Beamwidth Travel Time (sec).....	0.15

SUPPORT REQUIREMENTS:

Field of View (deg).....	0.12/35
Antenna Shape (ft).....	220/0.66
Pointing Accuracy (deg).....	0.50
Max. Roll/Yaw Rate (deg/sec).....	3200/110
Operating Power (watts).....	250
Data Rate (bits/sec).....	21,000
Radar Volume (cu. ft.).....	6.5
Antenna Weight (lbs).....	140
Radar Weight (lbs).....	100

COMMENTS:

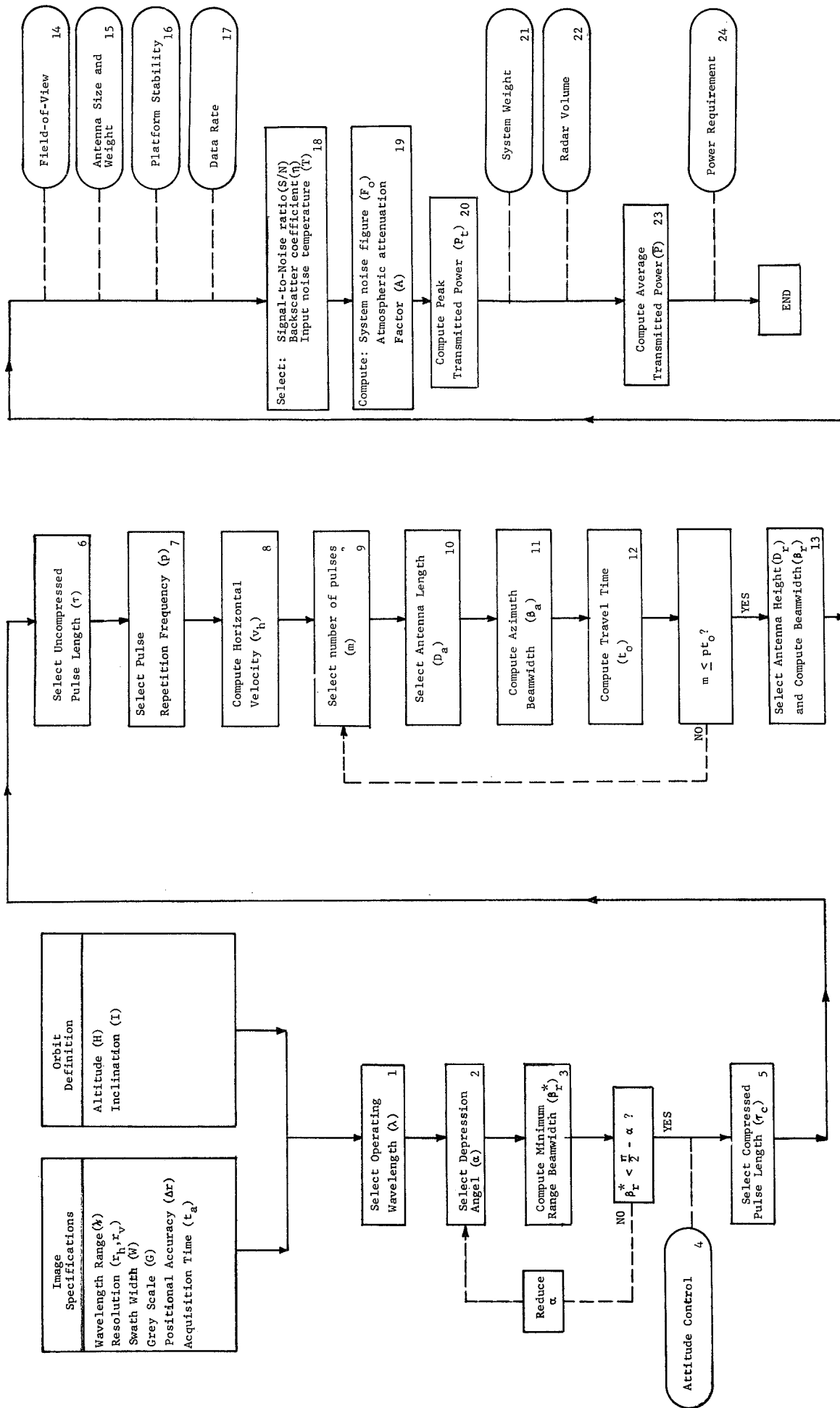


FIGURE 6-24. LOGIC DIAGRAM FOR SYNTHETIC APERTURE RADAR SYSTEMS

<p>1</p> <p>λ must be in range given by Image Specs. Suggested values are about 1 cm for Moon, Mars, Mercury, 10 cm for Venus, 30 cm for Jupiter.</p>	<p>2</p> <p>Suggested α near 45°, but $\alpha > \cos^{-1} \frac{R}{R_H}$</p> <p>$\delta = \frac{V}{2R}$</p> <p>$W' = \frac{V}{R} \sin \delta$</p> <p>$V_2 = \cos^{-1} \frac{R_H \cos \alpha}{R}$</p> <p>$V_2 = \frac{R \sin(\alpha - V_2)}{\cos \alpha}$</p> <p>$\beta_x^* = \tan^{-1} \left[\frac{W' \sin(V_2 + \delta)}{V_2 - W' \cos(V_2 + \delta)} \right]$</p>	<p>3</p> <p>$\Delta \theta = \frac{2\Delta E}{V_1 V_2}$</p> <p>where $R_1 = W' \sin(V_2 + \delta) / \sin \beta_x^*$</p>	<p>4</p> <p>If V_2 not given, $V_2 = W_2$.</p> <p>Shadowing: $V_2 = \frac{V_1 \tan V_1}{0.4W_2}$</p> <p>One-sided stereo: $V_2 = \frac{V_1}{H} (1 + \frac{R}{H}) (\alpha - \delta - V_2)$</p> <p>Two-sided stereo: $V_2 = V_1 (1 + \frac{R}{H}) (\alpha - \delta - V_2)$</p> <p>$\frac{10\lambda}{5 \times 10^{-12}} \leq \tau_c \leq \frac{2\tau_c \cos V_1}{20V_2}$</p> <p>where $V_1 = V_2 + \beta_x^* + 2\delta$</p> <p>$\tau_c$ normally chosen as large as possible.</p>	<p>5</p> <p>$\beta_x \leq \tau \leq 200 \tau_c$</p> <p>$\tau$ normally chosen as large as possible.</p>	<p>6</p> <p>where: $R_2 = R_1$ then $\frac{Q}{R_2 R_1}$</p> <p>$\leq H - c\tau$ $R_2 = R_1$</p> <p>$\geq 20c\tau$ $R_2 = H$</p> <p>none of above R_2</p> <p>P normally chosen as large as possible</p>	<p>7</p> <p>$a = R_1 \frac{R_1}{R_H} \left[\mu \left(\frac{2}{R_H R_1} - \frac{1}{R_1} \right) \right]^{\frac{1}{2}}$</p> <p>$V_0 = \frac{R_1}{R_H} \left[\mu \left(\frac{2}{R_H R_1} - \frac{1}{R_1} \right) \right]^{\frac{1}{2}}$</p> <p>$V_H = (V_0^2 + 2V_0 V_x \cos \lambda)^{\frac{1}{2}}$</p> <p>Note: V_H should be $> V_0$.</p> <table border="1"> <tr> <th>Planet</th> <th>$R_1 (m)$</th> <th>$\mu (m^2/sec^2)$</th> <th>$V_x (m/sec)$</th> </tr> <tr> <td>Moon</td> <td>1.74×10^6</td> <td>4.90×10^{12}</td> <td>-</td> </tr> <tr> <td>Mercury</td> <td>2.42×10^6</td> <td>2.17×10^{13}</td> <td>-</td> </tr> <tr> <td>Venus</td> <td>6.10×10^6</td> <td>3.25×10^{14}</td> <td>-</td> </tr> <tr> <td>Mars</td> <td>3.38×10^6</td> <td>4.30×10^{13}</td> <td>2.40×10^2</td> </tr> <tr> <td>Jupiter</td> <td>7.14×10^7</td> <td>1.27×10^{17}</td> <td>1.27×10^4</td> </tr> </table>	Planet	$R_1 (m)$	$\mu (m^2/sec^2)$	$V_x (m/sec)$	Moon	1.74×10^6	4.90×10^{12}	-	Mercury	2.42×10^6	2.17×10^{13}	-	Venus	6.10×10^6	3.25×10^{14}	-	Mars	3.38×10^6	4.30×10^{13}	2.40×10^2	Jupiter	7.14×10^7	1.27×10^{17}	1.27×10^4	<p>8</p> <p>$F_0 = \exp(1.30 - 0.344 \ln(100\lambda))$</p> <p>$A = \exp(a/\lambda^2 \sin V_2)$</p> <p>$a = 6.5 \times 10^{-4}$ for Venus, 0.066 for Jupiter, zero for Moon, Mercury, Mars</p>	<p>9</p> <p>$m \geq \frac{10V_2}{2R_1 V_H}$</p> <p>but $m \leq \frac{P}{V_H} (\beta_x^*)^{\frac{1}{2}}$ for unfocused systems</p>	<p>10</p> <p>$\frac{4V_H}{P} \leq D_a \leq \frac{1.25P\lambda R}{mV_H}$</p> <p>$2.5\lambda \cos^{-1} (R/R_1)$</p>	<p>11</p> <p>$\beta_a = \frac{1.25\lambda}{D_a}$</p>	<p>12</p> <p>$t_0 = \frac{2R}{V_H} \sin^{-1} \left[\frac{R_1 \sin(\beta_a/2)}{H + R_1 \sin(\alpha + \beta_a/2)} \right]$</p>	<p>13</p> <p>FOV is β_a by β_x</p> <p>Antenna Weight = $4.9 D_a^2 \lambda^2 \text{ kg}$.</p> <p>Antenna Area is D_a by D_x.</p>	<p>14</p> <p>$\beta = \frac{P\lambda}{m}$ $\beta = \frac{P\lambda}{m}$</p>	<p>15</p> <p>DR = $\frac{m\lambda G}{c^2 \epsilon_0} (\cos^2 V_1 + \cos^2 V_2)$</p>	<p>16</p> <p>S/N normally chosen as 10</p> <p>η normally chosen as 5×10^{-4}</p> <table border="1"> <tr> <th>Planet</th> <th>400</th> </tr> <tr> <th>Mercury</th> <th>700</th> </tr> <tr> <th>Mars</th> <th>300</th> </tr> <tr> <th>Jupiter</th> <th>200</th> </tr> </table>	Planet	400	Mercury	700	Mars	300	Jupiter	200	<p>17</p> <p>DR = $\frac{m\lambda G}{c^2 \epsilon_0} (\cos^2 V_1 + \cos^2 V_2)$</p>	<p>18</p> <p>$F_0 = \exp(1.30 - 0.344 \ln(100\lambda))$</p> <p>$A = \exp(a/\lambda^2 \sin V_2)$</p> <p>$a = 6.5 \times 10^{-4}$ for Venus, 0.066 for Jupiter, zero for Moon, Mercury, Mars</p>	<p>19</p> <p>$F_0 = \exp(1.30 - 0.344 \ln(100\lambda))$</p> <p>$A = \exp(a/\lambda^2 \sin V_2)$</p> <p>$a = 6.5 \times 10^{-4}$ for Venus, 0.066 for Jupiter, zero for Moon, Mercury, Mars</p>	<p>20</p> <p>$F_0 = \exp(1.30 - 0.344 \ln(100\lambda))$</p> <p>$A = \exp(a/\lambda^2 \sin V_2)$</p> <p>$a = 6.5 \times 10^{-4}$ for Venus, 0.066 for Jupiter, zero for Moon, Mercury, Mars</p>	<p>21</p> <p>Radar weight = $13.649 \ln(0.1P/\lambda)$ kg</p> <p>System weight = Radar weight + Antenna weight</p>	<p>22</p> <p>Radar volume = $0.0039 \times$ Radar weight</p>	<p>23</p> <p>$F = \frac{m\lambda}{\tau_c}$</p>	<p>24</p> <p>Power requirement = $100 + 3P$ watts</p>
Planet	$R_1 (m)$	$\mu (m^2/sec^2)$	$V_x (m/sec)$																																																				
Moon	1.74×10^6	4.90×10^{12}	-																																																				
Mercury	2.42×10^6	2.17×10^{13}	-																																																				
Venus	6.10×10^6	3.25×10^{14}	-																																																				
Mars	3.38×10^6	4.30×10^{13}	2.40×10^2																																																				
Jupiter	7.14×10^7	1.27×10^{17}	1.27×10^4																																																				
Planet	400																																																						
Mercury	700																																																						
Mars	300																																																						
Jupiter	200																																																						

FIGURE 6-25. SCALING LAWS FOR SYNTHETIC APERTURE RADAR SYSTEMS

To illustrate the design procedure, consider the image specifications and orbital parameters shown in Table 6-18. These values are appropriate for imagery of structure of features on a local scale at Venus, and have been obtained by using Table 4-1 and the appropriate worth curves. The experiment is similar to that used in the preceding section, except that local scale rather than regional scale imagery is desired. In particular, the minimum image size is 100 km, rather than 1000 km, and the resolution required, both horizontal and vertical, is 0.2 km, rather than 3 km. The selected orbit is more fully described by orbit data sheet #113 in Volume III, and is identical to the orbit selection for regional scale structure of features imagery.

Step 1: As with the previous example, an operating wavelength of ten cm is selected. The tradeoff between power requirement and antenna weight is somewhat different than for noncoherent systems. For synthetic aperture systems, the power requirement decreases with the cube of the wavelength while the antenna weight usually increases proportional to the wavelength. In the case of noncoherent systems, the power requirement was less sensitive, and the antenna weight more sensitive, to the wavelength.

Step 2: The antenna depression angle to the horizon is about 21.5 degrees, hence the depression angle selected should be greater than 21.5 degrees. A depression angle of 45 degrees may be tentatively selected.

Step 3: The half-angle δ subtended at the center of Venus by a 100 km swath width is 8.2 milliradians, and hence the chord length W' is essentially 100 km. The grazing angle ψ_2 at the far edge of the swath width is about 40.6 degrees, or 0.708 radians, while the range R_2 to the far edge of the swath width is 670 km. The antenna range beamwidth required to illuminate a 100 km swath width is then about 0.11 radians, or 6.3 degrees. This value is clearly less than ninety degrees minus the de-

Table 6-19

Image Specifications and Orbital Parameters
for Local Scale Structure of Features Imagery
(Venus)

Wavelength Range	1-100 cm
Ground Horizontal Resolution	0.2 km
Ground Vertical Resolution	0.2 km
Minimum Image Ground Size	100 km
Grey Scale	6 bits
Positional Accuracy	2 km
Maximum Acquisition Time	-
Orbit Periapse Altitude	454 km
Orbit Apoapse Altitude	454 km
Orbit Inclination	90 deg

pression angle, hence no iteration is required to ensure that the swath width fits between the subsatellite point and the apparent horizon.

Step 4: The slant range to the near edge of the swath width is 596 km. Thus the antenna pointing accuracy corresponding to 2 km on the ground is about 3.2 milliradians, or 0.2 degrees.

Step 5: The order of steps in the design procedure now departs radically from that appropriate to noncoherent systems. For synthetic aperture systems, the minimum antenna length is usually controlled by the pulse repetition frequency. Since the maximum pulse repetition frequency depends upon the transmitted pulse length, the pulse length must be determined before the antenna can be sized. The orbit selected provides sixty percent side overlap, hence operating in the one-sided stereo mode requires a ground range resolution of 17.6 meters. To achieve this range resolution, a compressed pulse length of about 79 nanoseconds is required. Since this value is larger than $10 \lambda/c$, as required, the system design may proceed using a 79 nanosecond compressed pulse length.

Step 6: Using a compression ratio of 200, the transmitted pulse length is about 16 microseconds.

Step 7: Since R_2 minus R_1 (74 km) is less than H minus $c\tau$ (449 km), the parameter Q has the value 74 km, and the maximum permissible pulse repetition frequency is about 1960 pulses per second. Since both the minimum antenna length and transmitted power per pulse are inversely proportional to the pulse repetition frequency, the design pulse rate is usually the maximum, in this case 1960 per second.

Step 8: As in the previous example, the ground speed of the antenna is 6.55 km/sec.

Step 9: The number of pulse returns which must be processed to provide an azimuth resolution of 0.2 km is 50 for a slant

range of 670 km. At closer ranges in the swath, a lesser number of pulse returns may be processed. The system need not be a focused system, that is, phase differences in the pulse returns need not be accounted for in the processing, since as many as 77 pulse returns per azimuth element can be accurately handled by an unfocused system, and this value is larger than the 50 pulses required. Thus m may be selected as 50.

Step 10: The antenna azimuth aperture, or length, must lie in the range 13.4 to 502 meters. However, the same state-of-art constraints as for noncoherent systems apply here. That is, the antenna cannot be manufactured and kept in alignment for lengths larger than the smaller of one thousand times the wavelength or 160 meters. Thus, in this case, the minimum antenna length is 13.4 meters while the maximum length is state-of-art limited to 100 meters. A 13.4 meter antenna may be tentatively selected.

Step 11: The antenna azimuth beamwidth corresponding to an aperture of 13.4 meters is 9.3 milliradians or about 0.5 degrees.

Step 12: The time required for a point target to travel through the antenna azimuth beamwidth is about 0.85 seconds for targets at the near edge of the swath. Since the pulse repetition frequency is 1960 pulses per second, nearly 1700 pulses can be transmitted during this time. If resolution requires more than can be transmitted during the travel time, some adjustment must be made in the system design parameters. If the necessary adjustment cannot be tolerated by the other design constraints, then no adequate system can be designed. A careful reader will note that the minimum number of pulses has been fixed by the azimuth resolution required at the far edge of the swath, while the travel time has been computed for targets at the near edge of the swath. This inconsistency is not usually troublesome since in those cases where synthetic aperture systems are appropriate, the swath widths tend to be small.

Step 13: Since the minimum antenna range beamwidth has been determined in Step #3 as 0.11 radians, the maximum antenna range aperture, or width, is 1.04 meters. If it appears that use of the maximum value for the range aperture will result in an excessively massive antenna, the range aperture can be reduced at the expense of system operating power. In this case, it appears that the antenna is not very large, hence a range aperture of 1.04 meters is selected, with a corresponding range beamwidth of 0.11 radians.

Step 14: The antenna field-of-view is 9.3 milliradians by 0.11 radians, or 0.5 by 6.3 degrees.

Step 15: The antenna area is 13.4 by 1.04 meters, and hence the antenna mass is about 68 kilograms, or 150 pounds.

Step 16: A time interval of about 25 milliseconds is required to transmit and receive 50 pulses. Assuming that the antenna should not move more than one beamwidth during this time implies that the antenna maximum allowable roll rate is about 20 deg/sec, while the maximum allowable yaw rate is about 250 deg/sec.

Step 17: The data acquisition rate is about 2.1×10^6 bits/sec assuming that 50 pulse returns must be acquired from each resolution element during 0.85 seconds, and that six binary bits are required to describe each resolution element.

Step 18: This step is the same as Step #20 in the previous example. That is, the required signal-to-noise ratio is taken as ten, the target backscatter coefficient as 5×10^{-4} , and the input noise temperature as 700 deg K.

Step 19: This step is also the same as Step #21 in the previous example, since the operating wavelength is the same. That is the system noise figure is 20 and the atmospheric attenuation factor is 1.33.

Step 20: The power transmitted by the antenna is estimated to be 0.56 megawatts per pulse. As with the previous example, this

value is well within the state-of-art limit of 40 megawatts. If the state-of-art constraint is exceeded, the system designer may, among other things, increase the operating wavelength (which will not only decrease the transmitted power but will increase the state-of-art limit as well as the antenna size) or decrease the antenna azimuth aperture by making the antenna longer.

Step 21: For the example design, the radar weight (excluding the antenna) is about 92 kilograms, or about 200 pounds. Thus the entire system, including the antenna, weighs about 350 pounds.

Step 22: The radar system volume (excluding the antenna) is estimated to be 0.36 cubic meters, or about 12 cubic feet.

Step 23: The average transmitted power is 525 watts. This estimate includes the dead time during which the antenna is not pulsing at the design rate. That is, the antenna transmits 50 pulses, each of 0.56 megawatts, at a pulse repetition rate of 1960 pulses per second. The antenna thus transmits all the required pulses in about 25 milliseconds. The average power transmitted during the transmitting cycle is then about 18 kilowatts. However, the transmitter is now turned off and waits 825 milliseconds until new targets come into view, and the cycle is repeated.

Step 24: The system average power requirement is about 1700 watts.

Table 6-20 summarizes the experiment support requirements for this illustrative design example. As pointed out earlier, the specific values generated by the scaling laws should be regarded as representative of a specific experiment. As should be clear by this time, sufficient design flexibility exists that one type of support requirement can usually be made less (or more) demanding at the expense (or gain) of some other type of support requirement. This is particularly the case with radar imaging systems. The following section summarizes the typical

Table 6-20

Sample Experiment Support Requirements
for Synthetic Aperture Radar Imaging Systems

PLANET: Venus

OBSERVABLE: Structure of Features (local)

FAMILY No. 18

RADAR TYPE: Synthetic Aperture (one-sided stereo)

ORBIT: Data Sheet Number..... 113
 Periapse/Apoapse Alt. (km).....454/454
 Inclination (deg)..... 90
 Imaging Altitude Range (km)..... 454
 Imaging On-Time (min)..... 97

IMAGE: Minimum Swath Width (km)..... 100
 Max. Ground Resolution (km).....0.2 (0.02 range)
 Positional Accuracy (km)..... 2

RADAR: Operating Wavelength (cm)..... 10
 Depression Angle (deg)..... 45
 Compressed Pulse Width (μ sec)....0.079
 Pulse Repetition Freq. (/sec).... 2000
 No. of Integrated Pulses..... 50
 Beamwidth Travel Time (sec)..... 0.85

SUPPORT REQUIREMENTS:	
Field of View (deg).....	0.5/6.3
Antenna Shape (ft).....	44x3.4
Pointing Accuracy (deg).....	0.2
Max. Roll/Yaw Rate (deg/sec).....	20/250
Operating Power (watts).....	1700
Data Rate (bits/sec).....	2.1×10^6
Radar Volume (cu.ft.).....	12
Antenna Weight (lbs).....	150
Radar Weight (lbs).....	200

COMMENTS:

experiment support requirements obtained by applying the imaging system scaling laws to specific sets of image specifications and specific orbit selections.

7. EXPERIMENT SUPPORT REQUIREMENTS

This section summarizes, for each spectral region, typical imaging experiment support requirements for planetary exploration. These support requirements are based upon a detailed analysis of the goals of space exploration and the scientific objectives which satisfy these goals. An imaging experiment has been defined for each observable property for which orbital imagery is useful. Each measurement definition has led to a conceptual experiment. An experiment is regarded as a specific sensor system operating in a specific mode from a specific orbit. The experiment support requirements are estimated by use of the sensor system scaling laws, together with an orbit description and a set of image specifications appropriate to the experiment. The sensor system scaling laws have been summarized in Section 6, the orbit selection process described in Section 5, and the image specifications given in Section 4.

In order to estimate typical support requirements, all variables which influence the requirements must be specified. For example, in the case of a television camera experiment to determine surface topography, a specific image ground size must be chosen on the basis of the science requirements. An acceptable range of image specification values are provided for each experiment by the worth curves of Section 4. In determining the support requirements, the value selected has been that value which would appear to result in the least demanding support requirements without degrading the scientific value of the experiment. In general, there is not a unique set of support requirements which can be associated with a specific planetary observable, orbit, and type of sensor system. That is, the sensor system designer has some freedom in designing a sensor system to procure specified imagery from a specified orbit, although the image specifications, the orbit parameters, and the current sensor system state-of-art tend to constrain the amount of design flexibility. For example, the television

system designer may elect to use a relatively large optical system to permit a short scene exposure time. This may result in a heavier optical system than necessary, but may ease the platform stability requirements. Because of this flexibility in system design, the experiment support requirements summarized here are properly regarded as representative, rather than definitive.

Detailed support requirements for each experiment are tabulated in Volume V (Support Requirements for Planetary Orbital Imaging), and are summarized here in order of spectral region. Support requirements are given for ultraviolet, visual, infrared, passive microwave, and radar imaging experiments in orbit about Mars, Venus, Mercury and Jupiter. Since no orbits have been selected for the Moon, no support requirements have been estimated for lunar missions. Similarly no support requirements are presented for radio frequency and multiband experiments, since no scaling laws are available.

7.1 Ultraviolet Scanning Systems

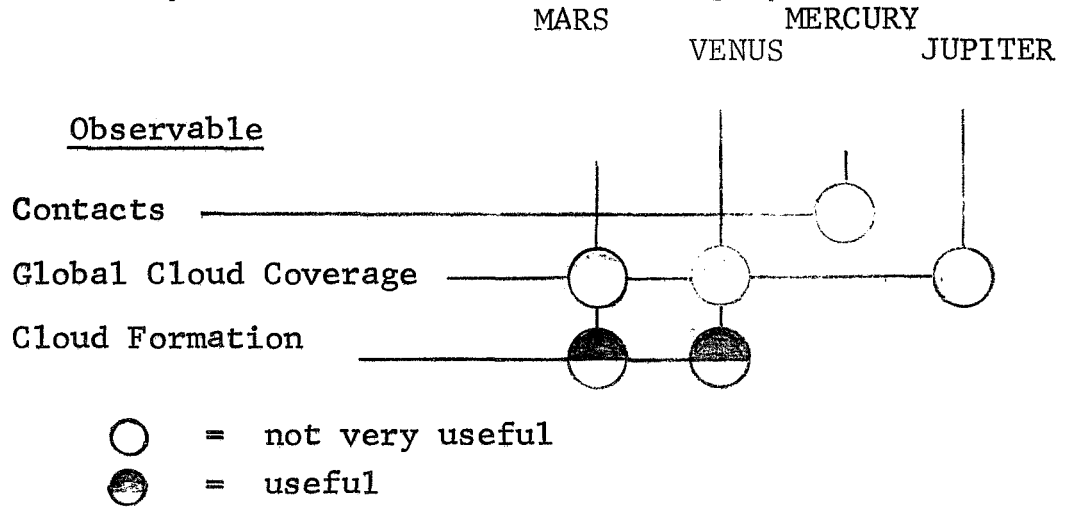
The analysis of planetary exploration scientific objectives presented in Volume II suggest that ultraviolet imaging systems are relatively useless. This denunciation is valid only in the context of orbital imaging experiments and the current state-of-art of image interpretation. Non-imaging ultraviolet systems, such as UV spectrometers, may indeed play a very useful role in planetary exploration; some UV spectrometer flyby experiments have already provided useful information on the possible composition of planetary atmospheres and ionospheres. Nonetheless, orbital UV imaging experiments appear to be useful only in the study of cloud formation processes at Venus and Mars. An assessment of the potential scientific value of orbital UV imaging experiments is summarized in Table 7-1. Only three types of planetary observables can be even marginally studied by UV imagers. The blank circles in the table indicate that orbital UV imaging experiments are expected to provide information which is not

IIT RESEARCH INSTITUTE

very useful in the study of the appropriate planetary observable. Similarly, the half-dark circles indicate that such experiments may be expected to provide useful data. The analysis presented in Volume II identified no cases in which orbital UV imagery could be expected to provide very useful data. For all other spectral regions, the analysis indicated that imagery could be expected to provide very useful data for the study of at least one type of planetary observable.

Table 7-1

Utility of Orbital Ultraviolet Imagery



Experiment support requirements have been estimated for all the planet-observable combinations identified in Table 7-1. These support requirements are listed in full by the data sheets in Volume V, and are summarized here in Table 7-2. In each case shown in the table, the sensor system design was predicated upon minimal achievement of the desired image specifications. For global cloud coverage experiments at Mars, for example, the image specifications provide nominal values for image ground size and resolution of 1200 and 10 km, respectively. The image worth curves for these specifications show that decreasing the image ground size to 1000 km and degrading the ground resolution to 20 km will not materially affect the

Table 7-2

Support Requirements for Ultraviolet Scanning Experiments

PLANET	OBSERVABLE	SCAN LENGTH (KM)	RESOLUTION (KM)	IMAGING ALTITUDE (KM)	WEIGHT (LBS)	POWER (WATTS)	DATA RATE (bits/sec)	TOTAL SCAN ANGLE (DEG)	SCANNING BEAM SIZE (DEG)
MARS	Global Cloud Coverage	1000	20	931	2	1	430	54	0.87
MARS	Global Cloud Coverage	1000	20	440-2749	2	1	6000	92	0.41
MARS	Cloud Formation	600	3	969	2	1	2200	34	0.15
VENUS	Global Cloud Coverage	1500	20	454	2	1	3500	112	0.71
VENUS	Global Cloud Coverage	1500	20	248-1297	2	1	26,000	129	0.35
VENUS	Cloud Formation	600	3	454	2	1	250,000	62	0.27
VENUS	Cloud Formation	600	3	255-2125	3	1	760,000	96	0.08
MERCURY	Contacts(regional)	600	3	500	2	1	1100	60	0.23
MERCURY	Contacts(regional)	600	3	500-1150	2	1	170,000	60	0.13
MERCURY	Contacts(local)	100	0.2	500	51	1	1.3 x 10 ⁶	11	0.02
MERCURY	Contacts(detailed)	0.5	0.005	500	-	-	-	-	-
JUPITER	Global Cloud Coverage	15,000	20	5.5-9.3radii	-	-	-	-	-
JUPITER	Cloud Formation	5,000	20	3.0-6.7radii	-	-	-	-	-

Note: A dash (non-entry) signifies that experiment is beyond the state-of-the-art.

scientific value of the imagery. Therefore, the sensor system design is based upon these less stringent image specifications, and these relaxed values appear in the table. The support requirement non-entries in the table indicate that the sensor system design requires components which are beyond the current state-of-art. The striking conclusion from Table 7-2 is that virtually all UV scanning systems which are within reach of the current state-of-art make rather modest demands upon the spacecraft support subsystems. This conclusion is substantiated by the more complete list of experiment support requirements given in Volume V. That is, the volume, pointing accuracy, and platform stability requirements of these experiments are equally lenient. The only feasible experiment with substantial support requirements is the Mercury experiment desired for study of lithologic contacts on a local scale. The detailed scale contacts experiment at Mercury, and the Jupiter experiments, all require optical systems of greater than one meter in diameter, which is considered to be the limit of current technological capability. In these cases, unreasonably large optical systems are required to collect sufficient detectable energy during the time available for observing each scene resolution element. The situation could be improved by developing more sensitive detectors with fast response times, and by operating at lower altitudes so that a moderately-sized optical system would intercept a larger fraction of the ultraviolet energy reflected by the planetary surface.

Photomultiplier detectors were found to be more suitable, in principle, than currently available solid-state detectors for each experiment studied. At the low scanning mirror rotation rates permitted by the relatively coarse resolution experiments, use of a photomultiplier detector permitted a smaller optical system than required by a solid-state detector. At the high scanning mirror rotation rates required by the finer resolution experiments, the solid-state

detectors do not have a sufficiently fast response time. However, for most of the experiments, in which structural integrity and electronics dominate the system weight, solid-state detectors could be used without increasing the experiment support requirements.

Only the Mercury local-scale contacts experiment satisfies, in all respects, the measurement achievement standards implied by the image specifications and the associated worth curves. At Mars, imaging experiments for determining the extent of global cloud coverage should cover at least 70 percent of the planet in one planetary day, and these coverages should be repeated twenty times per planetary year, with particular attention to the polar areas. The 931 km altitude circular orbit indicated in Table 7-2 results in 95 percent planetary coverage every three days, but the poles are not included in the coverage, while the elliptic polar orbit affords only 58 percent coverage every six days. Only one pole is in daylight at any time. The data acquisition rate is higher for the elliptic orbit because the smaller angular resolution, lower periapse altitude, and faster orbital speed while imaging require a faster scanning mirror rotation rate. Only ten percent planetary coverage at Mars is required for study of cloud formation, but each image should be acquired in less than one minute and the same area (or cloud formation process) should be imaged again in ten or fifteen minutes. Since the ground speed of an orbiting spacecraft is about two or three km/sec, approximately three to five minutes are required to traverse 600 km on the ground. Therefore, scanning systems require considerably more than one minute to collect data from an area 600 by 600 km. Very nearly the same area can be imaged on the next orbital pass, which occurs in about 2.4 hours. Use of an ultraviolet television camera would tend to solve these timing problems, since an image of the entire desired ground area could be acquired instantaneously and an image of nearly the same area could be procured one or two minutes later. Of

course, a standard television camera could, and undoubtedly, should, also be used.

Planetary coverage problems are even more severe at Venus, since Venus rotates only once in 120 Earth days. For global cloud coverage imagery at Venus, at least 70 percent planetary coverage is desired in 100 hours, and this coverage should be repeated ten times per planetary year (240 Earth days). Unless the orbit is changed during the mission, only 50% daylight planetary coverage is possible and requires 112 days. Section 5.5.2 has indicated that an impulse on the order of three km/sec is required for a suitable orbit change, and has also shown that sun-synchronous orbits (which would permit 100 percent coverage in 116 days) are probably not feasible for Venus. For study of cloud formation at Venus, a 600 x 600 km ground size image should be acquired in no more than one minute, and the same area should be viewed again in ten or fifteen minutes. Emphasis should be placed upon subsolar and polar areas. Use of the 454 km altitude circular polar orbit indicated in Table 7-2 requires 1.5 minutes to acquire the desired image of a 600 x 600 km area by using a scanning sensor system. The orbital period is 1.6 hrs. so the same area could be imaged again in 96 minutes. The elliptic orbit indicated in the table affords a faster spacecraft velocity during imaging operations, hence a single image can be acquired in one minute as required, but the orbital period is now 17 hours. As with Mars, a television sensor system would alleviate these problems.

Mercury also has a slow rotation rate, and similar coverage problems are encountered. These are especially severe in the case of imagery for the study of lithologic contacts, since a solar zenith angle of less than twenty degrees is desired for proper image interpretation. Only 34 percent of Mercury's surface is ever illuminated in this manner. Since at least 70 percent planetary coverage is desired for imagery of contacts on a regional scale, the desired experiment cannot be performed with a passive imaging system. However, for study of

contacts on a local scale, only ten percent coverage is required, and the desired experiment can be performed. As mentioned earlier, this is the only ultraviolet imaging experiment, using a scanning system, which completely satisfies all the image specifications.

The ultraviolet imaging experiments considered here are intended to supplement, rather than compete with, visual imaging experiments in support of the same scientific objectives. Nonetheless, it is interesting to compare the support requirements of UV imaging experiments to those of visual systems in support of the same objectives. The visual experiment support requirements are summarized in the next section. Comparison with the UV support requirements given above will show that, in general, the UV support requirements are less demanding than the corresponding visual experiment, provided the UV sensor system design is within the current state-of-art. For example, a visual imaging experiment, for studying the extent of global cloud coverage at Mars, using the same 931 km altitude orbit as for the UV experiment, will weigh about eight pounds, consume eight watts of power, and will collect data at 4500 bits/sec, compared with two pounds, one watt, and 430 bits/sec for the UV experiment. In other cases, the data acquisition rates may be of similar magnitude. Those readers searching for evidence of a universal system of justice will note that although the UV experiments place less demands upon the spacecraft support subsystems, they will also provide less useful data than visual systems if one is forced to measure one against the other. This is not the desire here, since the two types of imagery will in fact supplement each other.

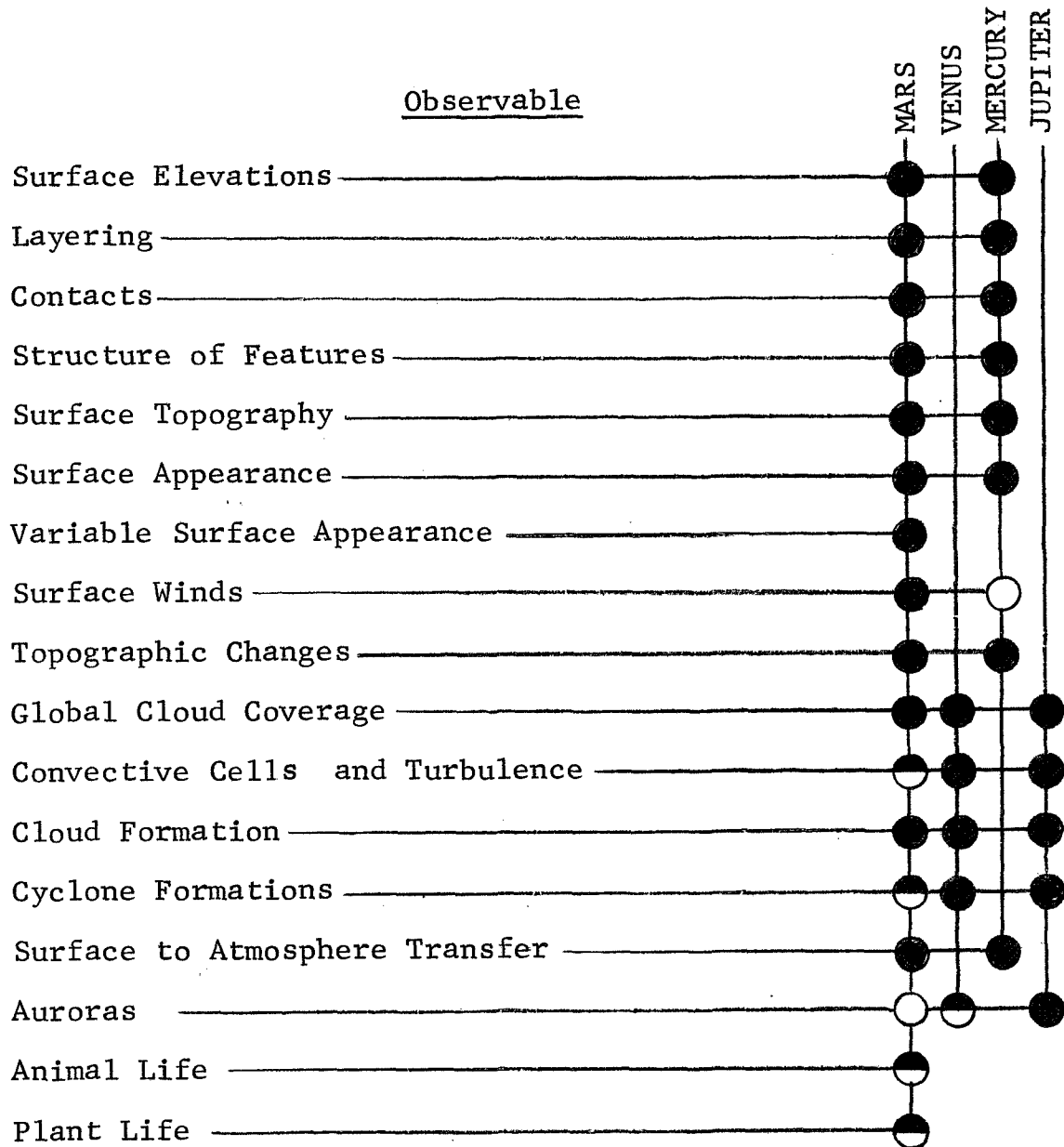
In summary, the support requirements demanded by ultraviolet orbital imaging systems are found to be rather modest. Systems affording ground resolutions of 3-20 km over scan lengths of 600-1500 km can be provided at the current state-of-art. These systems weigh about two pounds, consume one watt of power, and collect data at rates of less than 10^6

bits/sec. Some difficulty is encountered in providing the necessary planetary coverages, both in the extent of coverage and the times permitted to achieve and repeat the coverage, but these problems are not unique to ultraviolet imaging systems. Occasionally, the images cannot be acquired or repeated at the desired time intervals. These difficulties are common to all optical-mechanical orbital scanning systems.

7.2 Visual Imaging Systems

Imagery in the visible portion of the spectrum is more useful than imagery in any other single spectral region, in the sense that visual imagery contributes to the study of more observables than any other type of imagery. This is partly because visual imagery is usually easy to interpret and partly because both atmospheric and surface phenomena can be observed visually, at least if the atmosphere is not impenetrable. Table 7-3 lists the different planetary phenomena which might be observed visually at the different planets. The degree of usefulness is indicated by the blackness of the circles; the fully black circle signifies that visual imagery is expected to be very useful, the half-black circle signifies that visual imagery is expected to be useful, while the empty or white circle signifies that visual imagery is expected to be not very useful. The assessments shown in the table are substantiated in Volume II, which deals with the planetary phenomena individually. The usefulness of visual imagery in investigating both surface and atmospheric phenomena is shown quite clearly in the case of Mars. Mercury does not possess as many phenomena for which visual imagery is appropriate because of its virtually non-existent atmosphere and presumed lack of biological substances. Thus, at Mercury, the emphasis in the visible region is upon surface phenomena. At Venus and Jupiter, the emphasis is upon atmospheric phenomena, since both planets exhibit active atmospheres, and the surface can probably not be seen visually from orbit.

Table 7-3
 Utility of Orbital Visual Imagery



Experiment support requirements have been estimated for experiments suggested by all the observable/planet combinations indicated in Table 7-3. These support requirements are reported in detail by Volume V, and are summarized here for each planet. The support requirements are based on orbit selections described in Volume II, and on the image specifications given in Table 4-1 of this volume. In each case, the appropriate worth curves have been utilized to select those image specifications which would appear to result in the least demanding support requirements without appreciably degrading the scientific utility of the imagery. That is, the experiment support requirements are based on sensor system designs which will minimally satisfy the scientific requirements for imagery.

7.2.1 Mars

Because of the large number of visual imaging experiments considered at Mars, it is convenient to organize the experiment support requirements on the basis of the image scale: regional, local, and detailed. As shown earlier in Table 4-1, the image specifications reflect, for many observables, a hierarchy of investigation commencing with first-order, regional studies, usually covering seventy percent of the planet, contributing to a general identification or understanding of the phenomenon, and its large scale distribution in location or time. Second-order, or local, studies are aimed at developing a more detailed understanding, usually by more accurate investigations over ten to twenty percent of the planet. Finally, third-order, or detailed scale, imagery usually covers less than one percent of the planet and is expected to focus on observed anomalies or deviations. The minimum ground, or scene, area which should be covered in a single image, or frame, is related to the scale of the imagery. In particular, for Mars, the worth curves of Section 4 show that the minimum scene area is 600 x 600 km, or larger, for regional scale imagery, 100 x 100 km for local scale imagery, and about 0.5 x 0.5 km for detailed scale imagery. For example,

imagery procured for the study of lithologic contacts on a regional scale should consist of imaged areas no smaller than 600 x 600 km in a single image. With some exceptions, all visual imaging experiments which collect imagery of the same scale (regional, local, or detailed) tend to have similar support requirements. Further, the support requirements tend to place more demands upon the spacecraft, in terms of experiment weight, power, etc., as one goes from regional scale experiments to local scale experiments, or from local scale experiments to detailed scale experiments.

Regional Scale Experiments

Table 7-4 summarizes the weight, power, and data acquisition rate support requirements for regional scale visual imaging experiments at Mars. The values given in the table for the image ground size and the horizontal resolution have been obtained from the appropriate worth curves and represent the minimum acceptable values. Thus for global cloud coverage experiments, the minimum ground, or scene, area which should appear in a single image is 1000 x 1000 km, while the linear size of a resolution element in the processed imagery should correspond to a linear extent on the ground, or scene, of no larger than 20 km. In each case, the imaging system design satisfies, or even exceeds, these specifications. That is, ground size and resolution values in the table refer to the image specifications and not to the values actually achieved by the imaging experiment design.

Regional scale visual imagery at Mars requires sensor systems weighing from 10 to 30 pounds, consuming 10 to 35 watts (average) and collecting data at 10^3 to 10^6 bits/sec, assuming 64 shades of grey in the processed imagery. For similar experiments, use of stereoscopic coverage increases the support requirements, while use of a 3-color filter wheel may or may not increase the data acquisition rate. Film systems are not required, but may be useful, and may even result in less demanding support requirements than TV systems. The support requirements have been

Table 7-4
Support Requirements for Visual
Experiments-Mars (regional)

OBSERVABLE	STEREO	COLOR	IMAGING ALTITUDE (km)	IMAGE GROUND SIZE (km)	HORIZONTAL RESOLUTION (km)	CAMERA	WEIGHT (LBS)	POWER (WATTS)	DATA RATE (bits/sec)
Global Cloud Coverage	-	-	931	1000	20	1/2" VID	8	8	4.6 x 10 ³
Global Cloud Coverage	-	X	931	1000	20	1/2" VID	8	8	4.6 x 10 ⁴
Global Cloud Coverage	-	-	440-2568	1000	20	1 1/2" VID	24	24	1.2 x 10 ⁴
Global Cloud Coverage	-	X	440-2568	1000	20	1 1/2" VID	24	24	1.2 x 10 ⁴
Surface Winds	-	-	969	600	20	1/2" VID	8	8	4.6 x 10 ³
Convective Cells and Turbulence	-	-	969	600	20	1/2" VID	8	8	4.6 x 10 ³
Cyclone Formations	-	-	969	600	20	1/2" VID	8	8	4.6 x 10 ³
Auroras	-	-	969	600	20	1/2" VID	8	8	4.6 x 10 ³
Surface Elevations	-	-	969	600	20	1/2" VID	32	32	1.9 x 10 ⁴
Auroras	-	X	969	600	20	1/2" VID	8	8	4.6 x 10 ³
Auroras	-	-	425-6481	600	20	2" RBV	32	32	3.8 x 10 ⁵
Auroras	X	X	425-6481	600	20	2" RBV	32	32	5.1 x 10 ⁵
Surface Elevations	X	-	994	600	20	70mm(SO-243)	25	36	6.8 x 10 ⁵
Surface Elevations	X	-	400-580	600	20	3" RBV	48	48	4.9 x 10 ⁵
Contacts	-	-	969	600	3	1" VID	16	16	7.4 x 10 ³
Structure of Features	-	-	969	600	3	1" VID	16	16	7.4 x 10 ³
Surface Topography	-	-	969	600	3	2" RBV	32	32	3.8 x 10 ⁵
Surface Appearance	-	-	969	600	3	1" VID	16	16	7.4 x 10 ³
Variable Surface Appearance	-	-	969	600	3	1" VID	16	16	7.4 x 10 ³
Cloud Formation	-	-	969	600	3	1" VID	16	16	7.4 x 10 ³
Surface Appearance	-	X	969	600	3	1" VID	16	16	7.4 x 10 ³
Surface Appearance	-	X	425-952	600	3	2" RBV	32	32	4.1 x 10 ⁵
Surface Appearance	-	X	425-952	600	3	2" RBV	32	32	4.1 x 10 ⁵
Structure of Features	X	-	994	600	3	2" RBV	32	32	3.8 x 10 ⁵
Structure of Features	X	-	400-580	600	3	2" RBV	32	32	3.8 x 10 ⁵
Surface Topography	X	-	994	600	3	2" RBV	24	36	6.9 x 10 ⁵
Surface Topography	X	-	400-580	600	3	2" RBV	24	32	4.6 x 10 ⁵
Structure of Features	X	X	425-952	600	3	70mm(SO-243)	32	32	8.2 x 10 ⁵
Structure of Features	X	X	425-952	600	3	2" RBV	32	32	8.2 x 10 ⁵

estimated using scaling laws based on the current state-of-art. Advances in microminiaturization could easily lead to a four-fold reduction in weight and a two-fold reduction in power, but would have no effect on the data rates. With few exceptions, all the scientific requirements pertaining to regional scale imagery can be met. The exceptions arise, not from state-of-art limitations on the sensor system, but from basic incompatibilities between the orbit selections and the image specifications, most notably the coverage acquisition time and the image repetition rate.

The three groupings in Table 7-4 represent different combinations of scene size and horizontal resolution. The first grouping consists of all those experiments designed to provide 20 km resolution over a minimum area of 1000 x 1000 km. Only experiments for study of global cloud coverage require such large image ground sizes. Neglecting curvature of the planetary scene, not much more than 70 TV lines are required to achieve the necessary resolution. However, for low-contrast targets, even a $\frac{1}{2}$ -inch vidicon system will provide 275 TV lines. This excess resolution capability can be used to increase the imaged area and improve the resolution to the nominal values given in Table 4-1. Thus a $\frac{1}{2}$ -inch vidicon system operating in a circular orbit of 931 km altitude will actually provide 10 km ground resolution over an imaged area of 1200 x 1200 km. Use of a 3-filter color wheel to provide pseudo-color coverage does not increase significantly the support requirements, except for the total data load. For the non-color experiment, images are acquired approximately every 400 seconds. For the color experiment, three images are acquired in the same time, hence the image interval time is approximately 130 seconds. In either case, the image interval time is less than the maximum acceptable image tube storage time (100 sec). That is, the data acquisition rate is determined not by the image interval time, but by the need to remove the data from the tube faceplate before significant charge leakage occurs. In this situation, the data rate is not

affected by employment of a 3-color filter wheel.

If an elliptic orbit is used, with a fixed focal length system, an excess resolution capability must be provided at periapse, while a larger than necessary imaged area must be provided off-periapse. For a fixed orbit lifetime, an elliptic orbit will permit at least some imagery from lower altitudes than would be possible with a circular orbit. However, this may be a distinct disadvantage when large imaged areas are required. In viewing a 1000 x 1000 km area from an altitude of only 440 km with a fixed angular resolution, the effects of planetary curvature and oblique viewing angles near the edge of the field-of-view result in a ground resolution which varies by a factor of three across the imaged area. Thus about 200 TV lines are required for imagery of cloud coverage from a periapse altitude of 440 km. Since the camera system field-of-view is determined by the necessity of observing a 1000 x 1000 km area from a periapse altitude of 440 km, the same field-of-view will result in an unnecessarily large imaged area from 2568 km. Indeed, to obtain a ground resolution of 20 km throughout the central 1000 x 1000 km area, 430 TV lines are required for a low-contrast scene and a 1½-inch vidicon system is necessary, as compared to a ½-inch vidicon system, when essentially the same experiment is performed from a constant 931 km altitude. A ½-inch vidicon system with a zoom lens could be utilized for imagery from altitudes of 440 to 2568 km, but if a radar altimeter is used to control the focal length, the zoom lens imaging system would weigh more than a 1½-inch vidicon system with a fixed focal length. As with the circular orbit, use of a 3-color filter wheel does not increase the data acquisition rate because of the large imaged area, but does increase the data load.

Neither the circular orbit nor the elliptic orbit selected for global cloud coverage imagery provides the desired 70 percent planet coverage in one day. The 931 km circular orbit with the ½-inch vidicon system affords 95 percent daylight

planetary coverage every three days, while the elliptic orbit with the 1½-inch vidicon affords only 60 percent daylight planetary coverage every six days. By using a 2-inch RBV (return beam vidicon) system on a 931 km circular orbit, the field-of-view could be increased to cover an area of about 2200 x 2200 km per image, and 95 percent daylight planetary coverage could be achieved daily. Such a system would provide a ground resolution of about 5 km, but would weigh about 32 pounds, consume about 32 watts of average power, and acquire data at about 3.8×10^5 bits/sec.

The next experiment grouping shown in Table 7-4 consists of all those visual experiments requiring a ground resolution of 20 km over at least a 600 x 600 km area. Except for the surface elevations experiment, all these experiments can be performed from a circular 969 km altitude orbit by a ½-inch vidicon system of modest support requirements. In fact, for the first four experiments listed in this group (surface winds, convective cells, cyclone formations, and auroras), a ½-inch vidicon system provides a ground resolution of 7.3 km over a 1000 x 1000 km imaged area. For these image sizes, and the slow orbital speed associated with a circular orbit, color imagery can be obtained without an increase in the data acquisition rate. As with the global cloud coverage experiments, use of an elliptic orbit will generally result in increased support requirements. A 2-inch RBV system will provide 1.6 km ground resolution over a 1000 x 1000 km area from a periapse altitude of 425 km, but this degrades to 8.3 km resolution (which is still more than adequate) from 6481 km altitude. The higher ground speeds associated with the elliptic orbit mean that use of color filter wheels will slightly increase the data acquisition rate, even though large imaged areas are still involved.

For study of surface winds and auroras, time-lapse imagery is desired, i.e., the same area should be imaged again after an interval of two hours or less. Although orbit periods as short as nearly two hours can be achieved with a fifty year

lifetime orbit, Mars rotates about 2000 km under the orbit during this time, hence the same area cannot be observed every orbit. By increasing the image overlap along the orbit ground trace to 60 percent, rather than 20 percent, at least more than half the same area can be imaged again in two or three minutes. This type of time-lapse imagery may be adequate for the surface winds experiment, but will probably not reveal any temporal variations of auroras. On the other hand, it is unlikely that auroras will be observed at Mars anyway. Such time-lapse imagery will not increase the data acquisition rate, which is controlled by the vidicon storage time rather than the image overlap.

The surface elevations experiments demand a more stringent ground resolution capability than is apparent from a 20 km horizontal ground resolution requirement. In this case, the necessary resolution in the imagery is controlled by the desire to detect one km differences in vertical heights. The non-stereo surface elevations experiment utilizes low sun angles and long surface shadows to infer height differences. If the sun is 30 degrees above the horizon, a one km high surface feature will cast a shadow 1.7 km in length. Thus the ground resolution required is actually 1.7 km, rather than 20 km, and a 2-inch vidicon system is necessary. This assumes a low-contrast scene, and may not be the case for shadow measurements, hence the estimated support requirements may be unduly conservative. A 2-inch RBV system could also be used, providing a much better ground resolution at an increased data rate. If stereo coverage is obtained with an area of 600 x 600 km per image, the distance between camera stations is 360 km, and the image resolution must be equivalent to 0.24 km if stereo parallax is to indicate height differences of one km. Doubling the distance between camera stations permits a resolution twice as crude, but since the linear extent of the imaged area is also doubled, the same number of resolution elements per image is

required. In fact, if planetary curvature is accounted for, somewhat more resolution elements per image are required at larger image ground sizes. Thus stereo imagery for surface elevations experiments from the lowest feasible circular orbit requires a TV system of 4000 line capability, which is beyond the current state-of-art. Therefore a 70 mm film system has been selected with the support requirements summarized in the table. The system weight shown includes the weight of the film, on-board film processing, and radiation shielding. The increased resolution capability of the film system permits image ground sizes of 2300 x 2300 km and ground resolutions of slightly better than one km, which is required to detect the necessary amount of stereo parallax. An alternative mode is to use an elliptic orbit, imaging only in the vicinity of periapse. In this case, a 3-inch RBV system is adequate and provides 0.6 km ground resolution over an imaged area of 600 x 600 km at periapse. The support requirements are not radically different from the film system, and essentially the same amount of time is required to achieve 70 percent planetary coverage. The stereo experiment support requirements shown in the table are based on 60 percent image overlap in a direction normal to the orbit ground trace. That is, each stereo image pair consists of an image obtained from one orbit pass and an image obtained from a later orbit pass. Use of 60 percent forward overlap, rather than side overlap, would double the data acquisition rates, but a stereo pair would be obtained in a few minutes rather than one day as for side overlap.

The orbit selected for the non-stereo surface elevations experiment results in 74 percent planetary coverage at solar elevation angles of 15-30 degrees in five Martian days. For stereo coverage, a much different illumination regime is desired (solar zenith angles of 5-20 degrees) and, in a single Mars day, the area illuminated properly is small compared to that illuminated at larger zenith angles. In one day, only 35

percent of the Martian surface is illuminated at zenith angles of less than 20 degrees, hence to obtain 70 percent planetary coverage, one must wait for the Sun to move from one hemisphere to the other. In fact, if the Mars axis of rotation were normal to the ecliptic plane, only 35 percent planetary coverage could ever be obtained under the desired lighting conditions. However, the subsolar point on Mars moves from about 25 degrees South latitude to 25 degrees North latitude in one-half a Martian year, or about 340 Earth days. If stereo imaging operations are started at winter solstice, approximately 335 days will be required to obtain the desired 70 percent coverage. This is the minimum mission duration, and is independent of the orbit parameters and sensor system design as long as solar zenith angles of less than 20 degrees are desired. Thus in comparing mission modes of obtaining topographic information, 70 percent coverage requires five days for shadowing experiments and a minimum of 335 days for stereo experiments.

The last grouping in Table 7-4 consists of those imaging experiments requiring a three km horizontal resolution over an area of at least 600 x 600 km per image. In this grouping, the structure of features experiments and the surface topography experiments require vertical resolutions of three and one km, respectively. The first subset in the table (contacts, structure of features, surface topography, surface appearance, and variable surface appearance) is designed for solar elevation angles of 15 to 30 degrees, facilitating image interpretation or measurement of shadow lengths. With a ground resolution of three km, shadow measurements may be used to infer vertical height differences of about 1.7 km. This is inadequate for surface topography experiments, which require a 1.7 km ground resolution to infer height differences of one km from measurement of shadow lengths. Therefore, a one-inch vidicon system is not adequate for the surface topography shadow experiments. A two-inch vidicon would provide adequate resolution over a 600 x 600

km area, but by using a two-inch RBV considerably better resolution or larger imaged areas can be obtained at the expense of an increased data rate. The same orbit may be used for all these experiments, affording 74 percent planetary coverage every five days. However, this does not quite satisfy the scientific requirements for the variable surface appearance experiments, which demand 70 percent coverage in 100 hours (about four Martian days) and daily observation of selected areas. Note however that any area within the 74 percent coverage can be imaged at least once every five days. By using a two-inch RBV system providing single image areas of 2300 x 2300 km, over 70 percent coverage could be achieved daily.

Imagery for study of cloud formation processes can be performed during daylight; only ten percent planetary coverage is required. This implies that the necessary coverage can be obtained in less than one day, except that time-lapse imagery with an interval of about ten minutes is desired. As noted earlier, unless nearly full disk imagery is provided, image intervals of less than one day cannot be attained, except for high forward overlap situations with relatively short image interval times. In particular, with an image size covering 600 x 600 km from a 969 km circular orbit, 60 percent forward overlap permits more than half the same area to be pictured again in about 1.5 minutes. This image interval may be adequate for cloud formation experiments. The image interval could be lengthened to about six minutes by using a four-inch RBV system and an imaged area of about 2500 x 2500 km. This would, of course, greatly increase the experiment support requirements.

Color surface appearance experiments are best performed when the surface illumination results from a late morning or early afternoon sun. Thus the difficulties in obtaining 70 percent planetary coverage in a short time are similar to those described above in connection with the stereo surface elevations experiments. Since the lighting conditions desired for surface

color imagery are not quite as severe as for stereo (solar zenith angles of less than 40 degrees are acceptable for color, while stereo coverage should be obtained at zenith angles less than 20 degrees), the situation is not as bleak. Even without the propulsive investment required to enter a sun-synchronous orbit, very nearly 60 percent coverage can be achieved in ten days from the polar elliptic orbit referred to in the table. However, because imaging operations are conducted over an altitude range from 425 to 952 km, the one-inch vidicon system used on the 969 km circular orbit is inadequate, a two-inch RBV system is required. A two-inch vidicon system is adequate from altitudes near periapse, but will not provide the necessary resolution from 952 km. On the other hand, a two-inch RBV system has an excess resolution capability which increases the imaged area to 1250 x 1250 km at periapse while maintaining a three km ground resolution from 952 km. Daily observation of identical areas, as desired for study of variable surface appearance, cannot be provided by the selected orbit.

Finally, stereo coverage for structure of features and surface topography experiments can be obtained from either circular or elliptic orbits. These experiments are similar to the surface elevations experiments discussed above. The support requirements shown in the table indicate that use of an elliptic orbit need not result in more demanding support requirements than for a similar experiment on a circular orbit. If the altitude from which imaging is performed does not vary more than a factor of two or so, an elliptic orbit may actually decrease the support requirements. This is feasible with visual stereo experiments because the surface area which is properly illuminated is relatively small and the spacecraft altitude does not change greatly while flying over this small area.

Local Scale Experiments

Table 7-5 summarizes typical support requirements for visual imagery of Mars on a local scale, that is, when an imaged area 100 x 100 km (per image) satisfies the scientific requirements. Atmospheric imaging experiments require ground resolutions of three km, while surface imaging experiments require ground resolutions of 200 meters. Stereo surface experiments may require ground resolutions better than 200 meters, depending upon the vertical resolution desired and the distance between camera stations. The surface to atmosphere energy transfer imaging experiments require 70 percent planetary coverage; all the other experiments listed in the table can be satisfied with only ten percent planetary coverage.

A one-half-inch vidicon system is more than adequate for all the experiments in the first grouping in the table. Daily coverage of selected areas is desired for study of convective cells and atmospheric turbulence, and is provided by using an elliptic orbit having a period equal to one Mars day. Since local scale imaging experiments will presumably be preceded by regional scale coverage on an earlier mission, the results of the regional scale experiments can be utilized to select areas fruitful for local scale imagery. The local scale cyclone formations experiment is identical to the convective cells experiment, but the scientific requirements are not satisfied in this case because images of the same area cannot be obtained at intervals on one hour or so, at least not unless nearly full disk imagery is provided. The surface to atmosphere energy transfer experiments provide 75 percent planetary coverage in about 27 days, while 70 percent coverage in one day, ten times per year, is demanded by the scientific requirements. For the non-color experiment, where solar zenith angles of 30 to 60 degrees are desired, nearly 90 percent of Mars is properly illuminated each day. By using a 70 mm SO-243 film system, it should be possible to acquire more than 70 percent coverage daily with image ground

Table 7-5
Support Requirements for Visual
Experiments-Mars (local)

OBSERVABLE	STEREO	COLOR	IMAGING ALTITUDE(km)	IMAGE GROUND SIZE (km)	HORIZONTAL RESOLUTION (km)	CAMERA	WEIGHT (lbs)	POWER (watts)	DATA RATE (bits/sec)
Convective Cells and Turbulence	-	-	340-365	100	3	½" VID	8	8	2.3 x 10 ⁴
Cyclone Formations	-	-	340-365	100	3	½" VID	8	8	2.3 x 10 ⁴
Surface to Atmosphere Transfer	-	-	1016	100	3	½" VID	8	8	6.9 x 10 ³
Surface to Atmosphere Transfer	-	X	1016	100	3	½" VID	8	8	2.1 x 10 ⁴
Surface Winds	-	-	383-1115	100	0.2	2" RBV	32	32	1.9 x 10 ⁶
Contacts	-	-	340-976	100	0.2	2" RBV	32	32	2.0 x 10 ⁶
Contacts	-	-	383-2117	100	0.2	70mm(SO-243)	41	67	7.7 x 10 ⁶
Structure of Features	-	-	340-976	100	0.2	2" RBV	32	32	2.0 x 10 ⁶
Structure of Features	-	-	383-2117	100	0.2	70mm(SO-243)	41	67	7.7 x 10 ⁶
Surface Topography	-	-	340-976	100	0.2	2" RBV	32	32	2.0 x 10 ⁶
Surface Topography	-	-	383-2117	100	0.2	70mm(SO-243)	45	67	9.4 x 10 ⁶
Surface Appearance	-	-	340-976	100	0.2	2" RBV	32	32	2.0 x 10 ⁶
Surface Appearance	-	-	383-2117	100	0.2	70mm(SO-243)	41	67	7.7 x 10 ⁶
Variable Surface Appearance	-	-	340-976	100	0.2	2" RBV	32	32	2.0 x 10 ⁶
Variable Surface Appearance	-	-	383-2117	100	0.2	70mm(SO-243)	41	67	7.7 x 10 ⁶
Plant Life	-	-	383-1115	100	0.2	2" RBV	32	32	1.9 x 10 ⁶
Structure of Features	-	X	383-880	100	0.2	5"(SO-243)	36	51	2.6 x 10 ⁷
Surface Appearance	-	X	383-880	100	0.2	2" RBV	32	32	5.7 x 10 ⁶
Variable Surface Appearance	-	X	383-880	100	0.2	2" RBV	32	32	5.7 x 10 ⁶
Plant Life	-	X	383-880	100	0.2	2" RBV	32	32	5.7 x 10 ⁶
Surface Topography	X	-	383-485	100	0.2	5"(SO-243)	63	110	1.6 x 10 ⁷
Structure of Features	X	-	383-485	100	0.2	70mm(SO-242)	26	36	8.6 x 10 ⁶
Structure of Features	X	X	383-880	100	0.2	5"(SO-243)	40	51	4.9 x 10 ⁷

sizes of about 2500 x 2500 km. The experiment support requirements would then be similar to those of the regional scale stereo surface topography experiment. The color experiment could be done in the same manner, but only about 65 percent daily coverage could be achieved at the solar illumination desired for color imagery.

The second grouping in Table 7-5 actually contains three families of experiments which differ in the surface lighting conditions desired. The surface winds and plant life experiments should be conducted at solar zenith angles of 30 to 60 degrees, the color experiments at zenith angles of 10 to 40 degrees, and the remaining experiments at zenith angles of 60 to 75 degrees. The surface winds and plant life experiments are very similar, and can be performed with the same imaging system from the same orbit. To achieve a ground resolution of 200 meters over a 100 x 100 km area, at least 700 TV lines are required. For low-contrast targets, this exceeds the operational resolution of a two-inch vidicon system. A two-inch RBV system has excess capability which may be utilized by flying on an elliptic orbit and results in a less costly capture maneuver than would be required for a circular orbit. A ground resolution of 60 meters is attained at periapse (383 km), while at the maximum imaging altitude (1115 km) the ground resolution is 170 meters. For the surface winds experiment, the image specifications stipulate that the same ground area should be observed again after an interval of no more than two minutes. With a 20 percent image overlap at periapse, the image interval time is 20 seconds, and thus image interval times on the order of one minute are not possible. However, the interval time desired is dependent upon the ground resolution if wind velocities are being measured. Since 60 meter resolution is provided, increasing the overlap to 60 percent (and hence increasing the data rate to 3.8×10^6 bits/sec) would permit measurement of wind velocities in excess of about 20 km/hour, and thereby satisfy the scientific requirements.

The low-sun-angle family is designed for ease of image interpretation (contacts and surface appearance) and measurement of shadow lengths (structure of features and surface topography). The structure of features experiments require detection of 200 meter height differences, the surface topography experiments 100 meters. This difference does not affect the support requirements, since the required horizontal resolution of 200 meters will permit inference of 100 meter height differences throughout nearly all of the imaged areas. Both elliptic orbits selected provide about 75 percent planetary coverage in 50 days. The effect of imaging over an appreciable altitude range is clearly seen as imaging over the altitude range 340 to 976 km can be performed satisfactorily with a two-inch RBV system, while imaging over a range of 383-2117 km requires a 70 mm SO-243 film system with image motion compensation. Nearly 50 feet of film is required for ten percent planetary coverage.

A high-sun-angle family (surface appearance and plant life) designed to procure color imagery is shown in this grouping in the table. Since a two-inch RBV system provides adequate resolution over a 100 x 100 km area, the support requirements are similar to those of the experiments in the low-sun-angle family. Because a three-color filter wheel is used, the data acquisition rates are approximately triple those of the corresponding non-color experiments. The factor is not exactly three, because slightly different orbits and apparent ground speeds are involved. For all local scale experiments, where the imaged area is on the order of 100 x 100 km, the image interval time is controlled by the ground speed, image overlap, and image ground size, rather than the desire to avoid excessive resolution degradation due to long storage times on the image tube faceplate. Thus color imagery results in a data rate three times that of a non-color experiment, and 60 percent forward overlap (which would be used to obtain stereo coverage along the flight line) results in twice the data rate of 20 percent forward overlap imagery.

The only local scale experiments in which the imagery is intended to provide vertical height information are surface topography and structure of features. This may be accomplished by measurement of shadow lengths or stereo parallax. The shadowing experiments have been discussed briefly above; the stereo experiments form the last grouping in Table 7-5. The orbit selection is based on an imaged area of 100 x 100 km with a 60 percent side overlap of adjacent orbital imaged swaths. A retrograde orbit of 8.2 hour period affords the opportunity of observing a properly illuminated ground area from an altitude which does not change greatly (383 to 485 km) during imaging operations. The structure of features experiment has the more modest support requirements because only a 200 meter vertical resolution is demanded. Approximately 7000 TV lines are required, and hence a film system has been used. A 70 mm SO-243 film camera will provide adequate stereo parallax and ground resolution (125 meters at periapse) over an area of 600 x 600 km per image. The experiment could also be designed for a better ground resolution over a smaller ground area, but this would decrease the image interval or cycle time, and increase the data acquisition rate. The second half of each stereo pair is obtained one Mars day after the first half, but at essentially the same lighting conditions. A 60 percent overlap along the orbit trace would provide stereo coverage in the forward direction, with each stereo pair being obtained in about two minutes, but the data acquisition rate would increase to 8.6×10^6 bits/sec. The surface topography experiment requires a better ground resolution, to infer 100 meter vertical height differences, and a more capable imaging system is necessary. A five-inch SO-243 film system with image motion compensation provides the necessary resolution (60 meters at periapse) over an area of 550 x 550 km per image. For ten percent coverage, about 60 feet of film are required; the structure of features experiment requires only about 30 feet (of smaller film). Forward stereo could be used, but would double the data rate.

A structure of features stereo experiment could be included in the local scale color family described above, although the illumination provided is not quite that desired for stereo coverage, that is, there will be more shadows in the imagery than desired. Furthermore, because the color family operates over a wider range of imaging altitudes, a five-inch film system is required. The data rate of 4.9×10^7 bits/sec is based on obtaining a stereo pair in each of the primary colors, and is probably an upper limit. It may prove feasible to use the color triplets as two stereo pairs, or color triplets need not be obtained at all.

Detailed Scale Experiments

Table 7-6 summarizes the weight, average power, and data acquisition rates for detailed scale visual imagery at Mars. There are four natural groupings, which are based on the surface illumination desired. The first family is for color imagery at solar zenith angles of 10-40 degrees, the second is for stereo imagery at zenith angles of 5-30 degrees, the third is for low-sun-angle imagery at zenith angles of 60-75 degrees, and the last is for mid-morning or mid-afternoon imagery at zenith angles of 30-60 degrees. Except for layering and animal life experiments, the detailed scale experiments are presumed to have been preceded by local scale experiments in support of the same scientific objectives. These detailed scale experiments require something less than one percent planetary coverage, the exact planetary location of the coverage being determined by study of the local scale imagery obtained earlier. Even the layering and animal life experiments are part of the exploration hierarchy, since those areas of interest for study of layering will depend upon the results of the local scale structure of features and surface appearance experiments, while areas most promising for animal life searches might be selected from local scale plant life and variable surface appearance experiments.

Table 7-6
Support Requirements for Visual
Experiments-Mars (detailed)

OBSERVABLE	STEREO	COLOR	IMAGING ALTITUDE (km)	IMAGE GROUND SIZE (m)	HORIZONTAL RESOLUTION (m)	CAMERA	WEIGHT (lbs)	POWER (watts)	DATA RATE (bits/sec)
Surface Appearance	-	X	383-880	500	5	2" RBV	360	47	2.4 x 10 ⁸
Variable Surface Appearance	-	X	383-880	500	5	2" RBV	360	47	2.4 x 10 ⁸
Structure of Features	X	-	383-485	500	5	9½" (SO-230)	270	280	5.0 x 10 ⁸
Surface Topography	X	-	383-485	500	5	9½" (SO-230)	270	280	5.0 x 10 ⁸
Topographic Changes	X	-	383-485	500	5	9½" (SO-230)	270	280	5.0 x 10 ⁸
Structure of Features	X	X	383-485	500	5	9½" (SO-102)	400	280	1.2 x 10 ⁹
Contacts	-	-	383-2117	500	5	-	-	-	-
Structure of Features	-	-	383-2117	500	5	-	-	-	-
Surface Topography	-	-	383-2117	500	5	-	-	-	-
Surface Appearance	-	-	383-2117	500	5	-	-	-	-
Variable Surface Appearance	-	-	383-2117	500	5	-	-	-	-
Topographic Changes	-	-	383-2117	500	5	-	-	-	-
Layering	-	-	383-1115	500	0.3	-	-	-	-
Animal Life	-	-	383-572	300	0.2	-	-	-	-

The two color surface appearance experiments, which constitute the first family in Table 7-6, have identical support requirements. For study of variable surface appearance, both daily and seasonal repetitions are desired (and easily obtained for one percent coverage). The sensor system weight is dominated by the optical subsystem, which weighs about 300 pounds for the 36-inch aperture system. A need for image motion compensation adds slightly to the weight requirement and significantly to the power requirement. Although the resolution requirement could be met by a one-inch vidicon system, an eight meter focal length would result. It is therefore convenient to use the resolution capability of a two-inch RBV system, increasing the size of the imaged area to nearly 4 x 4 km, and reducing the focal length to about two meters. Further movement in this direction is not useful, since for a specific type of image tube, the image format size on the tube faceplate increases faster than the size on the ground of the imaged scene. That is, a three-inch RBV system, for example, would not have a shorter focal length. Even with a 4 x 4 km scene area, three color pictures must be taken in less than one second, before new areas come into view, and the data acquisition rate is 2.4×10^8 bits/sec. For non-color imagery, the data rate would decrease to 5.6×10^7 bits/sec.

The second family or grouping in Table 7-6 consists of stereo experiments for study of structure of features, surface topography, and topographic changes. Since the image specifications for these detailed scale experiments are very nearly identical, as shown in Table 4-1 and the associated worth curves, the experiment support requirements are nearly identical. The only difference in the support requirements is a more stringent pointing accuracy requirement for surface topography and topographic changes than for structure of features. The difference is not apparent in Table 7-6. The orbit selected for this family provides an opportunity for a second coverage of identical areas

one day after the first coverage and hence permit detection of changes in the surface topography. To detect vertical height differences of 50 meters, an imaging system must provide either 28,000 TV lines or 19,000 film lines and therefore a 9½-inch film system has been chosen for these experiments. Even with an IMC-equipped system, the exposure time must be less than about three milliseconds to prevent an unacceptable degree of image smear. To achieve such a short exposure time with the slow speed of SO-243 film, an f/1.3 optical system is required. By using the faster SO-230 film, an f/1.9 optical system of 15-inch aperture may be employed. However, more radiation shielding is required by the faster film, the net result is that the total system weight is very nearly the same whether SO-243 or SO-230 film is used. In either event, 230 feet of film is required for stereo coverage of one percent of Mars surface area. Since 9½-inch SO-230 film provides about 32,000 lines per frame, the excess resolution capability has been used to broaden the ground area per image to 125 x 125 km. This permits the procurement of stereo pairs either along or across the orbital ground trace. Forward stereo (along the ground trace) results in a data acquisition rate of 5.0×10^8 bits/sec, while side stereo (across the ground trace) results in a data acquisition rate of 2.5×10^8 bits/sec.

By using a faster film (SO-102) it is possible to obtain stereo color imagery. Because of the reduced resolution capability of the faster film, the maximum area per image is 105 x 105 km (at periapse) and a vertical resolution of 46 meters is possible. The imaging system weight is dominated by 180 lbs of radiation shielding and the 160 lb 14-inch aperture camera system. The data acquisition rate increases somewhat to 1.2×10^9 bits/sec, the decrease in the number of resolution elements per frame being more than compensated by the reduced image cycle time.

During this study, orbits were selected to satisfy

the image specifications with regard to proper lighting conditions, image overlap, planetary coverage, and mission duration (time required to achieve the desired planetary coverage). No detailed effort was made to minimize the experiment support requirements by varying the orbital parameters, although such considerations did play a role in orbit selection. In some cases, the orbit selected was a poor one, in the sense that the resulting imaging system design configurations were clearly beyond the current state-of-art. It is important to distinguish between two different situations. In the first, an orbit may be selected, and an attempt made to design the imaging system. The system designer may note that although system capabilities render the experiment unfeasible from one orbit, a somewhat different orbit would result in system configurations within the state-of-art. This is the case with the third family in Table 7-6, for which no support requirements are listed. Detailed scale visual imagery at Mars requires imaging systems which push current technologies to their limits, and hence adequate experiment design often depends upon a close communication between the imaging system designer and the orbit mechanistic, usually involving design iteration. Such detailed design can be adequately performed only within the context of a specific mission, where tradeoff criteria can be clearly defined, and consequently is beyond the scope of the research effort reported here. The second situation which arises is that no amount of iteration will result in imaging systems within the current state-of-art. This is the case for the last group of experiments given in Table 7-6. This type of situation can often be recognized without an undue amount of iteration, and this study attempts to point out such basic incompatibilities between scientific requirements, orbital mechanics, and imaging system design.

With this philosophical background, it is useful to consider the remaining two families of experiments listed in Table 7-6. The low-sun-angle family uses an elliptic sun-

synchronous orbit on which the spacecraft altitude varies from 383 to 2117 km as the spacecraft passes over the properly illuminated area on Mars. In attempting to achieve 5 meter ground resolution from an altitude of 2117 km under operational conditions, a television system will require an optical subsystem of greater than 2 meter aperture - clearly beyond the current state-of-art. A film system, on the other hand, because of a somewhat better system modulation transfer function, requires only a 1.5 meter aperture, but the optical system would then weigh about 900 pounds. Even with this massive optical system, a fast film (AEI greater than 40) is required, and no currently available fast film provides the necessary resolution. A slower film could be used, but only if the optical system diameter is increased to beyond 2 meters.

An alternative design approach would be to select a different orbit with less altitude variation over the illuminated surface area, or to restrict the altitude range of imaging operation on the originally selected orbit. For example, the orbit selected for this family of experiments using the arrival conditions appropriate to the 1988 launch opportunity is a 1027 km circular sun-synchronous orbit. From this constant altitude, a one meter aperture optical subsystem, weighing about 400 lbs, is required. A one-half-inch vidicon tube could be employed, but the small field-of-view would necessitate a seven meter focal length. By using a two-inch RBV system, with an image ground size of 9 x 9 km, the focal length is reduced to 2.5 meters. With an image cycle time of 2.9 seconds, the data acquisition rate is 1.4×10^7 bits/sec. The total system weight would be about 480 pounds, and the system average power consumption would be about 30 watts. For this family of experiments, there is no basic incompatibility between scientific requirements, orbital mechanics consideration, and imaging system design. However, experiment design iterations must be performed to keep the system

design within feasible limits.

For the fourth family of experiments in Table 7-6, an order of magnitude improvement in the ground resolution is required. Even from an altitude of 383 km, the required optical aperture is well in excess of two meters, if allowance is made for image degradation in the non-optical system components. That is, the classical diffraction limit is very nearly one meter optics, and it has been shown in Volume IV that any real system must use optical systems with apertures on the order of five times the classical diffraction limit. Since a 383 km orbit periapse is the lowest possible periapse from the standpoint of orbit decay, this family exhibits a basic incompatibility between scientific requirements and orbit mechanics. Visual imaging experiments for the study of surface layering or animal life cannot be performed from orbit about Mars.

In summary, all non-color visual imaging experiments for the study of atmospheric phenomena at Mars can be performed from orbit by a one-half-inch vidicon system (eight pounds, eight watts, 5000 - 25000 bits/sec), except for cloud formation experiments. Because of the combination of large imaged areas and high resolution, cloud formation experiments require a one-inch vidicon system (16 lbs, 16 watts, 7500 bits/sec). Color atmospheric experiments, performed by using a three-color filter wheel, have similar support requirements to the non-color experiments, except that the data rate may be increased by a factor of two. The support requirements for surface imagery experiments tend to fall within one of three groups, depending upon the size of the imaged area and the required ground resolution. Thus visual imaging systems capable of obtaining regional scale surface imagery weigh about 15 to 30 pounds, consume about 15 to 30 watts of power, and acquire data at the rate of 5,000 to 500,000 bits/sec. Imaging systems for local scale imagery weigh 30 to 60 pounds, consume 30 to 100 watts, and acquire data at 10^6 to 10^7 bits/sec. Imaging systems for detailed scale

imagery weigh 300 to 500 pounds, consume 30 to 300 watts, and acquire data at 10^7 to 10^8 bits/sec. Within each of these groups, color experiments have similar support requirements as non-color experiments, except that the data rate may be increased a factor of two. Also low-sun-angle experiments tend to have support requirements near the low end of the ranges given above, while stereo experiments tend to have support requirements near the high end.

Some basic incompatibilities between scientific requirements and orbital mechanics constraints have been identified by the experiment design analysis performed here. It is difficult to obtain visual imagery of large areas of Mars in a short time. Daylight coverage of 70 percent of the planet can only be achieved in one day by large field-of-view systems at low altitudes or by high resolution systems at high altitudes. In either case, the support requirements must be increased over those given above. The situation is aggravated when constraints are also imposed upon the desired surface illumination. Thus when solar zenith angles of less than 20 degrees are required, as is the case for stereo coverage, a minimum of approximately 335 days are required for illumination of 70 percent of the planet. When the same area of Mars is to be observed a second time to discover temporal variations in the surface or atmospheric phenomena, the second observation must follow quickly on the same orbital pass or must wait at least until the next pass one orbit period later (a minimum of 2-3 hrs. later). That is, image repetition times longer than a few minutes and shorter than a few hours are not possible for single spacecraft orbital missions. However, no severe difficulties are encountered in obtaining seasonal coverage as is desired for many imaging experiments at Mars.

7.2.2 Venus

As previously indicated by Table 7-3, visual imagery from orbit about Venus is expected to be useful only in the study of atmospheric phenomena. It is highly unlikely that the surface of Venus can be observed in the visible portion of the spectrum from orbital altitudes. Table 7-7 summarizes the weight, power, and data acquisition rates for visual imaging experiments at Venus. As with Mars, the support requirements for atmospheric imagery are relatively modest. Orbital imaging experiments at Venus are greatly influenced by the slow planetary rotation rate. The discussion in Section 5.2.2 has shown that from an inertial orbit only 50 percent daylight coverage can be achieved, unless a costly plane change is made sometime during the mission. Furthermore, more than 100 days in orbit are required to achieve the available 50 percent coverage. Sun-synchronous orbits could provide an opportunity for complete daylight coverage, but such orbits do not appear feasible for Venus. Thus, with the exception of cloud formation experiments, none of the regional scale experiments can be adequately performed at Venus, unless an expensive plane change maneuver is performed.

Another difference between Mars and Venus is the size of the planets, Venus being nearly twice the diameter of Mars. Thus for global cloud coverage experiments, the minimum scene area which is useful is larger for Venus than for Mars. An attempt to image such large areas from low altitudes is somewhat self-defeating, since near the edges of the imaged area the line-of-sight is nearly horizontal. For this reason, a 1½-inch vidicon system must be used in obtaining global cloud coverage imagery from a 454 km altitude circular orbit. Increasing the orbit altitude to about 1000 km would permit use of a one-half-inch vidicon system with decreased support requirements. With this in mind, the increase in support requirements resulting from imaging over a large range of orbit altitudes is more apparent than is immediately obvious from study of the first

Table 7-7
Support Requirements for Visual
Experiments-Venus

OBSERVABLE	COLOR	IMAGING ALTITUDE (km)	IMAGE GROUND SIZE (km)	RESOLUTION (km)	CAMERA	WEIGHT (lbs)	POWER (watts)	DATA RATE (bits/sec)
Global Cloud Coverage	-	454	1500	20	1½" VID	24	24	1.3 x 10 ⁴
Global Cloud Coverage	X	454	1500	20	1½" VID	24	24	2.2 x 10 ⁴
Global Cloud Coverage	-	248-1297	1500	20	2" RBV	32	32	3.8 x 10 ⁵
Global Cloud Coverage	X	248-1297	1500	20	2" RBV	32	32	6.2 x 10 ⁵
Convective Cells and Turbulence (regional)	-	454	600	20	½" VID	8	8	6.2 x 10 ³
Cyclone Formations (regional)	-	454	600	20	½" VID	8	8	6.2 x 10 ³
Auroras	-	454	600	20	½" VID	8	8	6.2 x 10 ³
Auroras	X	454	600	20	½" VID	8	8	1.9 x 10 ⁴
Convective Cells and Turbulence (regional)	-	255-2125	600	20	1" VID	16	16	1.5 x 10 ⁴
Cyclone Formations (regional)	-	255-2125	600	20	1" VID	16	16	1.5 x 10 ⁴
Auroras	-	255-2125	600	20	1" VID	16	16	1.5 x 10 ⁴
Auroras	X	255-2125	600	20	1" VID	16	16	4.5 x 10 ⁴
Cloud Formation	-	454	600	3	1½" VID	24	24	1.7 x 10 ⁴
Cloud Formation	X	454	600	3	1½" VID	24	24	5.0 x 10 ⁴
Cloud Formation	-	255-2125	600	3	2" RBV	32	32	7.2 x 10 ⁵
Convective Cells and Turbulence (detailed)	-	454	100	3	½" VID	8	8	3.8 x 10 ⁴
Cyclone Formations (detailed)	-	454	100	3	½" VID	8	8	3.8 x 10 ⁴

grouping in Table 7-7. As is the case at Mars, color imagery with television systems may or may not increase the data rate by a factor of three over the non-color rate, depending upon the image cycle time. Of course, the total mission or orbit data load would increase by a factor of three.

The other experiment groupings in Table 7-7 also show that the support requirements have this same dependence upon the altitude range from which the imagery is obtained and the use of a three-color filter wheel. It may be noted that no visual imaging experiment at Venus requires the use of film systems. In fact, except for cloud formation imagery, all the experiments are within reach of a one-half inch vidicon system. This was also the case at Mars, for atmospheric experiments.

In summary, visual imaging experiments at Venus have approximately the same support requirements as similar experiments at Mars. The essential differences are that more than half of Venus cannot be observed without changing the orbit, this coverage cannot be obtained more than twice per Venus year, but the same areas can be overflowed many times at intervals greater than 1.6 hours. This facilitates time-lapse imagery which is useful for studies of convective cells and turbulence, cyclone formations, and auroras. For cloud formation studies, these image interval times are longer than desired, but interval times of less than one minute can be achieved on the same orbital pass by increasing the amount of forward overlap.

7.2.3 Mercury

Table 7-8 summarizes weight, power, and data acquisition rate requirements for visual imaging experiments at Mercury. As with all the support requirements summarized in this section, a more detailed list is given in Volume V for each experiment. Since Mercury has no atmosphere, only surface imaging experiments are listed. The support requirements at Mercury are very similar to those found at Mars for analogous experiments. For example,

Table 7-8
Support Requirements for Visual
Experiments-Mercury

OBSERVABLE	STEREO	COLOR	IMAGING ALTITUDE (km)	IMAGE GROUND SIZE (km)	HORIZONTAL RESOLUTION (km)	CAMERA	WEIGHT (lbs)	POWER (watts)	DATA RATE (bits/sec)
Surface Winds (regional)	-	-	500	600	20	1/2" VID	8	8	3.9 x 10 ³
Surface Winds (regional)	-	-	500-2120	600	20	1/2" VID	8	8	3.9 x 10 ³
Surface Elevations	-	-	500	600	3	2" RBV	32	32	3.8 x 10 ⁵
Contacts (regional)	-	-	500	600	3	1 1/2" VID	24	24	1.2 x 10 ⁴
Structure of Features (regional)	-	-	500	600	3	1 1/2" VID	24	24	1.2 x 10 ⁴
Surface Topography (regional)	-	-	500	600	3	2" RBV	32	32	3.8 x 10 ⁵
Surface Appearance (regional)	-	-	500	600	3	1 1/2" VID	24	24	1.2 x 10 ⁴
Structure of Features (regional)	-	X	500	600	3	1 1/2" VID	24	24	1.6 x 10 ⁴
Surface Appearance (regional)	-	X	500	600	3	1 1/2" VID	24	24	1.6 x 10 ⁴
Surface Elevations	X	-	500	600	3	2" RBV	32	32	3.8 x 10 ⁵
Structure of Features (regional)	X	-	500	600	3	2" RBV	32	32	3.8 x 10 ⁵
Surface Topography (regional)	X	-	500	600	3	2" RBV	32	32	3.8 x 10 ⁵
Surface Elevations	-	-	500-2910	600	3	2 1/2" RBV	40	40	4.9 x 10 ⁵
Contacts (regional)	-	-	500-2910	600	3	2" RBV	32	32	3.8 x 10 ⁵
Structure of Features (regional)	-	-	500-2910	600	3	2" RBV	32	32	3.8 x 10 ⁵
Surface Topography (regional)	-	-	500-2910	600	3	2 1/2" RBV	40	40	4.9 x 10 ⁵
Surface Appearance (regional)	-	-	500-2910	600	3	2" RBV	32	32	3.8 x 10 ⁵
Surface to Atmosphere Transfer	-	-	500	300	3	1/2" VID	8	8	3.9 x 10 ³
Surface to Atmosphere Transfer	-	X	500	300	3	1/2" VID	8	8	1.1 x 10 ⁴
Contacts (local)	-	-	500	100	0.2	2" RBV	32	32	1.1 x 10 ⁶
Structure of Features (local)	-	-	500	100	0.2	2" RBV	32	32	1.1 x 10 ⁶
Surface Topography (local)	-	-	500	100	0.2	2" RBV	32	32	1.1 x 10 ⁶
Surface Appearance (local)	-	-	500	100	0.2	2" RBV	32	32	1.1 x 10 ⁶
Surface Winds (local)	-	-	500	100	0.2	2" RBV	32	32	7.6 x 10 ⁵
Structure of Features (local)	-	X	500	100	0.2	2" RBV	32	32	3.3 x 10 ⁶
Structure of Features (local)	X	-	500	100	0.2	70mm(SO-243)	44	36	2.5 x 10 ⁶
Surface Topography (local)	X	-	500	100	0.2	5" (SO-243)	96	50	9.6 x 10 ⁶
Contacts (detailed)	-	-	500	0.5	0.005	2" RBV	190	32	1.5 x 10 ⁷
Structure of Features (detailed)	-	-	500	0.5	0.005	2" RBV	190	32	1.5 x 10 ⁷
Surface Topography (detailed)	-	-	500	0.5	0.005	2" RBV	190	32	1.5 x 10 ⁷
Surface Appearance (detailed)	-	-	500	0.5	0.005	2" RBV	190	32	1.5 x 10 ⁷
Topographic Changes	-	-	500	0.5	0.005	2" RBV	190	32	1.5 x 10 ⁷
Structure of Features (detailed)	-	X	500	0.5	0.005	4 1/2" RBV	190	87	5.4 x 10 ⁷
Surface Appearance (detailed)	-	X	500	0.5	0.005	4 1/2" RBV	190	87	5.4 x 10 ⁷
Structure of Features (detailed)	X	-	508	0.5	0.005	9 1/2" (SO-243)	210	110	3.9 x 10 ⁷
Surface Topography (detailed)	X	-	500	0.5	0.005	9 1/2" (SO-243)	300	110	1.2 x 10 ⁸
Surface Topography (detailed)	X	-	500	0.5	0.005	9 1/2" (SO-243)	400	110	1.2 x 10 ⁸
Topographic Changes	-	-	500	0.5	0.005	-	-	-	-
Layering	-	-	500	0.5	0.003	-	-	-	-

local scale stereo experiments for study of surface topography can be performed at Mercury using a five-inch S0-243 film system just as at Mars. However, the film systems tend to weigh more at Mercury than at Mars because more massive amounts of radiation shielding is required. Also, the same trends are present in the support requirements - color experiments have support requirements similar to non-color experiments except the data rate is usually higher, stereo experiments weigh more, consume more power, and acquire data more rapidly than non-stereo experiments, and experiments performed from a range of altitudes have more demanding support requirements than analogous experiments performed from a circular orbit.

There are no incompatibilities between the scientific requirements and the orbital mechanics constraints for local and detailed scale experiments. (The layering experiment requires optical system of greater than two meters aperture and is thus not feasible). However, for regional scale experiments involving nearly noon-time solar illumination, the desired amounts of Mercury are not properly illuminated. Thus for color imagery, for which the solar zenith angle should be less than 40 degrees, only 64 percent of Mercury's surface is properly illuminated, and only about half of Mercury can be imaged from an inertial orbit. Similarly, for stereo coverage, for which the solar zenith angle should be less than 20 degrees, only 34 percent of Mercury's surface is properly illuminated, and thus only 15 percent of the surface can be properly imaged from orbit. At that, nearly two Mercury years (about 180 Earth days) are required to attain the available coverage. Time-lapse imagery, with image intervals of about two or more hours, is easily achieved, but is required for only a few of the experiments.

7.2.4 Jupiter

Atmospheric phenomena can be usefully imaged in the visible portion of the spectrum from orbit about Jupiter.

Table 7-9 summarizes typical weight, power, and data rate requirements for such experiments. The most obvious conclusion is that a two-inch RBV system is adequate for visual imagery at Jupiter. High orbital altitudes have been chosen to minimize the hazard from the Jovian radiation belts, hence the optical systems used with the RBV tend to be large. For those experiments requiring 20 km "ground" resolution, the optical system has a focal length from 20 to 60 cm and a lens aperture from 10 to 20 cm. For the three km ground resolution experiments, a 90 cm lens with a 2 meter focal length is used. Variations in experiment weight arise solely from variations in the optical system. In all cases, more than 100 seconds is required to fly from one area to a new area, and hence the use of a three-color filter wheel has no effect on the data rate. It does, of course, increase the total amount of data. Because of Jupiter's fast rotation rate, all the coverage and image interval time requirements can be achieved by proper orbit selection.

7.3 Infrared Scanning Systems

The usefulness of orbital infrared imagery in the exploration of Mars, Mercury, Venus and Jupiter is indicated in Table 7-10. The blackness of each circle is proportional to the usefulness of the imagery; a completely black circle indicating that imagery from orbit is expected to be very useful, a completely white circle indicating that imagery from orbit is not very useful. For details of these assessments, the reader is referred to Volume II (Definitions of Scientific Objectives). At Venus and Jupiter, infrared imagery is expected to be very useful in the study of nearly all atmospheric phenomena, while at Mars and Mercury, infrared imagery is expected to be very useful in the detection thermal anomalies on the surface and useful in the study of lithologic contacts. Although no distinction is apparent in the table, detection of both reflected solar and thermally emitted infrared energy is useful. In particular, reflected

Table 7-9
Support Requirements for Visual
Experiments-Jupiter

OBSERVABLE	COLOR	IMAGING ALTITUDE (radii)	IMAGE GROUND SIZE (km)	GROUND RESOLUTION (km)	CAMERA	WEIGHT (lbs)	POWER (watts)	DATA RATE (bits/sec)
Global Cloud Coverage	-	5.5-9.3	15,000	20	2" RBV	55	32	3.8×10^5
Global Cloud Coverage	-	2.5-5.0	15,000	20	2" RBV	37	32	3.8×10^5
Global Cloud Coverage	X	5.5-9.3	15,000	20	2" RBV	55	32	3.8×10^5
Global Cloud Coverage	X	2.5-5.0	15,000	20	2" RBV	37	32	3.8×10^5
Convective Cells and Turbulence (regional)	-	5.5-9.3	5,000	20	2" RBV	45	32	3.8×10^5
Convective Cells and Turbulence (regional)	-	4.0-7.5	5,000	20	2" RBV	40	32	3.8×10^5
Convective Cells and Turbulence (regional)	-	2.5-5.3	5,000	20	2" RBV	36	32	3.8×10^5
Cloud Formation	-	3.0-6.7	5,000	20	2" RBV	39	32	3.8×10^5
Cloud Formation	-	4.0-7.5	5,000	20	2" RBV	40	32	3.8×10^5
Cyclone Formations (regional)	-	5.5-9.3	5,000	20	2" RBV	32	32	3.8×10^5
Cyclone Formations (regional)	-	4.0-7.5	5,000	20	2" RBV	40	32	3.8×10^5
Cyclone Formations (regional)	-	2.5-5.3	5,000	20	2" RBV	36	32	3.8×10^5
Auroras	-	5.0-8.1	5,000	20	2" RBV	42	32	3.8×10^5
Cloud Formation	X	3.0-6.7	5,000	20	2" RBV	39	32	3.8×10^5
Cloud Formation	X	4.0-7.5	5,000	20	2" RBV	40	32	3.8×10^5
Auroras	X	5.0-8.1	5,000	20	2" RBV	42	32	3.8×10^5
Convective Cells and Turbulence (detailed)	-	3.0-6.7	1,000	3	2" RBV	280	32	3.8×10^5
Cyclone Formations (detailed)	-	3.0-6.7	1,000	3	2" RBV	280	32	3.8×10^5

infrared energy is expected to be useful in imagery of contacts, global cloud coverage, cloud formation, and cyclone formations, while thermally emitted infrared imagery is useful for all the phenomena listed in the table except contacts.

Table 7-10

Utility of Orbital Infrared Imagery

	MARS	MERCURY	VENUS	JUPITER
Contacts	●	●		
Surface Thermal Anomalies	●	●		
Atmospheric Thermal Anomalies	○		●	●
Global Cloud Coverage	○		●	●
Convective Cells & Turbulence	●		●	●
Cloud Formation	○		●	●
Cyclone Formations	○		●	●
Surface-to-Atmosphere Transfer	○		●	●

7.3.1 Mars

Weight, power, and data rate requirements for orbital infrared - imaging experiments at Mars are shown in Table 7-11. The experiments in the table are grouped according to minimum acceptable image ground size, or scan length on the planetary surface. These groupings correspond to regional, local, and detailed scale experiments. There is a very close correlation between the support requirements and the size of the scanning beam (system angular resolution). The scanning beam size in turn is directly related to the imaging altitude and the required ground resolution and indirectly to the scan length.

TABLE 7-11
SUPPORT REQUIREMENTS FOR INFRARED
EXPERIMENTS-MARS

OBSERVABLE	IMAGING ALTITUDE (km)	SCAN LENGTH (km)	RESOLUTION (km)	SCANNING BEAM SIZE (deg)	WEIGHT (lbs)	POWER (watts)	DATA RATE (bits/sec)
Convective Cells (regional)	969	600	20	1.0	2	2	300
Surface Thermal Anomalies (regional)	425	600	3	0.25	6	2	8400
Surface Thermal Anomalies (regional)	969	600	3	0.16	6	2	3300
Contacts (regional)	969	600	3	0.16	2	4	13000
Convective Cells (local)	340-370	100	3	0.45	6	2	3700
Surface Thermal Anomalies (local)	340-370	100	0.2	0.03	38	4	8300
Contacts (local)	340-976	100	0.2	0.012	410	28	2.8×10^6
Surface Thermal Anomalies (detailed)	340-370	0.5	0.005	—	—	—	—
Contacts (detailed)	383-2117	0.5	0.005	—	—	—	—

The regional scale experiments show surprisingly small weight, power, and data rate requirements. The convective cells and turbulence experiment design uses a thermistor operating in either the 6-14 μ band or the 20-40 μ band, avoiding the strong CO₂ absorption band at about 17 μ . The support requirements are the same in either case, and are based on a required temperature resolution of two deg K (appropriate for all thermal imagery experiments at Mars). The 969 km altitude circular polar orbit selected for this experiment affords complete planetary coverage every five days. Seasonal coverage is desired and easily obtained. Two surface thermal anomalies experiments are listed in the table, both using a thermistor detector over a broad band from 2 to 50 μ . The first uses an elliptic orbit with imaging performed only in the immediate vicinity of periapse at 425 km, the second a circular orbit of 969 km altitude with imaging performed over half the orbit. The higher ground speed of the elliptic orbit results in a higher data rate, but affords imagery of the same area after 25 hours as desired. The second provides an image interval of five days (actually complete planetary coverage every five days) with a less expensive capture maneuver and a lower data rate, because of the lower ground speed. The contacts experiment uses a PbS detector operating at 295 deg K from a sun-synchronous circular orbit providing 74 percent coverage every five days. A one-faced scanning mirror has been used. The data rate could easily be reduced a factor of two by using a two-sided scanning mirror with a very small increase in the system weight. Again, this emphasizes the amount of design flexibility available to the experiment designer, and the support requirements given here must be regarded as typical rather than optimized in any sense.

As with the regional scale experiment, the local scale convective cells experiment utilizes a thermistor operating either in the 6-14 μ band or in the 20-40 μ band. For local scale thermal anomalies, a better ground resolution, and hence

a more sensitive detector is required. An aluminum-doped silicon detector operating at 23 deg K has been chosen. The solid neon cooling system accounts for most of the sensor system weight. The deleterious effects of acquiring imagery over an appreciable range of altitudes is shown by the local scale contacts experiment. The angular resolution is set by the ground resolution which must be achieved even from an altitude of 976 km. The resulting small scanning beam size requires a large collecting aperture (31 cm) to collect enough energy when used with a linear array of 50 PbS detectors at 295 deg K. By operating the linear array at 195 deg K and using a radiation cooling system, the system weight could be reduced to about 100 pounds and the collector diameter to about 15 cm. The required operating power and data rate would remain unchanged.

The detailed scale experiments involve angular resolutions leading to diffraction-limited optical systems greater than one meter aperture, and hence beyond the current (and foreseeable) state-of-art. For Mars, the peak of the black body spectral emission curve occurs at about 15μ , and at this wavelength the collecting system must be at least 1.3 meters in diameter to achieve a five meter resolution from 370 km. Even if a sufficiently sensitive detector were available and the required optical system could be constructed, the sensor system would weigh well over 400 pounds. For the contacts experiment, a similarly sized optical system is necessary, the increase in orbit altitude counterbalancing the decrease in operating wavelength to about two microns.

In summary, infrared scanning experiments providing ground resolutions of 3 km weigh about five pounds, consume about three watts of power, and collect data at 10,000 bits/sec, or less. For ground resolutions of about 200 meters, a typical infrared imaging system might weigh 50-100 pounds, consume 5-30 watts, and collect data at 10^5 or 10^6 bits/sec. Detailed scale experiments at five meter resolution appear to be unfeasible.

In comparison with visual imaging experiments, infrared experiments appear to have support requirements roughly comparable to visual experiments on the regional and local scale, but the technology is not as well developed as for visual systems and thus detailed scale imagery is impossible at the current level of development. Of course, infrared systems can provide data on the thermal environment of the imaged scene, while visual systems cannot, except quite indirectly. Furthermore, a freedom from stringent illumination constraints permits greater latitude in orbit selection, facilitating achievement of coverage and time-lapse imagery requirements.

7.3.2 Venus

Table 7-12 summarizes some of the support requirements for orbital infrared scanning imagery at Venus. The thermal imaging experiments have been based on a required temperature resolution of five deg K. All the experiments desired at Venus are quite feasible, and have rather modest support requirements. This is because ground resolutions of only three km and temperature resolutions of only five deg K (compared to two deg K at Mars) are necessary. As with other imaging experiments, the support requirements are increased when imagery is obtained over a significant altitude variation, as compared to constant altitude imaging operations. Detector cooling is not necessary at Venus. Reflected sunlight imagery is obtained by PbS detectors, thermal imagery by thermistors. Virtually all the scientific requirements are met, except that complete planetary coverage cannot be achieved in less than about 120 Earth days.

7.3.3 Mercury

Table 7-13 summarizes the weight, power, and data rate requirements of orbital infrared imagery at Mercury. The support requirements for regional scale imagery (3 km ground resolution) are similar to those at Mars and Venus. The regional contacts experiment does not quite satisfy the scientific require-

TABLE 7-12
SUPPORT REQUIREMENTS FOR INFRARED
EXPERIMENTS-VENUS

OBSERVABLE	IMAGING ALTITUDE (km)	SCAN LENGTH (km)	RESOLUTION (km)	SCANNING BEAM SIZE (deg)	WEIGHT (lbs)	POWER (watts)	DATA RATE (bits/sec)
Global Cloud Coverage	454	1500	20	0.57	3	2	5400
Atmospheric Thermal Anomalies (regional)	454	1500	20	0.57	3	2	5400
Atmospheric Thermal Anomalies (regional)	248-1297	1500	20	0.35	8	3	19000
Convective Cells (regional)	454	600	20	1.7	2	2	630
Cyclone Formations (regional)	454	600	20	1.7	2	2	630
Surface-to-Atmosphere Transfer	454	600	20	1.7	2	2	630
Cyclone Formations (regional)	255-2125	600	20	0.52	2	4	8200
Surface-to-Atmosphere Transfer	255-2125	600	20	0.52	4	2	8200
Cloud Formation	454	600	3	0.25	2	4	7000
Atmospheric Thermal Anomalies (local)	454	100	3	0.37	3	2	4300
Convective Cells (local)	454	100	3	0.37	4	2	4300
Cyclone Formations (local)	454	100	3	0.37	4	2	4300

TABLE 7-13

SUPPORT REQUIREMENTS FOR INFRARED
EXPERIMENTS-MERCURY AND JUPITER

PLANET	OBSERVABLE	IMAGING ALTITUDE	SCAN LENGTH (km)	RESOLUTION (km)	SCANNING BEAM SIZE (deg)	WEIGHT (lbs)	POWER (watts)	DATA RATE (bits/sec)
MERCURY	Contacts (regional)	500 km	600	3	0.23	2	4	11000
MERCURY	Surface Thermal Anomalies (regional)	500 km	600	3	0.23	11	7	5300
MERCURY	Surface Thermal Anomalies (regional)	500-1540 km	600	3	0.10	11	7	12000
MERCURY	Contacts (local)	500 km	100	0.2	0.023	77	4	1.1×10^6
MERCURY	Surface Thermal Anomalies (local)	500 km	100	0.2	0.023	25	4	1.1×10^6
MERCURY	Contacts (detailed)	500 km	0.5	0.005	—	—	—	—
MERCURY	Surface Thermal Anomalies (detailed)	500 km	0.5	0.005	—	—	—	—
JUPITER	Global Cloud Coverage	2.5-5 radii	15000	20	0.003	1400	28	1.1×10^6
JUPITER	Atmospheric Thermal Anomalies (regional)	2.5-5 radii	15000	20	—	—	—	—
JUPITER	Cyclone Formations (regional)	2.5-5.3 radii	5000	20	0.003	1600	28	1.2×10^6
JUPITER	Atmospheric Thermal Anomalies (local)	5-8 radii	1500	3	—	—	—	—

ments in that only 63 percent (rather than 70 percent) planetary coverage is achieved, which is the most which can be attained with an inertial orbit. The support requirements for surface thermal anomalies are based on a five deg K temperature resolution. The weight of the local scale contacts experiment can probably be reduced to that of the local scale surface thermal anomalies experiment by operating the PbS detector at 195, rather than 295, deg K. The local scale thermal anomalies experiment employs a boron-doped silicon detector operating at 23 deg K. The cooling system is relatively small because of a short mission duration (60 days). The detailed scale experiments are not feasible at the current state-of-art. The contacts experiment requires an order of magnitude increase in detector sensitivity, the thermal anomalies experiment, (which demands a longer wavelength) has a diffraction-limited collecting system in excess of one meter aperture. Disregarding the detailed scale experiments, all the scientific requirements for infrared imagery at Mercury can be satisfied, except for the regional scale contacts experiment as noted above.

7.3.4 Jupiter

Table 7-13 also summarizes the support requirements implied by infrared imagery at Jupiter. In addition to the staggering support requirements, neither of the two feasible (?) experiments listed completely satisfy the scientific requirements. Infrared imagery of Jupiter is difficult to obtain from orbit because of the high orbital altitudes required to reduce exposure to the radiation belts, the small amount of both reflected solar and thermally emitted energy, and the two deg K temperature resolution required. Even using the best available detector (PbS at 195 deg K), the global cloud coverage experiment involves a large collecting aperture (80 cm) and a correspondingly massive scanning system. Furthermore, about 15 minutes is required to scan an area 15000 x 15000 km, exceeding the desired acquisition

time by nearly an order of magnitude. Because of Jupiter's low temperature, thermal imagery should be obtained at about 30 μ wavelength. Using the best available detectors, a collector aperture of two meters is required for imagery of thermal anomalies. The cyclone formations experiment is similar to the global cloud coverage experiment, except that the image acquisition time is reduced to about five minutes - one minute is required by the image specifications of Table 4-1.

7.4 Passive Microwave Scanning Systems

The analysis of planetary exploration scientific objectives presented in Volume II indicates that passive microwave imaging systems are potentially useful for the observation of both surface and atmospheric thermal anomalies, convective cells and turbulence, and surface to atmosphere transfer. This assessment is summarized in Table 7-14, where it is seen that passive microwave systems are of most value at Venus and Jupiter. This is primarily because Mars and Mercury have no significant atmosphere, hence the study of atmospheric structure and dynamics does not contribute materially to an understanding of these planets.

Table 7-14

Utility of Orbital Passive Microwave Imagery

<u>Observable</u>	MARS	VENUS	MERCURY	JUPITER
Surface Thermal Anomalies	●	●	●	●
Atmospheric Thermal Anomalies	○	●	●	●
Convective Cells and Turbulence		●	●	●
Surface to Atmosphere Transfer		●	●	●

Experiment support requirements have been estimated for all those planet-observable combinations identified in Table 7-14 as useful or very useful. These support requirements are summarized in Table 7-15, more detailed results are provided for these experiments in Volume V. For each experiment shown in the table, the support requirements are based upon minimal achievement of the appropriate image specifications, as determined by the various worth curves. In some cases, it is not possible to achieve the necessary temperature resolution because of state-of-art constraints on the sensor system design. These cases are identified in the table by the asterisk placed upon the desired temperature resolution values. The table shows that only at Venus can any of the desired imagery be obtained, within the constraints imposed by the orbital selections and current microwave system technology.

At Mars, only regional scale microwave experiments are at all feasible. Two alternate orbits have been chosen for the regional surface thermal anomalies experiment. The first is a circular polar orbit providing complete coverage of Mars every five days. The second is an elliptic polar orbit on which imagery is obtained only in the immediate vicinity of the 425 km periapse, thus sacrificing mission duration for a lower imaging altitude and a more economical capture maneuver. Approximately 120 days is required to achieve 70 percent planetary coverage. The lower imaging altitude results in a dramatic decrease in antenna weight, although the two experiments are not quite comparable. The first experiment provides a temperature resolution of 4.6 deg K, the second 7.4 deg K. A temperature resolution of two deg K cannot be achieved, even by a noise-free receiver. An electrically-scanned antenna has been used in both cases. The local and detailed scale experiments cannot be performed because the required antenna size and beam switching time exceeds the current state-of-art by orders of magnitude. It would appear that surface thermal anomalies at Mars are much easier

Table 7-15
Support Requirements for Passive
Microwave Imaging Experiments

PLANET	OBSERVABLE	SCAN LENGTH(KM)	SPATIAL RESOLUTION (KM)	TEMPERATURE RESOLUTION (DEG K)	IMAGING ALTITUDE (KM)	FREQUENCY (GHz)	WEIGHT (LBS)	POWER (WATTS)	DATA RATE (bits/sec)	TOTAL SCAN ANGLE (DEG)	SCANNING BEAM SIZE (DEG)
MARS	Surface Thermal Anomalies (regional)	600	3	2*	969	13	1200	110	1400	34	0.15
MARS	Surface Thermal Anomalies (regional)	600	3	2	425	13	600	100	3200	69	0.25
MARS	Surface Thermal Anomalies (local)	100	0.2	2	340-370	-	-	-	-	-	-
MARS	Surface Thermal Anomalies (detailed)	0.5	0.005	2	340-370	-	-	-	-	-	-
VENUS	Surface Thermal Anomalies (regional)	1000	3	5	454	-	-	-	-	-	-
VENUS	Surface Thermal Anomalies (local)	100	0.2	5	454	-	-	-	-	-	-
VENUS	Surface Thermal Anomalies (detailed)	0.5	0.005	5*	454	-	-	-	-	-	-
VENUS	Atmospheric Thermal Anomalies (regional)	1500	20	5	454	30	100	80	1700	112	0.57
VENUS	Atmospheric Thermal Anomalies (detailed)	100	3	5	454	65	40	70	440	66	0.38
VENUS	Convective Cells and Turbulence (regional)	600	20	5	454	30	17	12	230	66	1.7
VENUS	Convective Cells and Turbulence (detailed)	100	3	5	454	65	40	70	440	66	0.38
VENUS	Surface to Atmosphere Transfer	600	20	5	454	10	32	16	120	67	1.7
MERCURY	Surface Thermal Anomalies (regional)	600	3	5*	500	15	480	100	2100	60	0.23
MERCURY	Surface Thermal Anomalies (local)	100	0.2	5	500	-	-	-	-	-	-
MERCURY	Surface Thermal Anomalies (detailed)	0.5	0.005	5	500	-	-	-	-	-	-
JUPTER	Atmospheric Thermal Anomalies (regional)	15,000	20	2	2.5-5 radii	-	-	-	-	-	-
JUPTER	Atmospheric Thermal Anomalies (detailed)	1,500	3	2	3.5-7.5 radii	-	-	-	-	-	-
JUPTER	Convective Cells and Turbulence (regional)	5000	20	2	3.5-6.2 radii	-	-	-	-	-	-
JUPTER	Convective Cells and Turbulence (detailed)	1000	3	2	2.5-6.7 radii	-	-	-	-	-	-

*This temperature resolution is not achieved.

to observe in the infrared portion of the spectrum than in the microwave.

The surface of Venus cannot be adequately observed from orbit by any passive microwave system which is within reach of the current state-of-art. In order to penetrate the atmosphere, frequencies of less than ten GHz are necessary, implying antenna diameters of about 100 feet for three km resolution. Surprisingly enough, the detailed scale atmospheric thermal anomalies experiment has less demanding support requirements than the corresponding regional scale experiment. This is because the regional scale experiment actually contains more resolution elements per scan line, severely limiting the integration time per resolution element. The operating frequency must therefore be chosen to reduce the bandwidth rather than the antenna size. The regional scale experiment therefore operates at 30 GHz and an antenna size of 7 x 7 ft, while the detailed scale experiment utilizes a 2 x 2 ft antenna at 65 GHz. Even at that, the regional scale experiment provides a temperature resolution of slightly more than six deg K, while five deg K is desired. This design peculiarity does not occur for the convective cells experiments since the regional scale experiment requires scan lengths of only 600 km. This latter experiment is the only passive microwave experiment found for which a mechanically-scanned antenna is feasible. The surface to atmosphere energy transfer experiment does not satisfy the scientific requirements in that 120 days is required to obtain full planetary coverage, rather than 100 hours as desired. As noted with other imaging systems, this is a basic incompatibility between orbital operations and scientific requirements at Venus. Comparison of microwave to infrared imaging at Venus suggests, as at Mars, that for similar scientific objectives infrared imagery can be obtained more easily than passive microwave. However, different information is obtained and may be worth the increased support requirements.

At Mercury and Jupiter, no passive microwave imagery which completely satisfies the scientific requirements can be obtained by imaging systems within reach of the current state-of-art. The only feasible experiment is study of surface thermal anomalies on a regional scale at Mercury. Even operating at the optimum frequency (from the standpoint of the temperature resolution) produces imagery from which temperature differences of only seven deg K can be deduced, while five deg K resolution is required. At that, the relatively long wavelength requires an antenna 21 x 21 ft in size. By increasing the operating frequency, the antenna size could be reduced at the expense of temperature resolution. Enormous antennas are necessary at Jupiter to achieve the desired spatial resolutions from the orbital altitudes considered. The best that can be done with reasonably sized antennas is about 200 km "ground" resolution.

7.5 Radar Imaging Systems

An evaluation of the efficacy of radar imagery in exploring the planets from orbit is shown in Table 7-16. The table is based on data presented in Volume II of this report series. The black circles in the table signify that radar imagery is very useful, the half-black circles useful, the empty circles not very useful. Radar imagery at Venus is considered to be very useful, since it offers the only reasonable chance of observing the surface from orbit. The atmosphere at Jupiter is presumed to be so thick, and the presence of a surface so unknown, that radar imagery is regarded as not very useful. Experiment support requirements have been estimated for all the useful experiments suggested by the table. Only the weight, power, and data rate requirements are reported here. A complete set of support requirements for each useful experiment is given in Volume V. Because radar imagery is most important at Venus, a departure is made in the usual planetary order, and Venus experiments are discussed first here.

Table 7-16

Utility of Orbital Radar Imagery

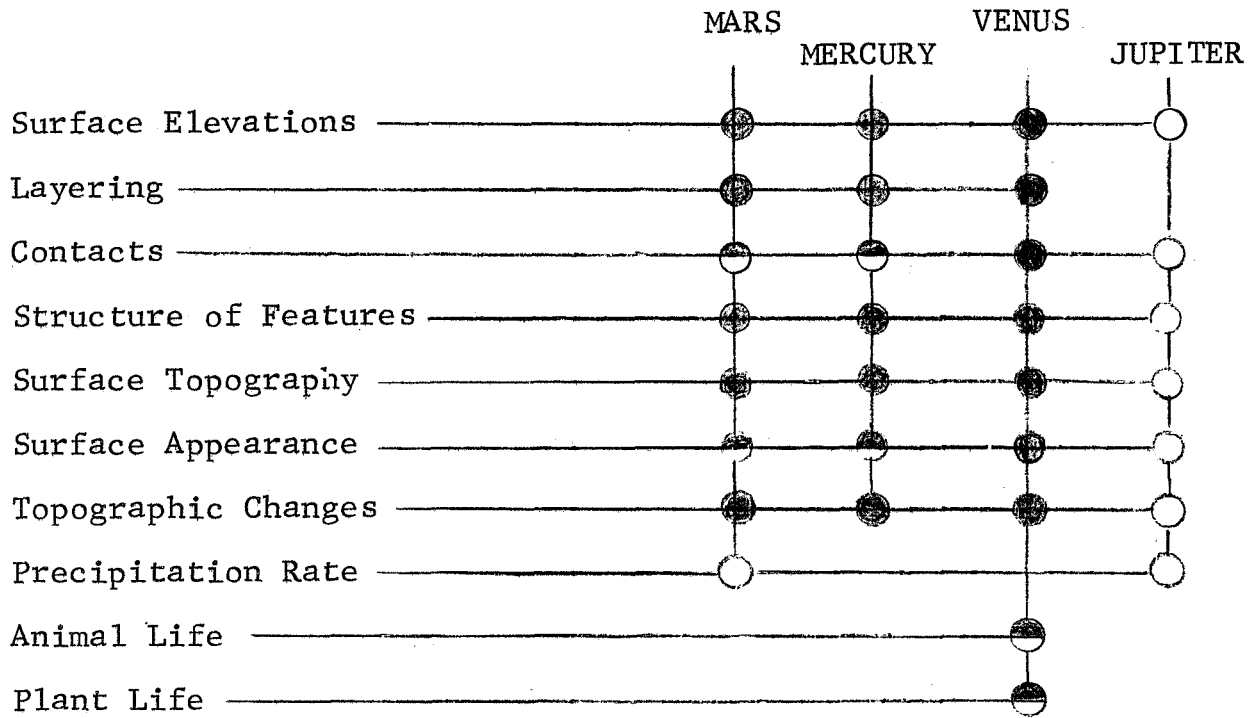


Table 7-17 presents the weight, power, and data rate requirements for various radar experiments at Venus, along with the antenna size and type of radar. Here NC signifies noncoherent radar, while SA indicates a synthetic aperture system. Noncoherent systems were used whenever possible, that is, unless the necessary antenna size exceeded the state-of-art limitations. Vertical height information can be obtained by stereo coverage or by measurement of radar shadow lengths. Only side-looking radar systems were considered. For such systems, stereo coverage can be obtained by passing by the same area twice, that is, by using two orbital passes. If both passes are on the same side of the imaged area, the stereo imagery is referred to as one-sided coverage and is identified in the table by a 1 in the stereo column. If the two passes are on opposite sides of the imaged area, the operation is referred to as two-sided stereo and identified by a 2 in the stereo column of the table. Two-sided stereo coverage provides superior vertical resolution, but requires a reorientation of the antenna during the mission and hence greatly increased command and control requirements. No detailed consideration has been given to the feasibility of such stereo coverage during a planetary mission.

The table lists experiment support requirements grouped into similar scientific requirements as to minimum useful image ground size (swath width) and horizontal ground resolution. A glance at the table shows that radar imaging experiments are generally heavier and more thirsty for power than any other imaging system considered. On the other hand, they offer the only possibility for penetrating thick atmospheres. The power requirements reflect the fact that radar systems are active remote sensors. All the other imaging systems considered in this study rely upon solar or thermal energy. It should also be emphasized that a great amount of design flexibility exists in the design of a radar system for this very reason. The support requirements given here are representative values and do not reflect

TABLE 7-17

SUPPORT REQUIREMENTS FOR RADAR

IMAGING EXPERIMENTS--VENUS

OBSERVABLE	STEREO	SWATH WIDTH (km)	HORIZONTAL RESOLUTION (km)	TYPE OF RADAR	ANTENNA SIZE (ft)	WEIGHT (lbs)	POWER (watts)	DATA RATE (bits/sec)
Surface Elevations	2	1000	20	NC	0.7 x 33	180	330	5.0×10^3
Surface Elevations	1	1000	20	NC	0.7 x 33	210	540	9.5×10^3
Contacts (regional)	-	1000	3	NC	0.7 x 220	240	230	1.9×10^4
Surface Appearance (regional)	-	1000	3	NC	0.7 x 220	240	230	1.9×10^4
Structure of Features (regional)	2	1000	3	NC	0.7 x 220	240	250	2.1×10^4
Surface Topography (regional)	2	1000	3	NC	0.7 x 220	270	330	3.2×10^4
Structure of Features (regional)	1	1000	3	NC	0.7 x 220	240	250	2.1×10^4
Surface Topography (regional)	1	1000	3	NC	0.7 x 220	300	540	6.3×10^4
Contacts (local)	-	100	0.2	SA	4 x 57	310	190	2.0×10^5
Surface Appearance (local)	-	100	0.2	SA	4 x 57	310	190	2.0×10^5
Structure of Features (local)	-	100	0.2	SA	4 x 55	310	210	2.1×10^5
Surface Topography (local)	-	100	0.2	SA	4 x 49	320	330	4.2×10^5
Structure of Features (local)	2	100	0.2	SA	4 x 57	310	190	2.0×10^5
Surface Topography (local)	2	100	0.2	SA	4 x 49	310	310	3.8×10^5
Structure of Features (local)	1	100	0.2	SA	4 x 43	360	450	2.1×10^6
Surface Topography (local)	1	100	0.2	SA	4 x 43	390	2800	4.3×10^6
Contacts (detailed)	-	0.5	0.005	SA	10 x 42	620	2.2×10^4	1.3×10^6
Surface Appearance (detailed)	-	0.5	0.005	SA	98 x 42	4200	320	1.3×10^6
Structure of Features (detailed)	-	0.5	0.005	SA	8 x 39	540	3.2×10^4	1.3×10^6
Surface Topography (detailed)	-	0.5	0.005	SA	84 x 39	3400	420	1.3×10^6
Surface Topography (detailed)	-	0.5	0.005	SA	8 x 39	540	3.2×10^4	1.3×10^6
Topographic Changes	-	0.5	0.005	SA	8 x 39	540	3.2×10^4	1.3×10^6
Layering	-	0.5	0.0003	SA	330 x 2	1000	9.4×10^4	3.5×10^8
Animal Life	-	0.3	0.0002	-	-	-	-	-

an optimized design in any sense.

Surface elevations experiments require only 20 km horizontal ground resolution, hence antenna lengths of only about 30 feet are required. The two-sided stereo mode affords a lower average power requirement and a decreased data rate as compared to the one-sided mode. As with all other Venus orbital imagery experiments, at least 120 Earth days are required to achieve 70 percent planetary coverage. Three km horizontal resolution is provided by noncoherent systems with antenna lengths of about 200 feet. Table 7-17 indicates that regional scale radar imagery at Venus can be provided by noncoherent systems weighing 200-300 pounds, consuming 300-500 watts of power, and collecting data at a rate of roughly 10,000 bits/sec. All local scale imagery requires synthetic aperture systems of 300-400 pounds with antenna lengths of about 50 feet. Power requirements range from about 200 to 3000 watts depending upon the required vertical resolution and the mode of coverage. If the one-sided mode of stereo coverage is rejected, the power requirements reduce to 200-300 watts. Data rates for local scale experiments are in the range of 10^5 - 10^6 bits/sec.

For detailed scale imagery, tradeoffs may be performed between the weight and power requirements by adjusting the antenna size. By using a large antenna to focus the transmitted power upon the desired ground area, the power requirement may be reduced at the expense of antenna weight. For example, contacts and surface appearance experiments require essentially the same imagery. By using a ten foot wide antenna, the system weight may be reduced to 600 pounds, but 20 kilowatts of power are required. Alternatively, by increasing the antenna width a factor of ten, the power requirement is reduced by a factor of 100, while the system weight is increased nearly a factor of ten. A reasonable compromise might result in system weights about 1000 pounds and power requirements of about one kilowatt. In any event, the data acquisition rate is about 10^6 bits/sec.

Experiments requiring less than one meter ground resolution are either prohibitively expensive (1000 pounds and 100 kilowatts) or are beyond the state-of-art.

Support requirements for radar imaging experiments at Mars and Mercury are similar to those at Venus. Noncoherent systems can be used for regional scale experiments, but local and detailed experiments demand synthetic aperture systems if the antenna length is to be kept within reasonable bounds. The scientific objectives for which radar imagery is useful at Mars and Mercury can also be achieved by visual imaging systems and at considerably reduced support requirements. Regional stereo coverage is the exception to this rule. That is, stereo visual coverage of 70 percent of Mars requires a mission duration of about 330 days, while stereo radar coverage of 70 percent of Mars can be acquired in less than ten days. Similarly at Mercury only 34 percent of the planet's surface is ever properly illuminated for visual stereo imagery. Radar stereo imagery of the entire surface can be achieved in 30 Earth days.

Radar imagery of Jupiter from the orbital altitudes considered in this study (higher than 2.5 Jupiter radii) does not appear feasible. Wavelengths of at least 30 cm will be required to penetrate the visible atmosphere to any appreciable depth. From an altitude of about 200,000 km, a noncoherent radar system will require an antenna nearly one kilometer in length to achieve a "ground" resolution of even 100 km. In addition, whether a noncoherent or synthetic aperture system is employed, the required transmitter powers are orders of magnitude beyond the foreseeable state-of-art.

8. CONCLUSIONS AND RECOMMENDATIONS

The study has provided a wealth of quantitative data on the subsystem requirements implied by an ongoing program of planetary orbiters. This data permits the mission analyst to define effective exploration plans and identify advanced technology needs. The results give the general subsystem support requirements and show the overall experimental trends, rather than the specific needs of an individual mission.

The research program has developed and implemented a method which yields meaningful subsystem requirements for a broad range of objectives, at many targets, and extending over a long period of planetary exploration. The very complex interrelationships between objectives, measurements, orbital operating conditions, instrument specifications, and spacecraft subsystem requirements have been understood and simplified effectively. This has been possible only because of the fundamental logic and the relative simplicity of the method.

Significant contributions have been made in each of the task areas. This is the first time that such detailed measurement specifications have been defined over so broad a spectrum of scientific disciplines. These specifications are unique in their depth, breadth, and freedom from mission or spacecraft design constraints. They bridge the chasm between the enunciated policies and goals of the scientific exploration of space and the detailed information required by the mission analyst in his planning of future planetary missions.

The study has provided a much better understanding of spacecraft orbits about Venus, Mercury, and Jupiter than previously existed. The first order motions and perturbations are now quite well defined. Of even greater importance is the understanding that has been obtained in selecting orbits to meet given measurement requirements.

The scaling laws, in most cases, provide the first formal synthesis of the criteria which are used in the design of experiments. They are based principally on the current state of the art and indeed, the study results can be used to define advanced technology development needs for the measuring instruments themselves. In the performance of the study, some insight in this direction has been gained. For instance, although no such instrument exists, an orbiting radio frequency imager would be invaluable for monitoring the bursts of decameter radiation at Jupiter. Also variable focal length systems of low distortion could be very effectively used over much of the electromagnetic spectrum.

The vast amount of data generated by this research effort cannot be summarized adequately without gross oversimplification. Nonetheless, some of the more important results of the study are recapitaled here to provide the reader with a broad appreciation of the need for orbital imagery in planetary exploration, the role played by various imaging sensor systems, the limitations of orbital imagery (both in principle and in practice), and requirements imposed upon spacecraft design by orbital imagery.

The analysis of scientific objectives has indicated that although no portion of the electromagnetic spectrum is without virtue, some portions are more useful than others. It is no surprise that the visible portion of the spectrum is the most useful for obtaining imagery from orbit. At Mars both surface and atmospheric phenomena demand visual imagery. The same would be true at Mercury, except it has no atmosphere. Venus and Jupiter both have active atmospheres which can be investigated in the visible, but the atmospheres are undoubtedly so dense that the surface cannot be seen from orbit. Radar imagery, which is the only active imagery considered in this study, is possibly the next most important type of imagery, since it provides the only chance of penetrating to the surface

of Venus. Unfortunately, radar systems tend to be heavy and consumers of power, and are probably not even feasible at Jupiter. Infrared imagery is useful for a wide variety of atmospheric studies and for detection and mapping of both atmospheric and surface thermal anomalies. Therefore infrared imagers are expected to be included in most orbiting payloads at Venus and Jupiter. Passive microwave systems are potentially useful for studying thermal anomalies (surface and atmosphere) and also for mapping convective cells and associated turbulence in the atmosphere. Ultraviolet imagers are not expected to contribute materially to the scientific data collected by orbiting missions, except for study of some anomalous atmospheric features which have been observed at Venus.

The scientific requirements for orbital imagery have been translated into specifications describing the desired imagery to provide a starting point for the imaging system designer. Nominal values for the image specifications have been provided in Table 4-1, and represent the imagery which is desired without regard to the ease (or difficulty) of obtaining the imagery. Recognizing that this may place an undue strain upon the imaging system designer, the nominal values have been supplemented by "worth curves" which suggest how far the nominal values may be relaxed without seriously jeopardizing the scientific value of the imagery. The experiment support requirements estimated during this study are based upon these "relaxed" specifications. These specifications imply an exploration hierarchy involving first, second, and even third generation missions aimed at acquiring data of increasing detail. That is, requirements for regional, local, and detailed scale imagery have been carefully defined. At Mars, Venus, and Mercury, the regional scale imagery requires minimum scene areas from about 600 x 600 km to 1500 x 1500 km with ground resolutions ranging from three to 20 km. Because of Jupiter's size, regional scale imagery at that planet demands minimum scene areas from 5000 x 5000 km to

15000 to 15000 km and acceptable ground resolutions of 20 to 100 km. Local scale imagery at Mars, Venus, and Mercury implies scene areas of about 100 x 100 km with a ground resolution of 200 meters for surface phenomena and three km for atmospheric phenomena. Since the nature of Jupiter's "surface" is unknown, no requirements have been defined for surface imagery except on a regional scale. Local scale atmospheric imagery at Jupiter should view areas of at least 600 to 1500 km on a side with a resolution of about three km. Detailed scale imagery has been defined for Mars, Mercury, and Venus and involves scene areas of about 500 x 500 meters and resolutions of five meters or less.

Some types of surface imaging experiments must supply vertical height information, if the scientific requirements are to be achieved. In general, regional scale experiments are directed towards detection of one to three km height differences, local scale 100 to 200 meters, and detailed scale 50 meters. Thermal mapping experiments require detection of five deg K temperature differences at Venus and Mercury, and two deg K at Mars and Jupiter. The fractional amount of the planet's area which must be imaged depends on the scale of exploration. That is, regional scale experiments generally require at least 70 percent coverage, local scale about ten percent, and detailed scale one percent or less. Finally, since most atmospheric phenomena are dynamic, nearly all of the regional scale atmospheric imaging experiments require rapid coverage of large areas, and many of the atmospheric experiments require repetitive imagery. This can be performed on a short period basis to detect temporal variations, or on a long period basis to detect seasonal variations.

Orbit selection for imaging experiments is controlled by the amount and location of the desired planetary coverage, applicable solar illumination constraints, the minimum acceptable ground area per image, and the amount of image overlap. The orbits selected during this study are representative of those orbits which are likely to be selected for specific orbital missions. Actual mission design involves launch vehicle and spacecraft constraints which have not been considered in any detail here. Nonetheless a number of basic incompatibilities between scientific requirements and orbital mechanics constraints have been identified. Most of these difficulties are associated with the amount of coverage required and the available solar illumination.

At Mars, the coverage required for regional scale imagery (70 percent) can be obtained from orbit in three to ten days, provided there are no solar illumination constraints or simply daylight illumination is required. A minimum of about 330 days is necessary to achieve 70 percent coverage at solar zenith angles less than 20 degrees, as is desired for visual stereo imagery. Image interval times (the time interval between opportunities for observing a specific location on the planet) are normally restricted to less than a couple minutes or greater than a couple hours. Seasonal repetitions are easily achieved.

At Venus 120 Earth days are required to obtain 70 percent coverage under daytime conditions, or if there are no solar illumination constraints. Most of the imaging experiments at Venus require only daylight illumination or are independent of the solar illumination. Therefore, regional scale coverage can be repeated at most twice a planetary year. It is difficult to provide image interval times greater than a few minutes and less than 1.5 hours.

At Mercury, 70 percent coverage can be achieved in 30 or 40 Earth days, provided there are no solar illumination constraints or at worst daylight constraints. The coverage can

be repeated every 30 or 40 days. However, only 64 percent of the surface is illuminated at solar zenith angles less than 40 degrees, and only 34 percent at zenith angles less than 20 degrees. Only about half the available area can be covered by an inertial orbit, and two Mercury years (about 180 Earth days) are required to obtain this coverage. Therefore, completely satisfactory visual color or stereo imagery at regional scale (70 percent coverage) cannot be obtained at Mercury.

At Jupiter, the desired imaging experiments have no stringent solar illumination constraints. Complete, or nearly complete, planetary coverage can be obtained easily in about 20 to 40 Earth days. Virtually any image repetition rate can be provided by proper orbit selection.

At each planet, the orbit selections have been used with the various imaging system scaling laws to estimate the experiment support requirements for those orbital experiments which are expected to be useful in achieving the scientific objectives. The estimated requirements are sensitive to the orbital parameters, the imaging system design, and, of course, the scientific requirements. Many tradeoffs in the analysis are possible, most of which affect the experiment support requirements, many of which are not immediately obvious. One of the more important tradeoffs found common to all the imaging systems studied is that imagery obtained from an elliptic orbit over any significant altitude range results in increased weight, power, and data acquisition rates as compared to use of a constant, or nearly constant, imaging altitude. Thus experiment support requirements can be traded off against the velocity change of the orbit capture maneuver and the mission duration required to achieve the desired amount of planetary coverage.

All the visual imaging experiments suggested by this study employ imaging systems which are within reach of the

current state-of-art, except for those few experiments which require ground resolutions of less than five meters. In fact, it appears that ground resolutions on the order of one meter are not feasible with any type of orbital imaging system. Most of the atmospheric imaging experiments at Mars and Venus can be performed by a one-half-inch vidicon system weighing eight pounds, consuming eight watts of power (average), and acquiring data at a rate of 25,000 bits/sec, or less, assuming six binary bits per resolution element. At Jupiter, the high imaging altitudes and elliptic orbits require a two-inch RBV (return beam vidicon) system using about 30 watts of power and a data rate of 4×10^5 bits/sec. For 20 km ground resolution, the system weighs about 50 pounds, but for 3 km ground resolution, the system grows to 300 pounds because of the large optical subsystem required. Support requirements for surface imagery at Mars and Mercury are 15-30 pounds, 15-30 watts, 5,000-500,000 bits/sec for regional scale imagery, 30-60 pounds, 30-100 watts, 10^6 - 10^7 bits/sec for local scale imagery, and 300-500 pounds, 30-300 watts, 10^7 - 10^8 bits/sec for detailed scale imagery.

Orbital radar imaging experiments are not feasible at Jupiter, at least from the orbital altitudes considered here, as enormous amounts of power are required. At Mars, Venus, and Mercury, the weight, average power, and data acquisition rates are 200-300 pounds, 300-500 watts, about 10,000 bits/sec for regional scale imagery, 300-400 pounds, 200-300 watts, 10^5 - 10^6 bits/sec for local scale imagery, and about 1000 pounds, 1000 watts, and 10^6 bits/sec for detailed scale imagery. Ground resolutions of less than five meters are not feasible

Except at Jupiter, all the atmospheric infrared imaging experiments can be performed by a scanning system weighing two to six pounds, consuming about two watts of power, and collecting data at a rate of less than 7,000 bits/sec. Regional scale surface imagery at Mars and Mercury requires 2-10 pounds, about five watts, and less than 15,000 bits/sec,

while local scale surface imagery requires 50-100 pounds, 5-30 watts, and about 10^6 bits/sec. Detailed scale imagery and atmospheric imagery at Jupiter do not appear to be feasible.

Surface passive microwave imagery from orbit is feasible only at Mars and Mercury, and then only for regional scale imagery. A typical imaging system is estimated to weigh about 500 pounds, consume 100 watts of power, and collect about 2000 data bits/sec. Atmospheric imaging experiments are applicable only to Venus and Jupiter. At Venus the atmospheric experiments require 20-100 pounds, 20-80 watts, and 200-2,000 bits/sec. At Jupiter the experiments desired are not feasible.

Ultraviolet scanning systems can be used at Mars, Venus, and Mercury. For three km ground resolution, a typical system weighs about two pounds, consumes only one watt of power, and collects data at rates from 2,000 to 250,000 bits/sec, depending upon the orbit. A ground resolution of 200 meters can be achieved by a 50 pound system with a 10^6 bit/sec data rate and one watt average power.

Multispectral scanning systems are likely to be very useful at Mars, Venus, and Mercury. Support requirements for such systems will be similar to those for infrared scanning systems, although the data acquisition rates will depend upon the number of channels required. Multifrequency radar systems might be useful at Mars and Venus, especially for study of atmospheric precipitation. The support requirements are likely to be somewhat more demanding than for monochromatic radar systems. Passive radiofrequency imaging systems would be especially useful at Jupiter, but the design of such systems is so speculative that scaling laws have not been derived during this study.

The recommendations which have resulted from the study can be summarized as follows:

The analytical techniques developed here should be reviewed and extended. At present they are a major first step, but include no tradeoffs between subsystem requirements nor any attempt at optimization.

The results should be carefully analyzed to identify the demands imposed on spacecraft subsystems, and the demands should be compared with projected subsystem capabilities.

The subsystem requirements for non-imaging orbital experiments should be developed and integrated with the imaging requirements.

The requirements for outer planet missions beyond Jupiter should be identified, since they may be more demanding on the subsystems than the closer planets.

The present analysis should be extended to atmospheric probe and lander experiments, since they may ultimately make the most severe demands on advanced technology developments.

REFERENCES

IIT RESEARCH INSTITUTE

REFERENCES

- Adams, J., et al., "A Strategy for Scientific Exploration of the Terrestrial Planets," JPL Cal. Inst. Tech., 1967.
- Anderson, D. L., and Kovach, R. L., "The Internal Structure of the Moon and Terrestrial Planets, JPL TM 32-66, pp. 84-91.
- Brandt, J.C., and Hodge, P. W., "Solar System Astrophysics," McGraw-Hill Book Co.
- Chandrasekhar, S., "Hydrodynamic and Hydromagnetic Stability," Oxford Univ. Press, London, 1961.
- Davidson, G.T., and Anderson, A. D., "Venus: Volcanic Eruptions May Cause Atmospheric Obscuration," Science, Vol. 156, 1729-1730, 1967.
- Dufour, L., and Defay, R., "Thermodynamics of Clouds," (Vol. 6 of International Geophysics Series) Academic Press, N.Y., 1963.
- Dungey, J. W., "Cosmic Electrodynamics," Cambridge Univ. Press, 1958.
- Efron, L., Jet Propulsion Laboratory, private communication.
- Ellis, G.R.A., and McCullough, P.M., "Decametric Radio Emission of Jupiter," Nature 198, 275, 1963.
- Fleagle, R.G., and Businger, J.A., "Atmospheric Physics," Academic Press, N.Y., 1963.
- Goody, R.M., "Atmospheric Radiation," Oxford University Press, 1964.
- Goudas, C.L., et al., "The Shape of the Moon as Deduced from the Orbiter Determination of Its Gravity Field," Boeing Scientific Research Labs., 1966.
- Hide, R., "On the Dynamics of Jupiter's Interior and the Origin of Its Magnetic Field" in "Magnetism and the Cosmos," Oliver and Boyd Ltd., Edinburgh, 1965.
- Hitchcock, D. R., and Lovelock, J.E., "Life Detection by Atmospheric Analysis," Icarus 7, 149-159, 1967.

REFERENCES (Continued)

- Jeffreys, H., "The Earth," Cambridge University Press, 1962.
- Kaula, W., "The Geometric and Dynamical Figures of the Moon," Univ. of Calif., 1966.
- Keene, G.T., "Venus: Uniformity of Clouds, and Photography," Science 159, 305, 1968.
- Kellogg, M.W., and Sagan, C., "The Atmospheres of Mars and Venus," Nat. Acad. of Sci., Nat. Res. Council, Publ. No. 44.
- Koenig, L.R., et al., "Handbook of the Physical Properties of the Planet Venus," National Aeronautics and Space Administration, p. 116, 1967.
- Kovach, R.L., "Lunar Seismic Exploration," Dept. of Geophysics, Stanford Univ., 1966.
- Kuiper, G.P., "Atmospheres of the Earth and Planets," Univ. of Chicago Press, 1952.
- Lamley, J. L., and Panofsky, H.A., "The Structure of Atmospheric Turbulence," (Vol. XII in Interscience Monographs and Texts in Physics and Astronomy), Interscience Publishers, N.Y., 1964.
- Lockheed Missile and Space Company, "Study of Technology Requirements for Near Mars/Venus Operations," Appendix to Volume III - Parametric Operations Analysis, pp. 3-29 to 3-31, February 1968.
- Manning, L.A., "Minimal Energy Ballistic Trajectories for Manned and Unmanned Missions to Mercury," TND-3900, National Aeronautic and Space Administration, April 1967.
- Michaux, C.M., edit., "Handbook of the Physical Properties of the Planet Jupiter," NASA SP-3031, 1967.
- Mintz, Y., "The General Circulation of Planetary Atmospheres," Appendix 8 of "The Atmospheres of Mars and Venus," (ed. Kellogg and Sagan), Nat. Acad. of Sci., NRC Publ. No. 944, 1961.
- Mintz, Y., "The Energy Budget and Atmospheric Circulation on a Synchronously Rotating Planet," Icarus, Vol. 1, 172-173, 1962.

REFERENCES (Continued)

- Mueller, R.R., "A Chemical Model for the Tower Atmosphere of Venus," *Icarus*, Vol. 3, 285-298, 1964.
- Muller, P.M., and Sjogren, W.L., "Mascons: Lunar Mass Concentrations," *Science* 161, 680-684, 1968.
- Newell, R.E., "Venus - A Contribution to the Greenhouse - Ionosphere Debate," *Icarus*, Vol. 7, 114-131, 1967.
- Opik, E.J., "The Aelosphere and Atmosphere of Venus," *JGR*, Vol. 66, p. 2807, 1961.
- Opik, E.J., "Jupiter: Chemical Composition, Structure and Origin of A Giant Planet," *Icarus*, Vol. 1, 200-257, 1962.
- Owen, T.C., "Comparisons of Laboratory and Planetary Spectra II. The Spectrum of Jupiter from 9700 to 11200 A," *Astrophys. J.*, Vol. 141, 444-456.
- Rosinski, J., "On the Origin of Ice Nuclei," *J. of Atm. and Terr. Phys.*, Vol. 29, 1202-1218, 1967.
- Runcorn, S.K., "Continental Drift," Academic Press, New York, 1962.
- Sagan, C., and Miller, S.L., "Molecular Synthesis in Simulated Reducing Planetary Atmospheres," *Astron. J.* 65, 499, 1960.
- Sagan, C., and Kellogg, W.W., "The Terrestrial Planets," *Annual Review of Astronomy and Astrophysics*, Vol. I, Annual Reviews, Inc., Palo Alto, Calif. pp. 235-266, 1963.
- Warwick, J.W., "Dynamic Spectra of Jupiter's Decametric Emission," *Astrophys. J.* 137, 41-60, 1963.

APPENDIX A
ORBIT SELECTION EXAMPLE

IIT RESEARCH INSTITUTE

APPENDIX A

ORBIT SELECTION EXAMPLE

To illustrate the use of the stereographic projection technique in selecting spacecraft orbits for a family of imaging measurement specifications, consider family number 7 (as defined by Table 5-3) at Mars. This family consists of regional scale imagery in support of the observables Contacts, Surface Winds, and Biochemical Systems. The family measurement specifications are summarized in Table A-1. The minimum acceptable scene area is 600 x 600 km, and the desired solar elevation angle is in the range 30-60 degrees.

Because of the solar illumination constraints, the most useful stereographic projection is one which uses the Martian subsolar point as the point of tangency. The primitive circle, which is the projection of a great circle every point of which is midway between the point projection source and the point of tangency, is then the projection of the terminator. The projection of the subsolar point appears as the center of the primitive circle or terminator. To locate the projection of Mars orbit plane, equator, and poles, specific arrival conditions must be considered.

Figure A-1 shows the stereographic projection appropriate to the arrival conditions (on October 13, 1984) for the selected 1984 interplanetary transfer. At this time, the subsolar point is at twenty degrees south latitude, and hence the projection of the South Pole appears within the primitive circle. It is nearly mid-summer in the Southern hemisphere. The projection of the heliocentric orbit plane of Mars appears in the figure as a straight line making an angle of 25 degrees with the equator, since the rotation axis of Mars is tipped at 25 degrees relative to the orbit plane. The vertical line shown

Table A-1

MEASUREMENT FAMILY SPECIFICATIONS

FAMILY OBSERVABLES.....	3 - Contacts (Regional)
	18 - Surface Winds (Regional)
	40 - Biochemical Systems
MINIMUM IMAGE SIZE.....	600 km
MINIMUM OVERLAP.....	20%
MINIMUM COVERAGE.....	70%
SOLAR ELEVATION RANGE.....	30 - 60 deg
COVERAGE DISTRIBUTION.....	--
TIME FOR COVERAGE.....	--
IMAGE INTERVAL.....	< 2 hr
COVERAGE INTERVAL.....	> 4/ yr

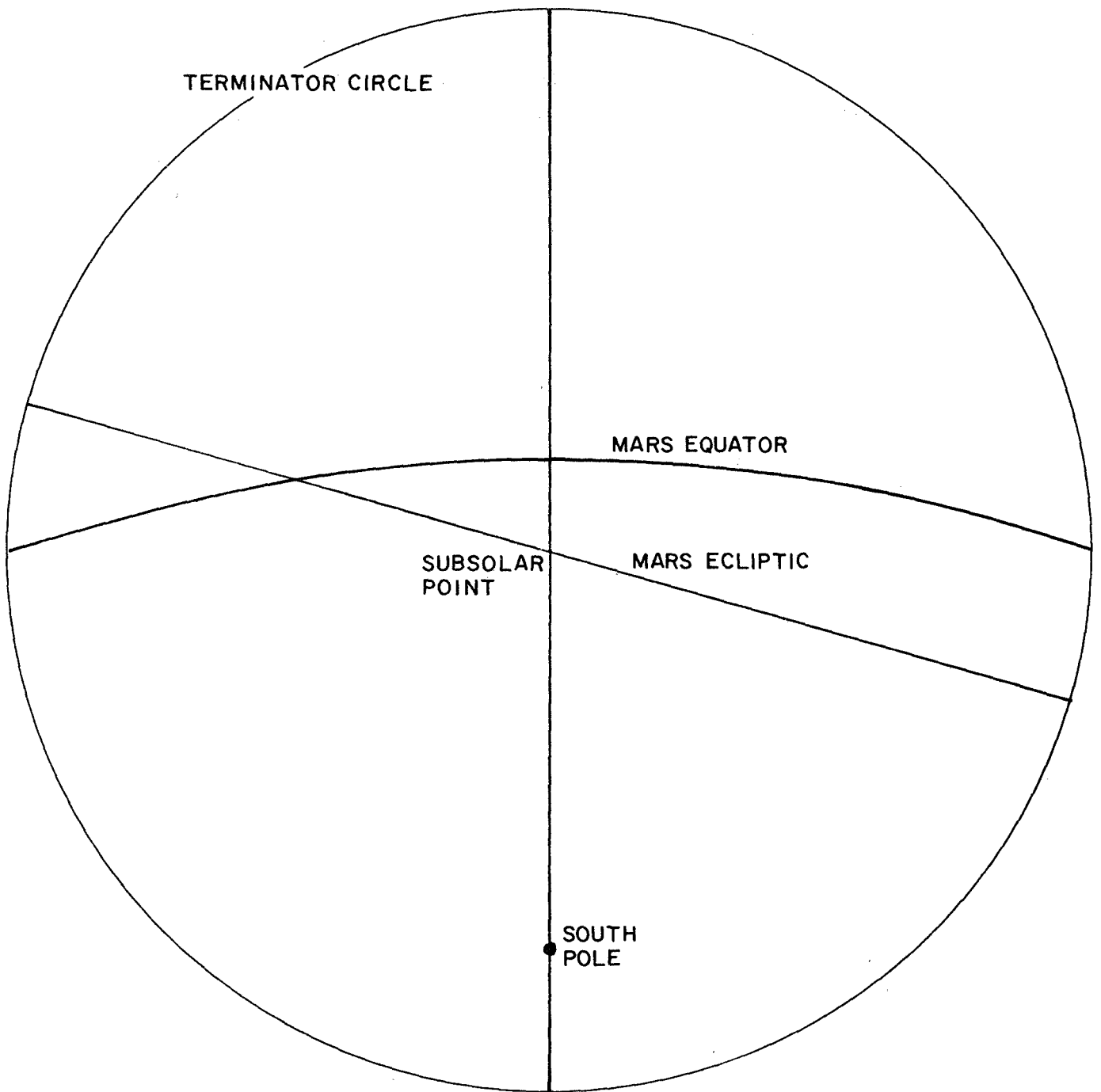


FIGURE A-I. STEREOGRAPHIC PROJECTION: ARRIVAL CONFIGURATION

in the figure represents a meridian passing through the subsolar point and the poles.

The planetary surface may be regarded as rotating underneath the stereographic projection, rotating once each Mars day. The planetary coverage which can be achieved at the desired solar illumination can be visualized by drawing the solar elevation limits on the stereographic projection. If the subsolar point has been used as the point of tangency, the locus of points of constant solar elevation angle is projected onto the stereographic projection as a circle about the subsolar point. At the subsolar point itself, the solar elevation angle is 90 degrees. Figure A-2 shows the solar illumination constraints for family number 7. In order to satisfy the measurement specifications, the imagery must be acquired from within the annular region bounded by the circles representing solar elevation angles of 30 and 60 degrees.

The direction of the approach asymptote may also be located on the stereographic projection. The interplanetary transfer parameters given in Table 5-1 show that, for the example considered here, the declination of the approach asymptote is 32.92 degrees below the equator while the angle between the subsolar point and the approach asymptote is 77.94 degrees. Thus the projection of the direction of the approach asymptote appears on the stereographic projection as shown in Figure A-2.

Assuming a coplanar periapse capture maneuver, possible locations of orbit subperiapse points form a minor circle on the planet surface centered on the direction of the approach asymptote. This minor circle may be projected onto the stereographic projection plane as illustrated in Figure A-2. The exact locus of periapse locations depends upon the specific value of the orbit periapse altitude. Three different orbit sizes, which are consistent with obtaining scene areas of 600 x 600 km with 20 percent overlap, are given in Table A-2. The periapse altitudes for these orbit sizes are sufficiently similar that the locus

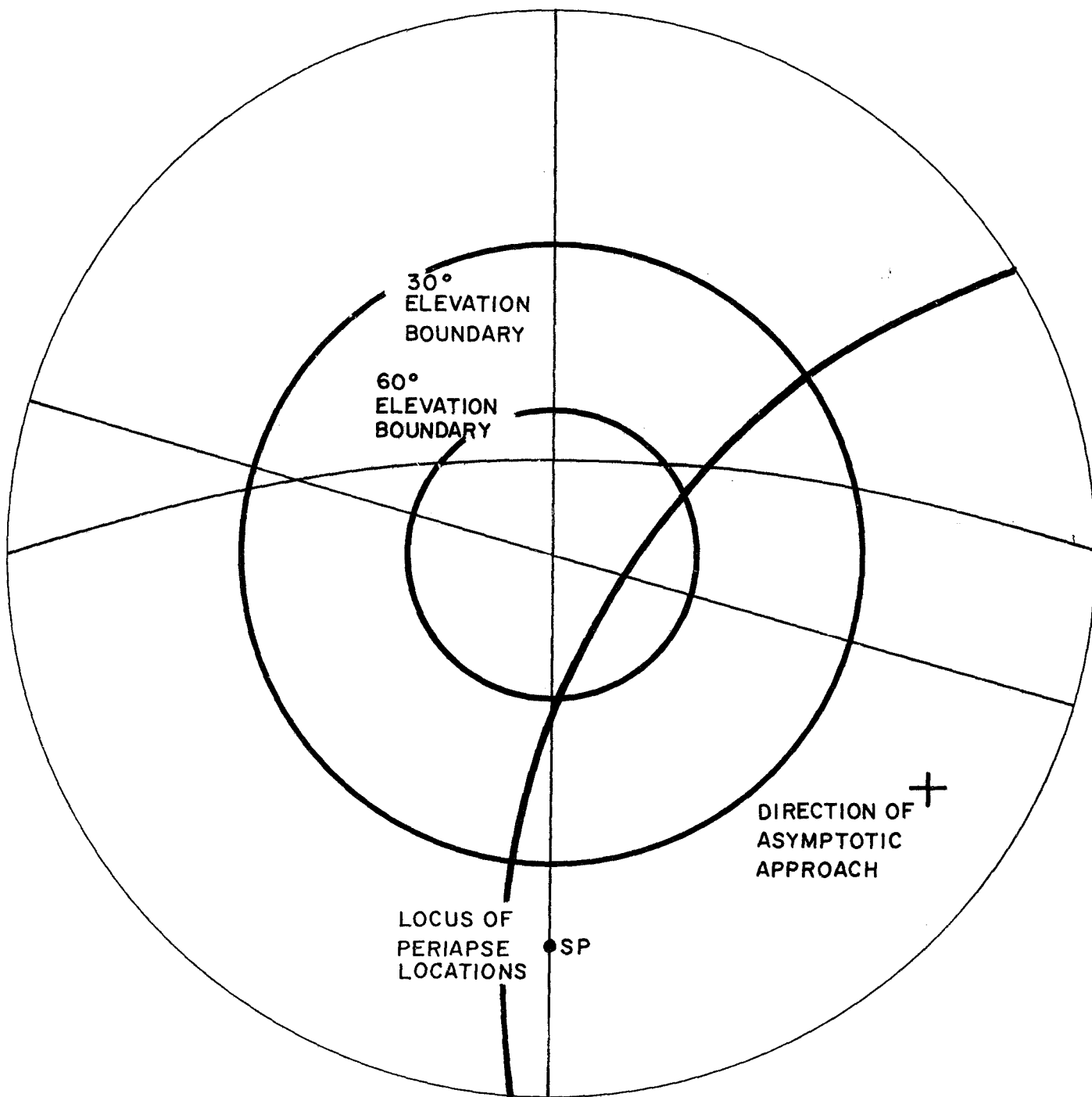


FIGURE A-2. STEREOGRAPHIC PROJECTION: CONSTRAINTS.

Table A-2

MARS CANDIDATE ORBIT SIZES

<u>Orbit Parameters</u>	<u>Orbit Number</u>		
	<u>1</u>	<u>2</u>	<u>3</u>
Eccentricity.....	0.0	0.4633	0.6115
Periapse Altitude.....	969	425	385
Maximum Altitude Ratio.....	1.0	16.4	31.8
Number of Orbits per day.....	10	5	3
Number of days to complete coverage....	5	10	15
Minimum Image Size.....	600	600	600
Minimum Overlap.....	30.6	27.8	23.1

of periapse locations shown in Figure A-2 is valid for all three orbit sizes.

Sufficient information is now given in Figure A-2 to facilitate orbit selection for the measurement family. Possible orbit selections appear on the stereographic projection plane as circular arcs which intersect the primitive circle (in this case the terminator circle) at two points which are 180 degrees apart. The projection of any orbit resulting from a direct coplanar capture maneuver must pass through the asymptotic approach direction point shown on the projection. In order to maximize the initial latitude coverage, the orbit arc should be oriented vertically on the projection and should be tangent to the inner solar elevation boundary. To maintain maximum coverage with increasing mission duration, the orbit should be sun-synchronous if solar illumination constraints are critical. This may be accomplished by selecting an orbit inclination such that oblateness perturbations move the orbit ascending node in the same direction and at the same rate as the Sun's motion. On the stereographic projection plane, the subsolar point appears to move along the line representing the orbit plane of Mars.

Using orbit size number two (as defined in Table A-2), two options which satisfy the factors discussed above are shown in Figure A-3. Both of the options shown precess correctly with the subsolar point motion, and both provide a large measurement arc within the area properly illuminated by the Sun. Option two, however, provides slightly more latitude coverage. The circular orbit (orbit size number one) could equally well have been selected and would yield somewhat different results. However, imagery would then be acquired from an altitude of 969 km. Using orbit size number two it is possible to acquire the imagery from a lower altitude. A sun-synchronous orbit of size number three requires a low orbit inclination and hence does not provide as much latitude coverage as the selections shown in Figure A-3. In the stereographic projection, the orbit inclination is simply

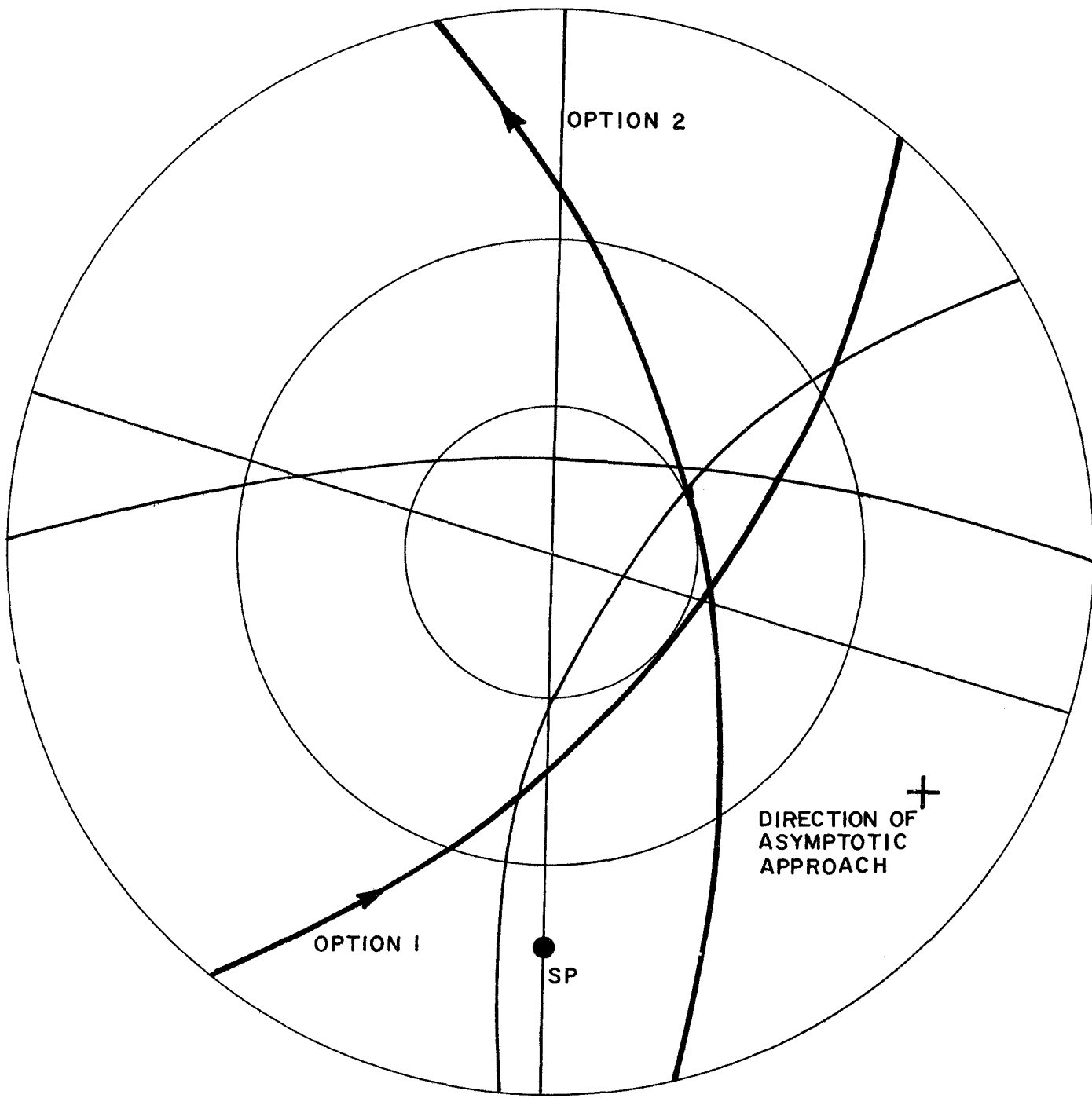


FIGURE A-3. STEREOGRAPHIC PROJECTION: ORBIT OPTIONS

the angle between the projected orbit arc and the projection of the equator. It should be noted that neither orbit option shown in Figure A-3 passes through the asymptotic approach direction point. That is, a coplanar periapse capture maneuver cannot be used to directly set up either option.

The stereographic projection is useful in determining an appropriate intermediate orbit. An initial capture maneuver injects the spacecraft into an intermediate (first) orbit, and at some later time a second impulse maneuver transfers the spacecraft from the intermediate orbit into the final orbit (either option one or two). The projection of the intermediate orbit must pass through the projected direction of asymptotic approach and must also intersect the projection of the final desired orbit. To minimize the impulse of a plane change maneuver, the periapse of the final orbit should occur at the projected intersection of the initial and final orbits. Furthermore, if the final orbit is elliptical, it is usually desirable to locate its periapse over the region of proper solar illumination in order that imagery may be acquired from low altitude. The point of intersection between the initial and final orbits should be on, or near, the arc representing the locus of periapse locations so that an efficient capture maneuver into the initial orbit can be made at, or near, the periapse of the hyperbolic approach trajectory. Finally, at the point of intersection, the angle between the two orbit projections should be small to minimize the extent of the required plane change.

One solution to the problem is illustrated in Figure A-4 in which orbit A is the initial, or intermediate, orbit and orbit B is the final orbit (equivalent to option two in Figure A-3). An initial orbit capture maneuver occurring 5.5 degrees past the approach trajectory periapse matches the peripase points of the initial and final orbits. Both orbits have the same periapse altitude (425 km), but the initial orbit has an eccentricity of 0.9. This permits an economical orbit transfer impulse at

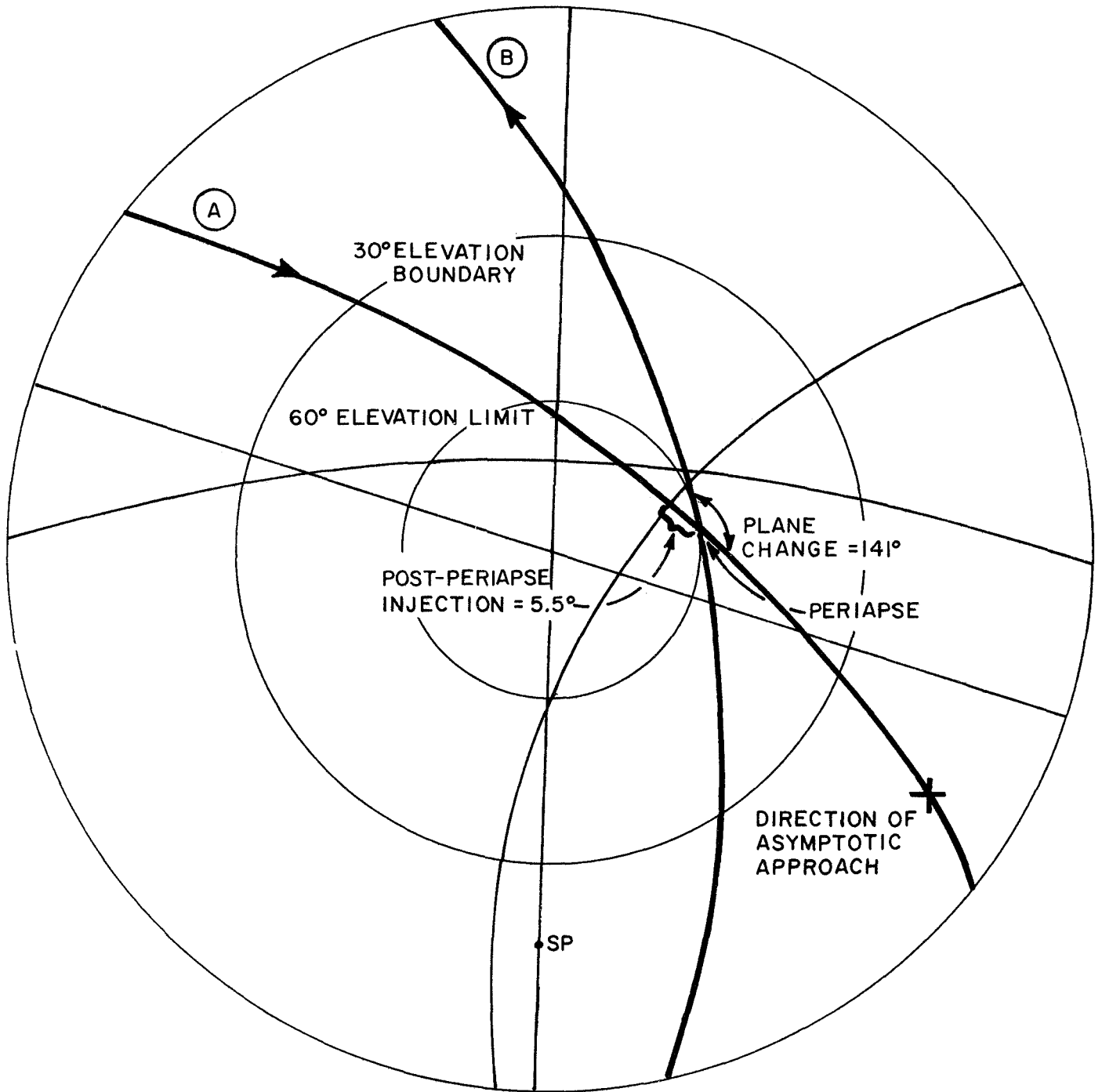


FIGURE A-4. STEREOGRAPHIC PROJECTION: ORBIT SELECTION.

apoapse of the initial orbit changing its plane (but not its size) 141 degrees to match the plane of the final orbit. At the next periapse passage, a final impulse maneuver is made reducing the eccentricity to 0.4633, thus establishing the final orbit. The required three impulses are:

1. off-periapse insertion - 1.36 km/sec
2. plane change - 0.46 km/sec
3. eccentricity change - 0.57 km/sec

and hence the total impulse required is 2.39 km/sec.

The maximum declination (southward) of the Sun occurs 60 days after the arrival date. Using the selected final (imaging) orbit, complete longitude coverage is obtained every ten days, assuming scene areas of 600 x 600 km and 23 percent scene overlap at the equator. Thus six complete longitude coverages can be achieved during the first 60 days of the mission. The orbit/illumination configuration at the end of this period is shown in Figure A-5. Further imagery obtained at this time would repeat the coverage previously obtained as the Sun moves back towards the Northern hemisphere.

This example demonstrates how the various factors of orbit selection were generally treated in the study. At times in the selection process it was necessary to modify this method of analysis to adapt to different planet characteristics and/or measurement specifications. The one notable change to this technique occurred at Mercury. The selection process was obvious and in all cases resulted in polar orbits. However, the degree of measurement achievement was difficult to determine from a stereographic projection because the planet rotates slower than the Sun's motion across its surface. Hence, actual ground traces with keyed solar elevation limits were constructed with the aid of a computer program for extended mission durations. The amount of coverage was then determined directly from these plots. A more detailed description of this analysis and ground trace plots are presented

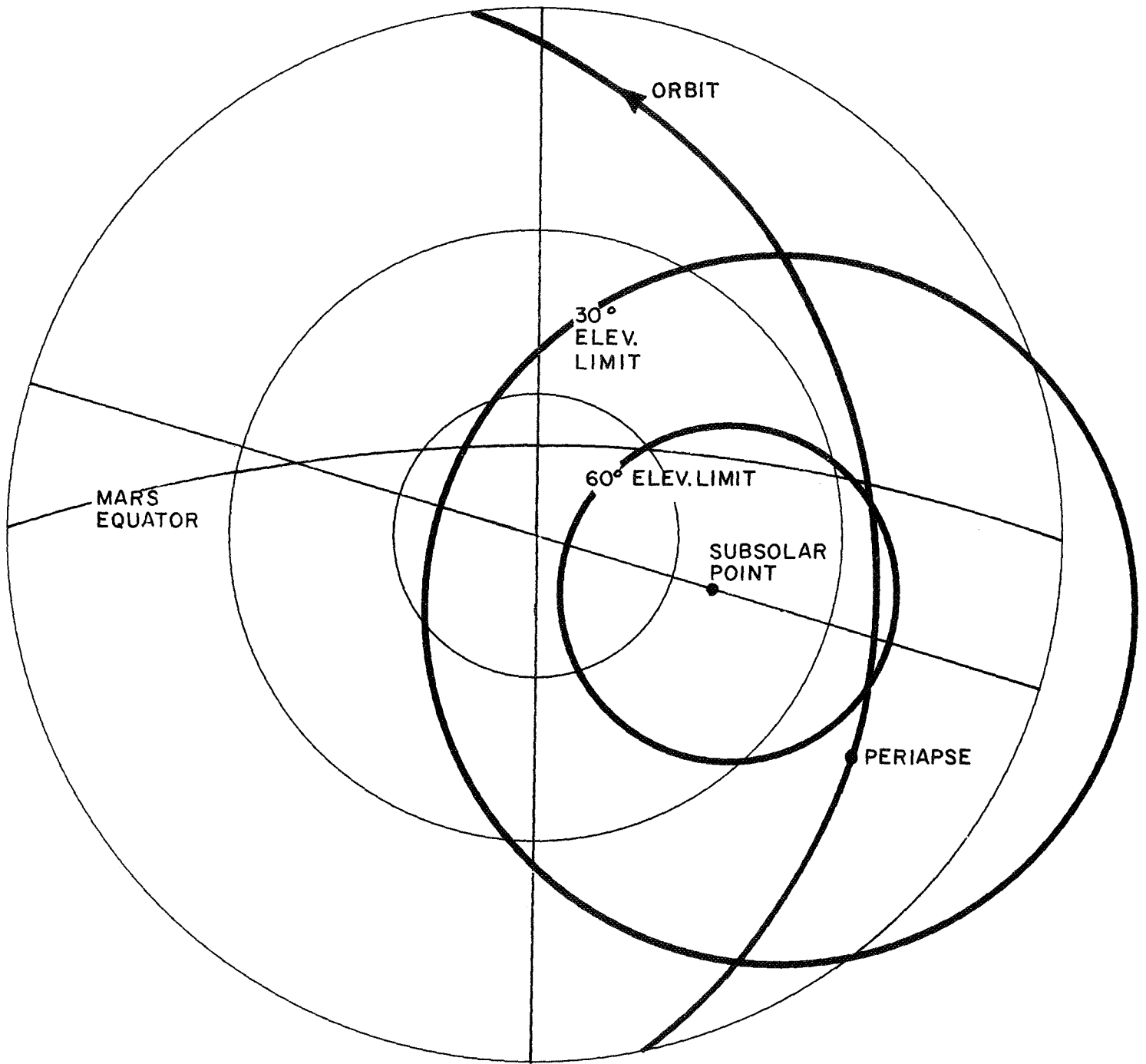


FIGURE A-5. STEREOGRAPHIC PROJECTION: 60 DAYS AFTER ARRIVAL

in the discussion of Mercury orbit selection results presented in Section 5 of this volume.